U.PORTO

DOCTORAL PROGRAMME IN PHARMACEUTICAL SCIENCES

PHARMACOLOGY AND PHARMACOTHERAPY SPECIALITY

Development of New Drug Combinations for Cancer Treatment

Diana Sousa Duarte

D

2023

U.PORTO
FACULDADE DE FARMÁCIA
UNIVERSIDADE DO PORTO

Development of New Drug Combinations for Cancer Treatment

Diana Sousa Duarte [1]

Doctoral Thesis in Pharmaceutical Sciences – Pharmacology and Pharmacotherapy Speciality (240 ECTS) submitted to the Faculty of Pharmacy of the University of Porto

Supervisor: Professor Doutor Nuno Filipe de Sousa Vale [2], Faculty of Medicine, University of Porto, Portugal

Co-Supervisor: Professor Doutor Jorge Manuel Moreira Gonçalves [3], Faculty of Pharmacy, University of Porto, Portugal

Porto, Portugal

January 2023

[1] up201201433@ff.up.pt [2] nunovale@med.up.pt [3] jgoncalves@ff.up.pt

This Doctoral Thesis was supported financially by *Fundação para a Ciência e Tecnologia* (FCT, Portugal) through the research grant [SFRH/BD/140734/2018].

The experimental work presented in this Doctoral Thesis was performed in the Department of Pharmacology of the Faculty of Pharmacy, University of Porto, Portugal, and in the Oncopharma Lab in the Department of Community Medicine, Health Information and Decision (MEDCIDS), Faculty of Medicine, University of Porto, Portugal.

“Para ser grande, sê inteiro: nada

Teu exagera ou exclui.

Sê todo em cada coisa. Põe quanto és

No mínimo que fazes.

Assim em cada lago a lua toda

Brilha, porque alta vive.” – Ricardo Reis

TABLE OF CONTENTS

ACKNOWLEDGMENTS

Este foi um percurso duro, de força, superação e acima de tudo, de muito trabalho. Foram 4 anos de altos e baixos, marcados pelo meio por uma pandemia e uma guerra. Sem todos os meus pilares de apoio durante esta longa viagem, não teria conseguido chegar até aqui.

Uma das pessoas mais importantes deste meu percurso académico foi, sem dúvida, o meu orientador, o Professor Doutor Nuno Vale. Quero agradecer-lhe toda a confiança depositada em mim durante estes anos, por todo o conhecimento que me transmitiu e por me ter guiado nesta viagem. Obrigada por todos os conselhos dados ao longo destes anos, quer a nível científico como pessoal, e por toda a motivação dada nos momentos em que eu estava mais em baixo. Obrigada por me chamar à razão quando assim era necessário e por me mostrar que o trabalho árduo compensa sempre.

Gostaria de agradecer também ao meu coorientador, o Professor Doutor Jorge Gonçalves, por me ter acolhido tão bem no seu laboratório nos dois primeiros anos do meu doutoramento e por ser sempre uma pessoa bastante correta comigo. Agradecer ainda à Céu, à Mónica e ao Dany por tudo o que ensinaram nos anos que estivemos juntos no laboratório da FFUP. Adorei partilhar conhecimento convosco e nunca me vou esquecer de tudo o que fizeram por mim nesses anos.

Não posso deixar de agradecer a todas as colegas de laboratório com quem convivi durante estes anos, especialmente à Sara e à Salomé, por todos os bons momentos que vivemos juntas durante estes últimos anos. Obrigada por todo o conhecimento que partilharam comigo no laboratório e fora dele, por todos os almoços e finais de tarde fantásticos. Obrigada pelas nossas conversas sem fim. Obrigada por estarem sempre lá nos bons e maus momentos. Sara, serás sempre a minha parceira preferida de laboratório e nunca irei esquecer estes últimos 6 anos que passamos juntas. Adoro-vos muito!

Quero deixar um agradecimento especial a todas as pessoas com as quais colaborei durante este percurso, especialmente à Professora Doutora Irina Amorim (ICBAS) e à Professora Doutora Sara Ricardo (i3S) por me acolherem nos seus laboratórios neste último ano. Obrigada por confiarem no meu trabalho e por contribuírem para o meu enriquecimento científico nas mais variadas áreas. Sou grata por todas as publicações que originaram das nossas colaborações.

Por fim, quero deixar um agradecimento especial à minha família. A família que está sempre lá, que nunca me falha. Mãe e Rui, obrigada por nunca me terem deixado desistir

e por me fazerem ver que eu posso ser sempre melhor, a cada dia que passa. Obrigada por terem lutado e trabalhado muito para que eu conseguisse chegar a esta etapa do meu percurso académico e nunca me ter faltado nada. Obrigada pelo orgulho que têm em mim, nunca vou conseguir agradecer-vos o suficiente por esta oportunidade. Ana, obrigada por seres sempre a pessoa mais sincera e mais verdadeira comigo. Obrigada por todo o orgulho que demonstras por mim. Espero pelo dia em que serás tu a agradecer-me nos agradecimentos da tua tese de doutoramento. Avó Guida e Avô Sousa, obrigada por terem feito de mim a pessoa que sou hoje e me terem transmitido sempre os valores mais acertados. Gosto muito de vocês.

Diogo, tu ♥. Sempre tu e só tu. Tu sabes por tudo o que te agradeço, porque te digo diariamente. Agradeço-te pelos bons momentos, pelo carinho, por toda a força, por toda a dedicação, pela entreajuda, pela compreensão e principalmente por nunca me deixares desistir. Por todos os conselhos, por toda a partilha de conhecimento e por me despertares o gosto pela ciência mesmo quando estou exausta. Por me chamares à razão, sempre que necessário e por me repreenderes quando sou injusta. Por seres o meu maior pilar e a minha maior motivação. Por tornares a minha vida mais leve e descomplicada, por me ensinares a importância do trabalho, mas também da vida. Meu companheiro de viagens, sem ti, não teria chegado até aqui. Obrigada por nunca me falhares. Esta tese é para todos nós.

PUBLICATIONS

This section presents all publications published within the scope of the Doctoral Thesis.

- Original research articles published in international peer-reviewed journals:

1. Duarte, D.; Vale, N. New Trends for Antimalarial Drugs: Synergism between Antineoplastics and Antimalarials on Breast Cancer Cells. *Biomolecules* **2020**, *10*, 1623, doi:10.3390/BIOM10121623.

2. Duarte, D.; Cardoso, A.; Vale, N. Synergistic Growth Inhibition of HT-29 Colon and MCF-7 Breast Cancer Cells with Simultaneous and Sequential Combinations of Antineoplastics and CNS Drugs. *Int. J. Mol. Sci.* **2021**, *22*, 7408, doi:10.3390/IJMS22147408.

3. Duarte, D.; Vale, N. Synergistic Interaction of CPP2 Coupled with Thiazole Derivates Combined with Clotrimazole and Antineoplastic Drugs in Prostate and Colon Cancer Cell Lines. *Int. J. Mol. Sci.* **2021**, *22*, 11984, doi:10.3390/IJMS222111984.

4. Duarte, D.; Vale, N. How Antimalarials and Antineoplastic Drugs Can Interact in Combination Therapies: A Perspective on the Role of PPT1 Enzyme. *Curr. Drug Metab.* **2021**, *22*, 1009–1016, doi:10.2174/1389200222666211118114057.

5. Duarte, D.; Rêma, A.; Amorim, I.; Vale, N. Drug Combinations: A New Strategy to Extend Drug Repurposing and Epithelial-Mesenchymal Transition in Breast and Colon Cancer Cells. *Biomolecules* **2022**, *12*, 190, doi:10.3390/BIOM12020190.

6. Duarte, D.; Falcão, S.I.; El Mehdi, I.; Vilas-Boas, M.; Vale, N. Honeybee Venom Synergistically Enhances the Cytotoxic Effect of CNS Drugs in HT-29 Colon and MCF-7 Breast Cancer Cell Lines. *Pharmaceutics* **2022**, *14*, 511, doi:10.3390/PHARMACEUTICS14030511.

7. Duarte, D.; Guerreiro, I.; Vale, N. Novel Strategies for Cancer Combat: Drug Combination Using Repurposed Drugs Induces Synergistic Growth Inhibition of MCF-7 Breast and HT-29 Colon Cancer Cells. *Curr. Issues Mol. Biol.* **2022**, *44*, 4930–4949, doi:10.3390/CIMB44100335.

8. Duarte, D.; Nunes, M.; Ricardo, S.; Vale, N. Combination of Antimalarial and CNS Drugs with Antineoplastic Agents in MCF-7 Breast and HT-29 Colon Cancer Cells: Biosafety Evaluation and Mechanism of Action. *Biomolecules* **2022**, *12*, 1490, doi:10.3390/BIOM12101490.

- Review articles published in international peer-reviewed journals:

1. Duarte, D.; Vale, N. Combining Repurposed Drugs to Treat Colorectal Cancer. Drug Discov. Today 2022, 27, 165–184, doi:10.1016/J.DRUDIS.2021.09.012.

2. Duarte, D.; Vale, N. Evaluation of Synergism in Drug Combinations and Reference Models for Future Orientations in Oncology. *Curr. Res. Pharmacol. Drug Discov.* **2022**, *3*, 100110, doi:10.1016/J.CRPHAR.2022.100110.

3. Duarte, D.; Vale, N. Antipsychotic Drug Fluphenazine against Human Cancer Cells. *Biomolecules* **2022**, *12*, 1360, doi:10.3390/BIOM12101360.

4. Duarte, D.; Vale, N. Antidepressant Drug Sertraline against Human Cancer Cells. *Biomolecules* **2022**, *12*, 1513, doi:10.3390/BIOM12101513.

- Communications in national congresses:

1. Duarte, D., Vale, N., 2021. New trends for antimalarial drugs: Synergism between antineoplastics and antimalarials on breast cancer cells. In: SPF Meeting 2021, held at the Faculty of Pharmacy of the University of Lisbon, from 17 to 19 February 2021. (abstract and oral presentation)

2. Duarte, D., Vale, N., 2021. New trends for antimalarial drugs: Synergism between antineoplastics and antimalarials on breast cancer cells. In: Ciência 2021 – Encontro com a Ciência e Tecnologia em Portugal, held at the Centro de Congressos de Lisboa (CCL), from 28 to 30 June 2021. (abstract and poster presentation)

3. Duarte, D., Vale, N., 2022. Synergistic growth inhibition of HT-29 colon and MCF-7 breast cancer cells with simultaneous and sequential combinations of antineoplastics and CNS drugs. In: 4º Encontro Nacional de Jovens Investigadores em Oncologia, held at Liga Portuguesa Contra o Cancro, at 24 September 2022. (abstract and poster presentation)

ABSTRACT

Chemotherapy represents the golden standard for cancer therapy in different types of cancer, including breast and colorectal cancer. Despite the advances in the design and synthesis of novel chemotherapeutic agents over the years, the development of drug resistance and the appearance of adverse side effects still compromise the efficacy rates of chemotherapy in oncological treatments. Therefore, the development of novel strategies for cancer combat is of urgent importance.

Drug repurposing, also known as drug repositioning, is a strategy that consists in discovering novel therapeutical indications for drugs that are already available in the market and represents a faster and more economical strategy for the discovery of novel chemotherapeutic agents, compared to the development of new drugs. Since these drugs have well-defined toxicological and pharmacokinetic profiles, the chances of these drugs to progress to clinical trials are increased. Moreover, as the majority of the repurposed drugs can be taken orally with good tolerance, and are generic medicines, they are more affordable than newly patented drugs.

Drug repurposing can be coupled to the approach of drug combination, a strategy that consists in the administration of cocktails of two or more drugs. This approach takes advantage of the different mechanisms of action of each drug, that can target different oncologic pathways at the same time, increasing the efficacy of the therapy and decreasing the chances of the development of drug resistance. The use of drugs in combination is even more advantageous when each of the drugs acts on a different target or signaling pathways and produce a synergistic effect, which helps to reduce the required drug concentrations for each individual drug. Therefore, the use of drug combinations can help increase the success rate of drug repurposing screens.

In this project, our group aimed to develop novel combination models for breast and colon cancer treatment. It was first performed an extensive drug screening to find drug classes with repurposing potential for breast and colorectal cancer therapy. It was studied the cytotoxic effect of drugs belonging to the class of antimalarial, central nervous system (CNS), antibiotics/ antifungal, and other drugs in two different cell lines: HT-29, a cell line representative of colorectal cancer cells, and MCF-7, representative of breast cancer cells. The results from these experiments demonstrated that the antimalarial and the CNS agents are the drug classes with the highest potential for drug repurposing against breast and colorectal cancer.

Next, four combination models were developed for breast and colorectal cancer combat: (I) combination models combining conventional antineoplastics and repurposed drugs; (II) combination models combining only repurposed drugs; (III) combination models combining peptides and chemotherapy and (IV) combination models combining peptides and repurposed drugs. It was found that the combination model consisting of repurposed drugs and chemotherapeutic agents induced the most cytotoxicity against MCF-7 and HT-29 colorectal cancer cells and had the most potential for further studies in breast and colorectal cancer. Specifically, it was found the combination of doxorubicin (DOX) + pyronaridine, DOX + chloroquine, DOX + artesunate, paclitaxel (PTX) + chloroquine, and PTX + artesunate had promising anticancer effects against MCF-7 breast cancer cells, with combined effects being stronger than each drug alone. Regarding the combination with CNS drugs, it was found that combinations of DOX + fluoxetine, DOX + thioridazine, DOX + benztropine, DOX+ quetiapine, PTX + fluoxetine, and PTX + thioridazine induced a significant decrease in cell viability compared to the treatments with each drug alone in breast cancer. Regarding colorectal cancer cells, it was found that the administration of the antimalarial artesunate prior to 5-fluorouracil (5-FU) produced better results in reducing HT-29 cell viability than the inverse drug schedule or the simultaneous combination. Moreover, these results demonstrated that fluphenazine, fluoxetine, and benztropine have enhanced anticancer activity when used alone as compared to being used in combination, making them ideal candidates for drug repurposing in colorectal cancer. Some combinations involving the use of peptides combined with antineoplastic agents also demonstrated promising anticancer effects in both cell lines.

Then, to find if these drug combinations achieved synergistic effects to allow for dose reduction, it was performed the synergism quantification by different reference models, such as the Chou-Talalay method as well as Zero Interaction Potency (ZIP), Highest Single Agent (HSA), Bliss independence, and Loewe reference models, using the CompuSyn and SynergyFinder software. It was found the combination of chloroquine, artesunate, and mefloquine with DOX and PTX to be synergic in MCF-7 cells, suggesting that antimalarials can act synergistically with DOX/PTX for breast cancer therapy. In the combination of CNS drugs with chemotherapeutic agents, it was found that the combination of fluoxetine, fluphenazine, and benztropine with PTX resulted in synergism for all concentrations below their half-maximal Inhibitory concentration (IC_{50}). In the case of HT-29 colorectal cancer cells, it was found that the simultaneous combination of the CNS drugs sertraline and thioridazine with 5-FU demonstrated the strongest synergism among all combinations. The drug combinations involving the use of peptides combined with antineoplastic agents also

demonstrated synergistic interactions in both cell lines; nevertheless, during this project, our studies were focused on the combination model using repurposed drugs and chemotherapeutic agents as this combination model produced enhanced cytotoxic effects on both cell lines.

After finding the most promising drug pairs, we aimed to evaluate the biosafety profile of these drug combinations against normal cells using a non-tumoral cell line (human fetal lung fibroblast cells (MRC-5)). It was demonstrated that these drug pairs are only cytotoxic for cancer cells, being safe for non-tumoral cells at lower concentrations, therefore supporting the use of antimalarial and CNS drugs in combination regimens with chemotherapeutic agents.

Finally, we attempted to determine the mechanisms of action behind these drug combinations to explain their enhanced cytotoxic effect against MCF-7 and HT-29 colorectal cancer cells. It was evaluated the effect of the combined pairs DOX + artesunate, DOX + chloroquine, PTX + fluoxetine, PTX + fluphenazine, PTX + benztropine, 5-FU + thioridazine and 5-FU + sertraline on the expression of epithelial-mesenchymal transition (EMT) biomarkers (E-cadherin, P-cadherin, vimentin, and β-catenin). This aimed to assess if these drug combinations affected the expression of these proteins and eventually reverted EMT. It was found that combination treatments increased E-cadherin expression while reducing P-cadherin, vimentin, and β-catenin expressions, suggesting that these treatments could indeed induce an EMT reversal. Then, it was also evaluated the expression of other proteins involved in the carcinogenesis process: palmitoyl-protein thioesterase 1 (PPT1), Ki67, cleaved-poly (ADP-ribose) polymerase (cleaved-PARP), multidrug resistance-associated protein 2 (MRP2), P-glycoprotein (P-gp), and nuclear factor-kappa-B (NF-kB) p65. These findings revealed that PPT1 may have an important role in the mechanism of action of these combinations, as demonstrated by their ability to decrease PPT1 expression.

Taken together, these results provide promising approaches for the design of novel drug combinations to treat breast and colon cancer patients and support the use of antimalarial and CNS drugs in combination regimens with chemotherapeutic agents; nevertheless, additional studies are recommended to further explore their complete mechanism of action and confirm their efficacy in more complex animal models.

KEYWORDS: drug combination, drug repurposing, drug synergism, cancer therapy

RESUMO

A quimioterapia desempenha um papel muito importante na terapia de diversos tipos de cancro, incluindo no tratamento do cancro da mama e do cancro colorretal. Apesar dos avanços que se têm verificado ao longo dos anos na área do desenvolvimento de novos quimioterápicos, a resistência farmacológica conjuntamente com o desenvolvimento de efeitos adversos em resposta à terapia, parecem comprometer os níveis de eficácia da quimioterapia nos tratamentos oncológicos. Assim, é de extrema importância que os investigadores se dediquem ao desenvolvimento de novas estratégias para o combate do cancro.

O reaproveitamento de fármacos, também denominado de reposicionamento de fármacos, é uma estratégia que consiste na descoberta de novas indicações terapêuticas para fármacos que já se encontram disponíveis no mercado, para além daquelas já originalmente descritas. Comparativamente ao desenvolvimento de novos fármacos, o reaproveitamento de fármacos representa uma estratégia mais rápida e mais económica para a descoberta de novos agentes quimioterápicos e, dado que esses fármacos já têm perfis toxicológicos e farmacocinéticos bem definidos na literatura, as chances de progredirem para ensaios clínicos são bastante mais elevadas. Adicionalmente, como a maioria destes fármacos reaproveitados têm boa tolerância quando administrados por via oral, e uma vez que a maioria são vendidos sob a forma de genéricos, tornam-se mais acessíveis à população, comparativamente a fármacos que tenham sido patenteados recentemente.

Esta estratégia pode ser acoplada à combinação de fármacos, uma estratégia que consiste na administração de dois ou mais fármacos em simultâneo. A combinação de fármacos tira vantagem dos diferentes mecanismos de ação de cada um dos fármacos, que coletivamente podem contribuir, de forma mais eficaz, para a atuação em diferentes vias oncológicas, aumentando, assim a eficácia da terapia e diminuindo as probabilidades do desenvolvimento de resistência aos fármacos. O uso de fármacos combinados é particularmente vantajoso quando cada um dos fármacos atua em alvos ou vias de sinalização diferentes, verificando-se sinergias entre os fármacos, que possibilitam a redução das concentrações de fármaco necessárias para a produção de um efeito terapêutico.

Neste projeto, o nosso grupo de investigação teve como principal objetivo desenvolver novos modelos de combinação para o tratamento do cancro da mama e do

cancro colorretal. Numa primeira fase, foi feita um extenso *screening* de fármacos de forma a encontrar classes de fármacos com potencial de reaproveitamento para a terapia destes dois tipos de cancro. Avaliou-se o efeito citotóxico de fármacos pertencentes a diferentes classes, tais como antimaláricos, fármacos do sistema nervoso central (SNC), antibióticos/antifúngicos, entre outros, em duas linhas celulares diferentes: HT-29, uma linha celular representante de células tumorais colorretais, e MCF- 7, representante de células tumorais de mama. Estes resultados permitiram concluir que os antimaláricos juntamente com os fármacos do SNC são as duas classes de fármacos com maior potencial para reaproveitamento em cancro de mama e colorretal.

Posteriormente, desenvolveram-se quatro modelos de combinação para o combate destes dois tipos de cancro usando (I) modelos de combinação de antineoplásicos convencionais e fármacos reaproveitados; (II) modelos de combinação de fármacos reaproveitados apenas; (III) modelos de combinação de peptídos e antineoplásicos e (IV) modelos de combinação de peptídos e fármacos reaproveitados. Os resultados desta fase permitiram concluir que o modelo de combinação de fármacos reaproveitados + agentes quimioterápicos é mais eficaz na indução de citotoxicidade contra as células MCF-7 e HT-29, tendo um elevado potencial para ser explorado em estudos posteriores. As combinações mais promissoras em células tumorais de mama demonstraram ser as de doxorrubicina (DOX) + pironaridina, DOX + cloroquina, DOX + artesunato, paclitaxel (PTX) + cloroquina e PTX + artesunato, DOX + fluoxetina, DOX + tioridazina, DOX + benzotropina, DOX+ quetiapina, PTX + fluoxetina e PTX + thioridazina. Em relação às células tumorais de colon, estes resultados demonstraram que a administração do antimalárico artesunato anteriormente à administração do quimioterápico 5-fluorouracil (5-FU) produz melhores resultados na redução da viabilidade de células HT-29 do que o esquema de combinação inverso ou a combinação simultânea. Além disso, estes resultados também permitiram concluir que os fármacos flufenazina, fluoxetina e benzotropina têm um efeito anti-tumoral mais pronunciado quando usados em monoterapia do que em combinação, tornando-os candidatos ideais para o reaproveitamento de fármaco em cancro colorretal. Algumas combinações de peptídos com fármacos antineoplásicos demonstraram, ainda, efeitos anti-tumorais promissores nas duas linhas celulares.

Para determinar se as combinações de fármacos previamente descritas produziam efeitos sinérgicos que permitissem a redução das doses terapêuticas, realizou-se, posteriormente, a quantificação do sinergismo recorrendo a diferentes modelos de referência, tais como o método de Chou-Talalay, Bliss, Loewe, entre outros, usando os softwares CompuSyn e SynergyFinder. Aqui, os resultados demonstraram que a

combinação da cloroquina, do artesunato e da mefloquina com a DOX e com o PTX é sinérgica em células MCF-7, sendo indicativo de que os antimaláricos podem, de facto, interagir sinergicamente com estes antineoplásicos em cancro da mama. Na combinação de fármacos do SNC, verificou-se que a combinação da fluoxetina, da flufenazina e da benzotropina com o PTX também resultou em sinergismo, especialmente em concentrações mais baixas. Em relação aos resultados nas células HT-29, verificou-se que os fármacos do SNC sertralina e tioridazina em combinação simultânea com o 5-FU foram os pares mais sinérgicos de todas as combinações testadas. As combinações que envolveram peptídos e fármacos antineoplásicos também demonstraram interações sinérgicas nas duas linhas celulares testadas; no entanto, ao longo deste trabalho, o nosso estudo focou-se nos modelos de combinação de fármacos reaproveitados e fármacos antineoplásicos, uma vez que esse modelo de combinação produziu efeitos citotóxicos mais pronunciados nas duas linhas celulares.

Depois de selecionar as combinações de fármacos mais promissoras, o próximo passo neste projeto passou por avaliar o perfil de biossegurança dessas combinações em células normais, usando uma linha de células não tumoral (células de fibroblastos pulmonares de fetos humanos (MRC-5)). Concluiu-se que estas combinações de fármacos são apenas tóxicos para células tumorais, tendo um perfil de segurança aceitável para células não tumorais, desde que usados em concentrações baixas. Desta forma, concluiu-se que o uso combinado de fármacos reaproveitados tais como antimaláricos e fármacos do CNS com antineoplásicos parece ser seguro para aplicação em terapias oncológicas.

Por fim, tentou-se determinar os mecanismos de ação por trás das combinações de fármacos mais promissoras, de forma a tentar explicar o efeito citotóxico mais pronunciado destas combinações em células tumorais de mama (MCF-7) e colon (HT-29). Para tal, avaliou-se o efeito das combinações DOX + artesunato, DOX + cloroquina, PTX + fluoxetina, PTX + flufenazina, PTX + benzotropina, 5-FU + tioridazina e 5-FU + sertralina ao nível da expressão de biomarcadores relacionados com a transição epitélio-mesenquimal (EMT): E-caderina, P-caderina, vimentina e β-catenina, com o objetivo de aferir se estas combinações poderiam afetar a expressão destas proteínas e eventualmente reverteram a EMT. Estes resultados demonstraram que os tratamentos com estas combinações de fármacos nestas linhas tumorais levam a um aumento da expressão da E-caderina, ao mesmo tempo que reduzem a expressão da P-caderina, vimentina e β-catenina, o que sugere que, de facto, estas combinações poderão induzir a reversão de EMT. Adicionalmente, foram também avaliados os efeitos destas combinações na expressão de outras proteínas envolvidas no processo de carcinogénese, incluindo a

palmitoil-proteína tioesterase 1 (PPT1), Ki67, PARP clivada, MRP2, P-glicoproteína (P-gp) e NF-kB p65. Os resultados parecem sugerir que a PPT1 pode ter um papel importante no mecanismo de ação destas combinações, dado que os tratamentos combinados demonstraram a capacidade de diminuir a expressão da PPT1.

Coletivamente, estes novos resultados fornecem informação valiosa para o futuro desenvolvimento de novas combinações terapêuticas para o tratamento de pacientes com cancro da mama e colorretal. Além disso, este trabalho suporta ainda a ideia de que alguns fármacos antimaláricos e do SNC têm potencial para serem reaproveitados nestas doenças, fornecendo evidências que suportam o estudo mais aprofundado destas combinações nas terapias do cancro da mama e do colón. De qualquer forma, são recomendados estudos adicionais que permitam perceber de forma detalhada o mecanismo de ação destas combinações nestes dois tipos de cancro e que comprovem a eficácia das mesmas em organismos mais complexos.

PALAVRAS-CHAVE: combinação de fármacos, reaproveitamento de fármacos, efeito sinérgico, terapia oncológica

GRAPHICAL ABSTRACT

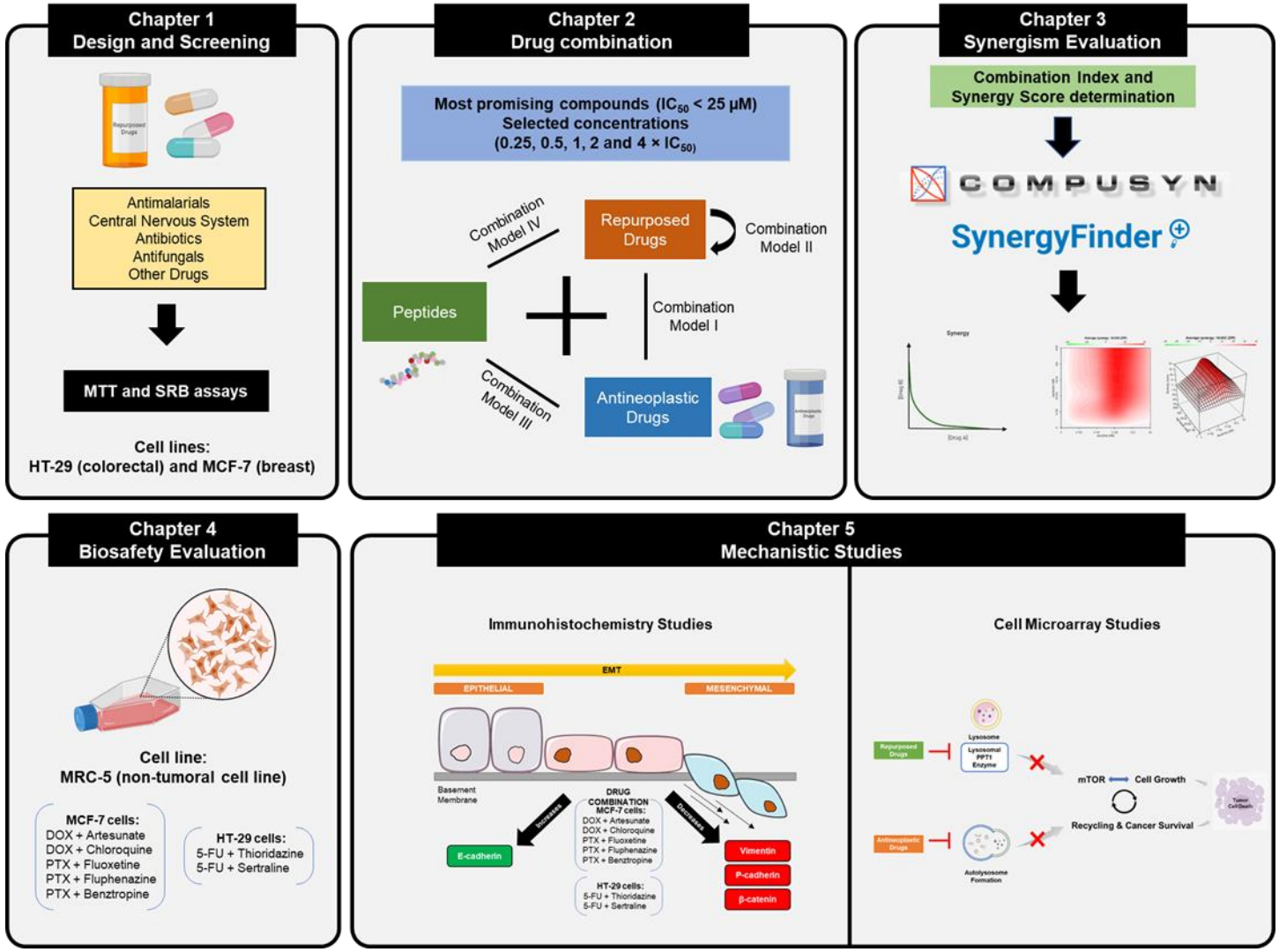

LIST OF FIGURES

CHAPTER I

CHAPTER II

FUTURE PERSPECTIVES

LIST OF SCHEMES

CHAPTER I

CHAPTER II

LIST OF TABLES

CHAPTER I

CHAPTER III

CHAPTER IV

CHAPTER V

LIST OF SUPPLEMENTARY FIGURES

CHAPTER I

control and represent mean ± SEM. Each experiment was done three times independently (n = 3); ** statistically significant vs. control at $p < 0.01$. **** statistically significant vs. control at $p < 0.0001$. 330

Figure S6. Cytotoxic effects of (**A**) piperazine and (**B**) quinidine on MCF-7 cells. Cells were cultured in the presence of increasing concentrations of the drug and after 48 h, the MTT assay was performed to measure cellular viability. Values are expressed in percentage of control and represent mean ± SEM. Each experiment was done three times independently (n = 3). 331

Figure S7. Effects of chloroquine on HT-29 cells. (**A**) Effect of chloroquine in cell viability and (**B**) dose-response curve. Cells were cultured in the presence of increasing concentrations of the drug and after 48 h, the MTT assay was performed to measure cellular viability. Values are expressed in percentage of control and represent mean ± SEM. Each experiment was done three times independently (n = 3); ** statistically significant vs. control at $p < 0.01$. **** statistically significant vs. control at $p < 0.0001$. 331

Figure S8. Cytotoxic effects of the CNS drugs (**A**) bromocriptine, (**B**) carbamazepine, (**C**) carbidopa, (**D**) entacapone, (**E**) tolcapone, (**F**) lamotrigine, (**G**) m-CPB and (**H**) nepicastat on HT-29 cells. Cells were cultured in the presence of increasing concentrations of the drug and after 48 h, the MTT assay was performed to measure cellular viability. Values are expressed in percentage of control and represent mean ± SEM. Each experiment was done three times independently (n = 3); ** statistically significant vs. control at $p < 0.01$. *** statistically significant vs. control at $p < 0.001$. **** statistically significant vs. control at $p < 0.0001$. 332

Figure S9. Cytotoxic effects of the CNS drugs (**A**) perampanel, (**B**) rivastigmine, (**C**) safinamide, (**D**) scopolamine, (**E**) selegiline and (**F**) edaravone on HT-29 cells. Cells were cultured in the presence of increasing concentrations of the drug and after 48 h, the MTT assay was performed to measure cellular viability. Values are expressed in percentage of control and represent mean ± SEM. Each experiment was done three times independently (n = 3); ** statistically significant vs. control at $p < 0.01$. *** statistically significant vs. control at $p < 0.001$. **** statistically significant vs. control at $p < 0.0001$. 333

Figure S10. Cytotoxic effects of the antibiotic drugs (**A**) amikacin, (**B**) vancomycin and (**C**) gentamicin on HT-29 cells. Cells were cultured in the presence of increasing concentrations of the drug and after 48 h, the MTT assay was performed to measure cellular viability. Values are expressed in percentage of control and represent mean ± SEM. Each experiment was done three times independently (n = 3). 334

Figure S11. Cytotoxic effects of (**A**) acamprosate, (**B**) atenolol, (**C**) atorvastatin, (**D**) furosemide, (**E**) glibenclamide, (**F**) metoprolol and (**G**) telmisartan on HT-29 cells. Cells

were cultured in the presence of increasing concentrations of the drug and after 48 h, the MTT assay was performed to measure cellular viability. Values are expressed in percentage of control and represent mean ± SEM. Each experiment was done three times independently (n = 3); * statistically significant vs. control at $p < 0.05$. ** statistically significant vs. control at $p < 0.01$. 335

ABBREVIATIONS

5-FU	5-Fluorouracil
ABC	ATP-Binding Cassette
AC	Combination of DOX and Cyclophosphamide
ACF	Anticancer Fund
AC-T	Combination of DOX and Cyclophosphamide, followed by PTX
ADME	Absorption, Distribution, Metabolism and Excretion
AIDS	Acquired Immunodeficiency Syndrome
AKT	Protein Kinase B
AMP	Adenosine Monophosphate
AMPA	α-Amino-3-Hydroxy-5-Methyl-4-Isoxazolepropionic Acid
AMPK	AMP-Activated Protein Kinase
ANOVA	Analysis of Variance
APC	Adenomatous Polyposis Coli
ATC	Anatomical Therapeutic Chemical
ATCC	American Type Culture Collection
ATG	Autophagy-Related Protein
ATP	Adenosine Triphosphate
BenzoTZ	2-Aminobenzothiazole
bFGF	Basic Fibroblast Growth Factor
BRAC1	Breast Cancer Gene 1
BRAC2	Breast Cancer Gene 2
BRAID	Bivariate Response to Additive Interacting Doses
BSA	Bovine Serum Albumin
BTZ5CA	2-Bromothiazole-5-Carboxylic Acid
BTZCA	5-Bromothiazole-2-Carboxylic Acid

C/EBPβ	CCAAT/Enhancer-Binding Protein β
CAF	Combination of Cyclophosphamide, DOX, and 5-FU
CAPOX	Combination of Capecitabine and Oxaliplatin
CDKs	Cyclin-Dependent Kinases
CI	Combination Index
CMA	Cell Microarray
CMF	Combination of Cyclophosphamide, Methotrexate, and 5-FU
CNS	Central Nervous System
COMT	Catechol-O-Methyl-Transferase
COX	Cyclooxygenase
COX-1	Cyclooxygenase-1
COX-2	Cyclooxygenase-2
CPPs	Cell-Penetrating Peptides
CSCs	Cancer Stem Cells
CXCL12	C-X-C Motif Chemokine Ligand 12
CXCR4	C-X-C Chemokine Receptor 4
DAB	Diaminobenzidine
DCIS	Ductal Carcinoma *in situ*
DCM	Dichloromethane
DIEA	*N*-Ethyl-*N,N*-Diisopropylamine
DMEM	Dulbecco's Modified Eagle's Medium
DMF	*N*,*N*-Dimethylformamide
DMSO	Dimethyl Sulfoxide
DNA	Deoxyribonucleic Acid
DOX	Doxorubicin
EAC	Ehrlich Ascites Carcinoma
EC_{50}	Half Maximal Effective Concentration

EDTA	Ethylenediaminetetraacetic Acid
EGFR	Epidermal Growth Factor Receptor
EMA	European Medicines Agency
EMT	Epithelial-Mesenchymal Transition
ER	Estrogen Receptor
ESI-IT MS	Electrospray Ionisation-Ion Trap Mass Spectrometry
ESMO	European Society for Medical Oncology
Fa	Fractional Effect
FAP	Familial Adenomatous Polyposis
FBS	Fetal Bovine Serum
FDA	Food and Drug Administration
FEC	Combination of 5-FU, Epirubicin, and Cyclophosphamide
Fli-1	Friend Leukemia Integration 1 Transcription Factor
FOLFIRI	Combination of Leucovorin, 5-FU and Irinotecan
FOLFOX	Combination of Leucovorin, 5-FU and Oxaliplatin
FOXO1	Forkhead Box O1
GABA	Gamma-Aminobutyric Acid
GMP	Guanosine Monophosphate
GPCRs	G-protein Coupled Receptors
H&E	Hematoxylin and Eosin
HBTU	Hexafluorophosphate Benzotriazole Tetramethyl Uronium
HDAC6	Histone Deacetylase 6
HER2	Human Epidermal Growth Factor Receptor 2
HMG-CoA	3-Hydroxy-3-Methylglutaryl-Coenzyme A
HNPCC	Hereditary Non-Polyposis Colorectal Cancer
HO-1	Heme Oxygenase-1
HPLC	High-Performance Liquid Chromatography

HPLC-DAD	High-Performance Liquid Chromatography with Diode Array Detection
HRP	Horseradish Peroxidase
HSA	Highest Single Agent
Hsp90	Heat Shock Protein 90
IBC	Invasive Breast Cancer
IBD	Inflammatory Bowel Disease
IC_{50}	Half-maximal Inhibitory Concentration
IHC	Immunohistochemistry
IL-10	Interleukin 10
IS	Internal Standard
IV	Intermediate Value
JNK	c-Jun N-terminal Kinases
KRAS	Kirsten Rat Sarcoma Virus
LC-MS	Liquid Chromatography–Mass Spectrometry
MAO-A	Monoamine Oxidase A
MAO-B	Monoamine Oxidase B
MAOI	Monoamine Oxidase Inhibitors
MAP4K4	Mitogen-Activated Protein Kinase Kinase Kinase Kinase 4
MAPK	Mitogen-Activated Protein Kinase
MeSH	Medical Subject Headings
miRNA	Micro RNA
MLH1	MutL Homolog 1
MLH6	MutL Homolog 6
mRNA	Messenger RNA
MRP1	Multidrug Resistance-Associated Protein 1
MRP2	Multidrug Resistance-Associated Protein 2
MSH2	MutS Homolog 2

mTOR	Mammalian Target of Rapamycin
mTORC1	Mammalian Target of Rapamycin Complex 1
MTT	Thiazolyl Blue Tetrazolium Bromide
MTZ	2-Amino-5-Methylthiazole
MuSyC	Multi-dimensional Synergy of Combinations
NADPH	Nicotinamide Adenine Dinucleotide Phosphate Hydrogen
NCCN	National Comprehensive Cancer Network
NDRI	Norepinephrine and Dopamine Reuptake Inhibitors
NF-kB	Nuclear Factor Kappa-Light-Chain-Enhancer of Activated B Cells
NMDA	N-Methyl D-Aspartate
Nrf2	Nuclear Factor Erythroid 2-Related Factor 2
NSAIDs	Non-Steroidal Anti-Inflammatory Drugs
NSCLC	Non-Small-Cell Lung Cancer
NTZ	2-Amino-5-Nitrothiazole
PABA	*para*-Aminobenzoic Acid
PARP	Poly (ADP-Ribose) Polymerase
PBS	Phosphate Buffered Saline
PDE5	cGMP-Specific Phosphodiesterase Type 5
Pen-strep	Penicillin-Streptomycin
PFA	Paraformaldehyde
P-gp	P-glycoprotein
PI3K	Phosphoinositide 3-Kinase
PPT1	Palmitoyl-Protein Thioesterase 1
PR	Progesterone Receptor
PTX	Paclitaxel
PyBOP	Benzotriazol-1-Yloxytripyrrolidinophosphonium Hexafluorophosphate
R&D	Research and Development

ReDO	Repurposing Drugs in Oncology Project
RNA	Ribonucleic Acid
ROS	Reactive Oxygen Species
RP-MPLC	Reverse-Phase Medium-Pressure Liquid Chromatography
SEM	Standard Error of the Mean
SNPs	Single Nucleotide Polymorphisms
SNRI	Serotonin and Norepinephrine Reuptake Inhibitors
SPPS	Solid-Phase Peptide Synthesis
SRB	Sulforhodamine B
SSRI	Selective Serotonin Reuptake Inhibitors
STAT3	Signal Transducer and Activator of Transcription 3
TAC	Combination of Docetaxel, DOX, and Cyclophosphamide
TBS	Tris-buffered Saline
TBTU	O-(Benzotriazol-1-yl)-N,N,N',N'-Tetramethyluronium Tetrafluoroborate
TCA	Tricyclic Antidepressants
TCTP	Translationally Controlled Tumor Protein
TFA	Trifluoracetic Acid
TGF-β	Transforming Growth Factor Beta
TIS	Thioanisole
TLC	Thin-layer Chromatography
TLR9	Toll Like Receptor 9
TMN	Tumor, Node, Metastasis System
TNBC	Triple Negative Breast Cancer
TNF	Tumor Necrosis Factor
TP53	Tumor Protein 53
TRAF1	Tumor Necrosis Factor Receptor-Associated Factor 1
TRAF2	Tumor Necrosis Factor Receptor-Associated Factor 2

UPLC	Ultra-Performance Liquid Chromatography
USA	United States of America
VEGF	Vascular Endothelial Growth Factor
WHO	World Health Organization
WNT	Wingless/Integrated
ZIP	Zero Interaction Potency

THESIS OVERVIEW

This Doctoral Thesis in Pharmaceutical Sciences – Pharmacology and Pharmacotherapy Specialty, Faculty of Pharmacy, University of Porto, entitled “Development of New Drug Combinations for Cancer Treatment”, is divided into five main chapters, namely:

I) Screening of repurposed drugs with potential antitumoral activity for breast and colorectal cancer therapy

II) Development of novel combination models for breast and colorectal cancer therapy

III) Evaluation of synergism in drug combinations and reference models for future orientations in oncology

IV) Evaluation of the biosafety profile of the most promising drug combinations

V) Mechanistic studies of the most promising drug combinations in breast and colon cancer cells

This thesis aimed to develop new drug combinations for breast and colorectal cancer therapy. Therefore, the following five specific objectives were established:

I) Finding drugs with repurposing potential for breast and colorectal cancer. In Chapter I, a screening of several drugs was performed for the evaluation of their potential for drug repurposing in breast and colorectal cancer. The cytotoxic effect of drugs belonging to the class of antimalarial, central nervous system (CNS), antibiotics/ antifungal, and other drugs was studied in two different cancer cell lines: colorectal HT-29 and breast MCF-7. The half-maximum inhibitory concentration (IC_{50}) value of each repurposed drug was calculated, and the most promising candidates were selected for further studies in Chapter II.

II) Developing novel combination models and achieve a set of drug combinations with anticancer potential in HT-29 and MCF-7 breast cancer cells. In Chapter II, four combination models for cancer combat were explored: (I) combination models combining conventional antineoplastics and repurposed drugs; (II) combination models combining only repurposed drugs; (III) combination models combining

peptides and chemotherapy and (IV) combination models combining peptides and repurposed drugs, to determine the most appropriate model of drug combination for breast and colorectal cancer therapy. The most promising drug combinations were subject of drug synergism evaluation in Chapter III.

III) Determining the drug interactions between the most promising drug combinations. In Chapter III, it was performed an evaluation of the drug interactions in the drug combinations previously tested in Chapter II, to determine possible synergistic interactions between drugs. The analysis of drug interactions was evaluated by different reference models, namely Chou-Talalay, Zero Interaction Potency (ZIP), Highest Single Agent (HAS), Bliss independence, and Loewe, using the CompuSyn and SynergyFinder software. The most synergistic drug combinations were selected for further studies in Chapter IV and V.

IV) Assessing the biosafety profile of the most promising drug combinations. In Chapter IV, the biosafety of the previously evaluated drug combinations was assessed using a non-tumoral human fetal lung fibroblast cell line (MRC-5). This aimed to confirm if the most promising drug combinations were safe against non-tumoral cancer cells and to validate their use in breast and colorectal cancer therapies.

V) Determining the mechanism of action of the most promising drug combinations. In the last chapter, to further clarify how these drugs act in combination and if some degree of epithelial-mesenchymal transition (EMT) is involved, the effect of most promising drug pairs on the expression of EMT biomarkers, such as E-cadherin, P-cadherin, vimentin, and β-catenin, was investigated. The expression of several proteins involved in the tumorigenesis process such as palmitoyl-protein thioesterase 1 (PPT1), Ki67, cleaved-poly (ADP-ribose) polymerase (cleaved-PARP), multidrug resistance-associated protein 2 (MRP2), P-glycoprotein (P-gp), and nuclear factor-kappa-B (NF-kB) p65 was also evaluated in both cell lines, to further depict the possible mechanisms of action behind these drug combinations.

The findings presented in this thesis demonstrated that the antimalarial and the CNS agents are the drug classes with the highest potential for drug repurposing against breast and colorectal cancer cells. Moreover, it was found that the combination model consisting of repurposed drugs and chemotherapeutic agents induces the most cytotoxicity against MCF-7 and HT-29 colorectal cancer cells and has the most potential for further studies in

breast and colorectal cancer. The combination of chloroquine and artesunate with doxorubicin (DOX) presented significant synergism in MCF-7 cells, suggesting that antimalarials can act synergistically with chemotherapeutic agents for breast cancer therapy. The combination of fluoxetine, fluphenazine, and benztropine with paclitaxel (PTX) also resulted in synergism for all concentrations. Regarding colon cancer cells, it was found that CNS drugs sertraline and thioridazine in simultaneous combination with 5-FU demonstrated the strongest synergism among all combinations. The biosafety studies demonstrated that these drug pairs are only cytotoxic for cancer cells, being safe for non-tumoral cells at lower concentrations, therefore supporting the use of antimalarial and CNS drugs in combination regimens with chemotherapeutic agents. Finally, mechanistic studies demonstrated that combination could indeed induce EMT reversal and that PPT1 may have an important role in the mechanism of action of these combinations.

CHAPTER I

SCREENING OF REPURPOSED DRUGS WITH POTENTIAL ANTITUMORAL ACTIVITY, FOR BREAST AND COLORECTAL CANCER THERAPY

1. SUMMARY OF CHAPTER I

Colorectal cancer represents the second leading cause of death by cancer in the United Stated of America (USA). In 2021, there were an estimated 149,500 newly diagnosed cases and 52,980 deaths caused by this type of cancer. Another type of cancer with elevated prevalence is breast cancer, which represents the second leading cause of death by cancer among women, with an estimated 281,550 new cases and 43,600 deaths in 2021 in the USA.

Although surgery and chemotherapy play a key role in the treatment of breast and colorectal cancers, the efficacy rate of these therapeutic approaches remains very low. It is, therefore, very important to find new therapeutic strategies that ensure the long-term survival and good life quality of these patients, by increasing the therapeutic efficacy of oncologic therapies, while reducing the therapeutic doses and toxicity of these treatments. However, the development of new drugs for cancer therapy is a process that is time-consuming, costly, and usually has low approval rates. Additionally, most of the new developed chemotherapeutics commonly present problems related to toxicity, which results in undesired side effects. Thus, it is important to develop and explore novel pharmaceutical strategies that help to overcome the obstacles associated with the development of new drugs for cancer therapy.

Drug repurposing (or repositioning) is an alternative approach to the *de novo* drug development that has been gaining attention from the scientific community in recent years. This strategy makes use of already-approved drugs to search for new therapeutic indications besides the original. This strategy presents advantages over the development of new drugs since repurposed drugs are already approved by the Food and Drug Administration (FDA) and have well-defined safety and toxicological profiles. This allows to save time and money, increasing the likelihood of these drugs entering clinical trials.

In this chapter, it was performed a screening of several drugs for drug repurposing in breast and colorectal cancer. We studied the cytotoxic effect of drugs belonging to the class of antimalarial, central nervous system (CNS), antibiotics/ antifungal, and other drugs in two different cell lines: HT-29, a cell line representative of colorectal cancer cells, and MCF-7, representative of breast cancer cells. To evaluate the anticancer potential of these drugs, both cell lines were incubated with increasing concentrations of each drug for a period of 48 h and cell viability was evaluated by thiazolyl blue tetrazolium bromide (MTT) and/or sulforhodamine B (SRB) assays.

These results demonstrate that the antimalarial and the CNS agents are the drug classes with higher potential for drug repurposing against breast and colorectal cancer. In MCF-7 breast cancer cells, mefloquine, tafenoquine, and pyronaridine demonstrated elevated cytotoxicity, with half-maximal inhibitory concentration (IC_{50}) values under 10 µM. Artesunate treatment also induced a significant reduction in MCF-7 cell viability and presented an IC_{50} value of 11.60 µM. Treatments with the CNS drugs fluphenazine, fluoxetine, sertraline, and thioridazine caused significant toxicity at all concentrations above 10 µM, which resulted in IC_{50} values of 2.682, 7.778, 5.723, and 2.217 µM, respectively. Benztropine induced a concentration-dependent reduction in cell viability, with an IC_{50} value of 21.71 µM. Treatment with antibiotic/antifungal and other classes of drugs did not produce any significant anticancer effect in this cell line.

Regarding the results in the HT-29 cell line, the antimalarial drugs mefloquine and artesunate successfully reduced the number of viable cells, with IC_{50} values under 20 µM. Treatment with the CNS drugs latrepirdine, fluphenazine, fluoxetine, benztropine, thioridazine, and sertraline resulted in strong inhibition of HT-29 cell growth, with IC_{50} values of 7.75, 1.86, 6.12, 18.23, 4.26 and 2.45 µM, respectively. Furthermore, clotrimazole, an antifungal agent, was able to induce a concentration-dependent reduction of cell viability, with a significant decrease in the number of viable cells at concentrations above 10 µM and an IC_{50} value of 21.64 µM. The antiarrhythmic drug amiodarone also demonstrated significant anticancer effects in this cell line, at concentrations above 10 µM, with an IC_{50} value of 7.297 µM.

Taken together, these findings demonstrate that several antimalarial and CNS drugs have strong repurposing potential for use in breast and colorectal cancer therapies as standalone agents. Moreover, other drug classes like antifungal and antiarrhythmic agents may also be promising candidates for drug repurposing in colorectal cancer.

2. INTRODUCTION OF CHAPTER I

The latest cancer statistics provided by the American Cancer Society estimate that, in 2022, more than 1,900,000 new cancer cases will be diagnosed and there will be about 600,000 cancer deaths, only in the USA [1]. Along with lung cancer, breast and colorectal cancers occupy the rank as the most diagnosed types of cancer, with an estimation of 43,780 cases and 52,580 estimated deaths in the USA, in 2022 [1].

In this section, we will provide a review of the main features related to breast and colorectal cancer, with reference to the most common therapeutic regimens for each type of cancer, highlighting the advantages and disadvantages of chemotherapy. We will then describe the development process of new drugs for oncology and present the strategy of drug repurposing as a faster and more economical strategy to the *de novo* drug development. Finally, evidence on some repurposed drugs with anticancer potential will be provided to further support our investigations.

2.1 Breast Cancer

Breast cancer is the most commonly diagnosed type of cancer in women and represents the second leading cause of death by cancer in women worldwide [2]. In developed countries, breast cancer is the second most mortal, just preceded by lung cancer. Although it is more frequent in women, breast cancer can also affect men, although to a much smaller extent (<1%) [3]. Even though the mortality rate of this cancer has declined over the last two decades, metastatic breast cancer still has a very reduced therapeutic efficacy, with a 5-year overall survival rate of only 23% [4].

2.1.1 Breast Cancer Etiology

Generally, cancer is a disease characterized by an increased and uncontrolled cell growth, with proliferative and metastatic capacity. Mutations in specific genes play a major role in the development of the disease and can occur in oncogenes, tumor suppressor genes, or genes involved in deoxyribonucleic acid (DNA) repair [5]. These mutations generally result in the inhibition of apoptotic mechanisms and uncontrolled proliferation of tumor cells.

Specifically for breast cancer, this disease can develop in response to DNA damage or genetic mutations, that can be influenced by exposure to estrogen [6]. Sometimes, it can also originate due to an inheritance of DNA defects or pro-cancerous genes like breast

cancer gene 1 (BRCA1) and breast cancer gene 2 (BRCA2). Therefore, a family history of ovarian or breast cancer can increase the risk for the development of breast cancer [6].

The risk factors for the development of breast cancer include age, gender, personal history of breast cancer, histologic risk factors, family history of breast cancer, genetic risk factors, reproductive risk factors, and the use of exogenous hormones [6].

2.1.2 Breast Cancer Classification

Currently, there are 20 major types and 18 minor subtypes of breast cancer that have been defined and included in the recently published World Health Organization (WHO) classification [7]. The traditional classification of the tumor can be done histologically, through the evaluation of morphological, anatomical, and physical properties, searching for abnormal cell changes. This classification is usually done using the tumor, node, metastasis (TMN) system, a classification system based on tumor size, nearby lymph node involvement, and tumor metastasis [8]. This classification groups breast cancer as *in situ*, subdivided into ductal or lobular, or as invasive carcinomas, that can be classified as tubular, ductal lobular, invasive lobular, infiltrating ductal, mucinous, medullary or infiltrating ductal (Figure 1) [9].

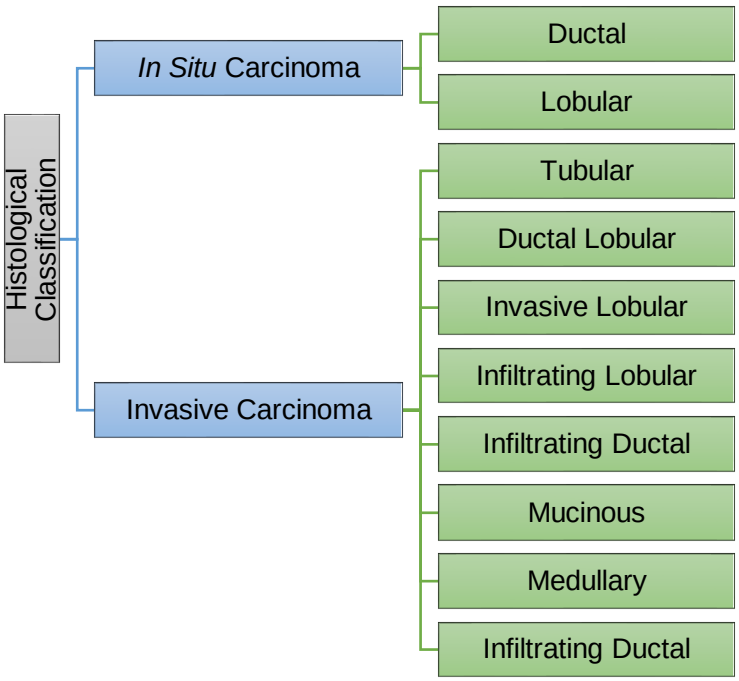

Figure 1. Histological classification of breast cancer subtypes.

However, advances in medicine have led to the creation of another tumor classification system based on molecular studies, primarily through the search for established biomarkers for breast cancer: the estrogen receptor (ER), the progesterone receptor (PR), and the human epidermal growth factor receptor 2 (HER2) [10]. Based on this classification, breast cancer can be classified into four different subtypes: luminal A (positive for ER and/or PR), luminal B (positive for ER and/or PR and HER2), HER2-enriched (amplification of the HER2, no expression of ER nor PR) and triple-negative breast cancer (TNBC) (negative for all) (Figure 2) [11]. It is estimated that 75% of all patients have tumors expressing the estrogen and/or progesterone receptors, the breast cancer subtype with a better prognosis [12]. Triple-negative breast cancers are the most difficult to treat and present worse prognosis, due to their lack of receptors for chemotherapeutic agents.

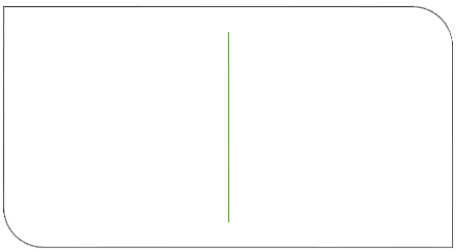

Figure 2. Molecular classification of breast cancer subtypes.

There is another type of breast cancer classification, called functional classification, that is based on the nature of tumor-initiating cells [9]. In this case, there are two proposed hypotheses: (A) either the heterogeneity seen in breast cancer arises from distinct mammary stem/progenitor cells or, (B) breast cancer heterogeneity is the result of a single mammary stem/progenitor cell being transformed by various oncogenes which give rise to various types of cancer [9].

2.1.3 Molecular Pathogenesis of Breast Cancer

In the normal breast terminal ductal lobular unit, there are lobules and ducts that consist of a bi-layered epithelium of luminal and myoepithelial cells [13]. The first phase of breast neoplasia begins with the formation of a premalignant lesion, named atypical hyperplasia, which is characterized by abnormal cell layers in these ducts or lobules. This condition is known as ductal carcinoma *in situ* (DCIS) and contains abnormal cells with non-

invasive ability. This condition can evolve into invasive breast cancer (IBC) unpredictably [14]. If cells invade, the risk of developing metastasis increases exponentially, being the lymph nodes adjacent to the tumor the primary site for breast cancer metastasis. When breast epithelial cells give rise to metastatic breast cancer, several events based on epigenetic and genetic changes occur in the microenvironment of the cells, mainly aberrations in the control of proliferation, differentiation, survival, migration, and interactions with tumor-stromal cells. Cells must enter and exit the vasculature while surviving in the absence of adhesion and establishing a new tumor in a foreign environment. Cancer stem cells also play an important role in breast cancer since they drive the initiation, progression, and recurrence of this cancer [15].

2.1.4 Therapeutic Management of Breast Cancer

For early-stage breast cancers, surgery is the standard treatment. The primary goal of surgery is the complete removal of the primary tumor, with negative margins to decrease the probability of local recurrences. The state of the tumor and the axillary lymph nodes are also evaluated, in order to estimate the prognosis of the disease [16]. There are two main types of surgery to remove breast cancer: breast-conserving surgery, where only the part of the breast containing the cancer is removed, and mastectomy, where the entire breast is removed, including all of the breast tissue and sometimes other nearby tissues [17].

Adjuvant chemotherapy may be given to the patients after surgery to try to eliminate any cancer cells that might have been left behind or that have spread but can't be detected, even on imaging tests [17]. Sometimes, neoadjuvant chemotherapy can be given to patients before surgery to try to shrink the tumor so it can be removed with less extensive surgery [17]. For metastatic breast cancer, surgery is no more effective, and systemic therapy (chemotherapeutic, hormonal and biological agents) and radiotherapy are the most common treatments [17].

In most cases, chemotherapy is the major player in oncologic therapy. This can be done using single drugs or a combination of two or more drugs. Anthracyclines, such as doxorubicin (DOX) and epirubicin, taxanes, such as paclitaxel (PTX) and docetaxel, 5-fluorouracil (5-FU) or capecitabine, cyclophosphamide and carboplatin are often used as adjuvant and neoadjuvant chemotherapeutic drugs [17]. For metastatic breast cancer, the most antineoplastic agents used are taxanes such as PTX, docetaxel and albumin-bound PTX, ixabepilone, eribulin, anthracyclines such as DOX, liposomal DOX and epirubicin, platinum agents such as cisplatin and carboplatin, vinorelbine, capecitabine and

gemcitabine [17]. Table 1 represents all chemotherapeutic drugs approved by the FDA for the prevention and treatment of breast cancer.

Table 1. Drugs approved by FDA for breast cancer therapy. Adapted from [18].

DRUGS FOR BREAST CANCER PREVENTION			
Raloxifene hydrochloride			
Tamoxifen citrate			
DRUGS FOR BREAST CANCER TREATMENT			
5-FU	Fulvestrant	PTX Albumin-stabilized Nanoparticle Formulation	Palbociclib
Abemaciclib	Gemcitabine Hydrochloride	Cyclophosphamide	Pamidronate Disodium
Ado-Trastuzumab Emtansine	Goserelin Acetate	Docetaxel	Pertuzumab
Anastrozole	Ixabepilone	DOX Hydrochloride	Ribociclib
Capecitabine	Lapatinib Ditosylate	Everolimus	Eribulin Mesylate
Olaparib	Letrozole	Exemestane	Thiotepa
Epirubicin Hydrochloride	Megestrol Acetate	PTX	Neratinib Maleate
Tamoxifen Citrate	Methotrexate	Vinblastine Sulfate	Talazoparib Tosylate
Trastuzumab	Trastuzumab and Hyaluronidase-oysk	Toremifene	

Combination therapy reduces the problems associated with mono-therapy because it allows to limit side effects and increases the anti-tumor capacity of the chemotherapeutics since the drugs act in several molecular pathways associated with carcinogenesis [19]. The main combinations approved by FDA for clinical use in breast cancer therapy are described in Table 2.

Table 2. Drug combinations approved by FDA for breast cancer therapy. Adapted from [18].

DRUG COMBINATIONS USED IN BREAST CANCER	DESCRIPTION
AC	Combination of DOX hydrochloride and cyclophosphamide
AC-T	Combination of DOX hydrochloride and cyclophosphamide, followed by PTX
CAF	Combination of cyclophosphamide, DOX hydrochloride, and 5-FU
CMF	Combination of cyclophosphamide, methotrexate, and 5-FU
FEC	Combination of 5-FU, epirubicin, and cyclophosphamide
TAC	Combination of docetaxel, DOX hydrochloride, and cyclophosphamide

Although surgical removal and chemotherapy play a key role in breast cancer therapy, being responsible for the long-term survival of patients [20], chemotherapy often has its effectiveness decreased due to the ability of tumor cells to offer intrinsic or acquired resistance to these therapeutic agents, making the treatment less effective [21]. Other problems related to chemotherapy involve the development of adverse side reactions, making cancer treatment less pleasant and narrowing the therapeutic window of antineoplastics [22].

2.2 Colorectal cancer

Colorectal cancer also represents one of the most common types of cancer worldwide and englobes the cancers that start in the colon and rectum, but the first ones are most frequent; for this reason, colorectal cancer is mainly referred to as colon cancer. Colorectal cancer is the third most frequently diagnosed cancer (excluding skin cancer), with an estimation of 1 to 2 million new cases each year globally [23]. It also represents the second leading cause of cancer-related deaths worldwide with an estimation of 881,000 deaths in 2018 [24], and this number is expected to continue to increase. Colorectal cancer is the second most common cancer in women (9.2%) and the third most common cancer in men (10%) [23]. More than half of colorectal cancer cases (55%) are detected in developed countries [24].

2.2.1 Colorectal Cancer Etiology

As in breast cancer, mutations in specific genes play a major role in the development of colorectal cancer. Based on the origin of the mutation, colorectal cancer can be divided into sporadic, inherited, and familial [25]. Sporadic colorectal cancer is the most common (70%) and results from successive point mutations, which start with the formation of adenomas and can progress to carcinomas [5]. The mutation often occurs in a tumor suppressor gene, namely adenomatous polyposis coli (APC), which leads to the formation of non-malignant adenomas (polyps). After this mutation, other mutations can occur, namely in Kirsten Rat Sarcoma Virus (KRAS), and Tumor Protein 53 (TP53), among others, which lead to the progression of adenomas to carcinomas [5].

Inherited cancers are less frequent and account for only 5% of all colorectal cancer cases [26]. In this type of cancer, one of the gene's alleles is already mutated (acquired hereditarily), and any point mutation may trigger the formation of tumor cells and lead to the formation of carcinoma. Inherited cancers can be classified into two groups: polyposis and non-polyposis forms. The first group is characterized by the formation of malignant polyps in the colon and results in familial adenomatous polyposis (FAP). The second group is characterized by mutations in the DNA repair mechanisms (MutS homolog 2 (MSH2), MutL homolog 1 (MLH1), MutL homolog 6 (MLH6), among others) and results in hereditary non-polyposis colorectal cancer (HNPCC) [26]. Familial colorectal cancer cancers account for 25% of total colorectal cancer cases and are also caused by hereditary mutations but have a different classification since they do not fall under the previously mentioned forms of inherited colorectal cancer [27].

Risk factors for colorectal cancer may be intrinsic (family history or genetic predisposition) or sporadic (derived from everyday habits, without a family history or genetic predisposition) (Figure 3). Hereditary conditions only account for a minority of all colorectal cancer (5% of all cases), being a much larger proportion due to sporadic risks [28]. Age, chronic diseases, and lifestyle are thought to be the main contributors for the increased incidence of colorectal cancer.

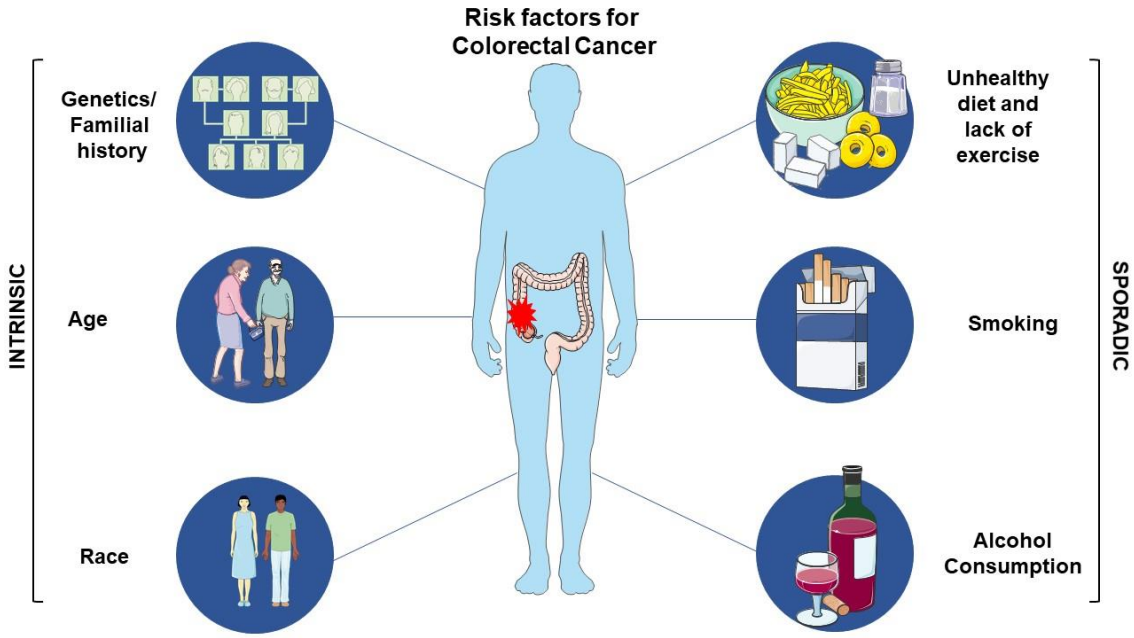

Figure 3. Colorectal cancer risk factors. Risk factors for this disease may be intrinsic, such as age, familial history, or race (left), or sporadic such as smoking, or alcohol consumption (right).

Age seems to be the main risk factor, as over 50 years of age the incidence of colorectal cancer cases increases considerably and below that age, cases are rare, except for hereditary cancers [29]. History of chronic diseases such as inflammatory bowel disease and Chron's disease are also important risk factors for the development of colorectal cancer [30]. Colorectal cancer cases in relatives under the age of 50 years also tend to be indicators of a higher risk of developing the disease. Lifestyle, especially habits related to diet and exercise can also contribute to an increased risk of developing colorectal cancer [31]. It is thought that this may be directly related to changes in the intestinal microbiome, which is directly involved in the regulation of metabolic pathways in the intestine and consequently may play a fundamental role in the maintenance of colorectal cells. Bad diet habits and lack of exercise can also be related to obesity, which is also another risk factor for colorectal

cancer [32]. Other risk factors include alcoholic consumption [33], smoking [34], etc. Racial and ethnic background may also play an important role for the predisposition of this disease, although the reasons are not fully understood [35].

2.2.2 Molecular Mechanisms of Colorectal Cancer

New genomic techniques have made it possible to understand which genomic aberrations are usually involved in colorectal cancer. Although the previously described mutations are much more common in this disease, chromosomal changes and translocations are also quite common in this disease. The main signaling pathways altered in colorectal cancer are Wingless/Integrated (WNT), Mitogen-activated Protein Kinase (MAPK) / Phosphoinositide 3-kinase (PI3K) and Transforming Growth Factor Beta (TGF-β). The WNT pathway is involved in stem cell differentiation and cell growth. In colorectal cancer, changes in the WNT pathway are related to the loss of adhesion of tight junctions, which leads to reduced cell adhesion and favors the migration of tumor cells [36]. The MAPK / PI3K pathway is involved in cell proliferation and survival and any alteration will lead to an uncontrolled increase in cell proliferation [25]. In turn, the TGF-β pathway is involved in processes such as cell growth, differentiation, and apoptosis. Changes in TP53 and cell cycle regulation are also frequent [37]. TP53 is a very important tumor suppressor gene and is involved in the regulation of the cell cycle [38]. Thus, mutations that affect one of these pathways will lead to an uncontrolled increase in cell growth and proliferation, a decrease in DNA repair mechanisms, and a consequent increase in the survival of these cells.

2.2.3 Molecular Pathogenesis of Colorectal Cancer

Most colorectal cancer cancers arise from neoplastic precursor lesions (called polyps). After a few years (10-15 years), polyps can evolve and progress to colorectal cancer. It is believed that the origin of colorectal cancer are stem cells that accumulate genetic and epigenetic alterations and result in the inactivation of tumor suppressor genes and activation of oncogenes. Stem cells are essential in the initiation and maintenance of tumor cells [39]. Depending on the genetic and epigenetic events, the development of colorectal cancer can occur through three main pathways: via adenoma-carcinoma, via serrated neoplasia, and microsatellite instability (Lynch syndrome) [37]. In most cases (70-90%), the development of colorectal cancer follows the classic adenoma-carcinoma pathway, so we will focus on this type of colorectal cancer.

The earliest stage colorectal cancer is called stage 0 and corresponds to carcinoma *in situ*, where the cancer cells are only in the mucosa, or the inner lining, of the colon or rectum. Then, colorectal cancer can be classified into 4 stages, ranging from I to IV depending on the development of the disease (Figure 4) [30]. Initially, there is an increasing in the proliferation of cells restricted to only one site (formation of small polyps). At this stage, the cells do not yet have malignant characteristics. Their accumulation leads to the formation of small clusters called adenomas. When they acquire malignant characteristics, they are called adenocarcinomas. These adenocarcinomas can successively increase in size by exaggerated cell growth and invade and spread to other parts of the body, especially to the lungs and liver, leading to the formation of metastases [40]. This occurs because the liver is very rich in blood supplements and has many humoral factors that promote cell growth. The lung is second place, after the liver, to be rich in blood supplements. This progression coincides with the previous mentioned key molecular alterations in important tumor suppressor genes, oncogenes, and other gatekeeper genes, impacting important signaling pathways responsible for the control of cell growth, proliferation, and malignancy [40].

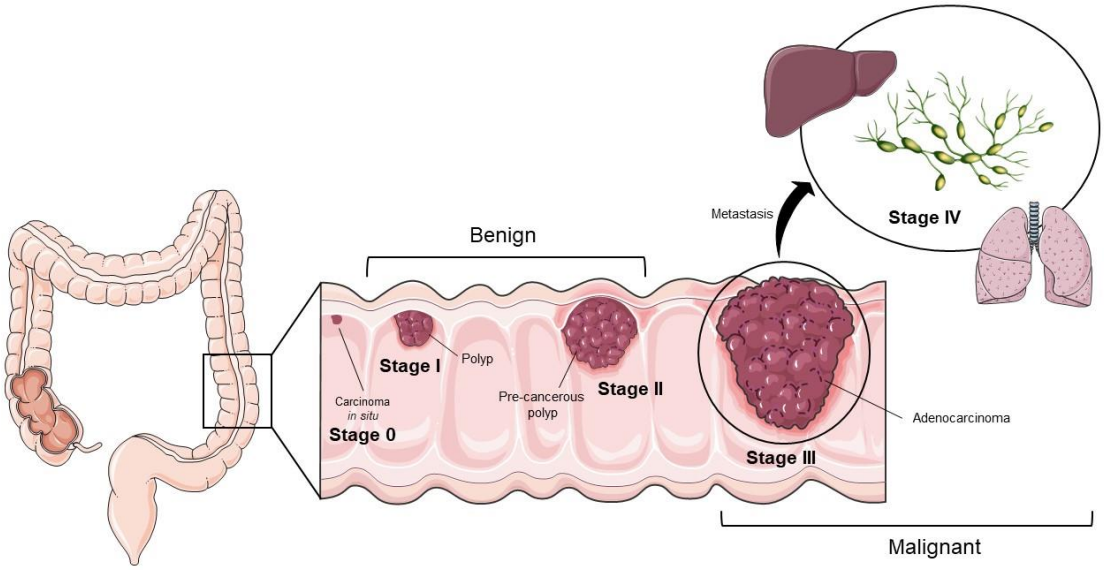

Figure 4. Adenoma-carcinoma stages in colorectal cancer. Cells of the normal epithelium mucosa grow abnormally and transform the gut epithelium into a hyper-proliferative epithelium, which can then form adenocarcinomas and invade other organs.

2.2.4 Therapeutic Management of Colorectal Cancer

Despite the advances in therapy, one of the main reasons that can be attributed to the high mortality of colorectal cancer is the failure of the current treatment options, since surgery can only be used in early stages and 20% of colorectal cancer cases are detected usually in advanced stages [41]. Tumor recurrence and metastasis are also frequent and cannot yet be effectively prevented. Treatment of colorectal cancer is a multimodal approach and depends on characteristics related both to the tumor and the patient. It is important to evaluate the presence or absence of metastases, the tumor progression, and the presence or absence of biomarkers, among others. It is also important to assess other diseases of the patient, age, prognosis, etc.

Colorectal cancer treatment can be done by surgery (removal of the primary tumor), radiotherapy (radiation exposure), or pharmacotherapy (cytotoxic chemotherapy or immunotherapy) (Figure 5) [42].

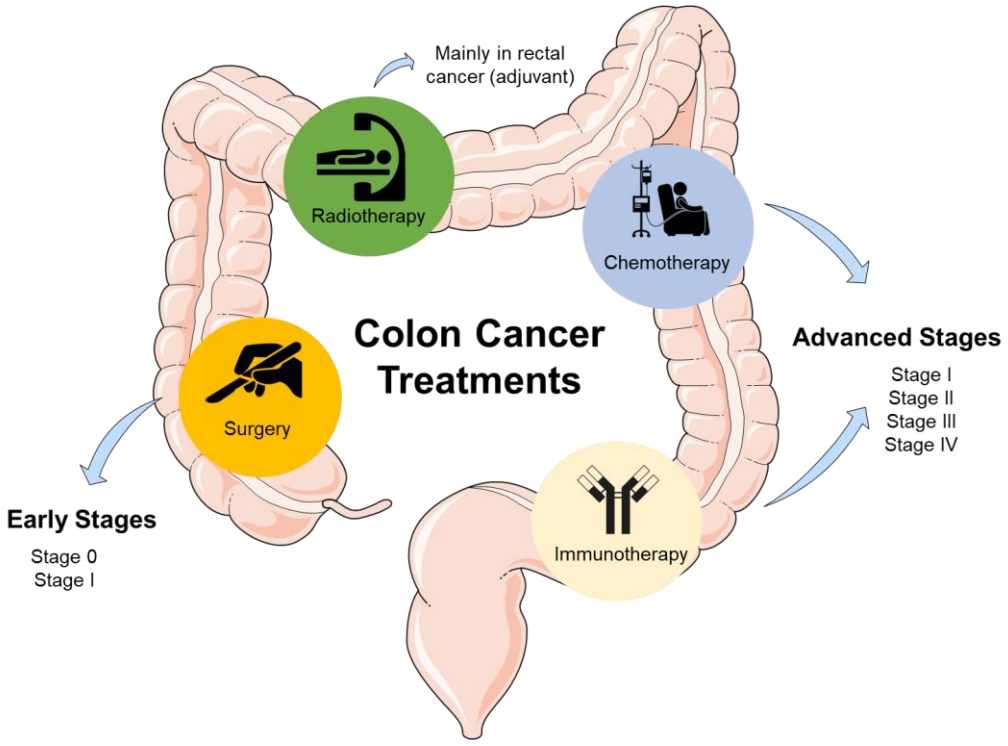

Figure 5. Current colorectal cancer treatments available. Surgery is usually the default treatment for early stages colorectal cancer while chemo- and immunotherapy are administered in advanced stages of the disease. Radiotherapy is usually used as adjuvant therapy for chemotherapy and surgery.

In clinical practice, colorectal cancer patients are divided into 4 groups. Group 0 corresponds to patients with no metastases or with resectable metastases in the lung or

liver and a good prognosis. In these cases, the most common treatment is surgery to remove the tumor and metastases [43]. Group 1 corresponds to patients with potentially resectable metastatic disease. Initially, these patients are treated with chemotherapy to decrease the number and reduce size of metastases that can be surgically removed later. Usually, double, or triple combinations of cytotoxic drugs combined with anti-vascular endothelial growth factor (VEGF) or anti-epidermal growth factor receptor (EGFR) strategies are used to decrease angiogenesis and metastasis of tumor cells [43]. In first-line treatment, the most common anti-VEGF strategy consists of using the monoclonal antibody Bevacizumab (which acts on circulating VEFG-A) and the recombinant protein Aflibercept (blocks VEGF-A, VEGF-B, and placental growth factors). Anti-EGFR treatments are only used in cases where there are no mutations in KRAS, with the most used monoclonal antibodies being Cetuximab and Panitumumab [43]. Group 2 corresponds to patients with disseminated but unresectable disease and the treatment intention is more palliative than curative. It is no longer a question of curing the disease but rather ensuring a reasonable quality of life for the patient, by reducing symptoms and aggressiveness of the disease. First-line treatment also consists of administering a dual combination of cytotoxic drugs with anti-VEGF or anti-EGFR strategies [43]. Group 3 corresponds to patients with unresectable disease and a lack of intensive treatment. The most common strategy is to combine a cytotoxic agent (such as fluoropyrimidine) combined with a biologically targeted agent [43]. Radiotherapy is mostly used in rectal cancers as an adjuvant to surgery and chemotherapy.

Based on National Comprehensive Cancer Network (NCCN) Clinical Practice Guidelines, first-line palliative chemotherapy consists of fluoropyrimidines (e.g., capecitabine or 5-FU) alone or in combination with leucovorin or other cytotoxic agents such as oxaliplatin (5-FU/leucovorin/oxaliplatin → FOLFOX), (capecitabine/oxaliplatin → CAPOX) or irinotecan (5-FU/leucovorin/irinotecan → FOLFIRI). Second-line chemotherapy is administered only to patients with good organ function and is administered when resistance occurs to the first-line treatment. Patients refractory to irinotecan are treated with FOLFOX or CAPOX (i.e. treatments with oxaliplatin) while those refractory to oxaliplatin are treated with irinotecan alone or FOLFIRI [43]. Table 3 represents all FDA-approved drugs for the treatment of colon cancer.

Table 3. Drugs approved by FDA for colon cancer therapy. Adapted from [44].

DRUGS FOR COLON CANCER TREATMENT	
5-FU	Oxaliplatin
Bevacizumab	Panitumumab
Capecitabine	Pembrolizumab
Cetuximab	Ramucirumab
Ipilimumab	Regorafenib
Irinotecan Hydrochloride	Trifluridine and Tipiracil Hydrochloride
Leucovorin Calcium	Nivolumab

2.3 Major Challenges in Breast and Colorectal Cancer Therapy

Advances in molecular biology allowed a better understanding of the mechanisms behind the formation of tumors and the acquisition of malignant characteristics by normal cells. Now, it is known that with carcinogenesis, populations of cells resistant to the therapy can be formed leading to the appearance of intra-tumor heterogenicity [45]. This heterogenicity causes the therapy to fail and, a drug that initially played a role in a metabolic pathway, may fail because of the cells' adaptation to therapy [46].

Although chemotherapy plays a key role in breast and colorectal cancer therapy, drug resistance and the development of undesired side effects make the treatment of these diseases less effective. These side effects include hair loss, nail changes, mouth sores, loss of appetite or weight changes, nausea and vomiting, diarrhea, fatigue, hot flashes, and/or vaginal dryness from menopause caused by chemotherapy and nerve damage [17]. Chemotherapeutic treatments can also affect the blood-forming cells of the bone marrow, which can lead to an increased chance of infections, easy bruising or bleeding and fatigue [17]. Some antineoplastic drugs, such as DOX, are also conditioned by cardiotoxicity [47]. In the case of PTX, the solvents used to solubilize this drug also difficult toleration of this drug and patients usually need to take pre-medications to minimize reactions to the solvents [48]. 5-FU use, for example, is also limited by the short half-life of this drug and its low bioavailability [49].

It is, therefore, very important to develop new methodologies and protocols that ensure the long-term survival and good life quality of these patients by increasing the therapeutic efficacy of these treatments, while reducing the doses and toxicity. Several approaches have been explored to overcome the disadvantages of traditional chemotherapy, such as the development of new oncologic drugs.

2.4 De novo Drug Development for the Search of New Anticancer Agents

Advances in medicine and technology have provided precious tools for the development of new drugs. Molecular biology has opened new doors to the knowledge of the molecular pathways involved in certain diseases and has allowed the development of new drugs more and more specific for certain pathologies [50].

The drug development process initiates with the *in silico* identification of potentially interesting compounds (between 5,000 and 10,000) during 3 and 5 years (Figure 6A). The most promising compounds enter the pre-clinical trials phase and their pharmacokinetic and pharmacodynamic properties are evaluated. The cytotoxicity of these compounds is further evaluated both *in vitro* and *in vivo*, in a process that may take between 1 and 2 years. At this stage, compounds that are toxic or have unfavorable absorption, distribution, metabolism, and excretion (ADME) properties are excluded (Figure 6B). At the end of this phase, the number of compounds under study is already reduced to approximately 5 candidates. For full drug approval, they must undergo clinical trials, which include 3 phases, in a process that takes about 6-7 years (Figure 6C). Being successful, a compound must be evaluated by the entities responsible for the approval of new drugs in a process that takes 1-2 years (Figure 6D). Only after this stage, the company can finally commercialize the new drug or medicine.

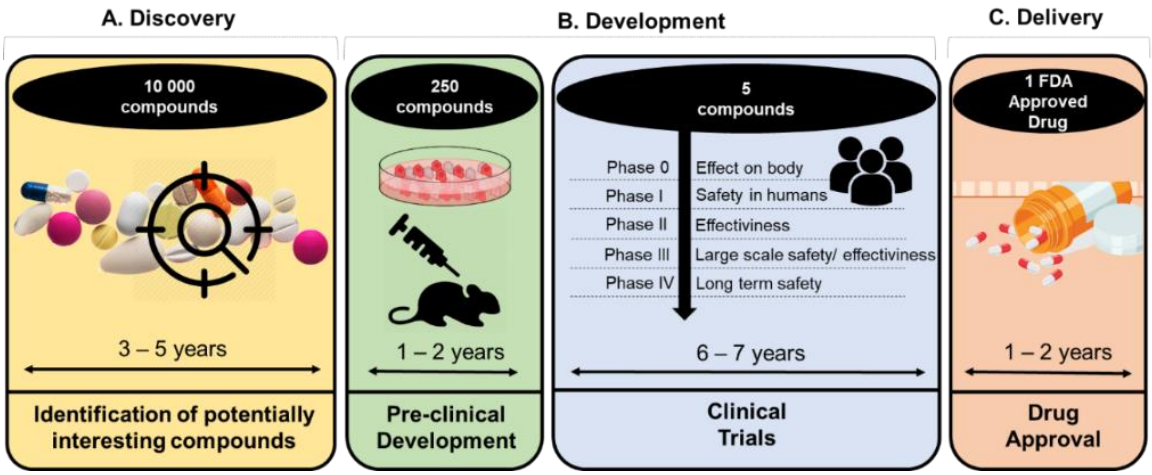

Figure 6. Timeline of the drug development process. A drug approval can take about 15 years and consists of four phases: drug discovery (**A**), development (pre-clinical and clinical trials) (**B**), and delivery (drug approval) (**C**). Most clinical trials fail at the beginning of the process.

Nevertheless, the costs associated with the process of developing new drugs are huge, as well as their design and approval time [51]. It is estimated that, specifically for cancer, the development of a new anti-neoplastic drug takes about 15 years and costs about 800 million dollars [52, 53]. Pharmaceutical companies often invest time and money

in drugs that never reach the market because they fail in the final clinical trials, leading to losses ascending to thousands of dollars. Currently, one of the main challenges in the pharmaceutical field is the development of cheaper, faster, and equally effective strategies that allow pharmaceutical companies to have high profits with low associated costs [54].

In oncology, the development of new drugs aims to find new candidates that are specific for tumor cells without causing significant damage to the normal cells that surround the tumor [55]. It is still a challenge to reach a high dose of antineoplastic at the tumor site, since the dose that usually reaches these cells is very reduced, enhancing the administration of higher doses to ensure the drug reaches the tumor, which leads to an increase in the side effects associated with chemotherapy [56].

In addition to the high costs and time necessary for the development of a new drug, the number of new drug approvals by the FDA, the entity responsible for the approval of new drugs in the USA, is diminishing over the years. In the oncological field, there are more than 10,000 ongoing clinical trials [57] but it is estimated that only 5% will progress to the next phases [58].

In 2016, 22 new drugs were approved by the FDA, compared to 45 approved in 2015 [59]. The number of novel cancer drugs approved followed the same trend and in 2016 only 4 new drugs were approved by FDA, compared to 14 in 2015 and 9 both in 2014 and 2013 [60]. Also, the European Medicines Agency (EMA) approved fewer drugs in 2016 than in previous years. This low approval rate, both of general drugs and drugs specially destined for the oncological area, demonstrates the constant need for the development of alternative methodologies to the development of new drugs. In 2017, FDA approved 46 novel drugs, with special emphasis on oncology (26%) and infectious diseases (17%) [61].

In 2016, as in previous years, the rate of FDA-approved drugs was similar to the rate of non-approved, which means half of the candidates that applied for FDA approval were rejected [62]. Because of this low approval rate, the drugs that reach the market are very expensive to allow pharmaceutical companies to recover the money invested in the clinical trials that have failed. As an example, the costs associated with the treatment of melanoma with the combination of ipilimumab and nivolumab may amount to $ 400,000 per patient [63, 64].

The increasing in Research and Development (R&D) expenditures by the pharmaceutical industries and the gradual decrease in the FDA's new drug approvals over the years, lead to a period of “innovation gap”, which means that alternatives to the *de novo*

development are needed. In the next section, we will present drug repurposing as an alternative strategy to the *de novo* drug development.

2.5 Drug Repurposing: An Alternative Strategy to the De Novo Drug Development

Currently, one of the main challenges in the pharmaceutical field is the development of cheaper, faster, and equally effective strategies that allow not only pharma companies to have high profits with low associated costs but also to decrease the costs associated with public health systems [54]. It is estimated that cancer treatment costs in the USA have doubled since 2012, making a total of $50 billion in 2017 [65]. There is, therefore, an urgent need for novel and innovative, cheaper, reliable, and easily applicable alternatives.

Drug repurposing (also described as drug repositioning, reprofiling, redirecting, switching, etc.) is a rapid methodology that has already been used in the clinic and allows to identify novel uses for drugs that are already commercialized in addition to its original medical indication [66]. Although the PubMed Medical Subject Headings (MeSH) term "Drug Repurposing" was only created in 2011, there has been an exponential increase in the number of publications in this database related to drug repositioning since 2004 (Figure 7) [67].

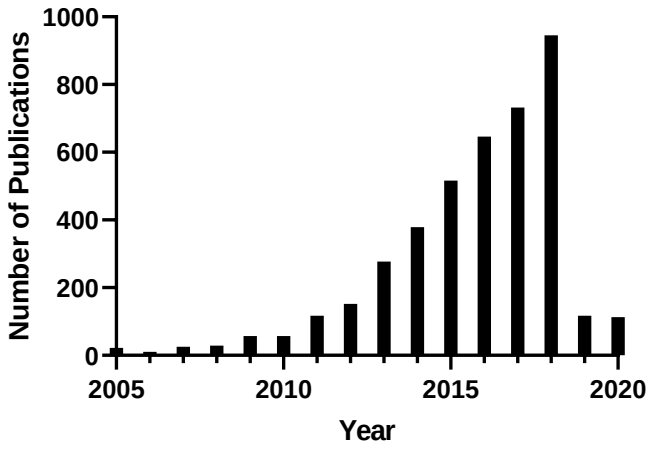

Figure 7. Number of publications related to “Drug Repurposing” in the database Pubmed, over the years (2005-August 2020). Publications related to drug repurposing have exponentially increased since 2005.

Although the initial definition of this strategy was restricted to the process of discovering new uses for drugs already on the market, over the years this definition has been expanded to include drugs that have failed clinical trials in their development process

due to high toxicity or ineffectiveness or drugs that have been withdrawn from the market for safety reasons. Nevertheless, this strategy can never include drugs that have not been subjected to clinical investigations.

Drug repurposing is based on the following scientific bases: (i) the discovery that different diseases share the same therapeutic targets and molecular features and (ii) the concept of pleiotropic drugs (i.e. drugs' actions other than those the drug was specifically developed) [68]. Currently, since most drugs are well characterized, it is possible to evaluate their therapeutic and side effects. In addition, and given that some diseases are also well-characterized, it is possible to molecularly understand the drugs' mechanism of action and adapt it to other diseases whose signaling pathways have similar patterns.

The main advantage of drug repurposing is the simplification of regulatory processes for drug approval for new therapeutical indications since the drug is already approved on the market and safety and toxicity profiles have already been extensively studied and approved [69]. In addition, these drugs have already described relevant clinical aspects such as dosage, drug interactions, and patient feedback. In addition, aspects related to pharmacokinetics, pharmacodynamics, mechanisms of action, molecular targets, and possible interactions with cells and tissues are also commonly described [69]. This brings economic advantages to pharmaceutical companies as the development of a new drug involves about 10-15 years of research, a brutal financial investment (estimated at 2-3 billion dollars in 2012), and a low success rate (about 2%) [70, 71]. This strategy is also useful in the discovery of new therapeutic targets and metabolic pathways [72].

It is estimated the development of a repositioned drug to be about 50-60% cheaper than a new drug and the chances of approval to be considerably higher (about 150%) [73]. Drug repurposing candidates usually have their patents expired and have been on the market for some time, leading to competition between pharmaceutical companies. This allows prices to remain low and brings benefits to public health systems in both developed and developing countries. In addition, repurposed drugs discovered by serendipity allow the discovery of new therapeutic targets and signaling pathways that remained unknown [74]. Together, the likelihood of the drugs to be accepted is greater and clinical trials are only required to confirm the benefits and effectiveness of the drug and to assess if there are no side effects other than those already described (Figure 8).

Figure 8. Advantages of drug repositioning in cancer therapy.

Drug repurposing has been adopted in several areas of medicine: one of the best-known examples is the case of sildenafil (sold under the commercial name of Viagra®), which was initially proposed for the treatment of angina and whose current therapeutic application is in the erectile dysfunction [75]. Another drug that has been studied in several therapeutic areas is saracatinib. This is an anticancer compound developed by AstraZeneca company that regulates tumor cell adhesion, migration, and invasion [76]. Phase II studies showed little benefits for oncological conditions [77, 78] and this drug is now being repurposed for Alzheimer's disease, as an analgesic to treat cancer-induced bone pain, as a therapeutic strategy for lymphangioleiomyomatosis and as a potential antipsychotic [79]. Another example is astemizole, an antihistamine that is currently used in the treatment of malaria [80]. In the treatment of Leishmaniasis, drugs from different classes, such as tamoxifen (an antitumor agent) [81] and amphotericin B (an antifungal) [82], were also repositioned. Raloxifene, an anti-neoplastic, has recently been repurposed for the treatment of osteoporosis [83]. Gemcitabine is also a classic that was initially proposed for the treatment of viral infections and is of increasing importance in cancer treatment [84]. Table 4 gives some examples of successful drugs that were repurposed for additional indications besides their original ones.

Table 4. Examples of successful repurposed drugs. Adapted from [79].

DRUG	ORIGINAL INDICATION	ADDITIONAL INDICATION AFTER REPURPOSING
Sildenafil	Angina	Erectile dysfunction
Astemizole	Antihistamine	Malaria
Tamoxifen	Anticancer	Leishmaniasis
Amphotericin B	Antifungal	Leishmaniasis
Raloxifene	Anticancer	Osteoporosis
Gemcitabine	Antiviral	Cancer
Zidovudine	Cancer	Acquired immunodeficiency syndrome (AIDS)
Minoxidil	Hypertension	Hair Loss
Thalidomide	Morning sickness	Multiple myeloma
Topiramate	Epilepsy	Obesity
Ketoconazole	Fungal infections	Cushing syndrome

In oncology, there has been a growing interest in repositioning drugs and there are more than 100 drug-relevant databases that support drug repurposing [85]. The Repurposing Drugs in Oncology (ReDO) project is a database whose objective is to identify drugs that are not used in cancer therapy with the potential to be repositioned as anti-tumor agents [86]. The ReDO project is funded by the Anticancer Fund (ACF) and is dedicated to the hard repurposing of cancer drugs, i.e. the use of non-neoplastic for cancer therapy [87]. By 2018, there were a total of 268 drugs in this database listed as potential candidates for cancer treatment. Repurposing candidates come from a wide range of areas of medicine and most of these drugs belong to the cardiovascular system family and the nervous system (Table 5).

Table 5. Number of repurposed drugs in the ReDO project according to Anatomical Therapeutic Chemical (ATC) Classification System. Adapted from [72].

ATC CLASSIFICATION	NUMBER OF DRUGS
Cardiovascular System	56
Nervous System	49
Alimentary Tract and Metabolism	39
Muscular-Skeletal System	31
Anti-infective for Systemic Use	26
Dermatological	23
Genito Urinary System and Sex Hormones	23
Sensory Organs	22
Antiparasitic Products, Insecticides, and Repellents	20
Blood and Blood-forming Organs	16
Antineoplastic and Immunomodulating Agents	12
Respiratory System	11
Systemic Hormonal Preparations, excl. Sex Hormones and Insulins	4
Various	4

Note that some drugs are included in multiple Anatomical Therapeutic Chemical (ATC) categories, and therefore the total is greater than the number of drugs in the ReDO dataset [72]. In all, 190 relevant late-stage trials were identified. Most of these drugs are studied for gastrointestinal and breast cancer, representing about 50% of the 190 trials registered with one of the drugs of the ReDO database (Table 6) [72].

Table 6. Type of cancer studied on the 190 trials registered with one of the drugs of the ReDO database. Adapted from [72].

CANCER TYPE	% OF TRIALS
Gastrointestinal	28
Breast	20
Hematologic	12
Lung	7
Gynecologic	6
Brain and CNS	5
Other	13
Pediatric	6
Not specified	12

A small number of drugs are currently under subject of intense clinical trial activity (i.e., 10 or more active late-stage trials) and should be considered to be well advanced in terms of a 'repurposing drugs pipeline' in oncology. Acetylsalicylic acid along with zoledronic acid are the drugs with the highest percentage of use in clinical trials involving drug repurposing (Table 7) [72].

Table 7. Drugs most studied on the 190 trials registered with one of the drugs of the ReDO database. Adapted from [72].

DRUGS WITH > 10 CLINICAL TRIALS	% OF TRIALS
Acetylsalicylic acid	14
Celecoxib	6
Cholecalciferol	6
Metformin	9
Olanzapine	5
Zoledronic acid	11

In terms of clinical trial sponsorship, the data show that very few trials have a commercial sponsor - less than 4% of trials in this dataset (Table 8). These clinical trials are largely carried out by public hospitals or universities, i.e., organisms with lower financial capacity and whose search for cheaper alternatives is always a priority [72]. Repositioning drugs enables public hospitals to lower the costs associated with the treatment of their patients and achieve better patient response rates. This strategy, on the other hand, also raises financial problems since the pharmaceutical industries have no interest in financing these projects, unless the drug is still patented and its eventual repurposing brings some financial benefit to these companies, i.e., the drug gives rise to new patents.

Table 8. Sponsors of the 190 trials registered with one of the drugs of the ReDO database. Adapted from [72].

CLINICAL TRIAL SPONSOR	% OF TRIALS
University and/or hospital	67
Research institute, organization, foundation, or network	28
Government	2
Small- and medium-sized pharmaceutical companies	3
Large pharmaceutical companies	1

2.5.1 Repurposed Drugs with Anticancer Potential

One of the best-known examples of cancer drug repurposing is propranolol. This drug was the first successfully synthesized beta-adrenergic blocker and is indicated for the treatment and prevention of myocardial infarction, angina, cardiac arrhythmias as well as migraine. In 2008, French doctors discovered that propranolol also had an unknown action on the biology of cells that make up the infant hemangioma, and, currently, propranolol is already used as therapy for this type of cancer. Propranolol is believed to decrease the expression of VEGF and basic fibroblast growth factor (bFGF), leading to endothelial cell apoptosis. Currently, propranolol has been studied for other cancers such as breast [88], prostate, and colon [89], among others [90–92].

Specifically, in oncology, there are already some repurposed drugs that seem to be good candidates for clinical use. Metformin, for example, has been associated with decreased cell viability in studies of hepatocellular, colorectal, prostate, and breast cancer, among others [93]. Verapamil, a calcium channel blocker that is used to treat cardiac arrhythmias, has been extensively studied for drug repurposing. It has been tested in gemcitabine-resistant pancreatic cells and has been able to inhibit tumor progression in this type of cell [94]. Other drugs, such as cimetidine or progesterone, have proven beneficial for the treatment of colorectal and breast cancer, respectively [95]. Despite the good results, only drugs such as thalidomide, tretinoin, also known as all-trans retinoic acid, zoledronic acid, and non-steroidal anti-inflammatory drugs (NSAIDs), like indomethacin and sulindac, are included in the guidelines of the European Society for Medical Oncology (ESMO) and the NCCN. The first three drugs were rebranded and reformulated by the pharmaceutical companies and, in the case of NSAIDs, they are used off-label [96, 97].

Figure 9 shows some repurposed candidates for tumor therapy and their main mechanism of action at the level of carcinogenesis. Many repurposed cancer drugs, like metformin, may act in various processes involved in tumorigeneses, such as in the dysregulation of cellular metabolism, proliferative signaling, or increased resistance to cell death [93]. Other examples include thalidomide, nelfinavir, or disulfiram. It should be noted that the drugs presented in Figure 13 belong to different pharmacological classes, ranging from anti-inflammatories, drugs for the treatment of diabetes and even for the treatment of alcohol dependence, among others, which demonstrates that any drug may be a good candidate for drug repurposing.

Figure 9. Relation between cancer repurposed drug candidates and the hallmarks of cancer. Reproduced from [93].

3. OBJECTIVES OF CHAPTER I

Here, we performed a screening of several drugs for the evaluation of their potential for drug repurposing in breast and colorectal cancer. We studied the cytotoxic effect of drugs belonging to the class of antimalarial, central nervous system, antibiotics/ antifungal, and other drugs in two different cancer cell lines: colorectal HT-29 and breast MCF-7. To evaluate the anticancer potential of these repurposed drugs, both cell lines were incubated with increasing concentrations of each drug for a period of 48 h and cell viability was evaluated by MTT and/or SRB assays. Finally, the IC_{50} value of each repurposed drug was calculated, and the most promising candidates were selected for further studies.

4. MATERIALS AND METHODS OF CHAPTER I

4.1 Materials and Reagents

Dulbecco's modified Eagle's medium (DMEM), McCoy's 5A Modified Medium, fetal bovine serum (FBS), and penicillin-streptomycin (pen-strep) solution were purchased from Millipore Sigma (Merck KGaA, Darmstadt, Germany). Other cell culture reagents were purchased from Gibco (Thermo Fisher Scientific, Inc, Waltham, MA, USA). MTT (cat. no. M5655) and SRB (cat. no. S1402) were obtained from Sigma-Aldrich (Merck KGaA, Darmstadt, Germany).

4.1.1 Antimalarial Drugs

Artesunate (cat. no. 11817) and cycloguanil (cat. no. 16861) were obtained from Cayman Chemical (Ann Arbor, Michigan, USA). Atovaquone (cat. no. 6358) was obtained from Tocris Bioscience (Bristol, UK). Pyronaridine (cat. no. P0049), tafenoquine (cat. no. SML0396), chloroquine (cat. no. C6628), lumefantrine (cat. no. L5420), primaquine (cat. no. 160393), sitamaquine (cat. no. SML1542) and 6-methoxy-nitroquinoline (cat. no. 206571) were obtained from Sigma-Aldrich (Merck KGaA, Darmstadt, Germany). Mefloquine (cat. no. sc-211784) was purchased from Santa Cruz Biotechnology (Dallas, Texas, USA).

4.1.2 CNS Drugs

Benztropine (cat. no. 16214), rufinamide (cat. no. 18870), thioridazine (cat. no. 14400), quetiapine (cat. no. 14152), lamotrigine (cat. no. 15428) and fluoxetine (cat. no. 14418) were obtained from Cayman Chemical (Ann Arbor, MI, USA). Ethosuximide (cat. no. PHR1413), latrepirdine (cat. no. D6196), perampanel (cat. no. P116), sertraline (cat. no. S6319), edaravone (cat. no. M70800), carbamazepine (cat. no. C4024), carbidopa (cat. no. PHR1655), entacapone (cat. no. SML0654), tolcapone (cat. no. SML0150), rivastigmine (cat. no. SML0881), safinamide (cat. no. SML0025), scopolamine (cat. no. PHR1470), selegiline (cat. no. M003) and fluphenazine (cat. no. F4765) were obtained from Sigma-Aldrich (Merck KGaA, Darmstadt, Germany). Primidone (cat. no. 0830), nepicastat (cat. no. 5037), and *m*-chlorophenilbiguanide (cat. no. 0440) were obtained from Tocris Bioscience (Bristol, UK). Bromocriptine was used in tablets and diluted in water before stock preparation.

4.1.3 Antibiotic/Antifungal Drugs

Natamycin (cat. no. 11634) and amikacin (cat. no. 15405) were obtained from Cayman Chemical (Ann Arbor, Michigan, USA). Dapsone (cat. no. A74807), clotrimazole (cat. no. C6019), and sulfamethoxazole (cat. no. S7507) were obtained from Sigma-Aldrich

(Merck KGaA, Darmstadt, Germany). Tobramycin (cat. no. 5390), gentamicin (cat. no. 6442), vancomycin (cat. no. 5506), and tunicamycin (cat. no. 3516) were obtained from Tocris Bioscience (Bristol, UK).

4.1.4 Other drugs

Piperazine (cat. no. P45907), amiodarone (cat. no. A8423), atenolol (cat. no. A7655), atorvastatin (cat. no. PZ0001), furosemide (cat. no. F4381), glibenclamide (cat. no. G0639), metoprolol (cat. no. M5391), telmisartan (cat. no. T8949) and quinidine (cat. no. Q3625) were obtained from Sigma-Aldrich (Merck KGaA, Darmstadt, Germany). Acamprosate (cat. no. 3618) was obtained from Tocris Bioscience (Bristol, UK).

4.2 Cell line and cell culture

4.2.1 MCF-7 cell line

Human breast cancer MCF-7 cell line was obtained from the American Type Culture Collection (ATCC; Manassas, VA, USA) and maintained according to ATCC's recommendations at 37 °C and 5% CO_2 in DMEM medium supplemented with 10% FBS and 1% pen-strep solution. Cells were always maintained in the logarithmic growth phase. The media was renewed every 2 days, trypsinized with 0.25% trypsin-ethylenediaminetetraacetic acid (EDTA) and subcultured in the same media.

MCF-7 cells (5,000 cells/well) were seeded in 96-well plates and allowed to adhere overnight prior to drug exposure. After that, the cell culture media were replaced with drug-containing media. Cells were exposed to drugs for 48 h, followed by SRB and/or MTT assays to evaluate drug treatments in the cell viability and protein synthesis rate of these cells.

4.2.2 HT-29 cell line

Human colorectal cancer HT-29 cell line was obtained from ATCC (Manassas, VA, USA) and maintained according to ATCC's recommendations at 37 °C and 5% CO_2 in an appropriate medium supplemented with 10% FBS and 1% pen-strep solution. Cells were always maintained in the logarithmic growth phase. The media was changed every 2 days and trypsinized with 0.25% trypsin-EDTA.

A total of 200 µL of HT-29 cells (7,500 cells/well) was seeded in 96-well plates and allowed to adhere overnight before drug exposure. After 24 h, the cell culture media were replaced with 200 µL of drug-containing media. Cells were exposed to drugs for 48 h, followed by MTT and/or SRB assays to evaluate drug treatments in the cell viability and protein synthesis rate of these cells.

4.3 Drug treatment

Both cell lines were treated with increasing concentrations of each drug for 48 h and then, based on the MTT results, the IC_{50} value was determined. The IC_{50} of the therapeutic drug was determined as each drug concentration showing 50% cell growth inhibition as compared with the control. All conditions were performed three times independently, in triplicate.

4.4 Cell viability assays

To determine the cytotoxic effects of each drug on MCF-7 breast and HT-29 colorectal cancer cells, MTT and/or SRB assays were used.

4.4.1 MTT assay

For the MTT protocol, after drug treatment, the cell medium was removed, and 200 µL/well of MTT solution (0.5 mg/mL in phosphate-buffered saline (PBS)) was added. Cells were incubated for 3 h and protected from light. After this period, the MTT solution was removed, and dimethyl sulfoxide (DMSO, 200 µL/well) was added to solubilize the formazan crystals. Absorbance was measured at 570 nm in an automated microplate reader (Sinergy HT, Biotek Instruments Inc., Winooski, VT, USA).

4.4.2 SRB assay

For the SRB assay, after treatments, the cultured cells were fixed with ice-cold 10% trichloroacetic acid for 30 min and stained with 0.4% SRB for 1h at room temperature. Excess dye was removed by rinsing several times with tap water. Protein-bound dye was dissolved with 400 µL 10 mM Tris base solution for the determination of absorbance with a microplate reader with a filter wavelength of 540 nm (Sinergy HT, Biotek Instruments Inc., Winooski, VT, USA).

4.5 Data Analysis

GraphPad Prism 9 (GraphPad Software Inc., San Diego, CA, USA) was used to produce all graphs from MTT and SRB assays as well as concentration-response curves by nonlinear regression analysis. The viability of cells treated with each drug was normalized to the viability of control cells and cell viability fractions were plotted versus drug concentrations in the logarithmic scale.

4.6 Statistical analysis

The results are presented as mean ± standard error of the mean (SEM) for *n* experiments performed. All data were assayed in three independent experiences, in

triplicate. Statistical comparisons between control and treatment groups, at the same time point, were performed with the Student's t-test and one-way analysis of variance (ANOVA) test. Statistical significance was accepted at p values < 0.05.

5. RESULTS AND DISCUSSION OF CHAPTER I

5.1 Drug Repurposing in Breast Cancer

5.1.1 Repurposing of Antimalarial Drugs for Breast Cancer

The consideration of antimalarial drugs as possible anticancer agents relies on their ability to interfere with important oncogenic pathways, such as WNT/β-catenin, signal transducer and activator of transcription 3 (STAT3) and nuclear factor kappa-light-chain-enhancer of activated B cells (NF-kB) along with the emerging role of mitochondria in mediating the anti-tumor effects of antimalarials [74]. Indeed, pre-clinical studies suggest that antimalarial drugs can have intrinsic anti-cancer activity, decrease cellular proliferation and induce apoptosis [98–104].

In this way, our group selected several antimalarials and structurally grouped them into two main groups: quinolinic-related derivatives (**1-7**, Scheme 1) and non-quinolinic-related derivatives (**8-11**, Scheme 1) to find the most promising antimalarial drugs for repurposing in breast cancer.

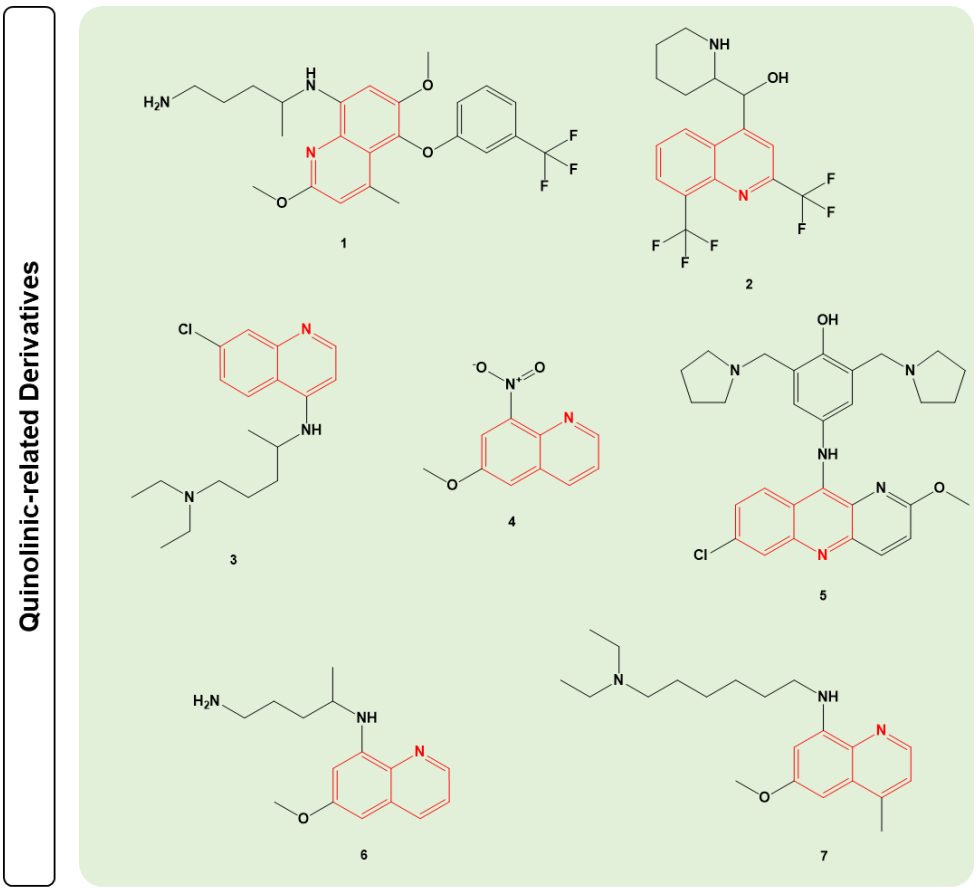

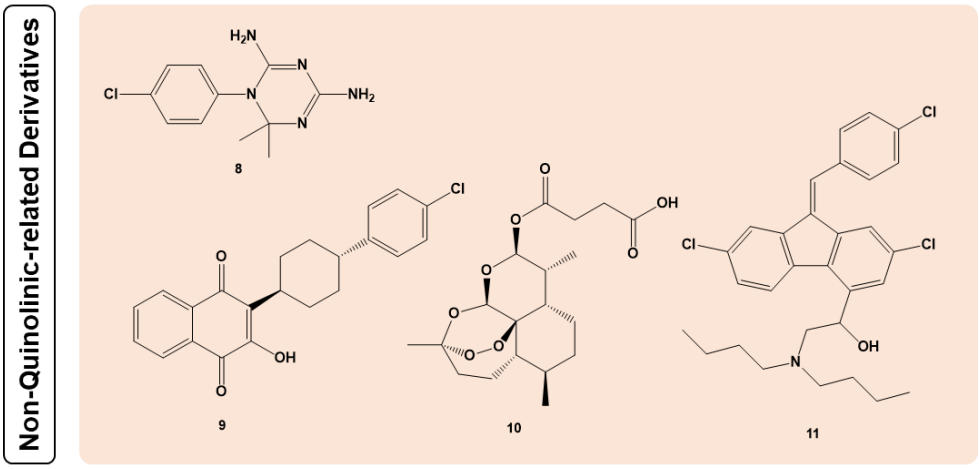

Scheme 1. Chemical structures of the antimalarial drugs evaluated in MCF-7 cells. Several compounds share a heterocyclic aromatic organic motif called quinoline (in red). Quinolinic-related derivatives: (**1**) Tafenoquine, (**2**) mefloquine, (**3**) chloroquine, (**4**) 6-methoxy-nitroquinoline, (**5**) pyronaridine, (**6**) primaquine and (**7**) sitamaquine; Non-quinolinic-related derivatives: (**8**) cycloguanil, (**9**) atovaquone, (**10**) artesunate and (**11**) lumefantrine.

First, the cytotoxic potential of several quinolinic-related derivatives, namely mefloquine, tafenoquine, 6-methoxy-nitroquinoline, pyronaridine, chloroquine, primaquine, and sitamaquine was analyzed in a human breast cancer cell line MCF-7 (non-invasive human breast cancer cell line, PR and ER-positive). These antimalarial drugs were grouped and chosen because they share a common structural feature: a quinolinic ring (**1-7**, Scheme 1).

Mefloquine (**1**, Scheme 1) is a quinolinic analog commonly used in combination with artemisinin in the treatment of malaria. Its mechanism of action is the inhibition of parasite protein synthesis by binding to the Pf80S subunit of the cytoplasmic ribosome of *Plasmodium falciparum* [105]. In cancer, mefloquine is believed to be involved in the modulation of the pathway induced by adenosine monophosphate-activated protein kinase (AMPK) via reactive oxygen species (ROS) production, as well as in lysosomal disruption [106]. Mefloquine also presents antitumor effects and has already been tested on tumor cell lines of the breast [107], prostate [106], etc. Specifically, in hormone receptor-positive T47D and negative MDA-MB-231 breast cancer cell lines, mefloquine inhibited autophagy, triggered endoplasmic reticulum stress, and caused cell death [107].

Tafenoquine (**2**, Scheme 1) is an 8-aminoquinoline derivative that was recently approved (2018) for the treatment of malaria caused by the parasite *Plasmodium vivax*. This drug is a primaquine analog and, although its mechanism remains unknown, it is

thought that its pharmacological activity is due to the metabolization catalyzed by the CYP450 complex, namely by CYP2D6 [108].

Chloroquine (**3**, Scheme 1) is a 4-aminoquinoline approved for the treatment of malarial infections and later for the treatment of discoid and systemic lupus erythematosus and rheumatoid arthritis. Chloroquine has been extensively studied both *in vitro* and in vivo in various cancer types, as monotherapy and combination therapy [109]. The mechanisms of action of chloroquine against the malarial *Plasmodium* parasite are well known [110]. Several hypotheses have been proposed on how chloroquine exerts its anti-cancer effect, but some preclinical studies refer that it influences the toll-like receptor (TLR9)/NF-kB signaling pathway, the C-X-C Motif Chemokine Ligand 12 (CXCL12)/ C-X-C chemokine receptor type 4 (CXCR4) signaling pathway, and the p53 pathway. Also, chloroquine might affect the autophagic flux at a late stage as it inhibits the fusion of the autophagosomes with the lysosomes and the subsequent degradation of the autolysosome [109]. Several pre-clinical studies also support the use of chloroquine in anti-cancer therapy, mainly combined with conventional chemotherapeutic drugs, such as 5-FU [111, 112]. Chloroquine has also been studied in different cancer cell types, such as lung [113], breast [98, 100], and colon [114], resulting in anti-cancer effects. Indeed, more than 30 clinical studies are currently evaluating the activity of this antimalarial drug combined with various standard treatments for different types of cancer. The idea behind this strategy is that chloroquine can increase tumor cells' sensibilization and therefore potentiate the therapeutic activity of chemotherapeutic drugs [109].

6-methoxy-8-nitroquinoline (**4**, Scheme 1) was also included in this study because it is also a quinoline derivative structurally very similar to the previous ones. No anticancer properties are reported for this drug in the literature.

Pyronaridine (**5**, Scheme 1) is a quinoline-related drug that inhibits the formation of β-hematin and promotes the lysis of blood cells. Its mechanism of action as an anti-malarial agent is based on the inhibition of the DNA polymerase II of the parasite *Plasmodium falciparum* through the formation of a stable complex with the DNA. In breast tumor cells, this drug exhibits cytotoxicity through the induction of apoptosis, by interfering with the progression of the cell cycle [115].

Primaquine (**6**, Scheme 1) is a substituted quinoline used in the treatment of malaria, mainly administrated in combination with chloroquine. This drug is effective against all four malarial species that infect humans [116, 117]. Its mechanism of action is not well understood but it is thought to interfere with the mitochondria of the parasite, by generating ROS or by interfering with the electron transport [118]. In a study published by Kim *et al*,

primaquine, in combination with mefloquine, has also demonstrated the ability to sensitize drug-resistant KBV20C cancer cells by increasing P-glycoprotein inhibition [102].

Sitamaquine (**7**, Scheme 1), also known as WR6026, is an 8-aminoquinoline with excellent efficacy against parasites and currently undergoing phase 2b clinical trials for the treatment of visceral leishmaniasis [119, 120]. Its mechanism of action involves inhibition of the respiratory chain complex II in parasites' mitochondria, by triggering ROS formation, ultimately leading to *Leishmania* parasites' apoptosis [121].

For the experiments, cells were treated with increasing concentrations of each previously described antimalarial drug (mefloquine, tafenoquine, 6-methoxy-nitroquinoline, pyronaridine, primaquine, and sitamaquine), starting from 1 µM to 100 µM to evaluate cell viability and cellular protein content after 48 h treatment, by MTT and SRB assays, respectively. These cell-based assays are among the most used in pharmacological studies involving cancer cell lines to evaluate the anti-cancer effect of different chemotherapeutic agents and provide important information regarding mitochondrial metabolism and cellular protein content. MTT assays measure the metabolic activity of cells, while SRB assays use an acidic protein-dye that binds electrostatically and pH-dependent to the basic amino acid residues of the proteins presented in the fixed cells, giving information about the cellular protein content.

Based on MTT results, the cytotoxic effects of mefloquine (Figure 10A) were significant even in concentrations of 1 µM, with higher concentrations causing a reduction in cell viability of more than 50% of the cells (Figure 10A). SRB results show a significant decrease in protein content inside these cells at all concentrations above or equal to 10 µM (Figure 10B). Both MTT and SRB assays for tafenoquine treatment demonstrate a strong cytotoxic effect of this antimalarial drug in MCF-7 cells for all concentrations tested above 10 µM (Figures 10C and D). Pyronaridine treatment also significantly decreased cell viability, from 1 µM to 100 µM, with a pronounced effect for all concentrations above 10 µM (Figure 10E). SRB results are not significative but demonstrate the same tendency as MTT results (Figure 10F). MCF-7 cells treated with primaquine at concentrations above 10 µM for 48 h, had little effect on cell viability and cellular protein content (Figure 10G and H). Above 50 µM, this drug caused a reduction of more than 50% in cell viability and protein synthesis. MTT and SRB assays for 6-methoxy-nitroquinoline, and sitamaquine demonstrated a lack of efficacy of these antimalarial drugs on the reduction of cell viability and protein content of this cell line (Supplementary Figure S1).

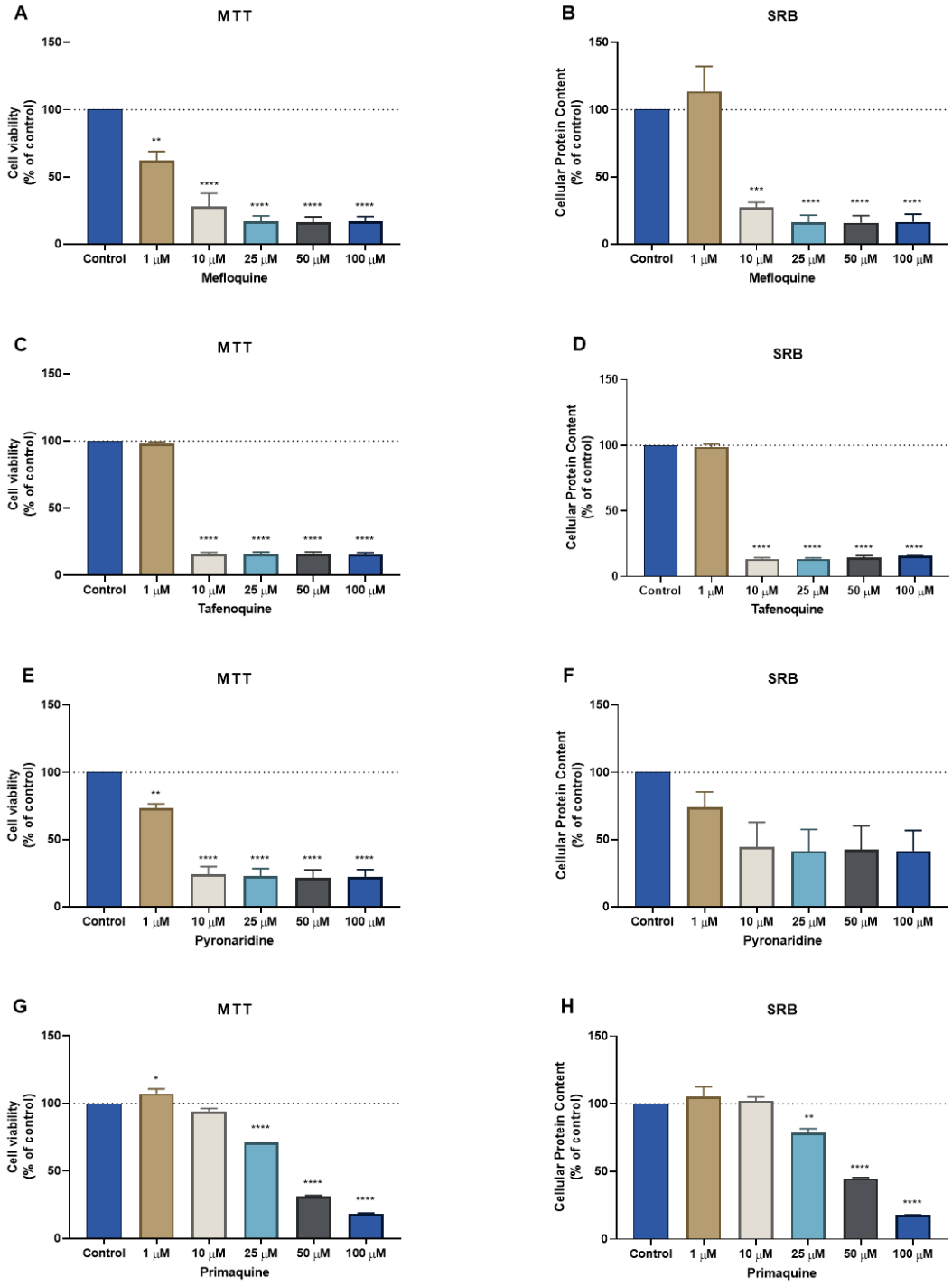

Figure 10. Effects of some antimalarial quinolinic derivates on MCF-7 cells. (**A**) Effect of mefloquine in cell viability and (**B**) protein content. (**C**) Effect of tafenoquine in cell viability and (**D**) protein content. (**E**) Effect of pyronaridine in cell viability and (**F**) protein content. (**G**) Effect of primaquine in cell viability and (**H**) protein content. Cells were cultured in the presence of increasing concentrations of each drug. After 48 h MTT and SRB assays were performed to measure cellular viability as well as protein content. Values are expressed in percentage and represent mean ± SEM. Each experiment was done three times independently (n = 3); *statistically significant vs. control at $p < 0.05$. **statistically significant vs. control at $p < 0.01$. ***statistically significant vs. control at $p < 0.001$. ****statistically significant vs. control at $p < 0.0001$.

As chloroquine anti-cancer activity has been evaluated several times in breast cancer cells, and its IC_{50} is well defined in the literature, the chloroquine cytotoxic effect was only evaluated by MTT assay and for a range of concentrations between 16 and 256 µM, i.e., tested for concentrations around its IC_{50} value described in the literature (64 µM) [100] (Figure 11).

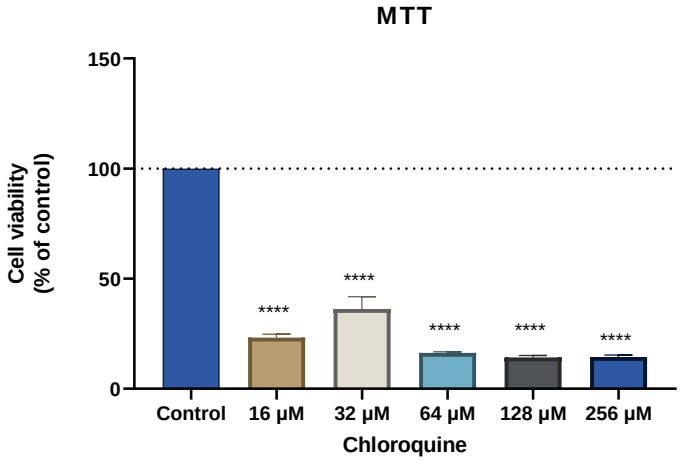

Figure 11. Effect of chloroquine on MCF-7 cells. Cells were cultured in the presence of increasing concentrations of chloroquine. After 48 h, an MTT assay was performed to measure cellular viability. Values are expressed in percentage and represent mean ± SEM. Each experiment was done three times independently (*n* = 3); ****statistically significant vs. control at $p < 0.0001$.

Next, the cytotoxic potential of four antimalarial non-quinolinic derivates, namely artesunate, lumefantrine, cycloguanil, and atovaquone was evaluated.

Cycloguanil (**8**, Scheme 1) is the active metabolite of proguanil, a prophylactic antimalarial drug. Proguanil is often administered together with chloroquine and atovaquone in the treatment of resistant malaria. Cycloguanil inhibits the enzyme dihydrofolate reductase in *Plasmodium falciparum* and *Plasmodium vivax,* which is involved in the reproduction of the parasites [122]. No reports on the anticancer activity of this antimalarial agent were found in the literature.

Atovaquone (**9**, Scheme 1) is an antimalarial drug approved for clinical use by FDA in 2000. It is used for the prevention of malaria and in the treatment of pneumocystis pneumonia and/or toxoplasmosis in immune-compromised patients [123, 124]. Atovaquone can be administered alone or in combination with Proguanil and targets the Co-enzyme Q10-dependence of mitochondrial complex III from *Plasmodium falciparum*, acting as a

competitive inhibitor of coenzyme Q10 [125]. Several studies demonstrated that atovaquone also has anti-tumoral activity against different types of cancer cells [126, 127], including breast cancer cells [128]. MCF-7 breast cancer cells treated with atovaquone demonstrated this drug inhibits oxygen-consumption and metabolically induces aerobic glycolysis and oxidative stress. Moreover, it was also found that atovaquone can also be potent and selective in mixed populations of cancer stem cells (CSCs) and non-CSCs [128].

Artesunate (**10**, Scheme 1) is a derivative of artemisinin which is also indicated in the treatment of malaria. This drug has a cytotoxic effect in different types of cells [129] and, specifically in gastric cancer, its effect is associated with a decrease in the expression of cyclooxygenase-2 (COX-2) [130]. In triple-negative breast cells, studies have shown a decrease in cell proliferation through the blocking of the cell cycle in G2/M (ROS-dependent) and G1 (ROS-independent) [131]. In addition, the same study suggested this drug is capable of inhibiting angiogenesis, reducing invasion and metastasis as well as altering lysosomal mechanisms [131].

Lumefantrine (**11**, Scheme 1) is a synthetic amino alcohol fluorene derivative, related to mefloquine [132]. It is an antimalarial agent used in the treatment of acute uncomplicated malaria. Usually, it is administered in combination with artemether for improved efficacy. This combination acts against the erythrocytic stages of the malaria parasite [122]. It can also be used to treat infections caused by *Plasmodium falciparum* and unidentified *Plasmodium* species, including those acquired in chloroquine-resistant. The exact mechanism of action of lumefantrine remains unknown but available data suggest that this drug inhibits the formation of β-hematin and inhibits nucleic acid and protein synthesis [122]. A recent study has demonstrated this drug can inhibit friend leukemia integration 1 transcription factor (Fli-1), a genetic element involved in brain cancer development and progression [133].

In this set of experiments, cells were treated as previous described. Based on MTT and SRB results, cytotoxic (Figure 12A) and protein synthesis effects (Figure 12B) of cycloguanil were significant for concentrations above 10 µM, but these effects were less pronounced compared to the previous tested antimalarial drugs. Artesunate treatment induced a higher reduction in cell viability (Figure 12C), at all concentrations above 10 µM, to a much higher extend than cycloguanil, with a reduction of more than 50% of cell viability in concentrations at 50 µM or more. SRB results for artesunate treatment were similar to those obtained by the MTT assay (Figure 12D). Neither atovaquone nor lumefantrine demonstrated good efficacy against MCF-7 cells, both in MTT and SRB assays (Figure S2).

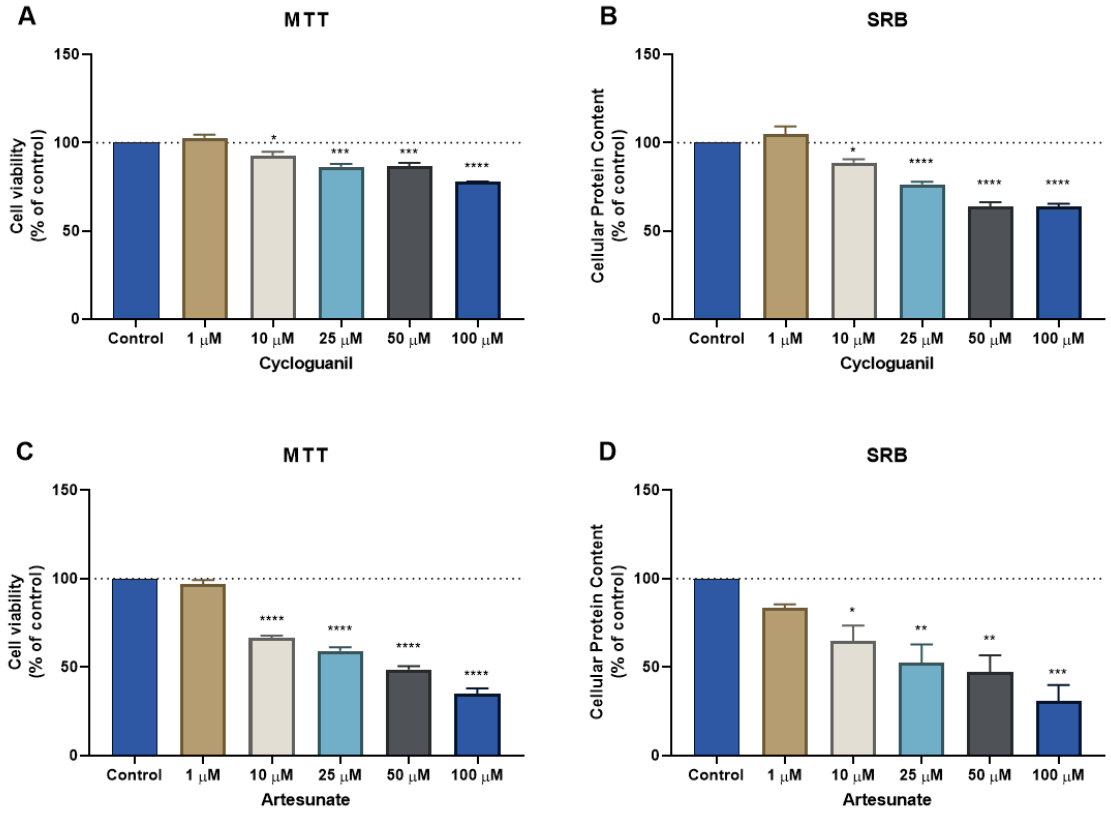

Figure 12. Effects of some antimalarial non-quinolinic derivates on MCF-7 cells. (**A**) Effect of cycloguanil in cell viability and (**B**) protein content. (**C**) Effect of artesunate in cell viability and (**D**) protein content. Cells were cultured in the presence of increasing concentrations of each drug. After 48 h, MTT and SRB assays were performed to measure cellular viability as well as protein content. Values are expressed in percentage and represent mean ± SEM. Each experiment was done three times independently (n = 3); *statistically significant vs. control at $p < 0.05$. **statistically significant vs. control at $p < 0.01$. ***statistically significant vs. control at $p < 0.001$. ****statistically significant vs. control at $p < 0.0001$.

Based on these results, it was concluded that, at this stage, the most promising antimalarials against MCF-7 cells were mefloquine, tafenoquine, primaquine, pyronaridine, chloroquine, artesunate, and cycloguanil. The first five are antimalarial quinolinic derivates and the last two are non-quinolinic derivatives. Therefore, after finding the most promising antimalarial drugs, based on the previous MTT and SRB results, we evaluated the IC_{50} for each drug.

Both mefloquine, tafenoquine and pyronaridine presented an IC_{50} lesser than 10 µM, with IC_{50} values of 1.241 µM, 2.595 µM, and 1.388 µM, respectively (Figure 13A, B, and D). Artesunate showed less cytotoxic activity than tafenoquine, with an IC_{50} of 11.60 µM (Figure 13E). Both primaquine and cycloguanil presented less ability than other antimalarial drugs to decrease the cell viability of MCF-7 cells, which resulted in higher IC_{50}, with IC_{50} values

of 29.90 µM and 20.30 µM, respectively (Figure 13C and F). Chloroquine IC_{50} was not calculated as this value was already available in the literature for this cell line [100], at the same experimental conditions. In general, the selected antimalarials showed great activity in reducing the cell viability of breast cancer cells, with very low IC_{50}. Table 9 summarizes the IC_{50} obtained for all antimalarial drugs tested in MCF-7 breast cancer cells.

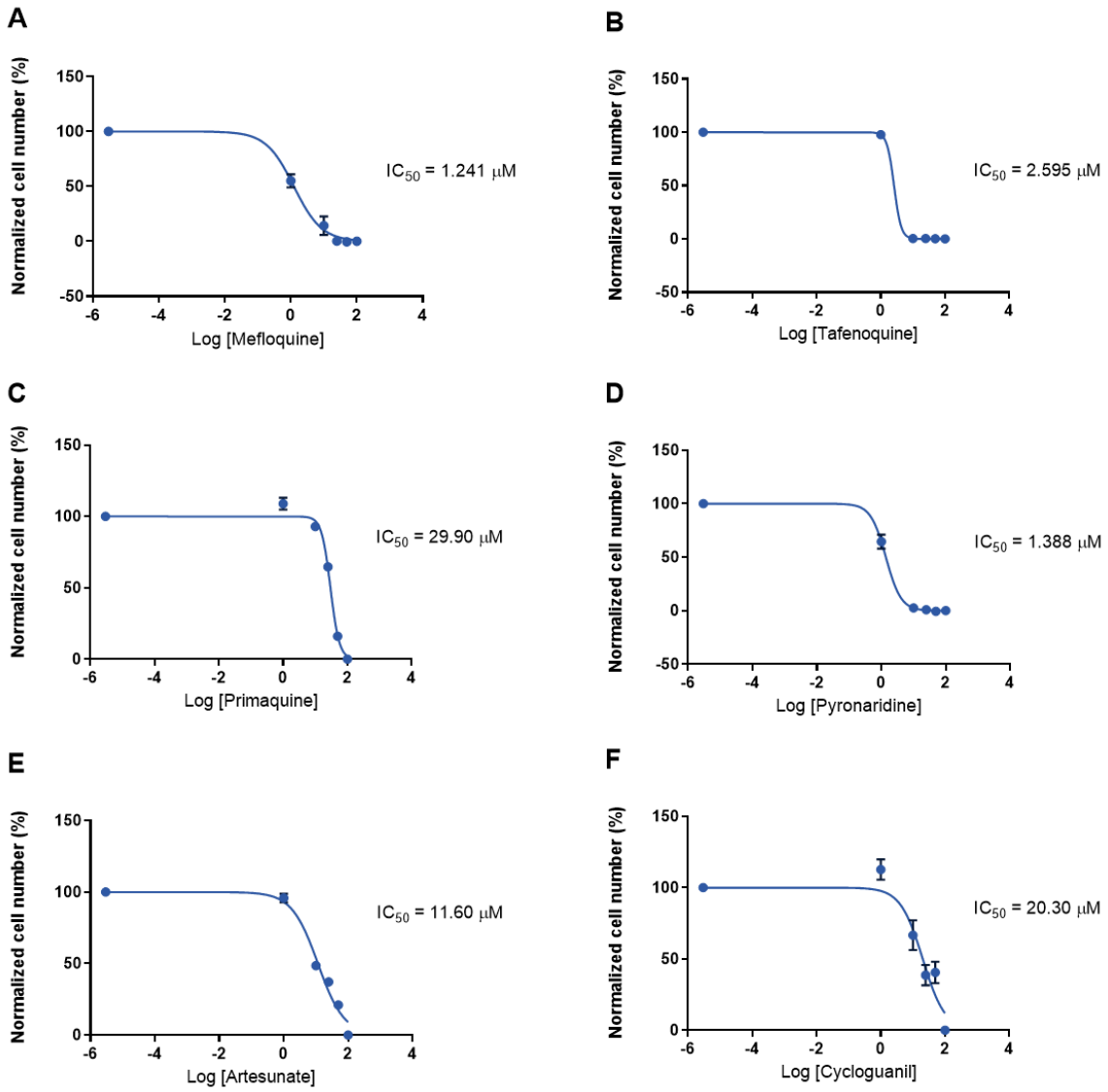

Figure 13. Concentration-response curves of (**A**) mefloquine, (**B**) tafenoquine, (**C**) primaquine, (**D**) pyronaridine, (**E**) artesunate and (**F**) cycloguanil on MCF-7 cells based on results obtained by MTT assay. The results represent the mean ± SEM of three independent experiments performed in triplicate.

Table 9. Cytotoxicity of all antimalarial drugs tested in MCF-7 breast cancer cells. IC_{50} values are given as mean. Chloroquine was not included in this table because its IC_{50} was obtained from the literature [100].

	Drug	IC_{50} (µM)
Quinolinic-related Derivatives	Mefloquine	1.241 ± 0.064
	Tafenoquine	2.595 ± 0.060
	6-methoxy-nitroquinoline	> 100
	Sitamaquine	> 100
	Primaquine	29.90 ± 0.02
	Pyronaridine	1.388 ± 0.216
Non-Quinolinic-related Derivatives	Artesunate	11.60 ± 0.04
	Atovaquone	> 100
	Lumefantrine	> 100
	Cycloguanil	20.30 ± 0.08

These results demonstrate that antimalarial drugs have the ability to decrease MCF-7 cell viability in a concentration-dependent manner, being good candidates to be used as standalone agents for breast cancer therapy.

5.1.2 Repurposing of CNS drugs in Breast Cancer

After demonstrating that antimalarial drugs can be promising candidates for drug repurposing in breast cancer, it was next hypothesized that another drug class, composed of different CNS drugs, could also display cytotoxic effects against MCF-7 breast cancer cells. Indeed, the repurposing of CNS drugs for cancer treatment has already been explored by the scientific community, and several studies have indeed demonstrated the effectiveness of this class of drugs in reducing the viability of different types of tumor cells [134–138].

CNS drugs can be divided into three main classes: antipsychotics, antidepressants, and anticonvulsants. Moreover, antipsychotics and antidepressants can also be subdivided

according to their mechanism of action in tricyclic antidepressants (TCA), monoamine oxidase inhibitors (MAOI), selective serotonin reuptake inhibitors (SSRI), serotonin and norepinephrine reuptake inhibitors (SNRI), norepinephrine and dopamine reuptake inhibitors (NDRI) and atypical antidepressants [138].

Several CNS drugs have demonstrated potential for drug repurposing, such as imipramine, phenothiazines, trifluoperazine, pimozide, and valproic acid. Imipramine, for example, has been studied in different types of cancer, such as glioma [137], breast [139], head and neck carcinoma [140], acute/chronic myeloid leukemia [141, 142], etc. Phenothiazines, a conventional antipsychotic drug family, which members work mainly as dopamine D2 antagonists, have also been studied in breast cancer [143], small-cell lung carcinoma [136], and oral cancer [144]. Trifluoperazine, an FDA-approved phenothiazine and a D2 receptor antagonist, was already studied in glioblastoma [145] and lung cancer [146]. Pimozide, another D2 blocking agent used for Tourette's Disorder, can be used to combat cancer cells, inducing apoptotic effects in cancer cells and decreasing the expression of Bcl-2 [147]. Valproate (Valproic acid) is an anti-epileptic drug that blocks Na^+ channels, gamma-aminobutyric acid (GABA) transaminase, and Ca^{2+} channels. This drug is used in epilepsy, migraine seizures, and acute manic episodes. Several studies suggest its beneficial role in fighting lymphoma [148], prostate [149], breast [150], bladder [151], and hepatocellular carcinomas [152], among others. Another recent study using different cell lines (malignant B, T, and myeloid cells) evaluated the effect of paroxetine and citalopram, two SSRI, and found these drugs are able to decrease cancer cell proliferation and induce apoptosis, in a concentration-dependent manner, in a mechanism serotonergic-independent [153]. Nevertheless, the authors found these drugs were nonselective for cancer cells, warning of their use as standalone chemotherapeutic agents [153]; however, they also concluded these drugs could be used in tolerable doses, preferentially in combination with antineoplastic drugs, supporting their use as chemosensitizer agents [153].

Therefore, four anticonvulsant drugs: ethosuximide (**1**, Scheme 2), perampanel (**2**, Scheme 2), primidone (**3**, Scheme 2) and rufinamide (**4**, Scheme 2), three antipsychotic drugs: fluphenazine (**5**, Scheme 2), thioridazine (**6**, Scheme 2) and quetiapine (**7**, Scheme 2), one for stroke and amyotrophic lateral: edaravone (**8**, Scheme 1), one for Parkinson's disease: benztropine (**9**, Scheme 2), another for Alzheimer's disease: latrepirdine (**10**, Scheme 2) and two antidepressant agents: fluoxetine (**11**, Scheme 2) and sertraline (**12**, Scheme 2) were selected to be evaluated in MCF-7 cell line.

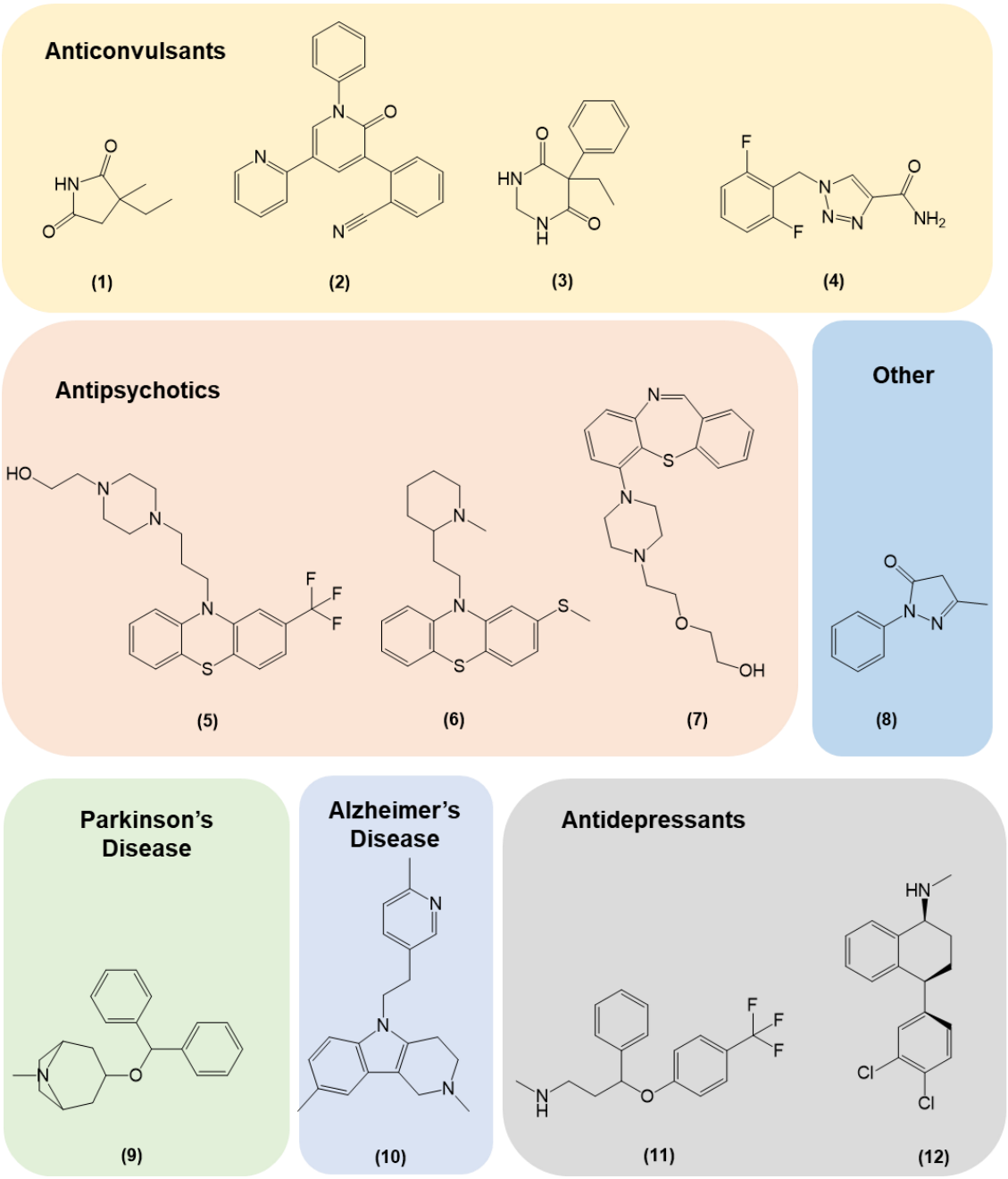

Scheme 2. Chemical structures of the CNS drugs evaluated in MCF-7 cells. (**1**) Ethosuximide, (**2**) Perampanel, (**3**) Primidone, (**4**) Rufinamide, (**5**) Fluphenazine, (**6**) Thioridazine, (**7**) Quetiapine, (**8**) Edaravone, (**9**) Benztropine, (**10**) Latrepirdine, (**11**) Fluoxetine, (**12**) Sertraline

Ethosuximide (**1**, Scheme 2) is an anticonvulsant drug approved in the USA in 1960, used for the management and treatment of absence epilepsy [154]. Its mechanism of action involves the decrease of the threshold of T-type calcium currents and the disruption of the oscillatory activity of thalamocortical circuitry by blockage of T-type calcium channels [155]. This drug is included in the List of Essential Medicines from the WHO and is currently

available as generic medication. In a study published by Abdul *et al*, this drug demonstrated ability to inhibit the growth of three prostate cancer cell lines, at clinically-relevant doses [156].

Perampanel (**2**, Scheme 2) is another anticonvulsant agent already approved in Europe and USA for the adjunctive treatment of partial-onset seizures (with or without secondary generalized seizures) in patients with epilepsy [157]. It is a non-competitive antagonist of the α-amino-3-hydroxy-5-methyl-4-isoxazolepropionic acid (AMPA) receptors, ligand-gated ion channels activated by glutamate. A recent study demonstrated that perampanel may also have promising antitumor effects in malignant glioma cells, through the induction of apoptosis [158].

Primidone (**3**, Scheme 2) is a first-generation barbiturate type antiepileptic medication developed to treat seizures, commonly for partial and generalized seizures [159]. It received its approval from FDA in 1954 for the treatment of epilepsy but nowadays this drug is not a first-choice drug [159]. The mechanism of action of this drug is not well-defined, but some studies suggest this drug binds to voltage-gated sodium channels, inhibiting the monotonous firing of action potentials [160]. Moreover, this drug also seems to activate the GABA-A receptor complex [161]. To date, no studies of this drug in cancer cells were found in the literature.

Rufinamide (**4**, Scheme 2) is a triazole derivative drug structurally unrelated to any other anti-seizure drugs. It was developed first in 2004 but was only approved by FDA in 2008, for the adjunctive treatment of seizures associated with Lennox Gastaut syndrome [162]. Its mechanism of action is still unknown but *in vitro* studies have demonstrated this drug stabilizes the inactive state of sodium channels, preventing sodium channels from returning to an activated state, therefore decreasing the neuronal hyperexcitability and action potential propagation [163]. No findings are reported regarding the use of this drug in cancer cells.

Fluphenazine (**5**, Scheme 2) is a typical antipsychotic used for the symptomatic management of psychosis in patients with schizophrenia. This drug **i**s part of a class of drugs known as first-generation antipsychotics or conventional antipsychotics [164]. Fluphenazine is an antagonist of the postsynaptic mesolimbic dopaminergic D1 and D2 receptors in the brain and depresses the release of hypothalamic and hypophyseal hormones [164]. Recently, using triple-negative breast cancer cells, fluphenazine demonstrated the ability to inhibit cancer cell growth, induce G0/G1 cell cycle arrest, and induce mitochondria-mediated apoptosis [165].

Thioridazine (**6**, Scheme 2) is an FDA-approved medication to treat schizophrenia and schizophrenia spectrum disorders and is similar to other first-generation, or typical antipsychotics [166]. Its mechanism of action involves the blockage of dopaminergic D1 and D2 receptors in the mesolimbic pathway, diminishing positive symptoms. Recently, it was found that this drug significantly suppresses the proliferation and invasion of colon cancer stem cells and induces cell apoptosis in a concentration-dependent manner. It was found that apoptosis genes such as Bax and caspase-3 were overexpressed after thioridazine treatment, while anti-apoptosis gene Bcl-2 was downregulated. Accordingly, the mitochondrial potential of these cells was also downregulated [167].

Quetiapine (**7**, Scheme 2) is an atypical antipsychotic drug that is used to treat schizophrenia and other neurologic disorders such as depression [168]. Recently, a study demonstrated that quetiapine is able to decrease the proliferation of brain cancer cells and induce glioblastoma-derived stem-like cell differentiation by inhibiting the WNT/β-catenin signaling pathway [169].

Edaravone (**8**, Scheme 2) is a pyrazolone derivative usually prescribed for the treatment of amyotrophic lateral sclerosis or after an acute cerebral infarction [170]. It was first approved in Japan and South Korea in 2015 and then in the USA in 2017 [171, 172]. Besides being a scavenger of oxygen free radicals, it also modules some transcription factors, repressing NF-kB and activating nuclear factor erythroid 2–related factor 2 (Nrf2), acting as an oxidative stress modulator [173]. Nrf2 is a transcription factor that plays an important role in the response of cells to oxidative stress since it regulates the expression of multiple antioxidant key genes [174]. Under oxidative stress, this transcription factor translocates into the nucleus and modulates the expression of the antioxidant enzymes heme oxygenase-1 (HO-1), thioredoxin-1, and peroxiredoxin genes family as well as enzymes implanted in glutathione synthesis [175]. In cancer cells, Nrf2 is an important player in the development of drug resistance, impairing drug-mediated oxidative stress and contributing to cancer cell survival, by inhibiting apoptosis and promoting cell proliferation [176, 177]. Nevertheless, some studies have been implicating this drug as a moderate anticancer agent [178–181]. A study demonstrated this drug has antiproliferative properties and is able to significantly enhance the anticancer and antimetastatic activities of irinotecan in a colon cancer model [178].

Benztropine (**9**, Scheme 2) is an FDA-approved drug for adjunctive therapy for all forms of parkinsonism. It is a selective inhibitor of dopamine transporter and presents affinity for histamine and M1 muscarine receptors [182]. Recent studies suggest that benztropine

reduces the activity of oncogenic signaling transducers and trans-activators for MMP9, including STAT3, NF-kB, and β-catenin [183].

Latrepirdine (**10**, Scheme 2) is an antihistamine drug that has been recently proposed for drug repurposing as a neuroprotective drug for the management and treatment of Alzheimer's disease [184]. This drug seems to operate through diverse mechanisms of action, involving the blockage of neurotoxic beta-amyloid proteins and inhibition of L-type calcium channels as well as modulation of AMPA and N-methyl D-aspartate (NMDA) glutamate receptors [185]. Its neuroprotective effect may involve mitochondrial pores [186]. Nevertheless, this drug has failed in several Alzheimer's disease clinical trials [187] as well as in a phase III trial for Huntington disease [188]. To our knowledge, this drug has never been studied in cancer cells.

Fluoxetine (**11**, Scheme 2) is an FDA-approved drug for major depressive disorder, obsessive-compulsive disorder, panic disorder, among other disorders. It exerts its effects by blocking the reuptake of serotonin into presynaptic serotonin neurons by blocking the reuptake transporter protein located in the presynaptic terminal [189]. Fluoxetine was found to significantly decrease the proliferation of several breast cancer cell lines by inducing apoptosis and autophagy-mediated cell death or endoplasmic reticulum stress and autophagy, respectively [190–193]. This drug has also demonstrated the ability to decrease the proliferation of PC-3, DU-145 and LNCaP prostate cancer cells, both *in vitro* and in animal models [194]. In other studies, this SSRI has also been able to induce apoptosis of C6 glioma [195] and neuroblastoma cells [196], in a mechanism involving the activation of MAPK/Jun N-terminal kinase (JNK) pathway, including phosphorylation of the c-Jun protein [196]. Another study observed a decrease in the cell viability of Jurkat malignant T cells after treatment with 20 μM of fluoxetine, demonstrating the potential of this drug to act as an anticancer agent [197].

Sertraline (**12**, Scheme 2) is a drug belonging to the class of SSRI, which are antidepressants commonly used in the management of psychiatric disorders [198]. This drug was among the first SSRI compounds to be approved by the FDA for clinical use, in 1992 [199]. This drug demonstrates efficacy in the treatment of depression, including major depressive disorder, anxiety, and eating disorders, and also premenstrual dysphoric disorders [199]. Its primary mechanism of action involves the inhibition of serotonin reuptake into the pre-synaptic nerve terminals, which causes the elevation of serotonin levels in the synaptic gap [200]. Several studies have reported the promising anticancer effects of sertraline, in different types of cancer cell lines [201–205]. It was found that sertraline decreases cell viability, proliferation, migration, and invasion, induces apoptosis, and

causes cell cycle arrest in different types of cancer cells, besides being an established P-glycoprotein modulator. It was also found that this drug is able to modulate autophagy, cause DNA fragmentation, and induce ROS formation. Moreover, it was found this drug targets important cellular pathways involved in tumorigeneses such as the tumor necrosis factor (TNF)/Mitogen-activated protein kinase kinase kinase kinase 4 (MAP4K4)/JNK pathway, the antiapoptotic pathway PI3K/Ak strain transforming (AKT)/mammalian target of rapamycin (mTOR), and the AMPK/mTOR axis. This drug also interferes with the translationally controlled tumor protein (TCTP)/p53 feedback loop and with the cytosolic free Ca^{2+} levels.

For this set of experiments and as previously described, MCF-7 cells were treated with increasing concentrations of each drug, and cell viability was evaluated by MTT and/or SRB assays after 48 h treatment. To perform a better accurate determination of the IC_{50} values of each drug, the range of concentrations for each drug was extended from 0.1 to 100 µM.

Based on the MTT results, it was found that several CNS drugs, such as fluoxetine, sertraline, thioridazine, fluphenazine, and benztropine displayed significant anti-tumor activity in MCF-7 cells. Specifically, cytotoxic effects of fluoxetine (Figure 14A) were significant in concentrations above 10 µM, with 7.78 µM causing a reduction of more than 50% of the cells (Figure 14B). The anti-tumor effect of sertraline was the strongest among all drugs tested alone, and concentrations above 10 µM killed almost all cells (Figure 14C). The IC_{50} value obtained for sertraline was the lowest, i.e., about 2.22 µM (Figure 14D). MTT results for thioridazine demonstrated a strong cytotoxic effect of this CNS drug in HT-29 cells for all concentrations tested above 10 µM (Figure 14E). The dose-response curve for thioridazine resulted in an IC_{50} value of 5.72 µM (Figure 14F). Fluphenazine showed significant anti-tumor effects similar to sertraline in concentrations above 10 µM (Figure 14G) and the IC_{50} value obtained was 2.68 µM (Figure 14H). Benztropine treatment significantly decreased MCF-7 breast cancer cell viability for all concentrations above 15 µM (Figure 14I) and an IC_{50} value of 21.71 µM (Figure 14J). Treatment with ethosuximide, rufinamide, and perampanel did not result in significant changes in the viability of MCF-7 cells (Figure S3). Only treatments with primidone and latrepirdine at doses of 100 µM and above 25 µM, respectively, had a significant effect on the cell viability (Figure S3), resulting in an IC_{50} value of more than 70 µM (Table 10). Treatments with 0.1 µM edaravone demonstrated a significant reduction of MCF-7 cell viability but in a lower extend (< 10%); moreover, only the highest concentration (100 µM) of quetiapine was able to decrease

significantly MCF-7 cellular viability (Figure S4). Table 10 summarizes the IC_{50} obtained for all CNS drugs tested in MCF-7 breast cancer cells.

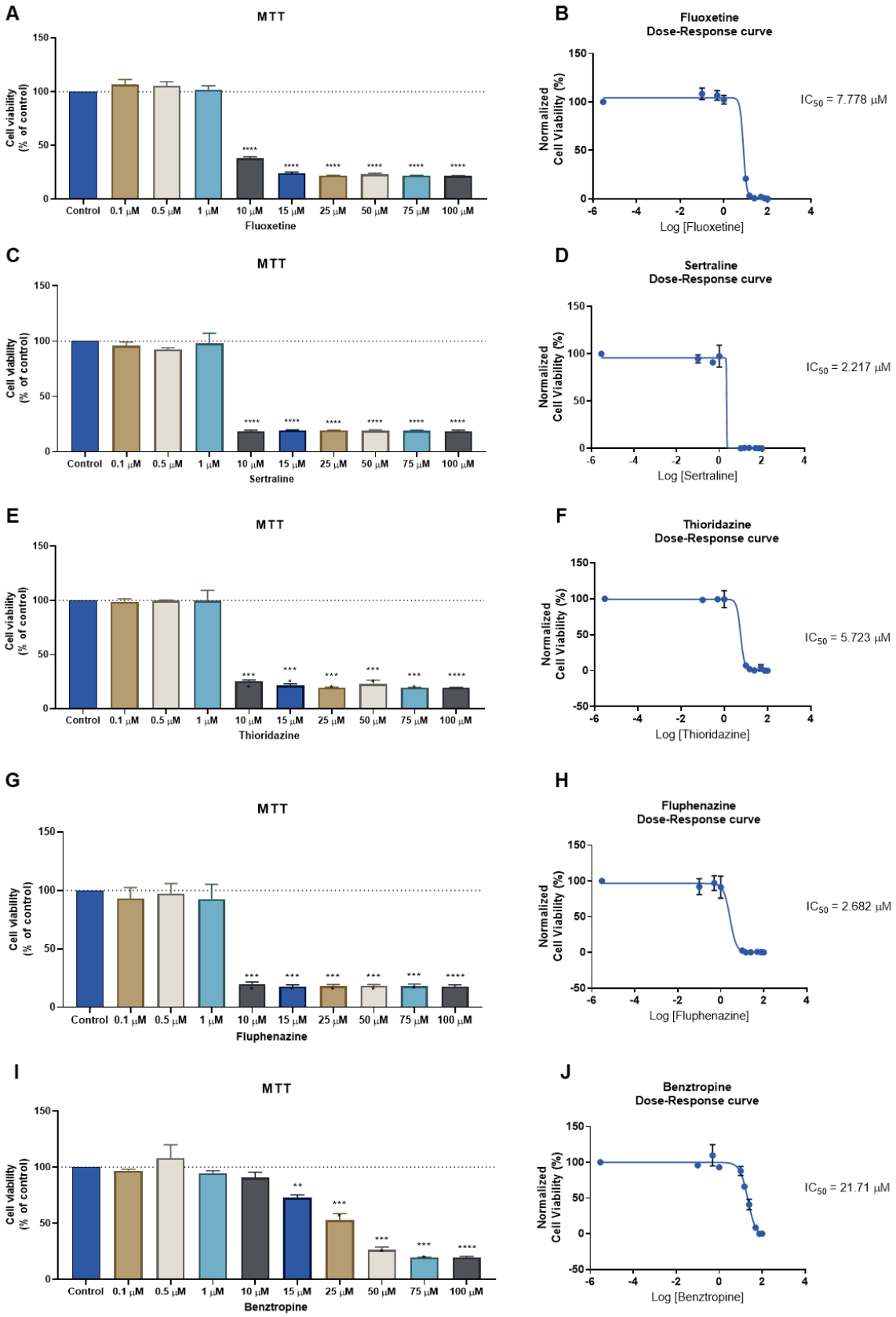

Figure 14. The effects of some CNS drugs on MCF-7 cells. (**A**) The effect of fluoxetine on cell viability and (**B**) the dose-response curve. (**C**) The effect of sertraline on cell viability and (**D**) dose-response curve. (**E**) The effect of thioridazine on cell viability and (**F**) the dose-response curve. (**G**) The effect of fluphenazine on cell viability and (**H**) the dose-response curve. (**I**) The effect of benztropine on cell viability and (**J**) the dose-response curve. Cells were cultured in the presence of increasing concentrations of each drug, and after 48 h, the MTT assay was performed to measure the cellular viability. Values are expressed in percentage of control and represent mean ± SEM. Each experiment was done three times independently (n = 3); * statistically significant vs. control at $p < 0.05$. ** statistically significant vs. control at $p < 0.01$. **** statistically significant vs. control at $p < 0.0001$.

Table 10. Cytotoxicity of all CNS drugs tested in MCF-7 breast cancer cells. IC_{50} values are given as mean.

Drug	IC_{50} (μM)
Fluphenazine	2.682 ± 0.268
Fluoxetine	7.778 ± 0.066
Benztropine	21.71 ± 0.05
Thioridazine	5.723 ± 0.594
Sertraline	2.217 ± 0.156
Ethosuximide	> 100
Perampanel	> 100
Primidone	> 100
Rufinamide	> 100
Quetiapine	> 100
Edaravone	> 100
Latrepirdine	75.37 ± 0.17

These results demonstrate that some CNS agents, such as fluoxetine, sertraline, benztropine, fluphenazine, and thioridazine, are good candidates to be used as standalone agents for breast cancer therapy.

5.1.3 Repurposing of Antibiotic/Antifungal Drugs for Breast Cancer Therapy

Next, it was selected and screened another class of drugs for repurposing in breast cancer. Based on evidence that demonstrated that several antibiotic and antifungal drugs may promote cancer apoptosis, inhibit cancer growth and prevent cancer metastasis [206, 207], four antibiotic drugs: tobramycin (**1**, Scheme 3), sulfamethoxazole (**2**, Scheme 3), dapsone (**3**, Scheme 3) and tunicamycin (**4**, Scheme 3) as well as one antifungal drug (natamycin, **5**, Scheme 3) were selected to be tested in the MCF-7 breast cancer cell line.

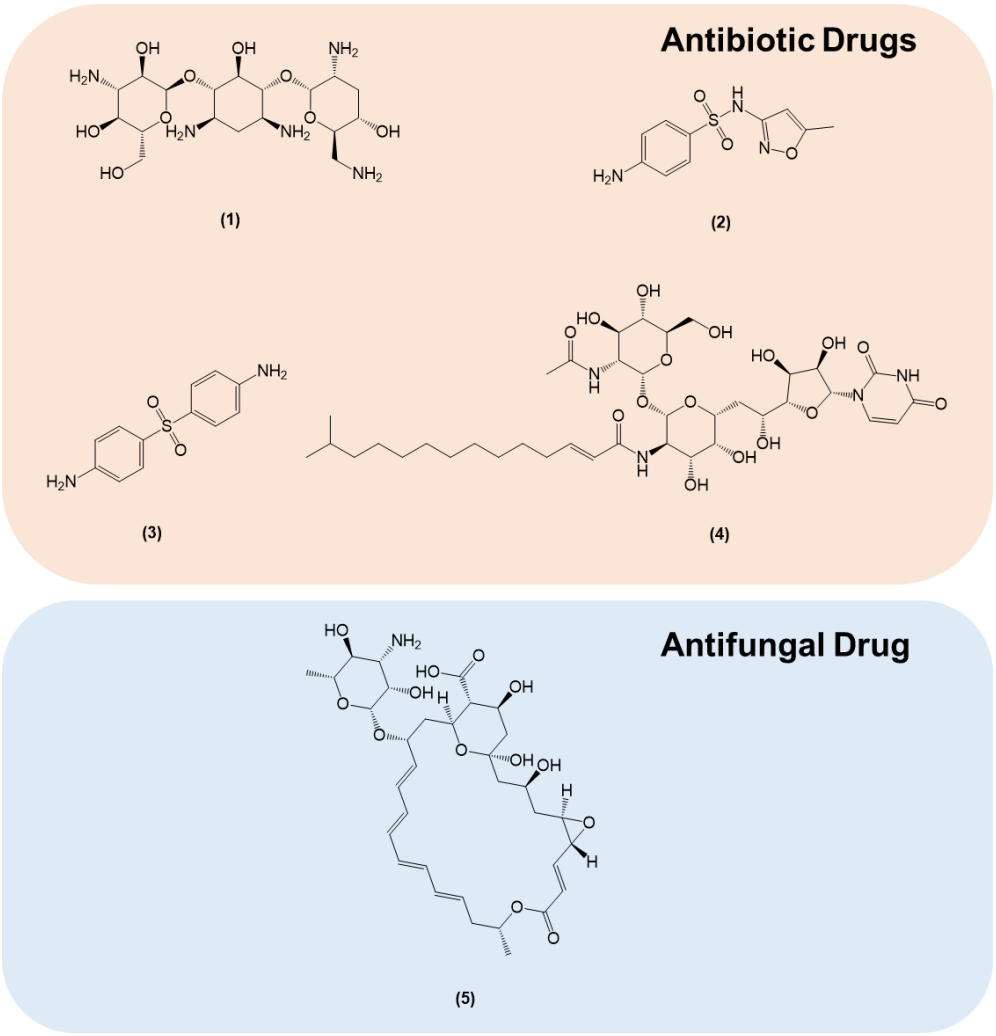

Scheme 3. Chemical structures of the antibiotic/antifungal drugs evaluated in MCF-7 cells. (**1**) Tobramycin, (**2**) Sulfamethoxazole, (**3**) Dapsone, (**4**) Tunicamycin, (**5**) Natamycin

Tobramycin (**1**, Scheme 3) is an antibiotic that belongs to the aminoglycosides, used for the management and treatment of systemic and ocular infections [208]. Its mechanism

of action involves the binding of the drug to the 16s ribosomal ribonucleic acid (RNA) of the bacterial 30s ribosomal unit, which leads to the inhibition of the initiation step of translation, which consequently results in incorrectly synthesized proteins and the disruption of the cell membrane [209]. To date, no reports have described anticancer properties for this antibiotic.

Sulfamethoxazole (**2**, Scheme 3) is a bacteriostatic sulfonamide antibiotic frequently used in combination with trimethoprim [210]. This combination is usually given for the treatment of a variety of bacterial infections, including those of the urinary, respiratory, and gastrointestinal tracts. Its mechanism of action is related to folic acid synthesis [210]. This drug has never been evaluated in cancer cells.

Dapsone (**3**, Scheme 3) is an antibiotic drug indicated for a variety of conditions, both dermatologic and non-dermatologic. The FDA-approved indications include leprosy and dermatitis herpetiformis [211]. It acts via inhibition of the folic acid pathway, by preventing bacteria from using para-aminobenzoic acid (PABA) for the synthesis of folic acid by competitively antagonizing PABA [212]. In a recent study, several dapsone derivatives demonstrated the ability to induce apoptotic cell death in Hep G2 and C6 human cancer cell lines [213].

Tunicamycin (**4**, Scheme 3) is a nucleoside antibiotic that acts as an inhibitor of glycosylation, impairing the protein folding machinery in eukaryotic cells and leading to the accumulation of unfolded proteins in the endoplasmic reticulum [214]. Several studies have demonstrated that tunicamycin exhibits anti-cancer potential [215–220].

Natamycin (**5**, Scheme 4) is an amphoteric macrolide antifungal antibiotic from *Streptomyces natalensis* or *S. chattanoogensis*, that is used for the treatment of a variety of fungal infections, mainly topically [221]. This drug is included in the WHO List of Essential Medicines. Its mechanism of action involves the binding of the drug to ergosterol in the plasma membrane, preventing ergosterol-dependent fusion of vacuoles, as well as membrane fusion and fission [222]. The anticancer potential of this drug has been already explored in prostate cancer [223] and hepatocellular carcinoma [224].

Despite the evidence of the anticancer potential of some drugs among this drug class, the results regarding the cytotoxic activity of tobramycin, sulfamethoxazole, dapsone, tunicamycin, and natamycin did not demonstrate promising anticancer profiles of these agents in MCF-7 breast cancer cells (Figure S5).

5.1.4 Repurposing of Other Drugs for Breast Cancer Therapy

Finally, the repurposing potential of two other drugs (piperazine and quinidine) was further evaluated in breast cancer cells. Piperazine (**1**, Scheme 4) is an anthelminthic especially useful in the treatment of partial intestinal obstruction caused by Ascaris worms, which is a condition primarily seen in children. Currently, there are several piperazine-based therapeutics, such as anti-depressants [225, 226], anti-viral [227, 228], anti-inflammatory [229, 230], and antioxidant agents [231, 232]. Additionally, several piperazine derivatives have also demonstrated significant anticancer activity on glioblastoma (U87) and cervix cancer (HeLa) cells [233].

Quinidine (**2**, Scheme 4) is one of the oldest known antiarrhythmics and is currently used in the management and treatment of specific arrhythmias and malaria [234]. Its mechanism of action involves the inhibition of the fast inward sodium current, depressing the phase 0 of the action potential hence dampening the excitability of cardiac muscles, which in turn prolongs the action potential and decreases automaticity [234]. As an antimalarial agent, this drug acts against the erythrocytic stage of the *Plasmodium* species [234]. To date, no studies have been done on the anticancer potential of this drug.

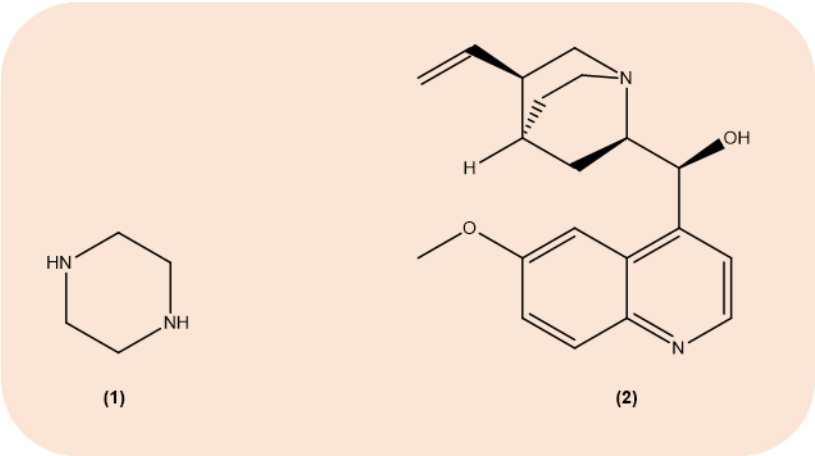

Scheme 4. Chemical structures of (**1**) piperazine and (**2**) quinidine.

The results regarding the cytotoxic activity of piperazine and quinidine demonstrated that both drugs do not induce significant cytotoxic effects against breast cancer cells (Figure S6).

5.2 Drug Repurposing in Colorectal Cancer

5.2.1 Repurposing of Antimalarial Drugs for Colorectal Cancer

Although the relationship between (familial) breast cancer and colorectal cancer is a controversial subject, recently, it was discovered that rare mutations in the *NTHL1* gene, which was originally associated with colorectal cancer, also cause breast cancer [235]. For this reason and to confirm if the previously tested drugs would maintain their anti-cancer activity in a different type of cancer, it was next selected some of the antimalarial drugs previously evaluated in MCF-7 cells and investigated their probable antitumor effects against the HT-29 colorectal cell line.

Based on the previous results, it was selected two quinolinic-related derivatives, mefloquine and chloroquine, and one non-quinolinic-related derivative, artesunate. Mefloquine was selected because this antimalarial drug demonstrated significant anticancer effects in MCF-7 cells, even at the lowest concentration tested (1 µM), which also resulted in this drug having the lowest IC_{50} value among all quinolinic-related derivatives. Artesunate was selected because it also presented the lowest IC_{50} among all tested non-quinolinic-related derivatives. Chloroquine was included due to the large literature data that indicate this drug can be a good candidate for drug repurposing in colorectal cancer.

HT-29 cells were treated with increasing concentrations of each drug, starting from 1 µM to 100 µM to evaluate cell viability after 48 h of treatment. Based on the MTT results, we found that mefloquine and artesunate displayed significant anti-tumor activity in HT-29 cells. All concentrations of the antimalarial drug mefloquine above 10 µM showed a strong effect on the cell viability of HT-29 cells, with more than 50% of the cells being not viable (Figure 15A). The dose-response curve resulted in a value of 11.49 µM for the IC_{50} (Figure 15B). Artesunate also demonstrated good efficacy against these cells at all concentrations above 10 µM (Figure 15C), with an IC_{50} value under 20 µM (Figure 15D). MTT assays for chloroquine demonstrated a lack of efficacy of this drug on the reduction of HT-29 cell viability for all concentrations under 25 µM, with an IC_{50} value above 20 µM (Figure S7). Table 11 summarizes the IC_{50} obtained for all antimalarial drugs tested in this cell line.

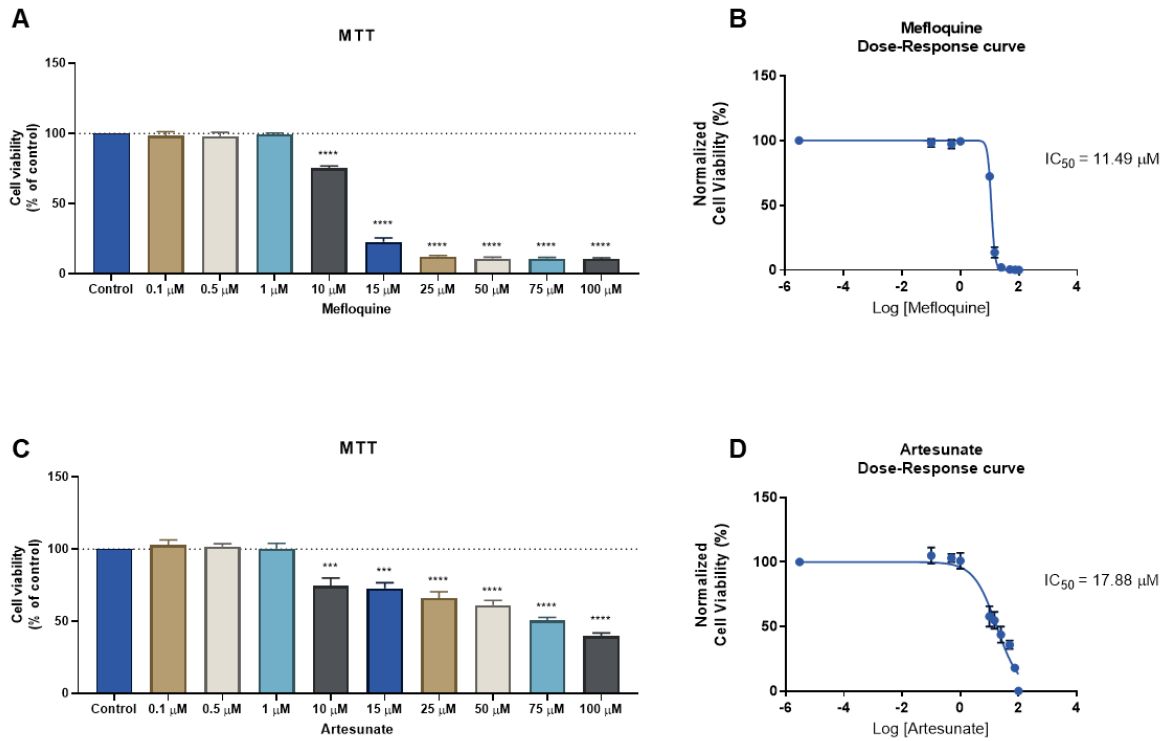

Figure 15. Effects of some antimalarial drugs on HT-29 cells. (**A**) Effect of mefloquine in cell viability and (**B**) dose-response curve. (**C**) Effect of artesunate in cell viability and (**D**) dose-response curve. Cells were cultured in the presence of increasing concentrations of each drug and after 48 h, the MTT assay was performed to measure cellular viability. Values are expressed in percentage of control and represent mean ± SEM. Each experiment was done three times independently (n = 3); *** statistically significant vs. control at $p < 0.001$. **** statistically significant vs. control at $p < 0.0001$.

Table 11. Cytotoxicity of all antimalarial agents evaluated in HT-29 colon cancer cells. IC_{50} values are given as mean.

Drug	IC_{50} (μM)
Chloroquine	32.13 ± 0.02
Mefloquine	11.49 ± 0.45
Artesunate	17.88 ± 0.05

These results also demonstrate that antimalarial drugs may also be used as antitumor agents in colorectal cancer, besides breast cancer. Nevertheless, comparing the IC_{50} values for both cell lines, it is possible to conclude that this class of drugs is more effective in breast cancer cells.

5.2.2 Repurposing of CNS drugs in Colorectal Cancer

Next, it was evaluated if CNS agents could also display significant anticancer activity against HT-29 colon cancer cells. To do so, the probable antitumor effect of different CNS drugs was investigated, namely the most promising ones previously tested in MCF-7 cells (benztropine, fluoxetine, sertraline, fluphenazine, latrepirdine and thioridazine (Scheme 2)) and some novel CNS drugs, namely carbamazepine, lamotrigine, *m*-chlorophenilbiguanide, selegiline, rivastigmine, entacapone, tolcapone, safinamide, carbidopa, scopolamine, nepicastat and bromocriptine (Scheme 5) in HT-29 colon cancer cells. Although edaravone, quetiapine, and perampanel did not demonstrate anticancer potential against breast cancer cells, these drugs were also included in this evaluation.

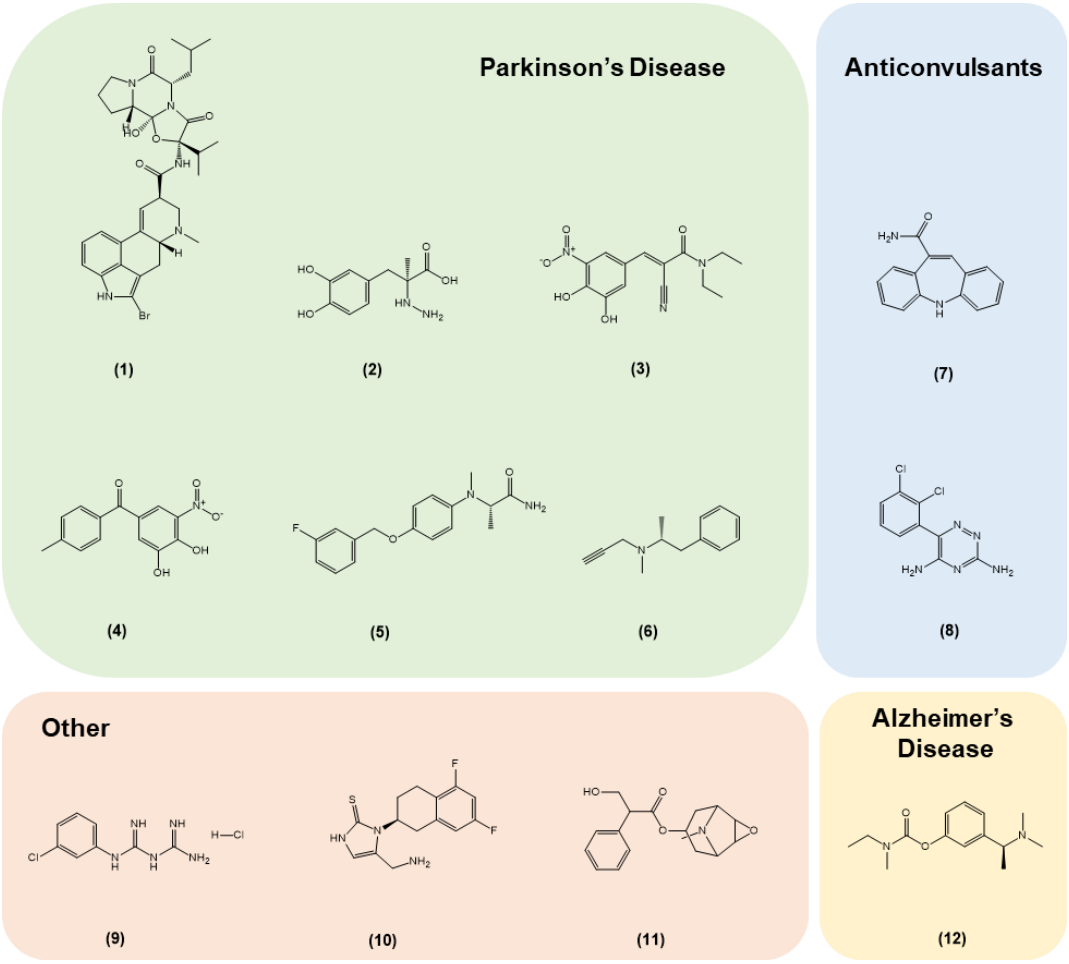

Scheme 5. Chemical structures of the CNS drugs evaluated in HT-29 colon cancer cells: (**1**) bromocriptine, (**2**) carbidopa, (**3**) entacapone, (**4**) tolcapone, (**5**) safinamide, (**6**) selegiline, (**7**) carbamazepine, (**8**) lamotrigine, (**9**) *m*-Chlorophenilbiguanide, (**10**) nepicastat, (**11**) scopolamine and (**12**) rivastigmine.

Bromocriptine (**1**, Scheme 5) is an agonist of dopaminergic D2 and D3 receptors in the brain, commonly used for the management and treatment of Parkinson's Disease [236]. The repurposing of this drug for cancer therapy has already been studied [237, 238].

Carbidopa (**2**, Scheme 5) is an inhibitor of the aromatic amino acid decarboxylase and the peripheral metabolism of levodopa. It is commonly administered in combination with levodopa for the treatment of Parkinson's Disease [239]. This drug has been demonstrated to suppress prostate cancer via aryl hydrocarbon receptor-mediated ubiquitination and degradation of androgen receptors [240] and to be a promising candidate for the therapy of pancreatic cancer [241].

Entacapone (**3**, Scheme 5) and tolcapone (**4**, Scheme 5) act as adjuvants to levodopa/carbidopa therapy and are reversible inhibitors of the catechol-O-methyltransferase (COMT) in peripheral tissues, altering the plasma pharmacokinetics of levodopa [242, 243]. Entacapone demonstrated the ability to enhance the antiproliferative activity of fruit-derived anthocyanins in different human cancer cell lines [244]. Tolcapone was also demonstrated to be cytotoxic to neuroblastoma cells through induction of oxidative stress, leading to apoptosis both *in vitro* and in animal models [245]. Moreover, entacapone and tolcapone combined with (-)-Epigallocatechin-3-gallate synergistically inhibited the growth of lung cancer cells in culture [246].

Safinamide (**5**, Scheme 5) is a reversible inhibitor of monoamine oxidase type B (MAO-B), blocks voltage-dependent Na^+ and Ca^{2+} channels, and inhibits glutamate release [247]. To our knowledge, this drug has no reports about its cytotoxic effects against cancer cells.

Selegiline (**6**, Scheme 5) is an irreversible inhibitor of MAO-B. It binds to MAO-B and blocks the microsomal metabolism of dopamine, enhancing the dopaminergic activity in the substantial nigra. It can also inhibit monoamine oxidase type A (MAO-A) [248]. Selegiline was also found to exert cytotoxicity towards acute myeloid leukemia through inhibition of mitochondrial respiration [249].

Carbamazepine (**7**, Scheme 5) inhibits sodium channel firing, treating seizure activity. In bipolar disorder, carbamazepine is thought to increase dopamine turnover and increase GABA transmission [250]. In SW480 colon cancer cell lines, carbamazepine treatment caused a decrease in β-Catenin and VEGF levels [251]. Moreover, in ER-positive breast cancer cell lines, this drug has shown significant anti-proliferation effects due to the enhancement of proteosome-mediated degradation of ERα and Cyclin D1 [252]. Carbamazepine was also found to promote HER-2 protein degradation in breast cancer

cells by modulating histone deacetylase 6 (HDAC6) activity and acetylation of heat shock protein 90 (Hsp90) [253].

Lamotrigine (**8**, Scheme 5) is used to treat the following partial seizures, primary generalized tonic-clonic seizures, bipolar I disorder maintenance, and Lennox-Gastaut syndrome. It binds selectively and inhibits voltage-gated sodium channels, stabilizing presynaptic neuronal membranes and inhibiting presynaptic glutamate and aspartate release [254]. No reports of lamotrigine in cancer cells have been found.

m-chlorophenilbiguanide (**9**, Scheme 5) is an allosteric agonist and modulator of the 5-HT_3 receptor and an antagonist of the α_{2A}-adrenergic receptor [255, 256]. Several biguanide derivatives have been studied for cancer therapy [257–259].

Nepicastat (**10**, Scheme 5) is an inhibitor of dopamine β-hydroxylase, an enzyme that catalyzes the conversion of dopamine to norepinephrine [260]. It has been studied as a possible treatment for congestive heart failure. In 2012, clinical trials to assess nepicastat as a treatment for post-traumatic stress disorder and cocaine dependence have been completed [261, 262]. Nevertheless, this drug has never been studies against cancer cells.

Scopolamine (**11**, Scheme 5) is a non-selective competitive inhibitor of G-protein-coupled muscarinic receptors, with anticholinergic action [263]. No reports are described regarding the anticancer effects of scopolamine.

Rivastigmine (**12**, Scheme 5) binds reversibly with and inactivates cholinesterase (e.g., acetylcholinesterase and butyrylcholinesterase), preventing the hydrolysis of acetylcholine, and thus, leading to an increased concentration of acetylcholine at cholinergic synapses [264]. To our knowledge, rivastigmine has no reports about its cytotoxic effects against cancer cells.

Based on the MTT results, it was found that latrepirdine, fluphenazine, fluoxetine, benztropine, thioridazine, and sertraline displayed significant anti-tumor activity in HT-29 cells. Cytotoxic effects of latrepirdine (Figure 16A) were significant even in concentrations of 1 µM, with 7.75 µM causing a reduction of more than 50% of the cells (Figure 16B). Fluphenazine's anti-tumor effect was the strongest among all tested drugs and concentrations above 10 µM killed almost all cells (Figure 16C). Indeed, the IC_{50} obtained for fluphenazine was the lowest and it was less than 2 µM (Figure 16D). The MTT assay for fluoxetine treatment demonstrated a strong cytotoxic effect of this CNS drug in HT-29 cells for all concentrations tested above 10 µM (Figure 16E). The dose-response curve for fluoxetine revealed an IC_{50} value of 6.12 µM (Figure 16F). Benztropine showed significant

anti-tumor effects in concentrations above 10 µM (Figure 16G) and the IC_{50} value obtained was 18.23 µM (Figure 16H).

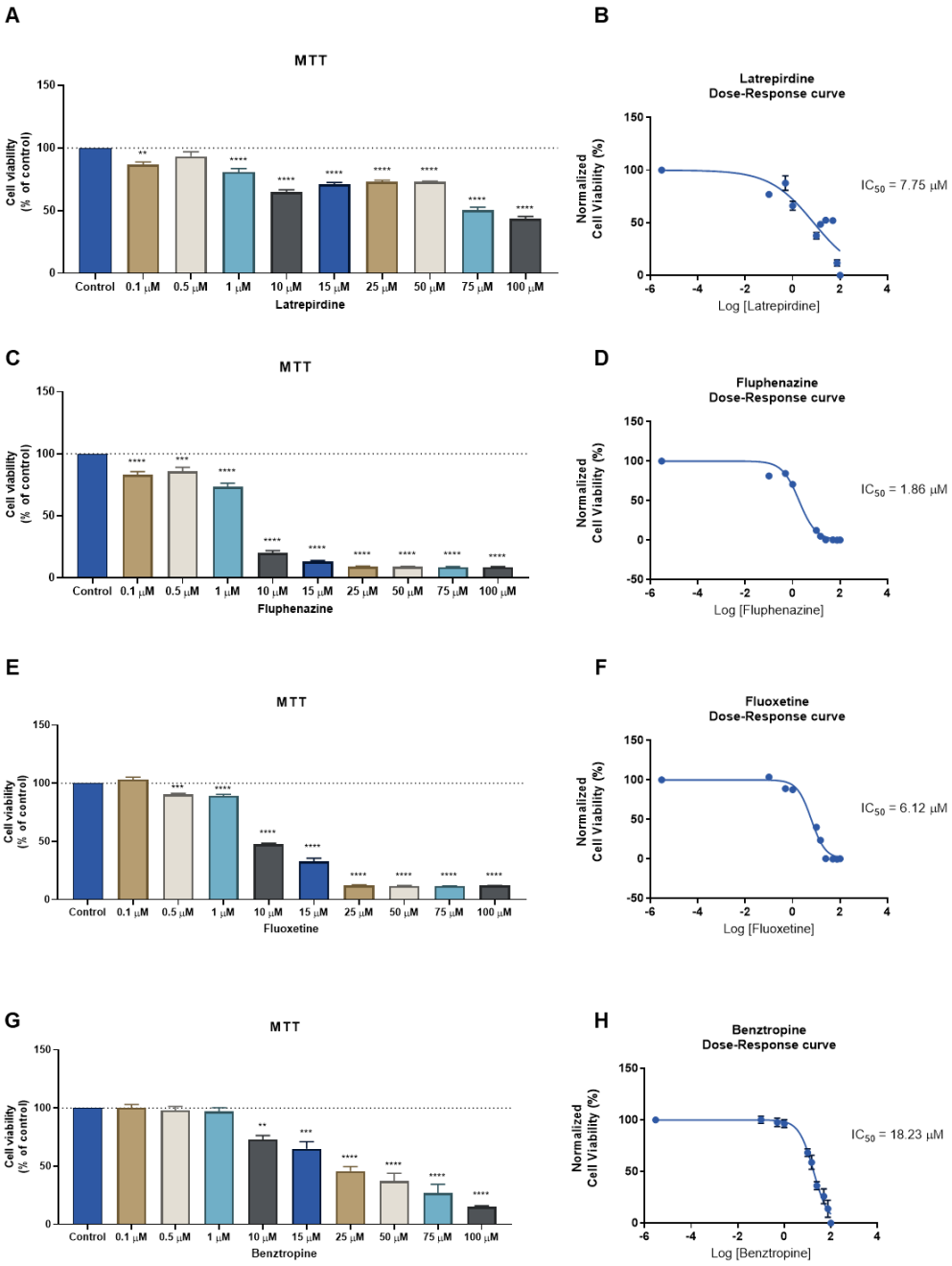

Figure 16. The effects of some CNS drugs on HT-29 cells. (**A**) The effect of latrepirdine on cell viability and (**B**) the dose-response curve. (**C**) The effect of fluphenazine on cell viability and (**D**) the dose-response curve. (**E**) The effect of fluoxetine on cell viability and (**F**) the dose-response curve. (**G**) The effect of benztropine on cell viability and (**H**) the dose-response curve. Cells were cultured in the presence of increasing concentrations of each drug, and after 48 h, the MTT assay was performed to measure the cellular viability. Values are expressed in percentage of control and represent mean ± SEM. Each experiment was done three times independently (*n* = 3); ** statistically significant vs. control at $p < 0.01$. *** statistically significant vs. control at $p < 0.001$. **** statistically significant vs. control at $p < 0.0001$.

Thioridazine treatment also significantly decreased HT-29 cell viability, from 1 µM to 100 µM, with more pronounced cytotoxic effects for all concentrations above 5 µM (Figure 17A) and an IC_{50} value of 4.26 µM (Figure 17B). Treatment with sertraline at doses above 1 µM for 48 h had a strong effect on the cell viability (Figure 17C), resulting in an IC_{50} value of less than 3 µM (Figure 17D).

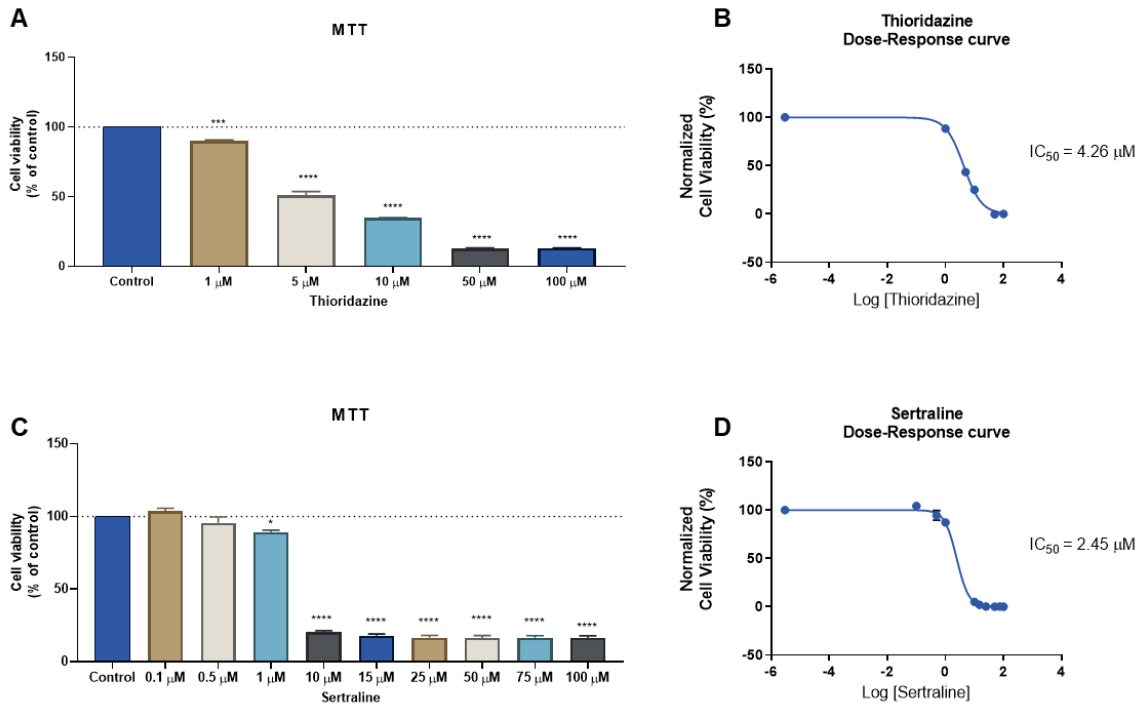

Figure 17. The effects of some CNS drugs on HT-29 cells. (**A**) The effect of thioridazine on cell viability and (**B**) the dose-response curve. (**C**) The effect of sertraline on cell viability and (**D**) the dose-response curve. Cells were cultured in the presence of increasing concentrations of each drug, and after 48 h, the MTT assay was performed to measure the cellular viability. Values are expressed in percentage of control and represent mean ± SEM. Each experiment was done three times independently (n = 3); * statistically significant vs. control at p < 0.05. *** statistically significant vs. control at p < 0.001. **** statistically significant vs. control at p < 0.0001.

Interestingly, and contrary to MCF-7 cells, quetiapine demonstrated the ability to induce a reduction in the viability of HT-29 colorectal cancer cells in a concentration-dependent manner (Figure 18A), with an IC_{50} value of 15.19 µM (Figure 18B).

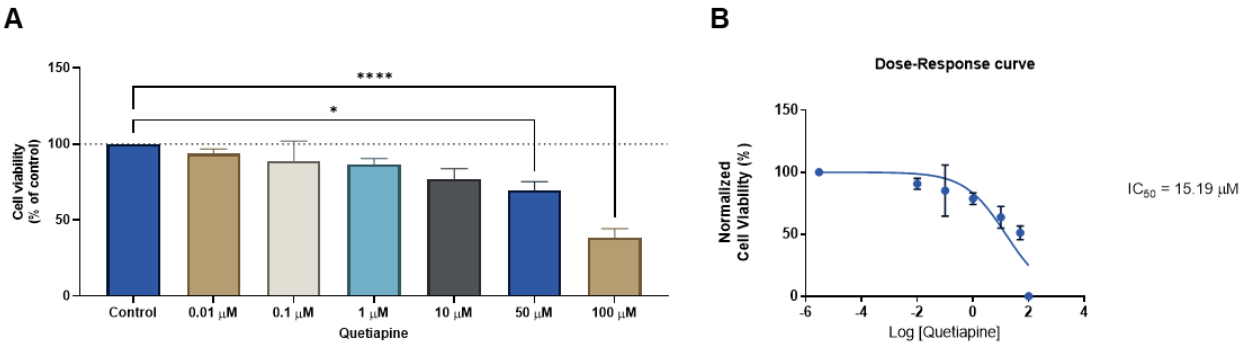

Figure 18. The effects of another CNS drug on HT-29 cells. (**A**) The effect of quetiapine on cell viability and (**B**) the dose-response curve. Cells were cultured in the presence of increasing concentrations of each drug, and after 48 h, the MTT assay was performed to measure the cellular viability. Values are expressed in percentage of control and represent mean ± SEM. Each experiment was done three times independently (n = 3); * statistically significant vs. control at $p < 0.05$. **** statistically significant vs. control at $p < 0.0001$.

MTT assays for other CNS drugs (bromocriptine, carbamazepine, carbidopa, entacapone, tolcapone, lamotrigine, *m*-chlorophenilbiguanide, nepicastat, perampanel, rivastigmine, safinamide, scopolamine, selegiline and edaravone) demonstrated a lack of efficacy of these drugs on the reduction of HT-29 cell viability or IC_{50} values above 20 μM (Figures S8 and S9). Table 12 summarizes the IC_{50} obtained for all CNS drugs tested in this cell line.

Table 12. Cytotoxicity of all CNS drugs tested in HT-29 colon cancer cells. IC_{50} values are given as mean.

Drug	IC_{50} (μM)
Selegiline	>100
Entacapone	40.89 ± 0.05
Tolcapone	35.47 ± 0.07
Latrepirdine	7.75 ± 0.14
Fluphenazine	1.86 ± 0.05
Safinamide	>100
Fluoxetine	6.12 ± 0.05
Benztropine	18.23 ± 0.03

Thioridazine	4.26 ± 0.02
Carbidopa	>75
Bromocriptine	>100
Nepicastat	61.24 ± 0.04
Scopolamine	>100
Carbamazepine	>100
Sertraline	2.45 ± 0.03
Rivastigmine	>100
m-Chlorophenilbiguanide	>100
Edaravone	> 50
Quetiapine	15.19 ± 0.20
Perampanel	>100
Lamotrigine	>100

These results demonstrate that some CNS agents, such as latrepirdine, fluphenazine, fluoxetine, benztropine, thioridazine, sertraline, and quetiapine can be good candidates as standalone agents for therapeutical use in colorectal cancer. Table 13 shows a comparison between the IC_{50} obtained for these drugs in both cell lines (MCF-7 and HT-29).

Table 13. Comparison between the IC_{50} of several CNS drugs in HT-29 and MCF-7 cancer cells. IC_{50} values are given as mean.

Drug	HT-29 IC_{50} (μM)	MCF-7 IC_{50} (μM)
Fluphenazine	1.86	2.68
Fluoxetine	6.12	7.78
Benztropine	18.23	21.71
Thioridazine	4.26	5.72
Sertraline	2.45	2.22
Latrepirdine	7.75	75.37
Quetiapine	15.19	> 100

Comparing these results, it is possible to verify that all IC_{50} values, except for sertraline, obtained for MCF-7 breast cancer cells are higher than the ones obtained for HT-29 colon cancer cells, demonstrating that this class of drugs has higher cytotoxic potential in colorectal cancer cells than in breast cancer cells.

5.2.3 Repurposing of Antibiotic/Antifungal Drugs for Colorectal Cancer Therapy

Although antibiotic and antifungal drugs have not demonstrated promising anticancer effects against breast cancer, it was still hypothesized that these classes of drugs could be effective against colorectal cancer cells. Therefore, the cytotoxic effect of three antibiotic drugs: amikacin (**1**, Scheme 6), gentamicin (*2*, Scheme 6), vancomycin (**3**, Scheme 6), and one antifungal drug: clotrimazole (**4**, Scheme 6) was further evaluated in the HT-29 colorectal cancer cell line.

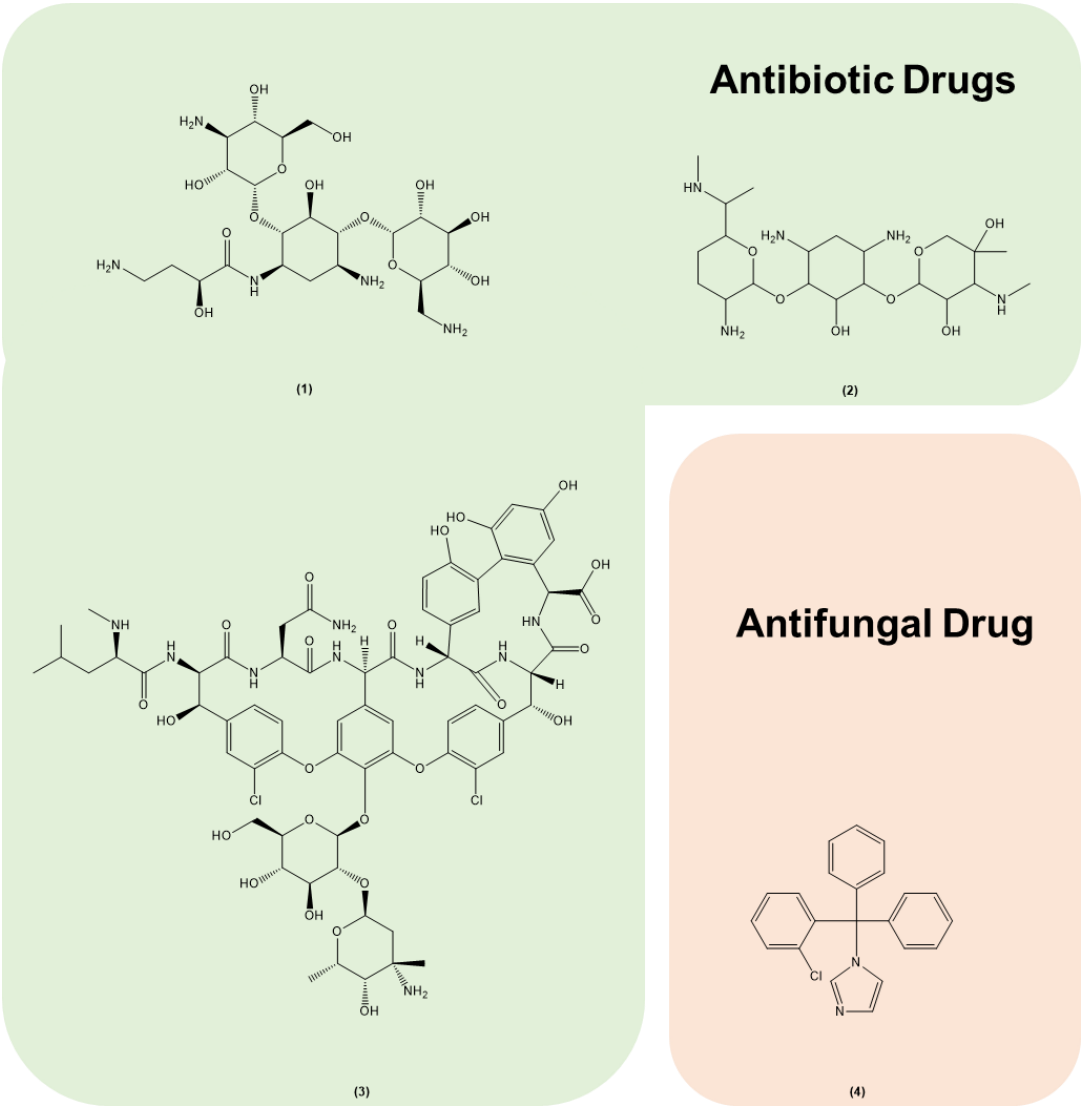

Scheme 6. Chemical structures of the CNS drugs evaluated in HT-29 colon cancer cells: (**1**) amikacin, (**2**) gentamicin, (**3**) vancomycin, and (**4**) clotrimazole.

Amikacin (**1**, Scheme 6) is an antimicrobial drug with activity against resistant gram-negative bacilli such as *Acinetobacter baumanii* and *Pseudomonas aeruginosa* [265]. It also has excellent activity against most aerobic gram-negative bacilli from the *Enterobacteriaceae* family, including *Nocardia sp.* and some *Mycobacterium spp* [265]. A recent study demonstrated that amikacin suppresses human breast cancer cell MDA-MB-231 migration and invasion [266].

Gentamicin (**2**, Scheme 6) is an aminoglycoside antibiotic that exhibits bactericidal activity against aerobic gram-negative bacteria and is used to treat several common infections [267]. This drug targets acid sphingomyelinase in human gastric cancer NCI-N87 cells [268] and has demonstrated the ability to arrest cancer cell growth on non-Hodgkin's T-cell human lymphoblastic lymphoma (SUP-T1) [269].

Vancomycin (**3**, Scheme 6) is a tricyclic glycopeptide antibiotic originally derived from the organism *Streptococcus orientalis* and used to treat and prevent various bacterial infections caused by gram-positive bacteria [270]. In a recent study, vancomycin treatment increased the efficacy of radiotherapy in animal models [271].

Clotrimazole (**4**, Scheme 6) is a synthetic imidazole with a broad spectrum of antimycotic activity, commonly used for the treatment of oral candidiasis, vaginal candidiasis, and dermatomycoses [272]. Additionally, clotrimazole has also been reported to have antitumor activity with minimal effect on normal cells [273].

Similar to the previous findings in MCF-7 cells, antibiotic treatment in the HT-29 colorectal cancer cell line demonstrated this class of drugs is not able to induce cytotoxicity in these cancer cells (Figure S10). However, clotrimazole treatment resulted in a strong reduction in the number of viable cells, with a significative decrease in HT-29 cell viability at concentrations above 10 µM (Figure 19A), with an IC_{50} value of 21.64 µM (Figure 19B).

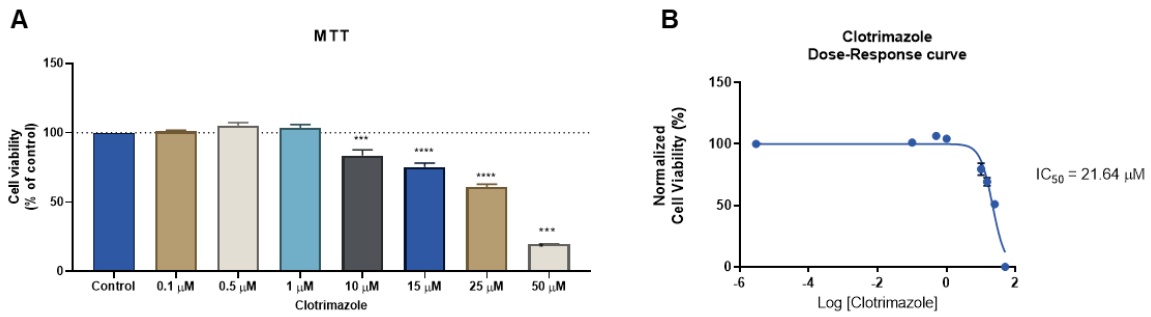

Figure 19. The cytotoxic effects of clotrimazole on HT-29 cells. (**A**) The effect of clotrimazole on cell viability and (**B**) the dose-response curve. Cells were cultured in the presence of increasing concentrations of each drug,

and after 48 h, the MTT assay was performed to measure the cellular viability. Values are expressed in percentage of control and represent mean ± SEM. Each experiment was done three times independently (n = 3); *** statistically significant vs. control at $p < 0.001$. **** statistically significant vs. control at $p < 0.0001$.

These results demonstrate that the repurposing of clotrimazole is plausible and that this drug can represent a promising candidate for colorectal cancer therapy.

5.2.4 Repurposing of Other Drugs for Colorectal Cancer Therapy

In the last set of experiments using repurposed drugs, diverse drugs that were not included in the previously described drug classes were selected and their possible anticancer effect was evaluated on HT-29 colorectal cancer cells. The following drugs were tested: acamprosate (**1**, Scheme 7), amiodarone (**2**, Scheme 7), atenolol (**3**, Scheme 7), metoprolol (**4**, Scheme 7), furosemide (**5**, Scheme 7), glibenclamide (**6**, Scheme 7), atorvastatin (**7**, Scheme 7) and telmisartan (**8**, Scheme 7).

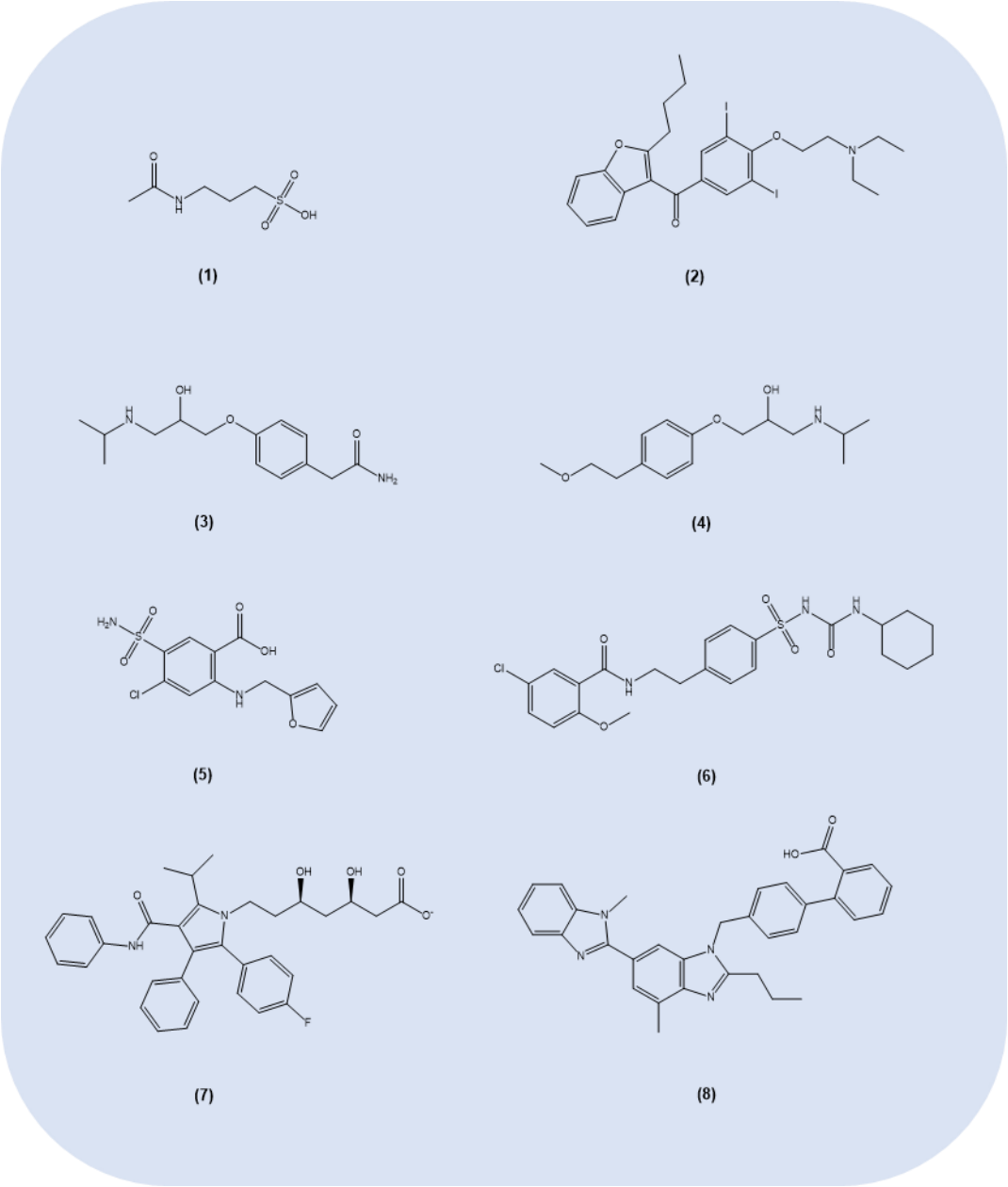

Scheme 7. Chemical structures of (**1**) Acamprosate, (**2**) amiodarone, (**3**) atenolol, (**4**) metoprolol, (**5**) furosemide, (**6**) glibenclamide, (**7**) atorvastatin and (8) telmisartan.

Acamprosate (**1**, Scheme 7) is a recent developed medication for the treatment of alcohol dependence [274]. Acamprosate is the third medication, after disulfiram and naltrexone, to receive FDA approval for post-withdrawal maintenance of alcohol abstinence. Acamprosate helps modulate and normalize brain activity, particularly in the glutamate and GABA neurotransmitter systems [274]. Although acamprosate's mechanism of action has not been clearly established, it may work by reducing symptoms of post-acute (protracted) withdrawal, such as insomnia, anxiety, and restlessness [274]. No studies of acamprosate in cancer cells have already been performed.

Amiodarone (**2**, Scheme 7) is one of the most commonly used anti-arrhythmic drugs. This drug works primarily by blocking potassium rectifier currents responsible for the repolarization of the heart during phase 3 of the cardiac action potential [275]. This potassium channel-blocking effect results in increased action potential duration and a prolonged effective refractory period in cardiac myocytes. Myocyte excitability is decreased, preventing reentry mechanisms and ectopic foci from perpetuating tachyarrhythmias [275]. Moreover, amiodarone also blocks beta-adrenergic receptors (e.g., beta-1), calcium channels, and sodium channels [275]. Pre-clinical studies suggest that amiodarone induces cytotoxicity in several types of cancer cells [276–279], thus making it a potential candidate for use as an anti-cancer treatment.

Atenolol (**3**, Scheme 7) and metoprolol (**4**, Scheme 7) are beta-1-selective adrenergic antagonists that reduce heart rate, blood pressure, and myocardial contractility [280, 281]. These drugs are FDA-approved and indicated for the treatment of hypertension, angina pectoris, and acute myocardial infarction [280, 281]. The use of antihypertensive drugs as coadjuvant therapy in cancer has already been explored [282, 283].

Furosemide (**5**, Scheme 7) is a widely used diuretic drug that has been approved for the treatment of conditions with volume overload and edema secondary to congestive heart failure exacerbation, liver failure, or renal failure, including the nephrotic syndrome [284]. Its mechanism of action involves the inhibition of tubular reabsorption of sodium and chloride in the proximal and distal tubules and the thick ascending loop of Henle by inhibiting the sodium-chloride cotransport system resulting in excessive excretion of water along with sodium, chloride, magnesium, and calcium [285]. This drug has shown the ability to diminish the proliferation of poorly differentiated human gastric cancer cells by affecting G0/G1 state [286] and to reverse multidrug resistance status in bladder cancer cells *in vitro* [287].

Glibenclamide (**6**, Scheme 7) is a second-generation sulfonylurea approved by the FDA for the treatment of type 2 diabetes mellitus [288]. This drug exerts its mechanism of action by increasing insulin secretion from beta cells in the pancreas [289]. Glibenclamide

has also been reported to inhibit cell growth and invasion in several cancer cell lines, including gastric, breast, ovarian, liver, prostate, and bladder cancer [290–293].

Atorvastatin (**7**, Scheme 7) is an 3-hydroxy-3-methylglutaryl-coenzyme A (HMG-CoA) reductase inhibitor (statin), a lipid-lowering medication used in the primary and secondary prevention of coronary heart disease [294]. Multiple lines of evidence indicate that certain cancers depend on the mevalonate pathway for growth and survival, and, therefore, are vulnerable to statin therapy [295].

Telmisartan (**8**, Scheme 7) is a nonpeptide angiotensin II receptor antagonist which selectively inhibits the angiotensin II AT1 receptor subtype without affecting other receptor systems involved in cardiovascular regulation, used for the treatment of hypertension [296]. This drug has demonstrated significative potential in the suppression of the proliferation of different cancer cells, both *in vitro* and in vivo [297–299].

Despite the promising anticancer profiles of the previously mentioned drugs, the only agent that presented significative effects on the reduction of HT-29 cell viability was amiodarone, with a strong cytotoxic effect at concentrations above 10 µM (Figure 20A), and an IC_{50} value of 7.297 µM (Figure 20B). Other evaluated drugs did not demonstrate anticancer potential in this cell line (Figure S11).

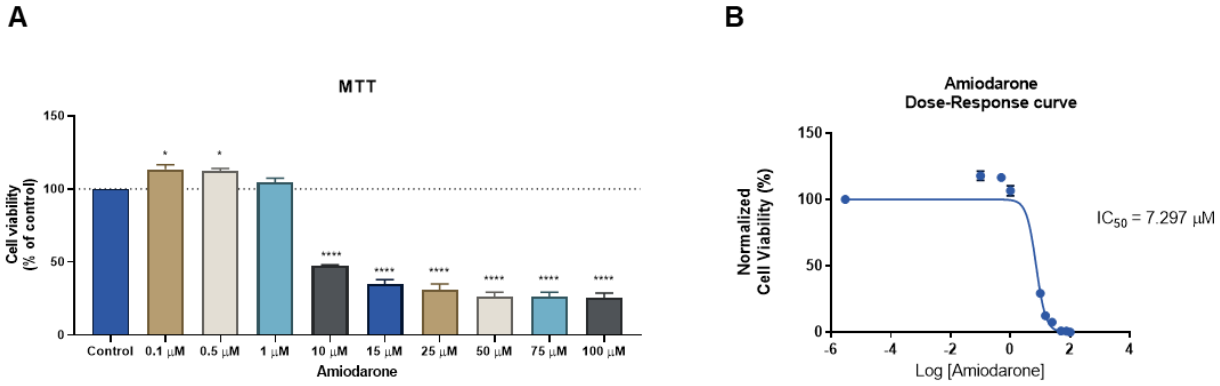

Figure 20. The cytotoxic effects of amiodarone on HT-29 cells. (**A**) The effect of amiodarone on cell viability and (**B**) the dose-response curve. Cells were cultured in the presence of increasing concentrations of each drug, and after 48 h, the MTT assay was performed to measure the cellular viability. Values are expressed in percentage of control and represent mean ± SEM. Each experiment was done three times independently (n = 3); * statistically significant vs. control at $p < 0.05$. **** statistically significant vs. control at $p < 0.0001$.

6. CONCLUSION OF CHAPTER I

Even though current protocols for breast and colorectal cancer treatments are quite effective, current strategies reside in the dose-limiting toxicity of the antineoplastic drugs that are used as adjuvant therapy [300]. Despite the good results of chemotherapeutic drugs in breast and colorectal cancer chemotherapy, side effects such as cardiotoxicity and acquired drug resistance are still major problems and limit the application of these treatments in cancer patients. To overcome these problems, higher doses and long-term use of antineoplastic drugs are necessary, which increases their side effects.

Drug repurposing has been gaining attention among the scientific community, as a faster and cheaper strategy to identify new potential anti-cancer therapies, compared to the de novo drug development. Repurposed drugs are already available on the market and have pharmacokinetics, pharmacodynamics, and toxicological profiles that are well established, which facilitates their approval for novel indications.

In this work, our research group aimed to find novel repurposed drugs for breast and colorectal cancer therapy. Therefore, several drugs belonging to different drug classes were screened and antimalarial and CNS agents were found to be the most promising drug classes against HT-29 and MCF-7 cancer cell lines.

These results demonstrated that several antimalarial drugs have the ability to decrease cell viability as standalone agents in a concentration-dependent manner in both cell lines tested in this work. In MCF-7 breast cancer cells, mefloquine, tafenoquine, pyronaridine, and artesunate demonstrated elevated cytotoxicity, with IC_{50} values under 20 µM. Regarding HT-29 cells, the antimalarial drugs mefloquine and artesunate successfully reduced the number of viable cells, with IC_{50} values also below 20 µM.

Moreover, MCF-7 treatment with the CNS drugs fluphenazine, fluoxetine, sertraline, benztropine, and thioridazine also caused significant toxicity at all concentrations above 10 µM. The same drugs were equally effective against HT-29 colon cancer cells. Additionally, in this cell line, the antifungal drug clotrimazole and the antiarrhythmic drug amiodarone were also able to induce a concentration-dependent reduction of cell viability.

Taken together, these results demonstrate the anticancer potential of antimalarials, CNS drugs, and other therapeutic agents against two different cell lines representative of breast and colorectal cancer. Therefore, we propose the repurposing of these drugs as a promising approach to treating breast and colorectal cancers. Since these drugs are already clinically available, their use in clinical practice for anti-cancer therapy is feasible and

facilitated. Moreover, the anticancer profile of these drugs may also contribute to enhance the effects of chemotherapy when used in combined treatments.

CHAPTER II

DEVELOPMENT OF NOVEL COMBINATION MODELS FOR BREAST AND COLORECTAL CANCER THERAPY

1. SUMMARY OF CHAPTER II

Drug combination, as well as drug repurposing, is an alternative strategy to the development of new drugs that consists on the administration of cocktails of two or more drugs, aiming to enhance the efficacy of treatments. In this way, after finding repurposed drugs with promising anticancer potential in Chapter I, our research group explored several new combination models for breast and colorectal cancer combat.

Here, several combination models for cancer combat were explored: (I) combination models combining conventional antineoplastics and repurposed drugs; (II) combination models combining only repurposed drugs; (III) combination models combining peptides and chemotherapy and (IV) combination models combining peptides and repurposed drugs.

In combination model I, it was evaluated the combination of chemotherapeutic drugs with several repurposed drugs (antimalarial and CNS agents) against MCF-7 breast and HT-29 colorectal cancer cells. Different schedules of administration were also tested on HT-29 colorectal cancer cells. The results in MCF-7 cells demonstrate that all antimalarial drugs have a higher ability than the antineoplastic drugs DOX and PTX to decrease cell viability at concentrations of IC_{50} and lower than their IC_{50}. Moreover, the combinations of DOX + pyronaridine, DOX + chloroquine, DOX + artesunate, PTX + chloroquine, and PTX + artesunate demonstrated promising anticancer profiles, with combined effects being stronger than each drug alone. Regarding the combination with CNS drugs, we found that combinations of DOX + fluoxetine, DOX + thioridazine, DOX + benztropine, DOX+ quetiapine, PTX + fluoxetine, and PTX + thioridazine induced a significant decrease in cell viability compared to the treatments with each drug alone. In HT-29 cancer cells, the simultaneous combination of antimalarial drugs with 5-FU did not demonstrate improvements compared to single treatments; however, we found that the administration of the antimalarial artesunate prior to 5-FU produced better results in reducing HT-29 cell viability than the inverse drug schedule or the simultaneous combination. Regarding CNS drugs, the results demonstrated that fluphenazine, fluoxetine, and benztropine have enhanced anticancer activity when used alone as compared to being used in combination, making them ideal candidates for drug repurposing in colorectal cancer. The combination of 5-FU + edaravone and 5-FU + quetiapine demonstrated significant anticancer effects when compared with each drug alone. These results demonstrate that some antimalarial drugs may be promising chemosensitizing compounds and that their use in combination can improve the anti-cancer activity of chemotherapeutic drugs, especially in breast cancer cells. Moreover, it was found that CNS drugs activity differs between the two selected cell lines, both alone and in combination.

In combination model II, the effect of treating both cell lines with a combination of two antimalarials (pyronaridine and mefloquine) or with a combination of two CNS drugs (sertraline and fluphenazine) was studied. In MCF-7 cells, it was not found any promising drug combinations for breast cancer therapy. However, in HT-29 cells the combination of sertraline at a fixed concentration with increasing concentrations of fluphenazine induced a significant reduction in the viability of this cell line, in comparison with both drugs alone, demonstrating the anticancer potential of these repurposed drugs to be used in combination regimens for colorectal cancer therapy.

In combination model III, it was evaluated if the combination of peptides with chemotherapeutic agents would result in enhanced anticancer effects. Melittin, a peptide that composes honeybee venom, was combined with DOX in MCF-7 cells and with 5-FU in HT-29 cells. The results demonstrated that honeybee venom is active against HT-29 colon and MCF-7 breast cancer cells, having better anti-tumor activity in MCF-7 cells. The combination of honeybee venom + DOX did not result in significant improvements compared to DOX and bee venom alone. On the other hand, the combination of honeybee venom with 5-FU in HT-29 cells resulted in enhanced cytotoxic effects than single treatments. These results support that the combination of honeybee venom with 5-FU can help improve the anti-cancer activity of the treatments in colorectal cancer therapy. The combination of a cell-penetrating peptide (CPP2) and its derivatives with 5-FU was also studied in HT-29 cells. The results demonstrate that BTZCA–CPP2 and BTZ5CA–CPP2 are the most promising CPP2 conjugates for decreasing the viability of HT-29 cells, with enhanced anticancer activity compared to 5-FU. However, these results suggest that the combination with 5-FU is not advantageous over the single treatment with CPP2–thiazole derivatives.

In combination model IV, we tested the combination of the aforementioned peptides with repurposed drugs. Specifically, the combination of Melittin was studied in combination with different CNS drugs (thioridazine, sertraline, fluoxetine, and fluphenazine) in both cell lines. The combination of MCF-7 cells with CNS drugs plus honeybee venom resulted in better anti-cancer efficacies than with DOX, notably for lower concentrations. In HT-29 cancer cells, the combination of honeybee venom with the repurposed drugs fluoxetine, sertraline, and thioridazine resulted in a significant reduction in the viability of HT-29 colon cancer cells compared to each drug alone, demonstrating that bee venom can help improve the anti-cancer activity of CNS drugs in colon cancer cells. The combination of CPP2 and its derivatives with clotrimazole was also studied in HT-29 cells. Nonetheless, these

combinations had not demonstrated promising results compared to the use of clotrimazole alone.

2. INTRODUCTION OF CHAPTER II

In cancer therapy, chemotherapy plays an important role. Regardless of all the efforts that have been made, and despite the increasing investment in this area, the response rate to chemotherapy is still greatly reduced and the unwanted side effects remain elevated. Therefore, it is urgent to adopt new strategies that allow greater effectiveness and selectivity of the treatments of patients.

Drug combination is an alternative strategy to the development of new drugs and has already been explored for the discovery of new treatment regimens for oncotherapy. This strategy is advantageous over the *de novo* drug development, representing a low-cost, rapid, and easy-to-apply alternative. The combination of antineoplastic agents is already being applied in cancer therapy, but the combination of repurposed drugs is still under-explored in pre- and clinical development. In this section, it will be provided an introduction to the drug combination approach, with evidence of the successful use of this strategy coupled to drug repurposing, exemplified with cases of application both in *in vitro* and *in vivo* studies, to further support the studies developed in this chapter.

2.1 Drug Combination

Drug combination is a strategy that consists of the administration of cocktails of two or more drugs [301]. The concept of drug combination was first proposed in 1965 by Emil Frei, James F. Holland, and Emil J. Freirich when they were trying to discover new therapies for the treatment of acute leukemia [302]. In oncology, this methodology is particularly useful because it allows to overcome intratumoral and intertumoral heterogeneity. With the evolution of the tumor, populations of cells resistant to the therapy can be formed leading to the appearance of intra-tumor heterogenicity [45]. This heterogenicity causes the therapy to fail in some types of cells within the tumor, which can survive and lead to cancer proliferation, acquiring different characteristics from the initial ones [303]. Thus, a drug that initially played a role in a metabolic pathway may fail to do so because of the cells' adaptation to therapy (i.e., acquirement of drug resistance) [46, 304, 305]. Therefore, strategies that allow to act simultaneously on multiple routes, such as the drug combination, lead to an increase in the effectiveness of the treatment. The intertumoral heterogeneity corresponds to the heterogeneity between patients with the same type of cancer which makes it difficult to predict the response of different patients to the same therapy [306].

Combination therapies may help to overcome the aforementioned problems and, indeed, several studies have demonstrated that they are more effective than monotherapy

[12, 55, 307–310]. The efficacy of the drug combination may depend on the schedule of administration (e.g., simultaneous or sequential) and on the design of the combination models [311, 312], to make the most of the interaction between the drugs. Pharmacologically, a combination of two or more drugs will be more effective the greater the synergism between the drugs, i.e., the greater the potentiation of its effectiveness compared to the two drugs alone [313]. Additionally, an ideal drug combination should allow to minimize the required therapeutic dose (and consequently its toxicity) while increasing the effectiveness of the treatment [314]. It is common to choose a concentration of the drugs around their IC_{50}, in an acceptable concentration range [315]. Some works still vary the time of the treatment and others vary the order of administration of the drugs [312]. This allows to study all the variables that can influence the effect of a treatment in which combinatorial therapy is employed.

Although combination therapies using repurposed drugs are more easily accepted by the FDA, since the drugs are already approved for this or other pathologies, the FDA also requires pre-clinical studies both *in vitro* and *in vivo* [316]. It is important to remember that the transition from *in vitro* studies to clinical practice is not always easy and does not always work, even in the cases of promising *in vitro* results. Also, in the case of the appearance of adverse reactions, it is not always possible to conclude its origin. Furthermore, advances in bioinformatics allow to evaluate, *in silico*, drugs that may be good candidates for a given treatment and, although they also require some experimentation, are tools that save time and resources to laboratories, being considerably faster than the traditional discovery of new drugs. Moreover, the passage to *in vivo* studies does not always run as expected given the number of factors to be taken into account when adopting this strategy: it is necessary to find the ratio between the two drugs that guarantees their best effect, the contact time as well as the order of the administration of the drugs, i.e., the drug schedule [311, 317].

Combination therapy for breast and colorectal cancers is already used in early and late-stage cancers and, usually, the maximum tolerated doses of each of the drugs are used [318]. This type of strategy reduces the problems associated with mono-therapy because it allows for limiting the side effects and increases the anti-tumor capacity of the chemotherapeutics since the drugs act in several molecular pathways associated with carcinogenesis [19]. Specifically, in oncology, the combination using two or more antineoplastic drugs is already an approved strategy and has shown good results in terms of treatment efficacy. It has been proven that the co-delivery of two or more antineoplastic drugs may have a synergistic effect on the inhibition of tumor growth both *in vitro* and *in*

vivo. Nevertheless, this strategy still presents some limitations. 5-FU, for example, a first-line chemotherapeutic drug in patients with advanced colorectal cancer, even when used in combination with other antineoplastics, only presents a response rate of only about 50% [319], which demonstrates the importance of developing novel models of drug combination for cancer combat.

2.2 Combination of Repurposed Drugs for Cancer Therapy

Different strategies rather than the traditional drug development and the drug repurposing have already been explored for the development of new cancer therapies (Figure 21). In the field of drug combination, specifically, some articles have already been studying the combination of hard repurposed drugs, i.e., by combining two or more drugs from non-cancer therapeutic areas as coadjuvant therapy (Figure 21); nevertheless, this field is still little explored. These pharmacological combinations are considered promising strategies for increasing the therapeutic index since single-drug systems are unsuitable for the treatment of drug-resistant cancers, a condition that is quite common for tumor cells [320]. These combinations usually include an agent that sensitizes the tumor cells and a second agent that takes advantage of this vulnerable state to increase its cytotoxic effect.

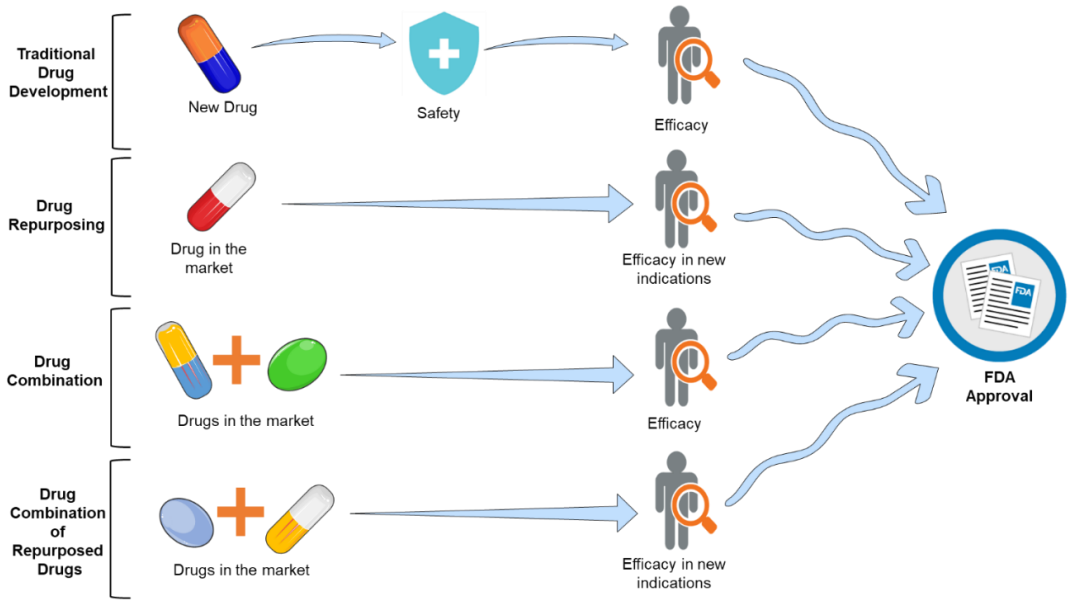

Figure 21. Strategies that can be explored for the development of new cancer therapies. The traditional development of new drugs is a thought process that involves steps such as determining the safety and efficacy of the new drug. FDA approval is time-consuming, and the cost of this process is high. Drug repurposing has been shown to be a promising approach, which allows the use of drugs that are already on the market in new therapeutic indications. Besides being cheaper, it is a faster process. The combination of drugs that are already approved for the same area has provided evidence of superior pharmacological effects compared to the effects

of each agent individually and is already being used in colon cancer therapy. The combination of repurposed drugs is still underexplored, and some *in vitro* studies have shown promising results, making it a good strategy to be explored in the future.

The simultaneous use of two or more drugs increases the effectiveness of the treatment of the disease even more if they are synergic, i.e., if their combined effect is greater than the sum of their effects individually. This strategy increases the sensitivity of the cells to the drugs and the treatment becomes more effective. However, if one of the drugs has significant toxicity, the toxicity in combination will always be lower when compared to monotherapy, since they will target complementary metabolic pathways and lower doses of the drug will be required to exert the same therapeutic effect. For that reason, combination therapy is already used in clinical practice and allows to overcome the disadvantages of monotherapy.

Several clinical trials already include combinations of chemotherapy, radiation therapy, hormone therapy, and immunotherapy. The combination of cytotoxic chemical compounds with biotherapy (monoclonal or polyclonal antibodies, vaccines, gene therapy, etc.) has also gained relevance in recent years [321]. Next, we will present some examples of repurposed drugs that have been included in combination models for cancer combat.

2.2.1 Sildenafil

Sildenafil was repurposed even before it reached the market and was initially proposed as an antihypertensive drug since it produced vasodilation and inhibited platelet aggregation by inhibition of cyclic guanosine monophosphate-specific phosphodiesterase type 5 (PDE5). During clinical trials, it was found this drug produced a side effect that resulted in penile erections, and in 1998 sildenafil was approved for the treatment of erectile dysfunction. Later, sildenafil underwent a new repositioning for the treatment of idiopathic form of pulmonary hypertension, a rare and potentially fatal condition, being approved for this new indication in 2005. PDE5 is frequently overexpressed in colorectal cancer [322], so Xiao-Long Mei *et al* evaluated the effect of sildenafil on human colorectal cancer both *in vitro* and *in vivo.* They have found this drug can significantly decrease cell growth, induce cell cycle arrest and apoptosis of colorectal cancer cells SW480 and HCT116. Sildenafil also induced an increase in intracellular ROS levels and proteins such as cyclin-dependent kinases (CDKs), cyclins, etc. In nude mice, this drug caused the reduction of xenograft models of human colorectal cancer [323]. Recently, another study used sildenafil in combination with DOX in 4T1 cells. The combination of these two drugs was found to be synergistic both *in vitro* and *in vivo* and resulted in a 4.7-fold reduction in tumor size when compared to DOX alone [300].

2.2.2 Metformin

Metformin is a biguanide (1,1-Dimethylbiguanid) and the first-line drug approved for the treatment of type 2 diabetes. It is also being used off-labeled (i.e., prescribed for indications that have not been approved by the FDA) for the treatment of polycystic ovary syndrome. This drug was discovered in 1922 and is currently at the top of the most prescribed drugs in the USA, occupying the fourth place in 2018 with more than 78 million prescriptions [324]. The mechanisms of this drug are not fully understood but metformin has been shown to act via both AMPK-dependent and AMPK-independent mechanisms and by inhibition of mitochondrial respiration. It is also believed this drug may inhibit the mitochondrial glycerophosphate dehydrogenase [325]. Over the years, several studies have examined the effect of metformin in cancer [326, 327], and doses of metformin have been shown to reduce cancer risk by about 37% [328]. It was found this drug effectively lowers the risk of several types of cancer such as breast, pancreas, colon, and prostate, both *in vitro* and *in vivo* [329, 330]. A study published in 2019 evaluated the combination of metformin with valproic acid, a drug used to treat epilepsy in transplant recipients on prostate cancer. The results demonstrated that this drug combination has a greater anti-tumor effect than each drug alone in clear renal cell carcinoma [331]. Recently, Mogaver *et al* studied the anti-cancer activity of metformin on colorectal cancer. This drug reduced HT-29 and HCT116 cell proliferation and migration by inducing cell cycle arrest in the G0/G1 phase, AMPK activation, and increasing the production of ROS [332]. Mussin *et al* published a study where metformin and some immunosuppressants were tested in three colorectal cell lines (HT-29, SW620, and HCT116) and viability assays showed a decrease in cell viability for all cell lines treated with sirolimus (an immunosuppressive drug used in the prophylaxis of acute rejection after renal transplantation), metformin and their combination. Cells treated with the combination of metformin and sirolimus showed synergistic effect comparing to cells treated with metformin or sirolimus alone [333]. Another study published by Miskimins *et al* tested the combination of phenformin (another biguanide, nearly 50 times as potent as metformin, that was introduced at the same time as metformin as an anti-diabetic drug) and oxamate (a lactate dehydrogenase inhibitor) for cancer therapy. Oxamate can be helpful in cancer therapy because lactate production by cells is a major side effect of biguanides. *In vitro* studies showed phenformin was more effective than metformin in increasing cell death of various cancer cell lines such as MCF-7 (breast cancer), B16F10 (melanoma), CT26 (colorectal cancer), A549 (lung cancer), and DU145 (prostate cancer). Also, the combination with oxamate produced synergistic anti-cancer effects by decreasing adenosine 5′-triphosphate (ATP) production and accelerating ROS production, resulting in a more rapid cancer cell death [334].

2.2.3 Propranolol

Another well-known example is the repositioning of propranolol, a non-selective beta-adrenergic receptor blocker indicated for the treatment and prevention of myocardial infarction, angina, cardiac arrhythmias as well as migraine. The beta-adrenergic receptors are a class of G-protein coupled receptors (GPCRs) that are the targets of the catecholamines epinephrine and norepinephrine and are reported to be overexpressed in several types of cancer. In 2008, French doctors accidentally discovered that propranolol also had an unknown action on the biology of the cells that make up the infant hemangioma, a benign tumor that affects babies starting in the first four weeks of life. Currently, propranolol is already used as therapy for this disease [335]. Propranolol is also believed to decrease the expression of VEGF and bFGF, leading to endothelial cell apoptosis. Therefore, propranolol has now been studied for other types of cancers such as breast [88], prostate, and colon [89], among others [90, 92]. Recently, Masur *et al* investigated the effect of norepinephrine (a catecholamine that functions as a hormone and neurotransmitter) and propranolol on SW480 colon carcinoma cells. They found that norepinephrine treatment caused an increase in cell migration, whereas combined treatment with propranolol abolished this increase [336]. Another study by Chin *et al* evaluated the effect of selective β2-adrenergic receptor antagonists, including propranolol, in several colorectal cancer cell lines (SW620, Colo205, and HT29 cells). They have found propranolol to significantly inhibit the viability of these colorectal cancer cells by inducing G1-phase arrest and apoptosis [337]. Moreover, this drug has also been studied in women with breast cancer, including in Phase II clinical trials, in combination with another repurposed candidate, etodolac. This combination demonstrated a decrease in transcription factors related to metastasis and inflammation, decreased epithelial-mesenchymal transition, and increased the number of tumor-infiltrating B cells [338]. Propranolol has also been tested in combination with other drugs, such as 5-FU or paclitaxel, and their combination has always been beneficial when compared to each drug alone [339].

2.2.4 Nonsteroidal anti-inflammatory drugs (NSAIDs)

NSAIDs are widely used drugs that are accessible without a prescription. The mechanism of action of these drugs is through the inhibition of cyclooxygenase (COX), which leads to the synthesis of prostaglandins that causes symptoms associated with inflammation, such as fever or pain. Most NSAIDs are specific for the COX-2 isoform and include drugs such as ibuprofen, celecoxib, among others. In addition to their anti-inflammatory effects, NSAIDs have been associated with a decreased risk of some types of cancer [340]. In fact, there is a well-defined link between cancer and inflammation [341,

342]. In various types of cancer, it is reported overexpression of COX-2, which is intimately linked to inflammatory processes. NSAIDs also have a pro-apoptotic effect on tumor cells, which involve the interference in pathways such as the WNT [343], p53, or MAPK [344]. Despite the extensive studies, the mechanisms of NSAIDs in cancer have not yet been fully clarified and the discovery of cancer preventive mechanisms of NSAIDs requires more research. To date, it is thought that chronic inflammation may facilitate the transition from a normal cell to a tumoral one and induce molecular pathways that constitute the initial steps of carcinogenesis for most sporadic cancers [345].

Acetylsalicylic acid (Aspirin®) is an NSAID that has been widely studied in cancer for its multiple biological actions. Aspirin and other NSAIDs have been associated with a decrease in the risk of colon cancer, and aspirin has recently been recommended for the prevention of colorectal cancer in patients with advanced colon polyps. It is the only orphan drug with positive phase III data for colorectal cancer [95]. Aspirin suppresses NF-kB, a transcription factor that controls genes related to inflammation, cell proliferation, survival, and prostaglandin production, inhibiting cyclooxygenase-1 (COX-1) and COX-2 and suppressing colorectal cancer growth. Studies in HT-29 cells, using the combination of aspirin with the anti-neoplastic drug 5-FU demonstrated synergism between these two drugs and consequently an increase in cell apoptosis in a time and concentration-dependent manner [346]. In a recent study, aspirin demonstrated the ability to inhibit epithelial-mesenchymal transition (EMT) in SW480 colorectal cancer cells, reducing cell viability and migration, including those induced by TGF-β, a protein related to chronic inflammation and involved in different pathways related to cell growth, proliferation, differentiation, and apoptosis [347, 348].

Isosorbide mononitrate is a drug commonly used for the treatment of cardiovascular diseases [349]. Nitric oxide plays a key role in cancer signaling as it can have both tumor-promoting and tumor-inhibiting effects, depending on its local tissue concentration. Isosorbide mononitrate is a prodrug that can be metabolized to nitric oxide and *in vivo* studies show it increases the intracellular concentrations of cyclic guanosine monophosphate [350]. Also, it was found isosorbide mononitrate inhibits angiogenesis, tumor growth, and metastasis in lung carcinoma [351]. Wang *et al* assessed the effect of this drug alone and in combination with aspirin in human colorectal cancer cells. Viability assays demonstrated that isosorbide mononitrate acts synergistically with aspirin in the inhibition of growth of HCT116 and SW620 colon cancer cells when compared with normal endothelial cells, whose growth was unaffected [352]. Indeed, in 2009, a group of researchers published a document stating the benefits of the use of aspirin and other

NSAIDs as tumor therapeutic agents [353]. Beneficial effects of aspirin for pancreatic, lung, prostate, and stomach cancer, among others, have been reported after 5 or more years of regular use of aspirin [354].

2.2.5 Antimalarial drugs

In the last few years, antimalarials have been gaining considerable notoriety in drug repositioning for various diseases. Chloroquine diphosphate is an antimalarial drug used worldwide and several studies seem to suggest a favorable action of this drug in cancer therapy [355, 356]. Sasaki *et al* evaluated the combination of chloroquine with 5-FU in HT-29 colorectal cancer cells and found this combination inhibited the proliferative activity of HT-29 cells by the arrest in G0/G1-phase and apoptosis induction [112]. In 2012, another study demonstrated that mice injected with colon26 cells, i.e., 5-FU resistant, were able to overcome this resistance and increase the effectiveness of the treatment if combined with chloroquine. This therapeutic combination resulted in higher apoptosis of the cells when compared to other treatments [357]. In the same year, another study directly evaluated the effect of the combination of these two drugs on DLD-1 cells. Cells were treated with 5-FU (10 µM) or chloroquine (100 µM) or a combination of both. It was concluded that chloroquine enhanced the anti-tumor effect of 5-FU via inhibition of the cell cycle in colon cells [111]. *In vivo* studies have shown that this drug can decrease the size of the primary tumor as well as the number and size of metastases and increase the survival time of mice with lung cancer [109]. Moreover, chloroquine has already shown promising results in Phase I clinical studies, either alone or in combination with other drugs for cancer therapy.

2.2.6 Statins

Statins are a class of drugs that lower the level of low-density lipoprotein cholesterol in the blood. They inhibit the rate-limiting enzyme HMG-CoA involved in the mevalonate pathway, the initial step in cholesterol synthesis. Statins also decrease chronic inflammation and fibrosis through TGF-β-independent pathways [358]. They also decrease NF-kB and apoptosis via TNF*α* receptor-associated factors 1 and 2 (TRAF1, TRAF2), which contribute to the carcinogenesis of several cancers [359]. In 2018, Zhou *et al* investigated the combination of atorvastatin, a drug that belongs to the statins, with phloretin (an antioxidant) on SW620 and HCT116 colon cancer cells. MTT results indicated that the combination of these drugs markedly reduced cell viability in both cell lines when compared with the drugs administered individually [360]. Zu *et al* investigated the effects of nobiletin (a citrus flavone) and atorvastatin both *in vitro* using colon cancer cells and macrophages and *in vivo* using an azoxymethane-induced colon carcinogenesis rat model. The results demonstrated that treatment with a combination of nobiletin and atorvastatin inhibited cell growth and

inflammation in the colon cancer cells and macrophages, respectively [361]. Another study published by Środa-Pomianek *et al* tested the anticancer activity of oxicam derivatives (PR17 and PR18), a class of NSAIDs, alone and combined with simvastatin, another statin, on doxorubicin-resistant colon cancer cells. Oxicam derivatives induced apoptosis through a caspase-3-dependent pathway, up-regulated Bax expression, and down-regulated Bcl-2 and COX-2 activity and expression. This study concluded that simvastatin combination with oxicam derivatives strongly potentiates their effect [362]. Jang *et al* aimed to combine statins with antineoplastic drugs to overcome irinotecan resistance. They evaluated the combination of simvastatin and irinotecan on HT-29 colon cancer cells with and without resistance to irinotecan and found that combination treatment with irinotecan and simvastatin decreased cell proliferation even in resistant cells and conclude simvastatin could act synergistically to overcome irinotecan resistance of colon cancer [363]. Recently, a novel approach to overcome the multidrug resistance of cancer cells has been proposed. Doxorubicin-resistant colon cancer cells were tested against three phenothiazine derivatives. These derivatives were tested alone and in combination with simvastatin. Cell growth, cell viability, and expression of COX-2 were investigated and it was found that the combination with simvastatin enhanced most doxorubicin cytotoxicity, compared to the treatment with the phenothiazine derivatives alone [364]. Statins were also tested on several breast cancer cell lines (such as MDA-IBC3, Sum149, and Sum190) and demonstrated good results, such as an increase in cell apoptosis and increased sensitivity to radiation, as well as inhibition of invasion and proliferation [365].

2.2.7 Natural compounds

Recently, several studies have addressed the use of bioactive natural compounds to overcome chemoresistance in cancer chemotherapy. Curcumin is a natural compound that has been studied in various diseases, particularly in oncology [366], because it is thought to function as a tumor cell sensitizer. Zhang *et al* investigated the effect of 5-FU alone or combined with curcumin in human colon cancer cell lines HCT116 and HT-29 and found that curcumin significantly increased the cytotoxicity of 5-FU and that the most effective combination was the pre-treatment of the cells with curcumin followed by 5-FU [367]. Nanoparticle-based combination chemotherapy can help achieve intracellular drug concentrations in cancer therapy. In this way, Xiao *et al* designed chitosan-functionalized camptothecin/curcumin-loaded polymeric nanoparticles. Camptothecin is a hydrophobic plant alkaloid extracted from *Camptotheca acuminate* and exhibits a broad spectrum of antitumor activity. It was found the combination of camptothecin and curcumin in a single nanoparticle enhanced the synergistic effects of the two drugs in colon26 cells and

decrease cell viability [368]. Dimethoxycurcumin, an analog of curcumin has also been shown to be active against colon cancer cells. Zhao *et al* investigated the antitumor effect of the combination of dimethoxycurcumin and 5-FU in SW480 and SW620 colon cancer cells. They found this combination induced apoptosis (by increasing Bax and cytochrome c and decreasing Bcl-2 expressions), cell cycle arrest, increased ROS levels, decreased mitochondrial membrane potential, and enhanced endoplasmic reticulum expansion, with better efficacy than either drugs alone [369].

Mycophenolate acid was initially proposed as an antibacterial, antifungal, and antiviral drug. Later, other properties continued to be explored, revealing the immunosuppressive effect of this drug. Mycophenolate mofetil is a prodrug of mycophenolate acid that has potent anti-inflammatory effects. Tacrolimus is a macrolide with immunosuppressive effects. Studies have shown that a combination of mycophenolate mofetil and tacrolimus is effective in the reversion of FAP in patients after kidney transplantation. Recently, mycophenolate mofetil and tacrolimus alone or in combination were also tested in a human colonic adenocarcinoma cell line. Mycophenolate mofetil in combination with tacrolimus induced changes in the cell cycle (S-phase arrest) and inhibited HT-29 cell viability, synergistically inhibiting the proliferation of the human colonic adenocarcinoma cell line [370].

Frondoside A is a triterpenoid glycoside isolated from an Atlantic Sea cucumber that consists of a pentaoside with one sulfate group and contains an aglycon ring with a xylose attached (3rd monosaccharide residue), 3-O-methylglucose (terminal monosaccharide) and an acetoxyl group (C-16 of the aglycon ring). Frondoside A has various anti-cancer properties such as pro-apoptotic, anti-proliferative, and anti-inflammatory effects, and has been tested both *in vitro* and *in vivo* against human pancreatic, breast, and lung cancer [371–374]. Recently, Attoub *et al* demonstrated that a combination of frondoside A, oxaliplatin, and 5-FU causes a concentration- and time-dependent decrease in the viability of HT-29 colon cancer cells. The authors demonstrated this apoptosis induction resulted from the inhibition of phosphorylation of the survival kinase AKT, which may lead to caspase-3 activation and poly (ADP-ribose) polymerase (PARP) inactivation, which ultimately leads to DNA damage [375].

Oxymatrine is a molecule extracted from the dry roots of *Sophora flavescens* and several studies have shown that it possesses anti-cancer effects. Liu *et al* evaluated the combination of oxymatrine and oxaliplatin both *in vitro* and *in vivo* and found that colon cancer lines (HT-29 and SW480) treated with this combination exhibited less proliferation and that it displayed synergistic effects, resulting in cell cycle arrest and apoptosis induction.

Furthermore, *in vivo* results showed an efficient reduction of tumor weight and volume on a SW480 xenograft mouse model after combined treatment [376].

Dietary intervention may help increase colorectal cells' sensitivity to chemotherapy. Recently, *in vivo* studies aimed to evaluate the effect of dihydromyricetin, a flavonoid component of herbal medicines, in combined treatments with two antineoplastic drugs: irinotecan and gemcitabine [377]. Dihydromyricetin displays several effects such as anti-inflammatory, antioxidant, antibacterial, antihypertensive, and antithrombotic. In addition, this drug has also potent antitumor activity, namely against breast, colon, and others [378–380]. For these experiments, colon cancer models were used and the obtained results seem to suggest that dihydromyricetin could act as a coadjuvant to irinotecan chemotherapy [377].

Taken together, the aforementioned studies demonstrate that the combination of drugs from totally different therapeutic areas may have applicability in the therapy of diseases like breast and colorectal cancers. Overall, studies addressing combination models using drugs with non-oncological indications have shown positive results in cancer therapy, both *in vitro* and *in vivo*, that further support the work developed in this chapter.

3. OBJECTIVES OF CHAPTER II

In this chapter, we aimed to explore four combination models for breast and colorectal cancer combat: (I) combination models combining conventional antineoplastics and repurposed drugs; (II) combination models combining only repurposed drugs; (III) combination models combining peptides and chemotherapy and (IV) combination models combining peptides and repurposed drugs. This aimed to determine the most appropriate models of drug combination for breast and colorectal cancer therapy.

4. MATERIALS AND METHODS OF CHAPTER II

4.1 Combination Model: Repurposed Drugs + Antineoplastic agents

4.1.1 Materials and Reagents

DMEM, McCoy's 5A Modified Medium, FBS, and pen-strep solution were purchased from Millipore Sigma (Merck KGaA, Darmstadt, Germany). Other cell culture reagents were purchased from Gibco (Thermo Fisher Scientific, Inc, Waltham, MA, USA).

MTT (cat. no. M5655), clotrimazole (cat. no. C6019), latrepirdine (cat. no. D6196), sertraline (cat. no. S6319), edaravone (cat. no. M70800), fluphenazine (cat. no. F4765), pyronaridine (cat. no. P0049), tafenoquine (cat. no. SML0396), 5-FU (cat. no. F6627), chloroquine (cat. no. C6628) and SRB (cat. no. S1402) were obtained from Sigma-Aldrich (Merck KGaA, Darmstadt, Germany). Artesunate (cat. no. 11817), benztropine (cat. no. 16214), thioridazine (cat. no. 14400), quetiapine (cat. no. 14152), fluoxetine (cat. no. 14418), DOX (cat. no. 15007) and cycloguanil (cat. no. 16861) were obtained from Cayman Chemical (Ann Arbor, Michigan, USA). Mefloquine (cat. no. sc-211784) was purchased from Santa Cruz Biotechnology (Dallas, Texas, USA). PTX (cat. no. 1097) was obtained from Tocris Bioscience (Bristol, UK).

4.1.2 Cell line and cell culture

Human breast cancer MCF-7 cell line was obtained from ATCC (Manassas, VA, USA) and maintained according to ATCC's recommendations at 37 °C and 5% CO_2 in DMEM medium supplemented with 10% FBS and 1% pen-strep solution. Cells were always maintained in the logarithmic growth phase. The media was renewed every 2 days, trypsinized with 0.25% trypsin-EDTA, and subcultured in the same media. MCF-7 cells (10,000 cells/well) were seeded in 96-well plates and allowed to adhere overnight prior to drug exposure. After that, the cell culture media were replaced with drug-containing media. Cells were exposed to drugs for 48 h, followed by SRB and/or MTT assays to evaluate drug treatments in the cell viability and protein synthesis rate of these cells.

Human colorectal cancer HT-29 cell line was obtained from ATCC (Manassas, VA, USA) and maintained according to ATCC's recommendations at 37 °C and 5% CO_2 in an appropriate medium supplemented with 10% FBS and 1% pen-strep solution. Cells were always maintained in the logarithmic growth phase. The media was changed every 2 days and trypsinized with 0.25% trypsin-EDTA. A total of 200 µL of HT-29 cells (7,500 cells/well) was seeded in 96-well plates and allowed to adhere overnight before drug exposure. After 24 h, the cell culture media were replaced with 200 µL of drug-containing media. Cells were

exposed to drugs for 48 h, followed by MTT and/or SRB assays to evaluate drug treatments in the cell viability and protein synthesis rate of these cells.

4.1.3 Drug treatment

Combination studies were performed by combining 5-FU or PTX and DOX (Drug A) according to each cell line, with different repurposed drugs (Drug B). 5-FU was selected as Drug A for HT-29 cells, while PTX and DOX were selected as Drug A for MCF-7 cells. Only drugs that presented a promising pharmacological profile (empirically defined as having IC_{50} < 25 µM) in Chapter I were tested in simultaneous combination with 5-FU or DOX/PTX. The concentration of both drugs in combination was variable and were combined in a fixed ratio of the IC_{50} values for each drug (0.25, 0.5, 1, 2, and 4 times the IC_{50}). Cells treated with vehicle (0.1% DMSO) were used as control.

The combinations of fluoxetine, fluphenazine, benztropine, and artesunate with 5-FU were also tested in sequential schedules of administration. For schedule A, cells were treated concomitantly with 5-FU and each repurposed drug for 48 h. For schedule B, cells were pre-treated with 5-FU for 24 h followed by each repurposed drug for another 24 h. For schedule C, cells were pre-treated with each repurposed drug for 24 h followed by 5-FU for another 24 h.

For the combined treatments with antineoplastic drugs plus quetiapine and edaravone, MCF-7 cells were treated with the IC_{50} value for DOX (0.17 µM) or PTX (0.44 nM) and combined with increasing concentrations (0.01–100 µM) of edaravone or quetiapine for 48 h. In the case of the HT-29 cells, the treatment consisted of the combination of 5-FU at IC_{50} (3 µM) with increasing concentrations (0.01–100 µM) of edaravone or quetiapine for 48 h.

4.2 Combination Model: Repurposed Drug + Repurposed Drug

4.2.1 Materials and Reagents

Cell culture reagents (cell culture medium, PBS, FBS, and pen-strep solution) were purchased from Millipore Sigma (Merck KGaA, Darmstadt, Germany). Other cell culture reagents were bought from Gibco (Thermo Fisher Scientific, Inc, Waltham, MA, USA). Fluphenazine (cat. no. F4765), pyronaridine (cat. no. P0049), and Thiazolyl Blue Tetrazolium Bromide (MTT, cat. no. M5655) were obtained from Sigma-Aldrich (Merck KGaA, Darmstadt, Germany). Sertraline (cat. no. 14839) was acquired from Cayman Chemical (Ann Arbor, MI, USA). Mefloquine (cat. no. sc-211784) was purchased from Santa Cruz Biotechnology (Dallas, TX, USA).

4.2.2 Cell Culture

Cytotoxicity of each treatment was performed using two cell lines: MCF-7 breast and HT-29 colon cancer (ATCC, Manassas, VA, USA). The MCF-7 and HT-29 cells were kept in DMEM and McCoy's cell culture medium, respectively, supplemented with 10% FBS and 1% pen-strep solution. Cells were maintained at 37 °C in an incubator with 95% air and 5% CO_2. Both cell lines were trypsinized using a 0.25% trypsin-EDTA solution when at 70–80% confluence.

4.2.3 Drug Treatment

On the day before cell treatment, 200 µL of MCF-7 and HT-29 cell suspension was seeded in 96-well plates at a density of 10,000 and 7,500 cells/well, respectively. Cells were allowed to grow and adhere for 24 h and then each well was aspirated and 200 µL of drug-containing media was added. All drugs were prepared in 100% DMSO and diluted to 0.1% DMSO using culture media. Control cells were treated with vehicle (0.1% DMSO). No significant changes were seen in control cells with and without vehicle.

For the combined treatments with the repurposed drugs, both cell lines were treated with a combination of two antimalarial drugs (mefloquine and pyronaridine) or two CNS drugs (fluphenazine and sertraline) for 48 h. Regarding the combination of antimalarial drugs, cells were incubated with mefloquine IC_{50} plus increasing concentrations (0.01–100 µM) of pyronaridine and vice-versa. The same experimental protocol was followed for the combination of CNS drugs. After 48 h treatment, morphological analysis was performed, and then cell viability was evaluated by an MTT assay.

4.3 Combination Model: Honeybee Venom + Antineoplastic Agents and Repurposed Drugs

4.3.1 Chemical Characterization of the Samples

4.3.1.1 Reagents and Materials

Apamin from bee venom (purity 98.3%) was obtained from CalBiochem (San Diego, CA, USA). Phospholipase A2 from bee venom (activity: 1775 units mg^{-1} solid), cytochrome c from equine heart (purity ≥ 95%), and melittin from bee venom (purity: ≥85%) were obtained from Sigma-Aldrich (St. Louis, MO, USA). Formic acid and High Performance Liquid Chromatography (HPLC) grade acetonitrile were obtained from Fisher Scientific UK (Loughborough, Leics, UK). Water was treated in a Milli-Q water purification system (TGI Pure Water Systems, Brea, CA, USA).

4.3.1.2 Honeybee Venom

The bee venom was gathered in 2018 from *Apis mellifera iberiensis* hives located in Bragança, Portugal. The sample was collected using a double-face bee venom collector, developed in our facilities with some specific features. The device was placed in the hives at one of the outmost opposite ends of the beehive nest. A mild electrical impulse shock was applied (increasing from 0V to 12V then decreasing to initial voltage). The optimum duration of bee venom collection in the beehive was set between 30 min to 60 min, early in the morning or at the beginning of the sunset. After the collection period, the venom was scraped off from the glass with a sharp scraper and conditioned in pharmaceutical-grade vials. The bee venom was then freeze-dried at −20 °C until further analysis.

4.3.1.3 LC-DAD-ESI/MSn Analysis

The Liquid chromatography coupled to diode array detection and electrospray ionization tandem mass spectrometry (LC-DAD-ESI/MS^n) study was performed on a Dionex Ultimate 3000 Ultra Performance Liquid Chromatography (UPLC) instrument (Thermo Scientific, San Jose, CA, USA) equipped with a diode-array detector and coupled to a mass detector. The chromatographic system consisted of a quaternary pump, an autosampler maintained at 5 °C, a degasser, a photodiode-array detector, and an automatic thermostatic column compartment. Chromatographic separation was carried out according to previously described work [381] on an XSelect CSH130 C18, 100 mm × 2.1 mm id, 2.5 µm XP column (Waters, Milford, MA, USA), and its temperature was maintained at 30 °C. Spectral data of all peaks were accumulated in the range of 190–500 nm. Cytochrome *c* was used as an internal standard (IS) and prepared in deionized water at the concentration of 25 µg/mL. For the analysis, the lyophilized HBV (3 g) was dissolved in 10 mL of IS solution. Each

sample was filtered through a 0.2 µm nylon membrane (Whatman). The standard solutions were prepared by dissolving the compound in IS solution, at the desired concentration. Quantification was achieved using calibration curves for apamin (4–60 µL/mL; $y = 0.031x + 0.021$; $R^2 = 0.998$), PLA2 (8–120 µL/mL; $y = 0.026x + 0.118$; $R^2 = 0.996$) and melittin (31–500 µL/mL; $y = 0.034x + 0.026$; $R^2 = 0.999$). The mass spectrometer was operated in the positive ion mode using a Linear Ion Trap LTQ XL mass spectrometer (Thermo Scientific, San Jose, CA, USA) equipped with an ESI source. Typical ESI conditions were nitrogen sheath gas 35 psi, spray voltage 3.5 kV, source temperature 300 °C, capillary voltage 20 V, and the tube lens offset was kept at a voltage of 74 V. The collision energy used was 30 (arbitrary units). Data acquisition was carried out with the Xcalibur® data system (Thermo Scientific, San Jose, CA, USA).

4.3.2 Cytotoxic Studies

4.3.2.1 Reagents and Materials

McCoy's 5A Medium powder (modified with L-glutamine, without sodium bicarbonate), DMEM, FBS, and pen-strep solution were purchased from Millipore Sigma (Merck KGaA, Darmstadt, Germany). Other cell culture reagents were purchased from Gibco (Thermo Fisher Scientific, Inc, Waltham, MA, USA). MTT (cat. no. M5655), SRB, (cat. no. S1402), 5-FU (cat. no. F6627), and fluphenazine (cat. no. F4765) were obtained from Sigma-Aldrich (Merck KGaA, Darmstadt, Germany). DOX (cat. no. 15007), thioridazine (cat. no. 14400), sertraline (cat. no. 14839), and fluoxetine hydrochloride (cat. no. 14418) were obtained from Cayman Chemical (Ann Arbor, MI, USA).

4.3.2.2 Cell Culture

Two different cell lines were used in this study (MCF-7 breast and HT-29 colon cancer cell lines). Both cell lines were obtained from ATCC (Manassas, VA, USA) and maintained, according to ATCC's recommendations, at 37 °C and 5% CO_2. HT-29 cells were grown in McCoy's 5a Medium Modified and MCF-7 cells were maintained in DMEM cell culture medium. All media were supplemented with 10% FBS and a 1% pen-strep solution. Cells were passaged using a 0.25% trypsin-EDTA solution when confluency reached 80–90% and were subcultured in the same culture media. Prior treatments, HT-29 cells (15,000 cells/well) and MCF-7 cells (10,000 cells/well) were seeded in 96-well plates and allowed to adhere overnight.

4.3.2.3 Drug Treatment

The cytotoxic effect of 5-FU, DOX, four different CNS drugs (fluphenazine, fluoxetine, sertraline, and thioridazine), and bee venom for single and combination studies

was evaluated after 48 h of treatment. First, the half-maximal inhibitory concentration (IC_{50}) value was determined for each drug alone both in HT-29 and MCF-7 cells. 5-FU, DOX, and CNS drugs' concentrations ranged from 0.1 to 100 µM for single-drug treatments. Bee venom was tested alone in concentrations of 6.25, 12.5, 25, 50, and 100 µg/mL. Additionally, combination studies were performed by combining 5-FU, DOX, or each CNS drug (Drug 1) at their IC_{50} value with bee venom at the same range of concentrations tested for the single treatment (Drug 2). Control cells were treated with 0.1% DMSO (vehicle). The combined effects of non-equipotent concentrations (non-fixed ratio) were evaluated by MTT and SRB assays.

4.4 Combination Model: CPP2-conjugates + with 5-FU and Clotrimazole

4.4.1 CPP2 and CPP2–Thiazole Conjugate Synthesis

4.4.1.1 Reagents and Solvents

All solvents used in this study were of analytical grade. Reagents and solvents were purchased from Novabiochem (Fmoc-amino acids and Fmoc-Rink Amide MBHA resin), Merck (Trifluoracetic acid (TFA), and other solvents), Sigma–Aldrich (coupling agents, piperidine, *N*-ethyl-*N, N*-diisopropylamine (DIEA) and all thiazole derivatives).

4.4.1.2 Synthesis of CPP2

The first peptide to be synthesized was CPP2. Only in this way would we be able to have available peptide to make the N-terminal modifications with the different thiazole derivatives. The peptide (C-terminal amide) was assembled by Fmoc/tBu solid-phase peptide synthesis (SPPS) methodologies. The resin (Fmoc-Rink Amide MBHA, 0.38 mmol/g loading capacity) was preconditioned for 20 min in *N*, *N*-dimethylformamide (DMF). After that, DMF was rejected, and the resin was swelled in dichloromethane (DCM) for another 15 min. The initial deprotection step (release of the free amino group of the Rink linker) was carried out using 20% piperidine in DMF (3 mL, 1 × 1 min + 1 × 20 min). After the deprotection, the resin was washed with DMF (3 mL, 3 × 1 min) and DCM (3 mL, 3 × 1 min), and a ninhydrin test was performed. Upon a positive ninhydrin test (dark blue resin beads and solution), the release of the free amine groups was confirmed and, therefore, the construction of the peptide chain could be initiated. Before coupling, amino acids were activated in solution for approximately 5 min before being transferred to the syringe to react with the resin or peptidyl-resin. This activation was accomplished by preparing a solution of Fmoc-AA-OH (5 eq.), coupling agent Hexafluorophosphate Benzotriazole Tetramethyl Uronium (HBTU) (5 eq.) and base DIEA (10 eq.) in DMF. Solvents were used in only sufficient volumes to ensure the proper solvation of the amino acids and the peptidyl resin beads, which is a crucial condition for efficient chain assembly. The activated amino acid solution was then transferred to the reaction vessel to react with the previously deprotected resin or peptidyl-resin for 1 h, under stirring. After this, the peptidyl-resin was washed with DMF (3 mL, 3 × 1 min) and DCM (3 mL, 3 × 1 min) to eliminate the excess of reagents, solvents, and side products, and a Kaiser test was performed to confirm the efficiency of the coupling. When the Kaiser test was negative, the following deprotection step was carried out using the deprotection solution (20% piperidine in DMF (3 mL, 1 × 1 min + 1 × 20 min)). Once deprotection was completed, the resin was washed again with DMF (3 mL, 3 × 1 min) and DCM (3 mL, 3 × 1 min), and another Kaiser test was performed. When the deprotection

was confirmed by a positive Kaiser test, the next Fmoc-AA-OH was coupled following the same aforementioned conditions. The peptide sequence was completed in the C→N direction by repeating the cycles of coupling of N-Fmoc amino acids and deprotection steps. When the peptide sequence was completed and after the final deprotection, the peptidyl-resin was subjected to a chemical treatment that cleaved the bond linking the peptide to the resin beads. First, a cleavage cocktail was prepared in the hood, containing 95% TFA, 2.5% H_2O, and 2.5% thioanisole (TIS) (v/v). Then, the dry peptidyl-resin was transferred to 15 mL Falcon tubes in 100 mg portions, and 1 mL of cleavage cocktail was added to each portion. The tubes were left under orbital stirring for 2 h at room temperature. After that, the peptide should be soluble in the solution and, thus, the contents of the tubes were filtered with a D4 funnel previously rinsed with TFA, and the resin beads were washed with TFA. The filtrate, containing the soluble peptide, was transferred to new Falcon tubes in 1 mL portions, and 14 mL of cold tert-butyl methyl ether was added to each tube. After slightly shaking the tubes, they were cooled to −22 °C for approximately 8 min and then centrifuged at 3500 rpm for 7 min at −5 °C. The ether was carefully rejected and “fresh” ether was added again. The addition of ether and centrifugation was repeated three more times and, finally, the tubes were left in a vacuum desiccator until the crude peptide was dry. Dry peptide pellets were then solubilized in 10% aqueous acetic acid and analyzed by HPLC and liquid chromatography–mass spectrometry (LC-MS).

4.4.1.3 Synthesis of the NTZ-C2-CPP2 and MTZ-C2-CPP2 Conjugates

To obtain these two conjugates, the last amino acid of the base sequence of CPP2 was deprotected and a Kaiser test was performed. When the deprotection was confirmed by a positive Kaiser test, a linker (C2) was coupled to this sequence. This step was carried out using succinic anhydride (10 eq.) and pyridine (2 mL) for 1 h under stirring. After this step, the resin was washed with DMF (3 mL, 3 × 1 min) and DCM (3 mL, 3 × 1 min) and divided into two halves. The 2-amino-5-nitrothiazole (NTZ) was coupled to one half and the 2-amino-5-methylthiazole (MTZ) to another using the coupling O-(Benzotriazole-1-yl)-N, N, N', N'-tetramethyluronium tetrafluoroborate (TBTU) (5 eq.) and base DIEA (10 eq.) in DMF for 2 h under stirring. Upon synthesis, the conjugates were cleaved and, once the products were dried in a vacuum desiccator, analyzed by HPLC and LC-MS.

4.4.1.4 Synthesis of the BenzoTZ-C2-CPP2 Conjugate

This strategy was based on the synthesis in solution of the derivative BenzoTZ-C2 and subsequent coupling to the peptide in the syringe. To this end, a suspension of BenzoTZ (0.2500 g) and C2 (2.4 eq.) in DMF (3 mL) was prepared at room temperature under magnetic stirring. DIEA (2 eq.) was added and allowed to react under these conditions

for 24 h. The reaction was monitored by thin layer chromatography (TLC) using a dichloromethane/acetone ratio of 4:1 as the eluent. Analyses were made for ESI-MS, the expected compound was confirmed to be obtained, and column purification was carried out. The tubes corresponding to the desired purified compound were selected and placed into a flask to be evaporated. The compound was then solubilized in water/methanol and lyophilized. Out of the syringe, in a small bottle, 2 eq. of purified BenzoTZ-C2, 2 eq. of benzotriazol-1-yloxytripyrrolidinophosphonium hexafluorophosphate (PyBOP), and 4 eq. of DIEA were placed together. Then, this solution was placed in the syringe and left overnight under shaking. After 24 h, the resin was cleaved and analyzed by LC-MS to confirm the formation of the conjugate.

4.4.1.5 Synthesis of the BTZCA-CPP2 and BTZ5CA-CPP2 Conjugates

To obtain these conjugates, the last amino acid of the base sequence of CPP2 was deprotected and a Kaiser test was performed. When the deprotection was confirmed by a positive Kaiser test, the resin was washed with DMF (3 mL, 3 × 1 min) and DCM (3 mL, 3 × 1 min) and divided into two halves. Then the 5-bromothiazole-2-carboxylic acid (BTZCA, 5 eq.) and the 2-bromothiazole-5-carboxylic acid (BTZ5CA, 5 eq.) were coupled using the coupling agent TBTU (5 eq.) and base DIEA (10 eq.) in DMF for 2 h under stirring. A Kaiser test was then performed to confirm the efficacy of the coupling. Upon synthesis, the conjugates were cleaved to separate the peptide from the resin and to remove the sidechain protecting groups. Once the products were dried in a vacuum desiccator, they were analyzed by HPLC and LC-MS, and it was found to correspond to the target conjugates.

4.4.1.6 General Analysis Procedure

The CPP2 and CPP2–thiazole conjugates' purity were determined by high-performance liquid chromatography with diode array detection (HPLC-DAD) on Merck–Hitachi LaChrom Elite equipment with a quaternary pump, automatic and thermostated by a Peltier effect injector and a diode detector. A reverse-phase Purospher star RP C-18 (octadecylsilane) column (125 × 4.0 mm), with a particle diameter of 5 µm, was used. The elution was performed with a variable gradient of acetonitrile in water containing 0.05% TFA, at a 1 mL/min flow and detection at a variable wavelength (220 or 270 nm). Synthetic crudes were purified by reverse-phase medium-pressure liquid chromatography (RP-MPLC), using a C18 Vydac® 218TP stationary phase, by Grace Vydac. MS analysis was performed on an LTQ Orbitrap™ XL hybrid mass spectrometer (Thermo Fischer Scientific, Bremen, Germany) controlled by LTQ Tune Plus 2.5.5 (Thermo Fischer Scientific, Bremen, Germany) and Xcalibur 2.1.0 (Thermo Fischer Scientific, Bremen, Germany). The electrospray ionization source settings were as follows: source voltage, 3.1 kV; capillary

temperature, 275 °C with a sheath gas flow rate at 40 and auxiliary gas flow rate at 10 (arbitrary unit as provided by the software settings). The capillary voltage was 36 V, and the tube lens voltage was 110 V. The direct electrospray ionization-ion trap mass spectrometry (ESI-IT MS) analysis was performed on a Finnigan Surveyor LCQ DECA XP MAX mass spectrometer from ThermoElectron Corporation (Waltham, MA, USA), and the LC-MS analysis was performed on the same equipment coupled to a Finnigan Surveyor HPLC equipped with a DAD Plus Detector, an Autosampler Plus, and an LC Pump Plus. MALDI-TOF/TOF matrix-assisted desorption/ionization mass spectrometry was performed using a Bruker Daltonics UltrafleXtreme (Bruker, MA, USA). MS data handling software (Xcalibur QualBrowser software, Thermo Fischer Scientific, Bremen, Germany) was used to obtain the confirmation of the synthetic peptides by their exact *m*/*z* value.

4.4.2 Cell Culture

4.4.2.1 Materials

McCoy's 5A Modified Medium, DMSO, FBS, and a penicillin-streptomycin solution were purchased from Millipore Sigma (Merck KGaA, Darmstadt, Germany). Other cell culture reagents were purchased from Gibco (Thermo Fisher Scientific, Inc., Waltham, MA, USA). 5-FU (cat. no. F6627), clotrimazole (cat. no. C6019), MTT (cat. no. M5655), and SRB (cat. no. S1402) were obtained from Sigma–Aldrich (Merck KGaA, Darmstadt, Germany).

4.4.2.2 Cell Line and Cell Culture

Human colorectal cancer HT-29 was obtained from ATCC (Manassas, VA, USA) and maintained according to ATCC's recommendations at 37 °C and 5% CO_2 in appropriate medium supplemented with 10% FBS and 1% pen-strep solution. Cells were maintained in the logarithmic growth phase at all times. The media were changed every 2 days and trypsinized with 0.25% trypsin–EDTA. A total of 100 µL of HT-29 cells (7,500 cells/well) were seeded in 96-well plates and allowed to adhere overnight before drug exposure. After 24 h, the cell culture media were replaced with 100 µL of drug-containing media. Cells were exposed to drugs/peptides for 48 h, followed by MTT and SRB assays to evaluate single and combination drug treatments in the cell viability and protein synthesis rate of these cells.

4.4.2.3 Cell Culture Treatment

The intermediate value (IV) was first determined for each conjugate alone in HT-29 cells. This IV was obtained by plotting the logarithm of concentration against the normalized values of cell viability, as in a dose-response curve, but did not necessarily represent the IC_{50} of each compound, as these peptides had reached a plateau of inhibition. Drug/peptide concentrations ranged from 0.1 to 50 µM for the single-drug treatment. Combination studies

were performed by combining 5-FU (Drug A) with each CPP2–thiazole conjugate (Drug B). Clotrimazole was also combined with each CPP2–thiazole conjugate. Only CPP2-conjugates that presented a promising pharmacological profile (defined as IV < 20 µM) were tested in simultaneous combination with 5-FU or clotrimazole. Both Drug A and Drug B concentrations were variable, and the combined effects of equipotent concentrations (fixed ratio) of the IV values for each drug were evaluated.

4.5 Microscopic Observation

After each treatment and before performing the MTT and/or SRB assays, cells were examined using a Leica DMI 6000B microscope coupled to a Leica DFC350 FX camera, and images were analyzed using Leica LAS X imaging software (v3.7.4, Leica Microsystems, Wetzlar, Germany).

4.6 Viability assays

To determine the cytotoxic effects of each combination on MCF-7 breast and HT-29 colorectal cancer cells, MTT and/or SRB assays were used. For the MTT protocol, after drug treatment, the cell medium was removed, and 200 µL/well of MTT solution (0.5 mg/mL in PBS) was added. Cells were incubated for 3 h and protected from light. After this period, the MTT solution was removed, and DMSO (200 µL/well) was added to solubilize the formazan crystals. Absorbance was measured at 570 nm in an automated microplate reader (Sinergy HT, Biotek Instruments Inc., Winooski, VT, USA). For the SRB assay, after treatments, the cultured cells were fixed with ice-cold 10% trichloroacetic acid for 30 min and stained with 0.4% SRB for 1h at room temperature. Excess dye was removed by rinsing several times with tap water. Protein-bound dye was dissolved with 400 µL 10 mM Tris base solution for the determination of absorbance with a microplate reader with a filter wavelength of 540 nm (Sinergy HT, Biotek Instruments Inc., Winooski, VT, USA).

4.7 Data Analysis

GraphPad Prism 9 (GraphPad Software Inc., San Diego, CA, USA) was used to produce all graphs from MTT and SRB assays as well as concentration-response curves by nonlinear regression analysis. The viability of cells treated with each drug was normalized to the viability of control cells and cell viability fractions were plotted versus drug concentrations in the logarithmic scale.

4.8 Statistical Analysis

The results are presented as mean ± SEM for *n* experiments performed. All data were assayed in three independent experiences, in triplicate. Statistical comparisons

between control and treatment groups, at the same time point, were performed with the Student's t-test and ANOVA test. Statistical significance was accepted at p values < 0.05.

5. RESULTS AND DISCUSSION OF CHAPTER II

5.1 Drug combination in Breast Cancer

5.1.1 Combination Model I: Repurposed Drugs + Antineoplastic agents in Breast Cancer

Drug combination is a strategy that allows the reduction of the drug concentrations needed for therapeutical effects. While many studies have identified promising drug pair candidates for specific cancer cells based on the combination of two or more antineoplastic agents, few report if antimalarials offer improved therapeutic benefits in drug combination schemes with antineoplastic agents.

Here, it was hypothesized that antimalarials could enhance the cytotoxic effects of DOX and PTX, two chemotherapeutic agents commonly used in the management of breast cancer. Therefore, it was proposed a new combination model that consisted of the combination of these two antineoplastic agents with different antimalarial drugs.

The main goal of this strategy is to have a safe starting point, such as an antineoplastic drug, whose antitumor activity is guaranteed in tumor cells. The combination with the repurposed drug, which has an acceptable toxicological profile, aims to improve the activity of the reference drug, and simultaneously reduce its therapeutic dose. Since the toxicological profile of repurposed drugs is already known, once their anti-cancer activity is better understood, the use of these drugs can be implemented clinically.

To allow the assessment of the efficacy of the drug combinations, it was first analyzed the cytotoxic potential of the antineoplastic drugs PTX and DOX as single agents, in the human breast cancer cell line MCF-7.

DOX is an antineoplastic drug belonging to the anthracycline class that is widely used in breast cancer [382]. Its mechanism of action is based on the intercalation with DNA, which leads to the cleavage of DNA by the enzyme topoisomerase II, and consequently, stops the cell cycle in the G2/M phase, resulting in cell death [383]. Also, studies suggest that the interconversion of DOX by cells to a semiquinone metabolite leads to the formation of ROS that interferes with lipid peroxidation and causes damage to DNA and cell membranes [383]. DOX is usually given in combination with other chemotherapy medicines, being used as adjuvant and neo-adjuvant therapy to treat advanced-stage breast cancer. However, the use of this drug in therapy is conditioned by its cardiotoxicity as well as the development of drug resistance by tumor cells, leading to a decrease in its effectiveness [47].

PTX is another antineoplastic used in the treatment of advanced-stage breast cancers and is a natural diterpene alkaloid, isolated from the *Taxus brevifolia* tree [384]. In addition to its use in breast cancer, PTX is also employed in the therapy of other types of cancers, such as ovary, lung, etc. [385]. The main target of PTX is β-tubulin, a protein responsible for stabilizing the microtubule polymers. When it binds to β-tubulin, PTX prevents its breakdown, and cells are blocked in phases G0/G1 and G2/M, which results in tumor cell death [386]. Several studies suggest that PTX can lead to increased expression of the forkhead box-O1 (FOXO1) gene, which may be involved in the inhibition of androgen receptors [387]. PTX also causes an increase in interleukin 10 (IL-10), an anti-inflammatory cytokine, as well as an increase in the production of ROS, by increasing the activity of nicotinamide adenine dinucleotide phosphate hydrogen (NADPH) oxidase [388]. The solvents used to solubilize this drug make PTX difficult to tolerate and patients usually need to pre-medications to minimize reactions to the solvents. Also, it causes other severe side effects such as low white blood cell count, susceptibility to infections, allergic reactions, hair loss, vomiting, and diarrhea, among others [389].

To evaluate the effects of DOX and PTX on the MCF-7 cell line, cells were treated with increasing concentrations of DOX (1-10 μM) and PTX (0.1–500 nM) for 48 h in MCF-7 cells. The percentage of cell survival was assessed by MTT assay and the percentage of cellular protein content was measured by SRB assay. The results of MTT and SRB assays are in agreement for DOX activity and are given in Figures 22A and B, respectively. These results reveal a significant activity of this drug at concentrations above 0.1 μM, with cells demonstrating a strong response to the cytotoxic effect of DOX, with 1 μM killing almost 50% of cells.

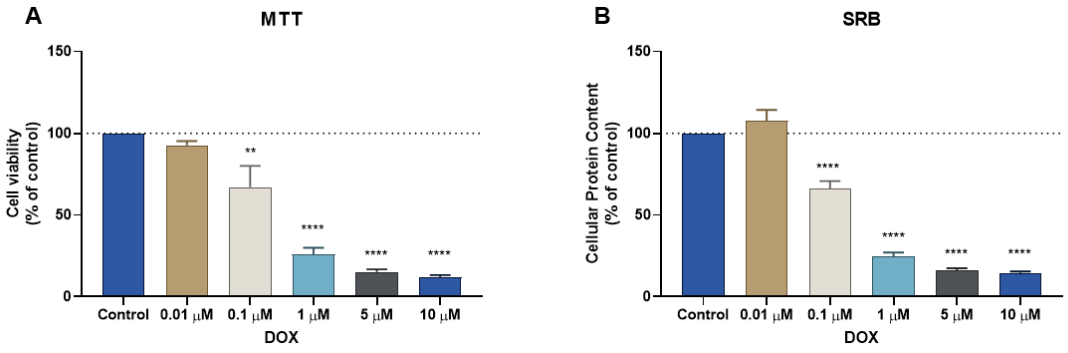

Figure 22. Effects of DOX on (**A**) cell viability and (**B**) cellular protein content. Cells were cultured in the presence of increasing concentrations of DOX. After 48 h MTT and SRB assays were performed to measure cellular viability as well as protein content. Values are expressed in percentage and represent mean ± SEM. Each experiment was done three times independently (n = 3); **statistically significant vs. control at $p < 0.01$. ****statistically significant vs. control at $p < 0.0001$.

The results concerning the PTX activity are given in Figures 23A and B for MTT and SBR assays, respectively, and demonstrate a great cytotoxic effect of this drug for concentrations above 1 nM, with 10 nM causing the reduction of almost 50% of the cells. This response is more pronounced in the SRB test, with a significant response from 1 nM.

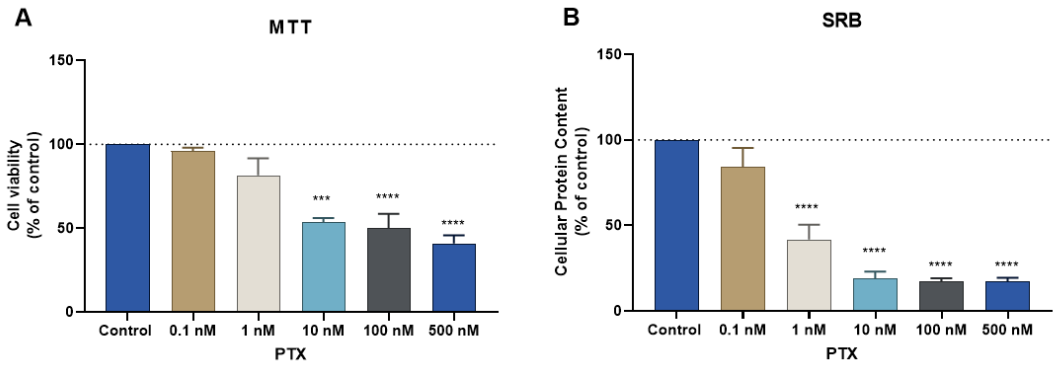

Figure 23. Effects of PTX on (**A**) cell viability and (**B**) cellular protein content. Cells were cultured in the presence of increasing concentrations of PTX. After 48 h MTT and SRB assays were performed to measure cellular viability as well as protein content. Values are expressed in percentage and represent mean ± SEM. Each experiment was done three times independently (n = 3), ***statistically significant vs. control at $p < 0.001$. ****statistically significant vs. control at $p < 0.0001$.

The dose-response curves for these drugs in MCF-7 breast cancer cells are represented in Figure 24. Compared to DOX, PTX demonstrated a higher efficacy in decreasing cell viability, which resulted in a lower IC_{50} of around 3 nM, compared to 0.1 µM for DOX (Figure 24).

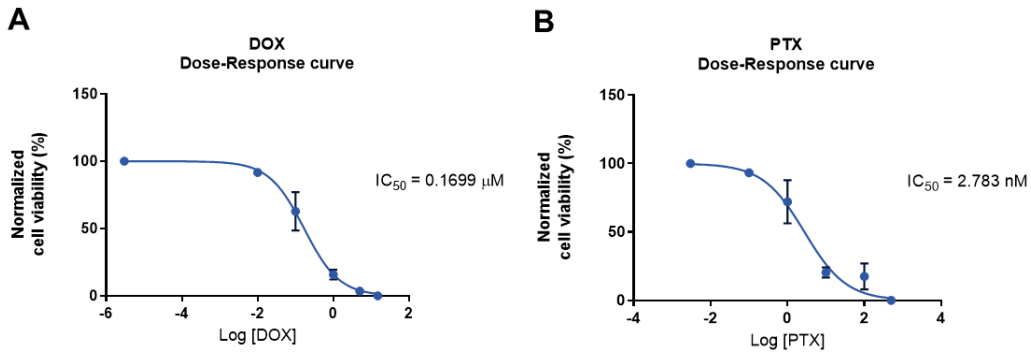

Figure 24. Concentration-response curves of (**A**) DOX and (**B**) PTX on MCF-7 cells based on results obtained by MTT assay. The results represent the mean ± SEM of three independent experiments performed in triplicate.

These results confirm the anti-cancer activity of these antineoplastic drugs against breast cancer cells, namely in estrogen-receptor-positive breast cancer. Given the elevated antitumor activity of these drugs at very low doses, these antineoplastics were considered good candidates to evaluate in combination models using antimalarial drugs.

5.1.1.1 Combination of DOX or PTX + Antimalarials in MCF-7 Cells

After finding the most promising antimalarial candidates for drug repurposing in breast cancer in Chapter I, it was designed a combination model consisting of one antineoplastic drug (Drug 1), and one antimalarial drug (Drug 2). MCF-7 cells were treated with both drugs alone and combined in a fixed ratio, in the concentrations of 0.25 × IC_{50}, 0.5 × IC_{50}, IC_{50}, 2 × IC_{50}, and 4 × IC_{50} as represented in Figure 25.

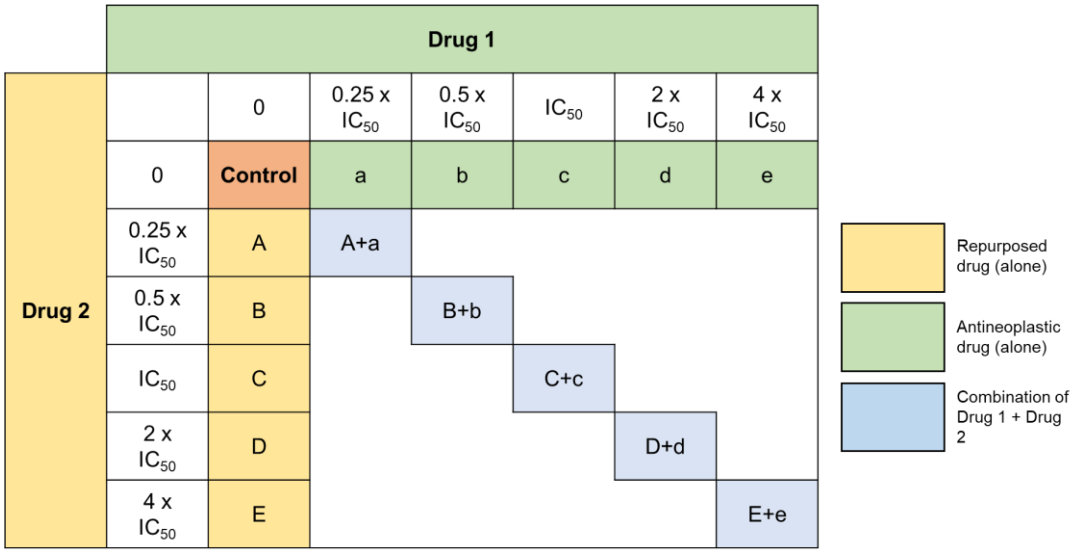

Figure 25. Representation of the design of the combination experiences. Drug 1 corresponds to the antineoplastic agent and Drug 2 corresponds to repurposed drugs. Cells were treated with Drug 1 and Drug 2 alone and in combination in a fixed ratio for 48 h, in the concentrations of 0.25 × IC_{50}, 0.5 × IC_{50}, IC_{50}, 2 × IC_{50}, and 4 × IC_{50}.

First, we evaluated the combinations of DOX + Artesunate, DOX + Mefloquine, DOX + Tafenoquine, DOX + Pyronaridine, and DOX + Cycloguanil by MTT assay (Figure 26). As chloroquine has been widely tested in several cell lines, we also included the combination of DOX + chloroquine in this study, using the IC_{50} value defined on the literature [100].

Analyzing the results obtained by the MTT assays, it is possible to verify that the treatment of DOX combined with mefloquine (Figure 26A) did not demonstrate an improved anticancer profile compared to both drugs alone. Nevertheless, this drug presented an enhanced anticancer effect than DOX alone for the concentrations of 0.5, 1, and 2 times IC_{50}. Combination of DOX + pyronaridine (Figure 26B) resulted in a significant reduction in the viability of MCF-7 cells compared to both drugs alone, at the concentrations of 0.25, 0.5, and 1 times IC_{50}. The combination of DOX plus tafenoquine (Figure 26C) did not result in any enhancement in the activity compared to both drugs alone. On the other side, the

combination of DOX + chloroquine (Figure 26D) at the concentration of 0.5 x IC_{50} demonstrated a significant reduction in the viability of MCF-7 cells in relation to both drugs alone. At other concentrations till 2 × IC_{50}, this combination was only advantageous over DOX alone. The combination of DOX and artesunate (Figure 26E) also demonstrated a promising anticancer profile, with the combinations of 0.5 and 1 × IC_{50} causing significant toxicity compared to both drugs alone. The combination of cycloguanil and DOX (Figure 26F) does not seem to be advantageous over the treatment with DOX alone.

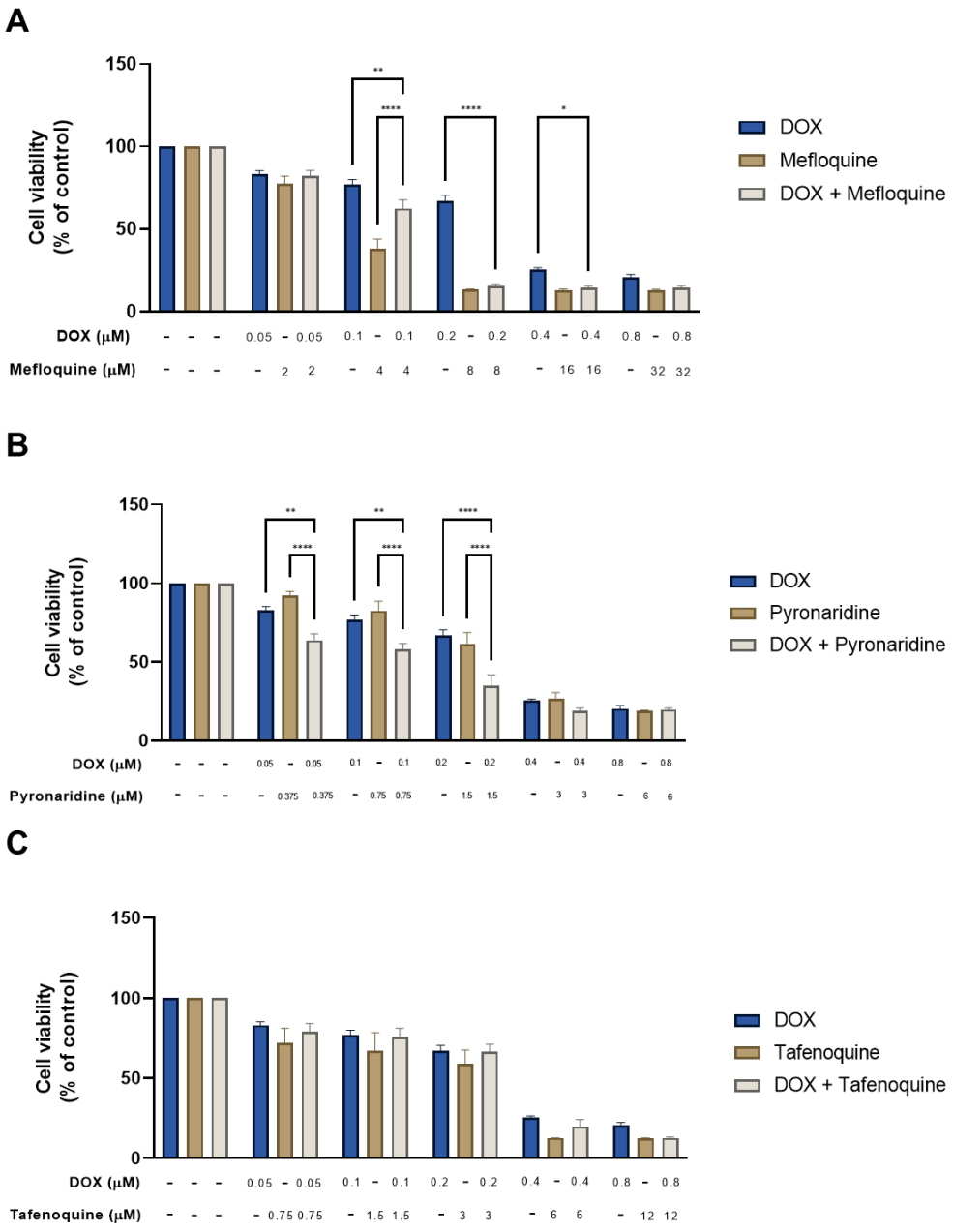

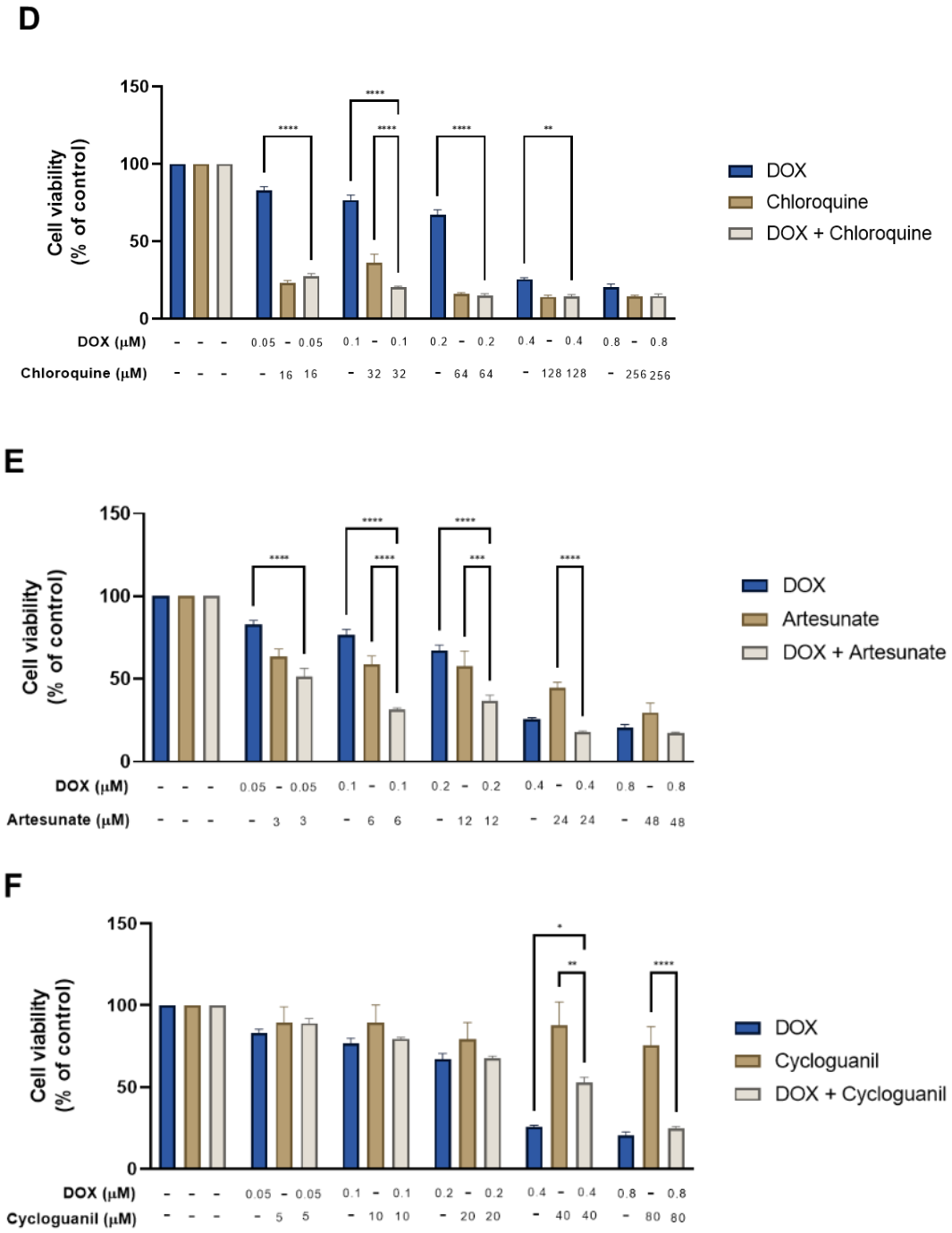

Figure 26. Growth inhibition of MCF-7 cells after 48 h treatment with a combination of DOX plus (**A**) mefloquine, (**B**) pyronaridine, (**C**) tafenoquine, (**D**) chloroquine, (**E**) artesunate, and (**F**) cycloguanil. Cells were exposed to concentrations of each drug of 0.25, 0.5, 1, 2, and 4 times their $IC_{50,}$ and cell viability was evaluated by MTT assay. The drugs in combination were co-administered at the same time. Values are expressed in percentage and represent mean ± SEM. Each experiment was done three times independently (n = 3); *statistically significant at $p < 0.05$. **statistically significant at $p < 0.01$. ***statistically significant at $p < 0.001$. ****statistically significant at $p < 0.0001$.

Next, to evaluate the influence of the antineoplastic agent, the same antimalarial drugs were combined with a different antineoplastic drug, PTX, using the same experimental design described in Figure 25. When compared to PTX as a single agent, at higher doses (2 × IC_{50} and 4 × IC_{50}), all drug combinations of PTX with antimalarial drugs, except for cycloguanil, demonstrated significant anti-cancer activity (Figure 27). Nevertheless, only the combination of PTX + chloroquine at the concentration of 0.5 x IC_{50} (Figure 27D) and the combination of PTX + artesunate (Figure 27F) at the concentrations of 0.5, 1, and 2 × IC_{50} demonstrated an improved anticancer profile in relation to both drugs alone.

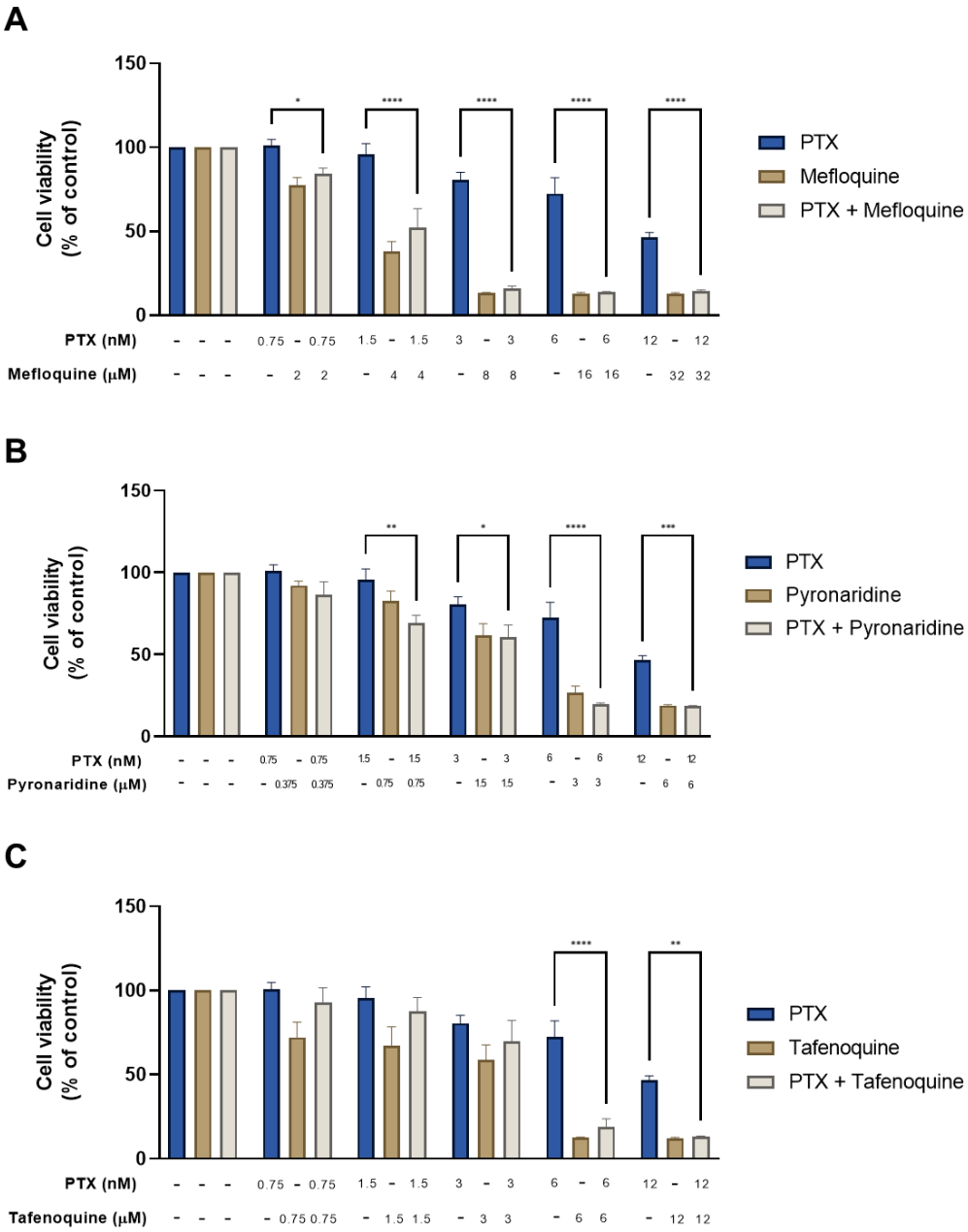

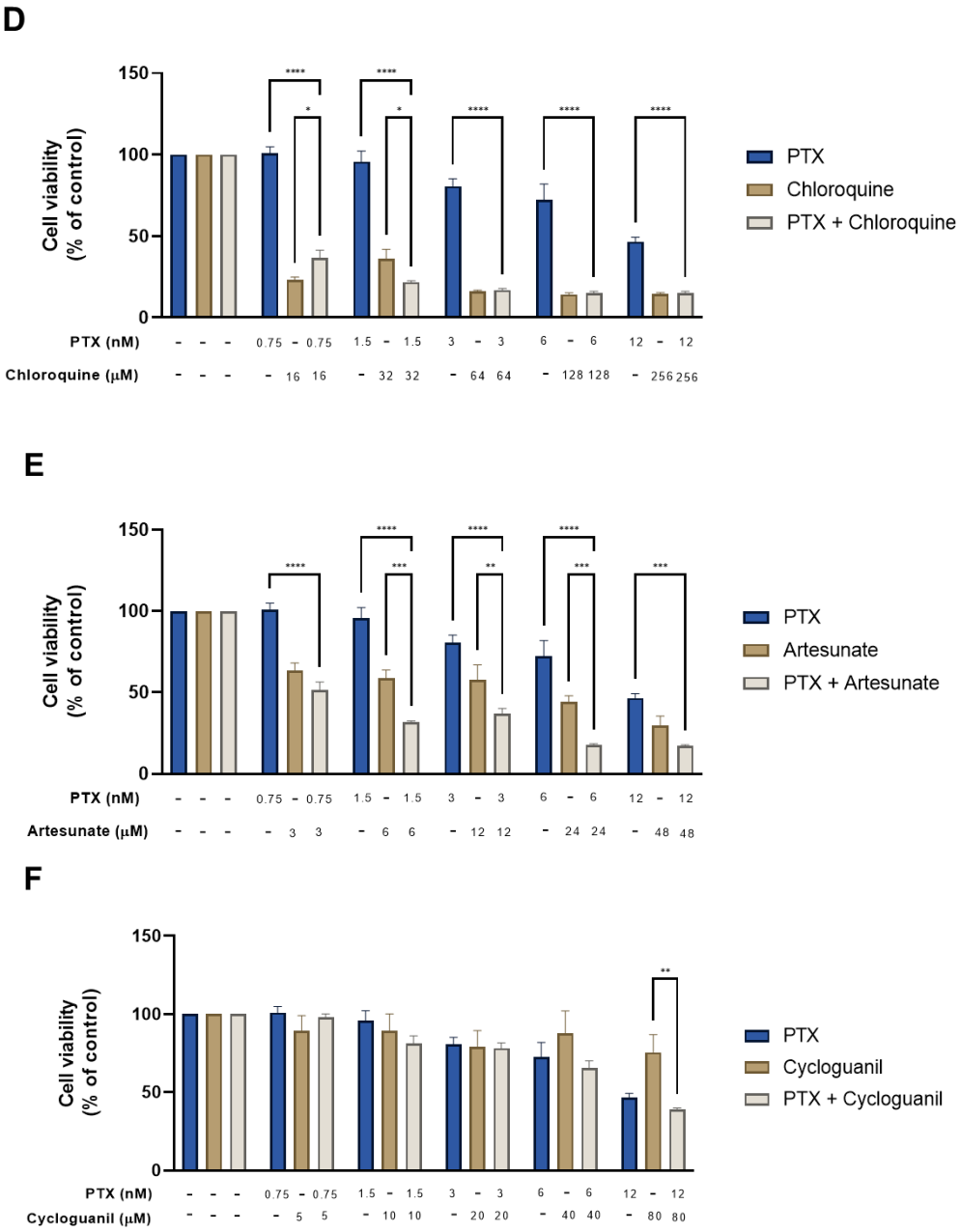

Figure 27. Growth inhibition of MCF-7 cells after 48 h treatment with a combination of PTX plus (**A**) mefloquine, (**B**) pyronaridine, (**C**) tafenoquine, (**D**) chloroquine, (**E**) artesunate, and (**F**) cycloguanil. Cells were exposed to concentrations of each drug of 0.25, 0.5, 1, 2, and 4 times their $IC_{50,}$ and cell viability was evaluated by MTT assay. The drugs in combination were co-administered at the same time. Values are expressed in percentage and represent mean ± SEM. Each experiment was done three times independently (n = 3); *statistically significant at $p < 0.05$. **statistically significant at $p < 0.01$. ***statistically significant at $p < 0.001$. ****statistically significant at $p < 0.0001$.

Taken together, these results demonstrate that some antimalarial drugs, such as artesunate, pyronaridine, and chloroquine, in combination can improve the anti-cancer activity of DOX or PTX in ER-positive breast cancer cells.

Compared to the previous results, the combination of antimalarial drugs with DOX seems to be preferable compared to the combination with PTX, with chloroquine and artesunate being promising antimalarial drugs to be used in combination with both antineoplastic drugs. These results also imply that some antimalarial drugs may act as chemosensitizing compounds for enhancing the cytotoxic effects of DOX or PTX in MCF-7 cells.

5.1.1.2 Combination of DOX or PTX + CNS Drugs in MCF-7 Cells

Next, the cytotoxic effect of the most promising CNS drugs in combination with PTX and DOX was evaluated. This time, the drugs thioridazine, benztropine, fluoxetine, fluphenazine, and sertraline were selected for evaluation in combination regimens, based on the results previously obtained in Chapter I that demonstrated these drugs to be the most promising candidates (IC_{50} under 25 µM) for drug repurposing.

After determining the IC_{50} value of each CNS drug in MCF-7 breast cancer cells in Chapter I, they were combined with increasing concentrations of DOX or PTX for 48 h, following the same experimental protocol described in Figure 25. This time, the obtained results were supported by two cell-based assays: MTT and SRB. Morphological evaluation of cells treated with each drug alone and in combination was also done.

Co-treatment of MCF-7 cells with fluoxetine and DOX at concentrations of IC_{50} demonstrated significant cytotoxicity, resulting in a decrease in cell viability compared to the treatments with DOX and fluoxetine alone (Figure 28A). No significant differences in the cellular protein content were observed in cells co-treated with fluoxetine and DOX (Figure 28B). The combination of sertraline and DOX proved to be less effective in promoting cytotoxic effects than each drug alone, for all concentrations tested, both by MTT and SRB assays (Figure 28C and D). Co-treatment of thioridazine with DOX proved to be effective and significantly different from thioridazine and DOX alone at the concentration of IC_{50} of each drug (Figure 28E). The combination of fluphenazine proved not to be advantageous over each drug alone, both by MTT and SRB (Figure 28G and H). Benztropine combined with DOX at the concentration of IC_{50} resulted in significant cell viability reduction compared to DOX and benztropine alone (Figure 28I). Linear regression analysis of the results obtained by MTT and SRB assays is represented in Figure 29 and demonstrate a good correlation between these assays. Morphologically, all treatments resulted in a lower number of viable cells compared to the control well and treatment with DOX alone (Figure 30).

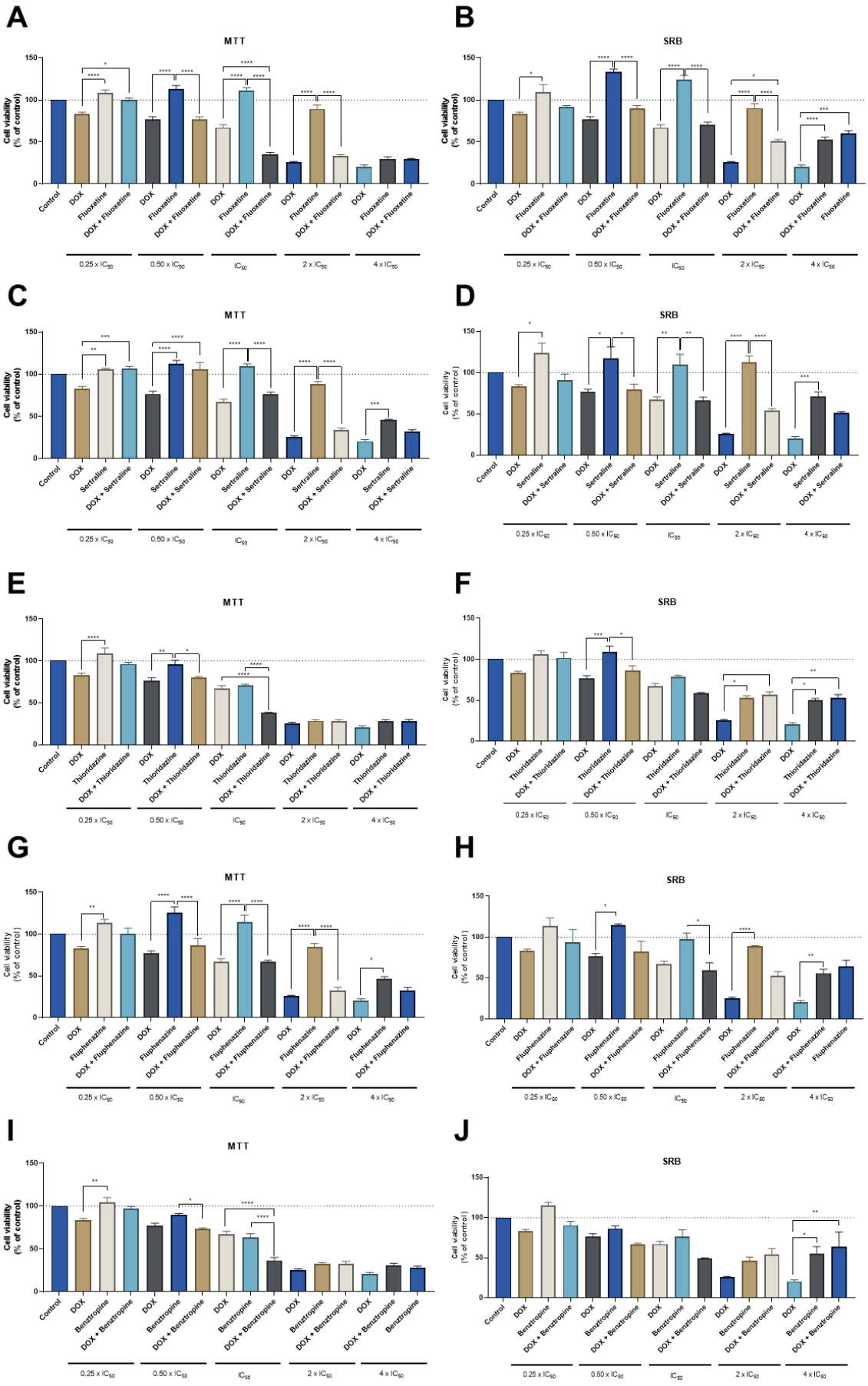
A
MTT
B
SRB
C
MTT
D
SRB
E
MTT
F
SRB
G
MTT
H
SRB
I
MTT
J
SRB
Cell viability (% of control)
Control
DOX
Fluoxetine
DOX + Fluoxetine
Sertraline
DOX + Sertraline
Thioridazine
DOX + Thioridazine
Fluphenazine
DOX + Fluphenazine
Benztropine
DOX + Benztropine
0.25 x IC50
0.50 x IC50
IC50
2 x IC50
4 x IC50

Figure 28. Cell viability of MCF-7 breast cancer cells treated with the combination of different CNS drugs and DOX, by MTT (left) and SRB assays (right). Cultured cells were seeded in 96-well plates and treated with concentrations of each drug of 0.25, 0.5, 1, 2, and 4 times their IC_{50} for 48 h. Cells treated with vehicle (0.1% DMSO) were used as the control. Cell viability was determined after the final treatment by MTT and SRB assays. The drugs were co-administered in combination. (**A**) The effect of DOX + fluoxetine on cell viability and (**B**) cell protein synthesis. (**C**) The effect of DOX + sertraline on cell viability and (**D**) cell protein synthesis. (**E**) The effect of DOX + thioridazine on cell viability and (**F**) cell protein synthesis. (**G**) The effect of DOX + fluphenazine on cell viability and (**H**) cell protein synthesis. (**I**) The effect of DOX plus benztropine on cell viability and (**J**) cell protein synthesis. Each point represents the mean ± SEM relative to the control cells. * Statistically significant at $p < 0.05$. ** Statistically significant at $p < 0.01$. *** Statistically significant at $p < 0.001$. **** Statistically significant at $p < 0.0001$.

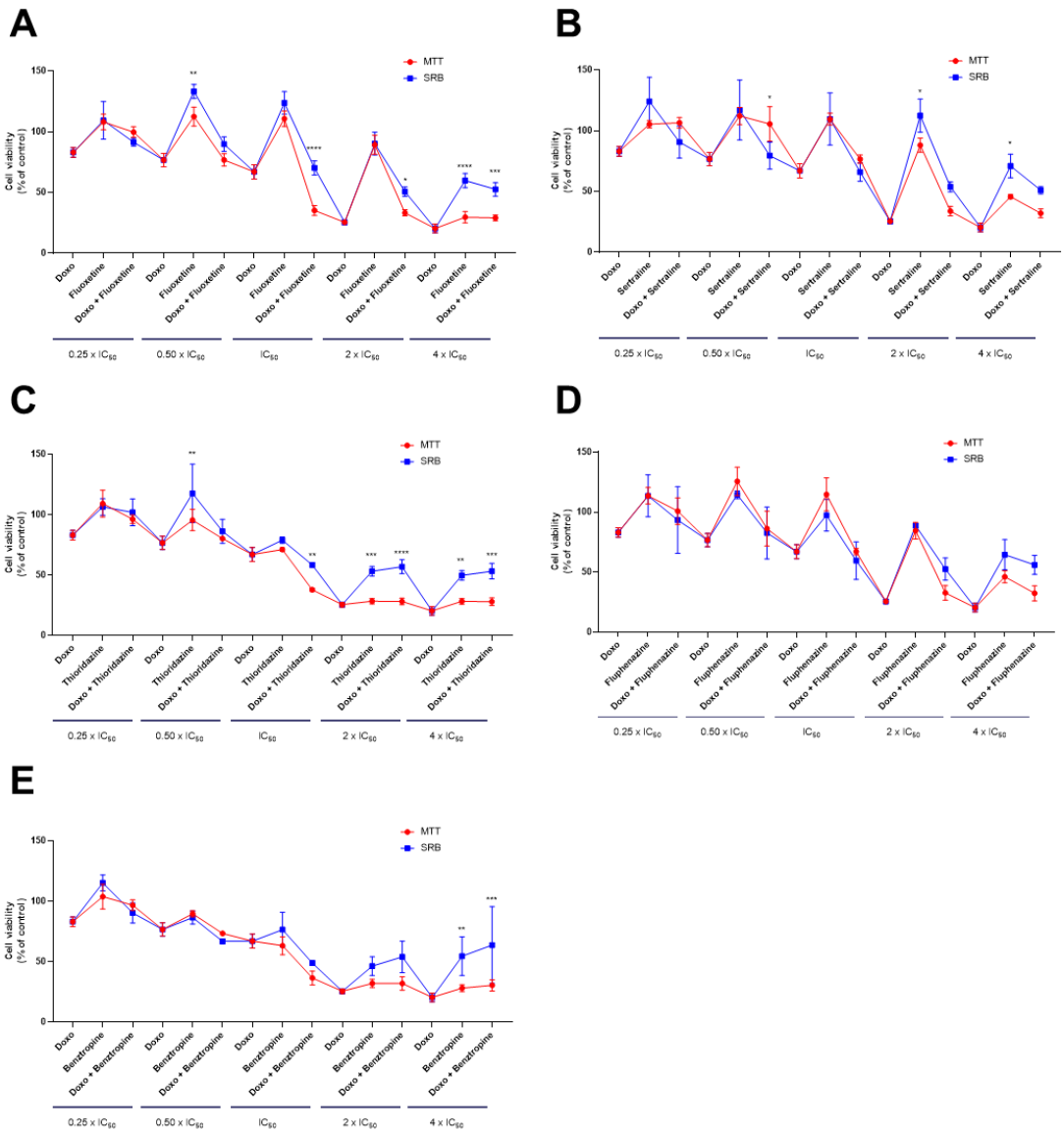

Figure 29. Linear regression analysis of the results obtained by MTT and SRB assays. The effect of (**A**) DOX + fluoxetine (**B**) DOX + sertraline (**C**) DOX + thioridazine (**D**) DOX + fluphenazine and (**E**) DOX + benztropine on cell viability. Each point represents the mean ± SD relative to the control cells. * Statistically significant at *p*

< 0.05. ** statistically significant at $p < 0.01$. *** statistically significant at $p < 0.001$. **** statistically significant at $p < 0.0001$.

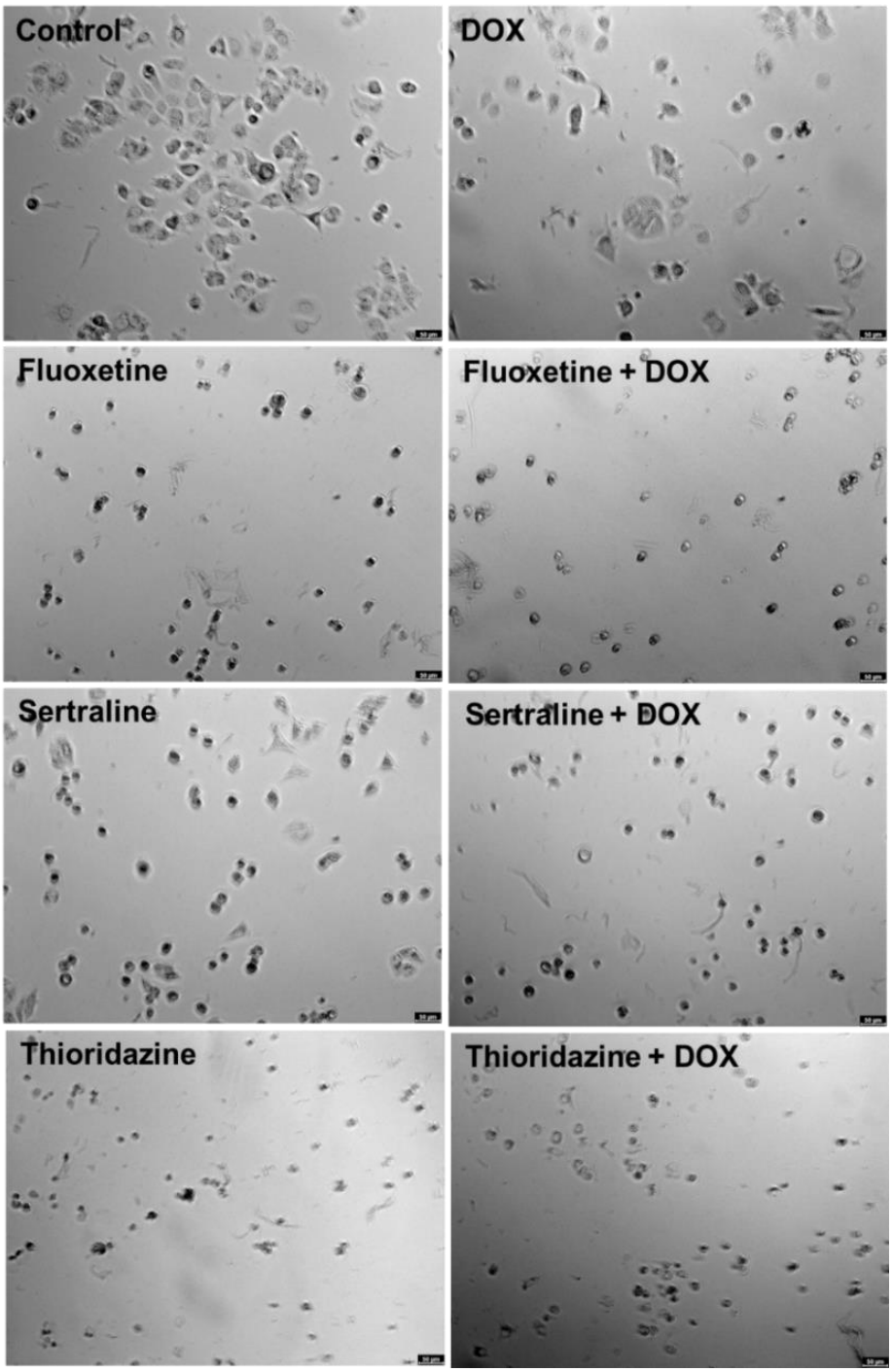

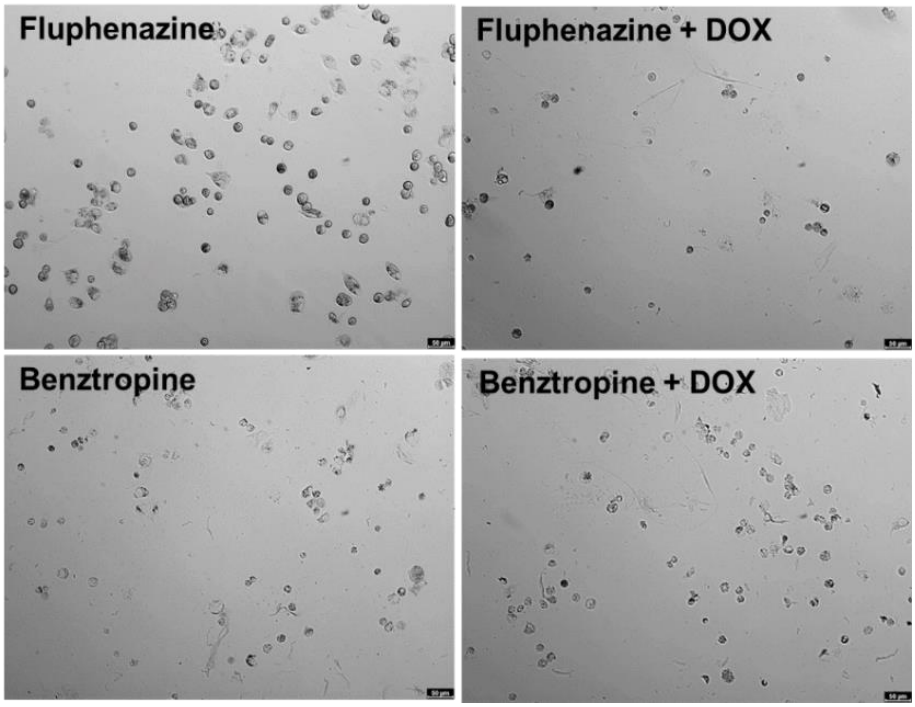

Figure 30. Microscopic cellular visualization of MCF-7 cells after treatment with the combination of different CNS drugs and DOX. Cells treated with vehicle (0.1% DMSO) were used as control. Scale bar: 50 µM.

These results demonstrate that fluoxetine, thioridazine, and benztropine combined with DOX at the concentrations of IC_{50} are the most promising drug pairs to further evaluate mechanistically and for dose adjustment.

Next, the combination of PTX with each CNS drug was also evaluated using the model of combination previously described in Figure 25. This aimed to understand if the choice of the antineoplastic agent could have an influence on the anticancer effects of these drug combinations. The combination of PTX plus fluphenazine, fluoxetine, benztropine, thioridazine, and sertraline was evaluated by MTT and SRB assays, as well as morphological analysis.

In combination with PTX, fluoxetine demonstrates significant anti-cancer effects both by MTT and SRB assays (Figure 31A and B, respectively), mainly at the concentration of 2 × $IC_{50,}$ where the combined effect was statistically significant compared to each drug alone. The combination with sertraline resulted in a similar reduction of cell viability and cell protein synthesis as PTX alone, at all concentrations. At the concentrations of IC_{50} and 2 × IC_{50}, the combination of PTX plus sertraline demonstrated significative anticancer effects compared to sertraline alone (Figures 31C and D). The combination with PTX and thioridazine demonstrated significant anticancer effects compared to both drugs alone, at

the concentration of IC_{50} (Figure 31E and F). The combination with fluphenazine resulted in all intermediate concentrations showing a greater anticancer effect than fluphenazine alone (Figure 31G and H). The activity seen for these combinations can be the result of the strong anticancer activity of PTX alone. The combination with benztropine resulted in a statistically significant reduction of cell viability at the concentration of IC_{50} compared to both drugs alone, and at the concentration of 2 × IC_{50} compared to PTX alone (Figure 31I and J), demonstrating that the activity of this combination can be the result of the repurposed drug alone, contrary to the previous combinations. Together, these results demonstrate that both CNS drugs and PTX can contribute to different pharmacological effects in the combined treatments. Morphologically, the results are in agreement with the MTT and SRB assays. At concentrations of 4 × IC_{50}, all combinations resulted in a decrease in cell number and smaller and rounder cells, compared to control cells and PTX, indicative of cell death (Figure 32).

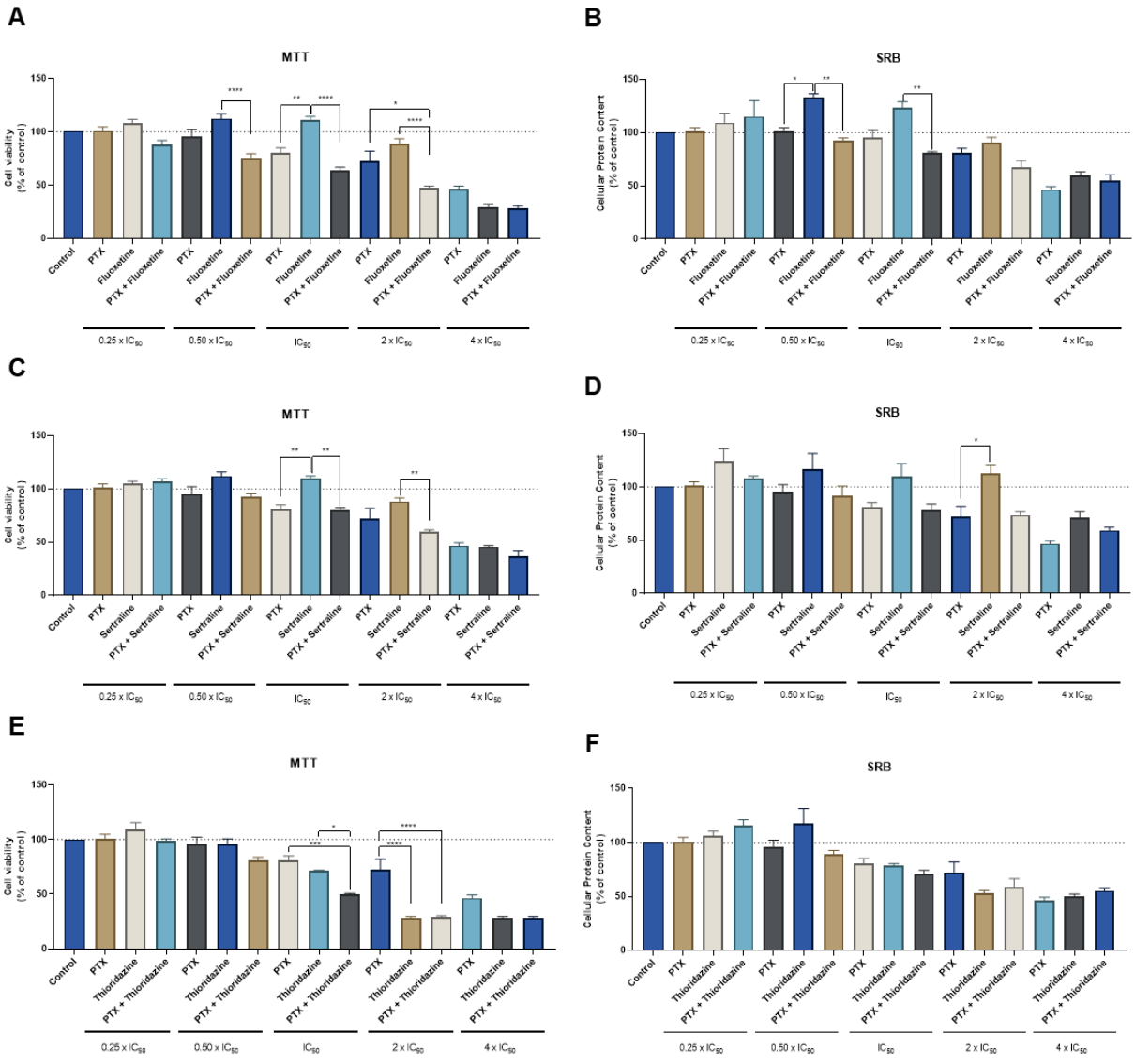

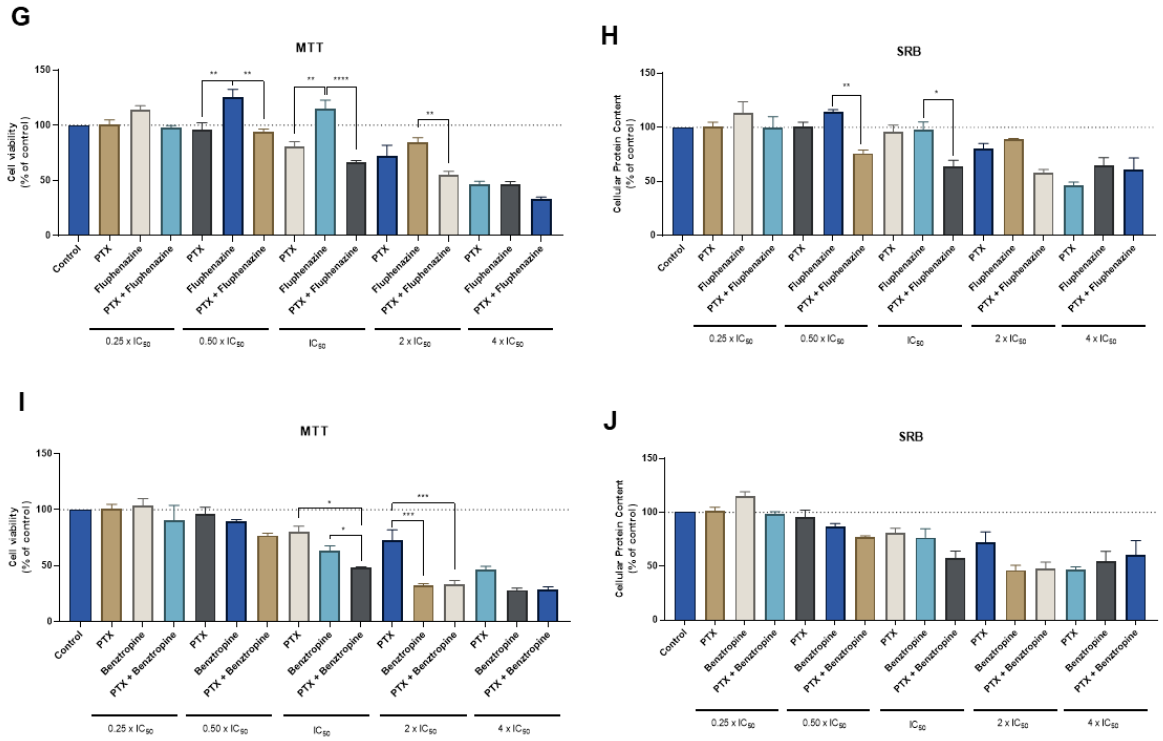

Figure 31. Growth inhibition of MCF-7 after 48 h of combination therapy with PTX, by MTT (**left**) and SRB assays (**right**). Cells were exposed to concentrations of each drug of 0.25, 0.5, 1, 2, and 4 times their IC_{50}, and the cell viability was evaluated by MTT and SRB assays. The drugs in combination were co-administered at the same time. (**A**) The effect of PTX plus fluoxetine on cell viability and (**B**) cell protein synthesis. (**C**) The effect of PTX plus sertraline on cell viability and (**D**) cell protein synthesis. (**E**) The effect of PTX plus thioridazine on cell viability and (**F**) cell protein synthesis. (**G**) The effect of PTX plus fluphenazine on cell viability and (**H**) cell protein synthesis. (**I**) The effect of PTX plus benztropine on cell viability and (**J**) cell protein synthesis. Values are expressed in percentage of control and represent mean ± SEM. Each experiment was done three times independently (n = 3); * statistically significant at $p < 0.05$. ** statistically significant at $p < 0.01$. *** statistically significant at $p < 0.001$. **** statistically significant at $p < 0.0001$.

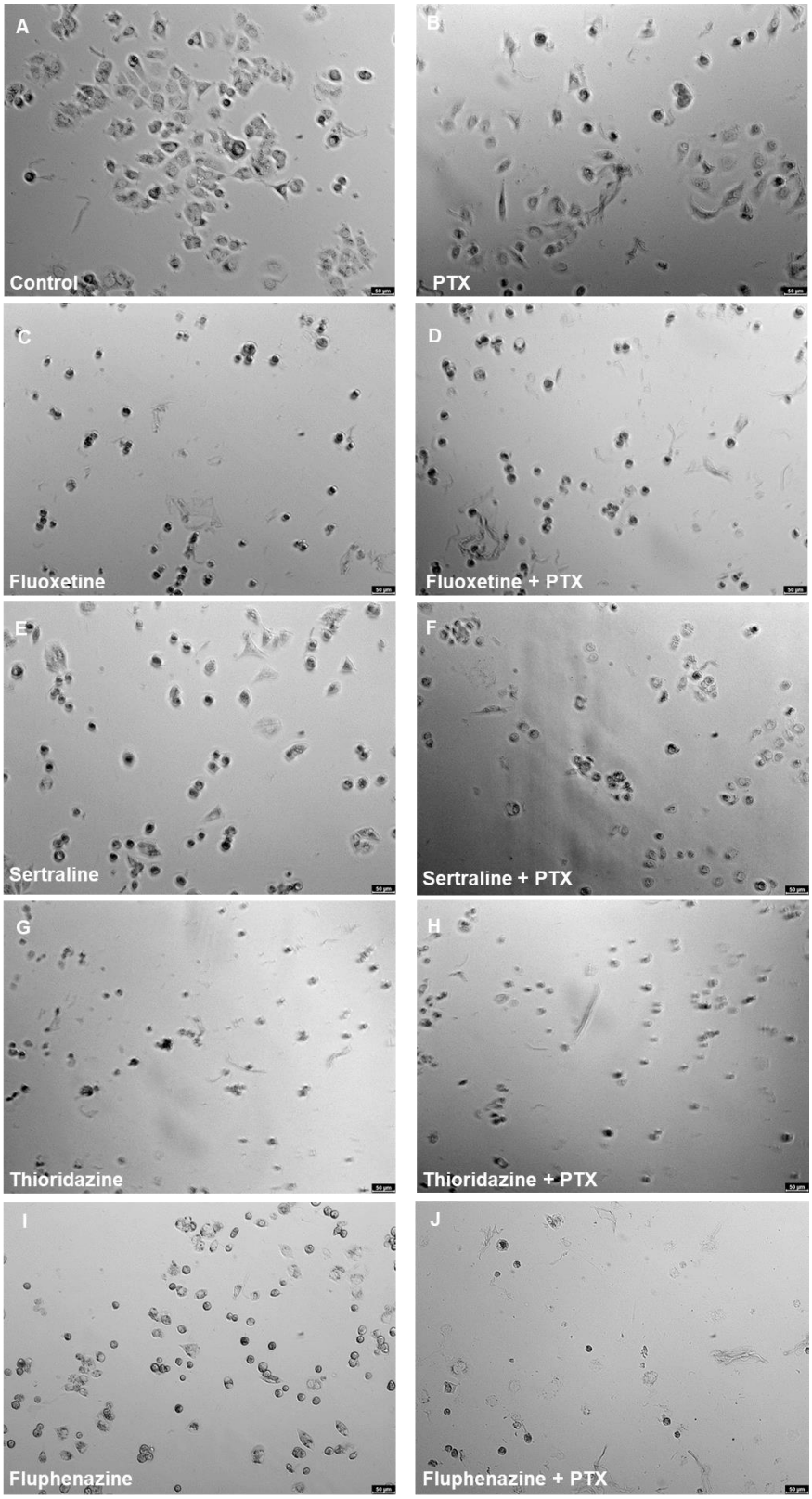

Figure 32. Microscopic cellular visualization of MCF-7 cells after 48 h of incubation with vehicle (**A**), PTX (**B**), fluoxetine (**C**), fluoxetine + PTX (**D**), sertraline (**E**), sertraline + PTX (**F**), thioridazine (**G**), thioridazine + PTX (**H**), fluphenazine (**I**) fluphenazine + PTX (**J**), benztropine (**K**) and benztropine + PTX (**L**) at concentrations of 4 × IC_{50} of each drug. Scale bar: 50 µm.

Compared to our previous results, these findings demonstrate that the combination of CNS agents with PTX has an anticancer potential similar to the combination with DOX. Nevertheless, as lower doses of PTX are necessary to exert similar therapeutic effects (as demonstrated by the IC_{50} of this drug), the combination of CNS drugs with this antineoplastic drug seems preferable than the combination with DOX.

Although the previous results from Chapter I demonstrated that quetiapine and edaravone were not adequate to be used as standalone agents for breast cancer therapy, their use as possible adjuvant agents in combination therapies was still investigated.

Therefore, the combination of PTX and DOX with edaravone and quetiapine was evaluated, to determine whether these repurposed drugs could effectively enhance the anticancer activity of these chemotherapeutic drugs. To do so, increasing concentrations (0.01–100 μM) of edaravone and quetiapine were combined with the IC_{50} values of PTX and DOX. Cell viability was assessed by an MTT assay as well as morphological evaluation.

The results regarding the combination of DOX plus edaravone are shown in Figure 33. Analyzing the morphological results (Figure 33A) and MTT results (Figure 33B), it was found that the combined effects of edaravone and DOX were very similar to the effect of DOX alone, for all concentrations, demonstrating that the cytotoxic effect seen for these combinations may be a result of the strong anticancer activity of DOX alone. The same conclusions can be applied to the combination of edaravone with PTX (Figure 34).

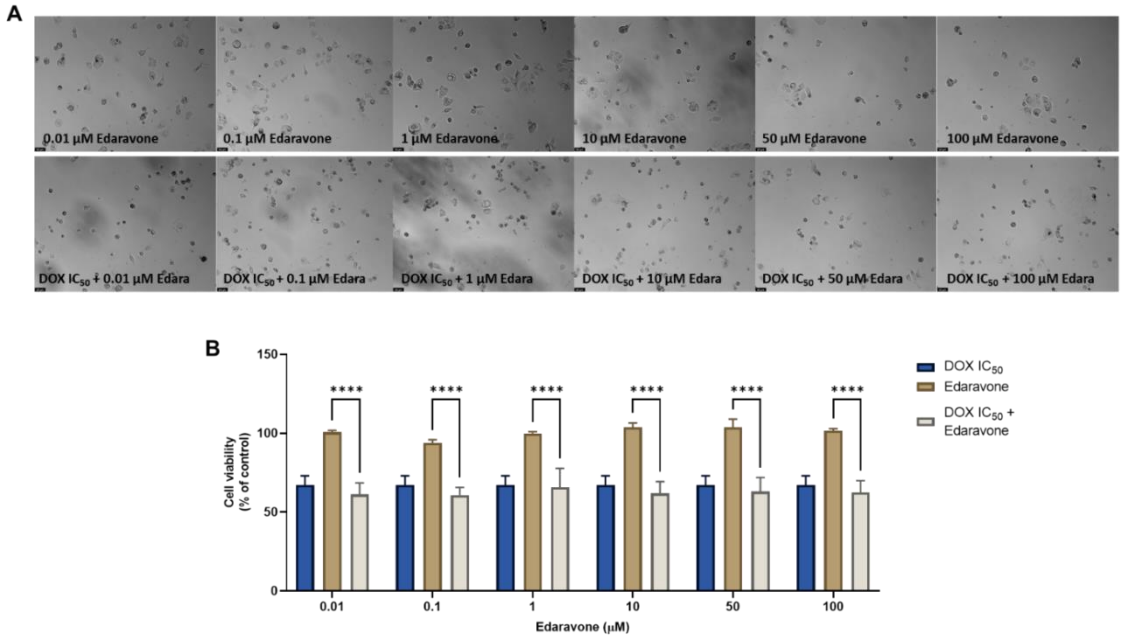

Figure 33. Morphological analysis (**A**) and cellular viability (**B**) results of MCF-7 cells after a single and combined treatment of DOX and edaravone. Cells were incubated with increasing concentrations of edaravone, alone and

combined with a fixed concentration (IC_{50}) of DOX for 48 h. Cell viability was evaluated using an MTT assay. Experiments were performed three times independently (n = 3). **** indicate significative results at $p < 0.0001$. Edara: edaravone

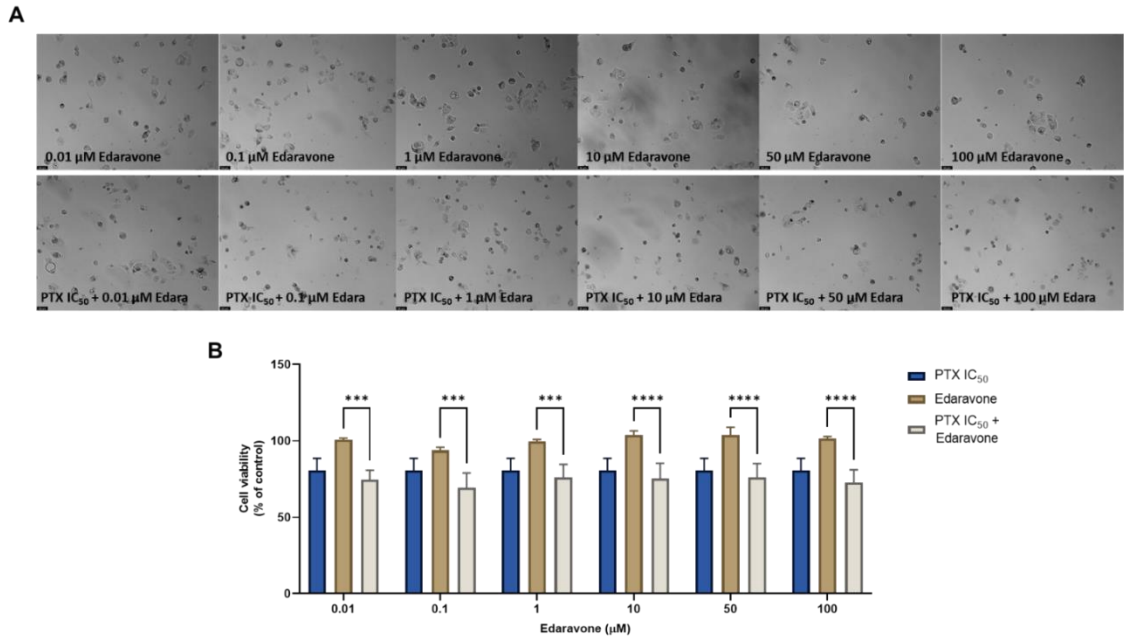

Figure 34. Morphological analysis (**A**) and cellular viability (**B**) results of MCF-7 cells after a single and combined treatment of PTX and edaravone. Cells were incubated with increasing concentrations of edaravone, alone and combined with a fixed concentration (IC_{50}) of PTX for 48 h. Cell viability was evaluated using an MTT assay. Experiments were performed three times independently (n = 3). *** and **** indicate significative results at $p < 0.001$ and $p < 0.0001$, respectively. Edara: edaravone

On the other hand, the combination of quetiapine and DOX revealed significant morphological changes in the cell structure and cell number of the MCF-7 cells (Figure 35A). These observations were compatible with the results obtained by the MTT assay (Figure 35B), where a significative reduction was found in the cell viability of the MCF-7 cells treated with the combination of DOX plus 0.1, 1, 10, and 50 µM of quetiapine compared with both drugs alone, demonstrating the promising anticancer profile of this drug combination against this cell line.

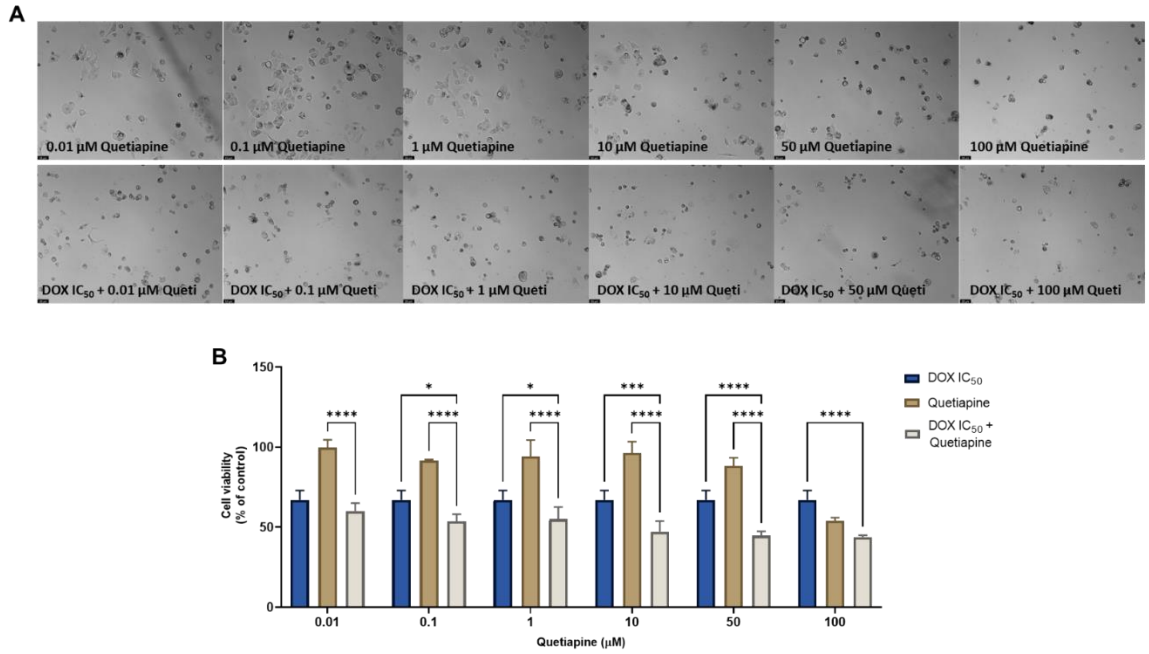

Figure 35. Morphological analysis (**A**) and cellular viability (**B**) results of MCF-7 cells after a single and combined treatment with DOX and quetiapine. Cells were incubated with increasing concentrations of quetiapine, alone and combined with a fixed concentration (IC_{50}) of DOX for 48 h. Cell viability was evaluated using an MTT assay. Experiments were performed three times independently (n = 3). *, *** and **** indicate significative results at $p < 0.05$, $p < 0.001$ and $p < 0.0001$, respectively. Queti: quetiapine

Regarding the combination of PTX + quetiapine, it was found this drug combination does not induce significant anticancer effects compared to PTX alone, either in the morphological analysis (Figure 36A) or in the MTT assay (Figure 36B), demonstrating only a significant reduction in cell viability in comparison with quetiapine alone. These results demonstrate the anticancer effect of the combination is mainly attributed to the anticancer activity of the antineoplastic drug.

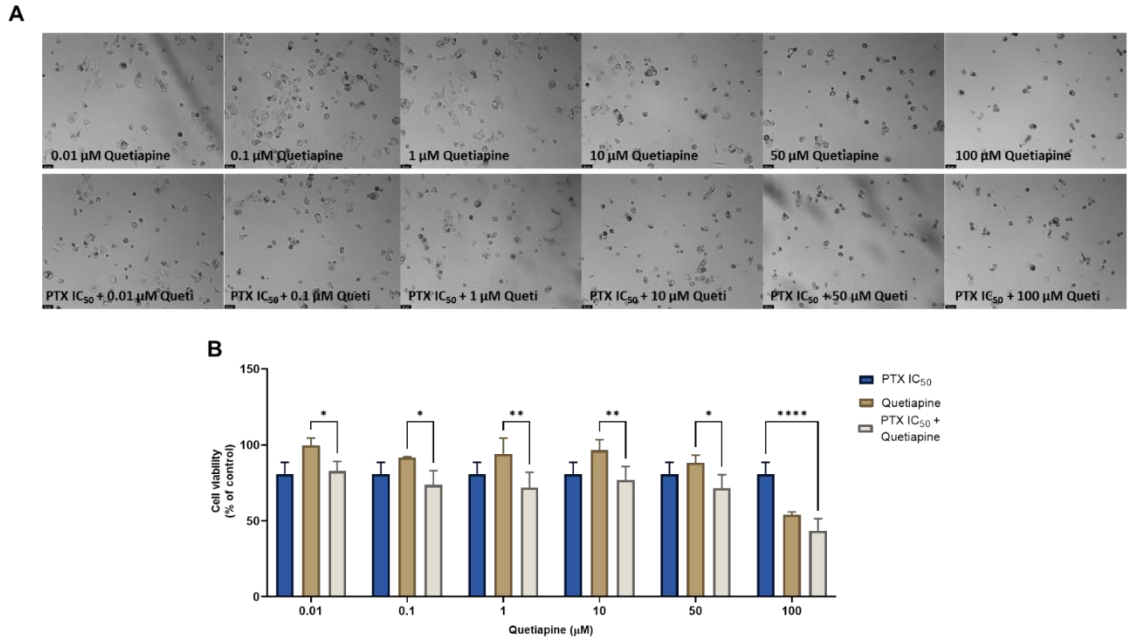

Figure 36. Morphological analysis (**A**) and cellular viability (**B**) results of MCF-7 cells after a single and combined treatment of PTX and quetiapine. Cells were incubated with increasing concentrations of quetiapine, alone and combined with a fixed concentration (IC_{50}) of PTX for 48 h. Cell viability was evaluated using an MTT assay. Experiments were performed three times independently ($n = 3$). *, ** and **** indicate significative results at $p < 0.05$, $p < 0.01$ and $p < 0.0001$, respectively. Queti: quetiapine

5.1.2 Combination Model II: Repurposed Drug + Repurposed Drug in Breast Cancer

Next, we aimed to develop a new model of drug combination consisting of two repurposed drugs. We selected repurposed drugs with promising anticancer profiles, taking into account the previous results regarding the screening of repurposed drugs with anticancer potential (Chapter I).

These drugs were selected based on their IC_{50}, assuming that the lower this value, the more their anticancer potential. We selected the two CNS and the two antimalarial drugs with the lowest IC_{50} values, to confirm the viability of this model of combination for application in breast cancer therapy.

This model of combination consisted in fixing the dose of one drug and varying the dose of the other drug. To do so, MCF-7 cells were treated with the combinations of fluphenazine plus sertraline (and vice-versa), and with the combination of mefloquine plus pyronaridine (and vice-versa) for 48 h. Cell morphology and viability were evaluated after each treatment.

First, the combination of mefloquine (IC_{50}) with increasing concentrations of pyronaridine on the cell morphology (Figure 37A) and viability (Figure 37B) of MCF-7 breast cancer cells was evaluated. The results demonstrate that this combination is not advantageous over mefloquine at all concentrations of pyronaridine, with mefloquine alone causing more than an 80% reduction in cell viability at its IC_{50} value.

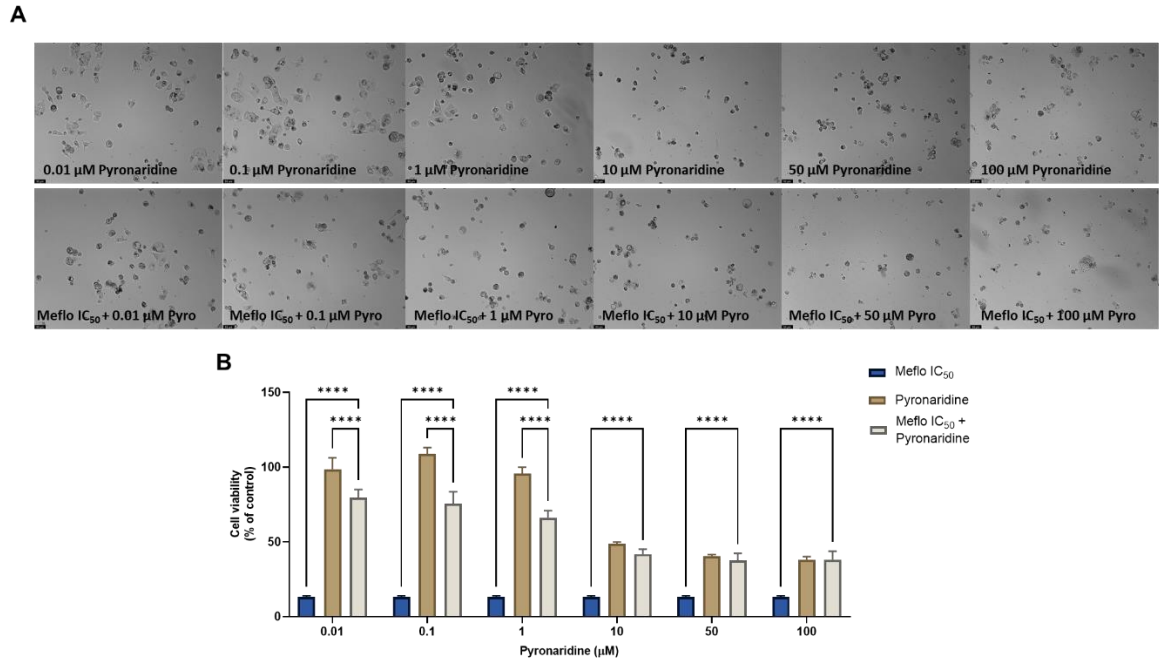

Figure 37. Morphological analysis (**A**) and cellular viability (**B**) results of MCF-7 cells after a single and combined treatment of mefloquine and pyronaridine. Cells were incubated with increasing concentrations of pyronaridine, alone and combined with a fixed concentration (IC_{50}) of mefloquine for 48 h. Cell viability was evaluated using an MTT assay. Experiments were performed three times independently ($n = 3$). **** indicate significative results at $p < 0.0001$. Pyro: pyronaridine; Meflo: mefloquine

Next, the order of the combination was inverted and the dose of pyronaridine was fixed and the concentrations of mefloquine varied. The results of the morphological analysis (Figure 38A) and for cellular viability (Figure 38B) demonstrate that the combination of 0.01, 0.1, and 1 of mefloquine with the IC_{50} for pyronaridine significantly reduced MCF-7 cell viability only when compared with mefloquine alone in these concentrations. No statistically significant combined pairs were found at any concentration compared to the use of both drugs alone, which demonstrates that this combination is not advantageous over single drugs.

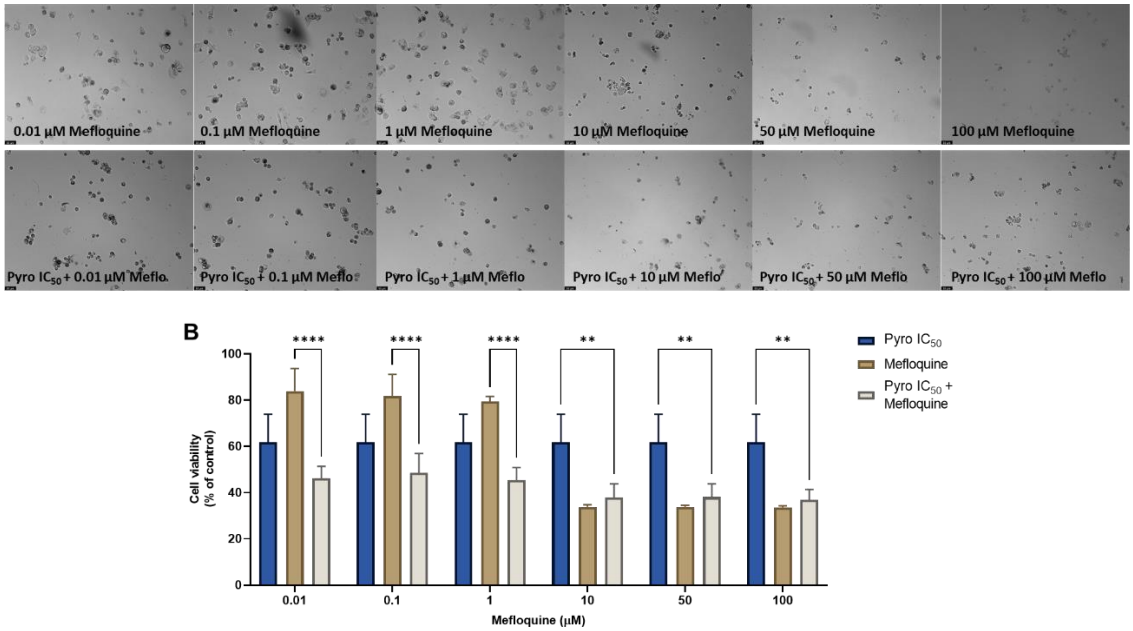

Figure 38. Morphological analysis (**A**) and cellular viability (**B**) results of MCF-7 cells after a single and combined treatment of pyronaridine and mefloquine. Cells were incubated with increasing concentrations of mefloquine, alone and combined with a fixed concentration (IC_{50}) of pyronaridine for 48 h. Cell viability was evaluated using an MTT assay. Experiments were performed three times independently (n = 3). ** and **** indicate significative results at $p < 0.01$ and $p < 0.0001$, respectively. Pyro: pyronaridine; Meflo: mefloquine

The same combination model previously described was then performed using the CNS drugs fluphenazine and sertraline. The results regarding the combination of sertraline IC_{50} and fluphenazine (0.01–100 µM) are shown in Figure 39. The results of the cell morphological analysis (Figure 39A) and MTT assay (Figure 39B) demonstrate this combination induced significant toxicity compared with sertraline alone, suggesting that the combined effect must be a result of the cytotoxicity of fluphenazine. The same conclusions can be applied to the inverse combination of fluphenazine IC_{50} and variable concentrations of sertraline (Figure 40), where it was found that the observed effect after the drug combination treatment is practically equal to the treatment with sertraline alone.

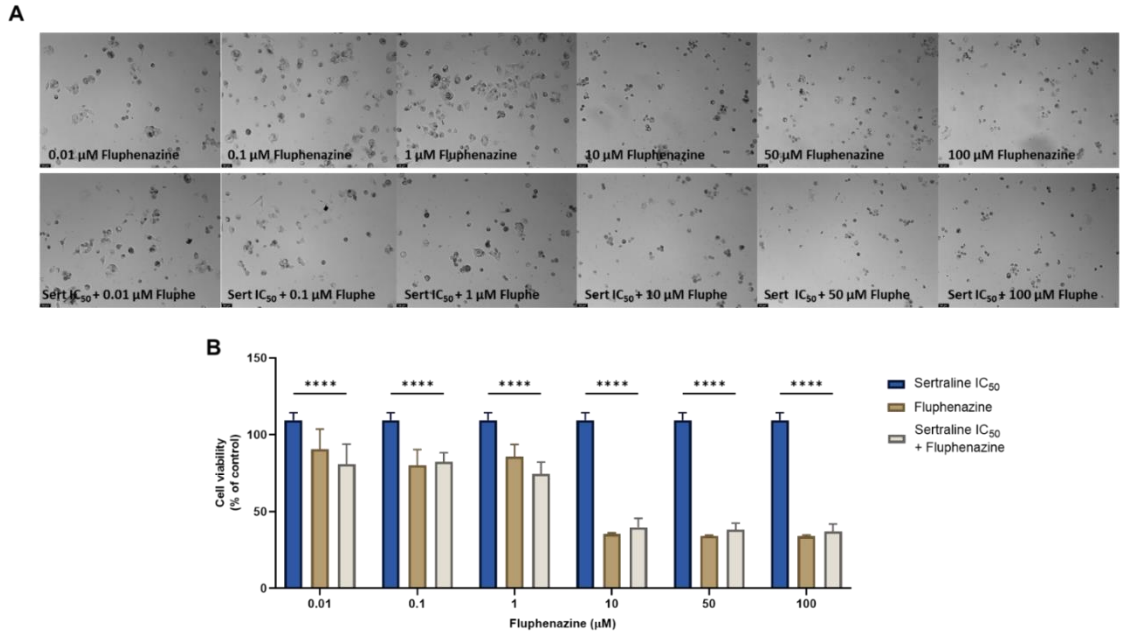

Figure 39. Morphological analysis (A) and cellular viability (B) results of MCF-7 cells after a single and combined treatment of fluphenazine and sertraline. Cells were incubated with increasing concentrations of fluphenazine, alone and combined with a fixed concentration (IC_{50}) of sertraline for 48 h. Cell viability was evaluated using an MTT assay. Experiments were performed three times independently (n = 3). **** indicate significative results at $p < 0.0001$. Fluphe: fluphenazine; Sert: sertraline

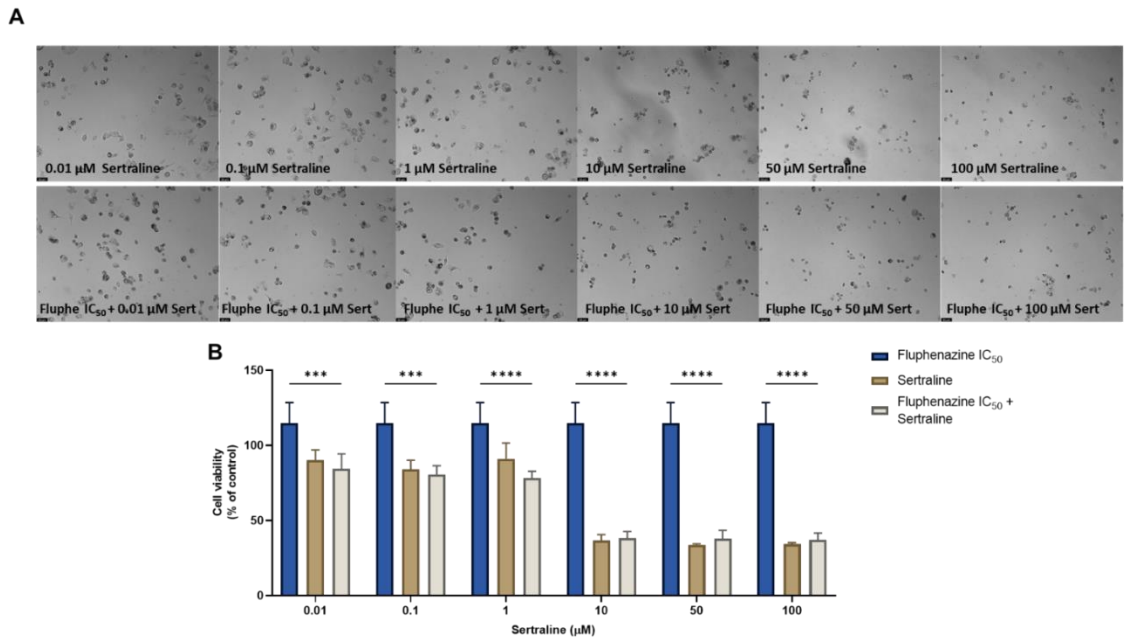

Figure 40. Morphological analysis (**A**) and cellular viability (**B**) results of MCF-7 cells after a single and combined treatment of sertraline and fluphenazine. Cells were incubated with increasing concentrations of sertraline, alone and combined with a fixed concentration (IC_{50}) of fluphenazine for 48 h. Cell viability was evaluated using an MTT assay. Experiments were performed three times independently (n = 3). *** and **** indicate significative results at $p < 0.001$ and $p < 0.0001$, respectively. Fluphe: fluphenazine; Sert: sertraline

5.1.3 Combination Model III: Peptides + Antineoplastic Drugs in Breast Cancer

After demonstrating that repurposed drugs can have promising anticancer potential in combination with chemotherapeutic drugs, it was decided to explore if other molecules, such as peptides, could also enhance the cytotoxic effect of antineoplastic agents. Therefore, the anticancer effects of Melittin (the most abundant peptide in honeybee venom) in combination with DOX were evaluated in breast cancer cells.

Honeybees secrete bee venom from a highly specific venom gland connected to the venom reservoir located in the abdominal cavity. Mainly composed of water, with a composition of 80%, bee venom is a complex mixture containing at least 18 pharmacological active compounds, which includes peptides like melittin, apamin, mast cell degranulating peptides, adolapin, enzymes such as phospholipase A2 and hyaluronidase, bioactive amines such as histamine and dopamine, amino acids, minerals and volatile compounds [390]. With a long tradition of applications in natural medicines to treat diseases such as arthritis, rheumatism, pain, tumors, and skin diseases, several studies describe the therapeutic potential of bee venom components as anti-inflammatory, anti-viral, and anti-cancer [390, 391]. Moreover, recent research also correlates bee venom to a variety of cancer management effects including induction of apoptosis, necrosis, cytotoxicity, and inhibition of proliferation in different cancer types, including prostate, breast, lung, liver, and bladder [391]. The rich composition in venom peptides, which are described to exhibit high specificity and selectivity towards cancer cells, with effects on cell proliferation, invasion, migration, and angiogenesis, as well as modulating immune responses [392], shows the increased potential of bee venom for targeted cancer therapy.

Here, a honeybee venom sample was chemically characterized and the differential modulations of the treatments with chemotherapeutics combined with honeybee venom on the cellular viability of MCF-7 breast cancer cells were investigated.

It was designed a combination model consisting of increasing concentrations of honeybee venom plus a fixed dose of a chemotherapeutic agent. DOX was used as a reference drug for MCF-7 cancer cells. Specifically, it was designed a combination model with variable doses (6.25–100 µg/mL) of honeybee venom combined with a fixed dose (IC_{50} value) of DOX. Cells were treated with each combination for 48 h and cell viability was evaluated by MTT and SRB assays. Morphology analysis was also performed in parallel with these cell-based assays.

The aim of this combination model was to find other compounds rather than repurposed drugs that also have the ability to enhance the anti-tumor effect of chemotherapeutic drugs for breast cancer therapy. This was achieved using a combination model consisting of a natural compound plus a therapeutic drug, instead of using two therapeutic drugs, as is usually done in drug combination studies for combatting cancer.

This work was initiated by the chemical characterization of the honeybee venom from *Apis mellifera iberiensis*, which is shown in Figure 41.

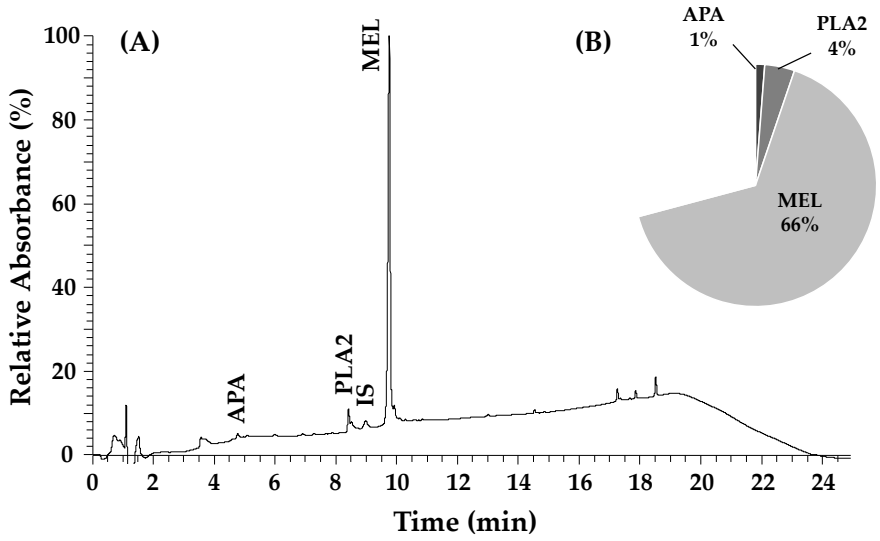

Figure 41. (**A**) Chromatographic profile of Apis mellifera iberiensis venom at 220 nm; (**B**) quantification of the main compounds of the honeybee venom; APA: apamim; PLA2: phospholipase A2; IS: internal standard (cytochrome c, 25 µg/mL); MEL: melittin.

These results demonstrated that the peptide melittin was the most abundant compound with a concentration of 65.6 ± 0.3%, followed by the enzyme phospholipase A2, with 4.0 ± 0.2%, and the peptide apamin with 1.2 ± 0.1%. Indeed, melittin has been reported by different authors as the main constituent of bee venom, accounting for 40–50% of its total dry weight [381, 391].

After the characterization of the honeybee venom, the anti-cancer effect of honeybee venom was analyzed in MCF-7 cells for 48 h and it was found that this compound was able to effectively reduce the cell viability of these cancer cells significantly in concentrations above 25 µg/mL (Figure 42A). This compound was also able to reduce the

cellular protein content of MCF-7 breast cancer cells in concentrations above 12.5 µg/mL (Figure 42B). Based on MTT results, a dose-response curve was plotted and the IC_{50} was calculated, giving a value of 12.18 µg/mL (Figure 42C).

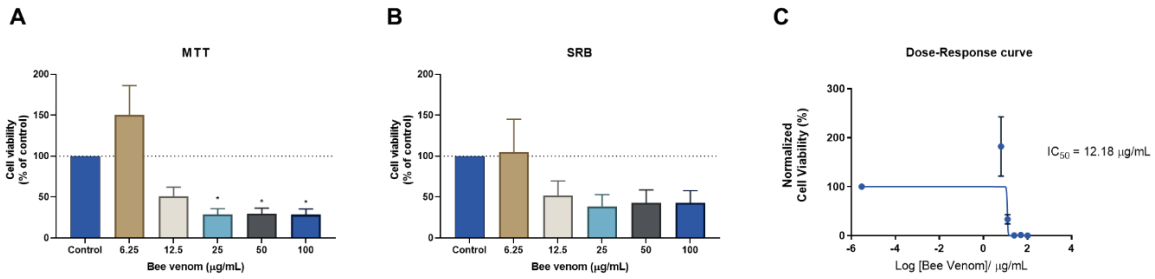

Figure 42. Cell viability of MCF-7 breast cancer cells treated with honeybee venom. (**A**) MTT assay, (**B**) SRB assay, and (**C**) the dose-response curve of MCF-7 cells cultured in 96-well plates and treated with increasing concentrations (6.25–100 µg/mL) of honeybee venom for 48 h. The dose-response curve was obtained by non-linear regression after the normalization of cell viability values. Each point represents the mean ± SEM relative to the control cells (0.1% DMSO) of three independent experiences. * Statistically significant vs. control at $p < 0.05$.

Next, MCF-7 breast cancer cells were treated with different combinations of DOX plus honeybee venom. This combination model included the treatment of cells with increasing concentrations of honeybee venom plus the IC_{50} value of DOX. The combination of DOX with bee venom did not result in significant improvements compared to DOX and bee venom alone, as demonstrated in the morphological analysis (Figure 43A), MTT (Figure 43B), and SRB (Figure 43C) assays.

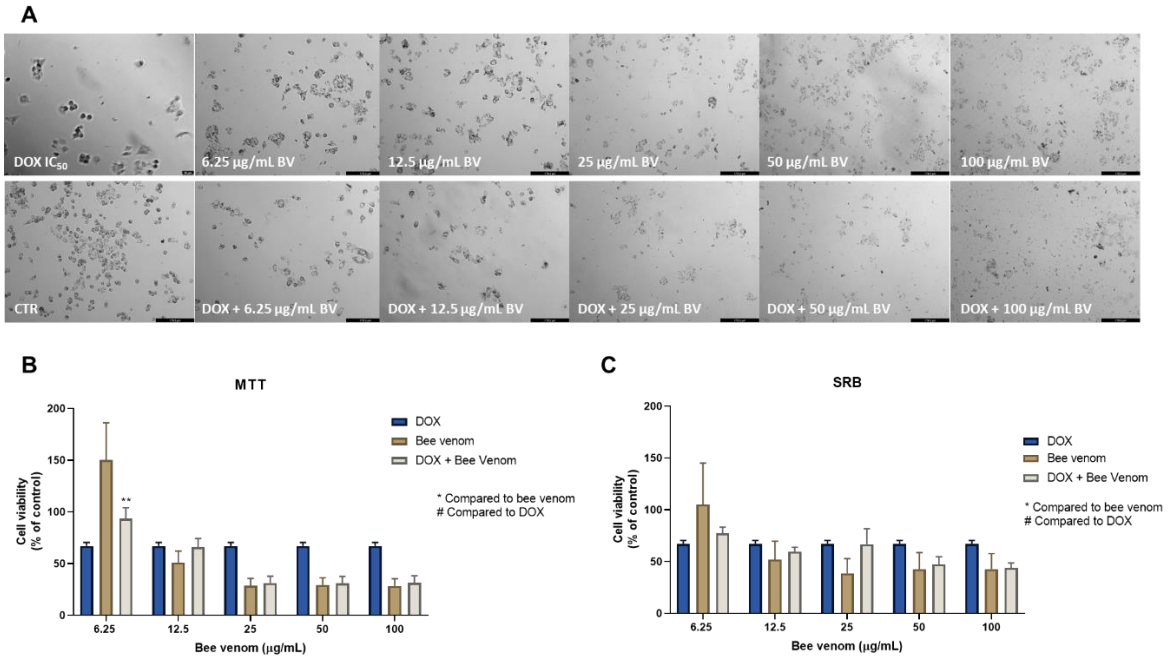

Figure 43. Effect of honeybee venom combined with DOX in MCF-7 breast cancer cells. (**A**) Morphological analysis; (**B**) MTT and (**C**) SRB assays. MCF-7 cells were cultured in 96-well plates and treated with each combination for 48 h. Cell viability was determined after the final treatment. Each point represents the mean ± SEM relative to the control cells (0.1% DMSO) of three independent experiences. ** Statistically significant vs. bee venom at $p < 0.01$; Scale bar: 179.3 µm; BV: bee venom.

Taken together, these results demonstrate that we successfully chemically characterized a honeybee venom sample from *Apis mellifera iberiensis*. Moreover, it was found that the peptide melittin was the most abundant compound in this sample, as reported by other authors. The cytotoxic evaluation of honeybee venom revealed that this compound has anti-cancer activity in the MCF-7 cell line, showing great potential in reducing cell viability even at lower concentrations (below 25 µg/mL). Together, these results support the anti-cancer potential of honeybee venom as a standalone agent in breast cancer.

5.1.4 Combination Model IV: Peptides + Repurposed Drugs in Breast Cancer

As the combination of honeybee venom with DOX did not result in significant improvements over bee venom and DOX alone, it was next decided to evaluate the combination of honeybee venom with four different CNS drugs that have demonstrated good anticancer profiles in Chapter I: fluphenazine, fluoxetine, sertraline, and thioridazine, to further evaluate if this drug class was able to enhance the cytotoxic activity of honeybee venom. This combination model consisted of the treatment of cells with increasing concentrations of honeybee venom plus the IC_{50} value of each repurposed drug.

Co-treatment of fluphenazine and 6.25 µg/mL of honeybee venom resulted in enhanced cell viability reduction, compared to both drugs alone. Higher concentrations of honeybee venom and fluphenazine only resulted in statistical differences compared to fluphenazine alone, demonstrating that the anti-cancer activity of the combination was mainly due to the effect of honeybee venom (Figure 44B). These results are supported by the morphological analysis (Figure 44A). The SRB assay did not demonstrate significant differences in protein cellular content (Figure 44C).

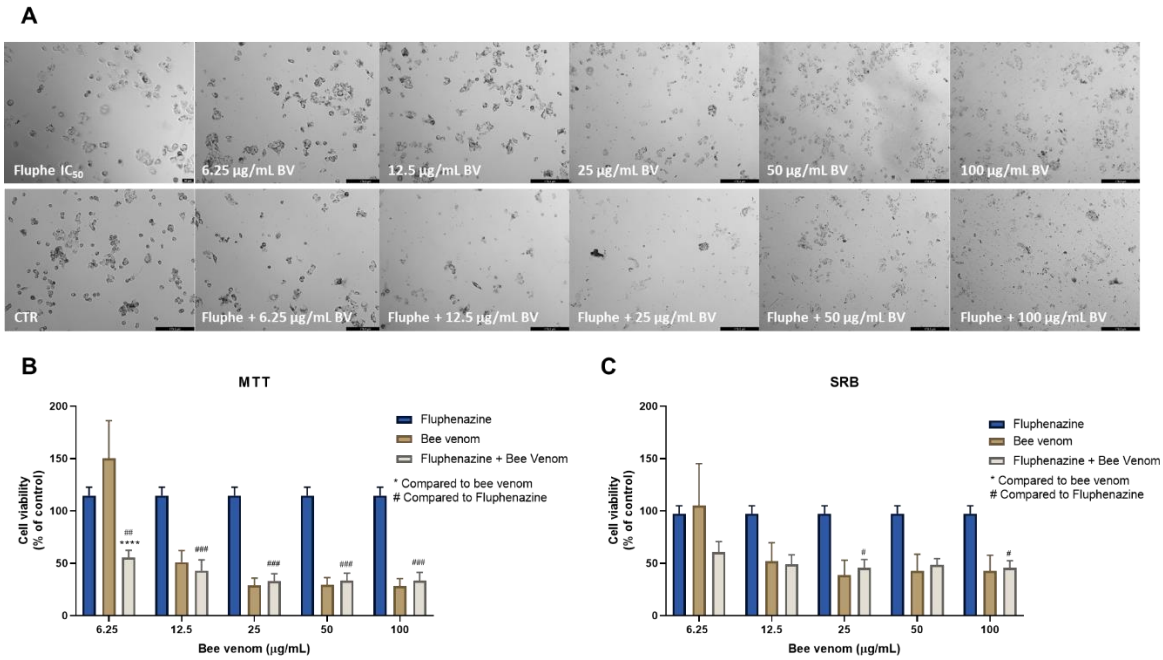

Figure 44. Effect of honeybee venom combined with fluphenazine in MCF-7 breast cancer cells. (**A**) Morphological analysis; (**B**) MTT and (**C**) SRB assays. MCF-7 cells were cultured in 96-well plates and treated with each combination for 48 h. Cell viability was determined after the final treatment. Each point represents the mean ± SEM relative to the control cells (0.1% DMSO) of three independent experiences. **** Statistically significant vs. bee venom at $p < 0.0001$; $^{\#}$ Statistically significant vs. fluphenazine at $p < 0.05$; $^{\#\#}$ Statistically significant vs. fluphenazine at $p < 0.01$; $^{\#\#\#}$ Statistically significant vs. fluphenazine at $p < 0.001$. Scale bar: 179.3 µm; BV: bee venom; Fluphe: fluphenazine

The combination of fluoxetine and sertraline with increasing concentrations of honeybee venom resulted in similar results (Figures 45 and 46, respectively). It was found that these combinations were statistically different from single treatments and effectively reduced MCF-7 cell viability and cellular protein content when 6.25 µg/mL honeybee venom were given in combination with the repurposed drug. These results were also supported by microscopy analysis. When using higher concentrations of bee venom, the observed result was only statistically different from the repurposed drug alone, demonstrating an anti-cancer effect similar to the treatment with bee venom alone.

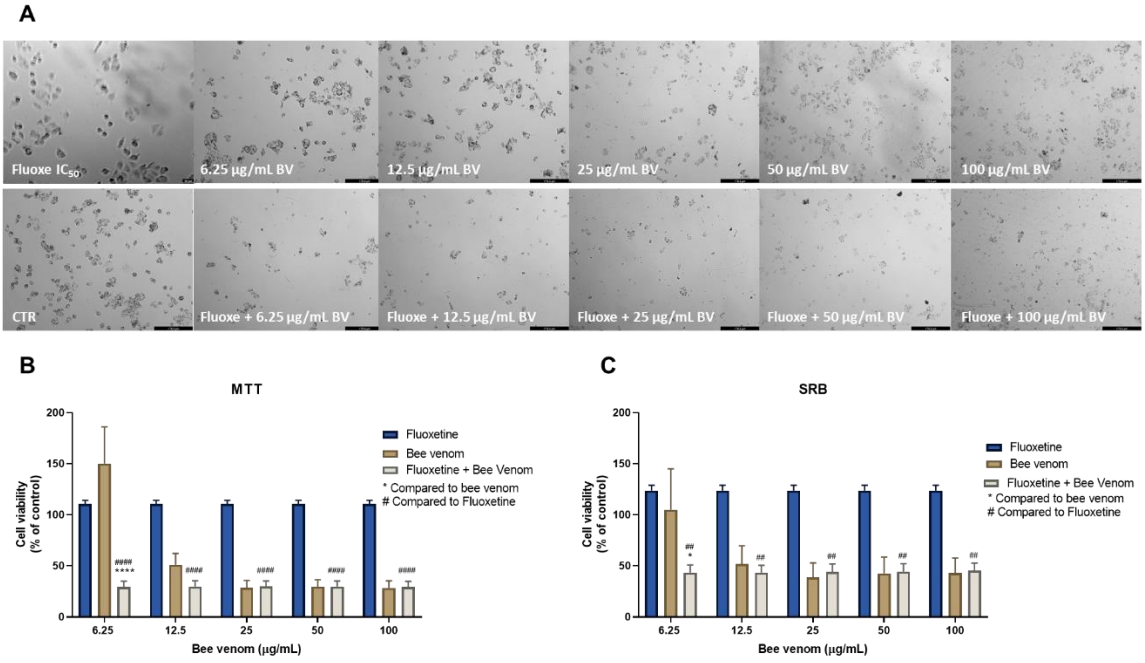

Figure 45. Effect of honeybee venom combined with fluoxetine in MCF-7 breast cancer cells. (**A**) Morphological analysis; (**B**) MTT and (**C**) SRB assays. MCF-7 cells were cultured in 96-well plates and treated with each combination for 48 h. Cell viability was determined after the final treatment. Each point represents the mean ± SEM relative to the control cells (0.1% DMSO) of three independent experiences. * Statistically significant vs. bee venom at $p < 0.05$; **** Statistically significant vs. bee venom at $p < 0.0001$; ## Statistically significant vs. fluoxetine at $p < 0.01$; #### Statistically significant vs. fluoxetine at $p < 0.0001$. Scale bar: 179.3 µm; BV: bee venom; Fluoxe: fluoxetine

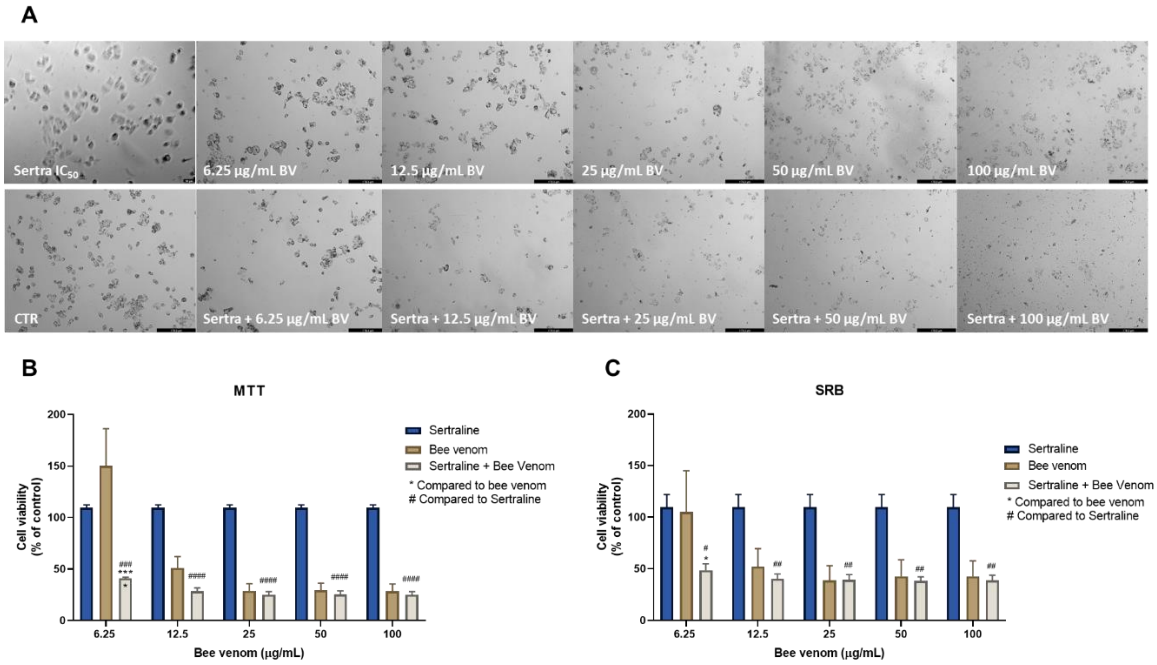

Figure 46. Effect of honeybee venom combined with sertraline in MCF-7 breast cancer cells. (**A**) Morphological analysis; (**B**) MTT and (**C**) SRB assays. MCF-7 cells were cultured in 96-well plates and treated with each combination for 48 h. Cell viability was determined after the final treatment. Each point represents the mean ± SEM relative to the control cells (0.1% DMSO) of three independent experiences. * Statistically significant vs. bee venom at $p < 0.05$; **** Statistically significant vs. bee venom at $p < 0.0001$; $^{\#}$Statistically significant vs. sertraline at $p < 0.05$; $^{\#\#}$ Statistically significant vs. sertraline at $p < 0.01$; $^{\#\#\#}$ Statistically significant vs. sertraline at $p < 0.001$; $^{\#\#\#\#}$ Statistically significant vs. sertraline at $p < 0.0001$. Scale bar: 179.3 µm; BV: bee venom; Sertra: sertraline

A low number of viable cells and cellular aggregates was seen in the combination treatment of thioridazine and bee venom (Figure 47A). MTT results demonstrated that co-treatment of thioridazine and 6.25 µg/mL honeybee venom significantly reduced breast cancer cell viability in relation to both drugs alone (Figure 47B). Protein content was significantly lower than bee venom only for the lowest concentration, being similar to bee venom in concentrations above 25 µg/mL (Figure 47C).

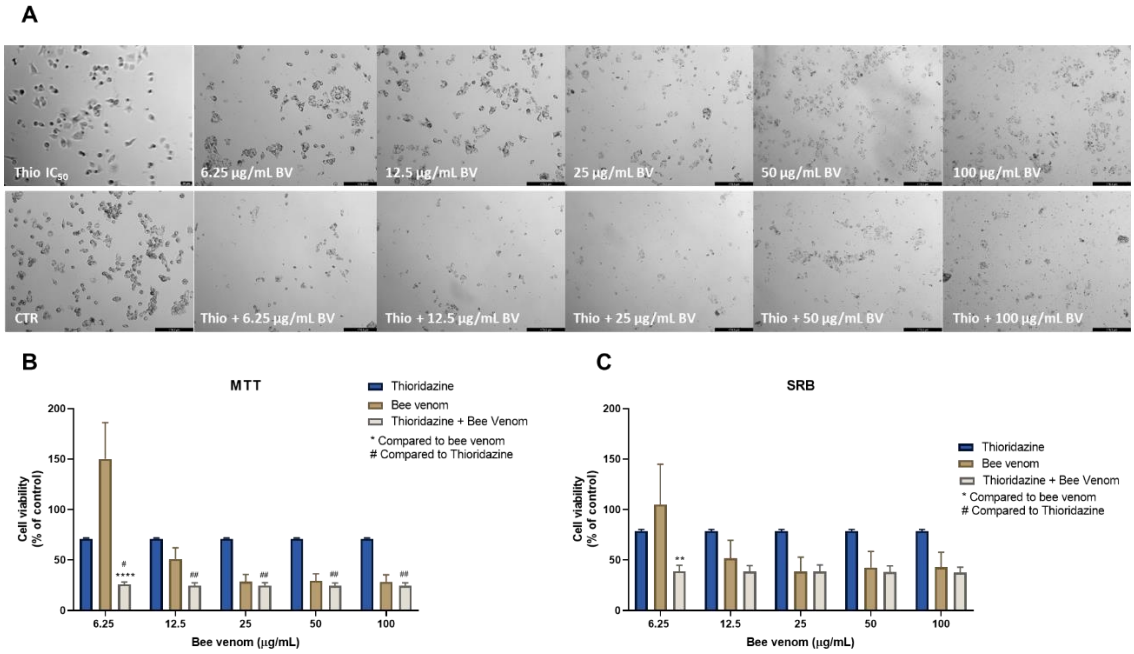

Figure 47. Effect of honeybee venom combined with thioridazine in MCF-7 breast cancer cells. (**A**) Morphological analysis; (**B**) MTT and (**C**) SRB assays. MCF-7 cells were cultured in 96-well plates and treated with each combination for 48 h. Cell viability was determined after the final treatment. Each point represents the mean ± SEM relative to the control cells (0.1% DMSO) of three independent experiences. ** Statistically significant vs. bee venom at $p < 0.01$; **** Statistically significant vs. bee venom at $p < 0.0001$; # Statistically significant vs. thioridazine at $p < 0.05$; ## Statistically significant vs. thioridazine at $p < 0.01$. Scale bar: 179.3 µm; BV: bee venom; Thio: thioridazine

These results demonstrate that the combination of honeybee venom with repurposed drugs is more effective in reducing MCF-7 cell viability than the combination of honeybee venom with DOX, notably for lower concentrations. Combinations of CNS drugs plus honeybee venom resulted in less than 40% of viable cells for all ranges of concentrations, supporting the idea that the combination of these repurposed drugs can help improve the efficacy of honeybee venom for breast cancer treatment.

5.2 Drug combination in Colorectal Cancer

5.2.1 Combination Model I: Repurposed Drugs + Antineoplastic Agents in Colorectal Cancer

Next, the same set of experiments was repeated in another type of cancer cells (HT-29), to determine if the previous combination models could also be employed for the treatment of another type of cancer (colorectal cancer). First, the anti-tumor potential of the antineoplastic drug 5-FU was analyzed in the HT-29 colorectal cancer cell line, to confirm the efficacy of this drug in colorectal cancer. Cells were treated with 5-FU in concentrations ranging from 0.1–100 μM for 48 h and cell survival was evaluated by MTT. The results of the MTT assay for 5-FU are given in Figure 48A. Based on these results, a dose-response curve was obtained and the IC_{50} value for 5-FU was calculated (Figure 48B). This value was further used in the combination studies.

These results revealed a significant activity of 5-FU at concentrations above 10 μM, with little differences in cell viability among the higher concentrations. The cells displayed a mild response to the cytotoxic effect of 5-FU, which resulted in an IC_{50} value of 3.79 μM after normalization of cellular viability results.

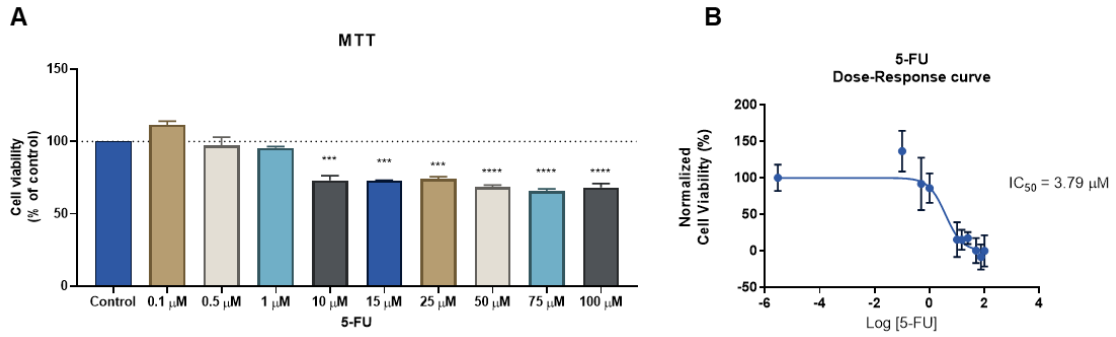

Figure 48. The effect of 5-FU on HT-29 cells. (**A**) Cell viability and (**B**) dose-response. Cells were cultured in the presence of increasing concentrations of 5-FU, and after 48 h, the MTT assay was performed to measure the cellular viability. Values are expressed in percentage of control and represent mean ± SEM. Each experiment was done three times independently (n = 3) *** statistically significant vs. control at $p < 0.001$. **** statistically significant vs. control at $p < 0.0001$.

These results support the anti-cancer activity of 5-FU in the treatment of colorectal cancer and justify its use in the combinations proposed in this study.

5.2.1.1 Combination of 5-FU + Antimalarials in HT-29 Cells

After finding the most promising antimalarials for drug repurposing in colorectal cancer therapy (mefloquine and artesunate) and their IC_{50} value in Chapter I, the combination of 5-FU with this class of drugs was next valuated, using the model of combination described in Figure 25. HT-29 cells were treated with both drugs alone or combined in a fixed ratio, in the concentrations of 0.25 × IC_{50}, 0.5 × IC_{50}, IC_{50}, 2 × IC_{50}, and 4 × IC_{50}, and two cell-based assays were performed: MTT and SRB. Morphological evaluation of cells treated with each drug alone and in combination was also done.

In the combination of 5-FU plus artesunate (Figure 49A and B), it was found that for a concentration of 2 × IC_{50}, the results of the combined drugs were worse than the repurposed drugs alone, demonstrating a kind of competition mechanism between the two drugs when administered together, mainly in the MTT assays. Additionally, for the highest concentrations (4 × IC_{50}), the results obtained for the combined drugs did not show improvements concerning the repurposed drugs alone (Figure 49A and B). Microscopically, at concentrations of 4 × IC_{50}, differences between cells were only found between 5-FU, control cells, and treated cells; differences between single drugs and drug combinations were very subtle and both treatments resulted in the decreasing of cell number, less aggregate formation and rounded cells (Figure 50). The combination with mefloquine resulted in all concentrations showing a greater anticancer effect than 5-FU alone (Figure 49C and D). The activity seen in these combinations can be the result of the strong anticancer activity of mefloquine alone. Morphologically, the results are in agreement with the MTT and SRB assays. At concentrations of 4 × IC_{50}, all combinations resulted in a decrease in cell number and smaller and rounder cells, compared with control cells and 5-FU, which is indicative of cell death (Figure 50).

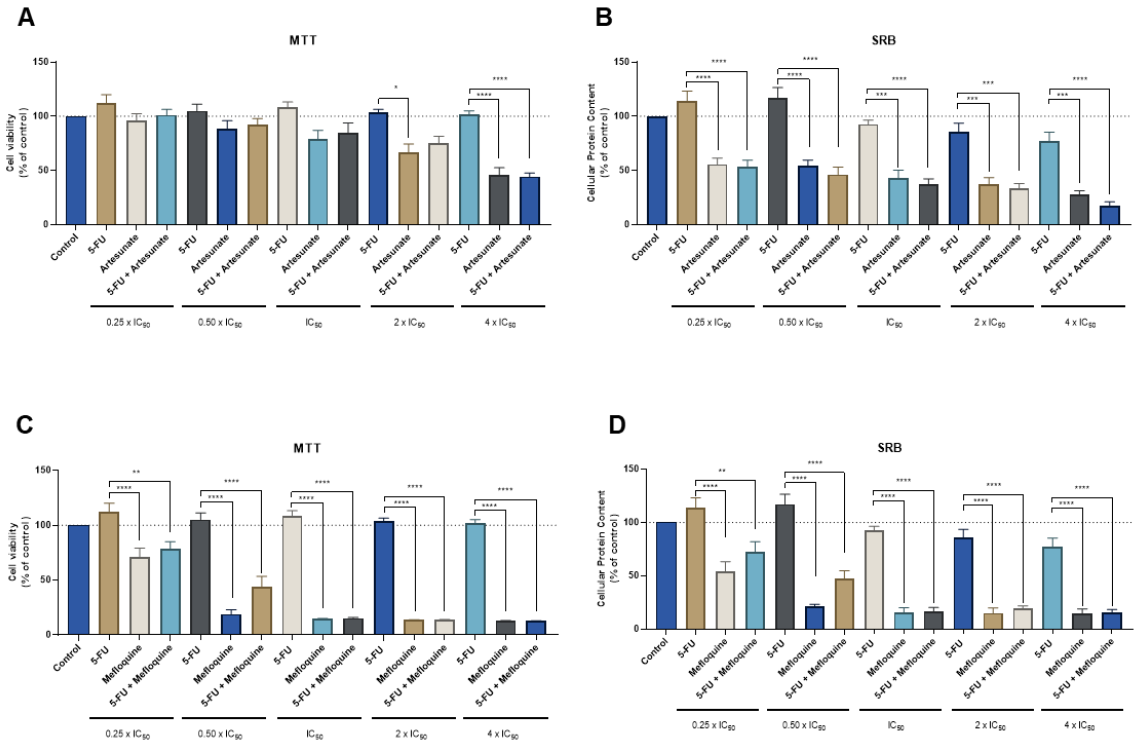

Figure 49. Growth inhibition of HT-29 after 48 h of combination therapy, by MTT (left) and SRB assays (right). Cells were exposed to concentrations of each drug of 0.25, 0.5, 1, 2, and 4 times their IC_{50}, and the cell viability was evaluated by MTT and SRB assays. The drugs in combination were co-administered at the same time. (**A**) The effect of 5-FU plus artesunate on cell viability and (**B**) cell protein synthesis. (**C**) The effect of 5-FU plus mefloquine on cell viability and (**D**) cell protein synthesis. Values are expressed in percentage of control and represent mean ± SEM. Each experiment was done three times independently (n = 3); * statistically significant at $p < 0.05$. ** statistically significant at $p < 0.01$. *** statistically significant at $p < 0.001$. **** statistically significant at $p < 0.0001$.

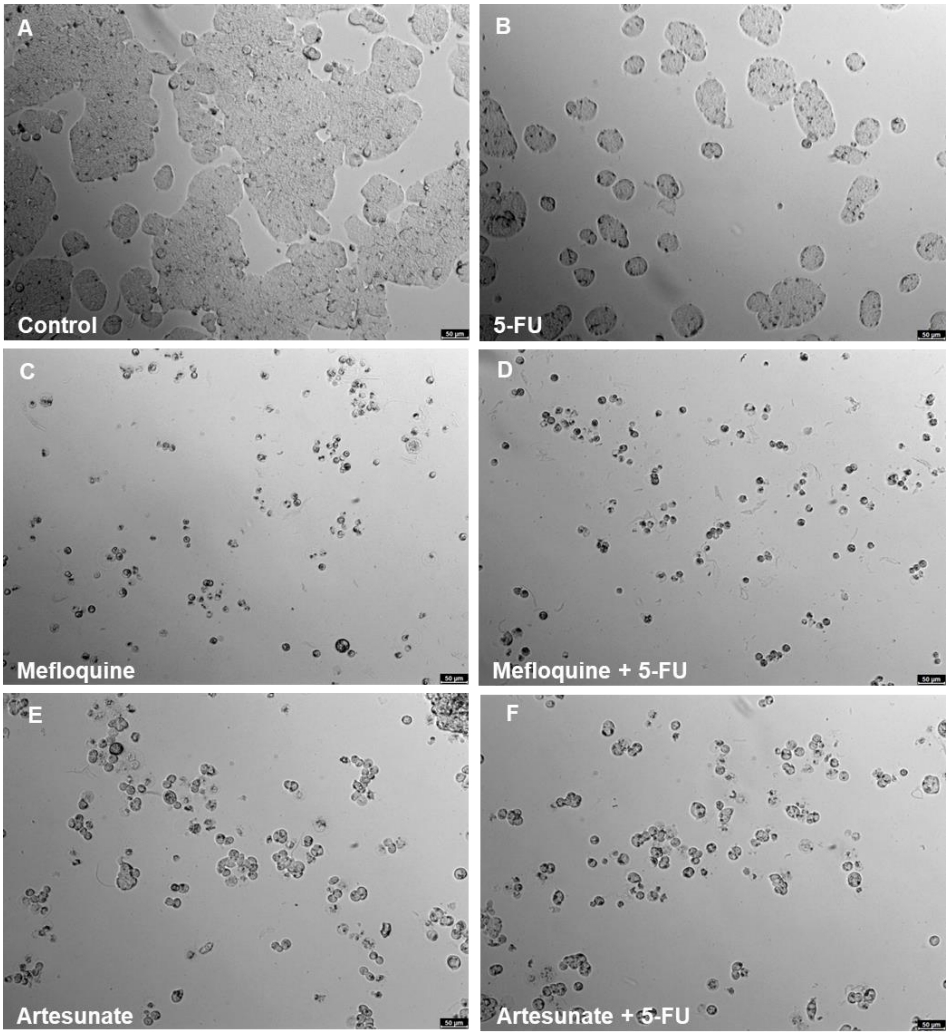

Figure 50. Microscopic cellular visualization of HT-29 cells after 48 h of incubation with vehicle (**A**), 5-FU (**B**), mefloquine (**C**), mefloquine + 5-FU (**D**), artesunate (**E**) and artesunate + 5-FU at concentrations of 4 × IC_{50} of each drug.

Based on the previous MTT assay results (Figure 49), the combination of 5-FU with artesunate seemed to demonstrate some kind of competition between these two drugs, with the results for the combination being worse than for the repurposed drug alone. Therefore, it was designed a new model of combination for these pairs of drugs to evaluate the influence of the choice of the drug schedule on HT-29 colon cancer cells.

It was hypothesized that if drugs were administered at different times (sequential), the results would be better, due to non-competition between the two drugs. To do so, three schedules (Figure 51) were tested: simultaneous administration (Schedule A), drug A prior to drug B (Schedule B), and drug B prior to drug A (Schedule C).

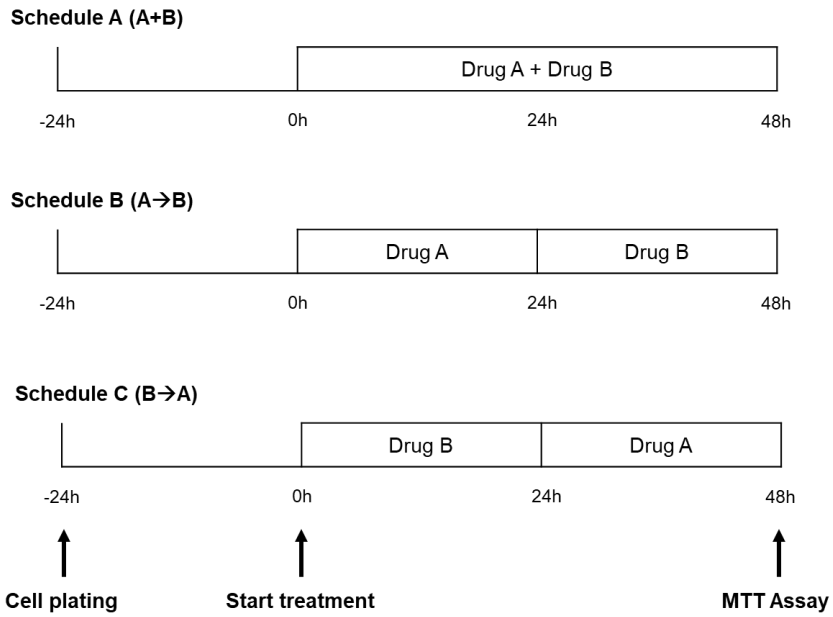

Figure 51. Three combination schedules were designed for evaluating 5-FU combination with some repurposed drugs. Schedule A represents cells treated concomitantly with 5-FU and each repurposed drug for 48 h. Schedule B represents cells pre-treated with 5-FU for 24 h followed by each repurposed drug for another 24 h. For schedule C, cells were pre-treated with each repurposed drug for 24 h, followed by 5-FU for another 24 h.

It was found that, for artesunate, the administration of artesunate prior to 5-FU produces better results than other drug schedules (Figures 52A and B).

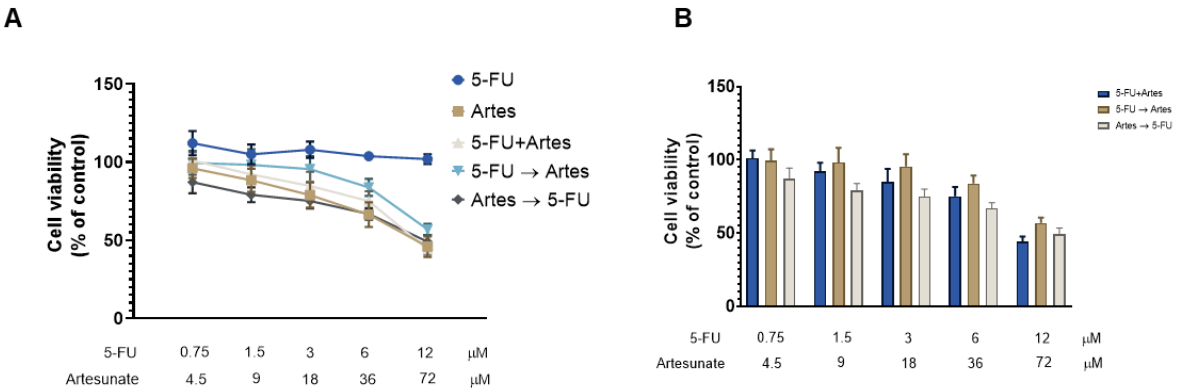

Figure 52. HT-29 cells were exposed to sequential 5-FU and (**A, B**) artesunate using constant ratios of the IC_{50} dose. Values are expressed in percentage of control and represent mean ± SEM. Each experiment was done three times independently (*n* = 3). Artes: artesunate

These results confirm that the choice of the drug schedule may produce different therapeutic outcomes when using drug combinations.

5.2.1.2 Combination of 5-FU + CNS Drugs in HT-29 Cells

After finding the most appropriate CNS agents for drug repurposing in colorectal cancer therapy and their corresponding IC_{50} value in Chapter I, next it was evaluated the combination of 5-FU with each repurposed drug using the model of combination previously described in Figure 25. The most promising CNS drugs were considered as having an IC_{50} value under 25 μM: latrepirdine, fluphenazine, fluoxetine, benztropine, thioridazine, and sertraline.

In combination with 5-FU, latrepirdine did not have any significant anti-cancer effects, at any concentration, both by MTT and SRB assay (Figure 53A and B, respectively). The combination with thioridazine resulted in a similar reduction of cell viability and cell protein synthesis as thioridazine alone, at concentrations higher than IC_{50}. At a concentration of $4 \times IC_{50}$, the combination of 5-FU plus thioridazine demonstrated enhanced but not significant anticancer effects than thioridazine (Figure 53C and D). The combination with 5-FU and sertraline also demonstrated significant anticancer effects compared to 5-FU alone, at a higher concentration, for both assays (Figure 53E and F). A small difference between sertraline and sertraline + 5-FU is seen at the concentration of $4 \times IC_{50}$, but this difference was not statistically significant. Morphologically, the results were in agreement with the MTT and SRB assays. At concentrations of $4 \times IC_{50}$, all combinations resulted in a decrease in cell number and smaller and rounder cells, compared with control cells and 5-FU, which is indicative of cell death (Figure 54).

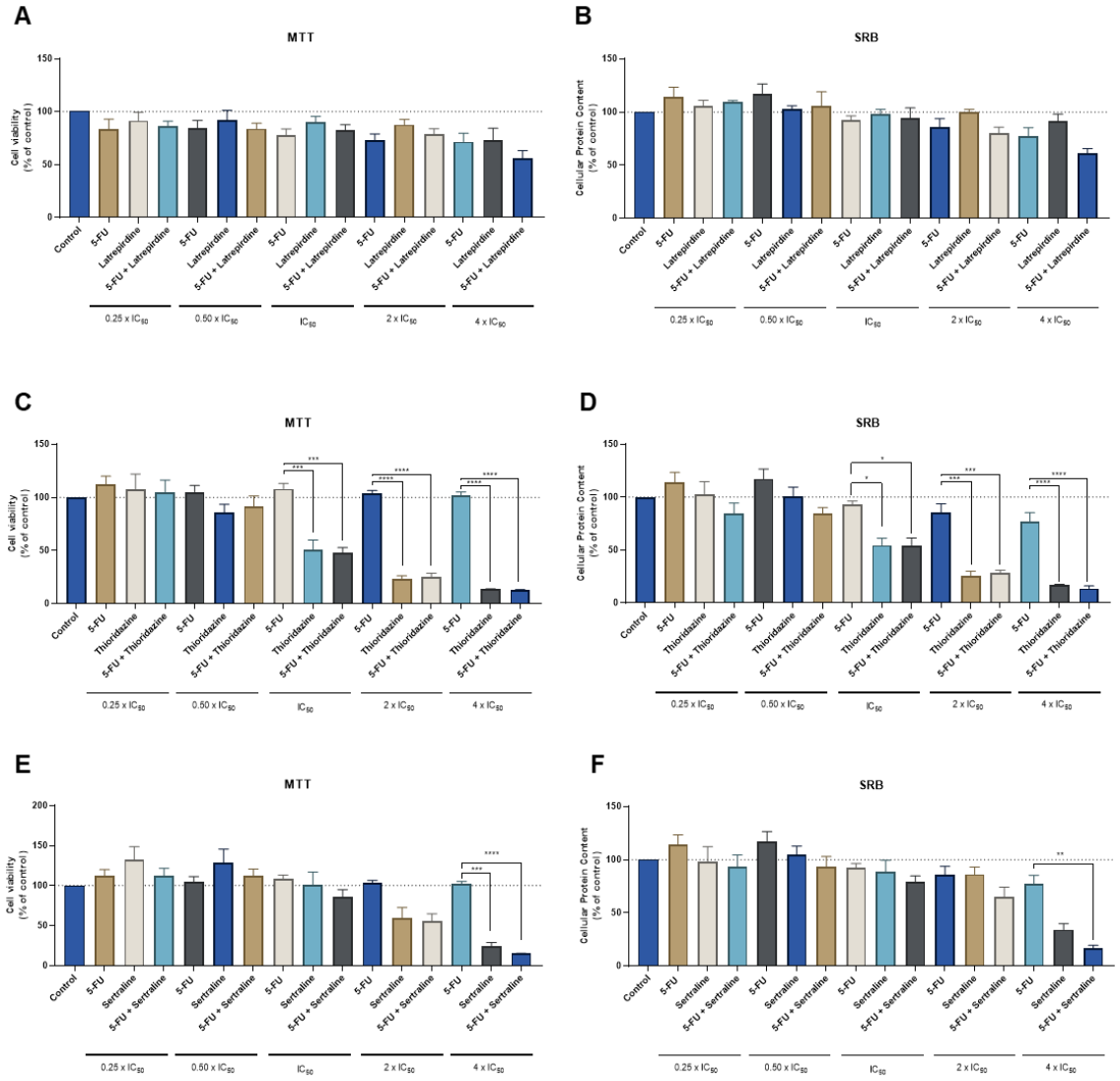

Figure 53. Growth inhibition of HT-29 after 48 h of combination therapy, by MTT (**left**) and SRB assays (**right**). Cells were exposed to concentrations of each drug of 0.25, 0.5, 1, 2, and 4 times their $IC_{50,}$ and the cell viability was evaluated by MTT and SRB assays. The drugs in combination were co-administered at the same time. (**A**) The effect of 5-FU plus latrepirdine on cell viability and (**B**) cell protein synthesis. (**C**) The effect of 5-FU plus thioridazine on cell viability and (**D**) cell protein synthesis. (**E**) The effect of 5-FU plus sertraline on cell viability and (**F**) cell protein synthesis. Values are expressed in percentage of control and represent mean ± SEM. Each experiment was done three times independently (n = 3); * statistically significant at $p < 0.05$. ** statistically significant at $p < 0.01$. *** statistically significant at $p < 0.001$. **** statistically significant at $p < 0.0001$.

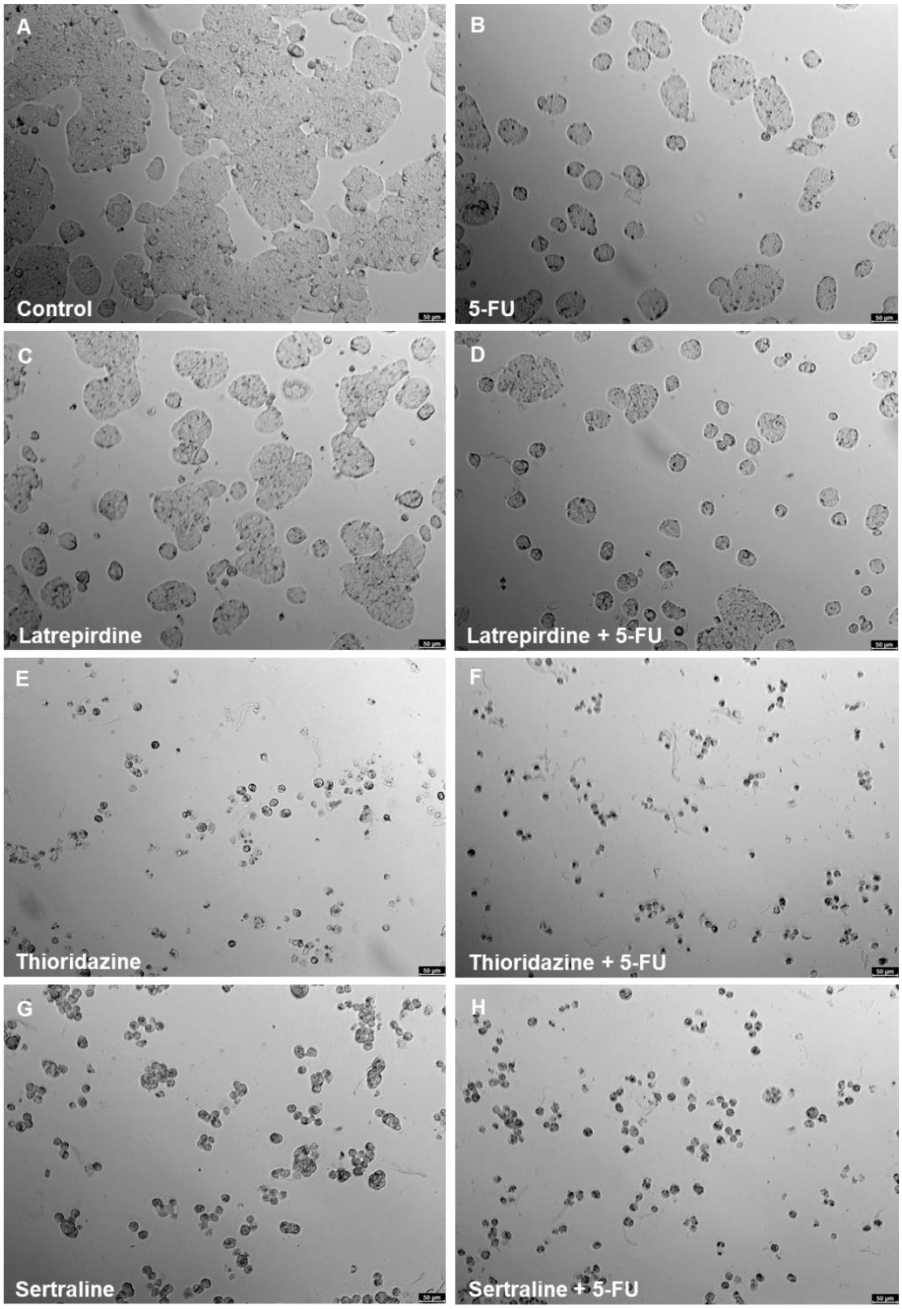

Figure 54. Microscopic cellular visualization of HT-29 cells after 48 h of incubation with vehicle (**A**), 5-FU (**B**), latrepirdine (**C**), latrepirdine + 5-FU (**D**), thioridazine (**E**), thioridazine + 5-FU (**F**), sertraline (**G**) and sertraline + 5-FU at concentrations of 4 × IC_{50} of each drug.

In the combination of 5-FU plus fluphenazine, fluoxetine, and benztropine, it was found that for a concentration of 2 × IC_{50}, the results of the combined drugs were worse than the repurposed drugs alone, demonstrating a kind of competition mechanism between the two drugs when co-administered, mainly in the MTT assays. Additionally, for the highest concentrations (4 × IC_{50}), the results obtained for the combined treatments did not show

improvements concerning the repurposed drugs alone (Figure 55). Microscopically, at concentrations of 4 × IC_{50}, differences between cells were only found between 5-FU, control cells, and treated cells; differences between single drugs and drug combinations were very subtle and both treatments resulted in the decreasing of cell number, less aggregate formation and rounded cells (Figure 56).

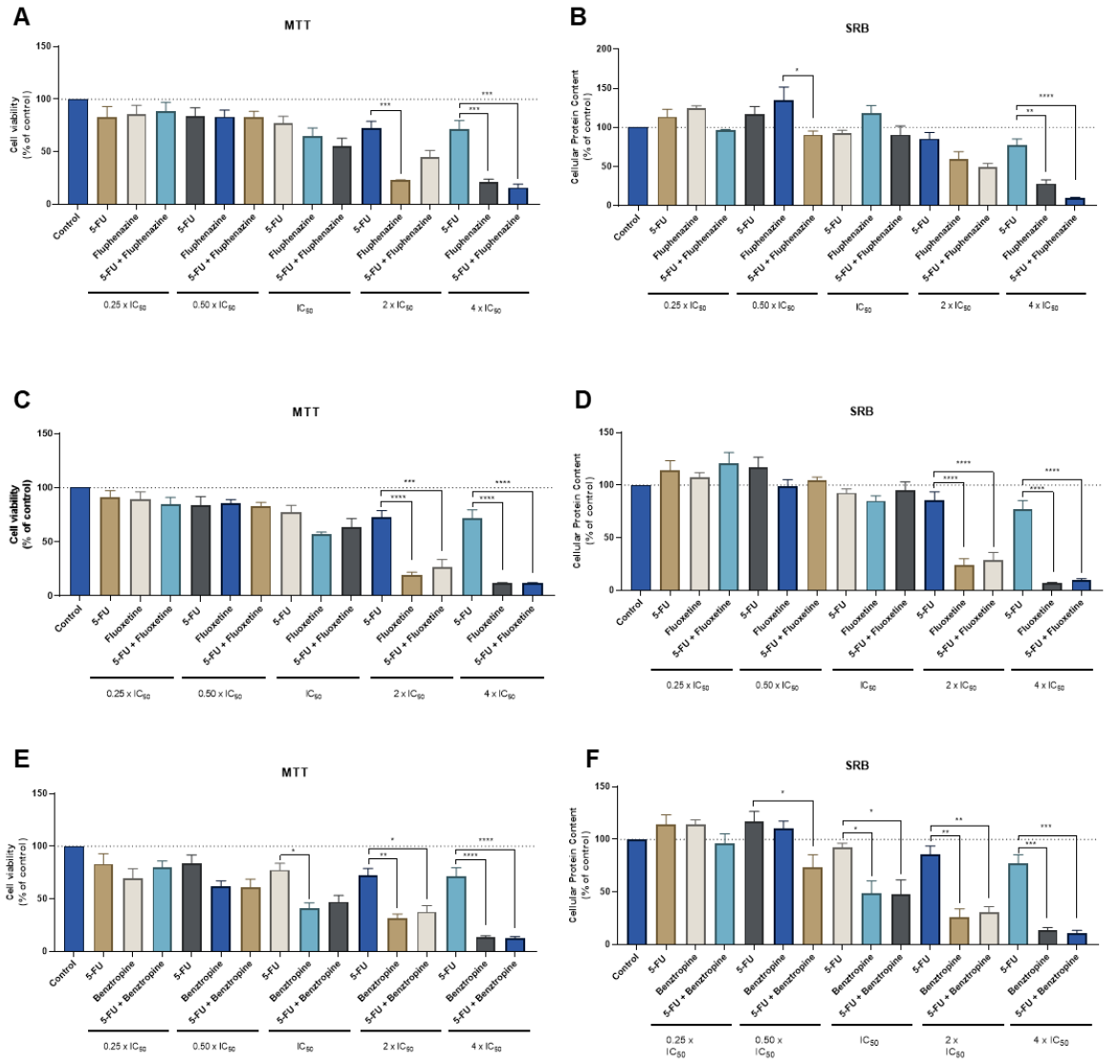

Figure 55. Growth inhibition of HT-29 after 48 h of combination therapy, by MTT (left) and SRB assays (right). Cells were exposed to concentrations of each drug of 0.25, 0.5, 1, 2, and 4 times their IC_{50}, and cell viability was evaluated by MTT and SRB assays. The drugs in combination were co-administered at the same time. (**A**) The effect of 5-FU plus fluphenazine on cell viability and (**B**) cell protein synthesis. (**C**) The effect of 5-FU plus fluoxetine on cell viability and (**D**) cell protein synthesis. (**E**) The effect of 5-FU plus benztropine on cell viability and (**F**) cell protein synthesis. Values are expressed in percentage of control and represent mean ± SEM. Each experiment was done three times independently (n = 3); * statistically significant at $p < 0.05$. ** statistically significant at $p < 0.01$. *** statistically significant at $p < 0.001$. **** statistically significant at $p < 0.0001$.

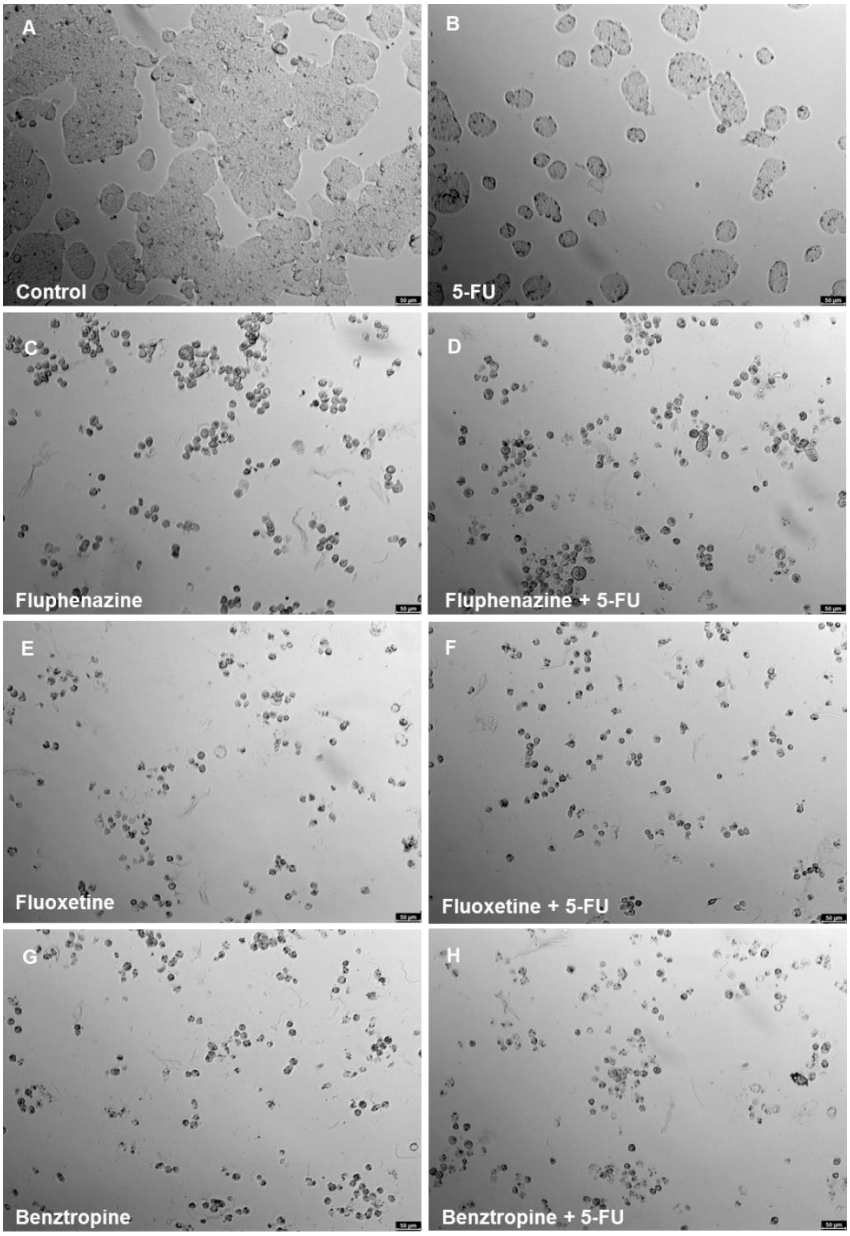

Figure 56. Microscopic cellular visualization of HT-29 cells after 48 h of incubation with vehicle (**A**), 5-FU (**B**), fluphenazine (**C**), fluphenazine + 5-FU (**D**), fluoxetine (**E**), fluoxetine + 5-FU (**F**), benztropine (**G**) and benztropine + 5-FU at concentrations of 4 × IC_{50} of each drug.

The combination of 5-FU with fluphenazine, fluoxetine, and benztropine seemed to demonstrate some kind of competition between these drugs. It was then hypothesized that the administration of these drugs at different times (i.e., sequential treatment), would result in better outcomes, due to non-competition between the two drugs. Therefore, the three schedules previously described in Figure 51 were also tested for these drug combinations.

The results for all CNS drugs tested in different combination schedules demonstrated that the simultaneous administration of 5-FU and these repurposed drugs resulted in enhanced anticancer effects (Figure 57), compared to sequential schedules; nevertheless, in any case, the single treatment with repurposed drugs revealed to be always advantageous over the combination regimens.

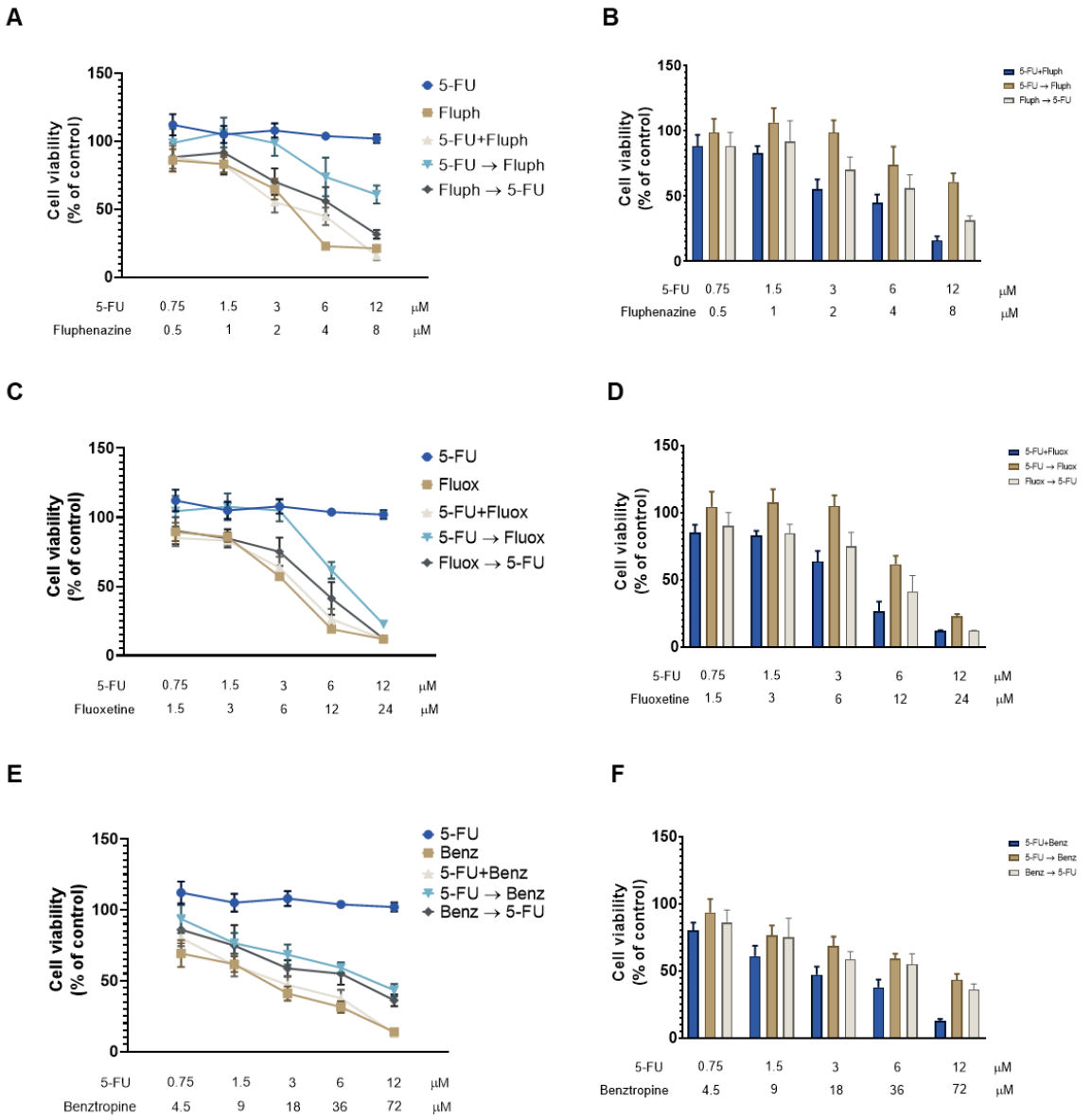

Figure 57. HT-29 cells were exposed to sequential 5-FU and (**A**, **B**) fluphenazine (**C**, **D**) fluoxetine, and (**E**, **F**) benztropine using constant ratios of the IC_{50} dose. Values are expressed in percentage of control and represent mean ± SEM. Each experiment was done three times independently (*n* = 3). Fluph: fluphenazine; Fluox: fluoxetine; Benz: benztropine

Taken together, these results demonstrate all CNS drugs as single agents have better antitumor activity than in combination, indicating these drugs are ideal candidates for drug repurposing in colorectal cancer.

Finally, it was also evaluated the combination of the CNS drugs edaravone and quetiapine with 5-FU, following the same methodology previously described for MCF-7 cells. Edaravone and quetiapine were combined in increasing concentrations with the IC_{50} value of 5-FU. This combination aimed to determine whether these repurposed drugs could enhance the anticancer effects of 5-FU.

Regarding the combination of edaravone and 5-FU, significant anticancer effects were found compared with each drug alone, when 0.1, 10, 50, and 100 µM of edaravone were combined with 5-FU, as demonstrated by morphological analysis (Figure 58A) and by MTT assay (Figure 58B). These results differ from those previously obtained for the MCF-7 cells, where it was found that the combination of edaravone and chemotherapeutic agents did not produce any significant effects on cell viability.

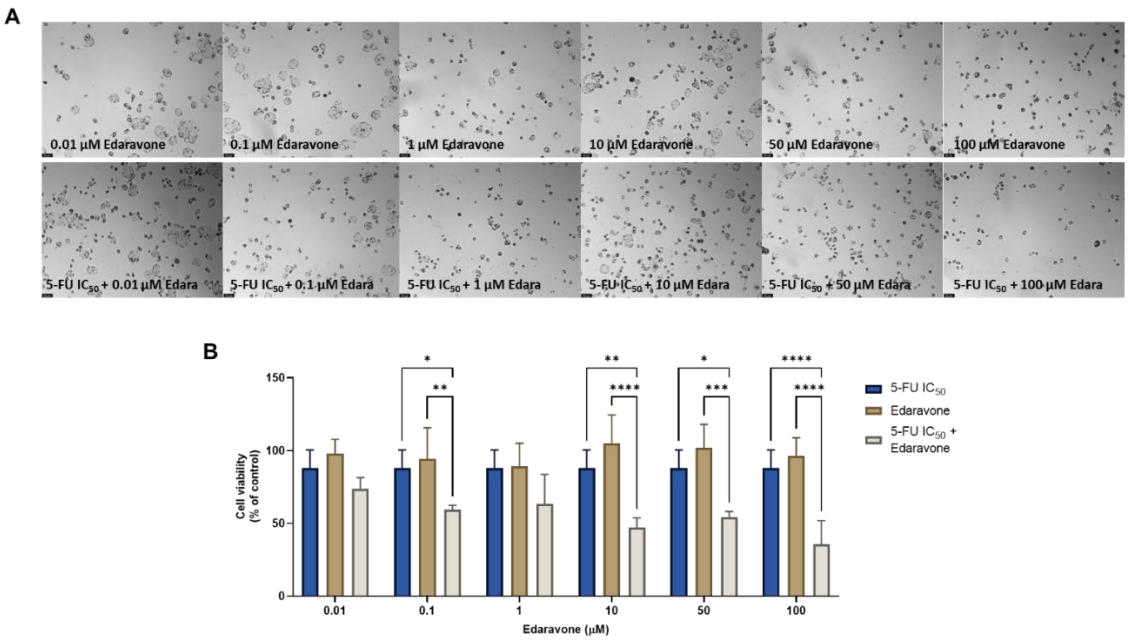

Figure 58. Morphological analysis (**A**) and cellular viability (**B**) results for HT-29 cells after a single and combined treatment with 5-FU and edaravone. Cells were incubated with increasing concentrations of edaravone, alone and combined with a fixed concentration (IC_{50}) of 5-FU for 48 h. Cell viability was evaluated using an MTT assay. Experiments were performed three times independently (n = 3). *, **, *** and **** indicate significant results at $p < 0.05$, $p < 0.01$, $p < 0.001$ and $p < 0.0001$, respectively. Edara: edaravone

The combination of 5-FU and quetiapine also resulted in significant anticancer effects compared with each drug alone, visible both in the analysis of cell morphology (Figure 59A) and in the MTT results (Figure 59B), for the combination of intermediate concentrations of quetiapine (0.1, 1, 10 and 50 µM). Additionally, for the combination of the highest concentration of quetiapine with the IC_{50} value for 5-FU, it was found the combined effect induced about 80% of cell death in this cell line.

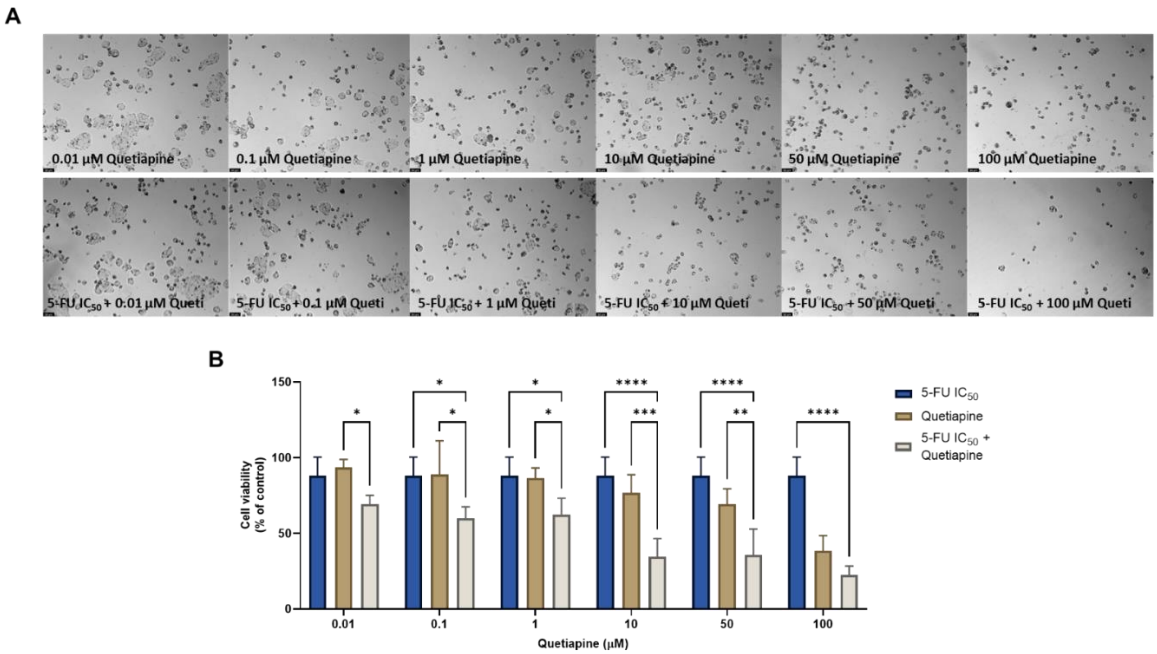

Figure 59. Morphological analysis (**A**) and cellular viability (**B**) results of HT-29 cells after a single and combined treatment with 5-FU and quetiapine. Cells were incubated with increasing concentrations of quetiapine, alone and combined with a fixed concentration (IC_{50}) of 5-FU for 48 h. Cell viability was evaluated using an MTT assay. Experiments were performed three times independently (n = 3). *, **, *** and **** indicate significant results at $p < 0.05$, $p < 0.01$, $p < 0.001$ and $p < 0.0001$, respectively. Queti: quetiapine

These results demonstrate that these repurposed drugs are promising adjuvant agents for combination therapies in colon cancer therapy. Taken together, the results obtained in the two cell lines (MCF-7 and HT-29) indicate that quetiapine is a more promising repurposed drug for cancer therapy, since it demonstrates anticancer activity both as a standalone agent against HT-29 cells and as an adjuvant agent in combination regimens with DOX and 5-FU against MCF-7 and HT-29 cells, respectively.

5.2.1.3 Combination of 5-FU + Antifungal Drugs in HT-29 Cells

Based on our findings in Chapter I, it was discovered that the antifungal drug clotrimazole was able to induce significant anticancer effects in HT-29 colorectal cancer cells. Therefore, the combination of clotrimazole with 5-FU in HT-29 cells was also evaluated, to determine if this combination could also display promising cytotoxic effects for cancer therapy.

The results regarding the combination of clotrimazole with 5-FU (Figure 60) seem to suggest that the anticancer activity from the combination is a result of the activity of clotrimazole alone, not demonstrating positive benefits of its use in oncotherapy.

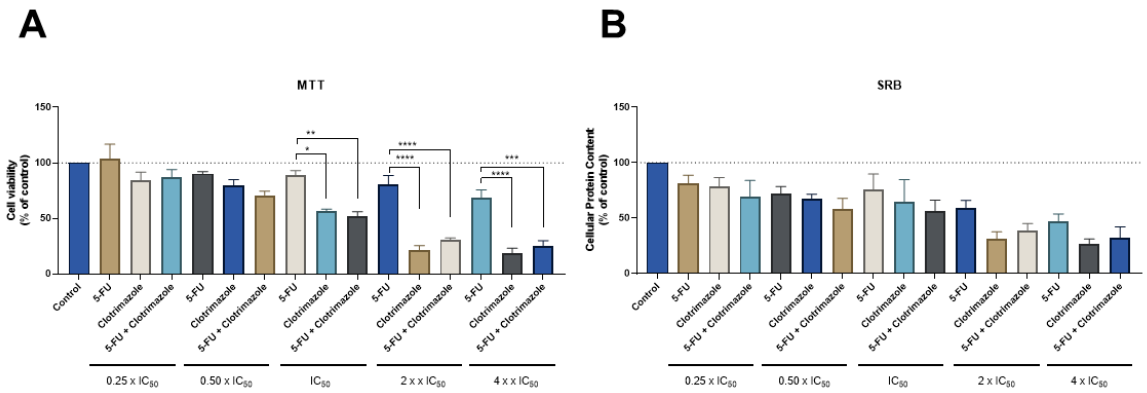

Figure 60. Cytotoxic effects of the combination of CLZ with (**A**, **B**) 5-FU on the viability (right panel) and cell protein (left panel) content of HT-29 cells. Cell viability and protein content were assessed by MTT and SRB assays, respectively, after 48 h of exposure to each treatment. The results are expressed in the percentage of cell viability relative to untreated control cells. *, **, *** and **** indicate $p < 0.05$, $p < 0.01$, $p < 0.001$ and $p < 0.0001$, respectively. All data are presented as the mean ± SEM of three independent experiments.

5.2.2 Combination Model II: Repurposed Drugs in Colorectal Cancer

Next, the combinations of repurposed drugs previously described for MCF-7 were examined in another cell line (HT-29) to evaluate whether these drug pairs would also have anticancer potential in another type of cancer.

The effect of the combination of mefloquine (IC_{50}) with increasing concentrations of pyronaridine on the cell morphology (Figure 61A) and viability (Figure 61B) of the HT-29 colon cancer cells indicates that this combination is only statistically significant when compared with the cytotoxic effect of pyronaridine alone at lower concentrations (0.01, 0.1, 1 and 10 µM). It was also found that the drug combination is not advantageous over mefloquine alone, with mefloquine alone causing more than an 80% reduction in cell viability at its IC_{50} value.

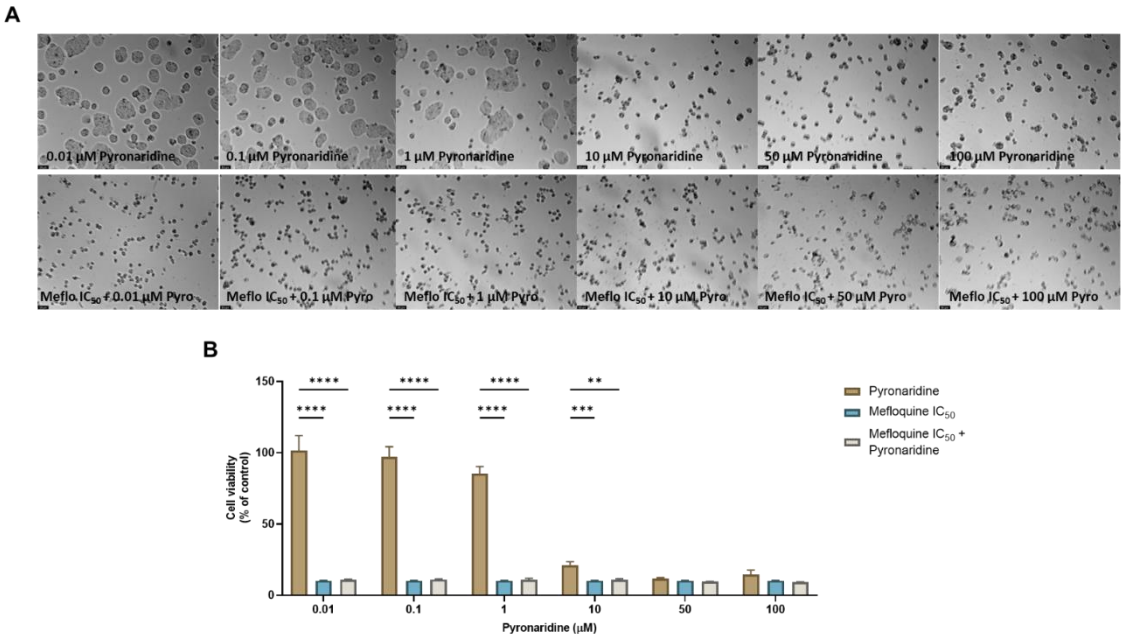

Figure 61. Morphological analysis (**A**) and cellular viability (**B**) results of HT-29 cells after a single and combined treatment of mefloquine and pyronaridine. Cells were incubated with increasing concentrations of pyronaridine, alone and combined with a fixed concentration (IC_{50}) of mefloquine for 48 h. Cell viability was evaluated using an MTT assay. Experiments were performed three times independently (n = 3). **, *** and **** indicate significative results at $p < 0.01$, $p < 0.001$ and $p < 0.0001$, respectively. Meflo: mefloquine; Pyro: pyronaridine

On the other hand, when analyzing the results of the reverse combination of a fixed concentration of pyronaridine (IC_{50}) and variable concentrations of mefloquine, both obtained after microscopic visualization (Figure 62A) and the viability assay (Figure 62B), it was found that the combination regimen only induced significant reductions in cell viability

compared with mefloquine, and for lower concentrations (0.01, 0.1 and 1 µM). Moreover, for the same range of concentrations, it was possible to conclude that the anticancer activity may be a result of the cytotoxic potential of pyronaridine, while at higher concentrations (>10 µM), the combined effect may be derived from the anticancer activity of mefloquine alone.

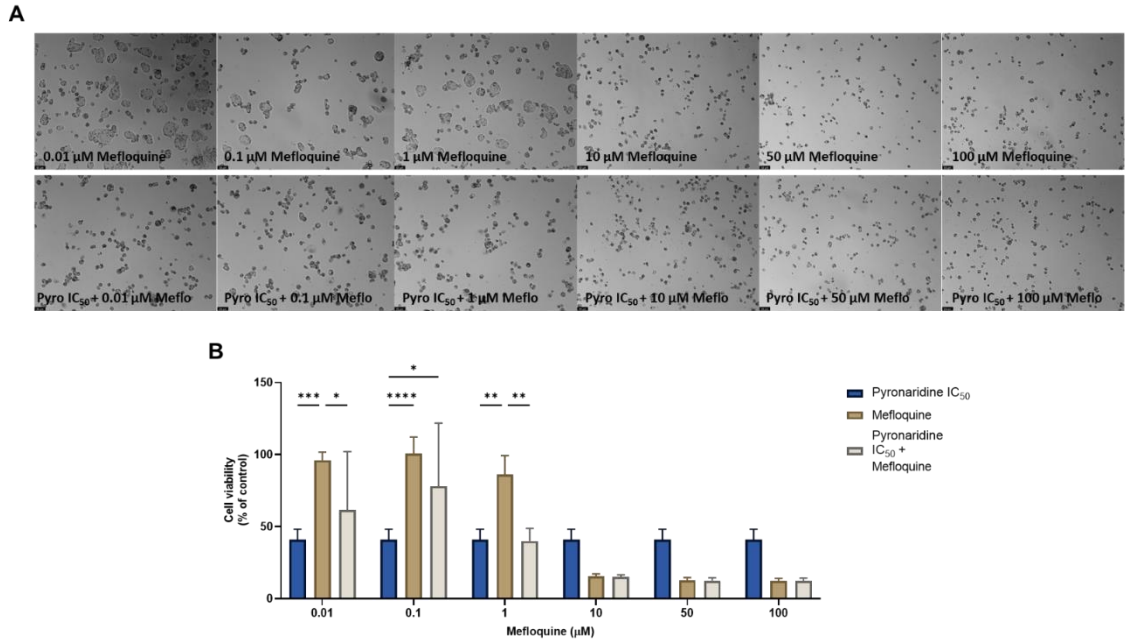

Figure 62. Morphological analysis (**A**) and cellular viability (**B**) results of HT-29 cells after a single and combined treatment of mefloquine and pyronaridine. Cells were incubated with increasing concentrations of mefloquine, alone and combined with a fixed concentration (IC_{50}) of pyronaridine for 48 h. Cell viability was evaluated using an MTT assay. Experiments were performed three times independently (n = 3). *, **, *** and **** indicate significative results at $p < 0.05$, $p < 0.01$, $p < 0.001$ and $p < 0.0001$, respectively. Meflo: mefloquine; Pyro: pyronaridine

Taken together, these results demonstrate that the combination of antimalarial drugs is not advantageous over a single treatment, for either cell line, indicating that these repurposed drugs are more promising as standalone agents in breast and colon cancer therapies than in combination with other repurposed drugs. Nevertheless, our previous results further support their use as chemosensitizers in combination models using antineoplastic agents.

Next, the two most potent CNS drugs were also combined in HT-29 colon cancer cells and the changes in cell morphology and cell viability were evaluated after a treatment of 48 h. First, it was evaluated the combination of sertraline at a fixed concentration of IC_{50} with increasing concentrations (0.01–100 µM) of fluphenazine. Analyzing both the microscopic images (Figure 63A) and the results obtained in the MTT assay (Figure 63B), it was possible to verify significant changes in the number and phenotype of the HT-29 cells treated with this combination, specifically when compared to the single treatment with fluphenazine at lower concentrations (< 1 µM). Indeed, the analysis of the MTT results demonstrates a significant reduction in the viability of this cell line at treatments with the combination of sertraline plus 0.01, 0.1, and 1 µM fluphenazine, compared to both drugs alone, demonstrating the anticancer potential of these repurposed drugs to be used in combination regimens.

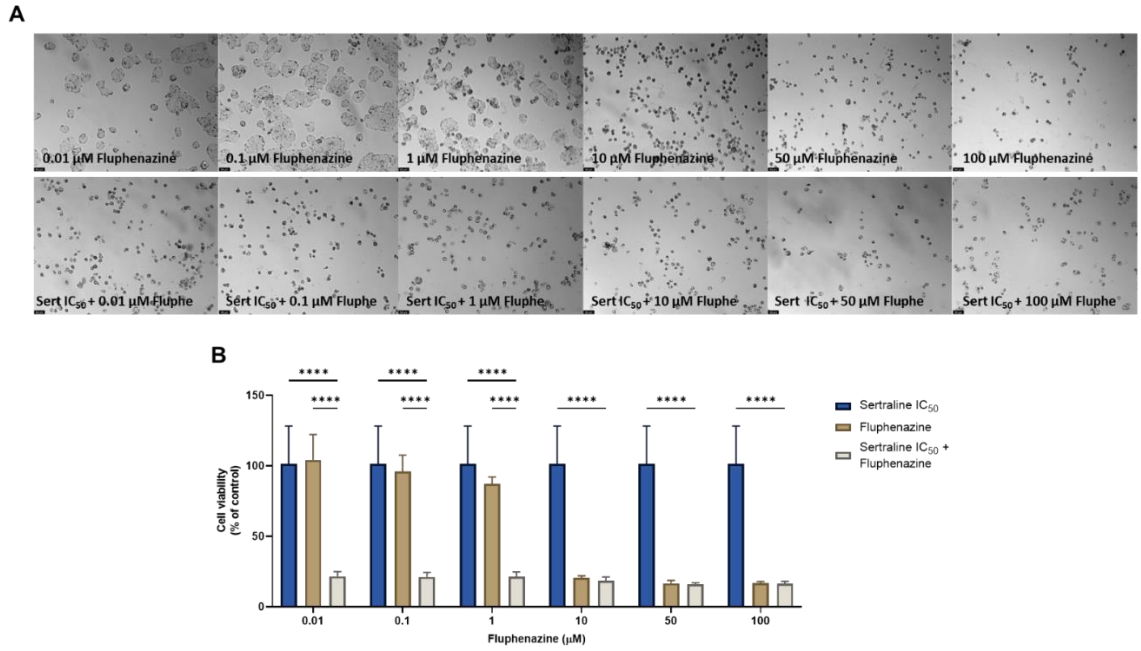

Figure 63. Morphological analysis (**A**) and cellular viability (**B**) results for HT-29 cells after a single and combined treatment with fluphenazine and sertraline. Cells were incubated with increasing concentrations of fluphenazine, alone and combined with a fixed concentration (IC_{50}) of sertraline for 48 h. Cell viability was evaluated using an MTT assay. Experiments were performed three times independently (n = 3). **** indicates significant results at $p < 0.0001$. Sert: sertraline; Fluphe: fluphenazine

On the other hand, when using the reverse combination, i.e., combining a fixed concentration of fluphenazine with increasing concentrations of sertraline, it was found that the combination was not able to induce significant cytotoxicity in the HT-29 cells, compared

to fluphenazine alone (for concentrations < 1 µM) or compared to sertraline alone at higher concentrations (>10 µM), demonstrating that the combination itself does not have improved anticancer activity compared to both drugs alone (Figure 64).

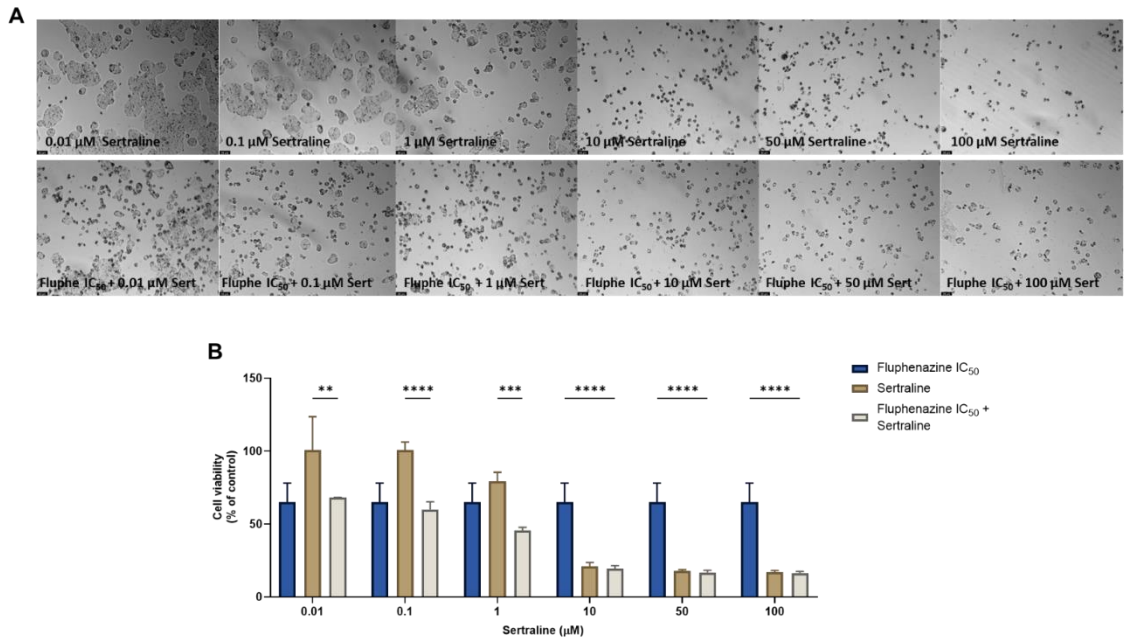

Figure 64. Morphological analysis (**A**) and cellular viability (**B**) results of HT-29 cells after a single and combined treatment of fluphenazine and sertraline. Cells were incubated with increasing concentrations of sertraline, alone and combined with a fixed concentration (IC_{50}) of fluphenazine for 48 h. Cell viability was evaluated using an MTT assay. Experiments were performed three times independently (n = 3). **, *** and **** indicate significative results at $p < 0.01$, $p < 0.001$ and $p < 0.0001$, respectively. Sert: sertraline; Fluphe: fluphenazine

Taken together, these results suggest that the combination of repurposed drugs, namely combining the CNS drugs sertraline and fluphenazine at lower doses, can be further investigated for colon cancer novel therapies. Nevertheless, these results also demonstrate the importance of the choice of the appropriate dose ratios used in combination regimens.

5.2.3 Combination Model III: Peptides + Antineoplastic Drugs in Colorectal Cancer

5.2.3.1 Melittin (a component of honeybee venom) in combination with 5-FU

Based on the experiments previously described in section 5.1.3., the same experiments were repeated in another cancer cell line, the HT-29 colorectal cancer cell line, to evaluate if these drug combinations would also have potential for application in colorectal cancer therapy.

First, it was examined the anti-cancer effect of honeybee venom in HT-29 colon cancer cells for a period of 48 h. Cells were treated with increasing concentrations of bee venom, and cell viability was evaluated by MTT and SRB assays. Control cells were treated with 0.1% DMSO, the vehicle used for stock preparation.

MTT results demonstrated that cells treated with honeybee venom in concentrations above 25 µg/mL had a significant reduction of viability (Figure 65A). The SRB assay demonstrated that cellular protein content was significantly reduced in cells treated with concentrations of bee venom above 6.25 µg/mL (Figure 65B). Based on MTT results, a concentration-response curve was plotted and an IC_{50} value of 24.25 µg/mL was obtained for bee venom (Figure 65C). Treatment with concentrations above 50 µg/mL of bee venom resulted in more than 80% cell reduction in both cell-based assays, demonstrating the great potential of this natural substance to reduce the viability of HT-29 colorectal cancer cells.

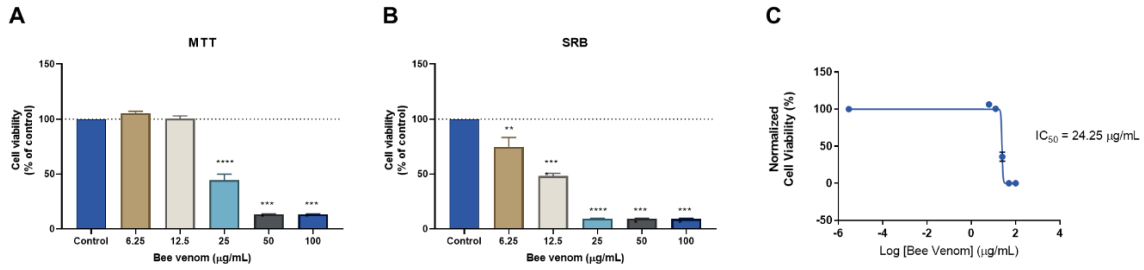

Figure 65. Cell viability of HT-29 colon cancer cells treated with honeybee venom. (**A**) MTT assay (**B**) SRB assay and (**C**) the dose-response curve of HT-29 cells cultured in 96-well plates and treated with increasing concentrations (6.25–100 µg/mL) of honeybee venom for 48 h. The dose-response curve was obtained by non-linear regression after the normalization of cell viability values. Each point represents the mean ± SEM relative to the control cells (0.1% DMSO) of three independent experiences. ** statistically significant vs. control at $p < 0.01$; **** statistically significant vs. control at $p < 0.0001$.

Next, and as previously done using MCF-7 cells, it was evaluated if honeybee venom could be used to further improve the anti-cancer activity of 5-FU, in the HT-29

colorectal cancer cell line. It was designed a combination model with variable doses (6.25–100 µg/mL) of honeybee venom combined with a fixed dose (IC_{50} value) of 5-FU. Cells were treated with each combination for 48 h and cell viability was evaluated by MTT and SRB assays. Morphology analysis was also performed in parallel with these cell-based assays.

MTT results demonstrated that honeybee venom in concentrations above 25 µg/mL had greater anti-cancer potential than 5-FU (at the concentration of its IC_{50}). Regarding the combination of honeybee venom with 5-FU, these results demonstrated an improved cytotoxic effect compared to single treatments with bee venom for concentrations ranging from 6.25 to 25 µg/mL. Particularly, for the combined pairs of 5-FU + 12.5 µg/mL of bee venom and 5-FU + 25 µg/mL of bee venom, results were even better than both 5-FU and bee venom alone (Figure 66B). The results of the SRB assay demonstrated that cellular protein content was significantly reduced when 5-FU was combined with 6.25 and 12.5 µg/mL of honeybee venom, compared to 5-FU and bee venom alone for the same concentrations (Figure 66C). Morphological analysis also confirmed that the combination of 5-FU + bee venom was effective in decreasing the number of tumor cells, especially at lower concentrations (Figure 66A).

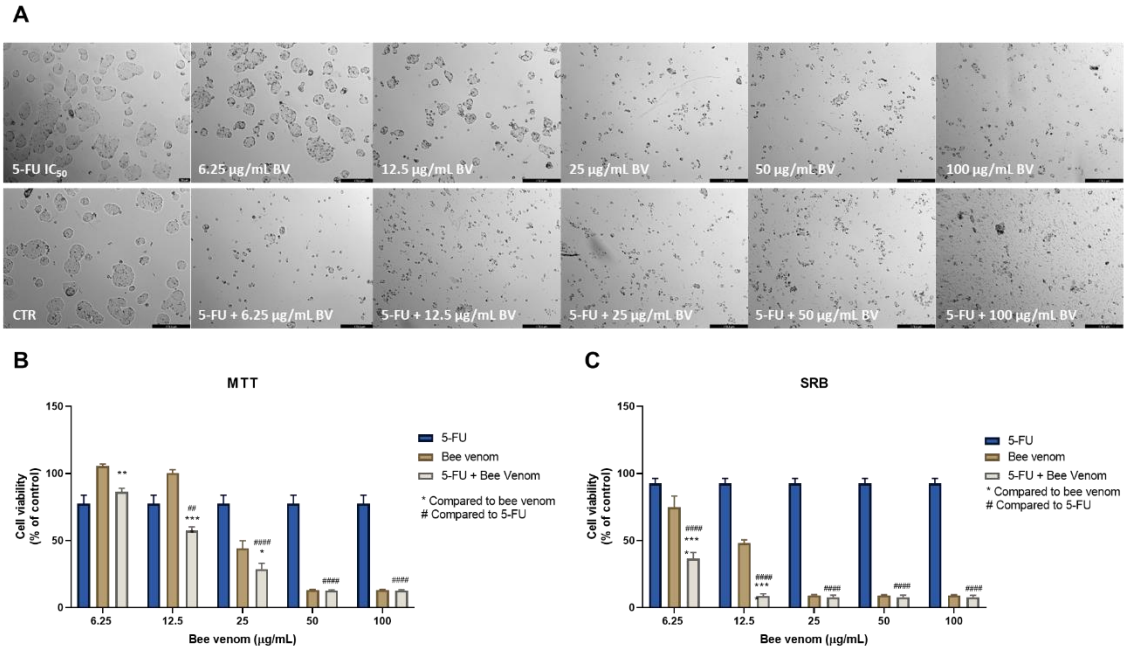

Figure 66. Effect of honeybee venom combined with 5-FU in HT-29 colon cancer cells. (**A**) Morphological analysis; (**B**) MTT and (**C**) SRB assays. HT-29 cells were cultured in 96-well plates and treated with each combination for 48 h. Cell viability was determined after the final treatment. Each point represents the mean ± SEM relative to the control cells (0.1% DMSO) of three independent experiences. * Statistically significant vs. bee venom at $p < 0.05$; ** Statistically significant vs. bee venom at $p < 0.01$; **** Statistically significant vs. bee venom at $p < 0.0001$; ## Statistically significant vs. 5-FU at $p < 0.01$; #### Statistically significant vs. 5-FU at $p < 0.0001$. Scale bar: 179.3 µm; BV: bee venom.

5.2.3.2 CPP2-conjugates in combination with 5-FU

Finally, and given the good results obtained with the combination models with honeybee venom, it was hypothesized that other peptides, such as cell-penetrating peptides (CPPs), could also be used to enhance the anticancer effects of chemotherapeutic agents. Therefore, several CPPs derivatives were tested in combination with 5-FU for colorectal cancer therapy.

CPPs are one of the most promising vehicles for the delivery of various types of cargo and have been extensively studied for the transport of different substrates to cancer cells [393]. CPPs are small peptides, usually 5–30 amino acids in length, and have the advantage of being able to translocate through the cell membrane via a non-toxic and apparently independent process of receivers or energy consumption [394]. CPPs are capable of transporting into the interior of living cells a wide variety of substrates such as drugs, peptides, proteins, liposomes, nanoparticles, or even nucleic acids [395]. There is currently a large panoply of CPPs that can be distinguished as to their origin as peptides derived from proteins, chimeric peptides (resulting from the fusion of two natural sequences), or synthetic peptides (designed based on experimental and/or computational studies) [396].

CPPs can be classified into three classes: cationic, amphipathic, and hydrophobic [397]. Currently, more than 100 different CPPs are patented with approximately 83% being cationic [398]. Hydrophobic CPPs are still very scarce and represent approximately 15% of all discoveries to date [399]. Although these peptides are rapidly assimilated, the different classes exhibit distinct behaviors, especially concerning endocytic internalization.

Cationic CPPs are composed of positively charged residues such as arginine and lysine. Thus, the total charge of the peptide is always positive in physiological conditions. These basic residues are responsible for the first interaction of electrostatic nature with the plasma membrane, particularly with the negatively charged polysaccharides and lipids which eventually lead to the internalization of the peptide in the cell [393]. Most cationic peptides are naturally occurring [398]; however, some artificial cationic peptides, such as homopolymers of lysine [400] and arginine [401], have already been synthesized. The use of cationic CPPs may be associated with the induction of side effects related to plasma membrane integrity and consequent cell viability, i.e., it may be associated with some degree of cell lysis [402].

One of the main applications of CPPs is in cancer therapy [395]. Since cancer is one of the greatest scourges in the world today, and since current therapy is strongly associated

with many side effects [403], CPPs represent a very plausible alternative for the destruction of cancerous cells. To date, more than 1800 kinds of CPPs have been developed to deliver cargo from basic research to clinics in therapeutics delivery, gene editing, and cell imaging [404].

Although CPPs are commonly used for the transport of different cargo, there are some specific amino acid sequences with intrinsic activity against tumor cells. For example, p28 (LSTAADMQGVVTDGMASGLDK-DYLKPDD) is a CPP that binds to wild-type and mutated p53, increasing its intracellular levels and inhibiting cancer cell proliferation. Indeed, this was observed in *in vitro* studies performed with colon, breast, ovarian, and other solid tumor cells [405]. Supported by these findings, a phase I clinical trial (NCT00914914) was concluded in 2014, where p28 was tested against a range of p53+ solid tumors. It was found that the peptide was well tolerated, and no patients exhibited any dose-limiting toxicities, significant adverse events, or immune response. Additionally, there was evidence of antitumor activity indicating a highly favorable therapeutic index [406].

Another study attempted to describe artificial CPPs that were selectively and efficiently incorporated into human tumor cells according to their lineage [407]. The authors obtained ten representative tumor lineage homing cell-penetrating peptides by a screening of a random peptide library constructed using messenger RNA display technology. Among the results, they were able to target specific tumor cell types with different CPPs. One of those CPPs was FITC–CPP2 (a conjugated form of CPP2 with fluorescein isothiocyanate), which showed highly efficient permeation of the colon adenocarcinoma cell line, LoVo, without any significant uptake by the other tumor cell lines. This strong permeation was corroborated in three additional colon adenocarcinoma lines, Sw620, Colo320, and WiDr, whereas other lineages, such as MCF-7 and NHDF, did not show significant permeation [407]. Despite the promising results, no CPPs or CPP/cargo complexes have yet been approved by the FDA [395].

In a previous study, our group reported the synthesis of novel CPP2–thiazole conjugates (Scheme 8) and evaluated their anticarcinogenic properties using Caco-2 colon and A549 lung cancer cells [408]. At the time, several thiazole conjugates were used: 2-amino-5-nitrothiazole (NTZ, **2**, Scheme 8), 2-amino-5-methylthiazole (MTZ, **3**, Scheme 8), 2-aminobenzothiazole (BenzoTZ, **4**, Scheme 8), 5-bromothiazole-2-carboxylic acid (BTZCA, **5**, Scheme 8) and 2-bromothiazole-5-carboxylic acid (BTZ5CA, **6**, Scheme 8). Of these, the first three were coupled to CPP2 by a linker (i.e., succinic anhydride); in contrast, BTZCA and BTZ5CA were directly coupled to CPP2. The results have demonstrated these conjugates have promising anticancer activity against these cancer cell lines [408].

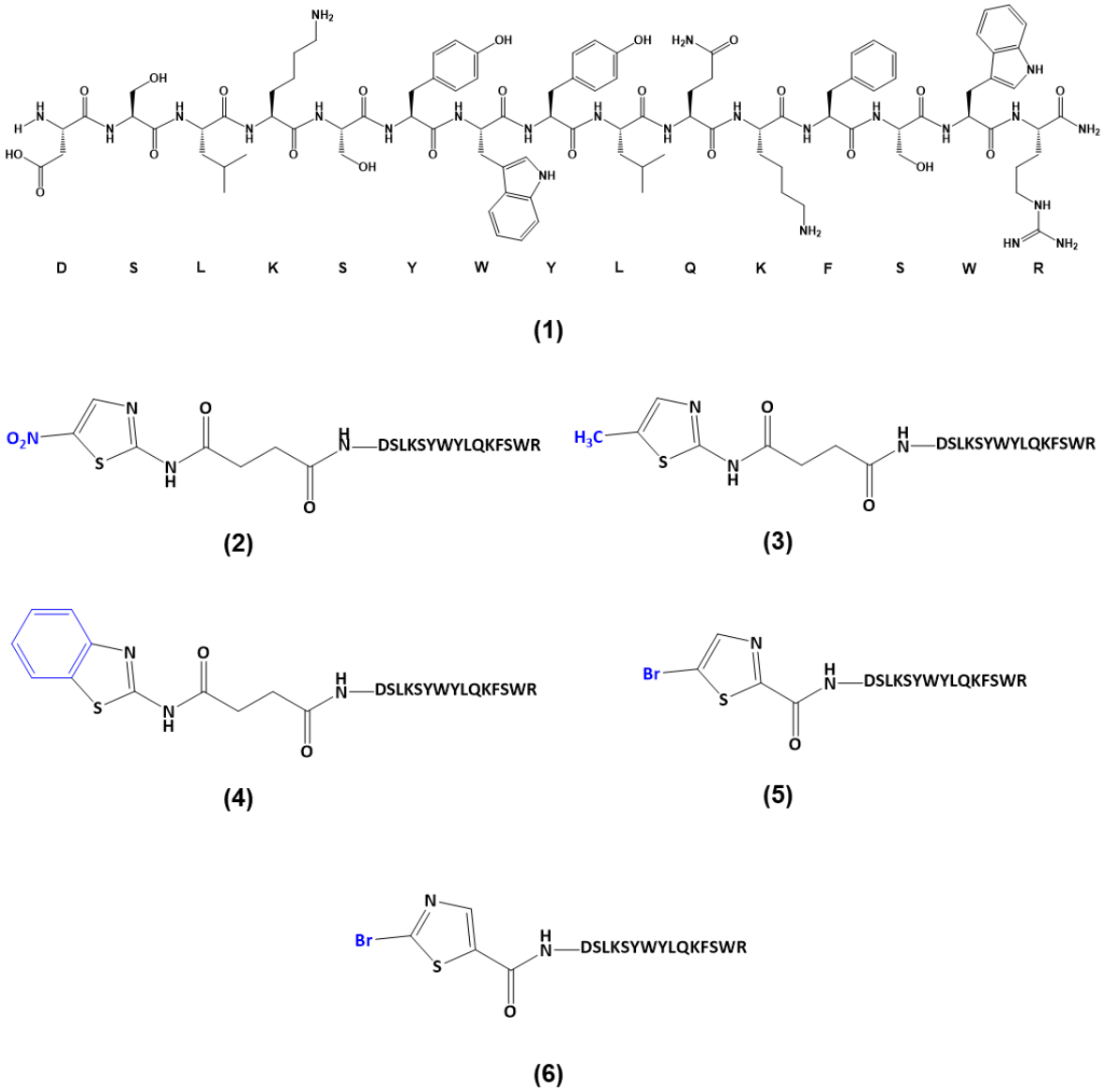

Scheme 8. Structure of the CPP2–thiazole conjugates previously synthesized by our group [408] and used in this work: (**1**) CPP2; (**2**) NTZ-C2-CPP2; (**3**) MTZ-C2-CPP2; (**4**) BenzoTZ-C2-CPP2; (**5**) BTZCA-CPP2; (**6**) BTZ5CA-CPP2.

Conventional chemotherapy has the main disadvantage of not being specific for tumor cells, acting both on normal and carcinogenic cells. In addition to its numerous side effects, the concentration of the drug that reaches the tumor site is quite low. Thus, this strategy of combining anticancer agents with CPPs may be very beneficial, since this synergism may increase the permeability of membranes for therapeutic agents and direct them toward the tumor's location, allowing for an increase in the concentration of drugs where they are strictly necessary, leading to an increase in treatment efficacy.

Therefore, in this work the previously synthesized CPP2–thiazole conjugates were combined with 5-FU in HT-29 colon cancer cells to investigate the cytotoxic effects of these combinations for cancer treatment. For that, it was first investigated the effect of each conjugate individually on HT-29 colon cells using increasing concentrations (0.1–50 µM) of CPP2 and five CPP2–thiazole conjugates for 48 h. Cell viability was evaluated by MTT assay.

The results demonstrated that BTZCA–CPP2 and BTZ5CA–CPP2 were the most promising CPP2 conjugates for decreasing the viability of these cells, with enhanced anticancer activity compared to 5-FU. Treatment with CPP2 did not result in a significant reduction in the viability of HT-29 cells. Cells treated with BenzoTZ-C2–CPP2, NTZ-C2–CPP2, and MTZ-C2–CPP2 did not result in significant changes compared to the treatment with 5-FU (Figure 66).

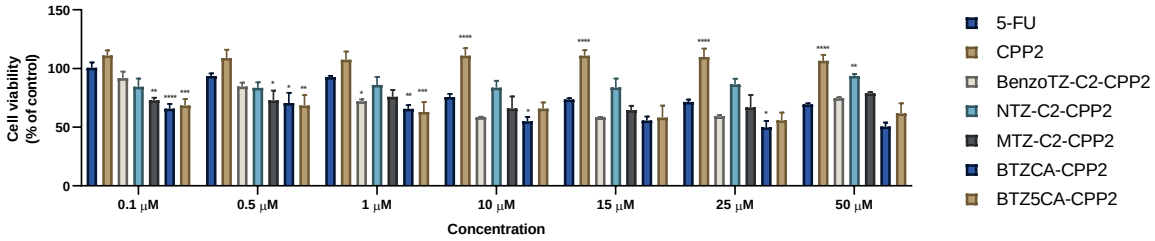

Figure 67. Cytotoxic effects of 5-FU, CPP2, and CPP2–thiazole conjugates on the viability of HT-29 cells. Cell viability was assessed by MTT assay after 48 h of exposure to each treatment. The results are expressed in the percentage of cell viability relative to untreated control cells. *, **, *** and **** indicate $p < 0.05$, $p < 0.01$, $p < 0.001$ and $p < 0.0001$, respectively, when compared with 5-FU. All data are presented as the mean ± SEM of three independent experiments.

Based on these results, it was found that most peptides did not achieve a 50% cell inhibition in this cell line, so it was next calculated an intermediate value (IV) for each compound individually by nonlinear regression using GraphPad software (Figure 68). This IV was obtained by plotting the logarithm of concentration against the normalized values of cell viability, as in a dose-response curve, but did not necessarily represent the IC_{50} of each compound, as these peptides had reached a plateau of inhibition. The calculation of this IV was necessary to have a method of comparison for the combination experiments. CPP2 treatment resulted in IV values higher than 50 µM, demonstrating a lack of activity against these cells. Treatment with NTZ– and MTZ-C2–CPP2 also resulted in poor anticancer effects. BenzoTZ-C2–CPP2 and the two conjugates without a linker (i.e., BTZCA–CPP2 and BTZ5CA–CPP2) resulted in IV values lower than 1 µM in HT-29 cells.

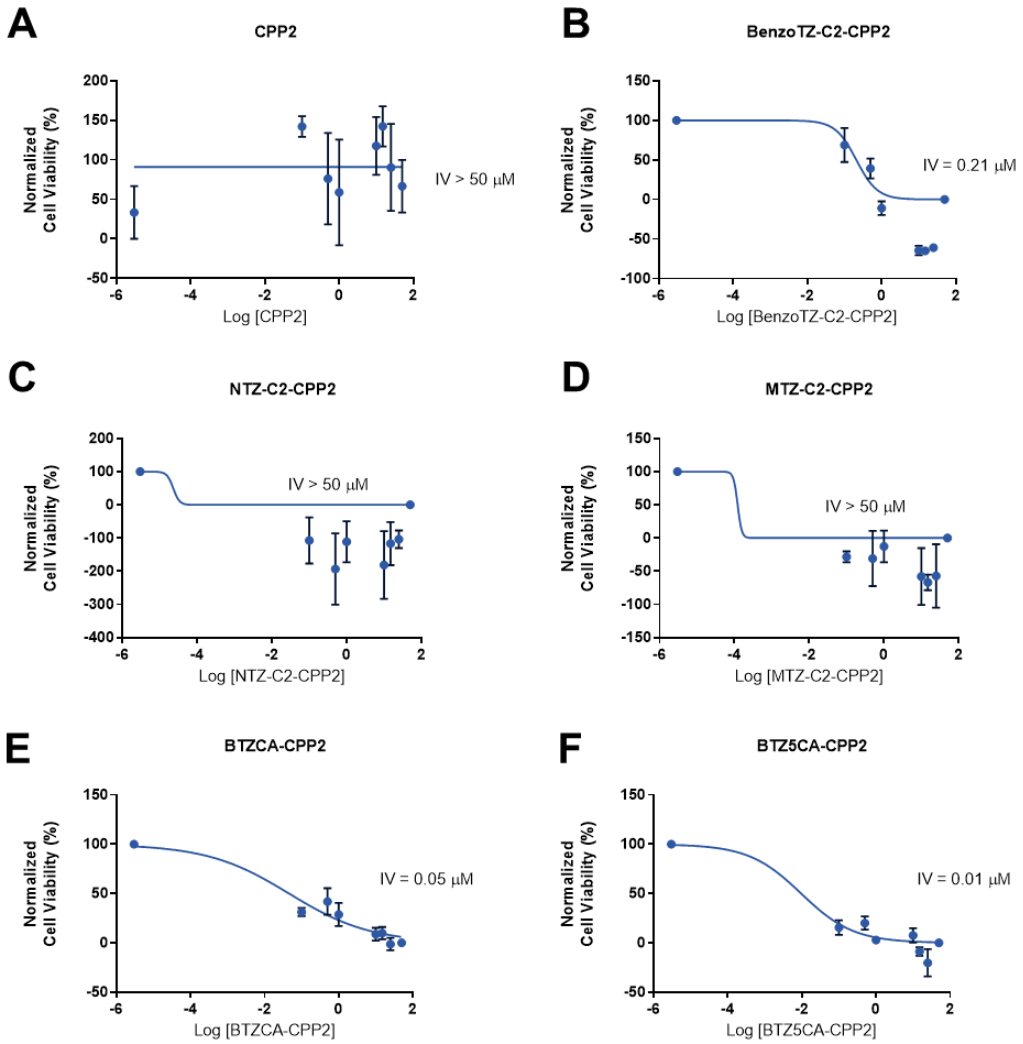

Figure 68. Concentration-response curves of CPP2 (**A**), BenzoTZ-C2-CPP2 (**B**), NTZ-C2-CPP2 (**C**), MTZ-C2-CPP2 (**D**), BTZCA-CPP2 (**E**) and BTZ5CA-CPP2 (**F**) on HT-29 cells based on the results obtained by MTT assay. The results represent the mean ± SEM of three independent experiments performed in triplicate.

CPP2 conjugates with an IV lower than 20 µM were further selected for combination treatments with 5-FU. Based on the results from Figure 68, three different CPP2–thiazole conjugates were selected for combination with 5-FU: BenzoTZ-C2–CPP2, BTZCA–CPP2, and BTZ5CA–CPP2. The *in vitro* cytotoxic effects of the selected CPP2–thiazole conjugates combined with 5-FU were assessed by MTT and SRB assays in HT-29 cancer cells. For that, five concentrations were selected, around the IV (0.25, 0.5, 1, 2, and 4 times IV) of each drug, both alone and combined, according to our previous combination model described in Figure 25.

The results between the MTT and SRB assays were in agreement and demonstrated a lack of significant antitumor activity for BenzoTZ-C2–CPP2 (Figure 69A and B) and BTZ5CA–CPP2 (Figure 69E and F) both alone and combined with 5-FU in HT-29 colon cancer cells. Moreover, treatment with 5-FU alone did not show significant modulation of the viability of these cells. Only cells treated with 5-FU + BTZCA–CPP2 (Figure 69C and D) demonstrated a significant reduction in cell viability, compared to 5-FU at the concentration of the IV of each drug, by MTT assay.

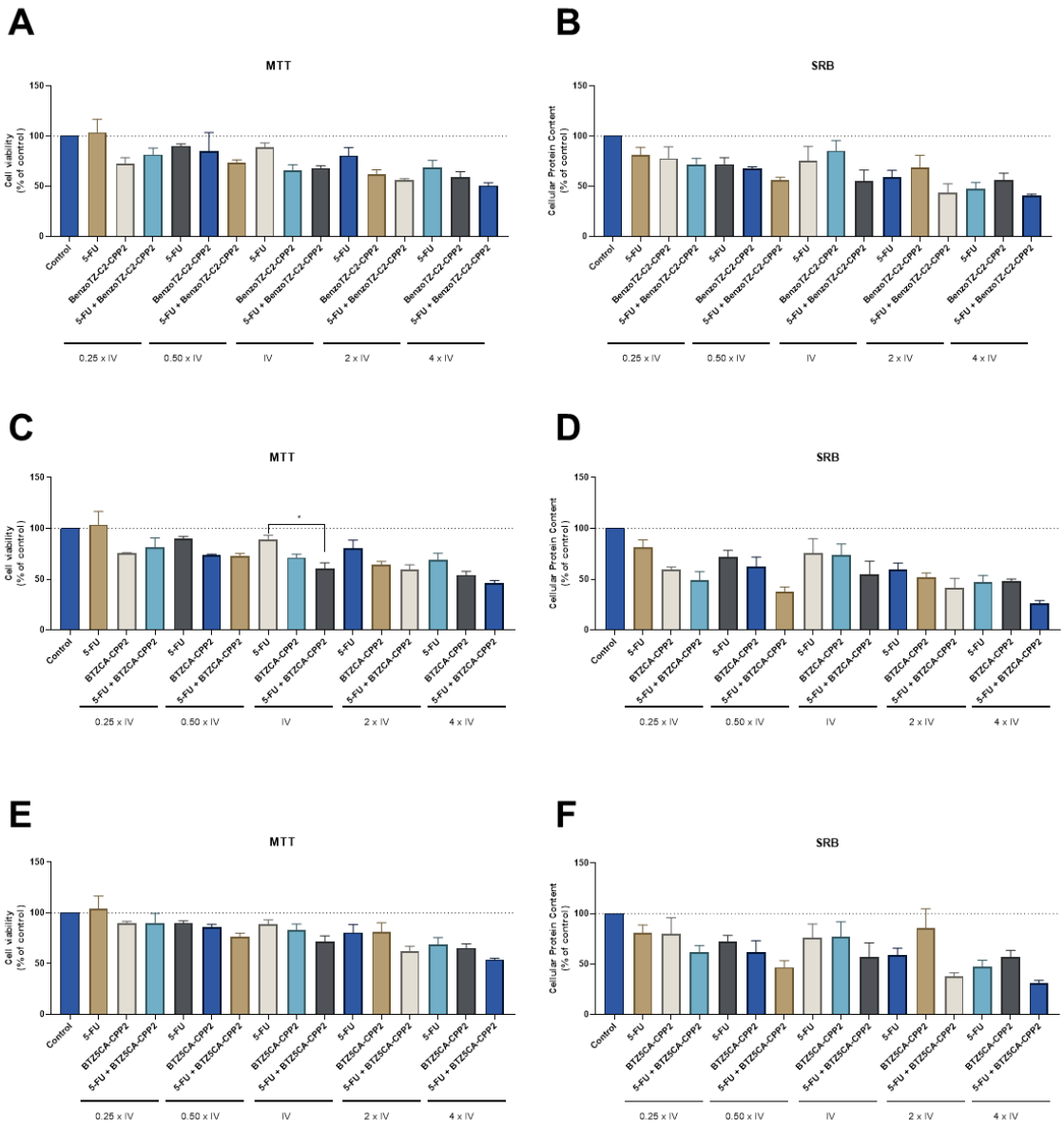

Figure 69. Cytotoxic effects of the combination of 5-FU with (**A**, **B**) BenzoTZ-C2-CPP2, (**C**, **D**) BTZCA-CPP2, and (**E**, **F**) BTZ5CA-CPP2 on the viability (right panel) and cell protein (left panel) content of HT-29 cells. Cell viability and protein content were assessed by MTT and SRB assays, respectively, after 48 h of exposure to each treatment. Results are expressed in the percentage of cell viability relative to untreated control cells. *

Indicates $p < 0.05$ when compared to control. All data are presented as the mean ± SEM of three independent experiments.

All previous treatments were confirmed by morphological analysis in HT-29 cells. No significant differences were noted among HT-29 cells treated with the CPP2–thiazole derivates alone compared to the control cells (Figure 70). Combination with 5-FU decreased cell number per well, but cell morphology was still maintained. Altogether, these results support the previous results obtained in the MTT and SRB assays.

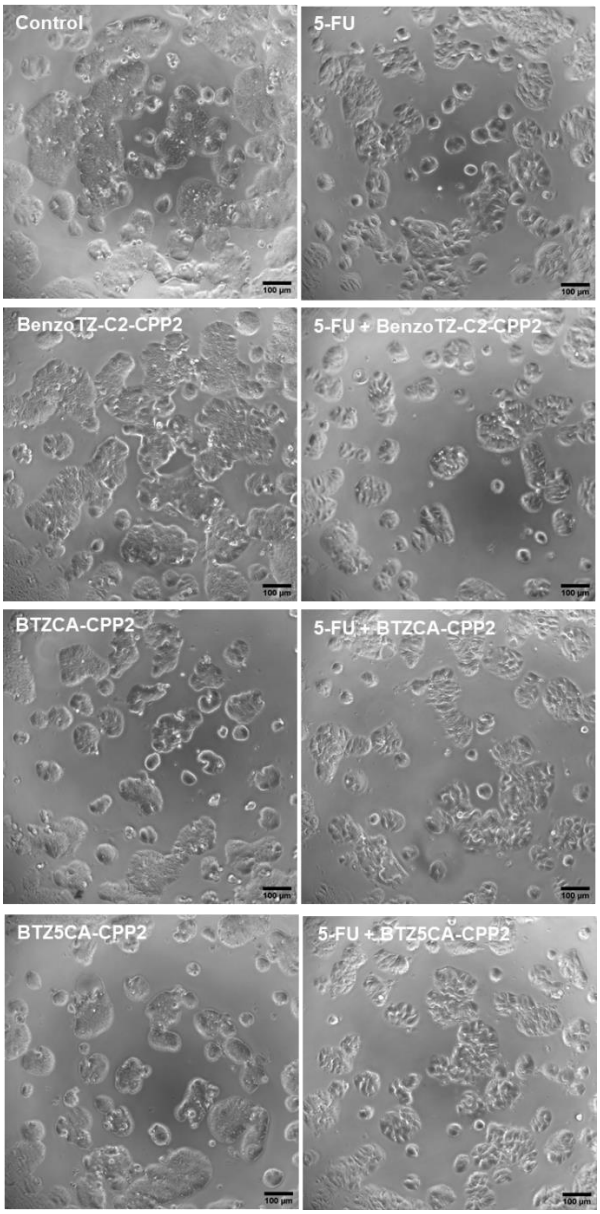

Figure 70. Microscopic visualization of HT-29 treated with CPP2-thiazole derivates, both alone and combined with 5-FU, at concentrations of 4 × IV. Representative images were obtained with a high contrast brightfield objective (10×) (LionHeart FX Automated Microscope) from three independent experiments. Scale bar: 100 µM.

Overall, these results suggest that the combination of CPP2-conjugates with 5-FU is not advantageous over treatment with CPP2–thiazole derivatives alone.

5.2.4 Combination Model IV: Peptides + Repurposed Drugs in Colorectal Cancer

5.2.4.1 Melittin (a component of honeybee venom) in combination with CNS drugs

After finding the favorable profile of the combination of honeybee venom with 5-FU, it was next hypothesized if several CNS drugs (fluphenazine, fluoxetine, sertraline, and thioridazine) could also have a promising anticancer profile in combination with this peptide. Therefore, these repurposed drugs were combined with honeybee venom in the same conditions as previously described.

Morphological analysis of HT-29 cells treated with fluphenazine plus increasing concentrations of honeybee venom resulted in a higher decrease in viable cells compared to bee venom alone, for the same range of concentrations (Figure 71A). Combinations with fluphenazine resulted in enhanced cytotoxic effects, with fluphenazine + 25 µg/mL of bee venom causing higher cytotoxicity than both corresponding drugs alone (Figure 71B). Cellular protein content was significantly reduced in HT-29 cells treated with fluphenazine + 6.25 µg/mL and fluphenazine + 12.5 µg/mL, compared to both compounds alone (Figure 71C).

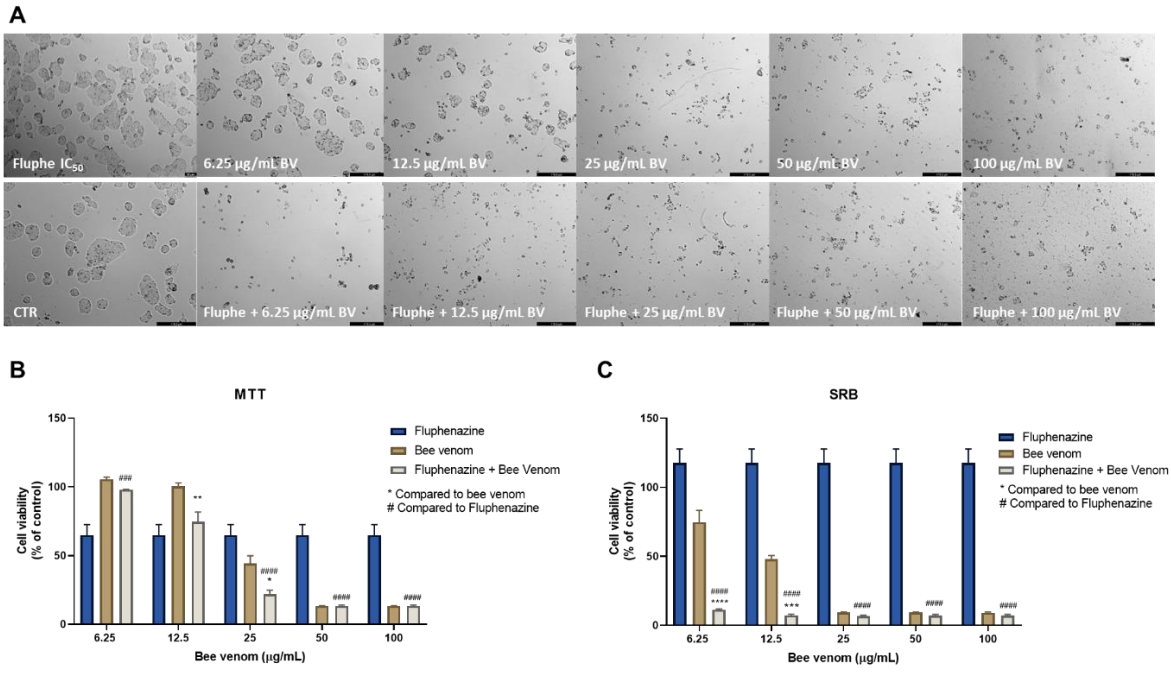

Figure 71. Effect of honeybee venom combined with fluphenazine in HT-29 colon cancer cells. (**A**) Morphological analysis; (**B**) MTT and (**C**) SRB assays. HT-29 cells were cultured in 96-well plates and treated with each combination for 48 h. Cell viability was determined after the final treatment. Each point represents the mean ± SEM relative to the control cells (0.1% DMSO) of three independent experiences. * Statistically

significant vs. bee venom at $p < 0.05$; ** Statistically significant vs. bee venom at $p < 0.01$; *** Statistically significant vs. bee venom at $p < 0.001$; **** Statistically significant vs. bee venom at $p < 0.0001$; ### Statistically significant vs. fluphenazine at $p < 0.001$; #### Statistically significant vs. fluphenazine at $p < 0.0001$. Scale bar: 179.3 µm; BV: bee venom; Fluphe: fluphenazine

The combination of fluoxetine and honeybee venom caused a higher reduction in the number of HT-29 viable cells (Figure 72A), compared to the single treatment with bee venom. Cell viability was significantly decreased in cells treated with a mixture of 6.25, 12.5, and 25 µg/mL of bee venom plus fluoxetine, being even lower than either drug alone (Figure 72B). Protein content inside cells in cells treated with the combination of 6.25 and 12.5 µg/mL of bee venom + fluoxetine was also lower than in cells treated with bee venom or fluoxetine alone (Figure 72C).

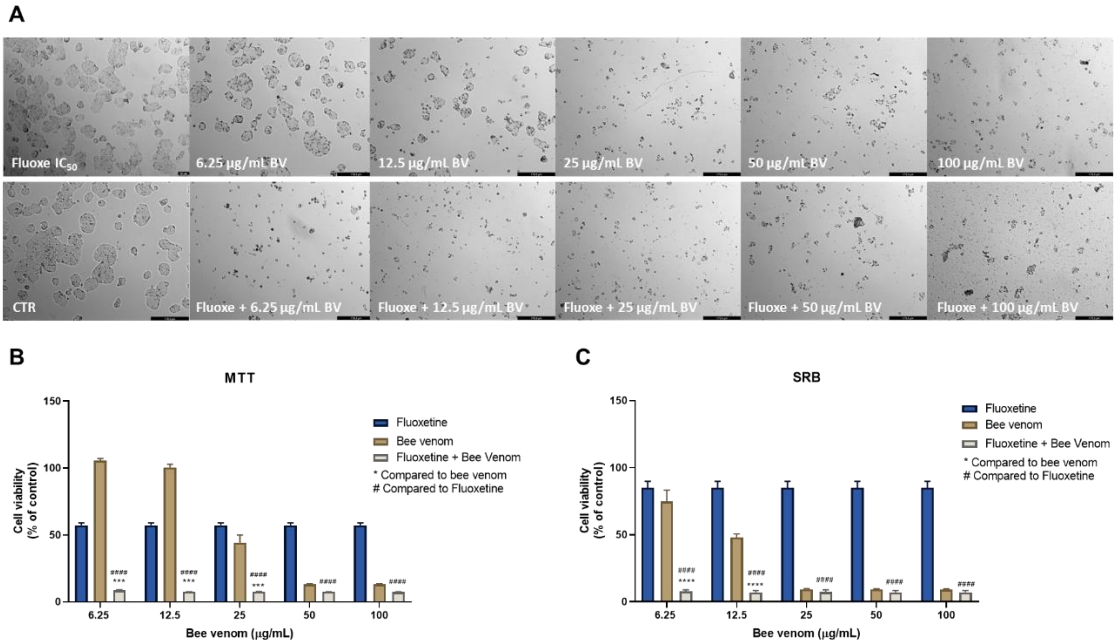

Figure 72. Effect of honeybee venom combined with fluoxetine in HT-29 colon cancer cells. (**A**) Morphological analysis; (**B**) MTT and (**C**) SRB assays. HT-29 cells were cultured in 96-well plates and treated with each combination for 48 h. Cell viability was determined after the final treatment. Each point represents the mean ± SEM relative to the control cells (0.1% DMSO) of three independent experiences. *** Statistically significant vs. bee venom at $p < 0.001$; **** Statistically significant vs. bee venom at $p < 0.0001$; #### Statistically significant vs. fluoxetine at $p < 0.0001$. Scale bar: 179.3 µm; BV: bee venom; Fluoxe: fluoxetine

Sertraline combined with honeybee venom also resulted in a significant decrease in cell viability, both seen by morphological analysis (Figure 73A) and MTT assay (Figure 73B). MTT results demonstrated that 6.25, 12.5 and 25 µg/mL of honeybee venom combined with sertraline produced better anti-cancer efficacy than each drug alone. For higher concentrations, results were significantly improved compared to sertraline alone. Cellular protein content in combined treatments was significantly lower than sertraline alone for all ranges of concentrations and lower than both drugs alone for the concentrations of 6.25 and 12.5 µg/mL of honeybee venom plus sertraline (Figure 73C).

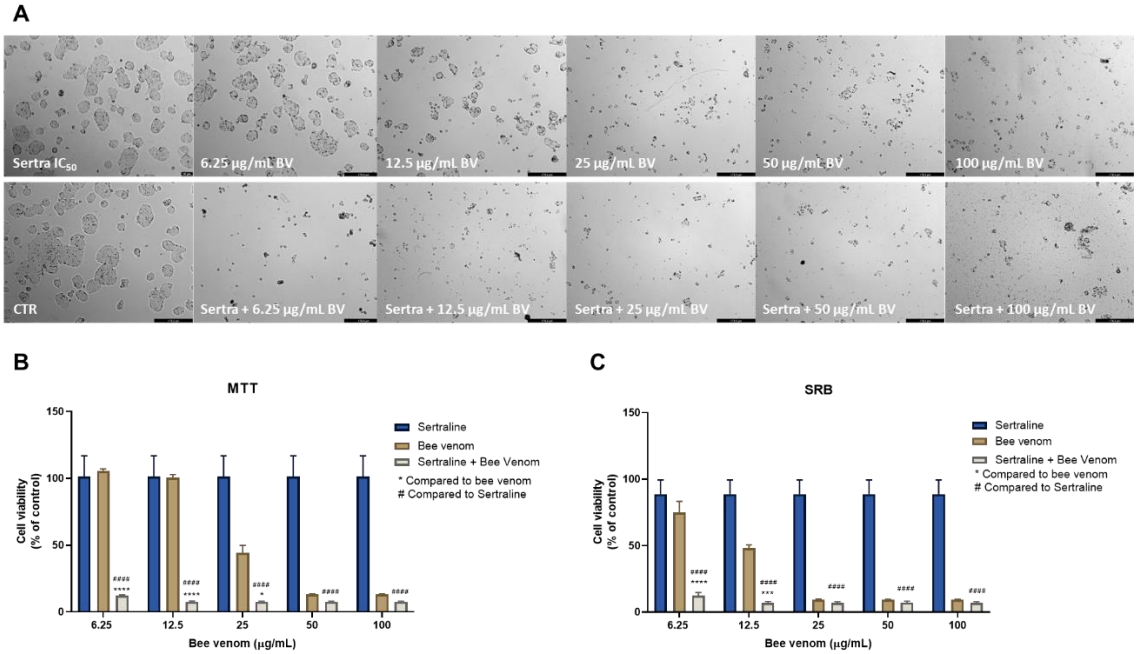

Figure 73. Effect of honeybee venom combined with sertraline in HT-29 colon cancer cells. (**A**) Morphological analysis; (**B**) MTT and (**C**) SRB assays. HT-29 cells were cultured in 96-well plates and treated with each combination for 48 h. Cell viability was determined after the final treatment. Each point represents the mean ± SEM relative to the control cells (0.1% DMSO) of three independent experiences. * Statistically significant vs. bee venom at $p < 0.05$; *** Statistically significant vs. bee venom at $p < 0.001$; **** Statistically significant vs. bee venom at $p < 0.0001$; #### Statistically significant vs. sertraline at $p < 0.0001$. Scale bar: 179.3 µm; BV: bee venom; Sertra: sertraline

The last repurposed drug used in HT-29 combination studies with honeybee venom was thioridazine. These combinations produced similar results to sertraline and fluoxetine plus honeybee venom, both by MTT and SRB assays. Compared to bee venom alone, the morphological analysis revealed a higher reduction of viable cells when thioridazine was combined with bee venom. These differences were seen mostly at lower concentrations of bee venom (Figure 74A). These results were in agreement with MTT assay results, where

it was found that the combination of thioridazine and honeybee venom in concentrations of 6.25, 12.5, and 25 µg/mL caused a significant reduction of viable cells, compared to each drug alone. For higher concentrations, the anti-cancer activity of the combinations was similar to bee venom alone (Figure 74B). Evaluation of the protein content of the cells treated with combinations of honeybee venom plus thioridazine also revealed a significant decrease for the two lowest concentrations (6.25 and 12.5 µg/mL of bee venom + thioridazine), compared to thioridazine and bee venom alone (Figure 74C).

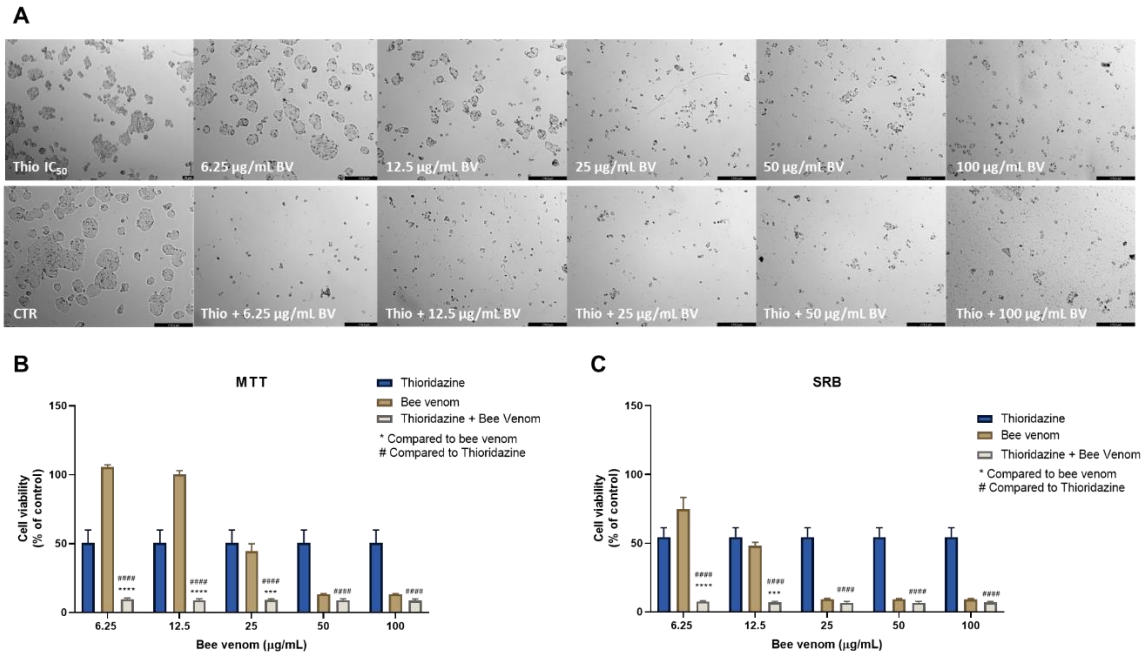

Figure 74. Effect of honeybee venom combined with thioridazine in HT-29 colon cancer cells. (**A**) Morphological analysis; (**B**) MTT and (**C**) SRB assays. HT-29 cells were cultured in 96-well plates and treated with each combination for 48 h. Cell viability was determined after the final treatment. Each point represents the mean ± SEM relative to the control cells (0.1% DMSO) of three independent experiences. *** Statistically significant vs. bee venom at $p < 0.001$; **** Statistically significant vs. bee venom at $p < 0.0001$; #### Statistically significant vs. thioridazine at $p < 0.0001$. Scale bar: 179.3 µm; BV: bee venom; Thio: thioridazine

Together, these results demonstrate that honeybee venom has anti-cancer activity against colon cancer cells, causing a significant reduction in cell viability in concentrations above 25 µg/mL. Moreover, the combinations of honeybee venom with CNS drugs (fluphenazine, fluoxetine, sertraline, and thioridazine) demonstrated greatest potential in reducing the number of viable cells than 5-FU, a common antineoplastic drug used for colorectal cancer.

Additionally, the combination of 6.25, 12.5, and 25 µg/mL of honeybee venom with the repurposed drugs fluoxetine, sertraline, and thioridazine resulted in significant

reductions in the viability of HT-29 colon cancer cells compared to each drug alone, demonstrating that CNS drugs can help improve the anti-cancer activity of bee venom in colon cancer cells.

5.2.4.2 CPP2-conjugates in combination with Clotrimazole

Since CPP2–thiazole conjugates combined with 5-FU did not result in many significant results in the HT-29 cell line, it was proposed another combination model using the combination of the repurposed drug clotrimazole plus CPP2-thiazole conjugates. This antifungal drug was selected because it presented significant anticancer activity against HT-29 colorectal cancer cells as a standalone agent. The experimental protocol was the same as presented in Figure 25. Cell viability and cellular protein content were evaluated by MTT and SRB assays, respectively, after a treatment period of 48 h.

These results suggest that clotrimazole has efficacy in the reduction of viability and protein synthesis of these cells, mainly at concentrations of IV and higher, demonstrating a greater anticancer potential than 5-FU in these cells (Figure 75). Nonetheless, the combination of CPP2–thiazole derivates did not demonstrated promising results compared to clotrimazole alone.

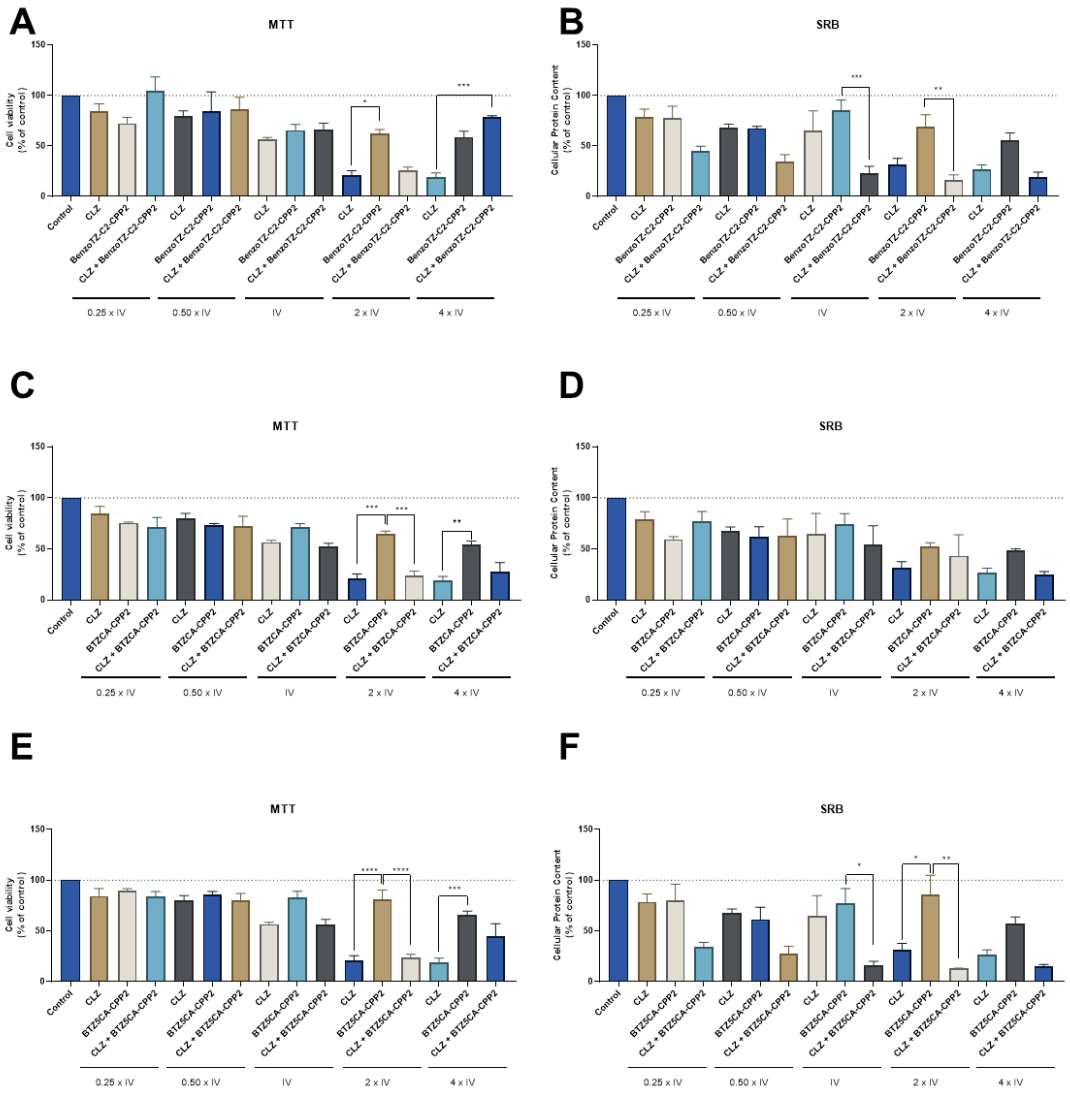

Figure 75. Cytotoxic effects of the combination of CLZ with (**A**, **B**) BenzoTZ-C2-CPP2, (**C**, **D**) BTZCA-CPP2, and (**E**, **F**) BTZ5CA-CPP2 on the viability (right panel) and cell protein (left panel) content of HT-29 cells. Cell viability and protein content were assessed by MTT and SRB assays, respectively, after 48 h of exposure to each treatment. Results are expressed in the percentage of cell viability relative to untreated control cells. *, **, *** and **** indicate $p < 0.05$, $p < 0.01$, $p < 0.001$ and $p < 0.0001$, respectively. All data are presented as the mean ± SEM of three independent experiments. CLZ: clotrimazole

The morphological analysis demonstrated that clotrimazole shows more potency than 5-FU in reducing cell numbers and promoting cell death. No significant differences were noted among HT-29 cells treated with the CPP2–thiazole derivates alone compared to the control cells. Combination with clotrimazole was very strong in reducing the number of viable cells and resulted in changes in the number and phenotype of these cells (Figure 76). Altogether, these results supported the previous results obtained in the MTT and SRB assays.

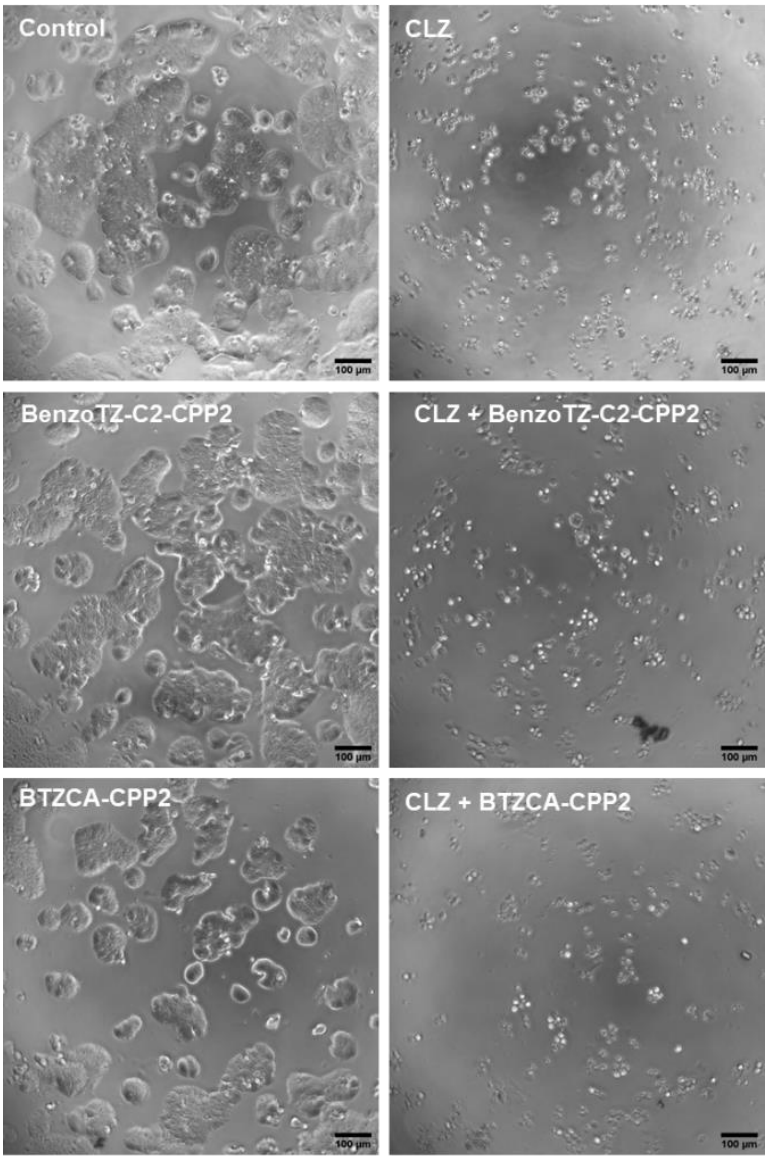

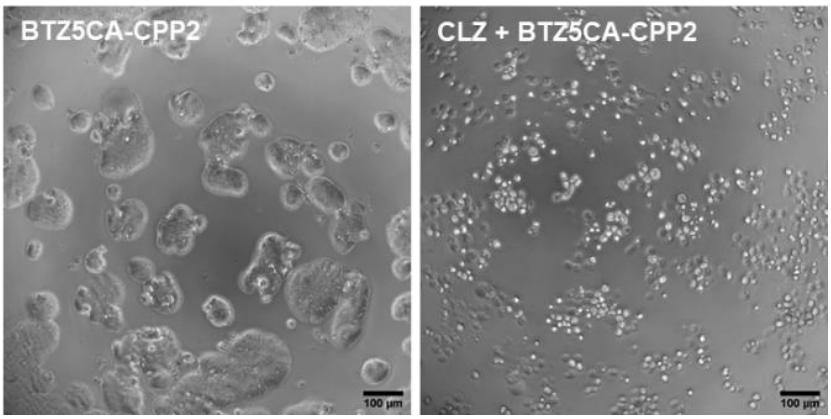

Figure 76. Microscopic visualization of HT-29 treated with CPP2-thiazole derivates, both alone and combined with CLZ, at concentrations of 4 × IV. Representative images were obtained with a high contrast brightfield objective (10×) (LionHeart FX Automated Microscope) from three independent experiments. Scale bar: 100 µM. CLZ: clotrimazole

These results suggest that the anticancer activity observed in these combinations resulted from the activity of clotrimazole alone and not from the thiazole derivates.

6. CONCLUSION OF CHAPTER II

Chemotherapy takes an important role in the treatment of colon cancer and has been subject of many advances over the years. Given the limitations of traditional new drug development, several strategies have gained attention such as drug repurposing, drug combination, and combination of repurposed drugs have been tested in both *in vitro* and *in vivo* studies for cancer therapy.

Here, the potential of four different combination models for breast and colorectal cancer therapy was evaluated. The combination model consisting of repurposed and antineoplastic drugs demonstrated that combined treatments using repurposed drugs can be advantageous for cancer therapy that it is ineffective or too toxic when chemotherapeutics are used as single agents. These results are encouraging for further research that considers antimalarials and CNS drugs as chemosensitizing agents of chemotherapeutic drugs for breast and colorectal cancer therapy. The combination model that combined only repurposed drugs demonstrated that the combination of antimalarial drugs is not advantageous over a single treatment, for both MCF-7 breast and HT-29 colorectal cancer cell lines, indicating that these repurposed drugs are more promising as standalone agents than in combination with other repurposed drugs. Nevertheless, the combination of CNS drugs demonstrated significant anticancer potential in colorectal cancer. In the combination model of peptides plus chemotherapeutic agents, these results demonstrated that 5-FU combined with honeybee venom, with peptide melittin as the principal component, is a promising drug combination for the chemotherapy of colorectal cancer. The last combination model consisted of the combination of repurposed drugs with peptides. It was found that CNS drugs can be used to enhance the cytotoxic activity of honeybee venom in both MCF-7 and HT-29 cell lines, especially at lower concentrations, which supports the anticancer potential of repurposed drugs and natural compounds in cancer therapies.

CHAPTER III

EVALUATION OF SYNERGISM IN DRUG COMBINATION MODELS FOR FUTURE ORIENTATIONS IN ONCOLOGY

1. SUMMARY OF CHAPTER III

One of the most important when designing and evaluating drug combinations is to achieve synergistic effects by demonstrating that the combined effects are greatly superior to the expected from the additive effects of the single drugs, allowing for dosage reduction and therefore decreasing toxicity. Nevertheless, synergism quantification is not a simple task due to the different definitions of additivity. Over the years, several reference models have been proposed based on different assumptions of additivity and with different mathematical frameworks.

In Chapter II, different novel combination models were developed and their cytotoxic effect was evaluated in two cancer cell lines: MCF-7 breast and HT-29 colorectal. Here, it is proposed the determination of the drug interactions between each drug in those combinations, aiming to find if the previously described drug combinations present synergistic interactions. This evaluation was performed by different reference models, such as the Chou-Talalay method as well as Zero Interaction Potency (ZIP), Highest Single Agent (HAS), Bliss independence, and Loewe reference models, using the CompuSyn and SynergyFinder software.

Regarding the combination of antimalarials and chemotherapeutic agents in MCF-7 cells, it was found that the combination of chloroquine, artesunate, and mefloquine with DOX and PTX to be synergic (combination index (CI) <1), which suggests that antimalarials can act synergistically with DOX/PTX for breast cancer therapy. Specifically, the combination of antimalarial drugs with DOX seems to result in more synergic drug pairs than the combination with PTX. In the combination of CNS drugs with chemotherapeutic agents, it was found that the combination of fluoxetine, fluphenazine, and benztropine with PTX resulted in synergism for all concentrations below IC_{50}. Also, it was found that the combination of DOX plus fluoxetine, benztropine, and thioridazine at their IC_{50} can improve the anticancer effect of DOX but to a lesser degree than when combined with PTX, resulting in most of the drug interactions being antagonist or additive. Moreover, it was also found that the use of quetiapine in combined therapies seems to synergistically enhance the anticancer activity of DOX but not PTX for the management of breast cancer. On the other side, the combination of repurposed drugs in this cell line did not result in synergism.

In the case of HT-29 colorectal cancer cells, it was found that the CNS drugs sertraline and thioridazine in simultaneous combination with 5-FU demonstrated the strongest synergism among all combinations. Both quetiapine and edaravone significantly improved the cytotoxic potential of 5-FU in HT-29 cells, but only quetiapine synergistically interacted with the antineoplastic drug in this combination. It was also found that the

antimalarial artesunate administration prior to 5-FU produced better results in reducing HT-29 cell viability than the inverse drug schedule or the simultaneous combination, with synergistic interactions between the two drugs for lower concentrations. Moreover, these results also allowed to conclude that antimalarial drugs as repurposed drugs have enhanced effects in MCF-7 breast cancer cells, while combination with CNS drugs seems to be more effective in HT-29 colon cancer cells. Regarding the combination of repurposed drugs, it was only found one synergic combination regimen (sertraline IC_{50} plus variable concentrations of fluphenazine) with anticancer potential against HT-29 colon cancer cells.

Regarding the combination of the peptide melittin with antineoplastic/repurposed drugs, it was found that bee venom combined with 5-FU and fluphenazine in HT-29 cells resulted in less cytotoxic effects compared to the co-treatment of fluoxetine, sertraline, and thioridazine plus bee venom, which resulted in less than 15% of viable cells for the whole range of concentrations, with all combined pairs being synergic, except for the higher concentration. Moreover, treatment of MCF-7 cells with the combination of repurposed drugs plus honeybee venom resulted in better anti-cancer efficacies and a higher number of synergistic pairs than with DOX, notably for lower concentrations.

Taken together, these results demonstrate that the choice of the antineoplastic drug in breast cancer influences the success of the drug combination and the drug interactions between the selected drug pairs. Moreover, it was found that CNS drugs activity differs between the two selected cell lines, both alone and in combination, which results in differences among the number of synergistic drug pairs. It was also found that the combination of repurposed drugs, specifically the CNS drugs sertraline and fluphenazine, may have an interesting profile for application in colon cancer novel therapies, with ability for further studies of dose optimization due to the presence of synergism among these drugs. The results regarding the combination of peptides support that honeybee venom in combination with repurposed drugs and chemotherapeutic agents can help improve their anti-cancer activity, especially for lower concentrations, in both cell lines, corroborating the enormous bioactive potential of honeybee venom for colon and breast cancer treatments, both alone and in combination with chemotherapy or repurposed drugs.

2. INTRODUCTION OF CHAPTER III

Drug combination exploits the susceptibility of different molecular pathways involved in the genesis of a certain disease to the different mechanism of actions of each individual drug. The main goal of this strategy is to improve the efficiency of the treatment, by decreasing cytotoxicity to normal cells and reducing the development of drug resistance [316]. Therefore, when combining two or more drugs, it is desirable to achieve positive interaction effects, by demonstrating superior evidence of the beneficial combination of two or more drugs compared to each drug individually [409]. Basically, achieving more with less. In this way, to make the best of the combination of drugs, it is important to efficiently find a way to prove that the drug combination has more benefits than both drugs alone. Over the years, research in this area resulted in several theoretical and experimental manuscripts [313, 410, 411], that described those interaction effects mostly as synergistic or antagonistic, that represent, respectively, more or fewer effects than the expected additive effect from each drug individually [316]. Nevertheless, defining additivity is not as simple as it may seem and throughout the years several authors have proposed different formal definitions and approaches to apply this concept in clinical practice [314, 412].

Here, it will be described the classical reference models that have been proposed for synergism evaluation, usually classified as effect-based and dose-effect-based methods (Figure 77), with a brief analysis of the current limitations of these models. It will also be provided the mathematical framework behind each reference model to perform the accurate evaluation of drug interactions in combination models. Moreover, novel methods for the accurate quantification of drug interactions in combined treatments will also be described. In addition, some of the most recent preclinical and clinical combination studies will also be covered to reflect the importance of the appropriate, accurate and precise application of the concepts and methodologies here described for the evaluation of synergism.

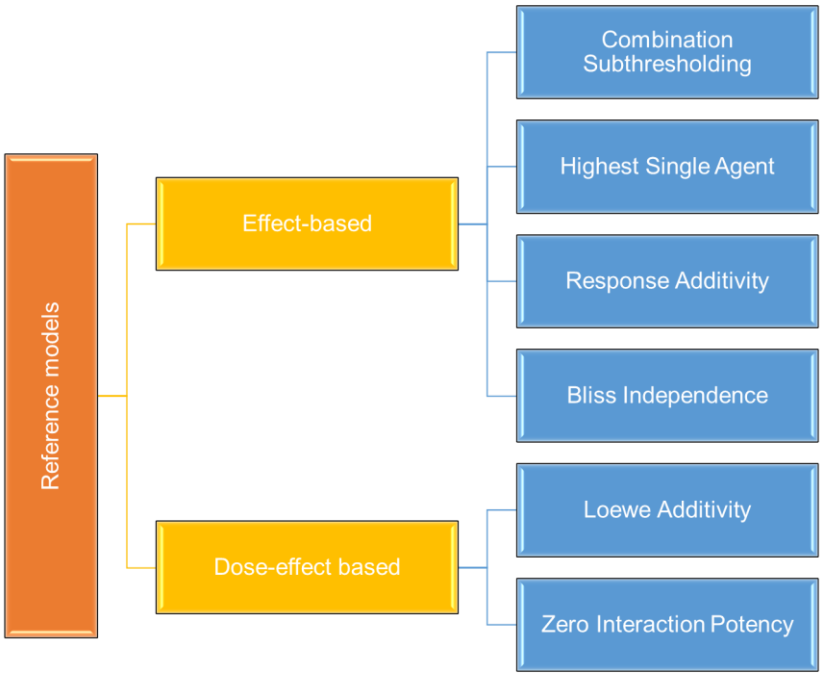

Figure 77. Most well-known reference models for the analysis of drug combinations. Current approaches can be divided into effect-based or dose-effect based and are described by different mathematical frameworks, based on different definitions of additivity.

2.1 Effect-Based Approaches

These methods are based on the effects of each individual drug within a combination to assess a positive interaction effect [316]. Effect-based strategies englobe four main strategies: Combination Subthresholding, HSA, Response Additivity, and Bliss Independence model [316]. The term "effect", sometimes referred to as response, is usually evaluated by cell death, viability, growth rate, among others, being indicative of the measured or phenotype effect. Throughout this chapter, the description of theorems assumes two drugs, A and B, given at doses a and b, with observed effects E_A and E_B. The effect of drug A combined with drug B is given by E_{AB} [316].

2.1.1 Combination Subthresholding

The Combination Subthresholding is the simplest approach based on the concept that the combination of ineffective doses of drugs generates significant effects. Contrary to other reference models, this significant effect is defined based on *p* values obtained from statistical tests by comparison with control (untreated groups) [316]. The observed effect is usually considered statistically significant when $p < 0.05$ (Figure 78). Although this approach

is sometimes still used, the observed effects may not be accurate enough and not necessarily be representative of significant differences if the difference between what is significant or not, is not necessarily significant [316, 413].

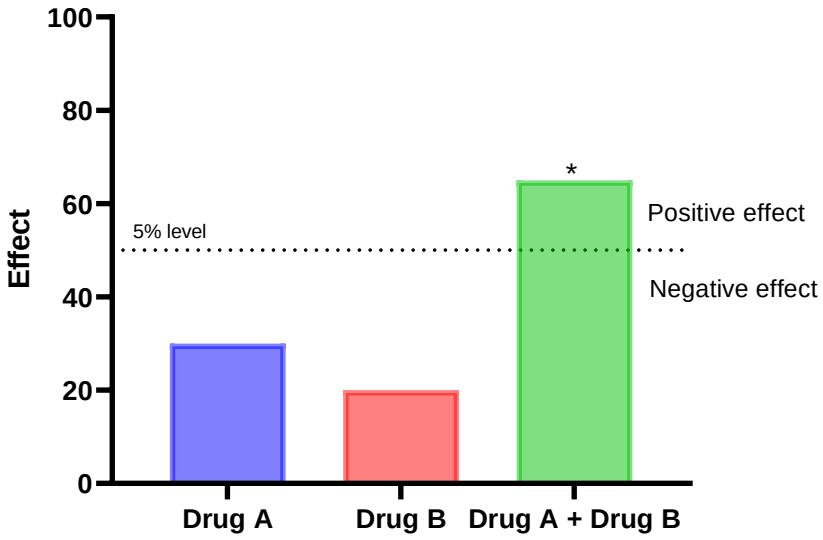

Figure 78. Demonstration of the Combination Subthresholding approach. This model assumes a positive interaction effect when $p < 0.05$. Based on E_A=30, E_B=20 and E_{AB}=65. Adapted from [316]. * significant at $p < 0.05$.

2.1.2 Highest Single Agent (HSA)

This reference model is also known as the Gaddum's noninteraction or cooperative effect [412, 414] and assumes a positive combination interaction when the drug combination elicits a greater response than the highest single agent ($E_{AB} > \max(E_A, E_B)$) (Figure 79). This represents an improvement of the Combination Subthresholding reference model as it allows the calculation of a CI by the following equation: $CI = \frac{\max(E_A, E_B)}{E_{AB}}$. If the value obtained for CI is positive, statistical significance is evaluated by comparing drug combination effects with the single drug more effective using the *p* value of the statistical test [316]. This reference model is more advantageous as it evaluates if differences are significant rather than the difference of significance. Nevertheless, this model only compares the drug combination effect to the most effective individual drug (highest single agent), not taking into account the expected additive effect of both drugs involved in the combination [316]. This makes this model suitable only for drug combinations where one of the drugs is inactive for all tested concentrations. Normally, this approach usually gives

more optimistic results because it has the lowest threshold for considering synergism among all reference models [415].

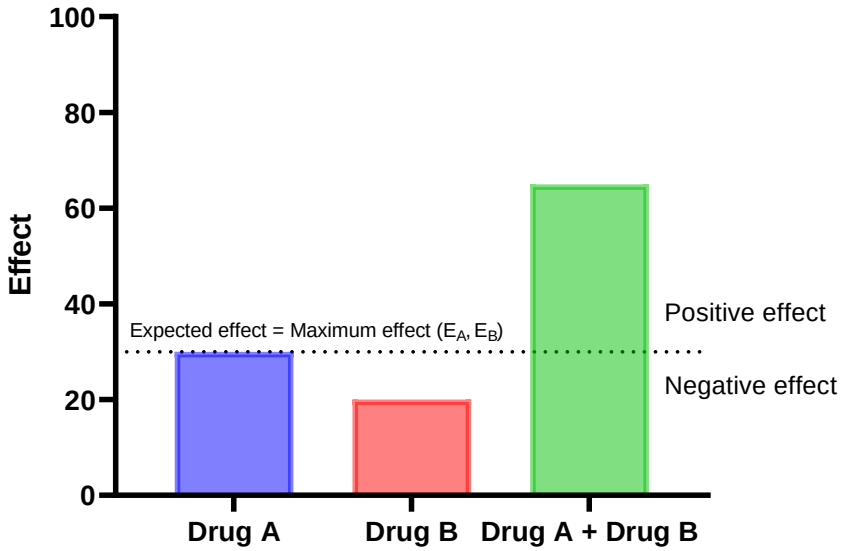

Figure 79. Demonstration of the Highest Single Agent approach. This model assumes a positive interaction effect when the drug combination induces a greater response than the highest single agent. Based on E_A=30, E_B=20 and E_{AB}=65. Adapted from [316].

2.1.3 Response additivity

This reference model is also known as Linear Interaction Effect [416] and assumes that a positive interaction occurs when the drug combination elicits a greater effect than the sum of the individual drugs' effects ($E_{AB} > E_A + E_B$) (Figure 80). The CI can be calculated as $CI = \frac{E_A + E_B}{E_{AB}}$, where the *p* value means the significance of the interaction effect in factorial analysis of variance of the individual and combined effects [416]. Compared to the previously mentioned reference model, the Response additivity approach represents an improvement as it compares the effects from the combination with the expected effects from both single drugs, assuming their effect to be addictive. Nevertheless, the determination of synergism using this model implies that both drugs have linear dose-effect curves, which may not be true for many drugs used in pharmacological studies [417].

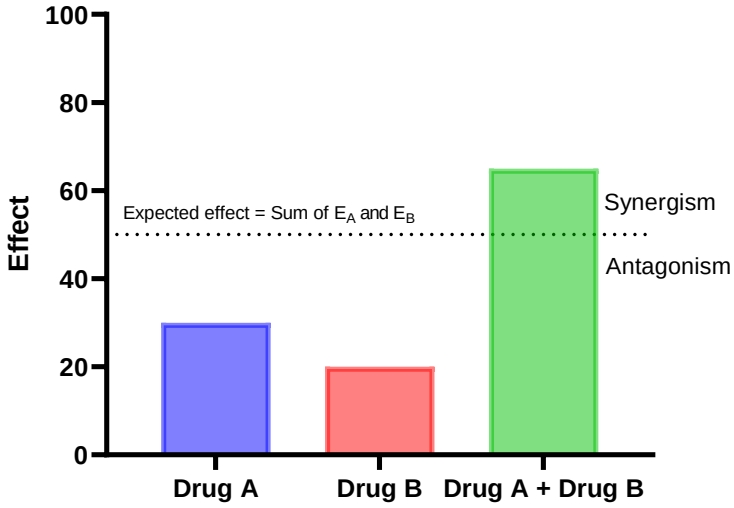

Figure 80. Demonstration of the Response Additivity approach. This model assumes synergistic effects when the drug combination induces a greater response than the sum of the individual drugs' effects. Based on E_A=30, E_B=20 and E_{AB}=65. Adapted from [316].

2.1.4 Bliss independence

This approach is one of the most popular models and was first introduced in the 1930s [412, 418–420]. This model assumes that both drugs used in drug combinations act independently and do not interfere with the other, assuming that drugs act on different sites of action [419]. Nevertheless, this model assumes both drugs contribute to the observed effect (Figure 81). In this approach, the drug effects from single and combined treatments are expressed in the form of a probability (0 ≤ E ≤ 1) and the expected combined effect is defined as: $E_{AB} = E_A + E_B(1 - E_A)$, where E_A and E_B represent the observed effects of drug A and B, respectively, and E_{AB} the effect of drug A combined with drug B. The calculation index for this approach can be calculated as $CI = \frac{E_A+E_B-E_AE_B}{E_{AB}}$, being indicative of synergy, antagonism or additivity when CI is under, above or equal to 1, respectively [316]. This model of non-interactivity is one of the effect-based approaches that has survived to the critics over time. Although this model is widely used in the pharmaceutical field and is more accurate than the previous ones, it still presents some limitations [421] such as: it depends on the knowledge of mechanisms of action, and most of the time drugs have several, intricate and possibly undetermined mechanisms of action [419]; moreover, this model also presumes that drugs follow an exponential dose-effect response, which may not be applicable for all drugs [420]; finally, this model only fits for effects that can be ranged in probabilities from 0 to 1 [316].

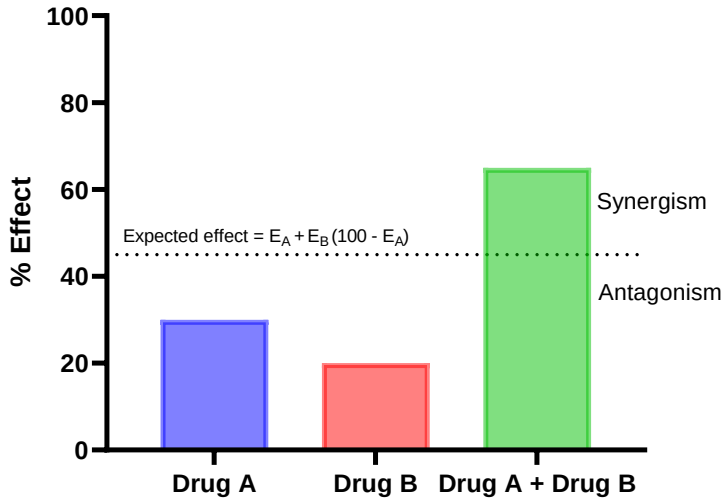

Figure 81. Demonstration of the Bliss Independence approach. This model assumes that both drugs act independently and do not interfere with each other. Based on E_A=30, E_B=20 and E_{AB}=65. Adapted from [316].

2.2 Dose-effect-Based Approaches

More recently, novel approaches have been proposed to surpass the limitations of the previously mentioned reference models. Especially for drugs that have nonlinear dose-effect curves, dose–effect-based approaches represent an improvement as they take into account the dose of each drug that results in the same quantitative effect [422]. These reference models consider the dose-effect curves of each drug and provide significant and unequivocal definitions of synergy, additivity, and antagonism [316]. Nevertheless, to evaluate if there is an interaction effect in a drug combination, it is essential to first define a non-interactive effect, which can be achieved by null reference models [410].

2.2.1 Loewe Additivity

The Loewe additivity model is a null reference model and the most well-known dose–effect-based approach. It was first mentioned by Frei in 1913 and further described using a mathematical framework by Loewe in 1926 [422–425]. This model is based on the isobole representation to define the additive effect. This reference model assumes the dose equivalence principle, meaning the dose a from Drug A is equivalent to the dose b_a of drug B and vice-versa, for any given effect. It also assumes the sham combination principle, meaning that dose b_a can be added to any dose b of drug B to achieve an additive effect, which is not a characteristic of other null reference models [410]. The additive effects depend on the dose curves of each drug and can be defined as $Effect\,(a+b) = E_A(a+a_b) = E_B(b+b_a) = E_{AB}$.

This model assumes that individual drugs have a constant potency ratio $(R = \frac{A}{B})$, meaning their doses have the same ratio at each level of effect. Graphically, this means the drugs have parallel dose-response curves and achieve the same maximum effects [426]. This interaction can be defined by the following mathematical equations: $a + a_b = A \leftrightarrow a + b \times R = A \leftrightarrow a + b \times \frac{A}{B} = A$, which is behind the Loewe Additivity equation and many other dose-based approaches that derived from this reference model: $\frac{a}{A} + \frac{b}{B} = 1$.

The CI derived from the Loewe Additivity is calculated by: $CI = \frac{a}{A} + \frac{b}{B}$ [422, 427, 428]. When CI is under 1, it means that the doses a and b that are necessary to produce a combined effect are lower than the ones predicted from additivity, which is indicative of synergistic interactions between the two drugs. When the CI value is above 1, the doses from each individual drug that produce a combined effect are greater than the ones predicted from additivity, meaning that drug interaction is antagonistic [422, 427, 428].

Isobologram analysis was first introduced in 1995 by Greco *et al* [419] and is a graphical approach to the Loewe Additivity model, allowing an easy interpretation of the interaction of two drugs in a given combination [426]. It is a graphical representation that has represented the doses of drug A and drug B in the x and y-axis and indicates the collection of all dose combinations of the drugs that achieve a desired percentage of effect.

In this graphical representation, there is a line with a negative slope that represents the additive effect (also known as additive isobole), where deviations from additivity indicate synergism or antagonism (Figure 82) [314, 429]. It represents the expected combined effect of a drug combination using doses a and b from two drugs A and B and can be calculated by the equation $b = B - \frac{B}{A} \times a$, where doses of A and B are represented on the x and y-axis. This means that when the doses from individual drugs necessary to achieve a combined effects are lower than the corresponding ones described from the additivity line (i.e., are located below the line), this can be translated as synergy (CI<1). A drug pair located on the additive isobole means that CI=1 and therefore indicates additivity, whereas a drug pair located above this isobole is indicative that higher doses of each individual drug are necessary to produce the expected combined effect and therefore are related with antagonism (CI>1) [316]. This approach does not rely on the drugs' dose-response relationship neither their mechanism of interaction, being only affected by the concentration of the drugs used in the combination. This means that one drug pair can be synergic for one dosage and antagonist for another therapeutic regimen [420].

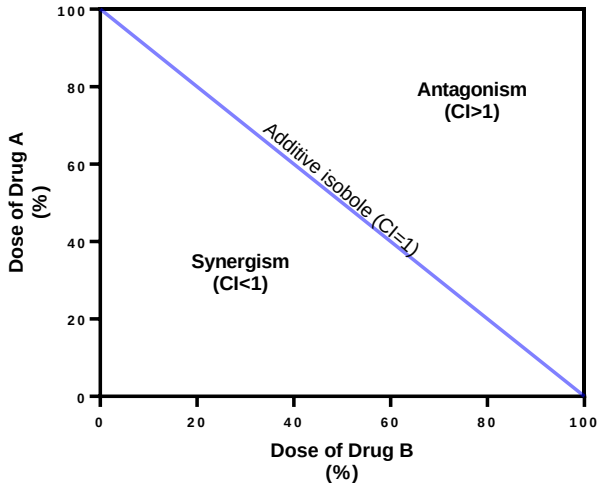

Figure 82. Demonstration of the Loewe Additivity approach (isobologram). The diagonal line represents the additive effect (also known as additive isobole) and deviations from additivity are indicative of synergism or antagonism. Adapted from [316].

Just like the previous reference models, the Loewe Additivity model also presents some limitations, mostly related to the dose-effect curves of each individual agent. It is only designed for drugs that have dose-response curves described by the Hill equation (also called sigmoid or logistic function) and sometimes the determination of these curves requires lots of data that can be time and money-consuming [430]. Also, some drugs have dose-response curves that are difficult to model, making the Loewe Additivity model useless [431]. In addition, many drugs do not fit in the isobole straight line: this can be a result of drugs that do not have a constant potent ratio, hence resulting in non-parallel dose-response curves and/or when the individual drugs do not achieve the same maximum effects [429].

Many null reference models are based on the concept of isoboles. The Chou-Talalay approach, proposed by Chou and Talalay is still one of the most used reference models in biological studies to quantify drug interactions. This reference model has been built based on the Loewe Additivity model [313, 314, 427, 428] and incorporates the median-effect equation, derived from the unified theory mass-action law principle, represented by the equation $\frac{fa}{fu} = (\frac{D}{Dm})^m$, where D represents the drug dosage or concentration, fa the inhibited fraction by the drug dose D, fu the unaffected fraction, Dm the dose that causes 50% inhibition, and m the coefficient indicating the shape of the dose-effect curve. The model is also described by an (r) value, that indicates the fitting of the data to the mass-action law. The values of (m), (Dm), and (r) for each single drug are the dose-effect

parameters required for the implementation of the Chou-Talalay theorem. In this way, the unified theory establishes the common link between single and multiple entities, and first order and higher-order dynamics. The general equation that describes this model, previously mentioned, is derived from the Michaelis-Menten, Hill, Henderson-Hasselbalch, and Scatchard equations, the most important ones in biochemistry and biophysics, which resulted in the development of the CI theorem, that offers a quantitative determination of synergism in drug combinations [313]. It has been improved by including the principle of mass action to analyze the combined effects of a given combination and is now the subject of a huge number of publications. The CI for a two-drug combination can be calculated as following: $CI = \frac{(D)_1}{(Dx)_1} + \frac{(D)_2}{(Dx)_2}$, where $(Dx)_1$ represents the dose of the drug D_1 alone that inhibits the growth of cells by x% and $(Dx)_2$ is the dose of the drug D2 alone that inhibits the growth of cells by x%. It has its own graphical representation consisting of a plot of CI versus the fractional effect (Fa), where CI<1, CI=1 and CI>1 indicate synergism, additivity and antagonism, respectively (Figure 83).

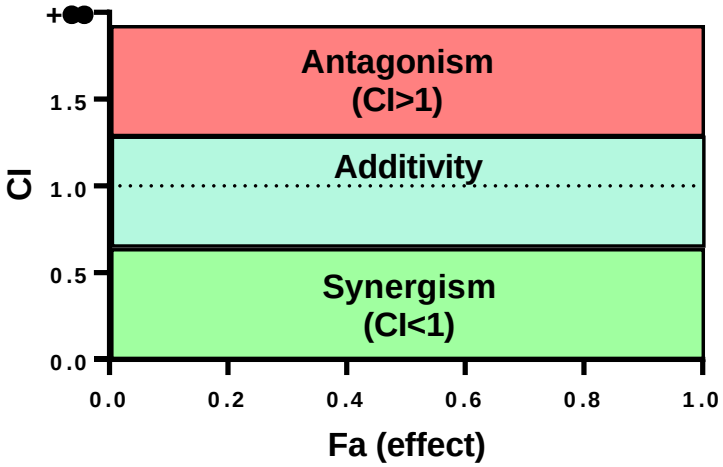

Figure 83. Fa-CI plot proposed by Chou and Talalay, based on the Loewe Additivity model. Fa indicates the observed effect and CI<1, CI=1, and CI > 1 indicate synergism, additivity, and antagonism, respectively. Adapted from [432].

2.2.2 Zero interaction potency (ZIP)

This is one of the most recent reference models proposed for the evaluation of expected responses in drug combinations, being a hybrid approach between the Bliss Independence and the Loewe Additivity models [433]. This approach evaluates the drugs' interactions by comparing changes in the potency of the dose-response curves between

individual and combined drugs, not being affected by the pharmacodynamics of the compounds in combination. It assumes that drugs are independent and do not interact with each other when combined, resulting in minimal changes in their response curves when combined [433]. This means that the accurate fitting of the dose-response curves is crucial for the determination of parameters like the relative half-maximal effect concentration (EC_{50}) and the slope, which can be a difficult challenge if data is of poor quality, for example [415].

Table 14 summarizes the advantages and disadvantages of the previously described reference models used to assess the pharmacological interaction in drug combinations, together with the mathematical framework behind the calculation of the expected additive effect and CI values for each model.

Table 14. Advantages, disadvantages, and mathematical framework of the reference models described in this manuscript used to assess the pharmacological interaction in drug combinations.

Reference model	Pros	Cons	Mathematical Framework
Combination Subthresholding	- Most simple approach	- Effect-based approach - Significant effects are defined based on *p* values - The observed effects may not be accurate and do not necessarily be representative of significant differences - Does not allow the calculation of a CI - Least accurate reference model	- The observed effect is considered statistically significant when $p < 0.05$
Highest Single Agent	- Allows the calculation of a CI	- Effect-based approach	- $E_{AB} = \max(E_A, E_B)$

	- Gives more optimistic results among all reference models	- Does not take into account the expected additive effect of both drugs involved in the combination - Suitable only for drug combinations where one of the drugs is inactive for all tested concentrations	- $CI = \frac{\max(E_A, E_B)}{E_{AB}}$.
Response additivity	- Allows the calculation of a CI - Considers the effects of both drugs in combination, assuming their effect to be additive	- Effect-based approach - Implies the drugs to have linear dose-effect curves	- $E_{AB} = E_A + E_B$ - $CI = \frac{E_A + E_B}{E_{AB}}$
Bliss Independence	- One of the most popular - Allows the calculation of a CI - Takes into account the effects of both drugs in the combination	- Effect-based approach - Depends on the knowledge of mechanisms of action of the drugs - Presumes that drugs follow an exponential dose-effect response - Only fits for effects that can be ranged in probabilities from 0 to 1	- $E_{AB} = E_A + E_B(1 - E_A)$ - $CI = \frac{E_A + E_B - E_A E_B}{E_{AB}}$

	- Assumes that both drugs act independently and do not interfere with the other - Allows combinations of more than 2 drugs		
Loewe Additivity	- Most well-known dose–effect-based approach - Allows the calculation of a CI - Take into account the dose of each drug - Assumes the dose equivalence and the sham combination principles - Graphical approach (isobologram)	- Only designed for drugs that have dose-response curves described by the Hill equation - Requires more data and sometimes raw data preprocessing - Only fit to drugs that have a constant potent ratio.	- $E_{AB} = E_A(a + a_b) = E_B(b + b_a)$ - $CI = \frac{a}{A} + \frac{b}{B}$

	- Does not rely on the drugs' dose-response relationship nor their mechanism of interaction - Allows combinations of more than 2 drugs		
Zero Interaction Potency	- One of the most recent reference models - Dose-effect-based approach - Assumes that drugs are independent and do not interact with each other when combined - It is not affected by the pharmacodynamics of the compounds in combination	- Requires accurate fitting of the dose-response curves - Requires data of good quality - Does not allow combinations of more than 2 drugs	- $E_{AB} = \frac{(\frac{[A]}{EC_{50,A}})^{\lambda A}}{1+(\frac{[A]}{EC_{50,A}})^{\lambda A}} + \frac{(\frac{[B]}{EC_{50,B}})^{\lambda B}}{1+(\frac{[B]}{EC_{50,B}})^{\lambda B}} - \frac{(\frac{[A]}{EC_{50,A}})^{\lambda A}}{1+(\frac{[A]}{EC_{50,A}})^{\lambda A}} \frac{(\frac{[B]}{EC_{50,B}})^{\lambda B}}{1+(\frac{[B]}{EC_{50,B}})^{\lambda B}}$

2.3 Current limitations of the classical combination models

As demonstrated in the previous sections, current reference models for the evaluation of synergism have been improved over the years but there are still some general limitations to the classical combination models [313, 316, 434].

The first limitation in the analysis of drug combinations is the misleading of the term "synergy" [411]. In most clinical studies and throughout the literature, this term is often used to justify the combination of drugs in therapy, but many times this term is not clearly defined and is commonly used without the proper knowledge underlying the concept and the methods necessary to evaluate it [410, 435]. Frequently, synergy is not evaluated nor calculated using the appropriate reference models and results are interpreted as synergism only by comparison of results obtained from simple experimental assays, rather than included in a mathematical approach and without information about the dose-effect curves for single drugs. For example, sometimes, better-observed effects in drug combinations are often described as synergy when indeed it is only a potentiation of the effects of the two drugs combined if only one drug is active alone [316].

Another limitation is that, to date, there is not a standard reference model to evaluate drug synergism. All available reference models have limitations and while some fail to provide clear definitions of additivity, others rely on data about the drug's mechanism of action, do not cover rare and specific cases like drugs that do not follow the ideal dose-response curves, or are not intuitive and user friendly [436]. The Loewe Additivity model is the most improved reference model, but it is also limited by the large amount of data required to make precise synergy analysis, which is particularly important when data is expensive or difficult to determine [316]. On the other hand, effect-based approaches are more limited but can still provide enough evidence of positive combination effects, with fewer data.

Another limitation is that, most of the time, the analysis of drug interactions in clinical trials involving drug combinations is impaired by intense practical and ethical constraints, which makes it hard to collect sufficient data to clearly and properly support synergy. Also, the choice of the reference model in each step of the investigational process must be tailored to the data available at each discovery step. For example, in *in vitro* studies, the HSA, Bliss Independence, and Loewe Additivity may be the most appropriate reference models to find promising drug pairs for evaluation of their mechanisms of action or to proceed for further clinical research [414, 437–441], whereas in further preclinical studies the Loewe Additivity with CI and Isobologram analysis may be more appropriate to determine more precisely the combination effects [316]. In clinical studies in humans, the

recommendations from the FDA [442] together with EMA [443] and the WHO [444] determine that there must be a strong and rational basis for the use of combination therapies supported by previous preclinical studies that also justify the use of combined agents over individual drugs and their improved safety profile for the proposed disease. Nevertheless, extrapolating *in vitro* results to animals or even humans is not well established and raise several questions, being far from being consensual among the scientific community [445]. Generally, drug combination clinical trials include four experimental groups that are treated with placebo, drug A, drug B or a combination of drug A + drug B and it must be clearly demonstrated that the combination therapy has greater efficacy than both drugs alone, using the same or even lower doses than the individual agents, while still maintaining a safety profile [313, 446].

The fourth limitation is related to the optimization of dose ratios. Since cells do not differentiate single drugs or their combination, two drugs combined at a given ratio could be considered as a third that has its own dose-effect relation [313]. So, rather than evaluating if a drug combination is synergistic, scientists must ask what dose ratio optimizes their synergy [447]. To do so, the design of experimental analysis must evaluate a different set of fixed ratios and explore what doses fit well to reach the desired synergistic effects [434]. These experiments should always be performed in preclinical studies before further clinical trials [316].

When analyzing drug combination results, one must also take into account that biological experiments regularly have associated some type of experimental error [316]. Although the Highest Single Agent and Response Additivity reference models take into account the statistical significance, the Bliss Independence and Loewe Additivity models do not allow statistical significance interpretation, because they do not have the mathematical background necessary for statistical evaluation [316]. In this way, the software CompuSyn (http://www.combosyn.com), based on the Chou-Talalay theory, which follows the Loewe Additivity model and assumes the Median-Effect approach of Chou and Talalay to assess the statistical significance of the experiments, represents an improvement over other approaches [313].

Another limitation when referring to the previously mentioned approaches is the use of drug combinations with more than two drugs, a common practice in cancer therapy, for example. Indeed, these approaches can be further extended for use of any drugs in combination. For example, for the Loewe Additivity model, the CI can be calculated by the following equation: $CI = \frac{a}{A} + \frac{b}{B} + \cdots + \frac{n}{N}$. Nevertheless, such generalization does not permit the quantification of each drug's contribution to the combination, implying that a synergistic

combination of three or more drugs could be the result of only two drugs, for example [316]. Therefore, it is really important to rationally design the experimental protocols to demonstrate that, for example, in a triple combination using drugs A, B, and C, A, and B are synergistic, and that the combination of A + B (considered as a new single agent) with the drug C is also synergistic [316].

2.4 Novel methods for directly quantifying drug synergism

Loewe additivity and Bliss independence approaches have been dominant in the field of synergism, together with the work proposed by Chou and Talalay. Still, there is no consensus among the scientific community regarding the appropriate use of these reference models. Recently, there has been an increase in the number of publications related to the definition of synergism, such as the "lack-of-fit" model [410] or the rediscovered Hand model [448, 449]. Novel ways to evaluate synergism in drug combination studies also appeared such as the ZIP model [433], Combenefit (SANE) [450], Bivariate Response to Additive Interacting Doses (BRAID) [451], Schindler's Hill partial differential equation [452], the SynergyFinder software [453], the Multi-dimensional Synergy of Combinations (MuSyC) [454], the effective dose model [455] and the copula model [456], for example. Next, we will describe some of the most recent methods for directly quantifying and evaluating drug synergism [434].

Response surface modeling is an approach based on a 3D plot representation to describe the interaction effects in drug combinations. Basically, doses of drugs A and B are plotted on the x and y-axis and the expected combined effects (response) are plotted on the z-axis, creating a 3D surface. Synergism or antagonism is measured as deviations from this surface and depends on the value of z. It allows the use of both Bliss Independence and Loewe additivity models for the estimation of the expected effects [434].

Recently, more user-friendly approaches have gained attention for the quantification of drug interactions. CompuSyn, a computer software based on the Chou-Talalay theorem, has been developed to make synergy determination more user-friendly, enhancing the usage of this reference model for the evaluation of drug interactions in combination studies. To use this software, raw data must be analyzed and normalized to convert responses in value between 0 and 1 [313].

Another approach is the Mixlow (i.e. Mixed-effects Loewe) methodology, developed by Boik, Newman, and Boik in 2008 [457]. This approach is based mainly on three elements: a nonlinear mixed-effects model for the estimation of the sigmoidal curve parameters from

the concentration-response curves, the Loewe index, and a method for the evaluation of statistical significance for the index. It is an improvement of the Chou-Talalay method as it is more accurate in the estimation of the parameters, includes the evaluation of confidence intervals, and dismisses the need for previous data processing [457].

More recently, Hennessey *et al* (2010) [458] proposed a novel model for the evaluation of dose-response curves and synergy determination. The Bayesian model uses hierarchical nonlinear regression to describe the variability between and within experiments and in the observed responses of the controls. To do so, the authors used Markov chain Monte Carlo (MCMC) for data fitting and a modified version of Loewe additivity to infer about synergism in drug combinations while incorporating variables related to variability and uncertainty related intrinsically to the experiments. The authors found this approach to be more precise in drug synergism estimation than the Chou-Talalay methodology [458].

2.5 Oncological preclinical studies based on combination models

The evaluation of synergism in preclinical trials involving *in vitro* assays is a common practice and nowadays many *in vivo* drug combination studies using animal models are based on the results obtained in studies using cell lines. Here, it was performed a search in the PubMed database using the terms '*in vivo*' and 'synergy' and 'cancer' and the results were limited to a period from 2019 to 2022. The selected studies will next be analyzed to find if *in vivo* combination studies make correct use of the term synergy and to evaluate which reference models they employ to assess drug interactions.

One of the reference papers for the evaluation of drug synergism in *in vivo* studies is the one published by Fu *et al* in 2016 [459], from the research group led by Ting-Chao Choug. The authors studied the combination of two anticancer drugs that target microtubule polymerization: Taxotere and T607 compound. They found these drugs were synergic against human colon carcinoma HCT-116 xenograft mice. The authors determine drug interactions quantitatively using the median-effect equation of the mass-action law and the CI theorem proposed by Chou-Talalay, demonstrating the basic concepts and experimental design aspects important for the quantitative analysis of drug interaction dynamics in complex biological systems [459].

A recent study from Skeberdyte [460] evaluated the effect of the combination of salinomycin and dichloroacetate in lung carcinoma. Salinomycin acts on cancer stem cells and dichloroacetate inhibits the pyruvate dehydrogenase kinase. The authors performed *in vitro* studies using two and three-dimensional cell cultures of Lewis lung carcinoma cells

(LLC1) and also *in vivo* studies using an LLC1-C57BL/6 mouse model. The authors successfully proved that this drug combination has synergistic effects *in vitro* using the Chou-Talalay method by testing several doses below IC_{50} from both monotherapies using a non-constant ratio drug design. The authors also proved this combination increased the survival rate of mice, reduced metastasis occurrence, and also decreased the population of cancer stem cells, proving the benefits of this combination both *in vitro* and *in vivo* [460].

Another study by Xu *et al* [461] attempted to evaluate the potential of the combination of ABT199 and irinotecan in RAS-mutant lung cancer cells. The authors selected this *in vitro* model as KRAS mutation is very frequent in non-small cancer lung cancer (NSCLC). Irinotecan is one of the most well-known chemotherapeutic drugs commonly used for metastatic colorectal cancer and ABT199 is an investigational drug with high efficacy of the Bcl-2 inhibitor. Using different human NSCLC cell lines (H441, A549, H838, and H522), the authors had successfully demonstrated that this drug combination inhibits lung cancer cell growth and enhances apoptosis, being synergistic with CIs under 0.7. Further *in vivo* studies suggested this combination induces tumor size and weight reduction, demonstrating the potent *in vivo* efficacy of the combination [461].

Ghosh *et al* [462] recently studied the anticancer effect of the combination of methylglyoxal, an agent with a well-established anticarcinogenic effect, and 5-FU, an antineoplastic agent commonly used for several types of cancer, including breast cancer treatment. This research group evaluated the effect of this drug combination both *in vitro* using MCF-7 breast cancer cells and *in vivo* and successfully found synergism using the Chou-Talalay theorem. *In vivo* studies revealed that EAC (Ehrlich Ascites Carcinoma) bearing mice and BALB/c mouse 4T1 breast tumor models exhibited tumor regression with fewer side effects when treated with this combination compared to single agents [462].

Buocikova and her colleagues [463] recently studied the combination of the DNA methyltransferase inhibitor decitabine with the anthracycline antibiotic DOX for breast cancer. They first evaluated the synergism of sequential decitabine + DOX treatment in three breast cancer cell lines (JIMT-1, MDA-MB-231, and T-47D) after assessing their influence on the cytotoxicity, genotoxicity, apoptosis, and migration capacity of these cells. The mathematical framework employed for drug synergism was based on the Chou-Talalay method using the CI to quantify drug interactions. They further confirmed these results using an orthotopic xenograft mouse model, demonstrating the potential of epigenetic drugs in the modulation of cancer cells' sensitivity to antineoplastic agents [463].

Another study combined Cisplatin-loaded poly(L-glutamic acid)-graft-methoxy poly(ethylene glycol) complex nanoparticles with different PD1/PD-L1 inhibitors and

evaluated their cytotoxic effect in different types of cells (LLC, H1299, A549, B16F10, ID8, and U14) and female C57BL/6 mice. They found this combination to cause tumor PD-L1 overexpression time-dependent *in vitro* and increased tumor PD-L1 signals after 72 h of treatment *in vivo*. Different from the previously mentioned studies, this work employed the Q value method of Zhengjun Jin to analyze the synergistic interaction of the combination group for tumor therapy (*in vivo*). Taken together, the authors demonstrated the potential clinical treatment of Cisplatin-loaded poly(L-glutamic acid)-graft-methoxy poly(ethylene glycol) complex nanoparticles with different PD1/PD-L1 inhibitors for cancer therapy [464].

In another study, the authors attempted to combine gemcitabine, a deoxycytidine nucleoside analog commonly used for the treatment of advanced or metastatic pancreatic cancer, with Troxacitabine (Troxatyl™), an unnatural L-nucleoside analog that demonstrates potent antitumor activity. The authors performed *in vitro* studies using different pancreatic adenocarcinoma cell lines (AsPC-1, Capan-2, MIA PaCa-2, and Panc-1) and evaluated synergism using the isobologram and CI methods of Chou and Talalay. The authors then evaluated the effects of both drugs, alone or combined in nude mice transplanted with human pancreatic (AsPC-1) tumors, and concluded that both drugs were more than additive at safer doses and schedules, being potential candidates for further evaluation in patients with advanced pancreatic cancer [465].

Sánchez *et al* [466] recently studied the combination of docetaxel, a chemotherapeutic agent, and capsaicin, an ingredient of hot chili peppers, for the treatment of prostate cancer. The authors used two prostate cancer cell lines (LNCaP and PC-3) for the *in vitro* studies and xenograft prostate cancer models to further evaluate this combination *in vivo*. Using the Chou-Talalay reference model, they found that docetaxel and capsaicin had synergistic effects in the inhibition of LNCaP and PC-3 cell growth, reflecting a CI under 1 for most of the combinations evaluated in the work. *In vivo* results reinforced the synergistic effects of this combination in the reduction of tumor growth in xenograft prostate cancer models [466].

Recently, another study aimed to study if the synergism between the drugs vincristine and irinotecan also extended to eribulin, another microtubule inhibitor for the treatment of childhood solid tumors. The authors combined vincristine or eribulin with irinotecan and studied their anticancer effect *in vitro* and xenograft models. CIs were calculated based on the Bliss model of independence and the Loewe additivity model. They found the eribulin combination to be very effective in these xenograft models, but not synergistic *in vitro* [467].

Despite the huge number of publications stating synergism in animal experiments, what was found is that most papers are not able to really prove drug synergism *in vivo*, assuming synergistic interactions based on the *in vitro* results and using only one reference model for assessing the drug interactions (usually the Chou-Talalay theorem). According to Chou [313], the quantification of synergy *in vitro* and in animals is based on the same principles, requiring a minimum of 65 nude mice for accurate results [313]. We believe that, for most of the combination studies, synergism is only determined *in vitro* because the determination *in vivo* is more expensive, time-consuming, and introduces more variability. Most of the studies then extrapolate the results from *in vitro* to animals, “which is a general and separate biomedical problem which is not expected to be solved by the Chou-Talalay method” [313].

2.6 Oncological clinical trials based on preclinical synergism evaluation

Most clinical trials are often supported by preclinical studies that state to have found synergistic drug combinations. Although synergism is the gold standard desired when referring to drug combinations in cancer therapy, this term is commonly misused, as we previously stated. Another aspect is that, even if one achieves synergism in a certain combination of drugs, this does not necessarily mean that the combination will be indeed useful for cancer therapy. The potential for clinical use of combining drugs in clinical trials should always be measured by the therapeutic index, a concept that relates the relative toxicity of an anticancer treatment to its toxicity in normal tissues, rather than only by the quantification of synergism [435].

In this way, a report from 2012 from Ocana *et al* [435] attempted to evaluate if clinical trials that frequently evaluate drug combinations were well designed and if they used correctly the term synergy, based on strong evidence from preclinical studies [435]. The authors found, at the time, that only 13.6% of the preclinical studies included the evaluation of synergism based on isobologram analysis and 7.6% based on the Chou-Talalay method. Regarding preclinical studies involving animal models, only 39% evaluated the therapeutic index, concluding that most phase I and II studies did not perform the appropriate background methods for correctly assessing synergism [435].

Also, a recent paper argued that synergism has not been proved in most clinical trials, especially those regarding studies that combine various checkpoint inhibitors with each other and with other antineoplastic drugs [468]. This review analyzed thirteen Phase III clinical trials and found no synergistic interactions, just additive effects of each therapy, only synergism previously supported in animal models. Although this is not necessarily a bad thing, it is still not the good thing that all scientists have been looking at and reflects, once again, the misuse of the term synergism among clinical studies [468].

Indeed, in a perspective published by Chou in 2010 [313], he stated that it is generally not possible to determine synergism in clinical trials, based on scientific, practical, and ethical reasons [313] that we already discussed previously. Furthermore, he claimed that most clinical trials that employ the term “synergism” are not well supported by the available data, especially in studies where only a single dose was tested for a single drug, mentioning the importance of preclinical evaluation for accurate and robust results to support clinical trials in humans [313].

Here, it was performed a Pubmed search using the same methodology as described by Ocana *et al* [435]. The terms ‘synergy’ or ‘synergistic’ and ‘cancer’ were searched and

limited to studies in humans, and clinical trials over the last year (2021-2022). Next, it will be mentioned some of the most recent clinical trials in oncology that are based on preclinical studies claiming synergism.

Kang *et al* [469] published the results from a recent randomized, multicenter, double-blind, placebo-controlled, phase II-III clinical trial (NCT02746796) for the evaluation of the combination of immune checkpoint inhibitor nivolumab and oxaliplatin versus placebo plus oxaliplatin. This combination is intended to be used as first-line therapy for the treatment of patients with HER2-negative, unresectable advanced, or recurrent gastric or gastro-esophageal junction cancer [469]. This study was based on previous preclinical studies that supported the additive or synergistic antitumor effects of the combination of immune checkpoint inhibitors with oxaliplatin. The authors found that a combination of nivolumab and oxaliplatin enhanced progression-free survival but not overall survival and concluded this drug combination has the potential to be used as a first-line treatment for patients with this type of cancer [469].

Jain *et al* [470] recently conducted a single-center, phase II nonrandomized trial (NCT02756897) to study the combination of ibrutinib and venetoclax in the treatment of chronic lymphocytic leukemia [470]. The study was based on preclinical studies that demonstrated synergism of Bruton tyrosine kinase inhibitors with the Bcl-2 inhibitor venetoclax. The authors found this combination can be advantageous for previously untreated patients with chronic lymphocytic leukemia [470].

Another study from Cousin *et al* [471] performed a single-arm, multicentric phase II trial (REGOMUNE) to assess regorafenib plus avelumab for the treatment of patients with microsatellite stable colorectal cancer, based on previous preclinical results that demonstrated that this combination is synergic. The authors concluded that regorafenib combined with avelumab successfully modulates antitumor immunity in some patients with this type of cancer [471].

A phase Ib randomized, open-label, multicenter study studied the combination of alpelisib with everolimus ± exemestane in solid tumors. This study claimed to be based on preclinical models that demonstrated a synergistic effect between and with alpelisib. Everolimus inhibits mTORC1, alpelisib acts on the phosphatidylinositol 3-kinase catalytic subunit p110α blockage, and exemestane is an antineoplastic drug already used for cancer therapy. The authors concluded that this combination was safe, manageable, and reversible and that the pharmacokinetics of each drug did not change significantly when in combination [472].

Another phase I clinical trial (NCT01677559) aimed to combine an aurora kinase A inhibitor (alisertib) and nab-PTX, a chemotherapeutic agent, for refractory high-grade neuroendocrine tumors. The authors refered that this trial was based on preclinical studies that have demonstrated that the combination of alisertib plus PTX was synergic in rapidly proliferative cancers. Moreover, the authors successfully found that the proposed combination was safe, manageable, and reversible and demonstrated promising preliminary efficacy [473].

Hong *et al* [474] recently published the results from a phase Ib study (NCT02124148) where it was evaluated the combination of prexasertib and samotolisib. Prexasertib is a CHK1 Inhibitor and samotolisib is a dual PI3K/mTOR inhibitor. This clinical trial was based on previous studies that demonstrated that prexasertib alone had moderate anticancer activity and other preclinical data in triple-negative breast cancer cells, MDA-MB-231 orthotopic xenograft tumors, and TNBC patient-derived xenograft mouse models that also supported this combination. The authors found this combination to be effective in preclinical models and preliminary effective, with some degree of toxicity associated [474].

Another phase I, open-label, dose-escalation study was performed by Amin *et al* [475], for the determination of the maximal tolerated dose of docetaxel in combination with temsirolimus for the treatment of refractory solid tumors. Temsirolimus selectively inhibits mTOR and docetaxel is an antineoplastic drug belonging to the class of taxanes. This trial was based on preclinical results that demonstrated the combination of taxanes and mTOR inhibitors to be additive or synergic in different types of cancer cells. The authors found this combination to be very toxic and not suitable for cancer treatment [475].

Taken together, the aforementioned clinical trials, usually phases I and II, demonstrated that synergism in preclinical studies is usually the justification for the clinical evaluation of drug combinations in cancer-related studies, clarifying the importance of the accurate and reliable drug interaction quantification in this type of studies. Therefore, in this chapter, we have evaluated synergism regarding the drug combinations previously studied in Chapter II, using the most common reference models (Chou-Talalay, ZIP, HSA, Bliss independence, and Loewe), to provide a more robust basis for further research of these drug combinations in future animal studies or clinical trials.

3. OBJECTIVES OF CHAPTER III

In this chapter, it was aimed to evaluate the drug interactions in the drug combinations previously tested in Chapter II, to find possible synergistic interactions between drugs. The analysis of drug interactions was evaluated by different reference models, namely Chou-Talalay, ZIP, HSA, Bliss independence, and Loewe, using the CompuSyn and SynergyFinder software.

4. MATERIALS AND METHODS OF CHAPTER III

4.1 Analysis of Drug Interactions

To quantify drug interaction in the drug combinations evaluated in Chapter II, the CI was estimated by the unified theory, introduced by Chou and Talalay [313] using the CompuSyn software (ComboSyn, Inc., New York, NY, USA). It was used the mutually exclusive model, based on the assumption that drugs act through entirely different mechanisms [411]. CI was plotted on the *y*-axis as a function of Fa on the *x*-axis to assess drug synergism between drug combinations. The CI is a quantitative representation of pharmacological interactions. CI < 1 indicates synergism, CI = 1 indicates additive interaction and CI > 1 indicates antagonism. For some drug pairs, the SynergyFinder software was also used to estimate the synergy scores of the proposed drug pairs by four different reference models: Bliss, Loewe, HSA, and ZIP. Synergy scores <−10 meant that the interaction between two drugs was likely to be antagonistic; scores from −10 to 10 meant the interaction between two drugs was likely to be additive, and scores >10 meant the interaction between two drugs was likely to be synergistic.

5. RESULTS AND DISCUSSION OF CHAPTER III

5.1 Analysis of Drug Interactions in Breast Cancer Cells

5.1.1 Synergistic Combinations of Antineoplastic and Antimalarial drugs

Experimental evidence suggests that some antimalarials exhibit synergism with other drugs with no increased toxicity toward normal cells. In this regard, the potential synergistic effects of several antimalarials with DOX and PTX were studied for the treatment of breast cancer. After evaluation of cytotoxic activity, seven antimalarials were selected for combination with DOX and PTX in Chapter II. Based on these results, here it was evaluated drug synergism using the Chou-Talalay method, which is based on the median-effect equation, derived from the mass-action law principle. This unified theory encompasses the Michaelis-Menten, Hill, Henderson-Hasselbalch, and Scatchard equations in biochemistry and biophysics and provides a quantitative definition for additive effect (CI = 1), synergism (CI < 1), and antagonism (CI > 1) in drug combinations.

Therefore, to investigate the synergistic effects of the combined antineoplastic drugs DOX and PTX with the antimalarial agents, the CI was calculated using the Chou-Talalay method. CI was plotted on the y-axis as a function of Fa on the x-axis to assess drug synergism. The fractional effect is a value between 0 and 1, where 0 means the drug had no effect on cell viability and 1 means the drug produced a full effect on decreasing cell viability.

Results for synergistic combinations are summarized in Table 15. The combination of DOX + chloroquine demonstrated more synergism than the combination with PTX. For lower doses of 0.05 µM + 16 µM, 0.1 µM + 32 µM, and 0.2 µM + 64 µM, corresponding to the concentrations of DOX and chloroquine, respectively, all combinations were synergic and produced effects between 0.724 and 0.851. The combination of 32 and 64 µM with 1.5 nM and 3 nM, respectively, also resulted in synergism, with Fa between 0.782 and 0.831 (Figure 84A). The combination of the IC_{50}s of DOX + mefloquine (8 µM and 0.2 µM, respectively) for 48h resulted in a synergistic effect (CI<1), with a fractional effect of 0.845. The combination of 3 nM of PTX and 8 µM of mefloquine also resulted in synergism, with a fractional effect of 0.841 (Figure 84B). The combination of artesunate with DOX resulted in more synergism than the combination of PTX with the same antimalarial drug, with CI<1 for almost all pairs of concentrations, with effects between 0.487 and 0.821. Only the combinations of 6 and 12 µM of artesunate with 1.5 and 3 nM of PTX were synergic but produced a lower fractional effect (Figure 84C).

Table 15. CI values and respective fractional effects of various combinations of DOX/PTX and mefloquine, chloroquine, and artesunate. CI in bold indicates concentrations of drug pairs that are synergic.

Combination (Drug A + Drug B)	Concentration (Drug A + Drug B)	Fractional Effect (Fa)	CI
DOX + chloroquine	0.05 µM + 16 µM	0.724	**0.965**
	0.1 µM + 32 µM	0.797	**0.676**
	0.2 µM + 64 µM	0.851	**0.560**
	0.4 µM + 128 µM	0.856	1.027
	0.8 µM + 256 µM	0.854	2.126
PTX + chloroquine	0.75 nM + 16 µM	0.636	2.886
	1.5 nM + 32 µM	0.782	**0.809**
	3 nM + 64 µM	0.831	**0.747**
	6 nM + 128 µM	0.850	1.091
	12 nM + 256 µM	0.851	2.146
DOX + mefloquine	0.05 µM + 2 µM	0.176	3.231
	0.1 µM + 4 µM	0.375	2.582
	0.2 µM + 8 µM	0.845	**0.729**
	0.4 µM + 16 µM	0.856	1.349
	0.8 µM + 32 µM	0.855	2.718

PTX + mefloquine	0.75 nM + 2 µM	0.158	2.939
	1.5 nM + 4 µM	0.479	1.501
	3 nM + 8 µM	0.841	**0.718**
	6 nM + 16 µM	0.863	1.252
	12 nM + 32 µM	0.857	2.602
DOX + artesunate	0.05 µM + 3 µM	0.487	**0.480**
	0.1 µM + 6 µM	0.684	**0.315**
	0.2 µM + 12 µM	0.631	**0.847**
	0.4 µM + 24 µM	0.821	**0.544**
	0.8 µM + 48 µM	0.828	1.035
PTX + artesunate	0.75 nM + 3 µM	0.337	1.044
	1.5 nM + 6 µM	0.453	**0.880**
	3 nM + 12 µM	0.544	**0.984**
	6 nM + 24 µM	0.617	1.289
	12 nM + 48 µM	0.726	1.448

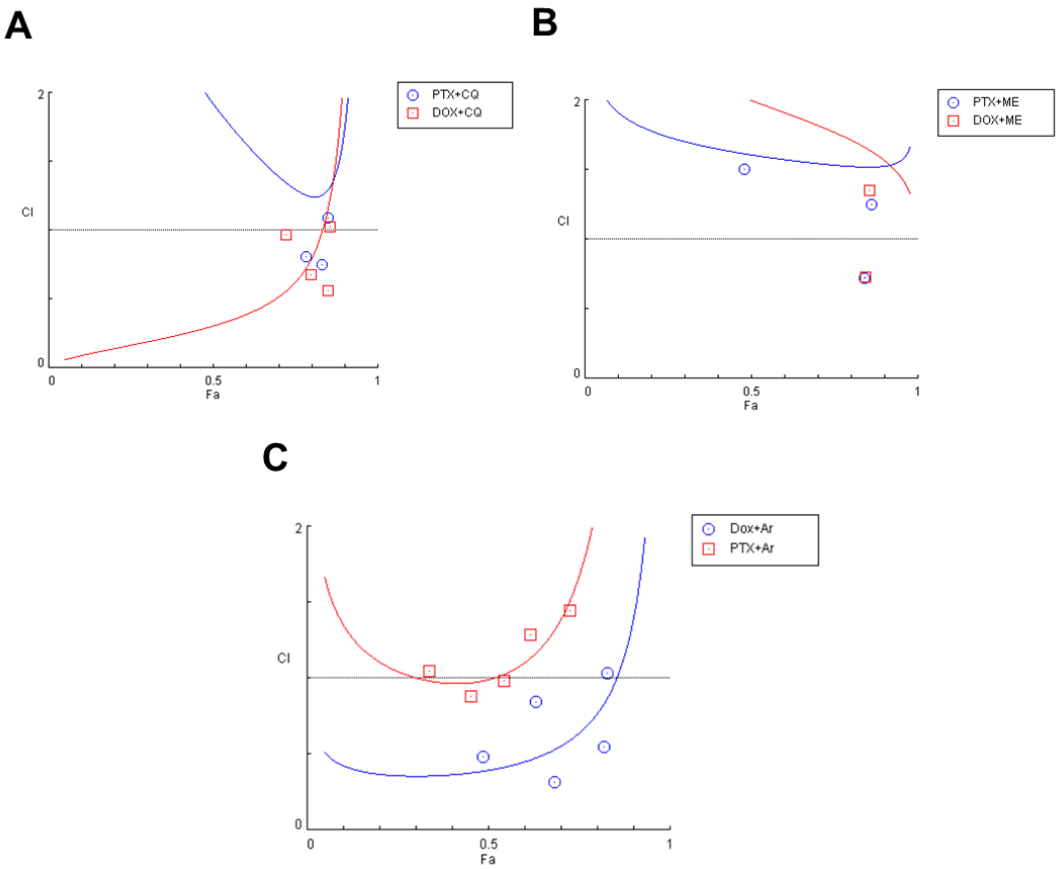

Figure 84. Chou-Talalay method Fa-CI plot of DOX/PTX and chloroquine (**A**), mefloquine (**B**) and artesunate (**C**). CI was plotted on the y-axis as a function of effect level (Fa) on the x-axis to assess drug synergism. CI<1, CI=1, and CI>1 indicate synergism, additivity, and antagonism, respectively. CQ: chloroquine; ME: mefloquine; Ar: artesunate

Together, these results demonstrate that non-quinolinic antimalarial derivates may be more promising to evaluate in future combinations (Figure 85). Other combinations were also performed but the results were not significant (Figure 86).

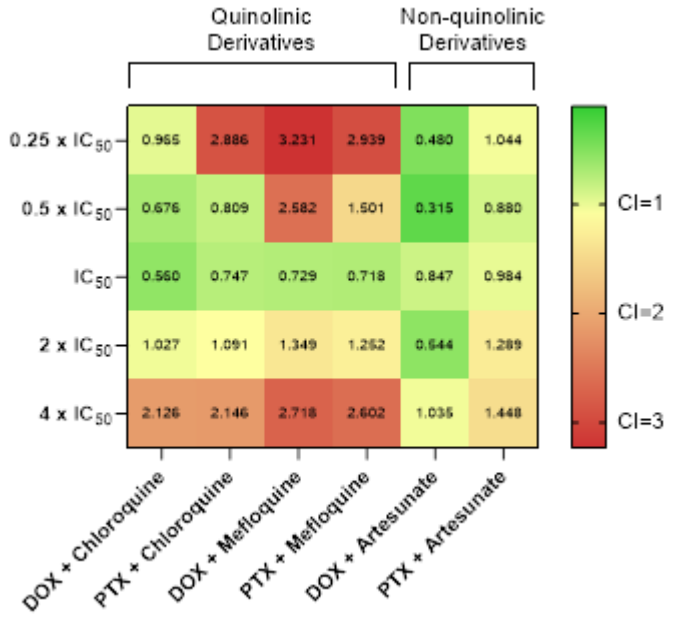

Figure 85. Synergy heat map compiling CI values. The squares in the figure indicate antagonism (CI > 1.2, red), additivity (0.9<CI<1.1, yellow), and synergism (CI<0.9, green) between DOX/PTX and chloroquine/mefloquine/artesunate against MCF-7 cells at combination settings described in Chapter II.

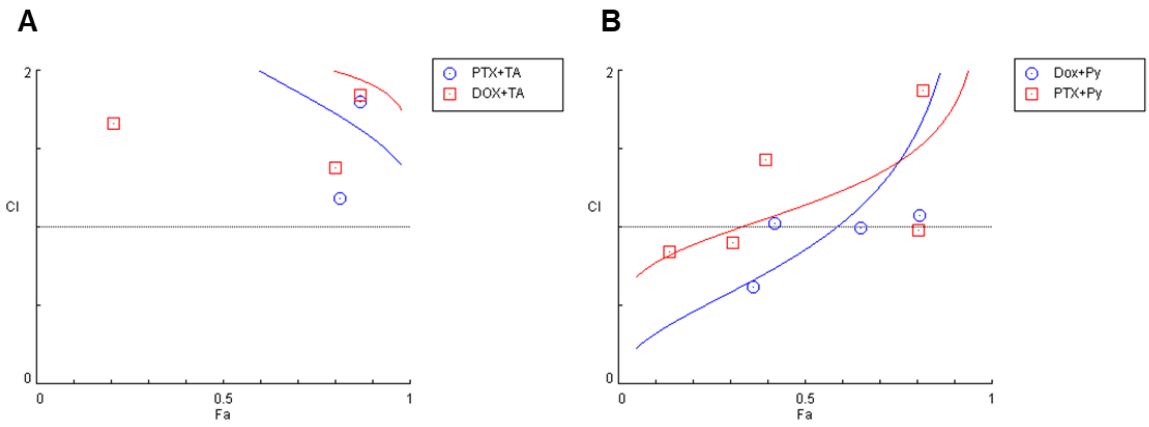

Figure 86. Chou-Talalay method Fa-CI plot of DOX/PTX and tafenoquine (**A**) and pyronaridine (**B**). CI was plotted on the y-axis as a function of effect level (Fa) on the x-axis to assess drug synergism. CI<1, CI=1, and CI>1 indicate synergism, additivity, and antagonism, respectively. TA: tafenoquine; Py: pyronaridine

Moreover, these results demonstrated that antimalarial drugs in combination can improve the anti-cancer activity of DOX and PTX in ER-positive breast cancer cells. It was demonstrated, for the first time, that the combination of artesunate, mefloquine, and chloroquine can synergistically inhibit breast cancer proliferation in MCF-7 cells. Furthermore, these results imply that antimalarial drugs may be promising chemosensitizing compounds for enhancing the cytotoxic effects of DOX and PTX in MCF-7 cells.

5.1.2 Synergistic Combinations of Antineoplastic and CNS drugs

Recent studies have investigated new drugs that can synergize with antineoplastic agents, but, to our knowledge, none have explored CNS drugs in combination with chemotherapeutic drugs for breast cancer therapy.

In Chapter II, it was studied the potential anticancer activity of different CNS drugs in MCF-7 breast cancer cells. Here, the potential synergistic effects of this class of drugs combined with PTX and DOX, two antineoplastic drugs used for breast cancer treatment, were evaluated. Drug synergism was evaluated synergism by two different methods: Chou-Talalay and Bliss independence. The Bliss independence model adopts a stochastic process in which two drugs produce their effects independently, and the expected combination effect can be calculated based on the probability of independent events [476].

First, the CI for the combinations of PTX + CNS drugs in MCF-7 cells was calculated. The combination of PTX plus fluoxetine demonstrated synergism for the lowest concentrations with three synergic pairs (Figure 87A), with Fa values of 0.1184, 0.2472, and 0.3621 (Table 16). The combination with sertraline resulted in only one synergic pair, for the lowest concentration (Figure 87B). The combinations of PTX plus thioridazine demonstrated synergism for two pairs (Figure 87C), with Fa values of 0.1895 and 0.5027 (Table 16). Combination with fluphenazine and benztropine resulted in three synergic pairs (Figure 87D and E, respectively), with Fa values lower than 0.60 (Table 16).

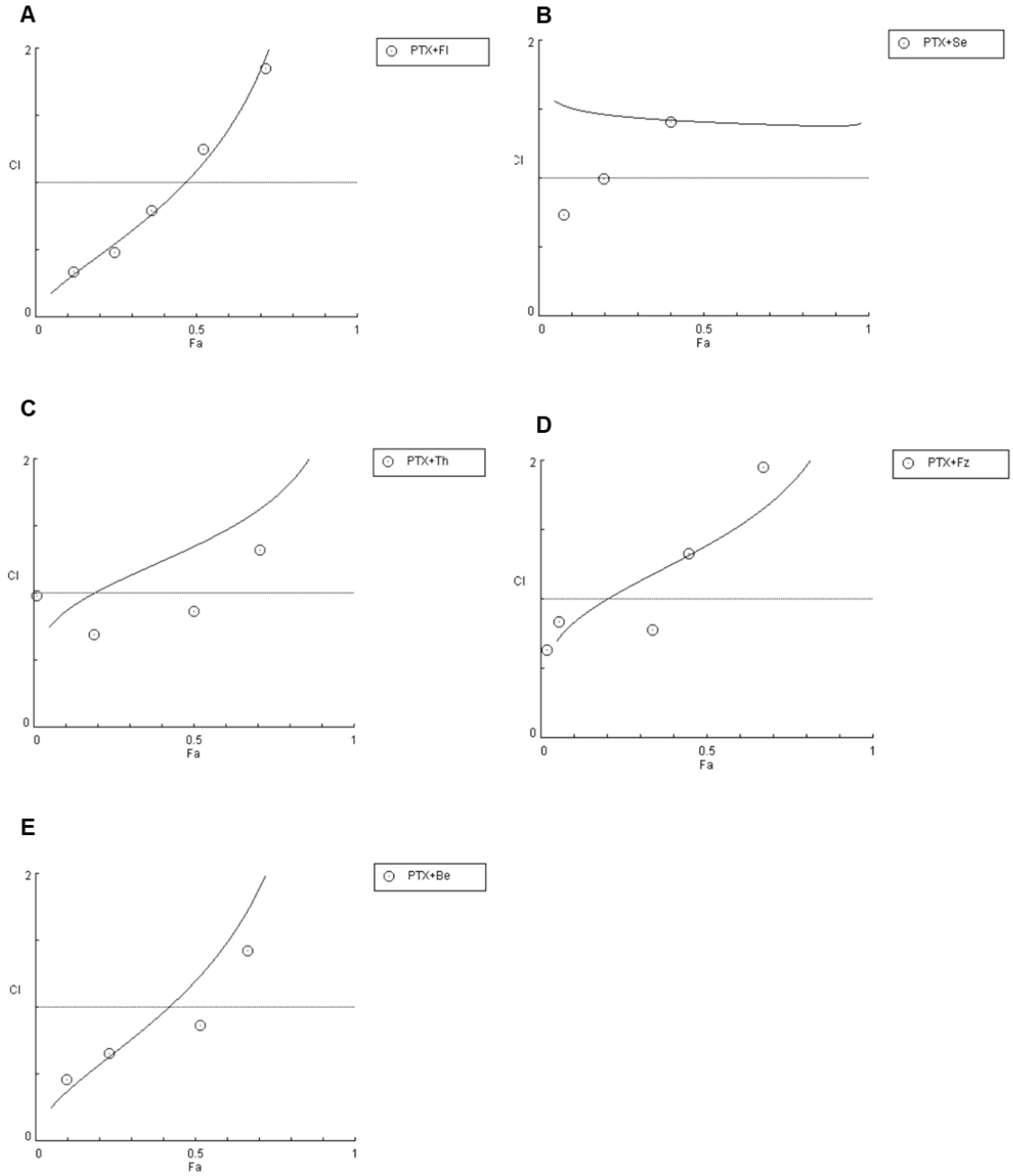

Figure 87. Chou-Talalay method Fa-CI plot of PTX plus fluoxetine (**A**), sertraline (**B**), thioridazine (**C**), fluphenazine (**D**), and benztropine (**E**). CI was plotted on the *y*-axis as a function of effect level (Fa) on the *x*-axis to evaluate drug synergism. CI < 1, CI = 1, and CI > 1 refer to synergism, additivity, and antagonism, respectively. Fl: fluoxetine; Se: sertraline; Th: thioridazine; Fz: fluphenazine; Be: benztropine

Table 16. CI values and respective fractional effect of different combinations of PTX plus CNS agents. CI in bold indicates concentrations of drug pairs that are synergic. Cells were treated with 0.25, 0.5, 1, 2, and 4 times the IC_{50} of each drug (total dose).

Combination (Drug A + Drug B)	Total Dose (Dose A + Dose B)	Fractional Effect (Fa)	CI Value
PTX + fluoxetine	2.75	0.1184	**0.33562**
	5.5	0.2472	**0.48322**
	11.0	0.3621	**0.79198**
	22.0	0.5227	1.24993
	44.0	0.7167	1.85505
PTX + sertraline	1.375	1.0×10^{-4}	5.01852
	2.75	0.0768	**0.73865**
	5.5	0.1987	0.99737
	11.0	0.4012	1.40860
	22.0	0.6326	2.04261
PTX + thioridazine	2.25	0.0109	0.98541
	4.5	0.1895	**0.69489**
	9.0	0.5027	**0.86789**
	18.0	0.7077	1.32210
	36.0	0.7128	2.62409
PTX + fluphenazine	1.5	0.01908	**0.63552**
	3.0	0.057	**0.83495**
	6.0	0.33804	**0.78096**
	12.0	0.44769	1.33256
	24.0	0.67095	1.95345

	6.25	0.09897	**0.45763**
	12.5	0.2321	**0.65346**
PTX + benztropine	25.0	0.51629	**0.86840**
	50.0	0.66485	1.42716
	100.0	0.71074	2.66897

Together, these results demonstrate that these CNS agents may be promising candidates to evaluate in future combinations.

Nevertheless, these drug interactions were also evaluated by the Bliss Independence method, using the SynergyFinder 2.0 software. This software is a web application for interactive analysis and visualization of multi-drug combination profiling data by different synergism evaluation methods. In this software, the synergy score for a drug combination is averaged over all the dose combination measurements, giving a positive or negative value, corresponding to synergism or antagonism, respectively. The 2D and 3D synergy maps highlight synergistic and antagonistic dose regions in red and green colors, respectively [476].

Fluoxetine combination with PTX analyzed with the Bliss model (Figure 88A) demonstrated the highest synergy score, in line with the Chou-Talalay results, indicating synergism for three pairs. Sertraline combination demonstrated synergism using the Bliss model, with a positive synergy score of 2.127 (Figure 88B). The combination of PTX with thioridazine also resulted in synergism using the Bliss method (Figure 88C) with a synergy score of 2.938. The combinations of PTX plus fluphenazine and benztropine resulted in the lowest synergy scores using the Bliss method, with scores of 0.569 and -8.262 (Figure 88D and E, respectively).

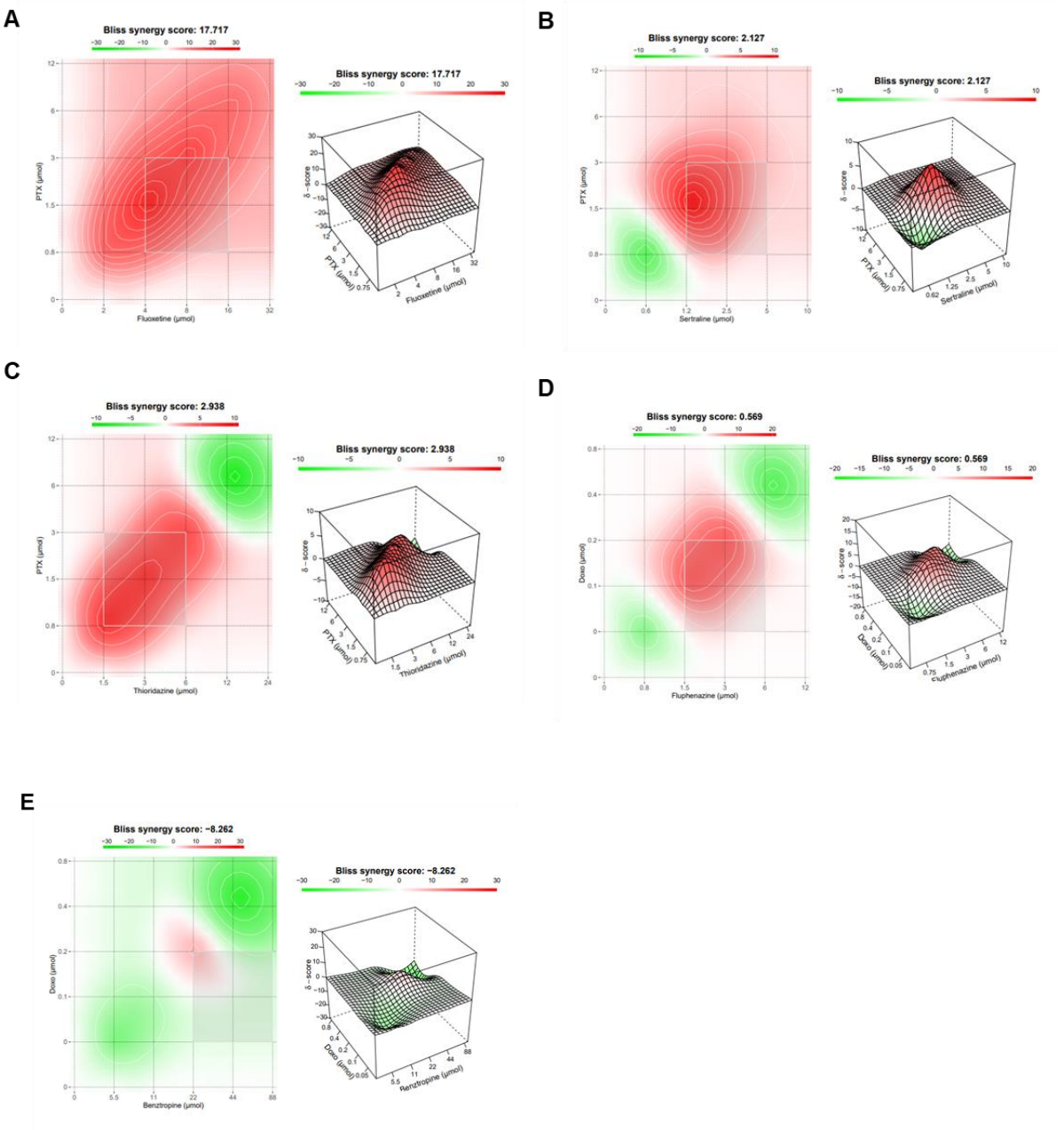

Figure 88. Bliss synergy plots of PTX plus fluoxetine (**A**), sertraline (**B**), thioridazine (**C**), fluphenazine (**D**), and benztropine (**E**).

The Bliss method results demonstrate slightly different results regarding the synergy evaluation of drug combinations compared to the Chou-Talalay results, especially regarding fluphenazine and benztropine combinations. Despite this, these reference models produce similar results most of the time.

Together, these results demonstrate that all tested CNS drugs can synergistically decrease MCF-7 cell viability when combined with PTX, with fluoxetine, benztropine, and

fluphenazine being the most promising drugs at lower concentrations. Curiously, when tested alone in MCF-7, sertraline was the most potent repurposed drug, but its combination with PTX resulted in only one synergistic pair. Taken together, these results imply that CNS drugs may be promising chemosensitizer compounds and enhance the cytotoxic effects of PTX in MCF-7 cancer cells.

PTX belongs to the taxanes drug class and acts by blocking cell mitosis through the stabilization of microtubules, leading to cell cycle arrest preferentially in the G2/M phase and apoptosis [477]. Some studies showed that drugs acting on serotonin (5-HT) signaling, including SSRI, inhibit tumor sphere formation in human breast tumor cells in *in vitro* and *in vivo* models [192]. Particularly, fluoxetine was found to significantly decrease the proliferation of several breast cancer cell lines by inducing apoptosis and autophagy-mediated cell death or endoplasmic reticulum stress and autophagy, respectively [190–193]. In triple-negative breast cancer cells, fluphenazine inhibited breast cancer cell growth and induced G0/G1 cell cycle arrest, and induced mitochondria-mediated apoptosis in breast cancer cells [165]. In the case of MCF-7 cells, as they do not express caspase-3, they do not undergo normal apoptosis and autophagy can represent the main alternative cell death pathway [478]. Recent studies suggest that benztropine reduces the activity of oncogenic signaling transducers and trans-activators for MMP9, including STAT3, NF-kB, and β-catenin [183]. In this way, we believe that the PTX mechanism of synergy in combination with CNS drugs can be related to enhanced cell cycle arrest, interference with important oncogenic signaling, and increased autophagy-mediated cell death. We also believe that CNS drugs can act as chemosensitizers by slowing down drug efflux, increasing drug accumulation. As several CNS drugs are substrates and modulators of the P-glycoprotein (P-gp) protein [479–481], we also believe they can inhibit P-gp to stop effusing drugs from intracellular, to increase the intracellular concentration of anticancer drugs such as PTX.

Then, and to complement our previous studies, it was hypothesized that the combination of CNS drugs would also synergistically increase the antitumor potential of DOX in breast cancer cells and that this combination would be preferable to the combination with PTX. However, as shown in Figure 89, the CI values of DOX and CNS drugs in combination were mostly higher than one, except for one pair of DOX + fluoxetine, suggesting that the growth inhibitory effect of these compounds in combination was mostly additive or antagonistic in MCF-7 cells.

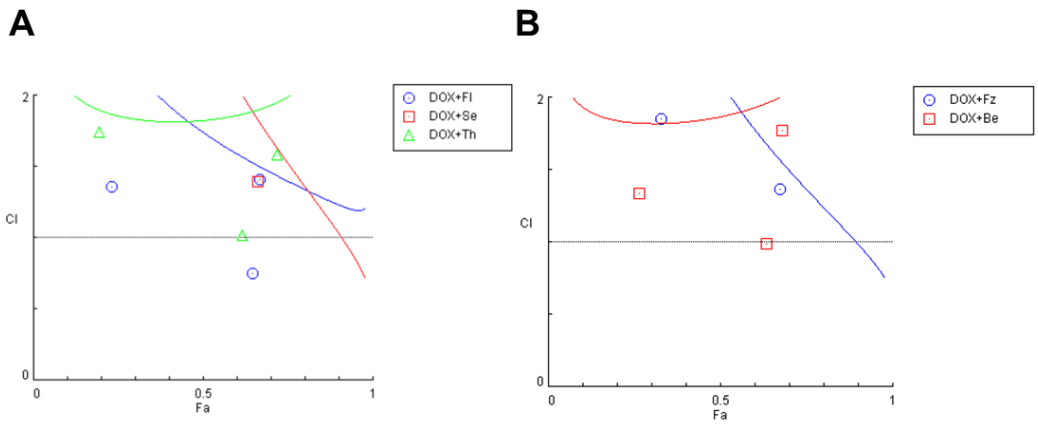

Figure 89. Fa-CI plot of combined treatments of DOX and different CNS drugs on MCF-7 breast cancer cells. For simplification, the results were split into two different plots. (A) Fa-CI plot of DOX+fluoxetine (blue), DOX+sertraline (red), and DOX+Thioridazine (green). (B) Fa-CI plot of DOX+fluphenazine (blue) and DOX+benztropine (red). CI was determined using CompuSyn software. CI < 1, = 1, and >1 indicate synergistic, additive, and antagonistic effects, respectively. Fl: fluoxetine; Se: sertraline; Th: thioridazine; Fz: fluphenazine; Be: benztropine.

In addition to CompuSyn results, it was also evaluated the drug interaction in these combinations with SynergyFinder, using the Bliss model. These results suggested that fluoxetine interacts most with DOX in intermediate concentrations, resulting in a synergy score of 10.675, indicative of synergism between the two drugs (Figure 90A). Sertraline combination with DOX also resulted in a positive Bliss score of 3.332, with synergic interactions with the reference drug for higher concentrations (Figure 90B). Both thioridazine and benztropine combinations with DOX resulted in negative scores of -3.284 and -8.262, respectively, indicative of antagonism (Figure 90C and E). Fluphenazine interaction with DOX gave a value of Bliss score near zero, indicating additivity (Figure 90D).

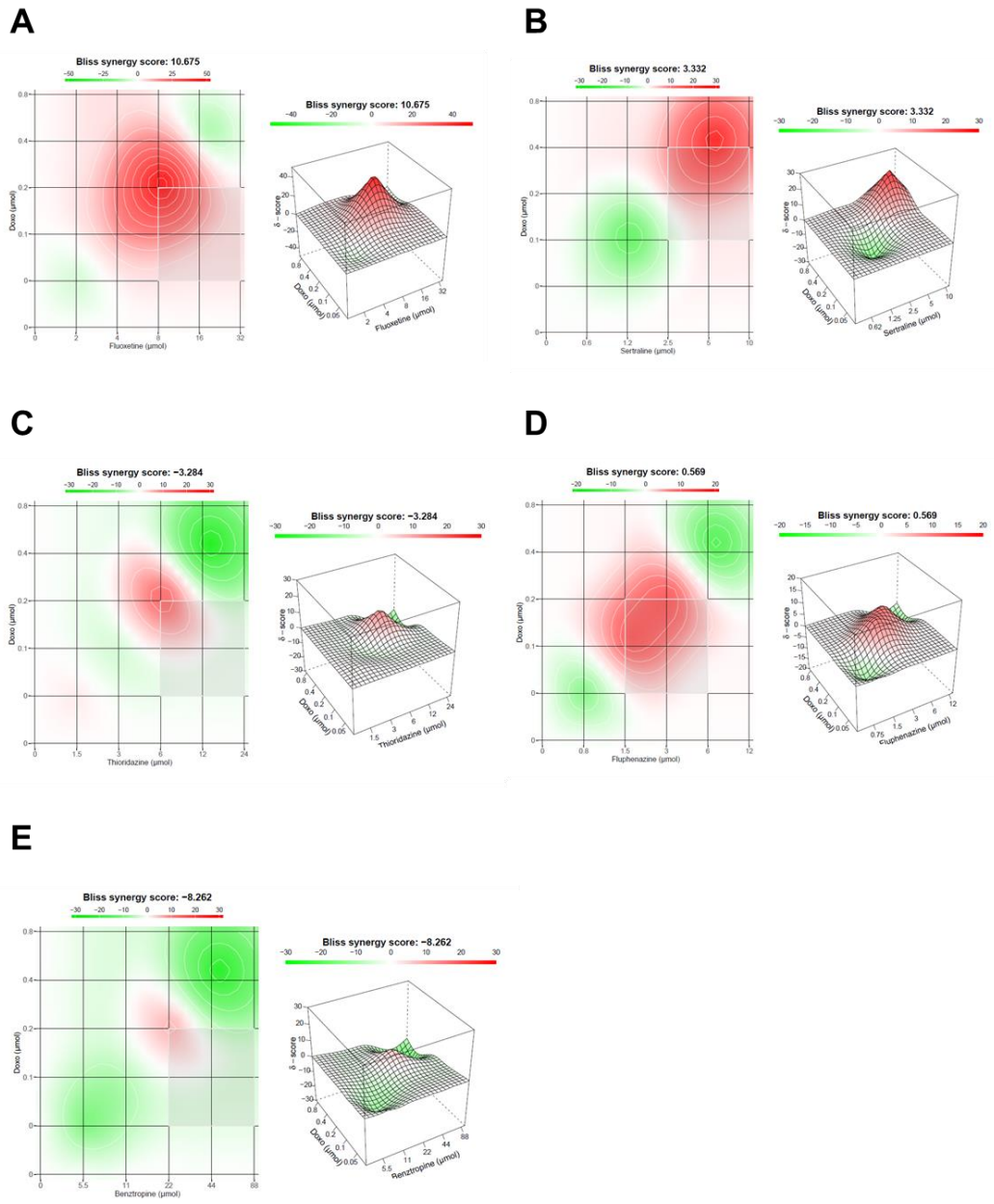

Figure 90. Bliss synergy plots of combined treatments of DOX and different CNS drugs on MCF-7 breast cancer cells. Bliss synergy plots of (**A**) DOX + fluoxetine, (**B**) DOX + sertraline, (**C**) DOX + thioridazine, (**D**) DOX + fluphenazine and (**E**) DOX + benztropine. The synergy score was calculated using SynergyFinder software. Positive or negative Bliss synergy scores indicate synergistic and antagonistic effects, respectively.

Compared to our previous findings, the combination of CNS drugs with PTX resulted in enhanced cell viability reduction compared to DOX, suggesting that these repurposed drugs should have some signaling pathway that may complement the mechanism of action of PTX but not DOX. These results also reinforce that the choice of the antineoplastic drug in different combination models with the same repurposed drugs can affect the results and

should be performed very carefully. Following these results, CI calculation also demonstrated that most drug pairs involving DOX presented an antagonistic or additive interaction, which supports our results from the viability studies. Moreover, these results demonstrate that using different reference models to evaluate the drug interactions between drug pairs can affect the synergism evaluation of these combinations.

It was next investigated the synergistic effects of the combinations of antineoplastic drugs DOX and PTX with CNS drugs quetiapine and edaravone using the Chou–Talalay method. These results are summarized in Figure 91 and Table 17.

In line with the previous MTT results obtained in Chapter II, it was found that the combinations of both chemotherapeutic drugs with edaravone resulted in all pairs being antagonists (CI > 10), with Fa values being very low (all under 0.5). As the *y*-axis in Figure 91 is under 2, these points are not displayed in the graph. On the other hand, the combination of DOX and PTX with quetiapine demonstrated promising results, with all pairs being synergistic. Nevertheless, the Fa values for these combinations are under 0.6, even when using the highest concentration of quetiapine, demonstrating that, although the drugs act synergistically, the combinations themselves cannot reduce cell viability by more than 60%.

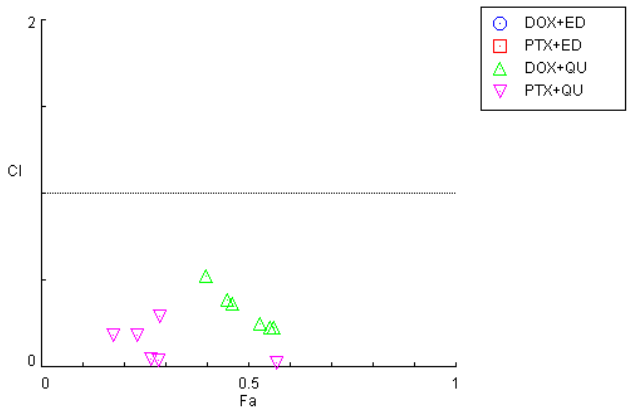

Figure 91. Graphical representation of CI plot obtained from the CompuSyn Report for the combinations of DOX + edaravone (blue), PTX + edaravone (red), DOX + quetiapine (green), and PTX + quetiapine (pink). ED: edaravone; QU: quetiapine

Table 17. CI values and the respective fractional effect of different combinations of antineoplastic drugs plus CNS agents in MCF-7 cells. CI in bold indicates drug pairs that are synergic.

Combination (Drug A + Drug B)	Dose A	Dose B	Fractional Effect (Fa)	CI Value
DOX + edaravone	IC_{50}	0.01	0.389	>10
		0.1	0.393	>10
		1	0.343	>10
		10	0.381	>10
		50	0.370	>10
		100	0.376	>10
PTX + edaravone	IC_{50}	0.01	0.255	>10
		0.1	0.307	>10
		1	0.240	>10
		10	0.247	>10
		50	0.240	>10
		100	0.274	>10
DOX + quetiapine	IC_{50}	0.01	0.399	**0.528**
		0.1	0.464	**0.363**
		1	0.451	**0.390**
		10	0.530	**0.252**
		50	0.554	**0.231**
		100	0.562	**0.232**
PTX + quetiapine	IC_{50}	0.01	0.173	**0.182**
		0.1	0.264	**0.049**
		1	0.283	**0.043**
		10	0.231	**0.186**

	50	0.287	**0.295**
	100	0.567	**0.027**

Taken together, these results demonstrate that the use of quetiapine synergistically enhances the anticancer activity of DOX and PTX for the management of breast cancer, although further studies of dose optimization are still necessary to guarantee the maximum therapeutic effects.

5.1.3 Synergistic Combinations of Antimalarial Drugs

The examination of the CI for the combination of two antimalarial drugs described in Chapter II demonstrates that some pairs interact synergistically, especially when the pyronaridine concentration is fixed and the mefloquine concentration is variable. Regarding the combination of the mefloquine IC_{50} plus variable pyronaridine, CI values of 0.205 and 0.664 were found for the combination with 10 and 50 µM of pyronaridine, respectively. The combination of pyronaridine IC_{50} plus variable mefloquine demonstrated synergism for lower concentrations of mefloquine (<10 µM). These results are shown in Figure 92 and Table 18.

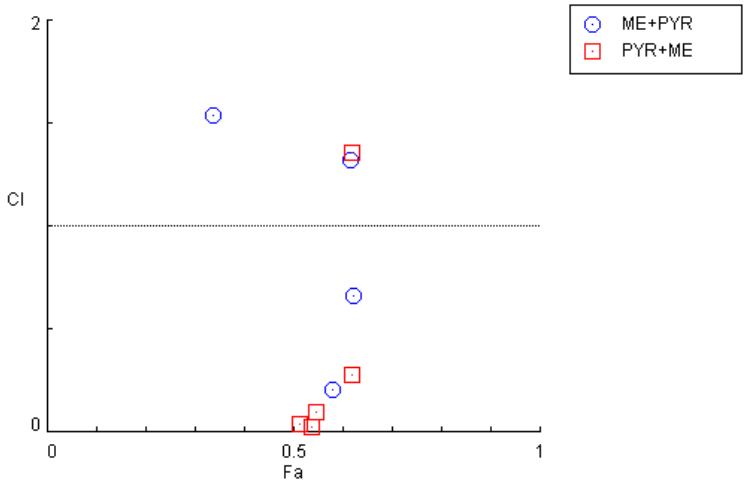

Figure 92. Graphical representation of CI plot obtained from the CompuSyn Report for the combinations of mefloquine IC_{50} + variable pyronaridine (blue) and pyronaridine IC_{50} + variable mefloquine (red). ME: mefloquine; PYR: pyronaridine

Table 18. CI values and the respective fractional effect of drug combinations using antimalarial drugs in MCF-7 cells. CI in bold indicates concentrations of drug pairs that are synergic.

Combination (Drug A + Drug B)	Dose A	Dose B	Fractional Effect (Fa)	CI Value
Mefloquine + Pyronaridine	IC_{50}	0.01	0.204	>10
		0.1	0.242	7.063
		1	0.339	1.537
		10	0.582	**0.205**
		50	0.623	**0.664**
		100	0.618	1.324
Pyronaridine + Mefloquine	IC_{50}	0.01	0.538	**0.025**
		0.1	0.514	**0.038**
		1	0.547	**0.096**
		10	0.621	**0.279**
		50	0.619	1.358
		100	0.632	2.272

5.1.4 Synergistic Combinations of CNS Drugs

The CI evaluation was then performed for the combination of CNS drugs using fluphenazine and sertraline. After calculation of the CI values and the respective fractional effects of the drug combinations using CNS drugs in MCF-7 cells (Figure 93 and Table 19), only one synergistic pair was found for the combination of sertraline IC_{50} plus 10 µM of fluphenazine and two pairs regarding the combination of fluphenazine IC_{50} and variable doses of sertraline (10 and 50 µM).

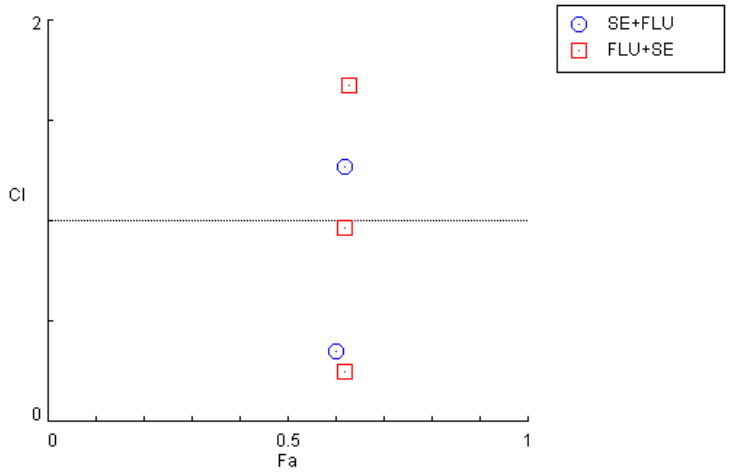

Figure 93. Graphical representation of CI plot obtained from the CompuSyn Report for the combinations of sertraline IC_{50} + variable fluphenazine (blue) and fluphenazine IC_{50} + variable sertraline (red). SE: sertraline; FLU: fluphenazine

Table 19. CI values and the respective fractional effect of drug combinations using CNS drugs in MCF-7 cells. CI in bold indicates concentrations of drug pairs that are synergic.

Combination (Drug A + Drug B)	Dose A	Dose B	Fractional Effect (Fa)	CI Value
Sertraline + Fluphenazine	IC_{50}	0.01	0.192	8.434
		0.1	0.177	>10
		1	0.255	5.102
		10	0.601	**0.351**
		50	0.618	1.269
		100	0.629	2.197
Fluphenazine + Sertraline	IC_{50}	0.01	0.156	>10
		0.1	0.196	>10
		1	0.218	>10
		10	0.619	**0.250**
		50	0.621	**0.967**
		100	0.630	1.676

5.1.5 Synergistic Combinations of Peptides and Antineoplastic/CNS Drugs

Next, the potential for synergistic cytotoxic activity between DOX, CNS drugs, and honeybee venom was also evaluated using the Chou–Talalay reference (Figure 94). The produced effect (Fa) and CI values for each combination are represented in Table 20. Based on the CI values, all drug combinations with CNS drugs indicated synergism for concentrations below 25 µg/mL of honeybee venom. The evaluation of drug interactions in cells treated with the combination of honeybee venom with DOX indicated mostly antagonism, except for DOX + 25 µg/mL honeybee venom.

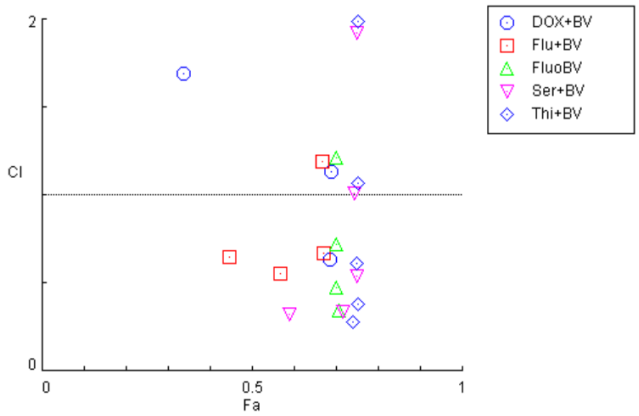

Figure 94. Fa-CI plot of combined treatments of DOX and CNS drugs combined with honeybee venom on MCF-7 breast cancer cells. The CI was calculated using CompuSyn software. CI < 1, = 1, and > 1 indicate synergistic, additive, and antagonistic effects, respectively. BV: bee venom; DOX: doxorubicin; Flu: fluphenazine; Fluo: fluoxetine; Ser: sertraline; Thi: thioridazine.

Table 20. The nature of drug interactions in MCF-7 breast cancer cells treated with CNS drugs and DOX combined with honeybee venom.

Drug A	Dose A (µM)	Sample B	Dose B (ug/mL)	Effect (Fa)	CI value	Interaction
DOX	0.17	Honeybee Venom	6.25	0.0656	30.74	Antagonism
			12.5	0.3388	1.69	Antagonism
			25	0.6877	0.63	Synergism
			50	0.6897	1.13	Antagonism
			100	0.6851	2.15	Antagonism

Fluphenazine	2.68	Honeybee Venom	6.25	0.4464	0.64	Synergism
			12.5	0.5691	0.55	Synergism
			25	0.6707	0.67	Synergism
			50	0.667	1.19	Antagonism
			100	0.6646	2.23	Antagonism
Fluoxetine	7.78	Honeybee Venom	6.25	0.7064	0.34	Synergism
			12.5	0.7025	0.47	Synergism
			25	0.7016	0.72	Synergism
			50	0.7022	1.21	Antagonism
			100	0.7076	2.18	Antagonism
Sertraline	2.22	Honeybee Venom	6.25	0.5892	0.32	Synergism
			12.5	0.716	0.33	Synergism
			25	0.7492	0.53	Synergism
			50	0.7442	1.01	Antagonism
			100	0.7497	1.92	Antagonism
Thioridazine	5.72	Honeybee Venom	6.25	0.7398	0.27	Synergism
			12.5	0.7523	0.38	Synergism
			25	0.7505	0.61	Synergism
			50	0.7545	1.06	Antagonism
			100	0.7545	1.98	Antagonism

The evaluation of drug interactions was also performed using the SynergyFinder software by other four reference models (ZIP, HSA; Bliss, and Loewe). The ZIP model evaluates the drug interactions' relationships by comparing the change in the potency (effect at a certain dose level) of the dose-response curves between individual drugs and their combinations, assuming that two non-interacting drugs were expected to incur minimal changes in their dose-response curves [433]. The Loewe additivity model calculates the expected response as if both drugs were the same [482]. The HSA model is one of the simplest reference models, which states that the expected combination effect is the maximum of the single drug responses at corresponding concentrations [316]. In these representations, synergy scores under −10, from −10 to 10, and above 10 indicate antagonism, additivity, and synergism, respectively.

These results also demonstrated that the combination of DOX plus honeybee venom was predominantly antagonistic (Figure 95), while combinations with CNS drugs were mostly additive (Figure 96–99). For the combined pair of thioridazine with honeybee venom, the ZIP synergy plot was not calculated by the software.

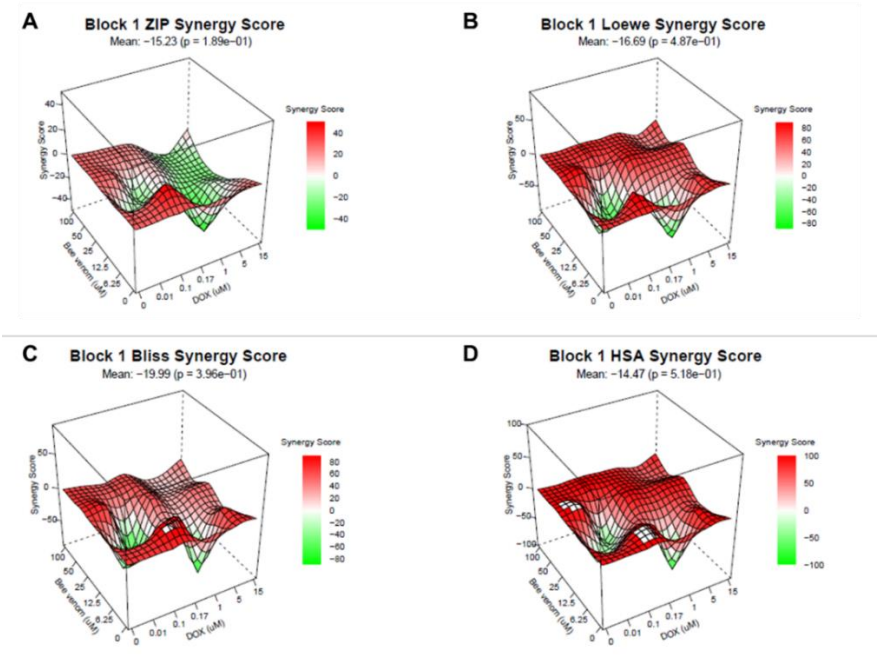

Figure 95. Synergy plots of combined treatments of DOX combined with honeybee venom on MCF-7 breast cancer cells calculated with (**A**) ZIP; (**B**) Loewe; (**C**) Bliss and (**D**) HSA reference models. These data were obtained using SynergyFinder software. Synergy scores < -10, from -10 to 10, and > 10 indicate antagonism, additivity, and synergism, respectively.

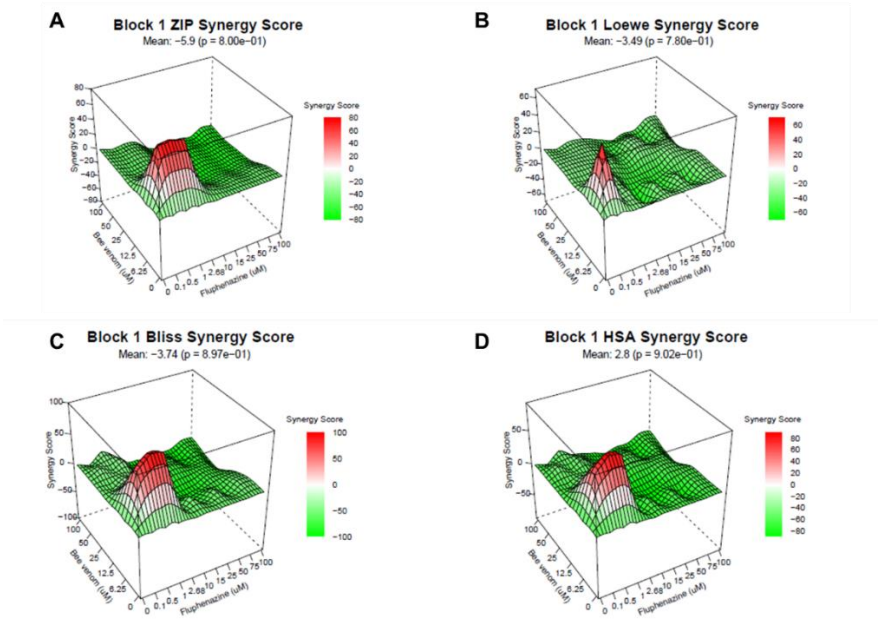

Figure 96. Synergy plots of combined treatments of fluphenazine combined with honeybee venom on MCF-7 breast cancer cells calculated with (**A**) ZIP; (**B**) Loewe; (**C**) Bliss and (**D**) HSA reference models. These data were obtained using SynergyFinder software. Synergy scores < -10, from -10 to 10, and > 10 indicate antagonism, additivity, and synergism, respectively.

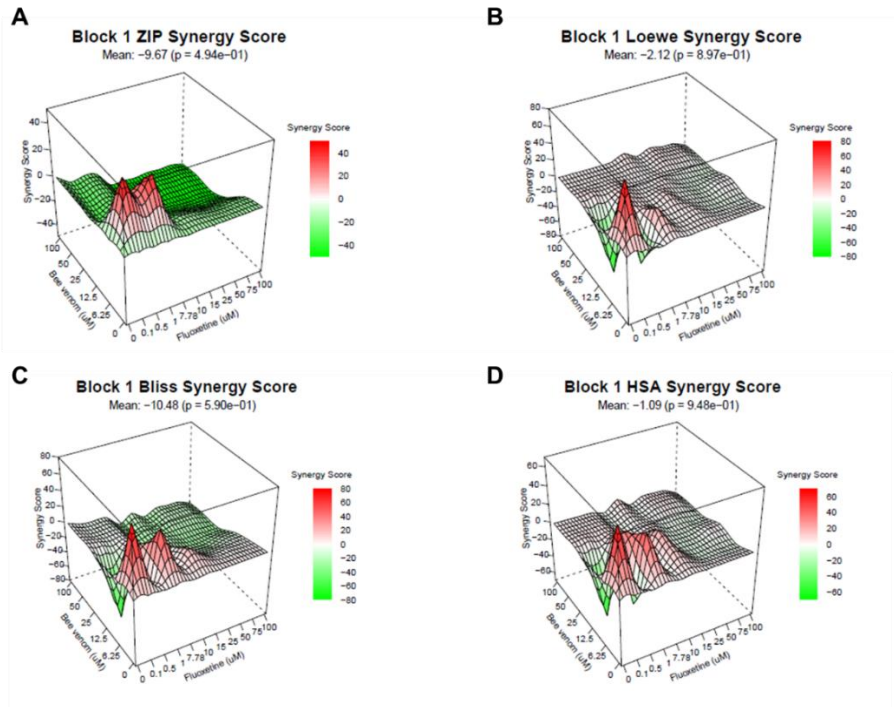

Figure 97. Synergy plots of combined treatments of fluoxetine combined with honeybee venom on MCF-7 breast cancer cells calculated with (**A**) ZIP; (**B**) Loewe; (**C**) Bliss and (**D**) HSA reference models. These data were obtained using SynergyFinder software. Synergy scores < -10, from -10 to 10, and > 10 indicate antagonism, additivity, and synergism, respectively.

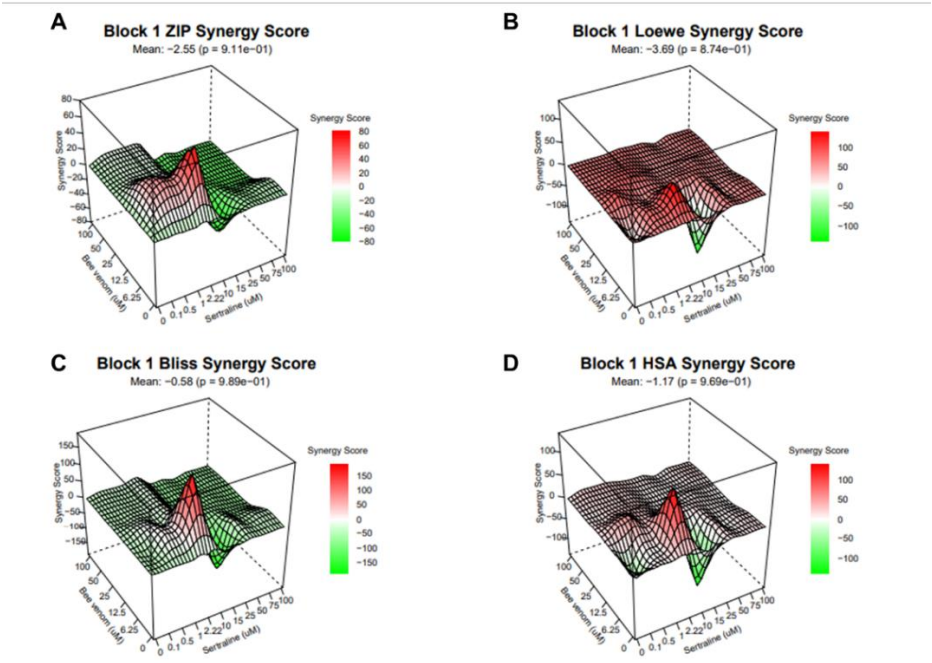

Figure 98. Synergy plots of combined treatments of sertraline combined with honeybee venom on MCF-7 breast cancer cells calculated with (**A**) ZIP; (**B**) Loewe; (**C**) Bliss and (**D**) HSA reference models. These data were obtained using SynergyFinder software. Synergy scores < -10, from -10 to 10, and > 10 indicate antagonism, additivity, and synergism, respectively.

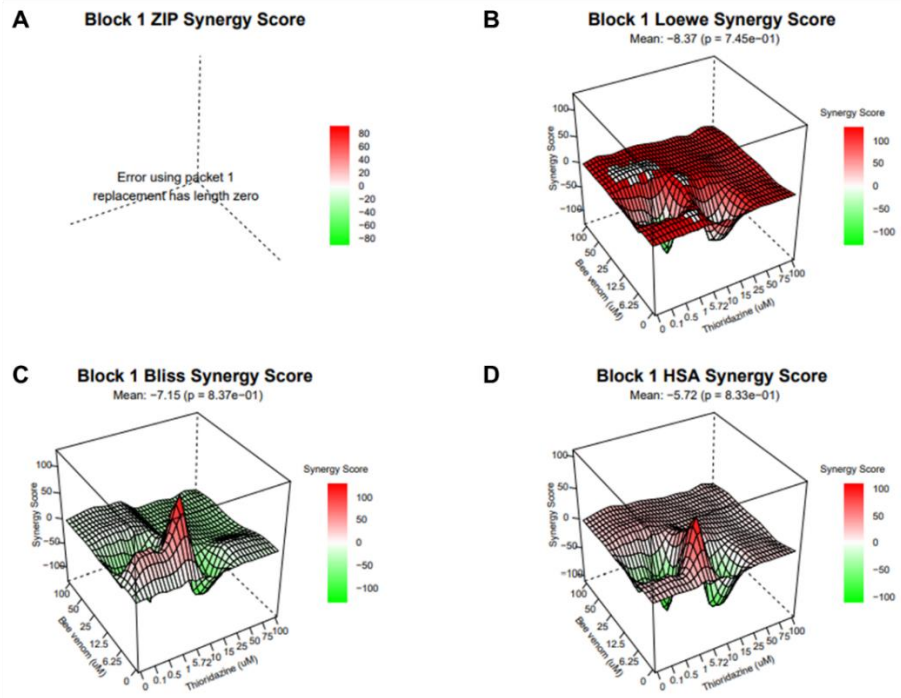

Figure 99. Synergy plots of combined treatments of thioridazine combined with honeybee venom on MCF-7 breast cancer cells calculated with (**A**) ZIP; (**B**) Loewe; (**C**) Bliss and (**D**) HSA reference models. These data were obtained using SynergyFinder software. Synergy scores < -10, from -10 to 10, and > 10 indicate antagonism, additivity, and synergism, respectively.

5.2 Analysis of Drug Interactions in Colorectal Cancer Cells

5.2.1 Synergistic Combinations of Antineoplastic and Antimalarial drugs

To investigate the effects of the combinations of 5-FU with the antimalarial drugs previously tested in Chapter II, the CI was calculated using the Chou-Talalay method, using the CompuSyn software. The combination of artesunate with 5-FU did not result in any synergism (Figure 100A), with CI > 1 for all pairs of concentrations (Table 21). The combination of 5-FU and mefloquine resulted in only one synergic pair (Figure 100B), with a Fa value of 0.848 (Table 21).

A **B**

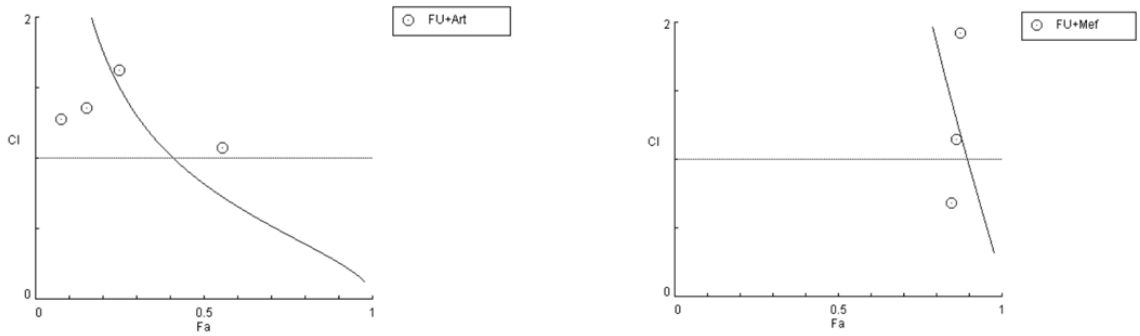

Figure 100. Chou-Talalay method Fa-CI plot of 5-FU plus artesunate (**A**) and mefloquine (**B**). CI was plotted on the *y*-axis as a function of effect level (Fa) on the *x*-axis to evaluate drug synergism. CI < 1, CI = 1, and CI > 1 refer to synergism, additivity, and antagonism, respectively. FU: 5-FU; Art: Artesunate; Mef: Mefloquine.

Table 21. CI values and the respective fractional effect of different combinations of 5-FU plus antimalarial drugs in HT-29 cells. CI in bold indicates concentrations of drug pairs that are synergic. Cells were treated with 0.25, 0.5, 1, 2, and 4 times the IC_{50} of each drug (total dose).

Combination (Drug A + Drug B)	Total Dose (Dose A + Dose B)	Fractional Effect (Fa)	CI Value
5-FU + mefloquine	3.625	0.2138	29.9325
	7.25	0.5659	4.07663
	14.5	0.8481	**0.68334**
	29.0	0.861	1.14685
	58.0	0.873	1.92463

	5.25	1.0E-5	1461.26
	10.5	0.0782	1.27561
5-FU + artesunate	21.0	0.1521	1.35742
	42.0	0.2489	1.62381
	84.0	0.5575	1.07643

Besides the Chou-Talalay method, drug interactions were also evaluated by the Bliss Independence and HSA methods, using the SynergyFinder 2.0 software. For mefloquine, no synergism was observed using the Bliss and HSA models (Figure 101A and B, respectively). Contrary to the previous results obtained by the Chou-Talalay method, the combination of 5-FU plus artesunate evaluated by the Bliss Method resulted in a positive synergy score of 0.411, with a red region on the 2D/3D plot in the lowest concentrations (Figure 101C). Using the HSA model, the synergy score was negative, demonstrating antagonism (Figure 101D).

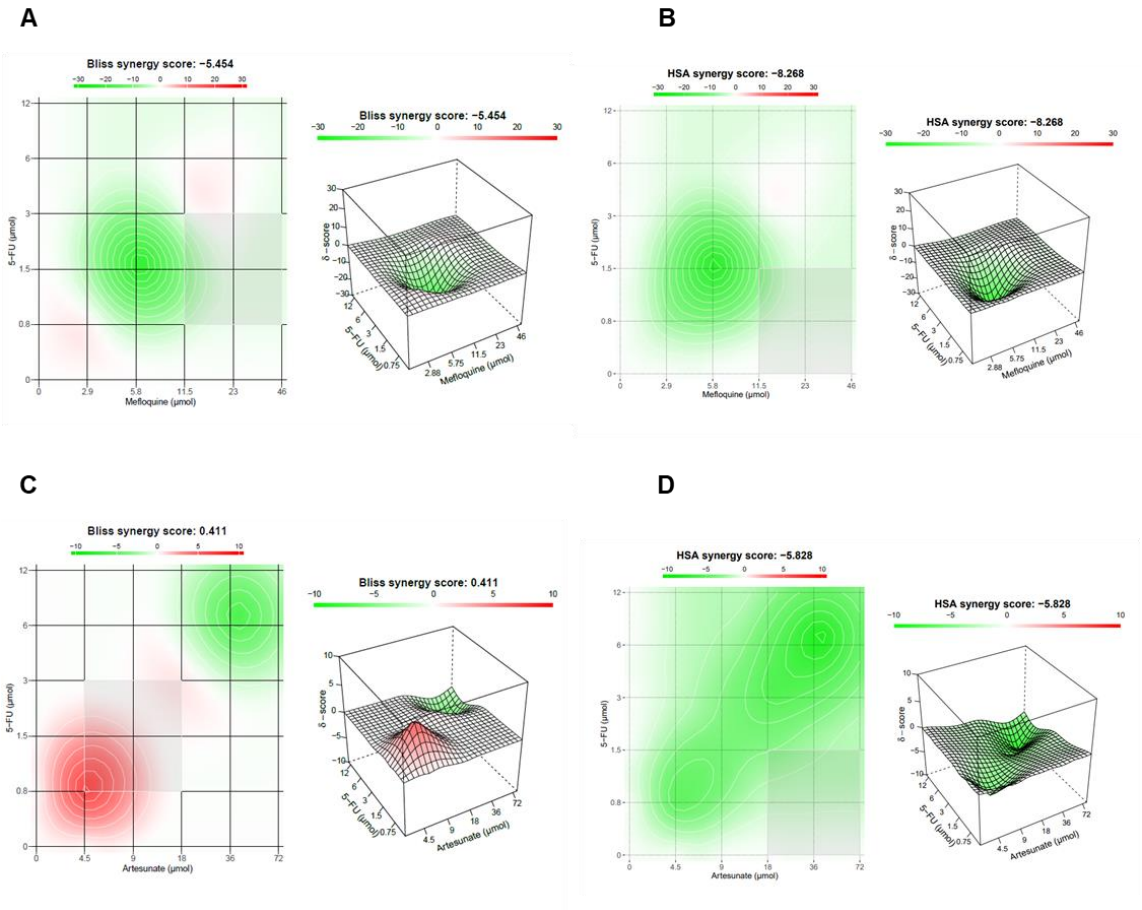

Figure 101. Bliss (**left**) and HSA (**right**) synergy plots of 5-FU plus mefloquine (**A**, **B**) and artesunate (**C**, **D**).

These results demonstrate that the choice of synergy evaluation model can give slightly different results regarding the synergy evaluation of drug combinations, although these reference models produce similar results most of the time.

5.2.2 Synergistic Combinations of Antineoplastic and CNS drugs

Next, the drug interactions between the combinations of CNS drugs with 5-FU were assessed both by Chou-Talalay method as well as Bliss and HSA reference models. The combination of 5-FU plus latrepirdine demonstrated little synergism with only one synergic pair (Figure 102A), with a Fa value of 0.44 (Table 22). Both combinations of 5-FU plus fluoxetine and benztropine demonstrated synergism just for one pair (Figure 102B and C, respectively), with Fa values of 0.73 and 0.87, respectively (Table 22). The combination with thioridazine was one of the most promising ones, with three synergic pairs (Figure 102D) and a Fa value reaching 0.75 (Table 22). For sertraline, all combinations were synergic (Figure 102E) and produced a Fa value of 0.85 (Table 22). A combination of

fluphenazine with 5-FU did not result in any synergism (Figure 102F), with CI > 1 for all pairs of concentrations (Table 22).

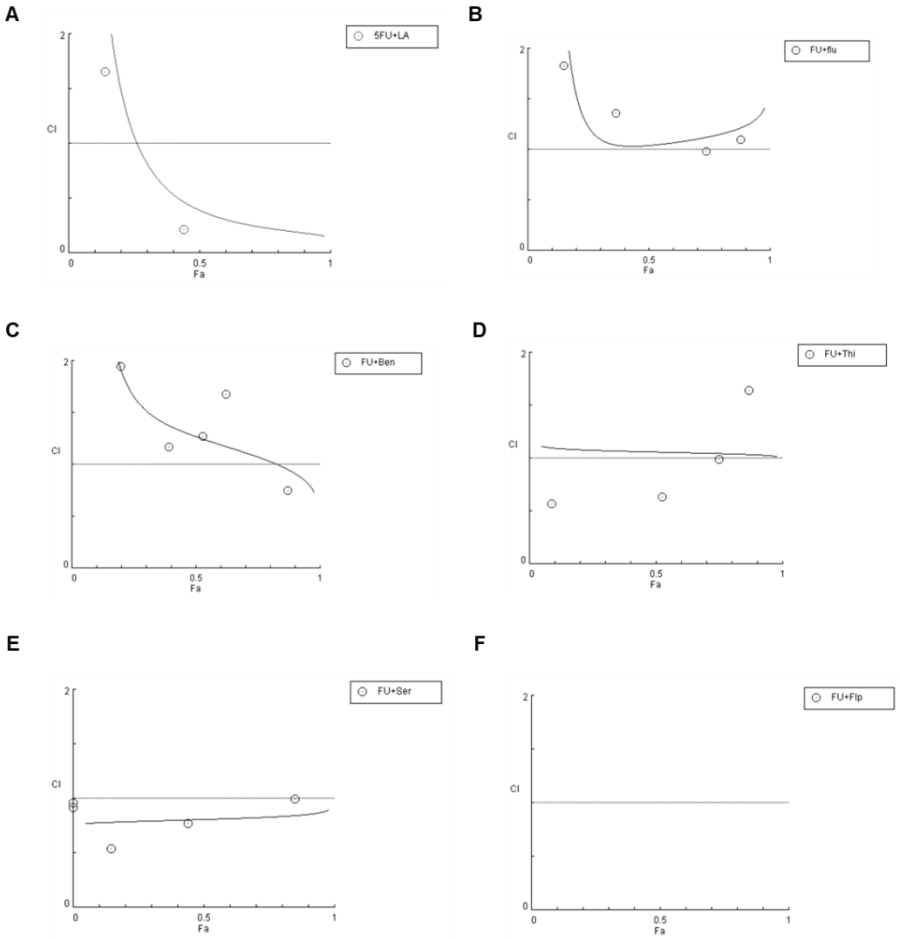

Figure 102. Chou-Talalay method Fa-CI plot of 5-FU plus latrepirdine (**A**), fluoxetine (**B**), benztropine (**C**), thioridazine (**D**), sertraline (**E**), and fluphenazine (**F**). CI was plotted on the *y*-axis as a function of effect level (Fa) on the *x*-axis to evaluate drug synergism. CI < 1, CI = 1, and CI > 1 refer to synergism, additivity, and antagonism, respectively. FU: 5-FU; LA: Latrepirdine; Flu: Fluoxetine; Ben: Benztropine; Thi: Thioridazine; Ser: Sertraline; Flp: Fluphenazine.

Table 22. CI values and the respective fractional effect of different combinations of 5-FU plus CNS agents. CI in bold indicates concentrations of drug pairs that are synergic. Cells were treated with 0.25, 0.5, 1, 2, and 4 times the IC_{50} of each drug (total dose).

Combination (Drug A + Drug B)	Total Dose (Dose A + Dose B)	Fractional Effect (Fa)	CI Value
5-FU + latrepirdine	2.75	0.14129	1.65359
	5.5	0.16103	2.00449
	11.0	0.17389	2.97604
	22.0	0.21248	2.69396
	44.0	0.44126	**0.21700**
5-FU + fluoxetine	2.25	0.1497	1.83049
	4.5	0.1688	2.64547
	9.0	0.364	1.36014
	18.0	0.73678	**0.98008**
	36.0	0.8799	1.09726
5-FU + benztropine	5.25	0.1984	1.94601
	10.5	0.3913	1.17167
	21.0	0.5293	1.27070
	42.0	0.6237	1.67649
	84.0	0.8716	**0.74841**
5-FU + thioridazine	1.75	1.0E-5	3.28032
	3.5	0.0882	**0.57237**
	7.0	0.5245	**0.63129**
	14.0	0.7502	**0.99126**
	28.0	0.8692	1.63800

5-FU + sertraline	1.375	1.0E-4	**0.91640**
	2.75	0.001	**0.95924**
	5.5	0.1469	**0.54137**
	11.0	0.4412	**0.76907**
	22.0	0.8507	**0.99970**
5-FU + fluphenazine	5.25	0.11608	11.6103
	10.5	0.17321	13.0845
	21.0	0.4477	8.40182
	42.0	0.5522	12.1699
	84.0	0.8399	8.04387

The results from SynergyFinder are represented in Figure 103. Latrepirdine in combination with 5-FU, both by Bliss and HSA models (Figure 103A and B, respectively), demonstrated a negative synergy score, in line with the Chou-Talalay results, indicating antagonism for all pairs. Thioridazine demonstrated synergism by the Bliss model, with a positive synergy score of 5.178 (Figure 103C). The results for the HSA model demonstrated antagonism, but some regions of synergy, as represented in red in Figure 103D. In line with the previous results, the combination of 5-FU with sertraline resulted in strong synergism, both in the Bliss (Figure 103E) and HSA models (Figure 103F), with synergy scores of 22.203 and 3.042, respectively. By the Bliss model, fluphenazine combined with 5-FU resulted in a negative synergy score, demonstrating antagonism (Figure 103G). By the HSA models, the general synergy score was also negative but with a region in the 2D/3D plot demonstrating a pair of concentrations with synergic behavior (Figure 103H). Fluoxetine (Figure 103I and J) and benztropine (Figure 103K and L) did not show any synergism in Bliss and HSA models, demonstrating an antagonistic behavior between these drugs and 5-FU.

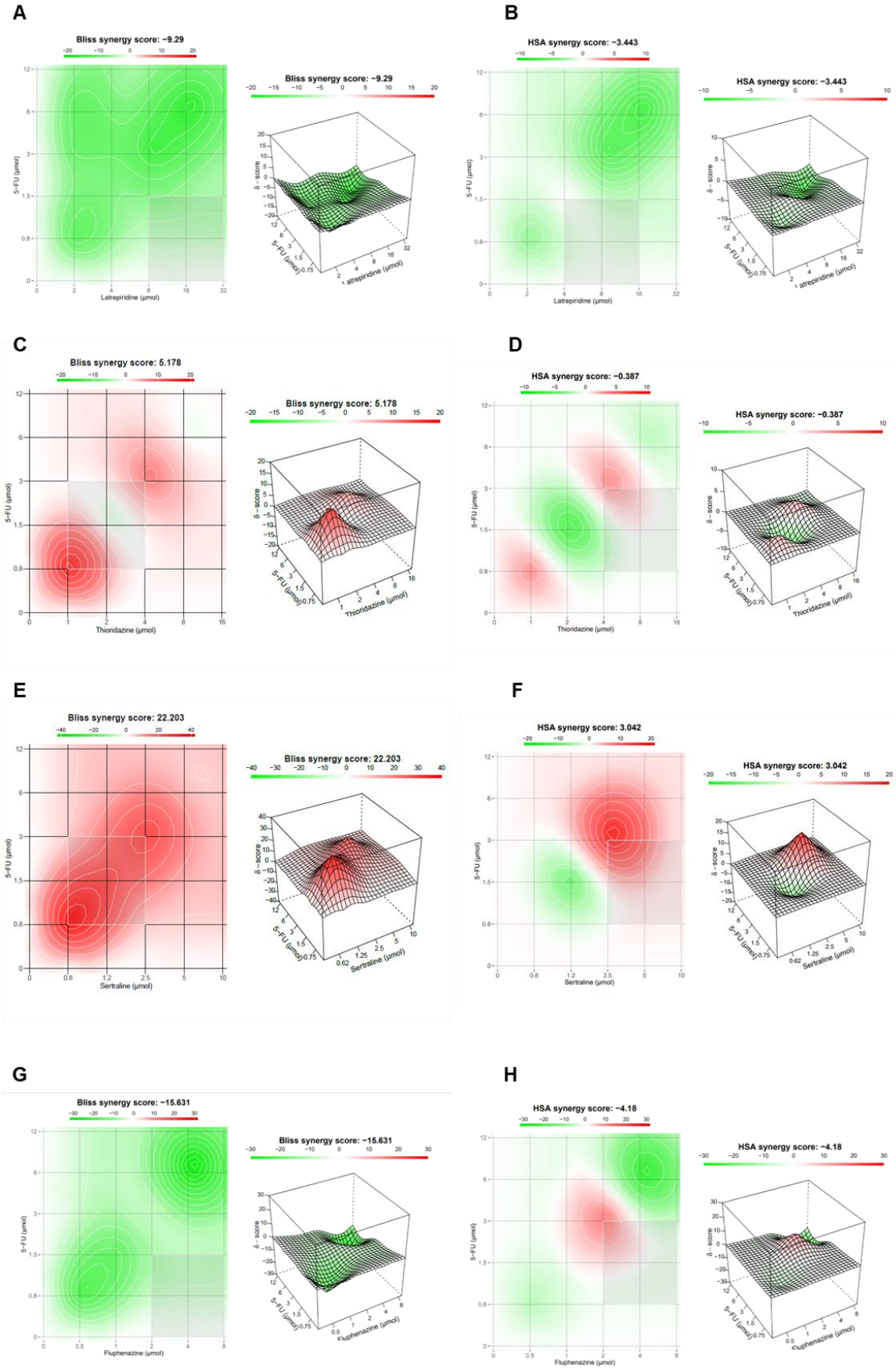
A
Bliss synergy score: −9.29
5−FU (μmol)
Latrepiridine (μmol)
δ − score
B
HSA synergy score: −3.443
C
Bliss synergy score: 5.178
Thioridazine (μmol)
D
HSA synergy score: −0.387
E
Bliss synergy score: 22.203
Sertraline (μmol)
F
HSA synergy score: 3.042
G
Bliss synergy score: −15.631
Fluphenazine (μmol)
H
HSA synergy score: −4.18

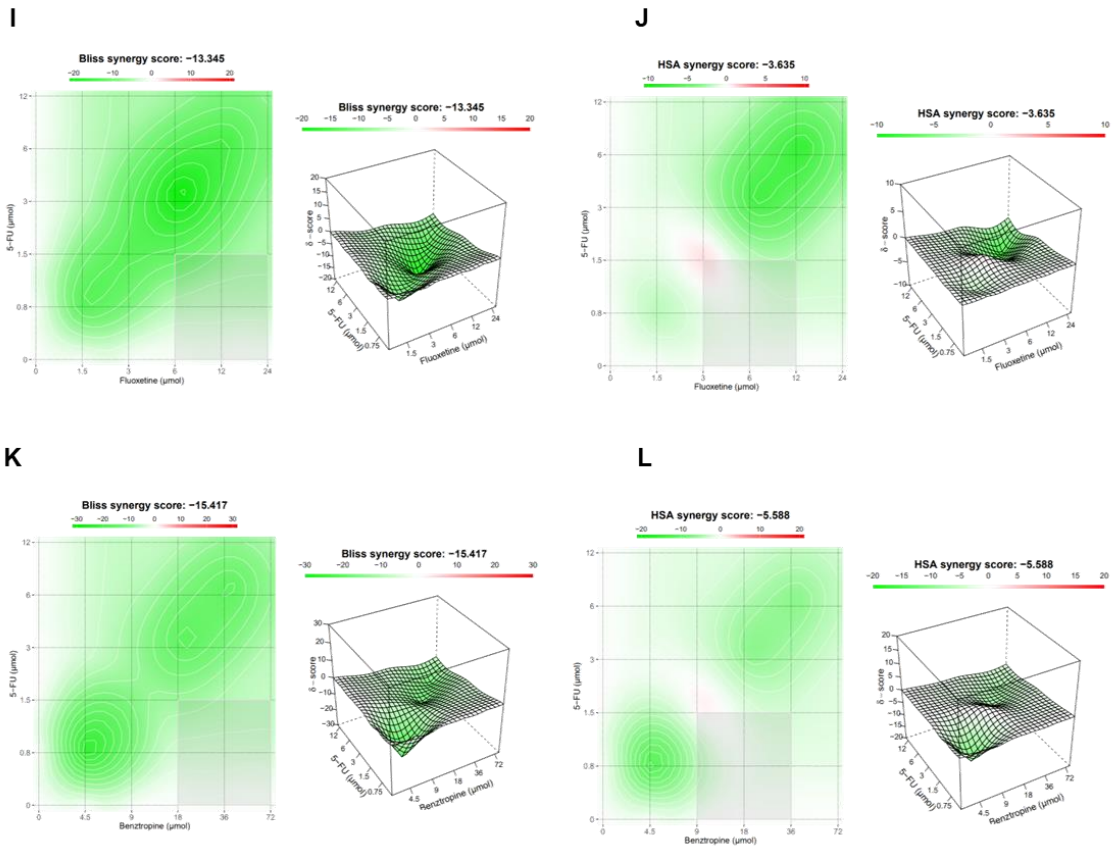

Figure 103. Bliss (**left**) and HSA (**right**) synergy plots of 5-FU plus latrepirdine (**A**, **B**), thioridazine (**C**, **D**), sertraline (**E**, **F**), fluphenazine (**G**, **H**), fluoxetine (**I, J**) and benztropine (**K, L**).

Together, these results demonstrate that some CNS agents, such as sertraline and thioridazine, may be promising to evaluate future combinations.

Drug synergism was further evaluated for the combinations of 5-FU with quetiapine/edaravone (Figure 104 and Table 23). It was found that all drug pairs for the combination of 5-FU with quetiapine present a CI value under 1, indicative of synergistic interactions. Additionally, for the combination of the highest concentration of quetiapine with the IC_{50} value for 5-FU, it was found the combined effect induced about 80% of cell death in this cell line. On the other hand, the CI values obtained for the combination of 5-FU and edaravone demonstrated all drug pairs to have values above 10, indicating antagonistic effects between the drugs (Figure 104 and Table 23).

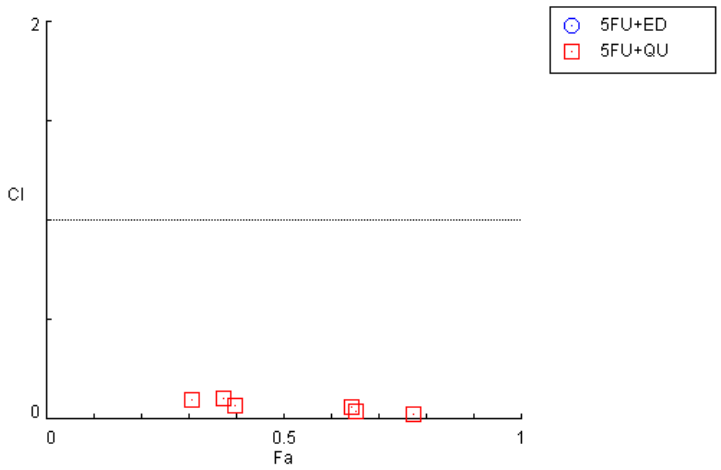

Figure 104. Graphical representation of CI plot obtained from the CompuSyn Report for the combinations of 5-FU + edaravone (blue) and 5-FU + quetiapine (red). 5FU: 5-FU; ED: Edaravone; QU: Quetiapine

Table 23. CI values and the respective fractional effect of different combinations of 5-FU plus CNS agents in HT-29 cells. CI in bold indicates concentrations of drug pairs that are synergic.

Combination (Drug A + Drug B)	Dose A	Dose B	Fractional Effect (Fa)	CI Value
5-FU + edaravone	IC_{50}	0.01	0.261	>10
		0.1	0.406	>10
		1	0.367	>10
		10	0.529	>10
		50	0.458	>10
		100	0.645	>10
5-FU + quetiapine	IC_{50}	0.01	0.307	**0.095**
		0.1	0.398	**0.072**
		1	0.374	**0.102**
		10	0.654	**0.036**
		50	0.643	**0.061**
		100	0.775	**0.026**

Comparing the results obtained in both cell lines, it is possible to conclude that CNS drugs work best in HT-29 colon cancer cells, both alone and combined with 5-FU, than in MCF-7 cells. When combined with PTX in MCF-7 cells, combination with CNS drugs resulted in higher combined efficacy than with DOX, revealing that the choice of the antineoplastic has an important role in the success of the combination. These results also allow to conclude that antimalarial drugs as repurposed drugs have enhanced effects in MCF-7 breast cancer cells, while combination with CNS drugs seems to be more effective in HT-29 colon cancer cells. These differences are visible when comparing the number of synergic pairs between the two cell lines and within the same line treated with different reference drugs (Table 24). Moreover, these results also demonstrate that quetiapine is a more promising repurposed drug than edaravone for breast and colorectal cancer therapy, demonstrating anticancer activity both as a standalone agent against HT-29 cells and as an adjuvant agent in combination regimens with DOX, PTX, and 5-FU against MCF-7 and HT-29 cells, respectively.

Table 24. Comparison of the number of synergic pairs in HT-29 and MCF-7 cell lines treated with the combination of CNS drugs (Drug B) and appropriate references (Drug A). N.D.: not determined

Drug A	Drug B	HT-29*	MCF-7
		Number of synergic interactions	Number of synergic interactions
5-FU	Mefloquine	1	N.D.
	Artesunate	0	
	Latrepirdine	1	
	Fluphenazine	0	
	Fluoxetine	1	
	Benztropine	1	
	Thioridazine	3	
	Sertraline	5	
	Edaravone	0	
	Quetiapine	6	

DOX	Artesunate	N.D.	4
	Chloroquine		3
	Mefloquine		1
	Pyronaridine		2
	Tafenoquine		0
	Fluoxetine		1
	Sertraline		0
	Thioridazine		0
	Benztropine		0
	Fluphenazine		0
	Edaravone		0
	Quetiapine		6
PTX	Artesunate	N.D.	2
	Chloroquine		2
	Mefloquine		1
	Pyronaridine		3
	Tafenoquine		0
	Fluoxetine		3
	Sertraline		2
	Thioridazine		3
	Benztropine		3
	Fluphenazine		3
	Edaravone		0
	Quetiapine		6

5.2.3 Synergism Evaluation of Different Combination Schedules of 5-FU and CNS Agents/Antimalarial Drugs

Next, it was analyzed the drug interactions in the different drug combinations schedules of 5-FU with antimalarial and CNS drugs previously evaluated in Chapter II, to evaluate if there were differences in the CI values between the three schedules of administration. For fluphenazine, there were no differences between the simultaneous administration and the sequential administration of the drugs, and all pairs were antagonists (Figure 105A). For fluoxetine, only one pair in the simultaneous administration was synergic, and in sequential administration, no synergism could be seen, so it was concluded that the simultaneous combination was advantageous over the sequential (Figure 105B). The same conclusions were found for benztropine and demonstrated a lack of efficacy in sequential administration (Figure 105C). Contrary to these drugs, the combination of 5-FU with artesunate in sequential form, with artesunate being given prior to 5-FU, seemed to produce better results compared to 5-FU prior to artesunate and simultaneous administration, resulting in three synergistic pairs (CI < 1) (Figure 105D). Table 25 shows the CI values obtained for each combination, depending on the drug schedule.

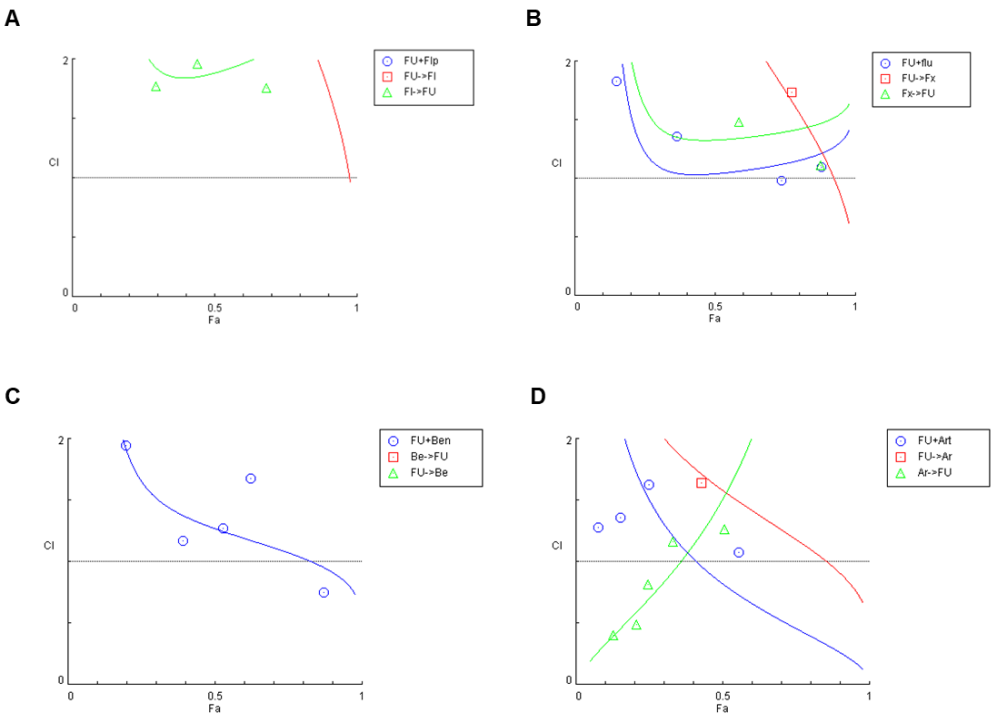

Figure 105. Chou-Talalay method Fa-CI plot of three schedule-dependent combinations of 5-FU plus fluphenazine (**A**), fluoxetine (**B**), benztropine (**C**), and artesunate (**D**). CI was plotted on the *y*-axis as a function of effect level (Fa) on the *x*-axis to evaluate drug synergism. CI < 1, CI = 1, and CI > 1 refer to synergism, additivity, and antagonism, respectively. FU: 5-FU; Ben: Benztropine; Art: Artesunate; Flp: Fluphenazine; Flu: Fluoxetine.

Table 25. CI values and respective fractional effect for three different combination schedules of 5-FU plus fluphenazine, fluoxetine, benztropine, and artesunate. CI in bold indicate concentrations of drug pairs that are synergic.

		CI for the Different Drug Combinations		
	Drug Combination (μM)	**Schedule A (CI)**	**Schedule B (CI)**	**Schedule C (CI)**
5-FU	*Fluphenazine*			
0.75	0.5	11.61	>100	4.09
1.5	1	13.08	>100	24.81
3	2	8.40	>100	1.77
6	4	12.17	4.36	1.96
12	8	8.04	4.68	1.76
5-FU	*Fluoxetine*			
0.75	1.5	1.83	>100	7.30
1.5	3	2.65	>100	3.53
3	6	1.36	>100	2.32
6	12	**0.98**	2.56	1.48
12	24	1.10	1.74	1.11
5-FU	*Benztropine*			
0.75	4.5	1.95	34.97	4.01
1.5	9	1.17	2.86	2.54
3	18	1.27	3.42	2.12
6	36	1.68	4.33	3.58
12	72	**0.75**	4.31	3.14

5-FU	*Artesunate*			
0.75	4.5	>100	7.88	**0.40**
1.5	9	1.28	4.85	**0.49**
3	18	1.36	4.22	**0.81**
6	36	1.62	2.56	1.16
12	72	1.08	1.64	1.26

5.2.4 Synergistic Combinations of Antimalarial Drugs

The evaluation of drug interactions regarding the combination of two antimalarial drugs in HT-29 cells (previous evaluated in Chapter II) is shown in Figure 106 and Table 26 and indicates that the combination of mefloquine IC_{50} plus pyronaridine acts synergistically when lower concentrations (< 10 µM) of pyronaridine are used. On the other hand, when combining pyronaridine at a fixed concentration plus variable concentrations of mefloquine, CI values under 1 were found for all concentrations, except for 100 µM of mefloquine, indicating synergistic interactions between these repurposed drugs.

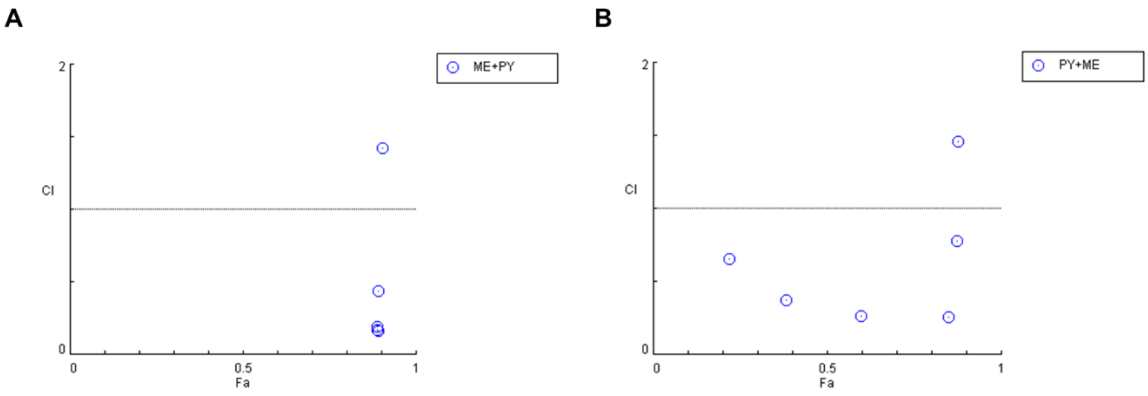

Figure 106. Graphical representation of CI plot obtained from the CompuSyn Report for the combinations of (**A**) mefloquine IC_{50} + variable pyronaridine and (**B**) pyronaridine IC_{50} + variable mefloquine. ME: mefloquine; PY: pyronaridine.

Table 26. CI values and the respective fractional effect of drug combinations using antimalarial drugs in HT-29 cells. CI in bold indicates concentrations of drug pairs that are synergic.

Combination (Drug A + Drug B)	Dose A	Dose B	Fractional Effect (Fa)	CI Value
Mefloquine + Pyronaridine	IC_{50}	0.01	0.891	**0.164**
		0.1	0.889	**0.169**
		1	0.891	**0.192**
		10	0.893	**0.439**
		50	0.904	1.426
		100	0.907	2.643
Pyronaridine + Mefloquine	IC_{50}	0.01	0.385	**0.373**
		0.1	0.219	**0.654**
		1	0.600	**0.263**
		10	0.850	**0.256**
		50	0.875	**0.777**
		100	0.877	1.460

5.2.5 Synergistic Combinations of CNS Drugs

The quantification of the CI for the combination of sertraline with fluphenazine demonstrated that, for concentrations under 10 µM, both combinations present synergism, with CI values under 1. Specifically, it was found that sertraline IC_{50} combined with 0.01, 0.1, 1, and 10 µM interact synergistically. The same occurred when fluphenazine IC_{50} was combined with 0.01, 0.1, 1, and 10 µM sertraline. These results are represented in Figure 107 and Table 27.

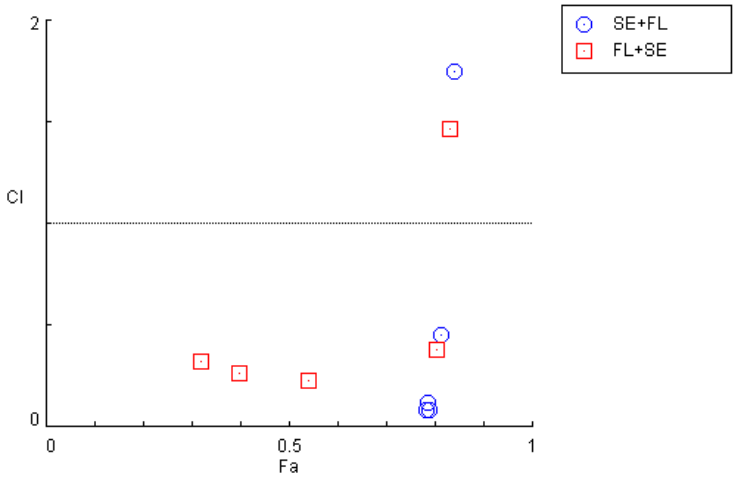

Figure 107. Graphical representation of CI plot obtained from the CompuSyn Report for the combinations of sertraline IC_{50} + variable fluphenazine (blue) and fluphenazine IC_{50} + variable sertraline (red). SE: sertraline; FL: Fluphenazine.

Table 27. CI values and the respective fractional effect of drug combinations using CNS drugs in HT-29 cells. CI in bold indicates concentrations of drug pairs that are synergic.

Combination (Drug A + Drug B)	Dose A	Dose B	Fractional Effect (Fa)	CI Value
Sertraline + Fluphenazine	IC_{50}	0.01	0.784	**0.081**
		0.1	0.789	**0.083**
		1	0.786	**0.122**
		10	0.815	**0.451**
		50	0.840	1.749
		100	0.838	3.464

Fluphenazine + Sertraline	IC_{50}	0.01	0.319	**0.322**
		0.1	0.399	**0.262**
		1	0.542	**0.230**
		10	0.805	**0.380**
		50	0.831	1.466
		100	0.836	2.814

5.2.6 Synergistic Combinations of Peptides and Antineoplastic/CNS Drugs

To evaluate the nature of the drug interactions in the combinations of honeybee venom with 5-FU and different CNS drugs, the CompuSyn software was also used, based on the Chou–Talalay method. The CI values of 5-FU and honeybee venom in combination were mostly lower than one, except for one pair (Figure 108), suggesting that the growth inhibitory effect of these compounds in combination was mostly synergistic in HT-29 cells. The same behavior was seen for combinations involving fluoxetine, sertraline, and thioridazine (Figure 108). Regarding the combination of fluphenazine and honeybee venom, it was found only two pairs presented synergism, while most of them were antagonists (Figure 108). Results obtained in the CompuSyn software are summarized in Table 28.

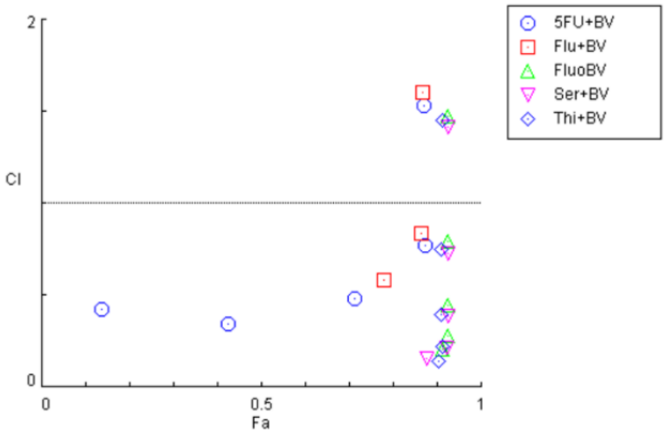

Figure 108. Fa-CI plot of combined treatments of 5-FU and CNS drugs combined with honeybee venom on HT-29 colon cancer cells. The CI was calculated using CompuSyn software. CI < 1, =1, and >1 indicate synergistic, additive, and antagonistic effects, respectively. BV: bee venom; 5FU: 5-FU; Flu: fluphenazine; Fluo: fluoxetine; Ser: sertraline; Thi: thioridazine.

Table 28. The nature of drug interactions in HT-29 colon cancer cells treated with CNS drugs and 5-FU combined with honeybee venom.

Drug A	Dose A (μM)	Sample B	Dose B (ug/mL)	Effect (Fa)	CI value	Interaction
5-FU	3.56	Honeybee Venom	6.25	0.1364	0.42	Synergism
			12.5	0.4246	0.34	Synergism
			25	0.7125	0.47	Synergism
			50	0.8731	0.77	Synergism
			100	0.8723	1.53	Antagonism
Fluphenazine	1.86	Honeybee Venom	6.25	0.0193	>100	Antagonism
			12.5	0.2529	4.39	Antagonism
			25	0.7797	0.58	Synergism
			50	0.866	0.83	Synergism
			100	0.867	1.60	Antagonism
Fluoxetine	6.12	Honeybee Venom	6.25	0.9125	0.20	Synergism
			12.5	0.9255	0.27	Synergism
			25	0.9244	0.44	Synergism
			50	0.9252	0.79	Synergism
			100	0.9256	1.47	Antagonism
Sertraline	2.45	Honeybee Venom	6.25	0.877	0.15	Synergism
			12.5	0.924	0.21	Synergism
			25	0.9249	0.38	Synergism
			50	0.9246	0.72	Synergism
			100	0.9247	1.41	Antagonism

			6.25	0.9034	0.13	Synergism
			12.5	0.9122	0.21	Synergism
Thioridazine	4.26	Honeybee Venom	25	0.911	0.39	Synergism
			50	0.912	0.75	Synergism
			100	0.913	1.45	Antagonism

Drug interactions in each combination were also analyzed by other four reference models: ZIP, Loewe, Bliss and HSA using the SynergyFinder software [476]. Synergy plots regarding the combination of 5-FU (Figure 109), fluphenazine (Figure 110), and fluoxetine (Figure 111) plus honeybee venom indicate mostly additivity, by all reference models. Analyzing the synergy plots of sertraline plus honeybee venom (Figure 112), it was found that the drug interaction in this combination was synergistic by ZIP, Bliss, and HSA models, with synergy scores of 12.04, 13.52, and 17.25, respectively. Thioridazine combined with honeybee venom was found to be predominantly additive, for all reference models (Figure 113).

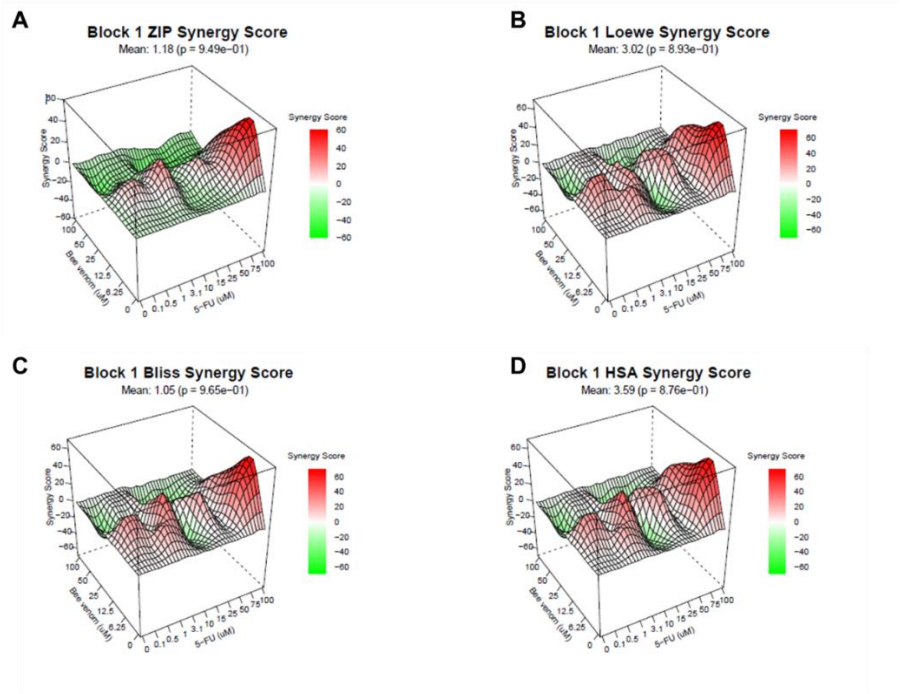

Figure 109. Synergy plots of combined treatments of 5-FU combined with honeybee venom on HT-29 colon cancer cells calculated with (**A**) ZIP; (**B**) Loewe; (**C**) Bliss and (**D**) HSA reference models. These data were obtained using SynergyFinder software. Synergy scores < −10, from −10 to 10, and > 10 indicate antagonism, additivity, and synergism, respectively.

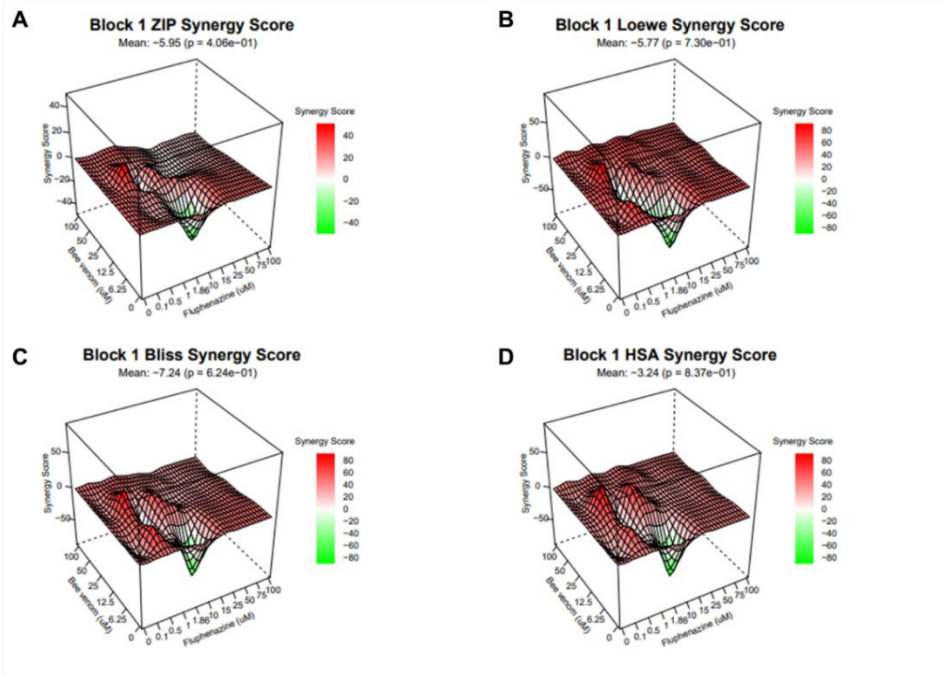

Figure 110. Synergy plots of combined treatments of fluphenazine combined with honeybee venom on HT-29 colon cancer cells calculated with (**A**) ZIP; (**B**) Loewe; (**C**) Bliss and (**D**) HSA reference models. These data were obtained using SynergyFinder software. Synergy scores < −10, from −10 to 10, and > 10 indicate antagonism, additivity, and synergism, respectively.

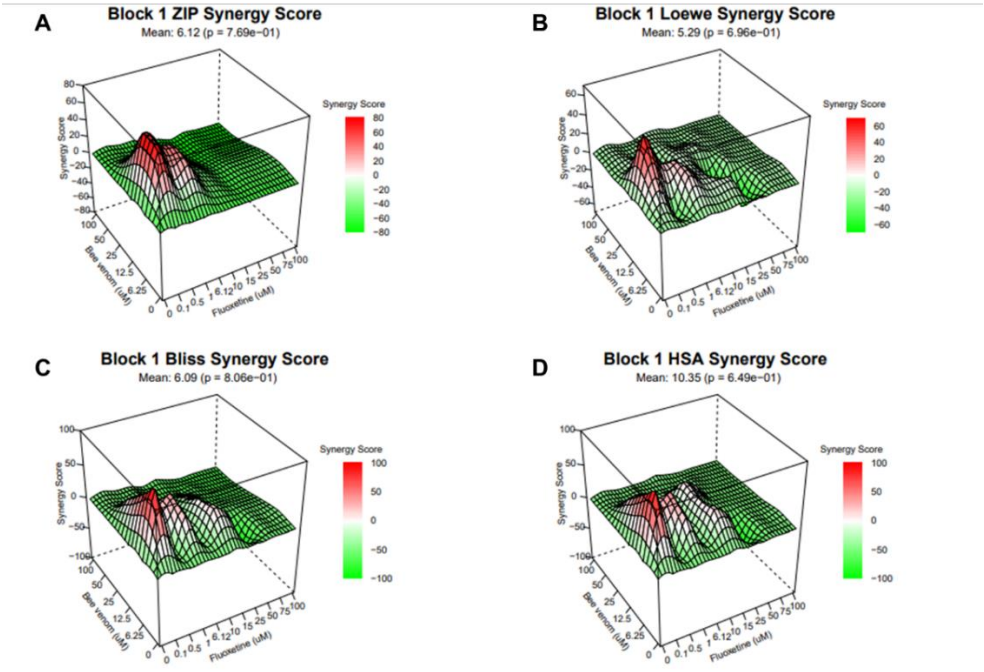

Figure 111. Synergy plots of combined treatments of fluoxetine combined with honeybee venom on HT-29 colon cancer cells calculated with (**A**) ZIP; (**B**) Loewe; (**C**) Bliss and (**D**) HSA reference models. These data were obtained using SynergyFinder software. Synergy scores < -10, from -10 to 10, and > 10 indicate antagonism, additivity, and synergism, respectively.

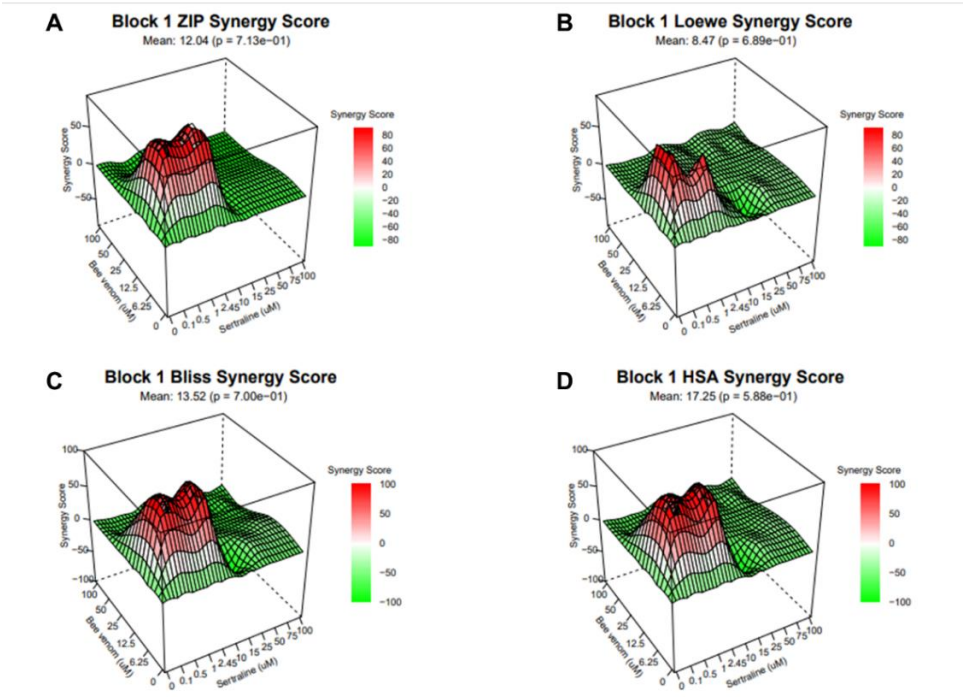

Figure 112. Synergy plots of combined treatments of sertraline combined with honeybee venom on HT-29 colon cancer cells calculated with (**A**) ZIP; (**B**) Loewe; (**C**) Bliss and (**D**) HSA reference models. These data were obtained using SynergyFinder software. Synergy scores < -10, from -10 to 10, and > 10 indicate antagonism, additivity, and synergism, respectively.

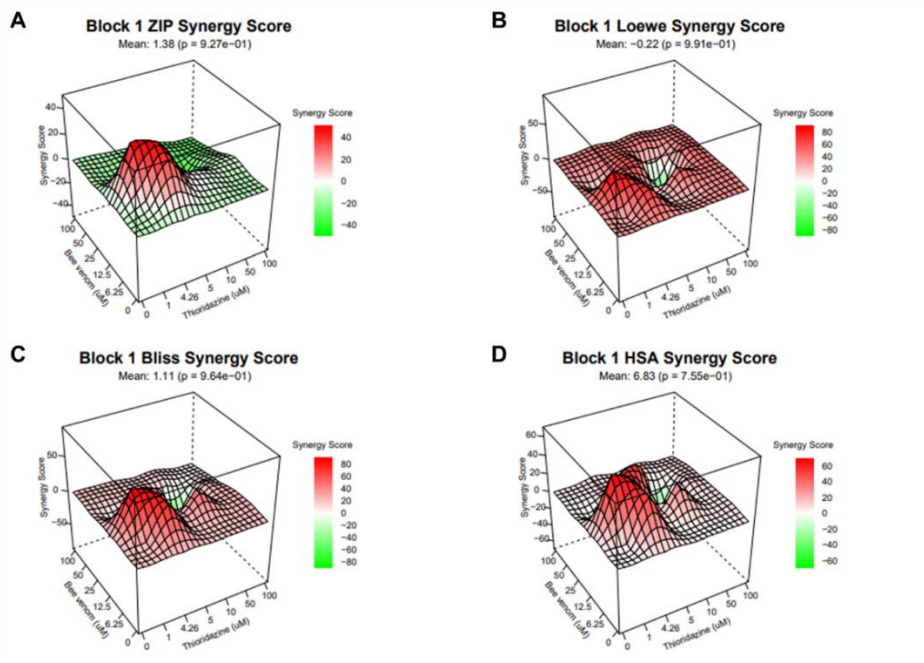

Figure 113. Synergy plots of combined treatments of thioridazine combined with honeybee venom on HT-29 colon cancer cells calculated with (**A**) ZIP; (**B**) Loewe; (**C**) Bliss and (**D**) HSA reference models. These data were obtained using SynergyFinder software. Synergy scores < -10, from -10 to 10, and > 10 indicate antagonism, additivity, and synergism, respectively.

Finally, the interaction between CPP2-thiazole derivatives and 5-FU as well as clotrimazole in HT-29 cells was evaluated, to confirm if these drug combinations presented synergism.

The combination of 5-FU + CPP2–thiazole derivatives in HT-29 cells demonstrated synergism only for the combinations of 5-FU plus BTZCA-CPP2 and BTZ5CA-CPP2 (Figures 114A). On the other side, the combination of clotrimazole with CPP2–thiazole derivatives in HT-29 cells resulted in synergistic pairs for the combinations with all CPP2-thiazole derivatives, at the concentration of 2 x IV (Figure 114B). These results are summarized in Figure 115.

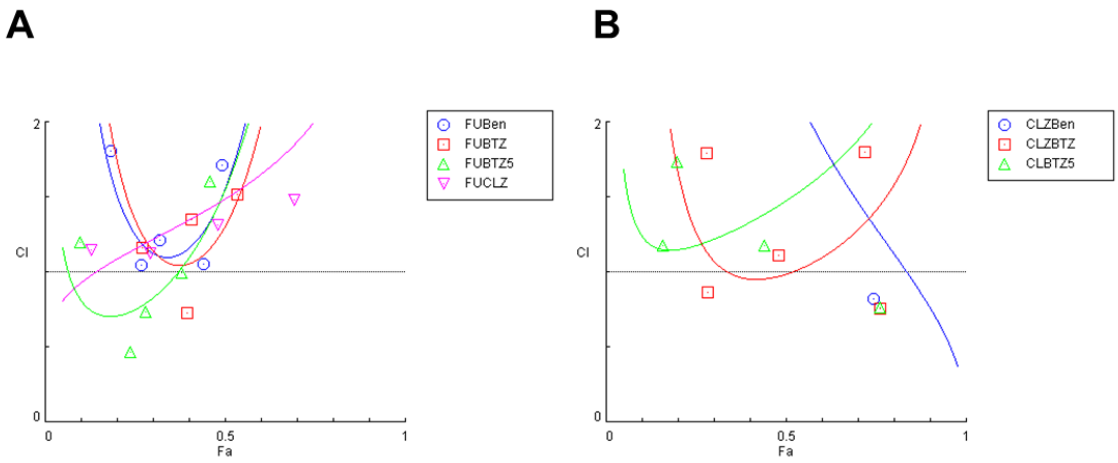

Figure 114. Chou–Talalay method Fa–CI plot of (**A**) 5-FU and (**B**) CLZ combined with CPP2–thiazole conjugates in HT-29 cells. CI is plotted on the *y*-axis as a function of effect level (Fa) on the *x*-axis to assess drug synergism. CI < 1, CI = 1, and CI > 1 indicate synergism, additivity, and antagonism, respectively. FUBen: 5-FU + BenzoTZ-C2-CPP2; FUBTZ: 5-FU + BTZCA-CPP2; FUBTZ5: 5-FU + BTZ5CA-CPP2; FUCLZ: 5-FU + CLZ; CLZBen: CLZ + BenzoTZ-C2-CPP2; CLZBTZ: CLZ + BTZCA-CPP2; CLZBTZ5: CLZ + BTZ5CA-CPP2.

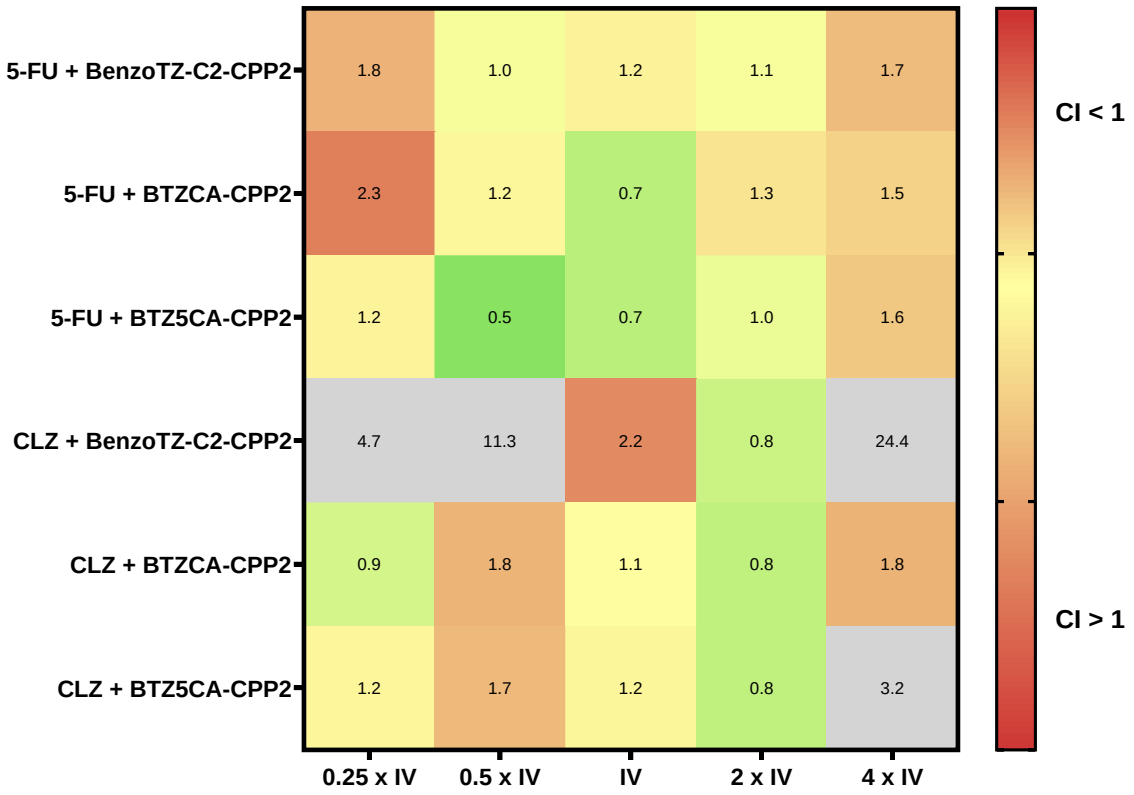

Figure 115. Synergy heat map compiling the CI values in HT-29 cells treated with the combination of CPP2–thiazole derivates plus the reference drug or CLZ. The squares in the figure indicate antagonism (CI > 1.2, red), additivity (0.9 < CI < 1.1, yellow), and synergism (CI < 0.9, green).

6. CONCLUSION OF CHAPTER III

There have been extensive efforts to enhance the efficacy of chemotherapy and find synergistic drug combinations for cancer therapy. While many studies have identified synergistic drug pairs for specific cancer cells based on the combination of antineoplastic agents, few reports if repurposed drugs offer improved therapeutic benefits in drug combination with antineoplastic agents. The synergistic combination of repurposed drugs with antineoplastic agents may allow for a decrease in the therapeutical doses, which can help to reduce the side effects of the treatments.

The novel combination model consisting of antimalarials and antineoplastic drugs developed by our research group demonstrated the potential for drug repurposing of antimalarials and found synergy between DOX/PTX and artesunate, mefloquine, and chloroquine which makes these combinations a promising approach to treat breast cancer, mainly the non-invasive and estrogen-receptor positive ones. It was also proved that artesunate has anticancer potential in HT-29 cells and that the combination with 5-FU is beneficial if given in a sequential schedule and prior to 5-FU.

Regarding the combination of CNS drugs with chemotherapeutic agents, it was found that all tested CNS drugs can synergistically decrease MCF-7 cell viability when combined with PTX, with fluoxetine, benztropine, and fluphenazine being the most promising drugs at lower concentrations. It was also concluded that sertraline and thioridazine in combination with 5-FU can synergistically decrease cancer viability in HT-29 colon cancer cells. Moreover, it was found that the use of quetiapine synergistically enhances the anticancer activity of DOX and PTX for the management of breast cancer. Edaravone and quetiapine significantly improved the cytotoxic potential of 5-FU in the HT-29 cells, with quetiapine synergistically interacting with the antineoplastic drug in this drug combination. Taken together, these results demonstrated that quetiapine can act as a chemosensitizer in combination therapies for breast and colon cancer. The mechanism of action behind these drug combinations should be further explored but studies suggest it may involve the WNT/β-catenin signaling pathway. Together, these results demonstrate that the use of CNS and antimalarial drugs, both alone and in combination, may lead to new therapeutic strategies for colon and breast cancer therapy.

Regarding the combination of antimalarial agents, it was found that the combination of antimalarials was not advantageous over a single treatment, for either cell line, indicating that these repurposed drugs are more promising as standalone agents in breast and colon cancer therapies than in combination with other repurposed drugs. Regarding the combination of CNS drugs, it was found that the combination of sertraline IC_{50} plus variable

concentrations of fluphenazine synergistically reduced the viability of HT-29 cancer cells, with significant anticancer potential at lower concentrations of fluphenazine. These results demonstrate that the combination of repurposed drugs, namely combining the CNS drugs sertraline and fluphenazine at lower doses, can also be further investigated for colon cancer novel therapies.

The results regarding the combination of honeybee venom support the idea that its combination with repurposed drugs and chemotherapeutic agents can help improve their anti-cancer activities, especially for lower concentrations, in both cell lines. These combinations also demonstrate greater potential for applications in colon cancer cells than in breast cancer therapy, with an indication of more synergistic interactions in HT-29 cancer cells. Together, these results demonstrate that chemotherapeutic and repurposed drugs combined with honeybee venom, with peptide melittin as the principal compound, are promising compounds for the chemotherapy of colorectal and breast cancer, being good candidates for employment in combination therapies.

The combination of CPPs with 5-FU and clotrimazole demonstrated that some CPP2–thiazole conjugates, such as BTZCA-CPP2 and BTZ5CA-CPP2, can be successfully combined with both drugs, resulting in enhanced anticancer effects and synergistic inhibition of cancer cell proliferation.

CHAPTER IV

EVALUATION OF THE BIOSAFETY PROFILE OF THE MOST PROMISING DRUG COMBINATIONS IN HUMAN NORMAL CELLS

1. SUMMARY OF CHAPTER IV

Drug combination and drug repurposing are two strategies that allow to find novel oncological therapies, in a faster and more economical process.

In the previous chapters, our research group developed a novel model of drug combination using antineoplastic and different repurposed drugs. It was demonstrated the combinations of DOX + artesunate, DOX + chloroquine, PTX + fluoxetine, PTX + fluphenazine, and PTX + benztropine induced significant cytotoxicity in MCF-7 breast cancer cells. Furthermore, it was found that 5-FU + thioridazine and 5-FU + sertraline could synergistically induce a reduction in the viability of the human colorectal adenocarcinoma cell line (HT-29).

Therefore, in this chapter, we aimed to evaluate the biosafety profile of these drug combinations against non-tumoral cells. To do so, human fetal lung fibroblast cells (MRC-5) were incubated for 48 h with all drugs, both alone and in combination in concentrations of 0.25, 0.5, 1, 2, and 4 times their IC_{50}. Cell morphology and viability were evaluated.

It was demonstrated that these combinations were cytotoxic for cancer cells and safe for non-tumoral cells at lower concentrations. These results support the use of antimalarial and CNS drugs in combination regimens with chemotherapeutic agents.

2. INTRODUCTION OF CHAPTER IV

In cancer treatment, one of the most important treatment regimens is chemotherapy; however, there are many problems regarding the use of many antitumor agents, including their hydrophobicity, low bioavailability, instability, high toxicity, severe side effects, and lack of targeted action [49, 483]. Therefore, an important area is the development and evaluation of new drug combination models for the treatment of tumors with higher efficiency and lower toxicity, that should always include their evaluation against non-tumoral cells.

Toxicological studies constitute one of the most important steps in the development of new drugs, as they allow to find possible adverse effects of these substances on the body, helping to prevent the appearance of undesired side effects [484, 485]. When referring to drug combinations, these should also be assessed for their toxicological profile in normal cells or animal models, even when using repurposing drugs, because their use in combined regimens can induce the crosstalk of novel pathways that can generate side effects. Biosafety studies may include both *in vitro* experiments or/ and *in vivo* toxicity testing [484, 485] and only in this way, the use of these new therapeutical drugs or drug combinations can be supported for clinical use, with the adequation of doses and modes of applications.

In oncology, the main aim of these studies is to assess the safety of these compounds or drug combinations and to determine if they do not induce significant cytotoxicity in normal cells while trying to guarantee maximum effectiveness against malignantly transformed cells.

In the previous chapters, new combination models involving the use of antineoplastic drugs and repurposed drugs were developed, aiming to improve the anticancer effects of chemotherapy in two different cancer cell lines: MCF-7, breast cancer, and HT-29, colorectal cancer. It was screened several repurposed drugs [11 antimalarial and 17 CNS drugs], that were selected based on literature findings that suggested the repurposing potential of these drug classes. For that, both cell lines were incubated with each repurposed drug alone, at increasing concentrations (0.1–100 µM), to find their IC_{50} value. Then, all repurposed drugs that presented an IC_{50} under 25 µM were considered to have a promising anticancer profile and therefore selected for the screening involving the drug combinations. Although the IC_{50} of chloroquine was above 25 µM, this drug was also included in the screening because approximately 30 clinical studies are currently evaluating the activity of this antimalarial drug combined with various standard treatments in different types of cancer.

In breast cancer cells, the selected repurposed drugs were combined with two different antineoplastic drugs (PTX and DOX). In colon cancer cells, the selected repurposed drugs were only combined with 5-FU. The cytotoxic effect of each drug pair was then evaluated by cell-based assays and the nature of drug interactions in each drug combination (additivity, synergism, or antagonism) was assessed. Drug combinations that demonstrated the ability to synergistically enhance the chemotherapeutic effect of the antineoplastic drug were considered promising drug combinations for cancer therapy.

Collectively, it was found that some combination regimens could effectively decrease the viability of these cell lines. Specifically, it was found the combinations of DOX + artesunate, DOX + chloroquine, PTX + fluoxetine, PTX + fluphenazine, and PTX + benztropine to be the most cytotoxic for MCF-7 cells and to act synergistically in this cell line. Regarding the results in HT-29 cells, it was found that 5-FU + thioridazine and 5-FU + sertraline were the drug combinations with the highest number of synergistic pairs in this cell line.

Therefore, in this chapter, it was evaluated the biosafety of the previously mentioned drug combinations in a non-tumoral human fetal lung fibroblast cell line (MRC-5) to determine their biosafety profile against non-tumoral cells.

3. OBJECTIVE OF CHAPTER IV

In this chapter, it was aimed to evaluate the biosafety of the previously evaluated drug combinations in Chapters II and III using a non-tumoral human fetal lung fibroblast cell line (MRC-5), to determine if the most promising drug combinations are safe for use in breast and colorectal cancer treatments.

4. MATERIALS AND METHODS OF CHAPTER IV

4.1 Cell Culture

MRC-5 human normal lung fibroblast cell line, obtained from the ATCC (Manassas, VA, USA), was used in passage 8 for the evaluation of biosafety of the most promising drug combinations found in previous chapters. These cells were maintained in DMEM cell culture medium supplemented with 10% FBS and 1% pen-strep solution, at 37 °C and 5% CO_2. Cell culture reagents were purchased from Millipore Sigma (Merck KGaA, Darmstadt, Germany). For subculturing, confluent cells were trypsinized using a 0.25% trypsin-EDTA solution (Gibco, Thermo Fisher Scientific, Inc., Waltham, MA, USA) and subcultured in the same culture media. On the day before treatments, 8,000 cells/well were seeded in 96-well plates and allowed to adhere for 24 h.

4.2 Drug Treatment

Based on our findings from Chapters II and III, the most promising drug combinations were selected for evaluation of their biosafety profile in normal cells. Previously, it was found that the combinations of DOX (cat. no. 15007, Cayman Chemical, Ann Arbor, MI, USA) + artesunate (cat. no. 11817, Cayman Chemical, Ann Arbor, MI, USA) and chloroquine (cat. no. C6628, Santa Cruz Biotechnology, Dallas, TX, USA), as well as PTX (cat. no. 1097, Tocris Bioscience, Bristol, UK) + fluoxetine (cat. no. 14418, Cayman Chemical, Ann Arbor, MI, USA), fluphenazine (cat. no. F4765, Merck KGaA, Darmstadt, Germany) and benztropine (cat. no. 16214, Cayman Chemical, Ann Arbor, MI, USA), resulted in significant cytotoxic effects in MCF-7 breast cancer cell line. On the other hand, for HT-29 colon cancer cells, the most promising drug combinations included the combination of 5-FU (cat. no. F6627, Merck KGaA, Darmstadt, Germany) + thioridazine (cat. no. 14400, Cayman Chemical, Ann Arbor, MI, USA) and sertraline (cat. no. 14839, Cayman Chemical, Ann Arbor, MI, USA).

Based on these findings, the cytotoxic effect of different drug combinations (DOX + artesunate, DOX + chloroquine, PTX + fluoxetine, PTX + fluphenazine, PTX + benztropine, 5-FU + thioridazine and 5-FU + sertraline) was evaluated in MRC-5 cells after 48 h of treatment. Cells were first incubated with each drug alone and then with each combination. MRC-5 cells were incubated with the following concentrations: 0.25, 0.5, 1, 2, and 4 times the IC_{50} value of each drug. These IC_{50} values were based on our previous results, where it was found the IC_{50} for each drug in HT-29 and MCF-7 cells (Table 29). Stock solutions were prepared in 100% DMSO and diluted to 0.1% DMSO on the day of the experiments.

Control cells were treated with vehicle (0.1% DMSO). No significant differences were seen between control cells with or without vehicle.

Table 29. Half-maximal inhibitory concentration (IC_{50}) of reference and repurposed drugs in MCF-7, breast cancer, and human colorectal adenocarcinoma (HT-29) cells. N.D.: not determined

Drug	HT-29	MCF-7
	IC_{50} (µM)	IC_{50} (µM)
DOX	N.D.	0.17
PTX	N.D.	2.78 (nM)
5-FU	3	N.D.
Fluoxetine	6.12	7.78
Benztropine	18.23	21.71
Thioridazine	4.26	5.72
Sertraline	2.45	2.22
Fluphenazine	1.86	2.68
Artesunate	17.88	11.60
Chloroquine	32.13	63.98

4.3 Morphological Analysis

Morphological analysis was performed for all conditions using a Leica DMI 6000B microscope coupled with a Leica DFC350 FX camera (Leica Microsystems, Wetzlar, Germany). Images were treated with the Leica LAS X imaging software (v3.7.4) (Leica Microsystems, Wetzlar, Germany).

4.4 MTT Assay

The cytotoxicity of each treatment was evaluated using the MTT assay. Briefly, after cell treatment, each well aspirated and 100 µL of MTT solution (0.5 mg/mL in PBS, cat. no. M5655, Merck KGaA, Darmstadt, Germany) was added. Plates were protected from light and incubated for a period of 3 h at 37 °C. Then, the MTT solution was removed and

replaced with 100 µL/well of DMSO to solubilize the formazan crystals. Absorbance was measured at 570 nm using an automated microplate reader (Tecan Infinite M200, Tecan Group Ltd., Männedorf, Switzerland).

4.5 Statistical Analysis

GraphPad Prism 9 (GraphPad Software Inc., San Diego, CA, USA) was used to obtain the cell viability representations. The results of three independent experiments are represented as the mean ± SEM. Statistical analysis was performed with one-way ANOVA tests by Dunnett's multiple comparisons between control and treatment groups. Statistical significance was accepted at p values < 0.05.

5. RESULTS AND DISCUSSION OF CHAPTER IV

5.1 Single Drug Treatments

In the previous chapters, it was developed a novel model of combination consisting of antineoplastic and repurposed drugs. These studies aimed to find repurposed drugs with promising anticancer activity that could, at the same time, be used in combination with antineoplastic drugs to improve their cytotoxicity against two different cancer cell lines: MCF-7 and HT-29. In these experiments, it was first determined the IC_{50} of every single drug and then selected the ones with the most promising pharmacological profiles (defined as having an IC_{50} < 25 µM, Table 29). Although the IC_{50} of chloroquine was above 25 µM, it was also included in the screening because approximately 30 clinical studies are currently evaluating the activity of this antimalarial drug combined with various standard treatments in different types of cancer. Next, it was combined simultaneously the antineoplastic drugs with the selected repurposed drugs in variable concentrations and evaluated the combined effects of equipotent concentrations (fixed ratio) of the IC_{50} values for each drug (0.25, 0.5, 1, 2, and 4 times IC_{50}). This experiment protocol for drug combinations was selected based on Chou-Talalay publications [313, 314], where it is recommended to use constant-ratio drug combinations and to select several data points above IC_{50} and below IC_{50} to determine drug interactions more accurately. It was successfully identified several antimalarial and CNS drugs with potential anticancer activity against these cell lines and demonstrated that the most promising drug combinations were DOX + artesunate, DOX + chloroquine, PTX + fluoxetine, PTX + fluphenazine, PTX + benztropine for MCF-7 cells, and 5-FU + thioridazine and 5-FU + sertraline for HT-29 cells.

Here, it was investigated if these drug combinations were safe against non-tumoral cells. First, to evaluate whether the antineoplastic drugs used in the previously proposed combinations were selective for cancer cells and non-cytotoxic for normal cells, each drug was tested, both alone and in combination, in a human normal lung fibroblast cell line (MRC-5). This cell line is commonly used in the production of vaccines, for biosafety evaluation and in other toxicological studies. To do so, the cytotoxic effect of each antineoplastic drug was evaluated, in a range of concentrations from 0.25 to 4 times their IC_{50} value for 48 h. Cell viability was assessed using an MTT assay. Drugs that did not cause significant reduction in the viability of MRC-5 cells were considered to have an acceptable toxicological profile and to be non-toxic for normal cells [486].

In our previous studies using tumoral cell lines, it was found an IC_{50} of 0.17 µM and 0.44 nM for DOX and PTX, respectively, in MCF-7 cells and 3.79 µM for 5-FU in HT-29 cancer cells. Here, using a non-tumoral cell line, it was demonstrated that all

chemotherapeutic drugs present an acceptable toxicological profile, at all concentrations below their IC_{50}. Significant toxicity was only found in the treatment with DOX in the concentration of 4 × IC_{50} (Figure 116A). Furthermore, treatment with 2 and 4 × IC_{50} of PTX also resulted in significant cytotoxicity for MRC-5 cells (Figure 116B). On the other hand, results regarding treatment with 5-FU did not demonstrate significant cytotoxicity at any concentration (Figure 116C). Together, these results demonstrate that DOX, PTX, and 5-FU are non-toxic for normal cells and support their use as anticancer agents.

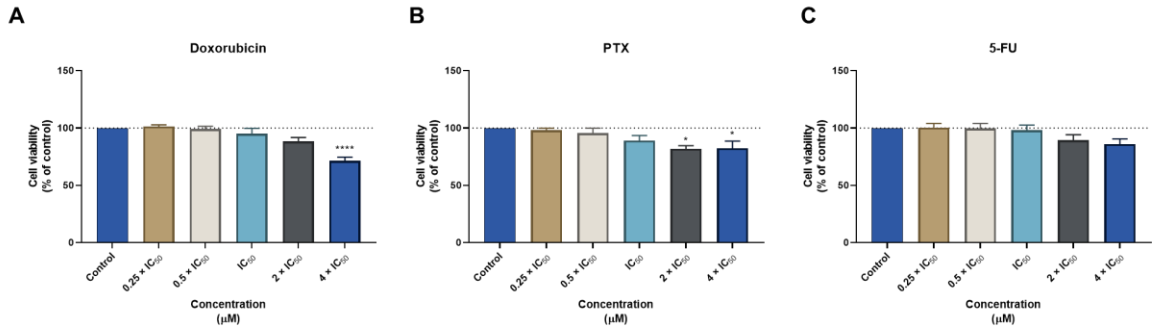

Figure 116. Cytotoxic effects of antineoplastic drugs in human fetal lung fibroblast cell line (MRC-5). MTT results of MRC-5 cells treated with increasing concentrations of (**A**) DOX, (**B**) PTX, and (**C**) 5-FU for 48 h. Results are represented as the percentage of control and represent mean ± SEM. Each experiment was done three times independently (n = 3). Statistically significant vs control at $p < 0.05$ * and $p < 0.0001$ ****.

Next, it was evaluated the cytotoxic effect of the antimalarial drugs used in the previously mentioned drug combinations. It was found these drugs were more cytotoxic for MCR-5 cells than the antineoplastic drugs DOX, PTX, and 5-FU. Artesunate treatment induced a significant reduction in cell viability at concentrations of IC_{50} and higher (Figure 117A). On the other side, chloroquine treatment demonstrated toxicity for all the ranges of concentrations tested for this cell line (Figure 117B). These results demonstrate that, although antimalarial drugs alone can be promising anticancer agents, they also induce cytotoxicity to normal cells, which warns their use as standalone therapeutics for cancer therapy.

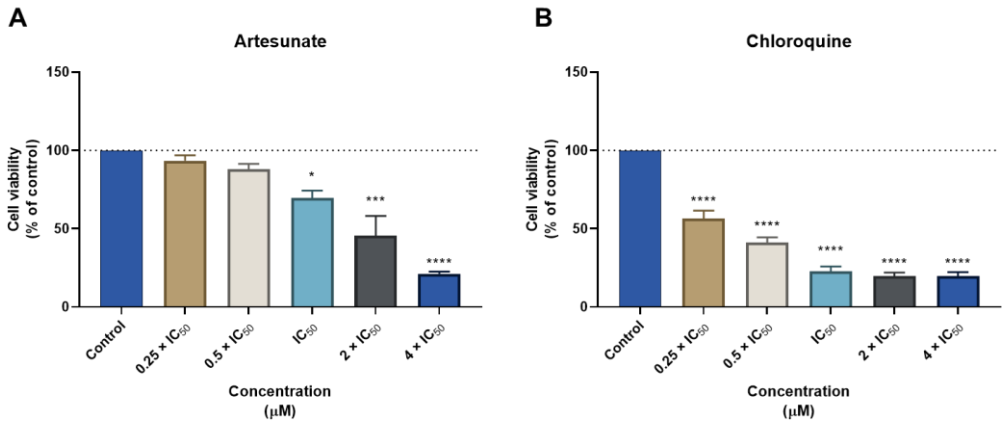

Figure 117. Cytotoxic effects of antimalarial drugs in MRC-5 human normal lung fibroblast cells. MTT results of MRC-5 cells treated with increasing concentrations of (**A**) artesunate and (**B**) chloroquine for 48 h. Results are represented as the percentage of control and represent mean ± SEM. Each experiment was done three times independently (n = 3). Statistically significant vs. control at $p < 0.05$ *, $p < 0.001$ *** and $p < 0.0001$ ****.

Then, the biosafety of CNS drugs was evaluated on MRC-5 cells. MTT results demonstrated that fluoxetine treatment did not induce cell cytotoxicity in concentrations under IC_{50} (Figure 118A). Moreover, treatment with fluphenazine resulted in a similar toxicological profile to fluoxetine, with an acceptable biosafety profile to MRC-5 cells at the concentrations of 0.25, 0.5, and 1 times IC_{50} (Figure 118B). On the other hand, benztropine treatment demonstrated a compatible cytotoxic profile to normal cells only at the lowest concentration (0.25 × IC_{50}) (Figure 118C). Indeed, benztropine was the most cytotoxic compound among all CNS drugs tested. Thioridazine treatment only induced significant reductions of cell viability in concentrations above IC_{50}, without significant cytotoxicity at the concentrations of 0.25, 0.5, and 1 times IC_{50} (Figure 118D). Sertraline, along with benztropine, was the second most cytotoxic compound for MRC-5 cells, with an acceptable biosafety profile only at the concentration below 0.5 × IC_{50} (Figure 118E). These results demonstrate that the selected CNS drugs have an acceptable toxicological profile, supporting their use as standalone or adjuvant compounds for cancer therapy, since used at lower dosages.

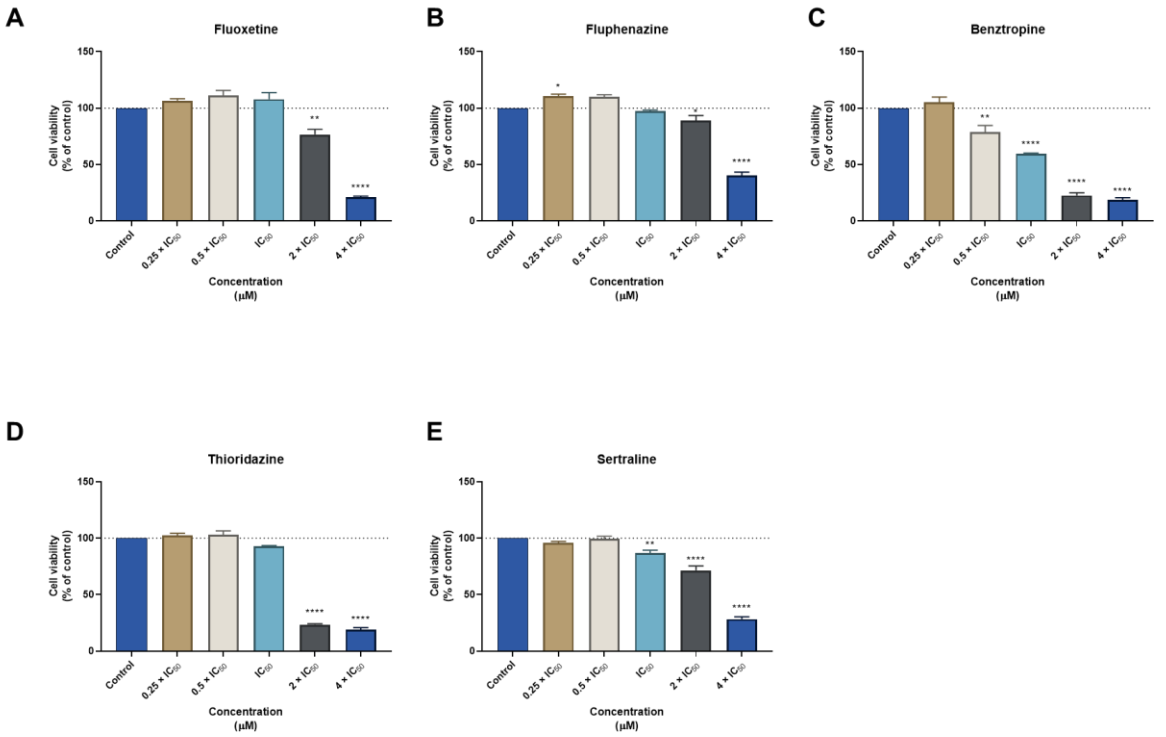

Figure 118. Cytotoxic effects of CNS drugs in MRC-5 human normal lung fibroblast cells. MTT results of MRC-5 cells treated with increasing concentrations of (**A**) fluoxetine, (**B**) fluphenazine, (**C**) benztropine, (**D**) thioridazine, and (**E**) sertraline for 48 h. Results are represented as the percentage of control and represent mean ± SEM. Each experiment was done three times independently (n = 3). Statistically significant vs. control at $p < 0.05$ *, $p < 0.01$ ** and $p < 0.0001$ ****.

Figure 119 summarizes the previously described results. Taken together, these results demonstrate that antineoplastic drugs are safe for normal cells, with an acceptable toxicological profile, at concentrations below their IC_{50}. Moreover, it was also demonstrated that antimalarial drugs are more cytotoxic than CNS drugs in MRC-5 human normal lung fibroblast cells, with chloroquine causing significant cell reduction even at lower concentrations. The selected CNS drugs only produced significant reductions in cell viability at higher concentrations, being safe for normal cells at concentrations below their IC_{50}.

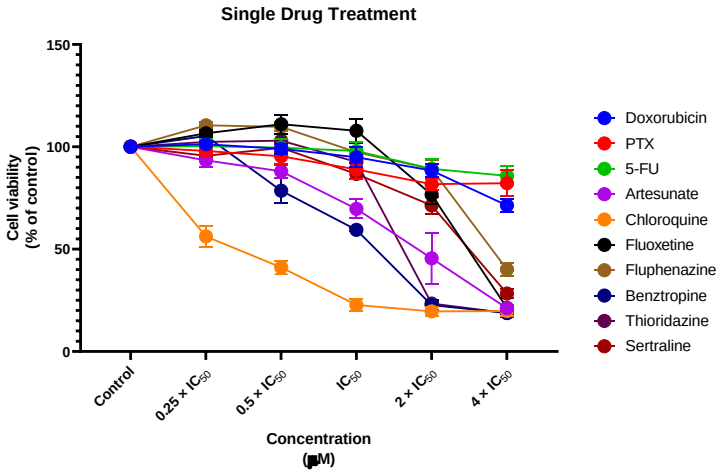

Figure 119. Comparison of the cytotoxic effect after single drug treatments with antineoplastic, antimalarial, and CNS drugs in MRC-5 human normal lung fibroblast cells. Results are represented as the percentage of control and represent mean ± SEM. Each experiment was done three times independently (*n* = 3).

5.2 Combination Treatments

Next, the safety of the drug combinations was evaluated in MCR-5 cells. MRC-5 cells were treated with the antineoplastic and repurposed drugs simultaneously, using a fixed ratio of concentrations: 0.25, 0.5, 1, 2, and 4 times the IC_{50} value of each drug. Cell morphology and viability were evaluated after 48 h incubation.

Although some repurposed drugs demonstrated cytotoxicity against normal cells as single agents, their biosafety profile was further evaluated in combination treatments to find if the combination of these drugs with antineoplastic agents could result in lower toxicity for normal cells. Regarding the combination of DOX + artesunate, it was found changes in the normal phenotype of MRC-5 cells treated with DOX + artesunate in concentrations above IC_{50} (Figure 120A). The MTT results demonstrated this drug combination only presented significant cytotoxicity in concentrations above IC_{50} (Figure 120B). Furthermore, the combination of these drugs presented less cytotoxicity than each drug alone in concentrations of 0.25 and 0.5 times IC_{50}, demonstrating that the association of artesunate with DOX can effectively decrease the toxicity of each drug. Moreover, it was found that, in some conditions (IC_{50} and 2 × IC_{50}), the toxicity of artesunate was reduced when combined with DOX, which was also supported by morphological analysis. Furthermore, compared to the results previously obtained in MCF-7, it was notorious the biosafety profile of this drug combination in MRC-5 cells and the selectivity of DOX + artesunate to cancer cells (Figure 120C).

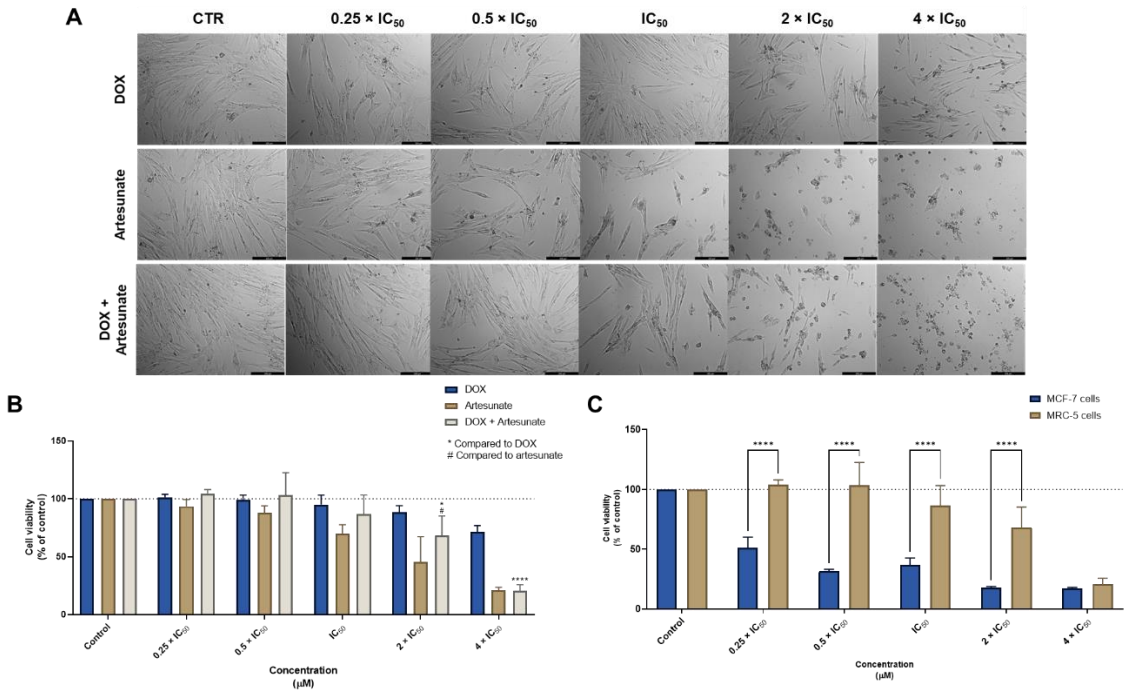

Figure 120. Cytotoxic effects of DOX + artesunate in MRC-5 human normal lung fibroblast cells. (**A**) Morphological analysis and (**B**) MTT results of MRC-5 cells treated with increasing concentrations of DOX, artesunate, and DOX + artesunate for 48 h. (**C**) Comparison of cytotoxicity of combined treatment with DOX + ART for 48 h in MCF-7 breast cancer cells and MRC-5 normal cells. Results are represented as the percentage of control and represent mean ± SEM. Each experiment was done three times independently ($n = 3$). Statistically significant at $p < 0.05$ * and $p < 0.0001$ ****. Statistically significant compared to artesunate at $p < 0.05$ #. Scale bar 200 µm.

As expected, and in line with the results obtained for single drug treatments, the combination of DOX + chloroquine resulted in higher cytotoxicity to MRC-5 cells than DOX + artesunate. The morphological analysis supported the toxic profile of the combination, with notorious changes in the cell morphology, even for the lowest concentrations (Figure 121A). Specifically, the combination of 0.25 × IC_{50} of DOX + 0.25 × IC_{50} of chloroquine did not produce significant cytotoxic effects in these normal cells (Figure 121B). Compared to the results in MCF-7, this combination seems to be safe in the concentrations of 0.25 and 0.5 times IC_{50}, while having potent anticancer activity against tumor cells (Figure 121C) and further supporting the study of this combination.

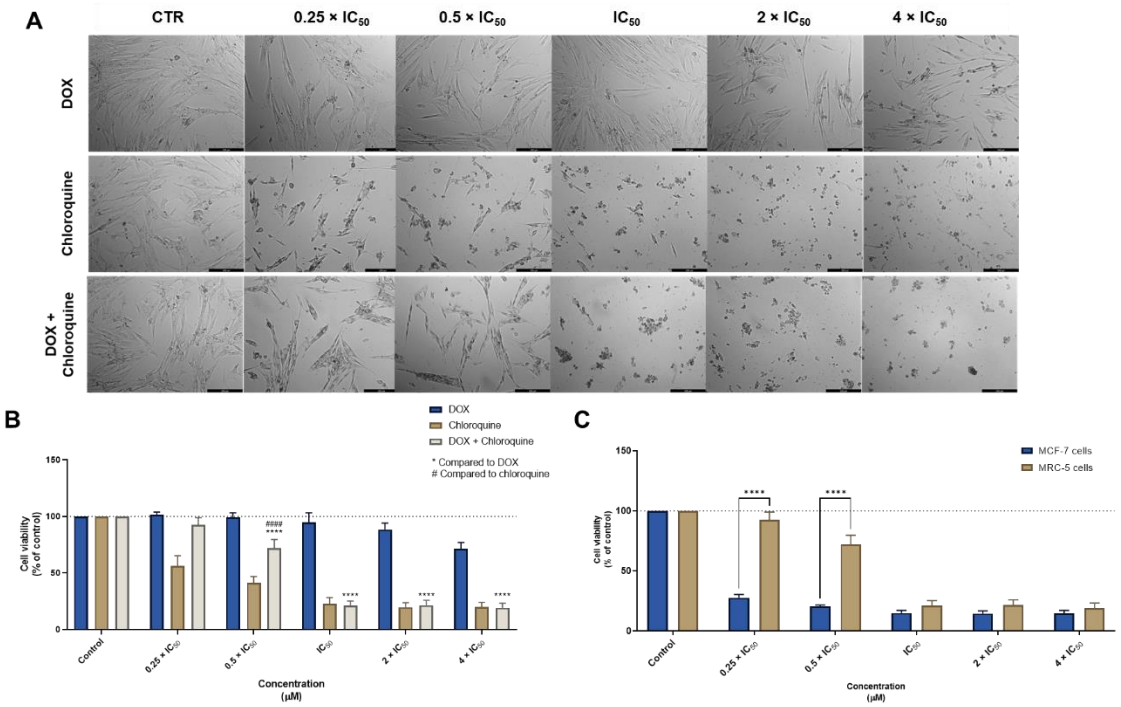

Figure 121. Cytotoxic effects of DOX + chloroquine in MRC-5 human normal lung fibroblast cells. (**A**) Morphological analysis and (**B**) MTT results of MRC-5 cells treated with increasing concentrations of DOX, chloroquine, and DOX + chloroquine for 48 h. (**C**) Comparison of cytotoxicity of combined treatment with DOX + CQ for 48 h in MCF-7 breast cancer cells and MRC-5 normal cells. Results are represented as the percentage of control and represent mean ± SEM. Each experiment was done three times independently (n = 3). Statistically significant at $p < 0.0001$ ****. Statistically significant compared to chloroquine at $p < 0.0001$ ####. Scale bar 200 µm.

The combination of PTX + fluoxetine did not produce significant alterations in cell viability at lower concentrations, which is supported by the microscopic images of morphological analysis (Figure 122A). The MTT results regarding the combination of PTX + fluoxetine revealed a promising safety profile of this combination, for all concentrations, except for 4 × IC_{50} (Figure 122B). Furthermore, compared to MCF-7 cells, it was demonstrated this drug is safe against MRC-5 cells, at all concentrations from 0.25 to 2 × $IC_{50,}$ and cytotoxic for cancer cells (Figure 122C). These results demonstrate that fluoxetine can be effectively used in combination with PTX, with a safety profile against normal cells and high efficacy against cancer cells.

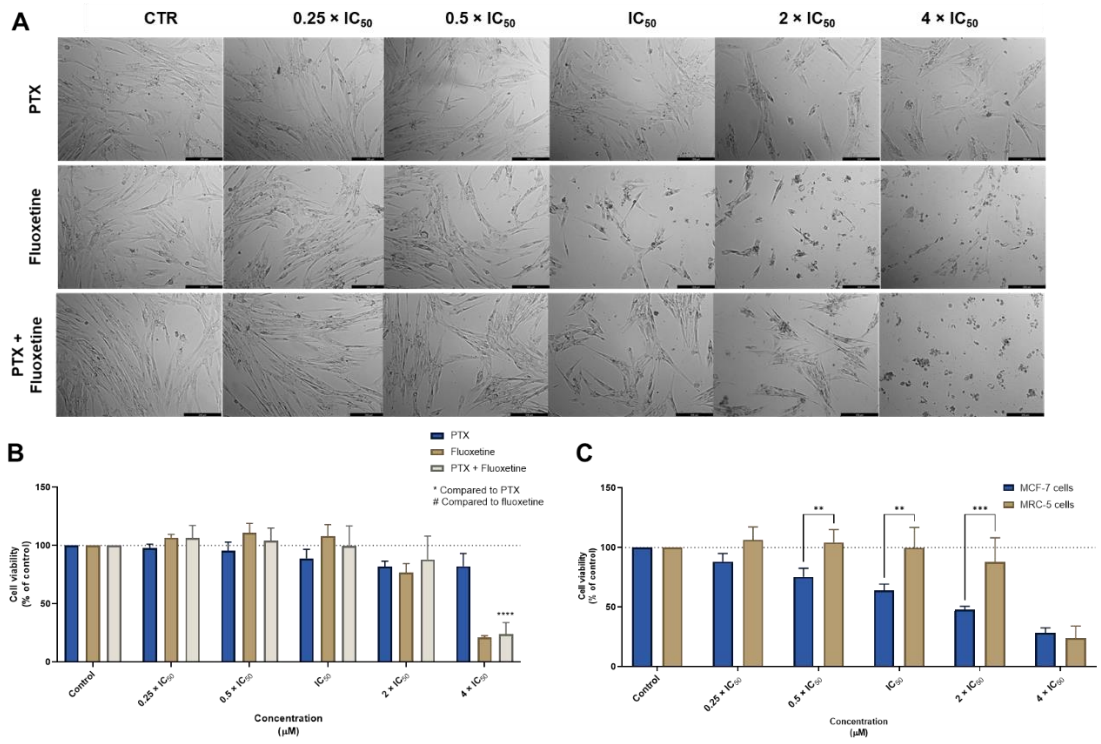

Figure 122. Cytotoxic effects of PTX + fluoxetine in MRC-5 human normal lung fibroblast cells. (**A**) Morphological analysis and (**B**) MTT results of MRC-5 cells treated with increasing concentrations of PTX, fluoxetine, and PTX + fluoxetine for 48 h. (**C**) Comparison of cytotoxicity of combined treatment with PTX + fluoxetine for 48 h in MCF-7 breast cancer cells and MRC-5 normal cells. Results are represented as the percentage of control and represent mean ± SEM. Each experiment was done three times independently (n = 3). Statistically significant at $p < 0.01$ **, $p < 0.001$ *** and $p < 0.0001$ ****. Scale bar 200 μm.

Next, the cytotoxic effect of the combination of PTX + fluphenazine was evaluated in MRC-5 cells. The results of cellular morphology analysis were in accordance with the MTT results, with significant changes in the phenotype of MRC-5 cells in the concentration of 4 times IC_{50} (Figure 123A). Analyzing the MTT results, it was possible to confirm this combination regimen is safe for this cell line in the concentrations of 0.25, 0.5, 1, and 2 times IC_{50} (Figure 123B). Moreover, the comparison of the cytotoxic effect between tumoral MCF-7 cells and non-tumoral MRC-5 cells demonstrated that, at lower concentrations, this combination has a promising toxicological profile, being safe for normal cells and effective against tumor cells (Figure 123C).

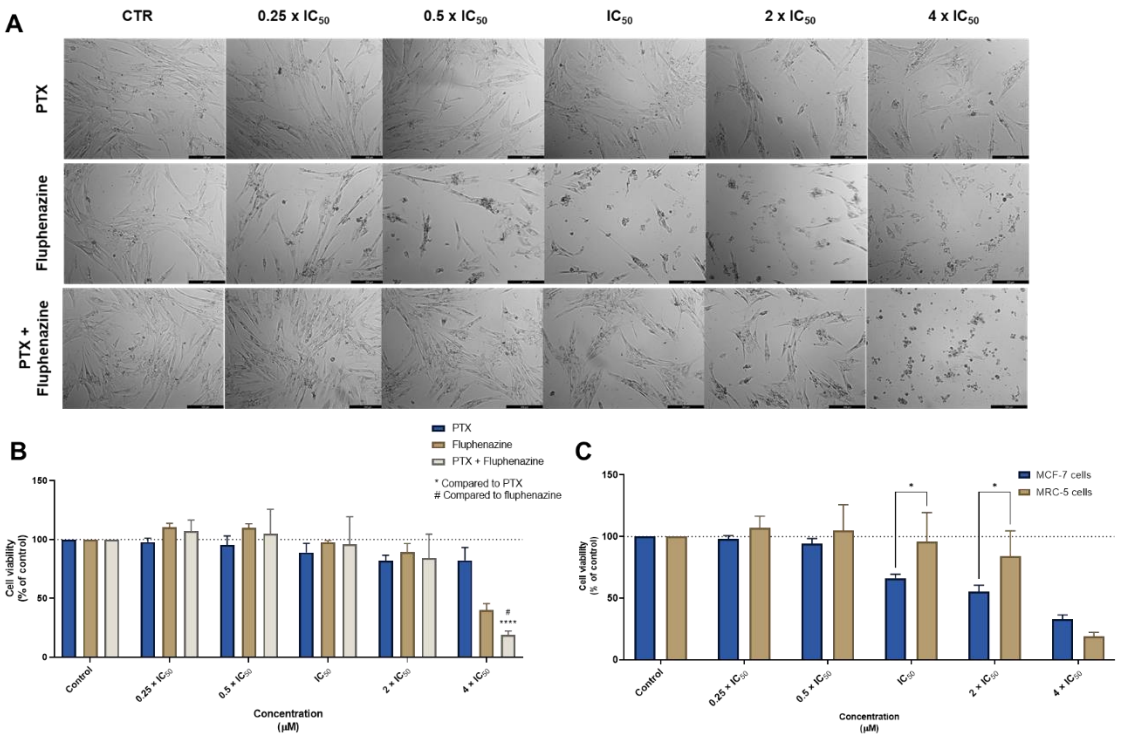

Figure 123. Cytotoxic effects of PTX + fluphenazine in MRC-5 human normal lung fibroblast cells. (**A**) Morphological analysis and (**B**) MTT results of MRC-5 cells treated with increasing concentrations of PTX, fluphenazine, and PTX + fluphenazine for 48 h. (**C**) Comparison of cytotoxicity of combined treatment with PTX + fluphenazine for 48 h in MCF-7 breast cancer cells and MRC-5 normal cells. Results are represented as the percentage of control and represent mean ± SEM. Each experiment was done three times independently (n = 3). Statistically significant at $p < 0.05$ * and $p < 0.0001$ ****. Statistically significant compared to fluphenazine at $p < 0.05$ $^{\#}$. Scale bar 200 µm.

Regarding the combination of PTX plus benztropine, it was found this combination to be more cytotoxic to MRC-5 cells than PTX + fluoxetine and PTX + fluphenazine, which was also in line with the previous results obtained for single-drug treatments. The morphological analysis demonstrated a reduction of cell viability and changes in cell morphology in the concentration of 0.5 × IC_{50} (Figure 124A), warning the use of this combination. Nevertheless, this combination demonstrated to have an acceptable toxicological profile at concentrations of 0.25 and 0.5 times IC_{50} (Figure 124B). The results of PTX + benztropine in MRC-5 and MCF-7 cells support the use of this combination at lower concentrations in cancer therapy (Figure 124C).

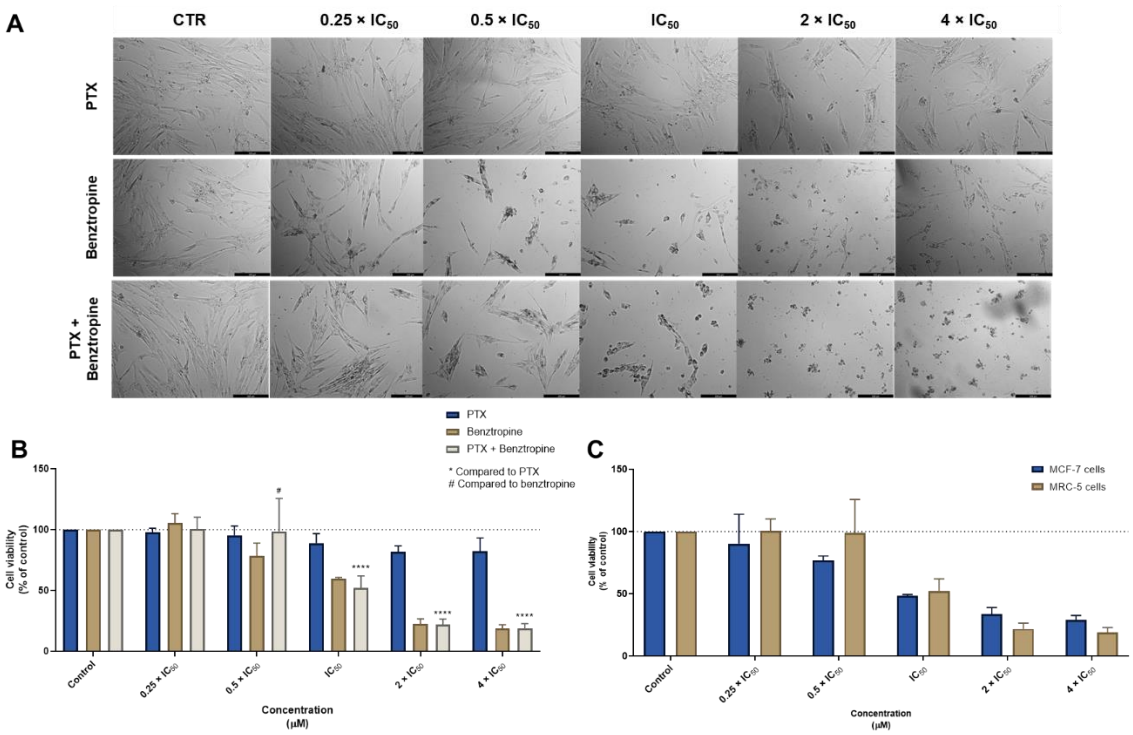

Figure 124. Cytotoxic effects of PTX + benztropine in MRC-5 human normal lung fibroblast cells. (**A**) Morphological analysis and (**B**) MTT results of MRC-5 cells treated with increasing concentrations of PTX, benztropine, and PTX + benztropine for 48 h. (**C**) Comparison of cytotoxicity of combined treatment with PTX + benztropine for 48 h in MCF-7 breast cancer cells and MRC-5 normal cells. Results are represented as the percentage of control and represent mean ± SEM. Each experiment was done three times independently (n = 3). Statistically significant at $p < 0.0001$ ****. Statistically significant compared to benztropine at $p < 0.05$ $^{\#}$. Scale bar 200 μm.

The combination of the antineoplastic drug 5-FU with thioridazine did not demonstrate significant changes in cell phenotype in concentrations under 2 × IC_{50} (Figure 125A). Regarding the MTT results, this combination demonstrated low cytotoxicity against MRC-5 cells in concentrations below the IC_{50}, with no significant changes in cell viability in this range of concentrations (Figure 125B). Comparing the cytotoxic effects of this combination between tumoral and non-tumoral cells (Figure 125C), it was found this drug significantly reduced the cell viability of HT-29 colon cancer, without affecting MRC-5 fibroblast cells. These results support the use of this combination in cancer therapies.

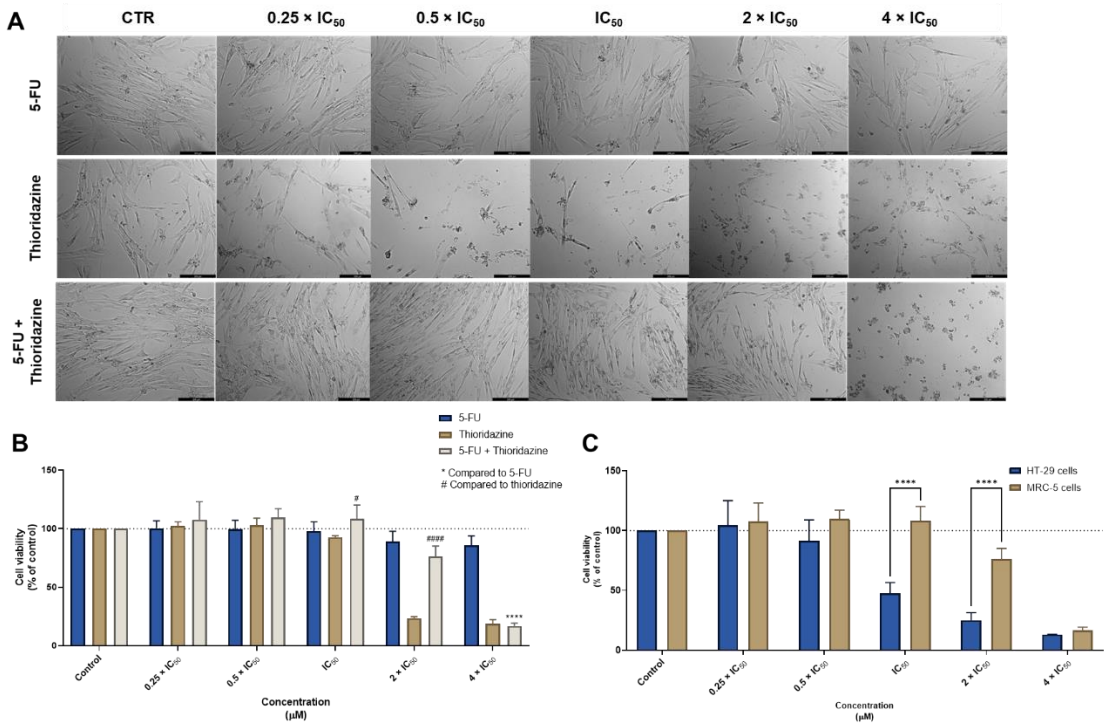

Figure 125. Cytotoxic effects of 5-FU + thioridazine in MRC-5 human normal lung fibroblast cells. (**A**) Morphological analysis and (**B**) MTT results of MRC-5 cells treated with increasing concentrations of 5-FU, thioridazine, and 5-FU + thioridazine for 48 h. (**C**) Comparison of cytotoxicity of combined treatment with 5-FU + thioridazine for 48 h in HT-29 colon cancer cells and MRC-5 normal cells. Results are represented as the percentage of control and represent mean ± SEM. Each experiment was done three times independently (n = 3). Statistically significant at $p < 0.0001$ ****. Statistically significant compared to thioridazine at $p < 0.05$ $^{\#}$ and $p < 0.0001$ $^{\#\#\#\#}$. Scale bar 200 μm.

Finally, the cytotoxic effect of 5-FU combined with sertraline was evaluated in MRC-5 cells. The results of the morphological analysis demonstrated some degree of cytotoxicity even in concentrations of 0.5 × IC_{50}, with a decrease in the cell number as well as changes in the cell phenotype (Figure 126A). Nevertheless, the MTT assay demonstrated this combination did not induce significant effects on the cell viability of this cell line, in concentrations below and equal to IC_{50} (Figure 126B). It is, therefore, advised to use this drug combination at lower concentrations (0.25 × IC_{50}). The results described in Figure 126C demonstrated that in the range of concentrations this combination was safe (0.25–1 × IC_{50}), there was almost no anticancer effect against HT-29 colon cancer cells, which suggests that the use of this drug combination in cancer therapy may not be totally adequate.

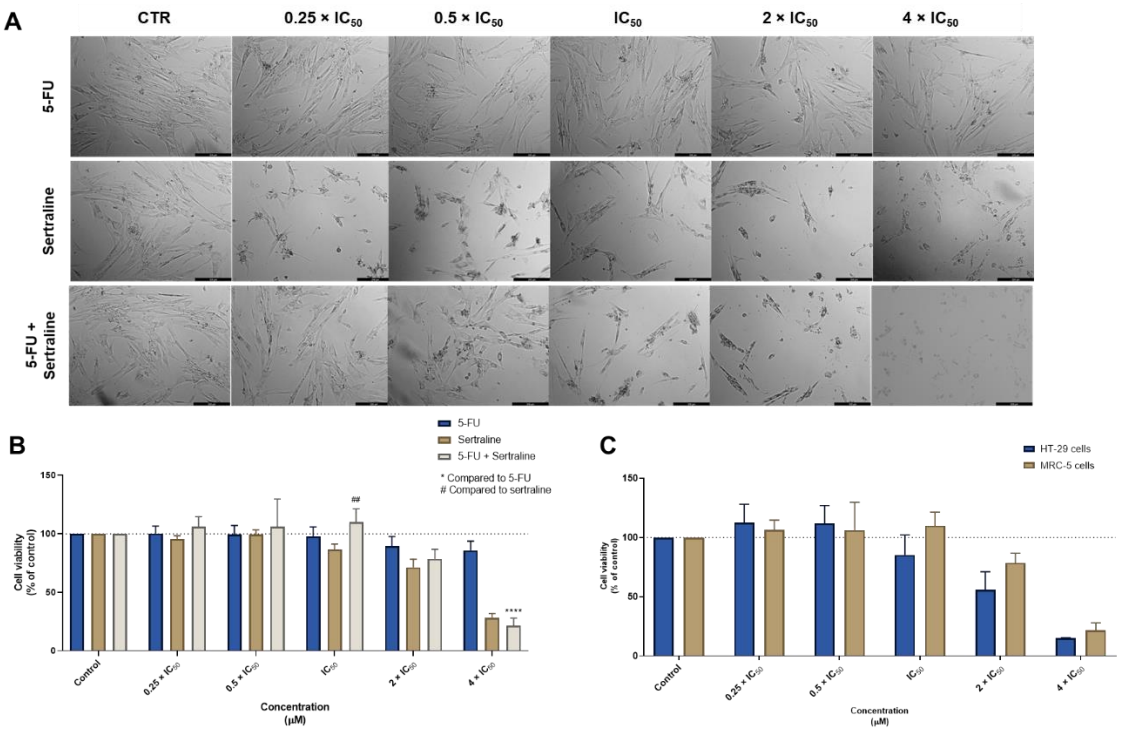

Figure 126. Cytotoxic effects of 5-FU + sertraline in MRC-5 human normal lung fibroblast cells. (**A**) Morphological analysis and (**B**) MTT results of MRC-5 cells treated with increasing concentrations of 5-FU, sertraline, and 5-FU + sertraline for 48 h. (**C**) Comparison of cytotoxicity of combined treatment with 5-FU + SERT for 48 h in HT-29 colon cancer cells and MRC-5 normal cells. Results are represented as the percentage of control and represent mean ± SEM. Each experiment was done three times independently (n = 3). Statistically significant at $p < 0.0001$ ****. Statistically significant compared to sertraline at $p < 0.01$ $^{\#\#}$. Scale bar 200 μm.

Figure 127 summarizes the previously described results. Taken together, these results are in line with the ones obtained for MRC-5 treated with single drugs. DOX + chloroquine is among the most cytotoxic drug combinations against this cell line and its use is only adequate at lower concentrations. PTX + benztropine is the second most cytotoxic drug combination and its use in cancer therapies is only possible in concentrations below 0.5 × IC_{50}. The remaining drug combinations present selectivity for tumoral cells and are safe for normal cells, especially at concentrations below their IC_{50}. At the concentration of 4 times IC_{50}, all tested drug pairs have significant cytotoxicity against MRC-5 normal cells. It was further demonstrated that these combinations help to reduce the cytotoxicity of the repurposed drugs alone. Taken together, these results support the use of these drug combinations in further studies, using animal models, although the use of lower doses is recommended.

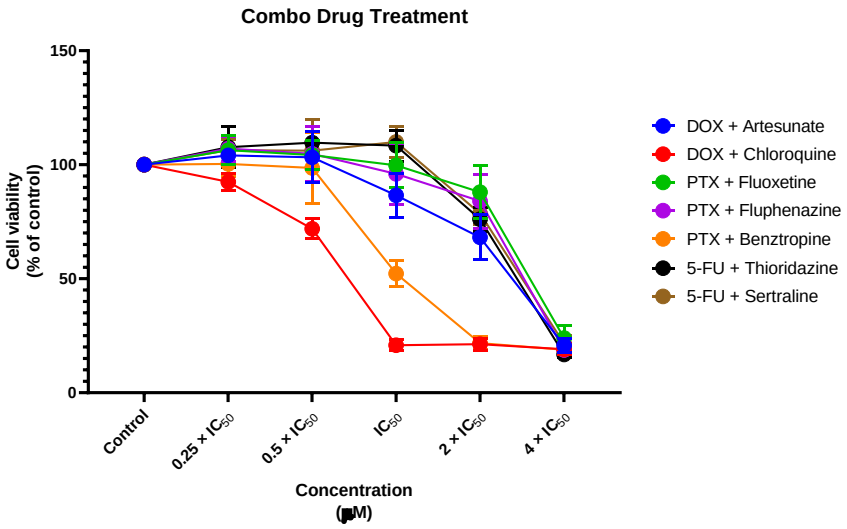

Figure 127. Comparison of the cytotoxic effect after combination treatments with antineoplastic and repurposed drugs in MRC-5 human normal lung fibroblast cells. Results are represented as the percentage of control and represent mean ± SEM. Each experiment was done three times independently (*n* = 3).

6. CONCLUSION OF CHAPTER IV

It was successfully demonstrated that the combinations of antineoplastic drugs with antimalarial and CNS drugs have an acceptable toxicological profile. By studying their cytotoxic evaluation on MRC-5 cells, it was demonstrated these combinations are safe at lower doses, without significant cell viability reduction of MRC-5 fibroblast cells. It was also proved these combinations induce cytotoxicity for cancer cells, even in the concentration range that is compatible with non-tumoral cells.

Taken together, it was demonstrated that antimalarial and CNS drugs can be safely used in combination regimens with chemotherapeutic agents. These results support further studies of these drug combinations in more complex systems such as animal models.

CHAPTER V

MECHANISTIC STUDIES OF THE MOST PROMISING DRUG COMBINATIONS IN BREAST AND COLON CANCER CELLS

1. SUMMARY OF CHAPTER V

In the previous chapters, our group proposed novel drug combinations for breast and colon cancer using repurposed drugs from different classes (antimalarial and CNS) and chemotherapeutic agents such as 5-FU, PTX and DOX and found promising results regarding the toxicity and biosafety profiles of these combined pairs. In this way, in this last chapter, we aimed to further study the mechanisms of action of the most promising drug combinations found in the previous experiments.

Therefore, the most promising drug combinations were selected for evaluation of the expression of EMT biomarkers (E-cadherin, P-cadherin, vimentin, and β-catenin) by immunohistochemistry (IHC) to assess if these drug combinations affect the expression of these proteins and eventually revert EMT. The IHC results demonstrated that combination treatments increase E-cadherin expression while reducing P-cadherin, vimentin, and β-catenin, suggesting that these treatments could induce EMT reversal.

Then, it was designed and constructed a cell microarray (CMA) to perform IHC studies for the evaluation of the expression of several proteins involved in the carcinogenesis process: palmitoyl-protein thioesterase 1 (PPT1), Ki67, cleaved-PARP, multidrug resistance-associated protein 2 (MRP2), P-glycoprotein (P-gp), and NF-kB p65 expression. It was found that PPT1 may have an important role in the mechanism of action of these combinations, as demonstrated by their ability to decrease PPT1 expression.

Taken together, these results support the use of antimalarial and CNS drugs in combination regimens with chemotherapeutic agents and implicate changes in EMT and PPT1 as having an impact in the action of these drug combinations; nevertheless, additional studies are recommended to further explore their complete mechanism of action.

2. INTRODUCTION OF CHAPTER V

In the last chapter, our research group explored the strategies of drug repurposing and drug combination for the development of novel cancer therapies, as they represent a novel way to identify new potential candidates for cancer combat. These strategies are advantageous as repurposed drugs have pharmacokinetics, pharmacodynamics, and toxicological profiles that are well established, making it easy for their approval for novel indications [487]. At the same time, if the combination with antineoplastic agents enhances their anticancer activity, it allows decreasing the therapeutical dose needed for the treatment and consequently the side effects [488]. We have studied the repurposing of antimalarial and CNS drugs for breast and colon cancer and have already found promising drug pairs for colon and breast cancer. Collectively, it was found DOX + artesunate, DOX + chloroquine, PTX + fluoxetine, PTX + fluphenazine, and PTX + benztropine to be the most promising combinations for breast cancer therapy [489, 490]. For colon cancer cells, we found 5-FU+thioridazine and 5-FU+sertraline to be the most effective drug pairs to reduce cell viability [489].

Here, it will be described the importance of EMT proteins and its link with cancer progression and explored further proteins involved in carcinogenesis such as PPT1, Ki67, cleaved-PARP, MRP2, P-gp, and NF-kB p65, to further describe the mechanisms of action behind the most promising drug combinations previously proposed in last chapters.

2.1 EMT proteins and cancer progression

Epithelial-mesenchymal transition (EMT) is a complex cellular process where cells lose their epithelial features and acquire mesenchymal characteristics. This phenomenon allows the cells to gain mobility and migrate from the primary tumor site, resulting in metastases [491]. Although EMT is normal in embryonic stages [492], in adults, EMT is usually related to the healing process or cancer metastasis [493]. EMT also explains the aggressive phenotype and malignancy of different types of cancer [494]. Different studies already suggested that EMT is linked to cancer progression [495–500].

Different biomarkers can be used in EMT studies through evaluation of their level of expression, distribution, and changes of function, which help to characterize the state in which cancer cells are. These biomarkers include growth factors, such as TGF-β and Wnts, transcription factors such as Snail and Twist, adhesion molecules such as cadherins, and molecules present in the cytoskeleton as vimentin [501].

TGF-β regulates cell proliferation and is one of the main regulators of EMT: it is a suppressor of epithelial cells and leads to the loss of epithelial proteins such as E-cadherin while increasing the expression of mesenchymal biomarkers such as vimentin [502]. Snail, a transcription factor induced by TGF-β, also increases the expression of mesenchymal phenotype while decreasing epithelial proteins such as E-cadherin [503]. Twist, another transcription factor, regulates the shift from E-cadherin to a less adhesive N-cadherin, a characteristic cadherin in mesenchymal cells [491]. P-cadherin is usually co-expressed with E-cadherin, and its expression is increased in some disease states, namely genetic disorders or cancer progression [504]. Another marker of EMT is the β-catenin expression, which is overexpressed in more advanced cases with worse prognoses [505]. Vimentin is a cytoskeleton protein, typically overexpressed in mesenchymal cells, and its increased expression has been observed in several carcinomas such as breast and colon, associated with malignancy and metastasis [506–508]. Therefore, the study of the expression of these proteins may give information about cancer progression or regression.

2.2 PPT1 enzyme and its relationship with repurposed drugs in cancer

Autophagy is a cellular process responsible for the degradation and elimination of misfolded proteins and damaged organelles [509]. Autophagy role is the adaption to starvation, development, cell death, and tumor suppression [510–512]. It is a pathway mediated by double-membrane vesicles called autophagosomes that collect damaged cell components and deliver them to the lysosomes. Lysosomes recycle these components under stress and confer protection to the cells from damaged proteins and toxins, promoting cell survival. In stress conditions such as nutrient deprivation, autophagy aims to provide nutrients (energy supply), increasing cell survival [511–513].

This process is tightly regulated by proteins: mTOR is one of the most important ones and is involved in the regulation of cell proliferation, stress, and cancer progression. Activated mammalian target of rapamycin complex 1 (mTORC1), a complex of mTOR, is involved in the phosphorylation of autophagy-related protein (ATG) that inhibits the autophagic process. Under stress conditions, mTORC1 is inhibited, which leads to increased AMPK and the autophagic process is increased [512, 514, 515]. The role of mTORC1 in autophagy is not completely understood [516].

Autophagy also plays an important role in cancer. Some studies suggest autophagy can regulate the expression of some oncogenes and tumor suppressor genes [513, 517]. Its role is controversial as some studies suggest that autophagy plays a dual role: it can

promote tumorigenesis and it can also be involved in cancer inhibition [512, 518, 519]. On one hand, it may suppress carcinogenesis by inhibiting cancer cell survival and inducing apoptosis; on the other hand, it can induce tumorigenesis by improving the proliferation and growth of tumor cells [520, 521]. mTOR and AMPK are the negative regulators of tumor suppressor genes, promoting autophagy and suppression of cancer initiation. mTOR also regulate oncogenes and activate them, inhibiting autophagy and enhancing cancer progression [513, 517]. For these reasons, the regulation of autophagy is a very important target in cancer therapy. Drugs targeting the mTOR are already been used in several types of cancer, such as breast [522], brain [523] and kidney [524], although their efficacy has been limited. AstraZeneca also developed an mTOR inhibitor (vistusertib) but trials in several types of cancer resulted in different outcomes and the drug has been abandoned [525].

Recent studies have pointed out the role of antimalarials in several types of cancer, including breast [526], lung [527] and other solid tumors [528]. According to ClinicalTrials.gov, approximately 20 clinical trials are evaluating the role of chloroquines in cancer [529]. Indeed, antimalarial drugs have gained crescent interest in the scientific community because of their promising results in cancer. Until recently, their mechanism of action in cancer has not been completely understood.

Recently, researchers at the University of Pennsylvania discovered that chloroquine and its derivates target the PPT1, an enzyme localized in the lysosomes [530]. PPT1 depalmitoylates proteins in the lysosome before their degradation; it also regulates the mTOR and consequently the autophagic process [531]. In this work, they found this enzyme is overexpressed in several types of cancer, including breast, colon and other solid tumors. In most advanced stages, PPT1 expression was even higher and associated with worse outcomes. Using the CRISPR-Cas9 gene editing, researchers were able to knockout PPT1 from cancer cells, and it resulted in slowed tumor growth. Melanoma cells treated with chloroquine and derivates confirmed that PPT1 is the target these drugs are targeting [530].

PPT1 expression and importance in cancer are not completely understood. Rebecca *et al* found that PPT1-dependent depalmitoylation may be important for the stabilization of v-ATPase subunits in the lysosomes. This v-ATPase complex maintains lysosomal acidity and provides the machinery needed for mTOR activation. They found that dynamic palmitoylation is involved in the stabilization of autophagy-lysosome function and consequent mTOR signaling, via v-ATPase. Moreover, they found that inhibiting PPT1 activity suppresses v-ATPase function and, consequently, autophagy [530]. The loss of PPT1 protein activity also leads to upregulation of lysosomal biosynthesis and mitochondrial

dysfunction, increasing ROS production. It was also found that these pathologies can be mitigated by the addition of exogenous PPT1 [532]. These results describe a novel target in cancer cells and demonstrate the potential of PPT1 inhibition in cancer therapy. A recent study also found that PPT1 interactome affects neuronal morphology and function, suggesting this enzyme may be involved in the regulation of neurodegenerative diseases as well [533].

Lysosomal activity is elevated in advanced cancers and regulates mTORC1-dependent protein translation and autophagy. It was found that DOX co-localizes with lysosomes and autophagosomes in breast cells resistant to doxorubicin. Also, it was found that inhibitors of lysosomal function such as chloroquine potentiate the anticancer effect of doxorubicin in hepatic cancer cells. Studies also demonstrate that PTX inhibits endosomal-lysosomal membrane trafficking, by inducing early accumulation of protein and endocytic markers in endosomes and later accumulation in a subdomain of lysosomes. Also, reports suggest that enhanced lysosomal function is responsible for PTX resistance in cancer cells and that this drug resistance can be reverted using artesunate or other inhibitors of lysosomal function. Taken together, these results suggest that other antimalarial drugs besides chloroquine and CNS drugs may also interact in lysosomal metabolism, mainly through the inhibition of the PPT1 enzyme. This interaction can help to decrease the accumulation of the antineoplastic drugs in the lysosome and cell resistance, enhancing their bioavailability, and increasing the antitumor effect of these drugs, explaining their synergism in breast cancer cells.

Recently, our group found that antimalarials and CNS could act synergistically with DOX and PTX in MCF-7 breast cancer cells and with 5-FU in HT-29 colorectal cancer cells but the mechanism behind these interactions remains unknown [490]. Following the results obtained by Rebecca *et al* [530], we hypothesized that other antimalarial drugs besides chloroquine as well as CNS drugs, could also target lysosomal enzyme PPT1 in breast and colorectal cancers. We believe that mefloquine, artesunate and different CNS drugs can also target PPT1, inhibiting the mTOR pathway and playing a role in the regulation of autophagy.

2.3 Other proteins involved in carcinogenesis

Here, it was constructed a cell microarray (CMA) to evaluate the expression of several proteins in MCF-7 and HT-29 cells exposed to each treatment, by immunohistochemistry. The CMA is a single paraffin block that allows side-by-side

comparations between different cell lines, diverse conditions, biomarker expression, and cytolocalization evaluation at the same time [534]. It was evaluated the expression of the PPT1, P-gp, MRP2, Ki67, cleaved-PARP and NF-kB p65 after treatment with drugs, both alone and combined, in both cell lines.

These proteins were studied for their implication in cancer: NF-kB p65 is a protein complex that regulates DNA transcription, cytokine production, and cell survival/death. Its inactive form is located in the cytoplasm and, upon activation, it migrates to the nucleus, enabling DNA transcription [535]. In cancer cells, a higher expression of NF-kB p65 is associated with a worse prognosis [535]. The P-gp, also known as multidrug resistance associated protein 1 (MRP1), is a glycoprotein expressed in the cellular membrane and is involved in the efflux of drugs to the outside of cells [536]. Therefore, it has an important role in the development of drug resistance, being overexpressed in tumor cells [536]. The MRP2 protein is a member of the ATP-binding cassette (ABC) transporters and has a similar function as P-gp [537]. Higher levels of MRP2 are related to chemoresistance [537]. The Ki67 is a marker for tumor cell proliferation; this protein is located in the nucleus and is involved in the regulation of mitosis [538]. This protein is used as a prognostic predictive biomarker in cancer patients, being an indicator of metastasis and tumor stage [538]. The PARP1 is a protein that is cleaved during apoptosis, being generated by the activation of caspases 3 and 7 [539]. This protein is involved in DNA repair and chromatin structure modulation. It is a nuclear protein and its levels are elevated in different types of cancer [539].

3. OBJECTIVE OF CHAPTER V

In the previous chapters, it was evaluated the combination of CNS drugs with PTX, DOX and 5-FU, in MCF-7 breast and HT-29 colon cancer cells and it was found that some drug pairs could synergistically decrease the proliferation and viability of cancer cells. This work is a follow-up to our previous experiments and here our group hypothesized that the combination of antineoplastic agents and repurposed drugs could help reverse the EMT in breast and colon cancer cells. To understand how the drugs act in combination and if EMT is involved, it was evaluated the most promising drug pairs since the beginning of this project, regarding the use of repurposed drugs (antimalarial and CNS agents) combined with antineoplastic agents in two different cell lines (HT-29 and MCF-7 cells), for the expression of EMT biomarkers, such as E-cadherin, P-cadherin, vimentin, and β-catenin, to assess if all drug pairs would affect EMT the same way, using different classes of repurposed drugs and different cell lines. MCF-7 breast and HT-29 colon cancer cells are widely used cell lines, with epithelial characteristics. Some studies suggest they can acquire mesenchymal features under malignancy and drug resistance.

It was also studied the expression of the proteins PPT1, P-gp, MRP2, Ki67cleaved-PARP and NF-kB p65 after treatment with drugs, both alone and combined, in both cell lines, to further evaluate the possible mechanisms of action behind these drug combinations.

4. MATERIALS AND METHODS OF CHAPTER V

4.1 Evaluation of EMT Biomarkers

4.1.1 Materials and Reagents

Cell culture reagents such as McCoy's 5A Modified Medium, DMEM, FBS, and a mixture of pen-strep solution were obtained from Millipore Sigma (Merck KGaA, Darmstadt, Germany). Other cell culture reagents were brought from Gibco (Thermo Fisher Scientific, Inc, Waltham, MA, USA). Fluphenazine (cat. no. F4765), latrepirdine (cat. no. D6196), 5-FU (cat. no. F6627), Bovine Serum Albumin (BSA, cat. no. A8531), Entellan mounting medium (cat. no. 107960), and (3-Aminopropyl)triethoxysilane (silane, cat. no. A3648) were obtained from Sigma-Aldrich (Merck KGaA, Darmstadt, Germany). Benztropine (cat. no. 16214), sertraline (cat. no. 14839), thioridazine (cat. no. 14400), fluoxetine (cat. no. 14418), artesunate (cat. no. 11817), and doxorubicin (cat. no. 15007) were acquired from Cayman Chemical (Ann Arbor, Michigan, USA). Chloroquine (cat. no. C6628) was purchased from Santa Cruz Biotechnology (Dallas, Texas, USA). PTX (cat. no. 1097) was obtained from Tocris Bioscience (Bristol, UK). Perampanel was purchased from Eisai Co., Ltd. (Tokyo, Japan). Novolink Max-Polymer detection system was bought from Novocastra (Newcastle, UK).

4.1.2 Cell Line and Cell Culture

This protocol was carried out using two different cell lines: MCF-7 and HT-29 cell lines (ATCC, Manassas, VA, USA). MCF-7 and HT-29 cells were maintained in DMEM and McCoy's cell culture medium, respectively, in the same conditions described in the previous chapters. After reaching 70–80% confluence, cells were prepared for immunohistochemistry.

4.1.3 Preparation of Cells for Immunohistochemistry (IHC)

It was first adapted the protocol for IHC for 24 well plates, using adherent cells. Sterile 13 mm coverslips were placed in 24-well plates and coated with silane 2% in acetone for 1 h at room temperature. Before cell seeding, silane coverslips were washed with PBS and allowed to dry for 2 h. Next, MCF-7 and HT-29 cells were seeded with a density of 12,500 and 37,500 cells/well, respectively, and incubated for 24 h at 37 °C. After that period, cells were incubated with single and combination treatments for 48 h. Cells treated with vehicle (0.1% DMSO) were used as control. Cells were then washed with PBS and incubated with a solution of paraformaldehyde (PFA) 4% in PBS for 15 min at room temperature, for cell fixation. Next, cells were washed three times with PBS-0.1% Tween 20 and maintained in PBS at 4 °C until the beginning of the IHC protocol.

4.1.4 Immunohistochemistry Protocol

For the IHC protocol, a Novolink Max-Polymer detection system was used, according to the manufacturer's instructions. The detailed protocol is described in Figure 128. Primary antibodies included anti-E-cadherin (4A2C7; 1:1000 in bovine serum albumin (BSA) 5%; Invitrogen, MA, USA), anti-P-cadherin (56/P-Cadherin; 1:150 in BSA 5%; BD Biosciences, NJ, USA), anti-β-catenin (CAT-5H10; 1:900 in BSA 5%; Invitrogen, MA, USA), and anti-vimentin (V9; 1:1000 in BSA 5%; Dako, Denmark). The negative control refers to cells that were not incubated with the primary antibody. After IHC protocol, each coverslip was removed from the 24-well plate using a small pair of broad-tipped forceps and rinsed in water, counterstained in hematoxylin for 30 sec, washed again for 5 to 10 min, dehydrated (at increasing concentrations of ethanol), and diaphanized in xylene, and the slides were mounted using Entellan. Each slide was analyzed using a Nikon Eclipse E600 microscope coupled to a digital camera (Nikon Digital Sight DS-Fi2, Tokyo, Japan). Images were then captured using the Imaging Software NIS-Elements AR Version 4.30.0 (Nikon, Tokyo, Japan).

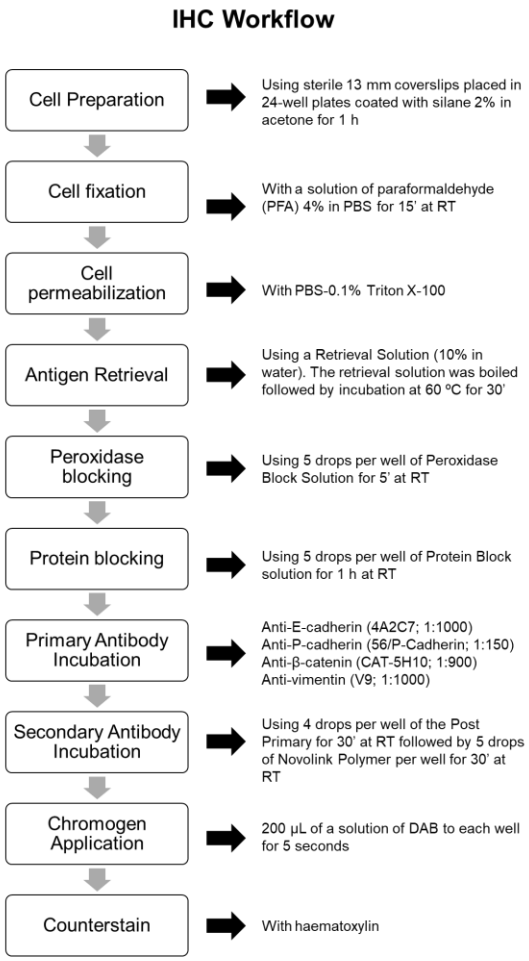

Figure 128. Detailed protocol of immunohistochemistry technique used in this work. Briefly, sterile 13 mm coverslips were placed in 24-well plates and coated with silane 2% in acetone for 1 h at room temperature. Before cell seeding, silane coverslips were washed with PBS and allowed to dry for 2 h. Next, cells were seeded and incubated for 24 h at 37 °C. After that period, cells were incubated with each treatment for 48 h. Cells were then washed with PBS and incubated with a solution of PFA 4% in PBS for 15 min at room temperature, for cell fixation. Next, cells were permeabilized with PBS-0.1% Triton X-100. Antigen retrieval (unmasking) was performed using a Retrieval Solution (10% in water). The retrieval solution was boiled and 500 µL were transferred to each well, followed by incubation at 60 °C for 30 min. After that, cells were washed twice in Tris buffered saline (TBS) for 5 min. Endogenous peroxidase was blocked using 5 drops per well of Peroxidase Block Solution for 5 min at room temperature and washed twice in TBS for 5 min. Next, protein block was performed using 5 drops per well of Protein Block solution for 1 h at room temperature. Slips were then washed twice in TBS for 5 min. Afterwards, the coverslips were incubated with agitation overnight, at 4 °C with 200 µL of each primary antibody. Next, cells were washed twice in TBS, for 5 min and 4 drops of the Post Primary solution was added to each well, following an incubation time of 30 min at room temperature. Once again, the slips were washed twice in TBS, for 5 min. After this time, they were incubated with 5 drops of Novolink Polymer per well for 30 min and then washed twice in TBS for 5 min. Next, the peroxidase activity was developed by adding 200 µL of a solution of diaminobenzidine (DAB) to each well. Finally, each coverslip was removed from the 24-well plate using a small pair of broad-tipped forceps and rinsed in water, counterstained in hematoxylin for 30 sec, washed again for 5 to 10 min, dehydrated, diaphanized in xylene, and the slides were mounted. RT: room temperature

4.2 Evaluation of PPT1, Ki67, cleaved-PARP, MRP2, P-gp, and NF-kB p65 expression

4.2.1 Cell culture and Drug Treatment

Experiments were carried out using two cancer cell lines: MCF-7 breast and HT-29 colon (ATCC, Manassas, VA, USA). MCF-7 and HT-29 cancer cells were maintained in DMEM and McCoy's (Merck KGaA, Darmstadt, Germany) cell culture medium, respectively, both supplemented with 10% FBS and 1% of a pen-strep solution (1000 U/mL; 10 mg/mL, Merck KGaA, Darmstadt, Germany). Cells were grown in T75 cm^2 flasks and kept at 37 °C in a humidified atmosphere with 95% air and 5% CO_2. Cell media was changed twice a week. When cell confluence reached 70–80% and for cell seeding prior experiences, cells were washed with PBS (Gibco, Thermo Fisher Scientific, Inc., Waltham, MA, USA) and trypsinized using a solution of 0.25% trypsin-EDTA.

Before drug treatment, MCF-7 and HT-29 cells were plated in 6-well plates using a density of 7.5×10^5 cells/well and incubated at 37 °C and 5% CO_2 to adhere. After 24 h, cell media were replaced with drug-containing media for 48 h. For each condition, three wells were used. Based on the previous results, MCF-7 cells were treated with vehicle (0.1% DMSO), PTX, DOX, artesunate, chloroquine, fluoxetine, fluphenazine, and benztropine

alone and with the combinations of DOX + artesunate, DOX + chloroquine, PTX + fluoxetine, PTX + fluphenazine and PTX + benztropine, at the concentration of 0.25 times their IC_{50} (Table 29). This concentration was selected so that we could have, simultaneously, some cytotoxic effect and an acceptable number of viable cells, to allow for marker quantification. HT-29 cells were treated with vehicle (0.1% DMSO), 5-FU, thioridazine, and sertraline alone and with the combinations of 5-FU + thioridazine and 5-FU + sertraline, at the concentration of 0.25 times their IC_{50}. Cells were incubated with drugs alone or combined for 48 h. All drugs were dissolved in DMSO and kept at −20 °C until the experiments. No significant differences were seen between control cells with or without vehicle.

4.2.2 Collection, Fixation, and Histogel™ Processing of Cultured Cells

After 48 h, cells were scraped from culture dishes, washed three times with ice-cold PBS and fixed with 10% (*v/v*) neutral-buffered formaldehyde (AppliChem GmbH, Darmstadt, Germany), and fixed for 1 h at room temperature with gentle agitation. Then, the cells' pellet was re-suspended in liquefied HistoGel™ (Thermo Fisher Scientific, Inc., Waltham, MA, USA), according to the manufacturer's instructions, followed by standard histological processing and paraffin embedding. To confirm that all conditions tested were appropriate for the CMA construction, each block was sectioned with a microtome, and hematoxylin and eosin (H&E) staining was performed.

4.2.3 CMA Construction and Immunocytochemistry Expression Analysis

All conditions were arrayed in a CMA block, in the same way as previously described by Nunes *et al* [540]. After designing the cell block, it was constructed and finally sectioned using a microtome. For the immunocytochemistry protocol, the slides were deparaffinized and hydrated. Next, the antigen retrieval (unmasking) was performed by heat-induction (98 °C), using a citrate buffer solution (1:100 at pH 6.0; Thermo Fisher Scientific, Inc, Waltham, MA, USA) or EDTA (1:100; Thermo Fisher Scientific, Inc, Waltham, MA, USA) for 40 min. Then, the activity of endogenous peroxidase was blocked using a hydrogen peroxide solution 3% (*v/v*) (Thermo Fisher Scientific, Inc, Waltham, MA, USA) for 10 min. Finally, each slide was incubated with the specific primary antibodies (conditions described in Table 30). Then, was detected using a secondary antibody with horseradish peroxidase (HRP)-labeled polymer (Dako REAL™ EnVision™ Detection System Peroxidase/DAB+, Rabbit/Mouse) for 30 min. DAB was used to develop the activity of peroxidase according to the manufacturer's instructions. Hematoxylin staining was also performed to stain the nucleus of the cells. In the last step, slides were dehydrated, clarified, and cover slipped using a mounting medium for microscopic visualization and analysis. The staining pattern

(nuclear, cytoplasm, or membrane) and the percentage of cells stained (0%, 1–10%, 11–25%, 26–50%, 51–75%, and 76–100%) were evaluated and validated by three independent observers.

Table 30. List of antibodies used for immunohistochemistry studies. mAb—monoclonal antibody; pAb—polyclonal antibody; RT—room temperature.

Antigen	Clone	Origin	Animal origin	Antigen retrieval buffer	Dilution	Incubation conditions	Localization
MRP2	4C9.2	Sigma-Aldrich	Mouse mAb	EDTA	1:50	60´ RT	Membrane
NF-kB p65	C-20	Santa Cruz Biotechnology	Rabbit pAb	Citrate at pH 6	1:600		Cytoplasm
Cleaved-PARP	Asp214 D64E10	Cell Signaling Technology	Rabbit mAb	Citrate at pH 6	1:50		Nuclear
PPT1	-	Thermo Fisher Scientific	Rabbit pAb	Citrate at pH 6	1:500		Cytoplasm
Ki67	SP6	Thermo Fisher Scientific	Rabbit mAb	Citrate at pH 6	1:100		Nuclear
P-gp	C219	Thermo Fisher Scientific	Mouse mAb	EDTA	1:25		Membrane

5. RESULTS AND DISCUSSION OF CHAPTER V

5.1 Evaluation of EMT biomarkers expression

5.1.1 MCF-7 results

After finding the most promising drug pairs for MCF-7 and HT-29 cancer cell lines, it was evaluated if these drug combinations would affect the expression of some EMT biomarkers and if it was related to some degree of EMT reversion. Previously, in MCF-7 breast cancer cells, it was found that both artesunate and chloroquine resulted in significant cell viability reduction, especially when combined with DOX [490]. To evaluate EMT biomarkers expression, IHC studies were performed using the antibodies anti-E-cadherin, anti-P-cadherin, anti-β-catenin, and anti-vimentin. As these treatments resulted in a large decrease in the number of viable cells, it was necessary to adapt the traditional IHC protocol to minimize cell loss during the experiments. The traditional protocol of IHC using cells involves growing them in T-flasks, followed by trypsinization and centrifugation steps to obtain a pellet to embed in paraffin, creating cell blocks. Instead, we seeded the cells in glass coverslips placed in 24-well plates, fixed and permeabilized them, and then performed the antigen retrieval, blocking, antibody incubations, and DAB reveal steps directly in each well. This allowed to avoid morphological changes and cell losses due to the trypsinization and centrifugation steps needed for the cell blocks. After these steps, each coverslip was taken from each well with the help of forceps and was counterstained with hematoxylin, dehydrated, and permanently mounted in glass slides. This adapted protocol is also advantageous because it decreases the density of cells needed to obtain cell blocks and uses less volume of reagents.

Results regarding E-cadherin expression (Figure 129) demonstrated that negative control did show any labelling, confirming the success of the methodology. Single-drug treatments showed similar expression of E-cadherin to the control cells (represented in the insert), except for chloroquine, whose treatment resulted in an increased expression of this protein. Results regarding the combination treatments DOX demonstrated higher expression of E-cadherin compared to control cells. There was also a smaller number of viable cells, with a pronounced change in morphology in the combined treatments. Chloroquine treatments also resulted in morphological changes at the nucleus.

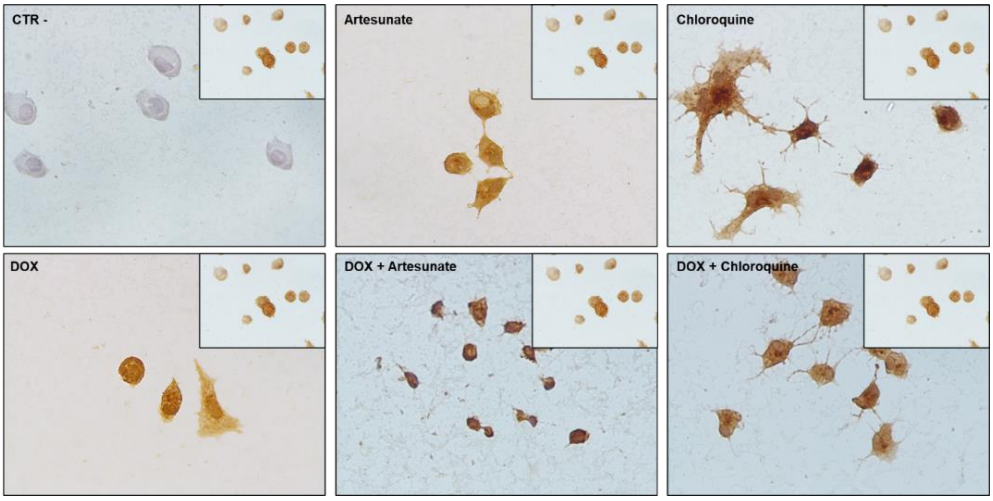

Figure 129. Expression of E-cadherin in MCF-7 cells, by IHC. Treatments are described in the upper left corner of each image. All images were obtained at a magnification of 400x. Insert represents control cells (treated with 0.1% DMSO). CTR -: negative control.

The negative control of cells incubated with anti-P-cadherin did not show P-cadherin labelling, as expected. Similar labelling to the control cells (insert) was seen for all treatments both alone and in combination. In the combination of DOX + artesunate, there were some cells with a loss of expression of this protein (Figure 130).

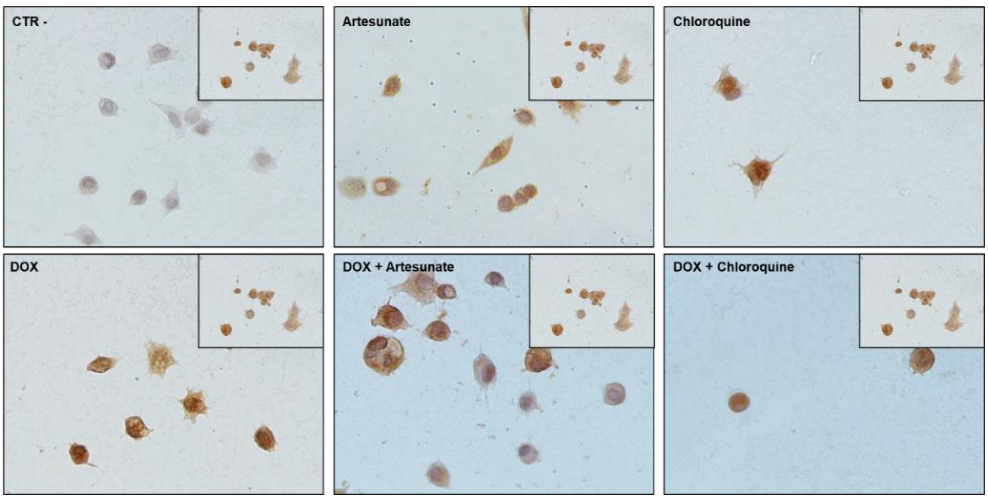

Figure 130. Expression of P-cadherin in MCF-7 cells, by IHC. Treatments are described in the upper left corner of each image. All images were obtained at a magnification of 400x. Insert represents control cells (treated with 0.1% DMSO). CTR -: negative control.

Figure 131 represents the β-catenin labelling of MCF-7 cells treated with artesunate and chloroquine combined with DOX, to complement the previous results. For cells treated with each drug alone and combined, it was found less protein labelling compared to control cells (insert), except for chloroquine.

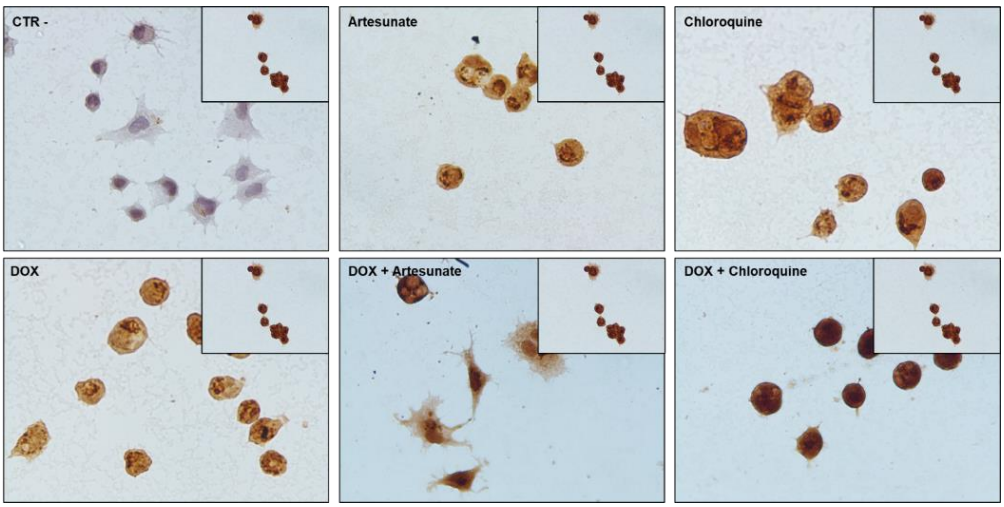

Figure 131. Expression of β-catenin in MCF-7 cells, by IHC. Treatments are described in the upper left corner of each image. All images were obtained at a magnification of 400x. Insert represents control cells (treated with 0.1% DMSO). CTR -: negative control.

Finally, it was also evaluated the labelling of vimentin, a biomarker of mesenchymal cells that is related to increased malignancy of cancer cells. It was found no labelling of this protein in all treatments, except for cells treated with DOX alone, where slight labelling occurred (Figure 132). This may be due to the fact that some cells acquire resistance to this antineoplastic agent, becoming more aggressive.

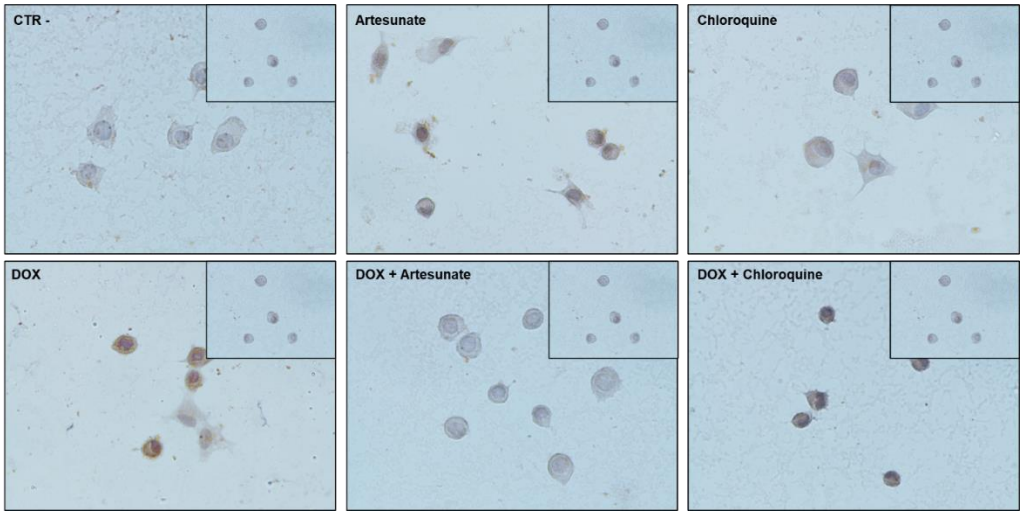

Figure 132. Expression of vimentin in MCF-7 cells, by IHC. Treatments are described in the upper left corner of each image. All images were obtained at a magnification of 400x. Insert represents control cells (treated with 0.1% DMSO). CTR -: negative control.

Next, the same EMT biomarkers were evaluated in MCF-7 treated with another class of repurposed drugs (CNS agents), combined with PTX. Regarding E-cadherin, it was found similar labelling of this protein compared to control cells (insert) in all single treatments. In combination with PTX, there was a more intense expression of E-cadherin, mainly in the combination of PTX with fluoxetine. There was also a smaller number of viable cells, with changes in morphology (Figure 133).

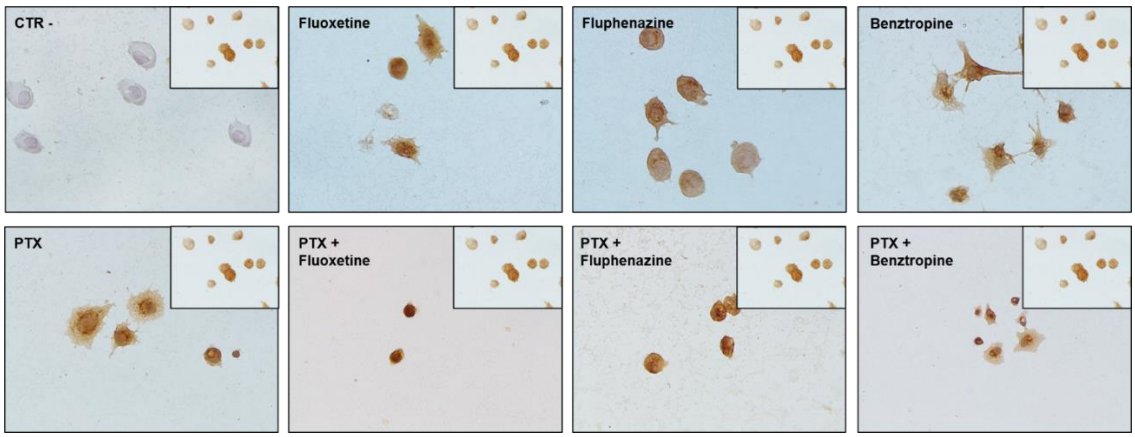

Figure 133. Expression of E-cadherin in MCF-7 cells, by IHC. Treatments are described in the upper left corner of each image. All images were obtained at a magnification of 400x. Insert represents control cells (treated with 0.1% DMSO). CTR -: negative control.

Next, it was evaluated P-cadherin labelling in these cells and it was found a similarity between the control cells and the various treatments both alone and in combination (Figure 134). Treatment with fluoxetine and benztropine demonstrated some cells with loss of P-cadherin expression.

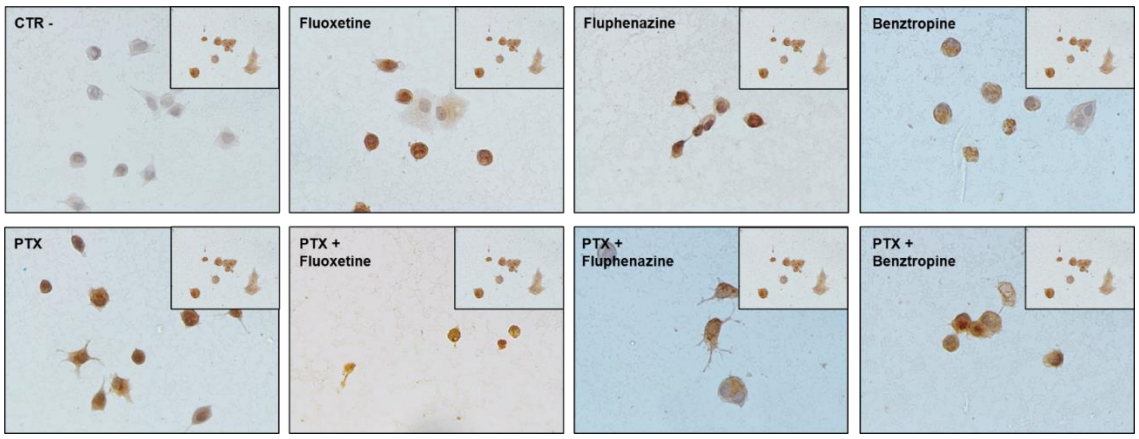

Figure 134. Expression of P-cadherin in MCF-7 cells, by IHC. Treatments are described in the upper left corner of each image. All images were obtained at a magnification of 400x. Insert represents control cells (treated with 0.1% DMSO). CTR -: negative control.

Results regarding β-catenin labelling demonstrated less labelling than control cells in the various treatments with each drug alone. In combination with PTX, there was a lower expression of protein labelling for all treatments compared to control cells, except in the combination of PTX and fluoxetine, whose labelling was similar to the control (Figure 135).

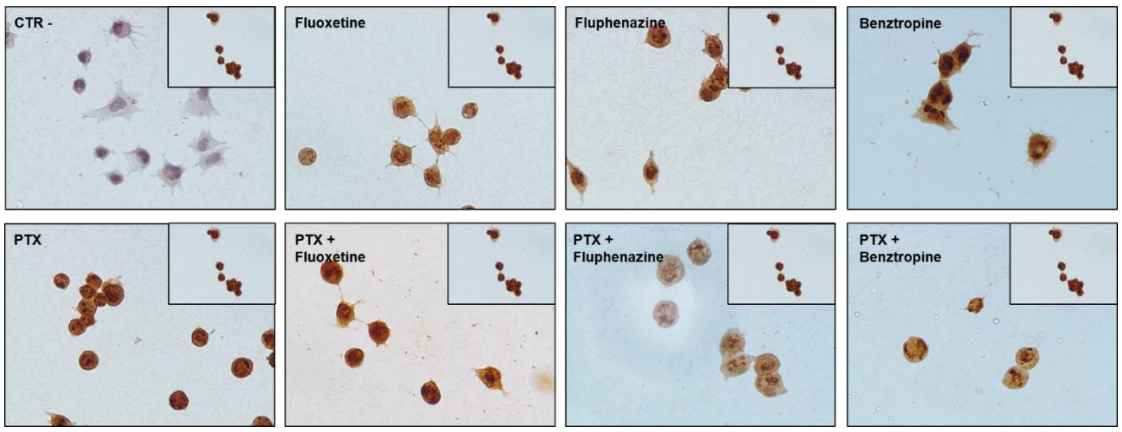

Figure 135. Expression of β-catenin in MCF-7 cells, by IHC. Treatments are described in the upper left corner of each image. All images were obtained at a magnification of 400x. Insert represents control cells (treated with 0.1% DMSO). CTR -: negative control.

There was no labelling of vimentin protein in any treatment, both alone and combined, except for MCF-7 cells treated with benztropine, where slight labelling was found. Interestingly, this marking was reversed when the cells were treated with benztropine in combination with PTX (Figure 136).

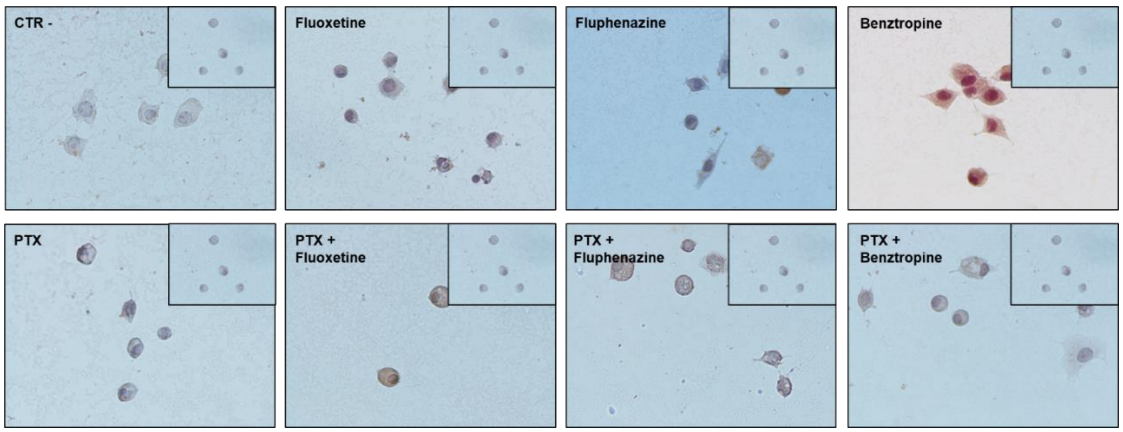

Figure 136. Expression of vimentin in MCF-7 cells, by IHC. Treatments are described in the upper left corner of each image. All images were obtained at a magnification of 400x. Insert represents control cells (treated with 0.1% DMSO). CTR -: negative control.

5.1.2 HT-29 results

Next, these EMT biomarkers were also evaluated in HT-29 colon cancer cells treated with the most promising drug combinations using CNS agents. Similar E-cadherin labelling to the control cells was seen in the various treatments with each drug alone. There was more intense labelling in the combination treatments with 5-FU and all repurposed drugs. There was also a smaller number of viable cells with less aggregation ability, with a more pronounced change in morphology, especially in the combined treatments (Figure 137).

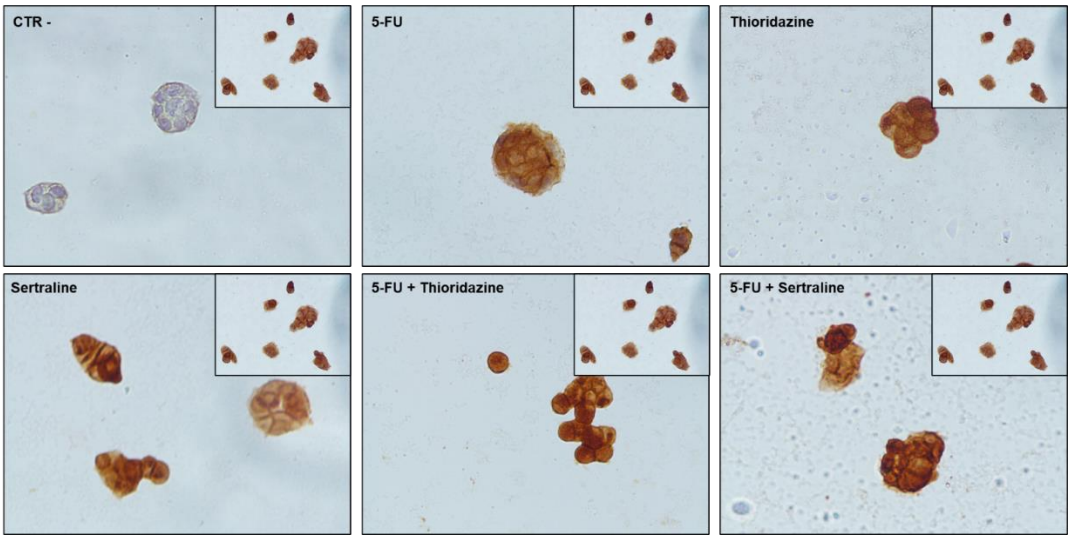

Figure 137. Expression of E-cadherin in HT-29 cells, by IHC. Treatments are described in the upper left corner of each image. All images were obtained at a magnification of 400x. Insert represents control cells (treated with 0.1% DMSO). CTR -: negative control.

Regarding P-cadherin labelling, similar results were found between the control cells and 5-FU and sertraline treatments alone. There was an intense expression of P-cadherin in thioridazine treatments alone and combined with 5-FU, with lower intensity in the combination. There was also a smaller number of viable cells, especially in combination treatments, with smaller aggregates. In the combination of 5-FU with sertraline, it was found only a few viable cells (Figure 138).

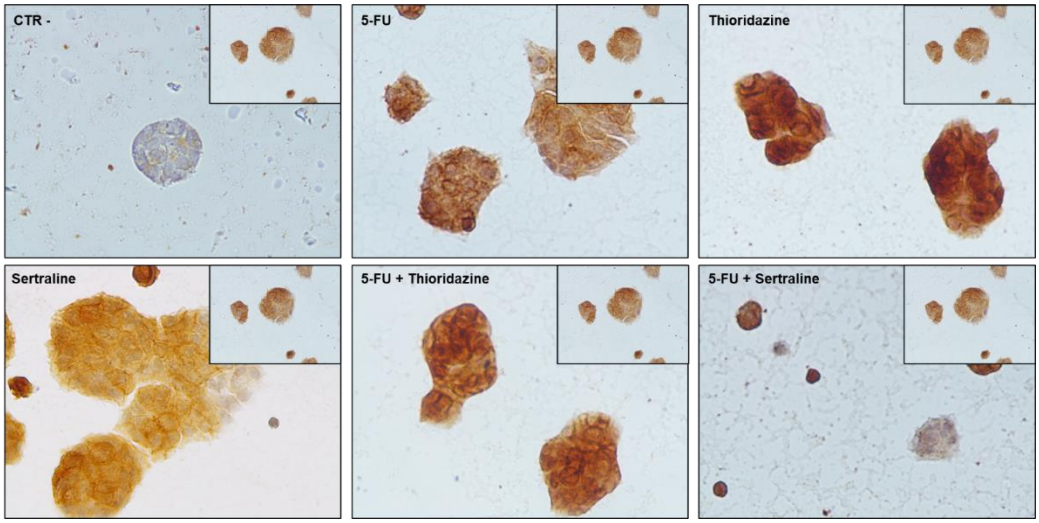

Figure 138. Expression of P-cadherin in HT-29 cells, by IHC. Treatments are described in the upper left corner of each image. All images were obtained at a magnification of 400x. Insert represents control cells (treated with 0.1% DMSO). CTR -: negative control.

There was a similar expression of β-catenin in the control cells and the treatment with 5-FU alone. Intense β-catenin labelling was seen in cells treated with thioridazine and sertraline alone; on the other hand, there was a reduction of the expression of this protein in the cells treated with these drugs combined with 5-FU. In all combination treatments, there was a notable change in cell morphology (Figure 139).

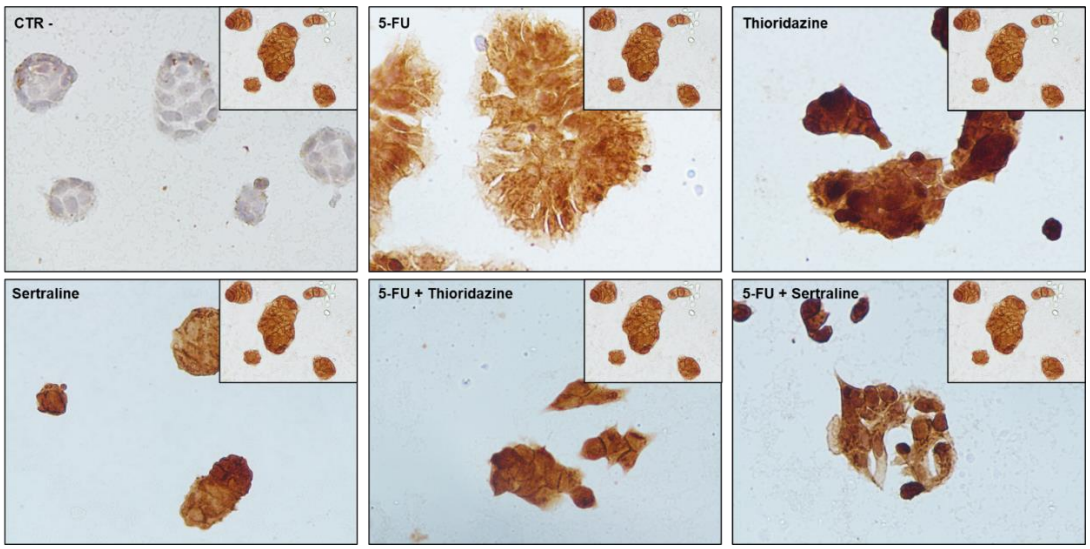

Figure 139. Expression of β-catenin in HT-29 cells, by IHC. Treatments are described in the upper left corner of each image. All images were obtained at a magnification of 400x. Insert represents control cells (treated with 0.1% DMSO). CTR -: negative control.

There was some labelling of vimentin protein in control cells and 5-FU alone, demonstrating a slight change in the characteristics of these cells, with some degree of transformation to a mesenchymal phenotype. This protein expression was reduced in all treatments with drugs both alone and combined (Figure 140).

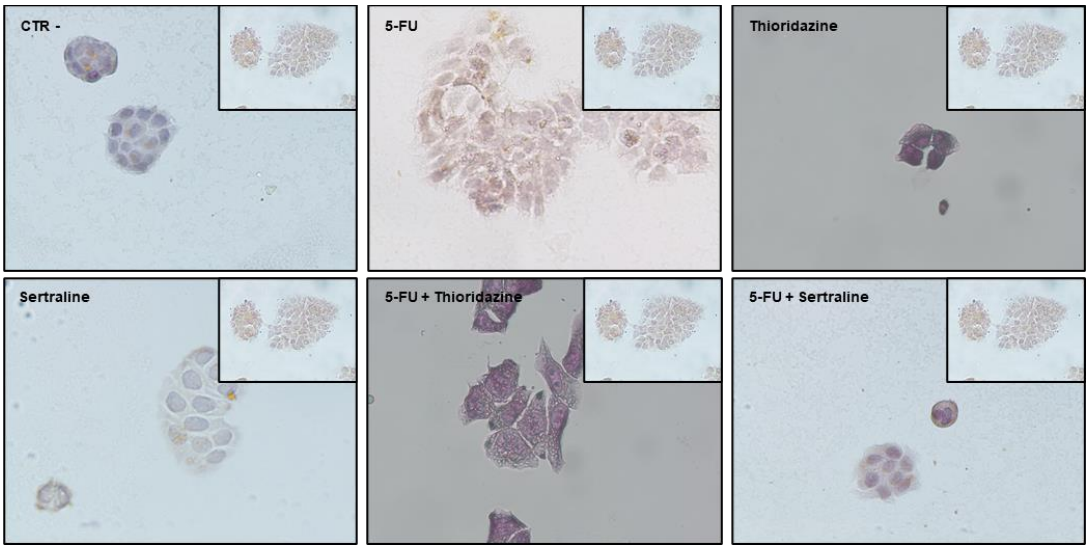

Figure 140. Expression of vimentin in HT-29 cells, by IHC. Treatments are described in the upper left corner of each image. All images were obtained at a magnification of 400x. Insert represents control cells (treated with 0.1% DMSO). CTR -: negative control.

5.2 Evaluation of PPT1, Ki67, cleaved-PARP, MRP2, P-gp, and NF-kB p65 expression

After proving that the proposed drug combinations have an acceptable toxicological profile against non-tumoral cancer cells while retaining significant anticancer effects against different tumoral cancer cells and that some degree of EMT reversal was involved in the mechanism of action of these drug combinations, it was next aimed to evaluate the expression of different proteins related to carcinogenesis after treatment with these drug pairs. To do so, MCF-7 breast cancer cells were cultured and treated with the corresponding drug combinations: DOX + artesunate, DOX + chloroquine, PTX + fluoxetine, PTX + fluphenazine, and PTX + benztropine for 48 h. HT-29 cells were treated with the combinations of 5-FU plus thioridazine and sertraline. Cells were treated with a concentration of 0.25 × IC_{50} of each drug, to ensure enough viable cells for the IHC evaluation. A CMA composed of positive controls and each condition was constructed and used to perform IHC evaluation using the following antibodies: MRP2, P-gp, Ki67, NF-kB p65, cleaved-PARP, and PPT1. Figure 14 represents the IHC results of a liver used as a positive control for PPT1, MRP2, and P-gp. As expected, it was found an abundant expression of PPT1 in the cytoplasm of liver cells (Figure 141A), as this enzyme is involved in lysosomal degradation. On the other side, regarding P-gp (Figure 141B) and MRP-2 (Figure 141C), since these proteins are involved in the efflux of drugs to the outside of cells, it was found an abundant expression in the cell membrane. These results support the selectivity of these antibodies and demonstrate that the IHC protocol has been correctly performed.

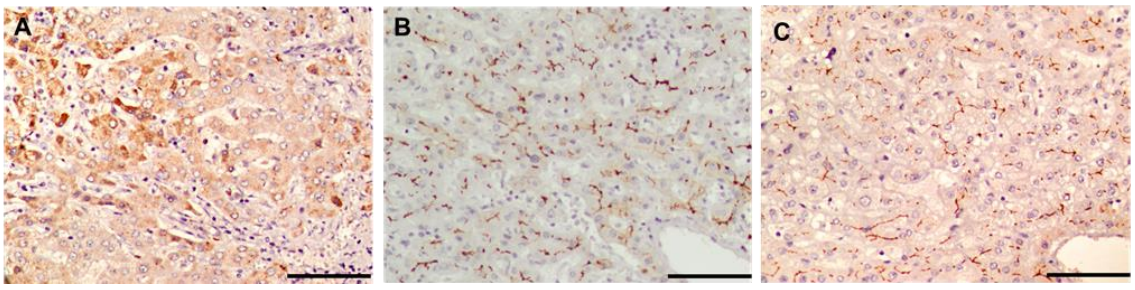

Figure 141. Representative IHC images for (**A**) PPT1; (**B**) P-gp and (**C**) MRP2 in a positive control (liver). All the images are taken at magnification of 200x. Scale bar 100 µm.

5.2.1 MCF-7 results

First, it was evaluated the expression of Ki67, cleaved-PARP, and NF-kB p65 in MCF-7 cells treated with a combination of DOX plus the antimalarial drugs artesunate and chloroquine (Figure 142).

Ki67 is a nuclear protein that marks active cell proliferation, both in normal and tumoral cells [541]. Specifically, this protein is used as a marker for the classification, prognosis, and prediction of therapeutic response in breast cancer [541]. This protein is expressed in all active phases of the cell cycle and decreases its expression after mitosis, in G0 phase [542]. Here, it was hypothesized if these drug combinations could effectively reduce cell proliferation and consequently the expression of Ki67. As expected, in the control condition it was found abundant nuclear expression (51–75%) of this protein in MCF-7 cells (Figure 142). On the other side, MCF-7 treated with DOX alone demonstrated a decreased expression of Ki67 (26–50%) when compared to control (Figure 142). Nevertheless, treatment with antimalarial drugs alone did not cause a decrease in MCF-7 cell proliferation; treatment with artesunate alone demonstrated a similar expression of Ki67 to control cells, and treatment with chloroquine alone caused an elevated expression of Ki67 (76–100%) compared to control cells (51–75%) (Figure 142). The combination treatment of DOX + artesunate resulted in similar results to control cells regarding Ki67 expression (51–75%) (Figure 142). Interestingly, when DOX was combined with chloroquine it was found a decrease in Ki67 expression (26–50%), both compared to control cells and to the treatment with chloroquine alone, which demonstrates this combination can reduce MCF-7 cell proliferation (Figure 142).

PARP is a protein involved in DNA repair and chromatin modulation, being overexpressed in cancer [543]. Therefore, PARP is an important target for cancer therapy. Here, we hypothesize if these drug combinations can act as PARP inhibitors. It was not found significant changes in cleaved-PARP expression among treatments with single and combined drugs, with all cleaved-PARP expression results being negative or <1% (Figure 142). NF-kB is a well-known signaling pathway in oncogenesis and aberrant activation of this pathway is already described for different types of cancer [544]. The results found with respect to NF-kB p65 expression were similar to those regarding PARP expression, which indicates these combinations do not target the NF-kB pathway (Figure 142).

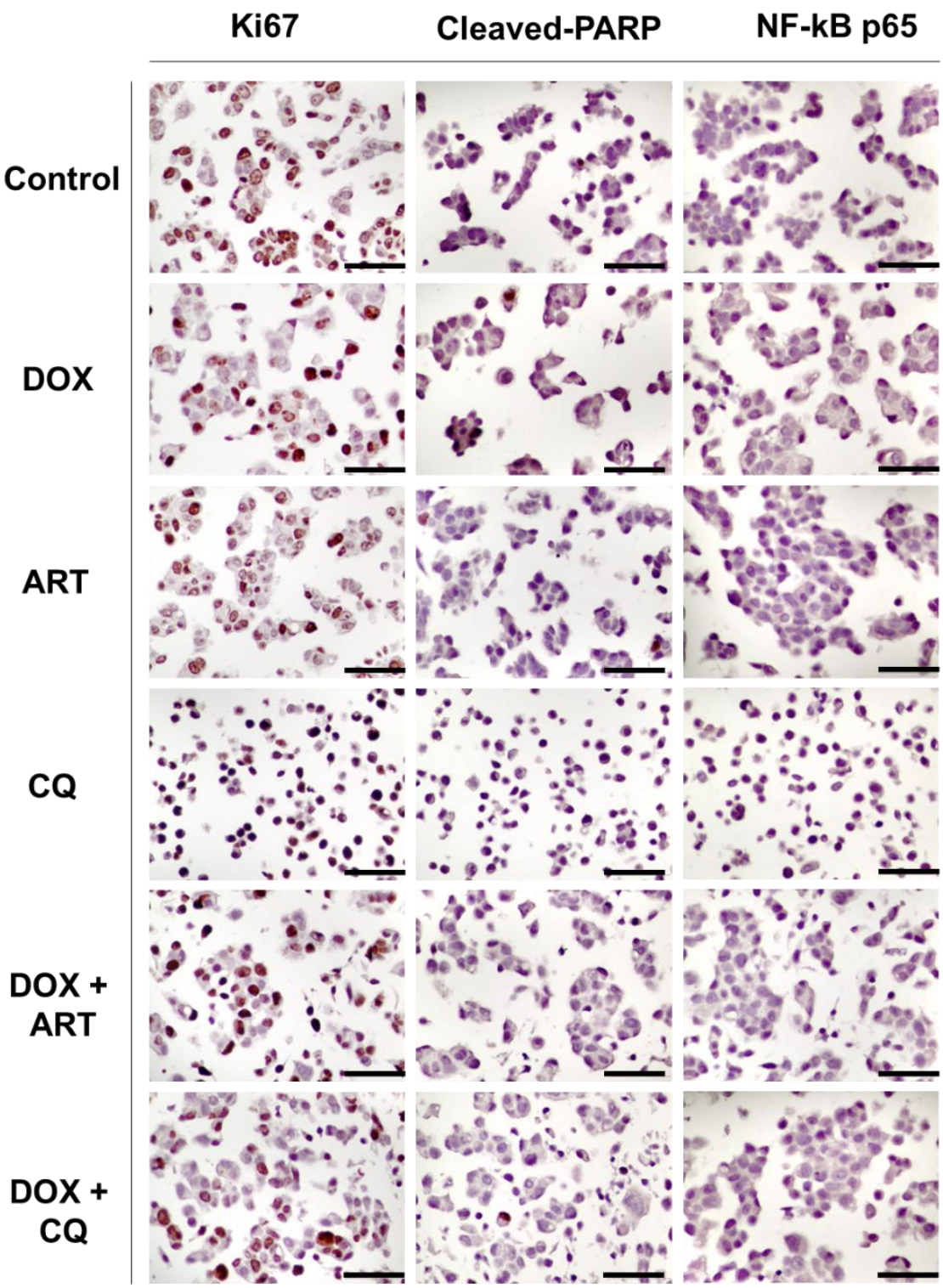

Figure 142. Representative IHC images for Ki67, cleaved-PARP, and NF-kB p65 expression in MCF-7 cells treated with antimalarial drugs (artesunate and chloroquine), alone and in combination with DOX. All images are taken at magnification of 400x. Scale bar 50 µm. ART: artesunate; CQ: chloroquine

Next, it was evaluated the expression of PPT1, P-gp, and MRP-2 in MCF-7 cells treated with a combination of DOX plus the antimalarial drugs artesunate and chloroquine (Figure 143).

PPT1 is an enzyme involved in lysosomal degradation and is overexpression in different types of cancer. CQ is known to inhibit this enzyme [530, 545]. The activity of PPT1 in cancer cells involves the depalmitoylation of the V0a1 subunit of v-ATPase, which facilitates the v-ATPase assembly on the lysosomal membrane [546]. Then, the V1 subunit of v-ATPase interacts with Ragulator, enabling the formation of the mTORC1 complex on the lysosome and activating mTORC1. This activation induces protein synthesis and inhibits the autophagic process [546]. PPT1 can also remove palmitate from palmitoylated proteins prior to their degradation in the lysosome. PPT1 inhibition impairs the depalmitoylation of the V0a1 subunit of v-ATPase, disrupting the assembly of v-ATPase and causing lysosomal deacidification [546]. Furthermore, the interaction between the V0a1 subunit of v-ATPase and Ragulator is lost, causing the inhibition of mTORC1, which inhibits protein synthesis and stops cell proliferation and tumor growth, and impairs autophagy [546]. In this work, it was hypothesized if the proposed drug combinations could inhibit PPT1 enzyme. In MCF-7 control cells, it was found low expression (11–25%) of PPT1 (Figure 143). Treatment with DOX and artesunate alone led to an increase in PPT1 expression to 26–50%, while treatment with chloroquine resulted in 75–100% of MCF-7 expressing this protein, contrary to what was expected (Figure 143). Results of MCF-7 cells treated with DOX + artesunate demonstrated a similar expression of PPT1 to DOX and artesunate alone (Figure 143). Nevertheless, results regarding the combination of DOX + chloroquine resulted in a significant decrease in PPT1 expression (11–25%), demonstrating the ability of the combination to inhibit PPT1 expression (Figure 143).

P-gp, also known as MDR1, is an ATP binding cassette transporter (ABCB1) that is expressed in the cell membrane and is involved in the efflux of drugs to the outside of cells, contributing to the development of drug resistance [547]. Many types of cancer overexpress Pgp which prevents cancer drugs from reaching their cellular targets [548]. Antineoplastic drugs that interfere with the DNA replication process, such as doxorubicin, are especially vulnerable to P-gp overactivity [549]. On the other hand, novel drugs that inhibit P-gp can be promising agents for cancer cell growth inhibition and overcoming multidrug resistance [549]. Ras, c-Raf, p53, and other oncogenes are reported to affect the regulation of P-gp expression [550]. Moreover, it is described that epigenetic modifications play a role in the activation of P-gp-mediated drug resistance [551]. CCAAT/enhancer-binding protein β (C/EBPβ) has also been shown to induce P-gp expression in MCF-7 breast cancer cells.

Furthermore, it has been demonstrated that hypertonic and hypoxic stress increases P-gp expression [552, 553]. Here, it was hypothesized these drug combinations could effectively inhibit P-gp activity, contributing to retaining drugs inside cells. Control cells did not demonstrate any expression of this protein. Treatment with DOX resulted in an increased expression of P-gp (11–25%) (Figure 143). Interestingly, it was found marking of this protein in the cytoplasm in all conditions, although this protein is usually located in the cell membrane. We could not find any explanation for this event, as there are no studies that describe the migration of this protein to the cytoplasm. Treatment with artesunate did not change PPT1 expression compared to control but the combination of DOX + artesunate resulted in higher expression of this protein (11–25%) (Figure 143). On the other side, MCF-7 cells treated with chloroquine alone and combined with DOX revealed a higher expression of PPT1 (26–50%) (Figure 143).

The MRP2 protein is a member of the ABC transporters and has a similar function as P-gp. MRP2 is expressed in various tissues such as hepatocytes, kidney proximal tubules, intestine, nerves, bladder, placenta, and CD4+ lymphocytes [554]. *In vivo* studies using MRP2−/− mice demonstrated that MRP2 knockdown decreases hepatobiliary excretion of drugs and toxins as well as their metabolites, suggesting that MRP2 may play a role in eliminating endogenous and xenobiotic metabolites [555]. Moreover, additional studies have demonstrated that single nucleotide polymorphisms (SNPs) greatly influence the function of MRP2, such as substrate effluxing and microRNA (miRNA) recognition [556]. Several studies implicate MRP2 in the chemoresistance of some types of cancer [557]. Indeed, in tumor cells, it was found that MRP2 messenger RNA (mRNA) levels are related to resistance to chemotherapeutic drugs such as vincristine, cisplatin, and doxorubicin [558]. It was then hypothesized if the combination pairs could target MRP2 and inhibit this protein. Results regarding MRP-2 expression demonstrated this protein is not expressed in these cells in any treatment (Figure 143).

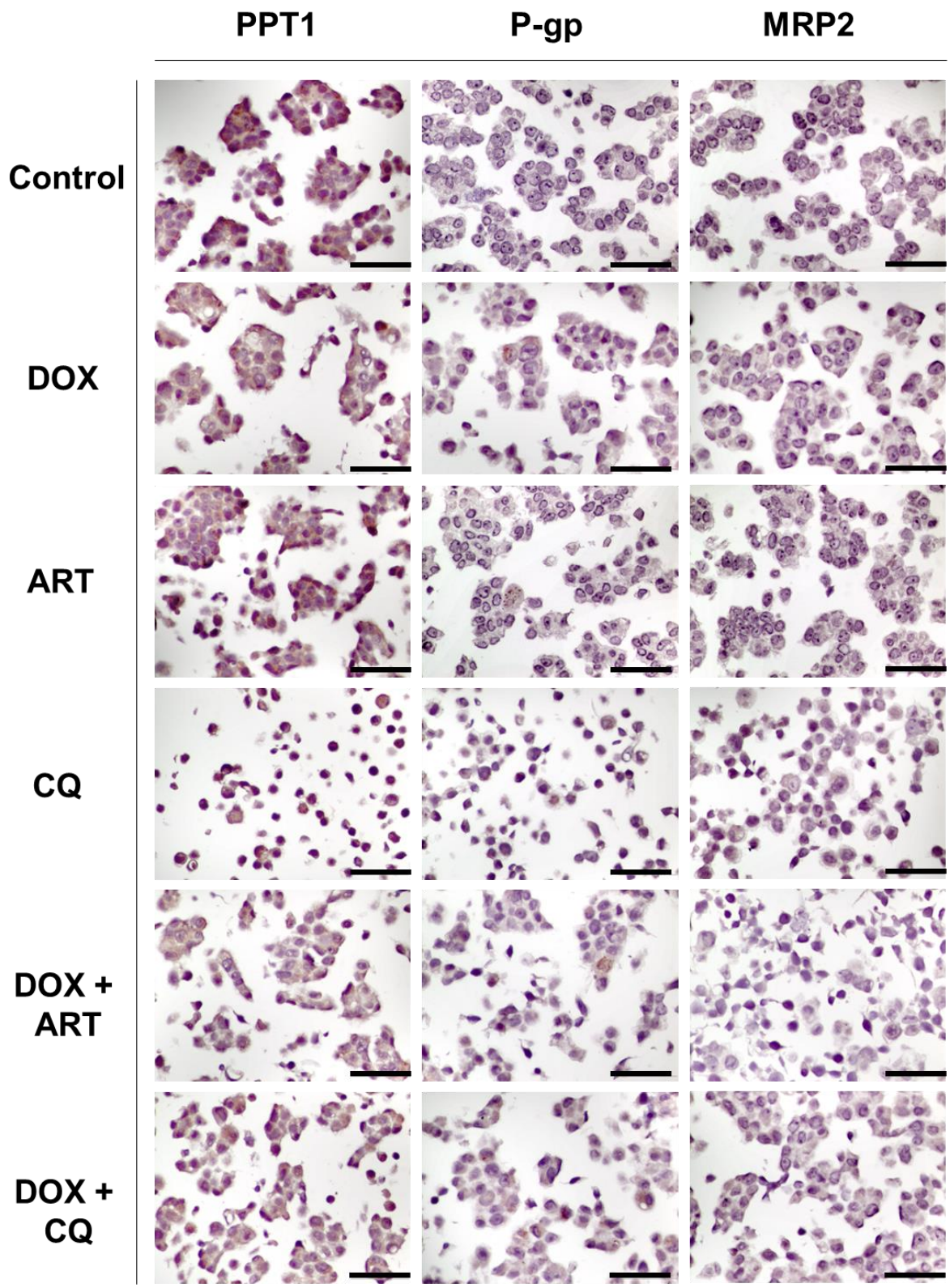

Figure 143. Representative IHC images for palmitoyl-protein thioesterase 1 (PPT1), P-glycoprotein (P-gp), and multidrug resistance-associated protein 2 (MRP2) expression in MCF-7 cells treated with antimalarial drugs (artesunate and chloroquine), alone and in combination with DOX. All images are taken at magnification of 400×. Scale bar 50 µm. ART: artesunate; CQ: chloroquine

Then, we evaluated the expression of Ki67, cleaved-PARP, and NF-kB p65 in MCF-7 cells treated with a combination of PTX plus the CNS drugs fluoxetine, fluphenazine, and benztropine (Figure 144). It was found an abundant expression (51–75%) of Ki67 in the nucleus of MCF-7 control cells. On the other side, all treatments with PTX and CNS drugs, both alone and combined, presented higher Ki67 expression (76–100%) (Figure 17). It was not found significant changes in cleaved-PARP and NF-kB p65 expression among treatments with single and combined drugs, with a negative or <1% expression (Figure 144).

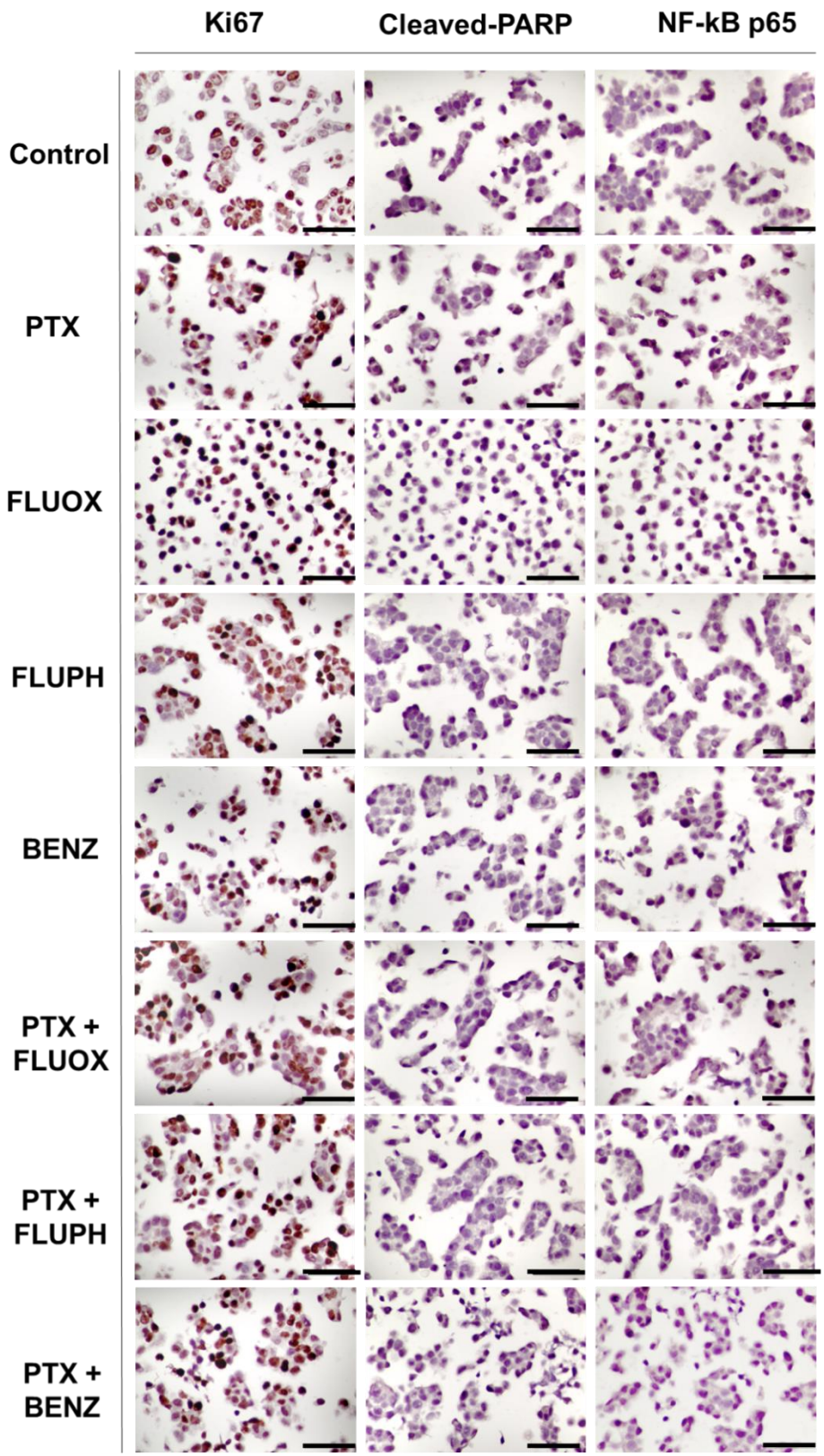

Figure 144. Representative IHC images for Ki67, cleaved-PARP, and NF-kB p65 expression in MCF-7 cells treated with CNS drugs (fluoxetine, fluphenazine, and benztropine), alone and in combination with PTX. All images are taken at magnification of 400×. Scale bar 50 µm. FLUOX: fluoxetine; FLUPH: fluphenazine; BENZ: benztropine

Finally, it was evaluated the expression of PPT1, P-gp, and MRP-2 in MCF-7 cells treated with a combination of PTX plus CNS drugs fluoxetine, fluphenazine, and sertraline (Figure 145). It was found low expression (11–25%) of PPT1 in MCF-7 cells treated with PTX and fluphenazine alone (Figure 145). Treatment with fluoxetine alone led to an increase in PPT1 expression to 76–100%, while treatment with benztropine resulted in only 1–10% of MCF-7 expressing this protein (Figure 145). Results of MCF-7 cells treated with PTX + fluoxetine and PTX + benztropine demonstrated 11–25% of positive cells for this marker (Figure 145). Interestingly, the combination of PTX + fluphenazine demonstrated the capacity to inhibit PPT1, with negative expression of this protein (Figure 145). Treatment with PTX, fluphenazine, and benztropine alone resulted in 11–25% positive cells for PPT1 expression. Treatment with fluoxetine revealed a higher expression (51–75%) of the protein (Figure 145). MCF-7 cells treated with PTX + benztropine revealed a similar expression of PPT1 protein to each drug alone (11–25%). The combination of PTX + fluoxetine also demonstrated a reduction in the percentage of positive cells (26–50%) (Figure 145). On the other side, MCF-7 cells treated with PTX + fluphenazine revealed an increased expression of PPT1 (26–50%), compared to both drugs alone (Figure 145).

It was found low expression of P-gp in MCF-7 cells treated with PTX, fluphenazine, and benztropine alone (11–25%) (Figure 145). Treatment with fluoxetine alone led to an increase in P-gp expression to 51–75%. Results of MCF-7 cells treated with PTX + benztropine demonstrated 11–25% of positive cells for this marker, similar to the treatment with each drug alone (Figure 145). On the other side, the combination of PTX + fluoxetine demonstrated the ability to reduce P-gp expression (26–50%) (Figure 145). In the treatment of PTX + fluphenazine, it was found an increase in P-gp expression compared to single drugs, with 26–50% positive cells (Figure 145). Results regarding MRP-2 expression demonstrated this protein is not expressed in these cells in any treatment (Figure 145).

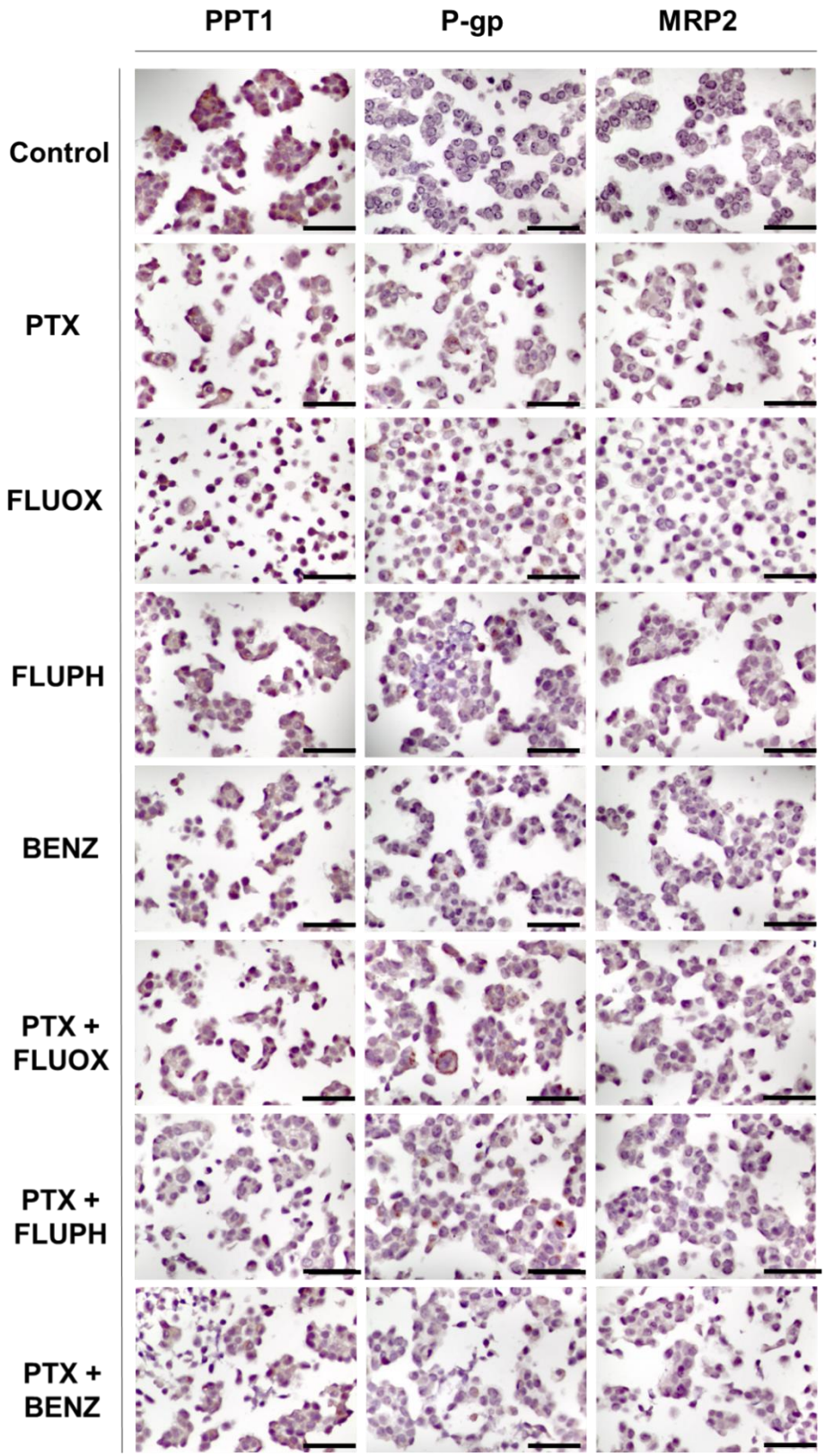

Figure 145. Representative images of PPT1, P-gp, and MRP2 IHC results of MCF-7 cells treated with CNS drugs (fluoxetine, fluphenazine, and benztropine), alone and in combination with PTX. All images are taken at magnification of 400×. Scale bar 50 µm. FLUOX: fluoxetine; FLUPH: fluphenazine; BENZ: benztropine

The results regarding Ki67, cleaved-PARP, and NF-kB p65 expression in MCF-7 cells are summarized in Figure 146. Results about PPT1, P-gp, and MRP-2 expression in MCF-7 cells treated with antineoplastic and repurposed drugs are summarized in Figure 147.

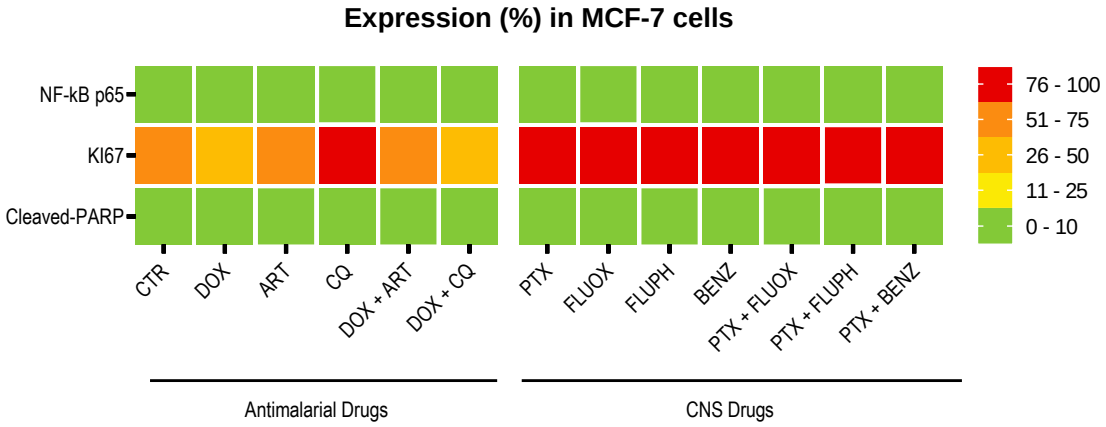

Figure 146. Heat map showing the percentage of positive cells for Ki67, cleaved-PARP and NF-kB p65 for all the conditions tested. MCF-7 cells were treated with antineoplastic (DOX and PTX) and repurposed drugs (artesunate, chloroquine, fluoxetine, fluphenazine, and benztropine), both alone and in combination. The color key represents the percentage of positive cells for each marker. ART: artesunate; CQ: chloroquine; FLUOX: fluoxetine; FLUPH: fluphenazine; BENZ: benztropine

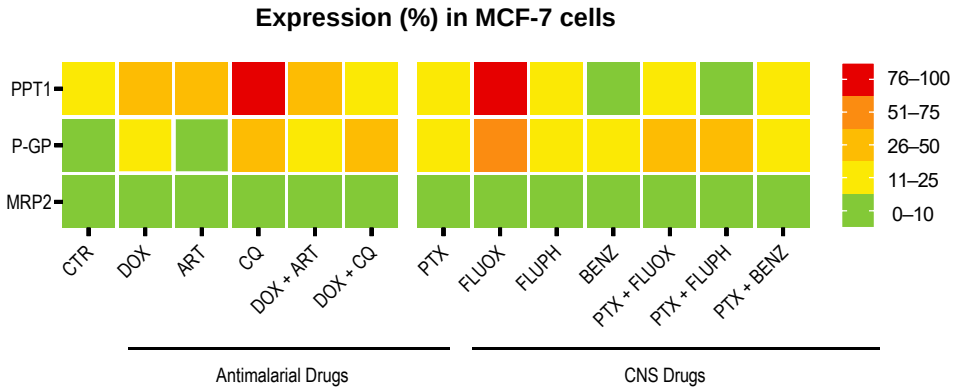

Figure 147. Heat map showing the percentage of positive cells for PPT1, P-gp, and MRP-2 for all the conditions tested. MCF-7 cells were treated with antineoplastic (DOX and PTX) and repurposed drugs (artesunate, chloroquine, fluoxetine, fluphenazine, and benztropine), both alone and in combination. The color key represents the percentage of positive cells for each marker. ART: artesunate; CQ: chloroquine; FLUOX: fluoxetine; FLUPH: fluphenazine; BENZ: benztropine

5.2.2 HT-29 results

Next, it was evaluated the expression of Ki67, cleaved-PARP, and NF-kB p65 markers in HT-29 cells treated with a combination of 5-FU plus the CNS drugs thioridazine and sertraline (Figure 148). In HT-29 control cells, it was found an abundant nuclear expression (76–100%) of Ki67. Except for the treatment of HT-29 cells with 5-FU, all conditions demonstrated a similar percentage of Ki67 positive cells to the control (Figure 148). Treatment with the antineoplastic drug 5-FU induced a reduction in cell viability, as demonstrated by a decrease (26–50%) in Ki67 expression (Figure 148).

It was not found significant changes in cleaved-PARP and NF-kB p65 expression among treatments with single and combined drugs, with the expression of both markers being negative or <1% (Figure 148).

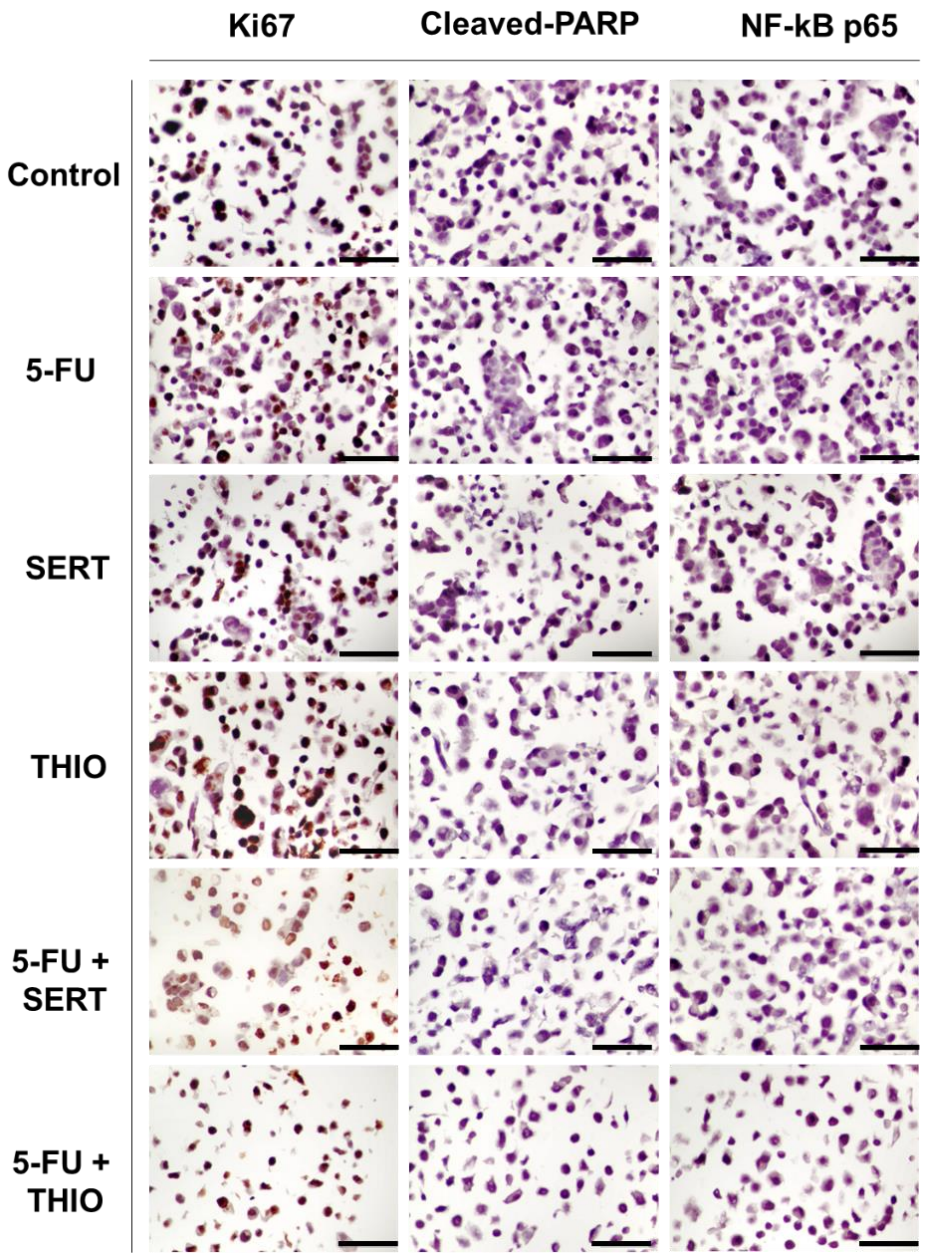

Figure 148. Representative IHC images for Ki67, cleaved-PARP, and NF-kB p65 expression in HT-29 cells treated with antimalarial drugs (sertraline and thioridazine), alone and in combination with 5-FU. All images are taken at magnification of 400x. Scale bar 50 µm. SERT: sertraline; THIO: thioridazine

Regarding the expression of PPT1, P-gp, and MRP-2 in HT-29 cells treated with a combination of 5-FU plus CNS drugs thioridazine and sertraline (Figure 149), it was found high (51–75%) expression of PPT1 in HT-29 control cells (Figure 149). Interestingly, treatments with single drugs and in combination seemed to inhibit this enzyme, with almost no HT-29 cells expressing this protein. Results regarding MRP-2 and P-gp expression demonstrated these proteins were not expressed in these cells in any treatment (Figure 149).

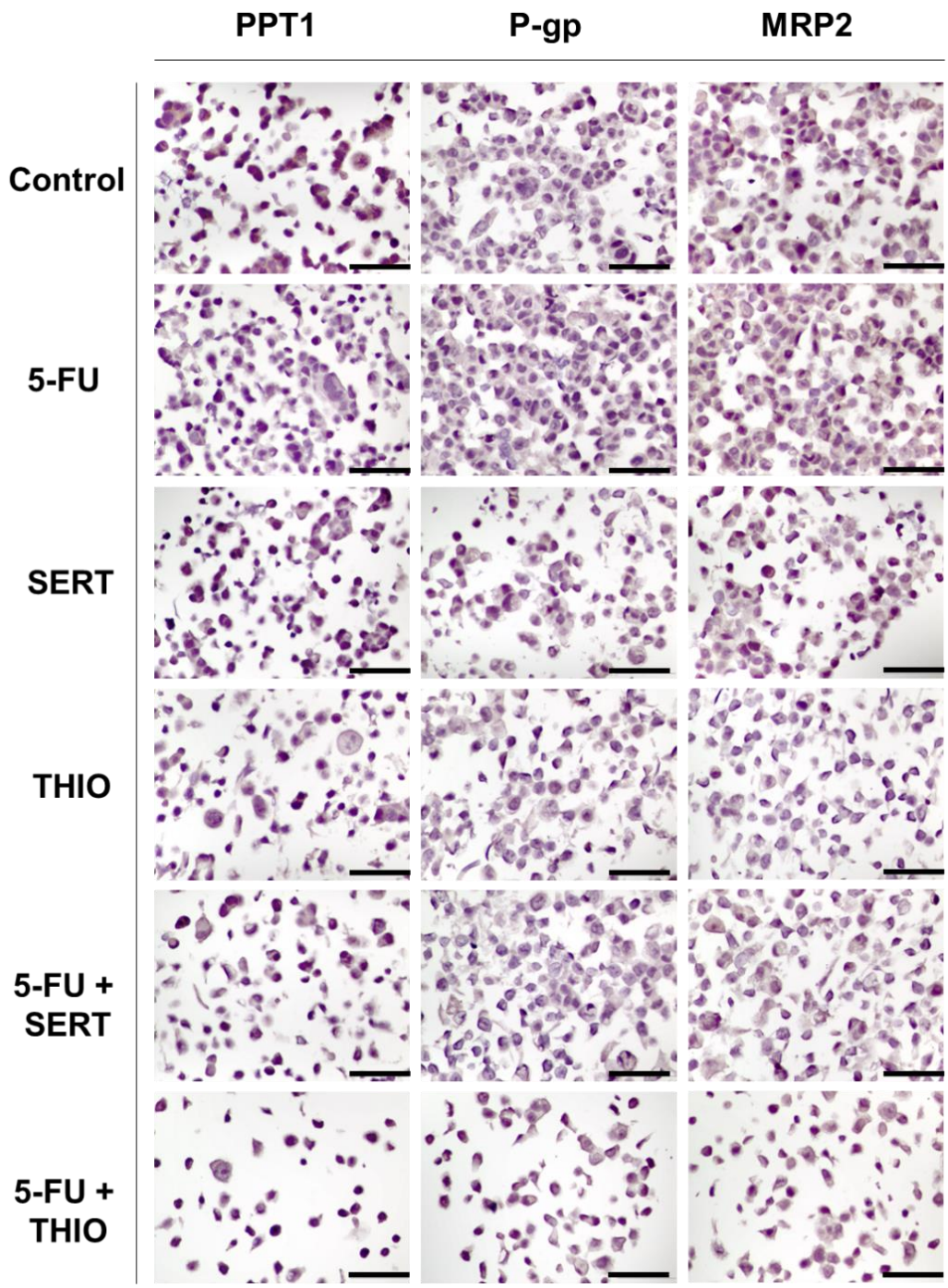

Figure 149. Representative IHC images for PPT1, P-gp, and MRP2 expression in HT-29 cells treated with antimalarial drugs (SERT and THIO), alone and in combination with 5-FU. All images are taken at a magnification of 400×. Scale bar 50 µm. SERT: sertraline; THIO: thioridazine

The results regarding Ki67, cleaved-PARP, and NF-kB p65 expression in HT-29 cells are summarized in Figure 150. Results about PPT1, P-gp, and MRP-2 expression in HT-29 cells treated with antineoplastic and repurposed drugs are summarized in Figure 151.

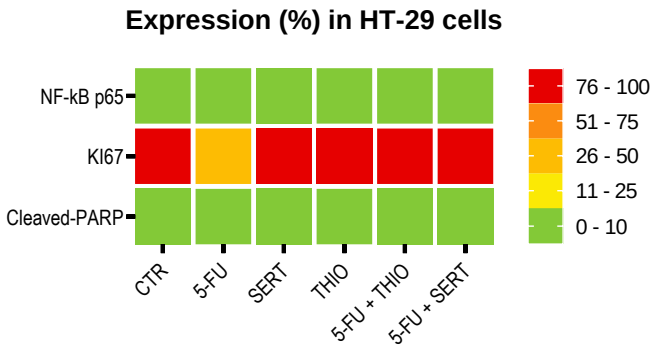

Figure 150. Heat map showing the percentage of positive cells for Ki67, cleaved-PARP and NF-kB p65 for all the conditions tested. HT-29 cells were treated with antineoplastic (5-FU) and repurposed drugs (sertraline and thioridazine), both alone and in combination. The color key represents the percentage of positive cells for each marker. SERT: sertraline; THIO: thioridazine

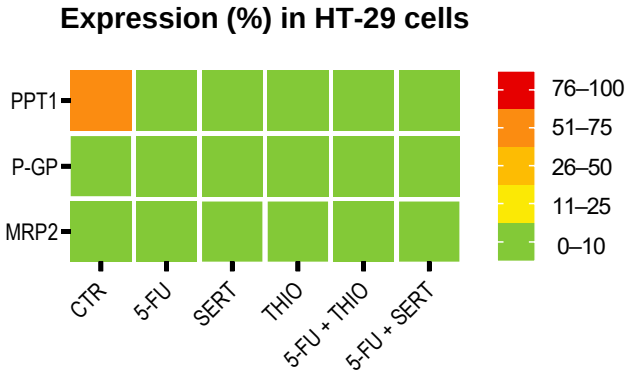

Figure 151. Heat map showing the percentage of positive cells for PPT1, P-gp, and MRP-2 for all the conditions tested. HT-29 cells were treated with antineoplastic (5-FU) and repurposed drugs (sertraline and thioridazine), both alone and in combination. The color key represents the percentage of positive cells for each marker. SERT: sertraline; THIO: thioridazine

We have suggested in a prospective study that other antimalarial agents besides chloroquine, may interact with PPT1 and therefore inhibit the mTOR signaling and the autophagic flux [545]. In that study, our group hypothesized that PPT1 inhibition by antimalarial drugs could result in changes in the lysosomal metabolism that contribute to less accumulation of antineoplastic drugs in lysosomes, increasing the bioavailability of the antineoplastic agents. Indeed, several studies indicate that doxorubicin co-localizes with lysosomes and autophagosomes in breast cells resistant to doxorubicin [559]. Furthermore, it was found that inhibitors of lysosomal function such as chloroquine potentiate the anticancer effect of doxorubicin in hepatic cancer cells [560]. Moreover, it was also demonstrated that paclitaxel inhibits endosomal-lysosomal membrane trafficking, by

inducing early accumulation of protein and endocytic markers in endosomes and later accumulation in a subdomain of lysosomes [561]. Other studies demonstrated that enhanced lysosomal function is responsible for paclitaxel resistance in cancer cells and that this drug resistance can be reverted using artesunate or other inhibitors of lysosomal function [562]. Similar findings were reported in relation to 5-FU, where the inhibition of the autophagy process, either by chloroquine or lysosomal photodamage, contributed to increased sensitivity of pancreatic cancer cells to 5-FU [563].

Here, we demonstrated that not only antimalarial drugs but also CNS drugs can target PPT1 and inhibit this protein. To explain the synergistic effect among antineoplastic and repurposed drugs in breast and colon cancer cells, we propose that (1) antineoplastic drugs such as 5-FU, PTX, and DOX inhibit autophagy, resulting in cell death; nevertheless, some cells resist autophagy and survive, leading to cancer progression (2) the repurposed drugs affect lysosomal metabolism, mainly through the inhibition of the PPT1 enzyme and consequently mTOR, helping decrease the accumulation of the antineoplastic drug in the lysosomes and consequently reducing the chance of drug resistance, enhancing their bioavailability, and increasing the antitumor effect of these drugs.

6. CONCLUSION OF CHAPTER V

Our research group has been exploring the strategies of drug repurposing and drug combination as they represent a novel way to identify new potential candidates for cancer therapy. We make use of repurposed drugs, i.e., drugs already available on the market for other diseases than the original indication, and combine them with drugs already used in cancer therapy (antineoplastic agents) [67]. These strategies are advantageous as repurposed drugs have pharmacokinetics, pharmacodynamics, and toxicological profiles that are well established, making it easy for their approval for novel indications [487]. At the same time, if the combination with antineoplastic agents enhances their anticancer activity, it allows decreasing the therapeutical dose needed for the treatment and consequently the side effects [488]. We have been studying the repurposing of antimalarial and CNS drugs for breast and colon cancer and have already found promising drug pairs for colon and breast cancer. Previously, we have combined different antimalarial drugs with 5-FU for the colon and with DOX and PTX for breast cancer therapy [489, 490]. Regarding the CNS drugs class, we have already tested the combination of these agents with 5-FU in HT-29 colon and with PTX in MCF-7 breast cancer cells. These studies aimed to evaluate if these drugs showed anticancer activity and mainly if their combination with antineoplastic drugs would enhance their cytotoxic effect on these cells. Collectively, we have found DOX + artesunate, DOX + chloroquine, PTX + fluoxetine, PTX + fluphenazine, and PTX + benztropine to be the most promising combinations for breast cancer therapy [489, 490]. For colon cancer cells, we found 5-FU+thioridazine and 5-FU+sertraline to be the most effective drug pairs to reduce cell viability [489].

Next, we compiled all results from our previous combination models with antimalarial and CNS drugs in HT-29 and MCF-7 cells and selected the most promising drug pairs to evaluate if these treatments resulted in changes in the expression of some EMT biomarkers such as E-cadherin, P-cadherin, vimentin, and β-catenin. The EMT is a process usually associated with cancer progression, where cells lose their epithelial features and acquire mesenchymal characteristics [564]. This phenomenon allows the cells to gain mobility and migrate from the primary tumor site, resulting in metastases. Different studies already suggested that EMT is linked to cancer progression [495–500]. TGF-β is involved in the regulation of cell proliferation and regulates the EMT by suppressing epithelial cells, leading to the loss of E-cadherin, an epithelial protein, while increasing the expression of mesenchymal biomarkers such as vimentin [565]. P-cadherin is another EMT biomarker that is usually co-expressed with E-cadherin and associated with poor prognosis, being associated with tumors with high metastatic potential [566]. On the other hand, β-catenin is usually overexpressed in more advanced staged cancers [567]. Vimentin is another protein

that is overexpressed in mesenchymal cells and its increased expression is associated with malignancy and metastasis [568].

Generally, the findings presented in this chapter demonstrate that the most promising combination treatments resulted in increased expression of E-cadherin and reduced expression of vimentin, β-catenin, and P-cadherin when compared to control cells, in both cell lines, which is indicative of a reversal in EMT, with cells expressing a typical profile of epithelial cells (Figure 152). Collectively, these results support that combination therapies can help reduce cell malignancy.

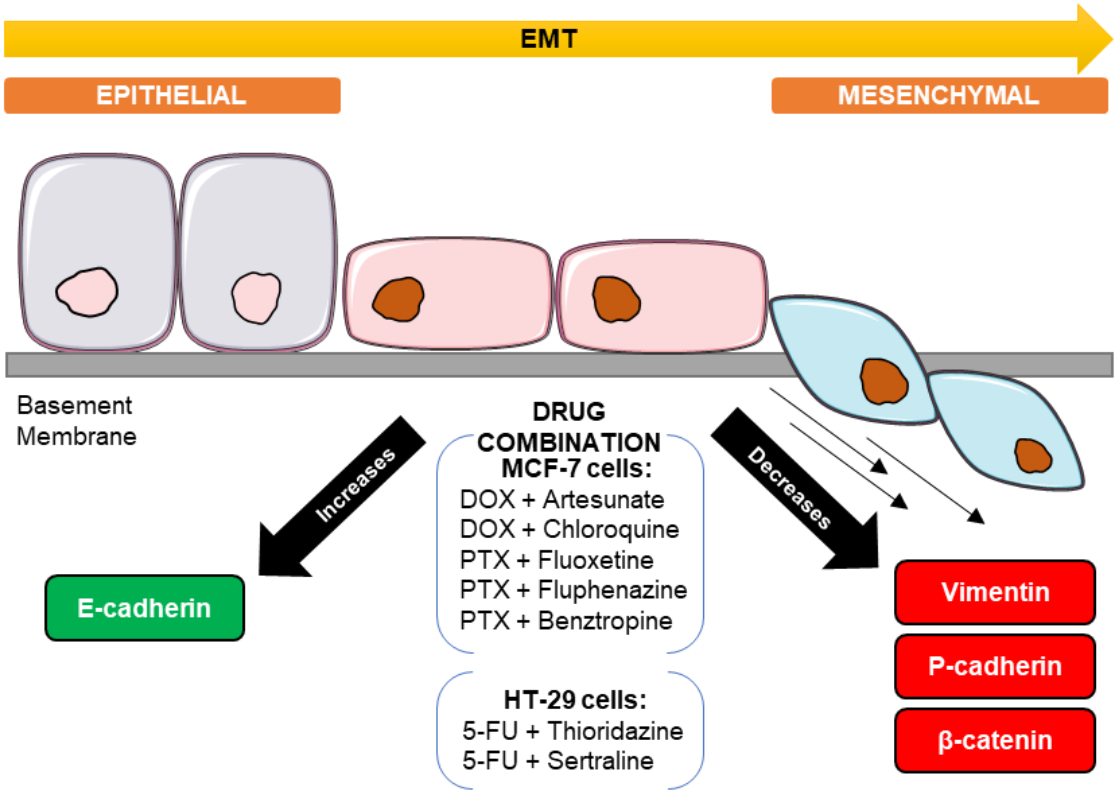

Figure 152. Main findings regarding the evaluation of the effect of the most promising drug combinations on EMT proteins. These findings demonstrate that combination treatments increase E-cadherin expression while reducing P-cadherin, vimentin, and β-catenin, suggesting that these treatments could induce EMT reversal.

Moreover, these results also demonstrate that PPT1 might be involved in the mechanism of action of the aforementioned drug combinations and demonstrate that both antimalarial and CNS drugs in combination with chemotherapeutic agents can decrease the PPT1 expression in MCF-7 breast and HT-29 colon cell lines. These results suggest that PPT1 may be a target not only of antimalarial drugs, as already described in previous studies, but also of CNS drugs, both alone and in combination. We propose a model for the action of these combination therapies in breast and colon cancer in which the antineoplastic

drugs inhibit autophagy, resulting in cell death, with the simultaneous targeting of PPT1 by the repurposed drugs, leading to mTOR inactivation and consequently decreasing the cellular protein synthesis and cancer cell growth (Figure 153).

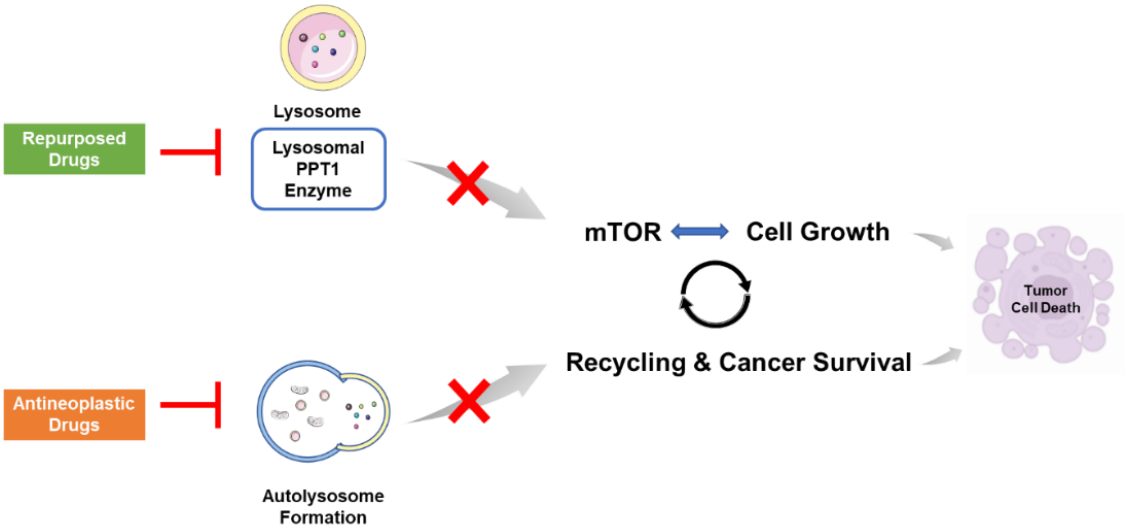

Figure 153. Proposed model for the action of combination therapies using repurposed and antineoplastic drugs in PPT1, a lysosomal enzyme. Antineoplastic drugs such as 5-FU, PTX, and DOX can inhibit autophagy, resulting in cell death. Nevertheless, some cells can be resistant to autophagy and survive, leading to cancer progression. Combination with repurposed drugs can generate a deeper response by inhibiting PPT1. This inhibition leads to mTOR inactivation, decreasing cellular protein synthesis and cell growth.

FUTURE PERSPECTIVES

The results obtained in this study provide compelling evidence for the pharmacological potential of drug combinations involving repurposed drug and antineoplastic agents in the field of oncology, specifically for the treatment of breast and colon cancer. Over the last four years, extensive research has been conducted, yielding promising outcomes that pave the way for further investigation in more advanced animal models and even in future clinical trials. However, deeper mechanistic studies are strongly recommended in the future to evaluate the anticancer mechanisms behind these drug combinations. These experiments should also be performed in other types of cancer, such as pancreatic, prostate, lung, etc., and further confirmed on animal models and clinal trials.

These findings also suggest that the continuation of this research in sophisticated animal models holds great promise for eventual application and testing in clinical settings. To ensure the most optimized implementation of these findings, researchers may employ in silico tools, which allow for the fine-tuning of therapeutic doses and the prediction of expected tumor regression in these specific study models. Moreover, these studies have the potential to shed light on the pharmacokinetic parameters associated with these drug combinations, both in animal models and in patients with the disease. Understanding the pharmacological behavior of these combinations in different contexts can aid in the development of more effective treatment strategies and improve patient outcomes.

By leveraging the insights gained from this research, clinicians and scientists can potentially identify novel therapeutic approaches that harness the benefits of repurposed drugs and antineoplastics. Ultimately, this may lead to the development of innovative and personalized oncology therapies, bringing new hope to individuals affected by breast and colon cancer.

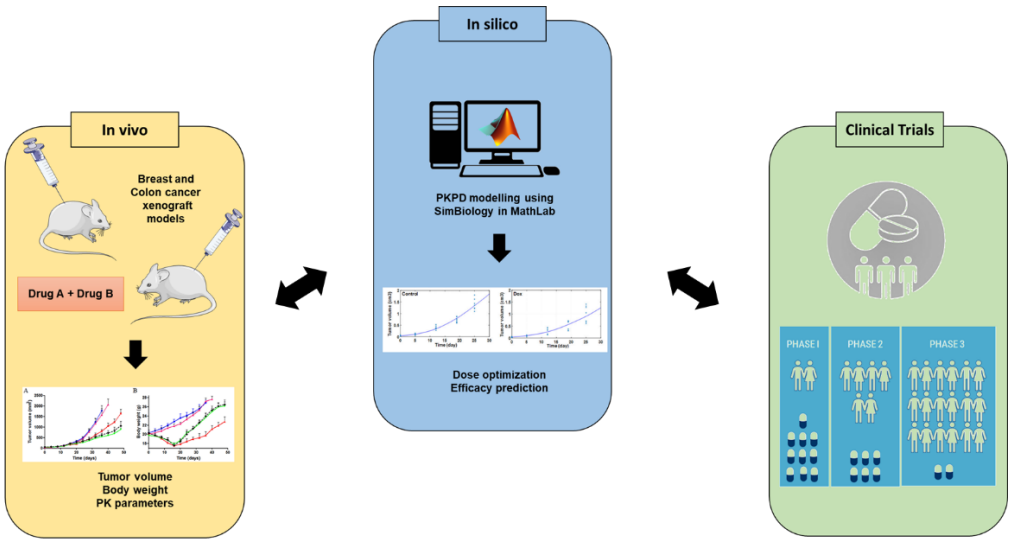

Figure 154. Representation of the potential avenues of exploration within the scope of this doctoral thesis.

SUPPLEMENTARY MATERIAL

CHAPTER I

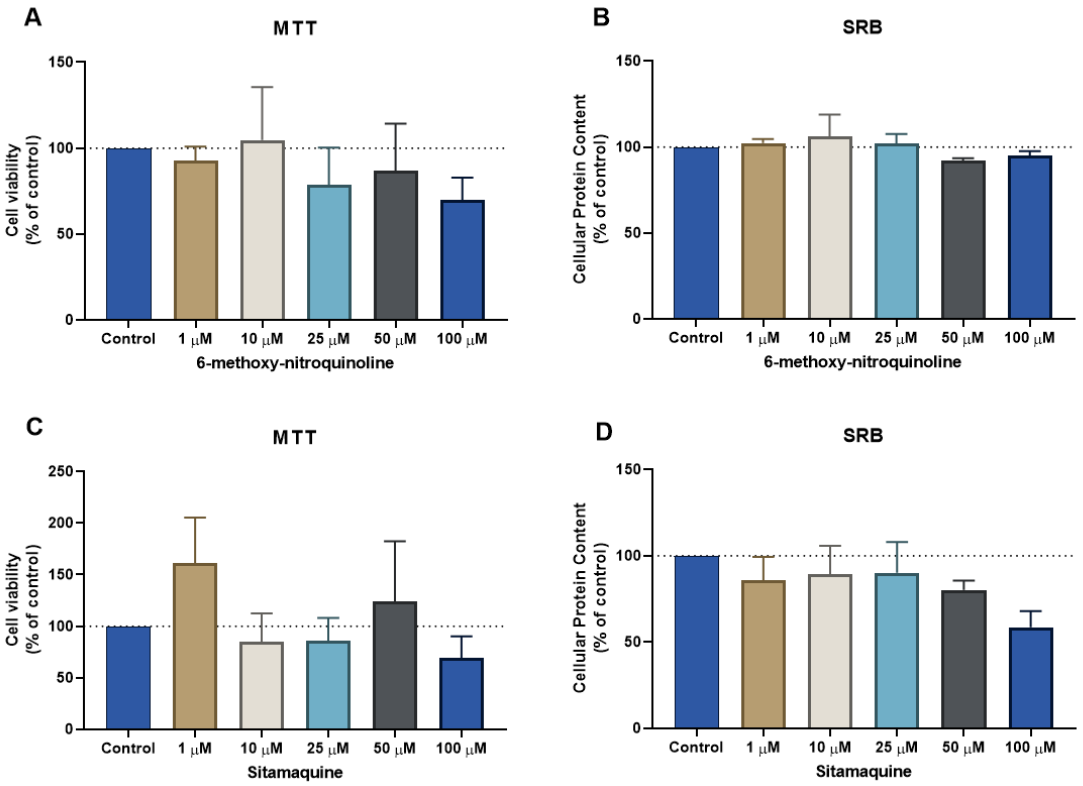

Figure S1. Effects of some antimalarial quinolinic derivates on MCF-7 cells. (**A**) Effect of 6-methoxy-nitroquinoline in cell viability and (**B**) protein content. (**C**) Effect of sitamaquine in cell viability and (**D**) protein content. Cells were cultured in the presence of increasing concentrations of each drug. After 48 h MTT and SRB assays were performed to measure cellular viability as well as protein content. Values are expressed in percentage and represent mean ± SEM. Each experiment was done three times independently (n = 3).

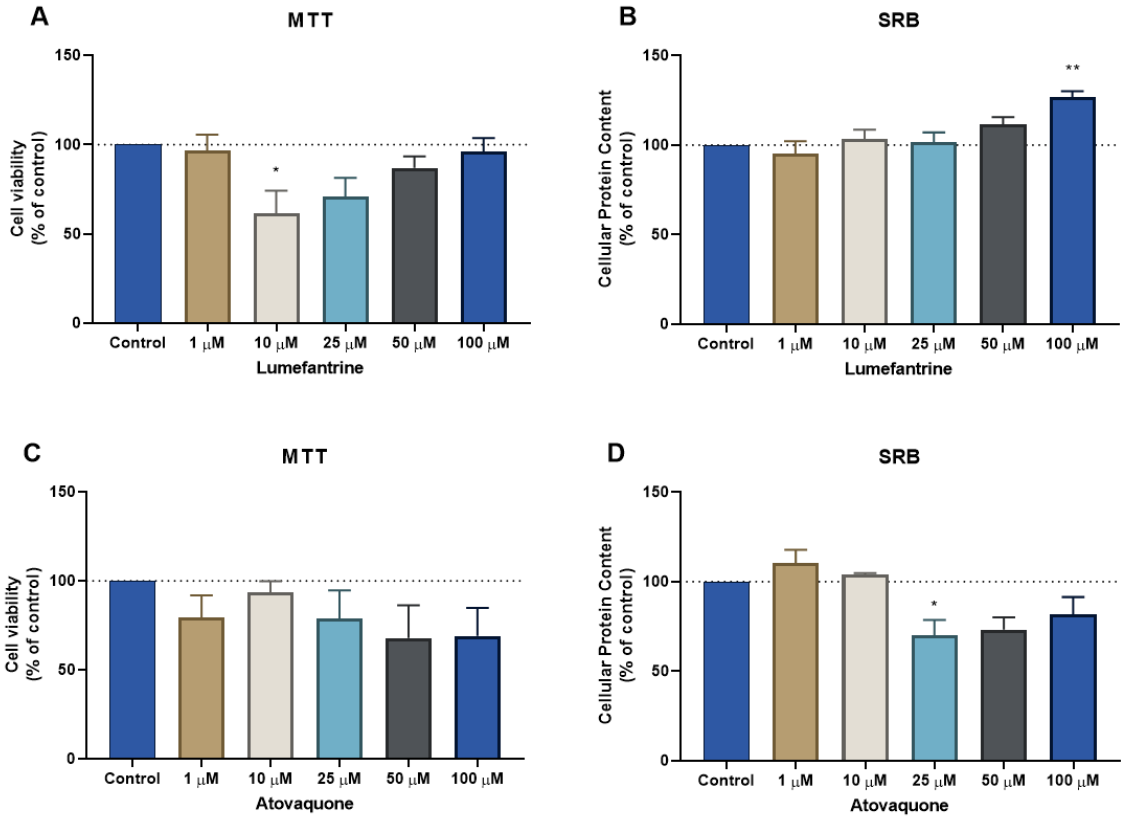

Figure S2. Effects of some antimalarial non-quinolinic derivates on MCF-7 cells. (**A**) Effect of lumefantrine in cell viability and (**B**) protein content. (**C**) Effect of atovaquone in cell viability and (**D**) protein content. Cells were cultured in the presence of increasing concentrations of each drug. After 48 h MTT and SRB assays were performed to measure cellular viability as well as protein content. Values are expressed in percentage and represent mean ± SEM. Each experiment was done three times independently (n = 3). * statistically significant vs. control at $p < 0.05$. ** statistically significant vs. control at $p < 0.01$.

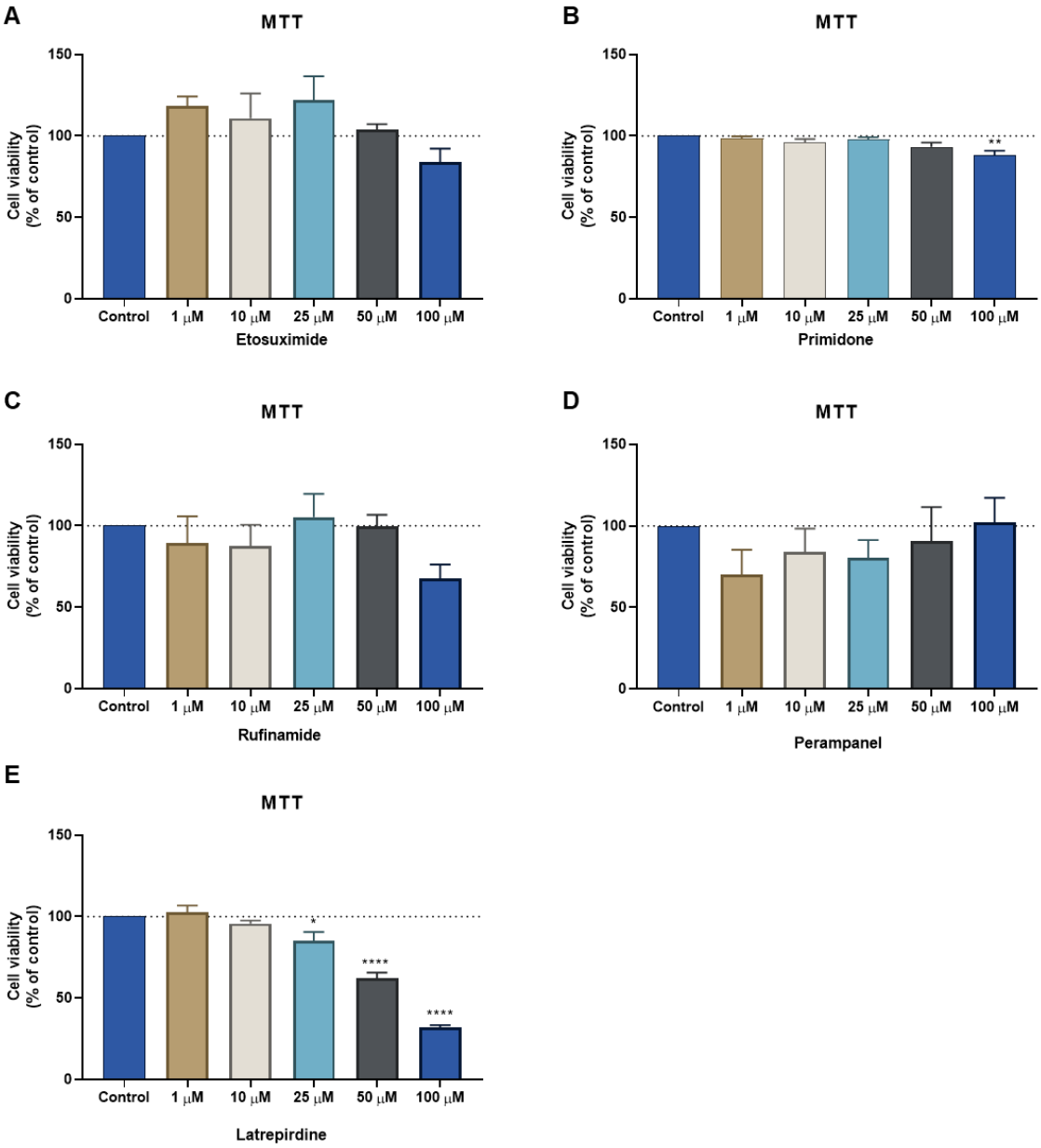

Figure S3. Effects of the CNS drugs (**A**) ethosuximide, (**B**) primidone, (**C**) rufinamide, (**D**) perampanel and (**E**) latrepirdine on MCF-7 cells. Cells were cultured in the presence of increasing concentrations of the drug and after 48 h, the MTT assay was performed to measure cellular viability. Values are expressed in percentage of control and represent mean ± SEM. Each experiment was done three times independently (n = 3); * statistically significant vs. control at $p < 0.05$. ** statistically significant vs. control at $p < 0.01$. **** statistically significant vs. control at $p < 0.0001$.

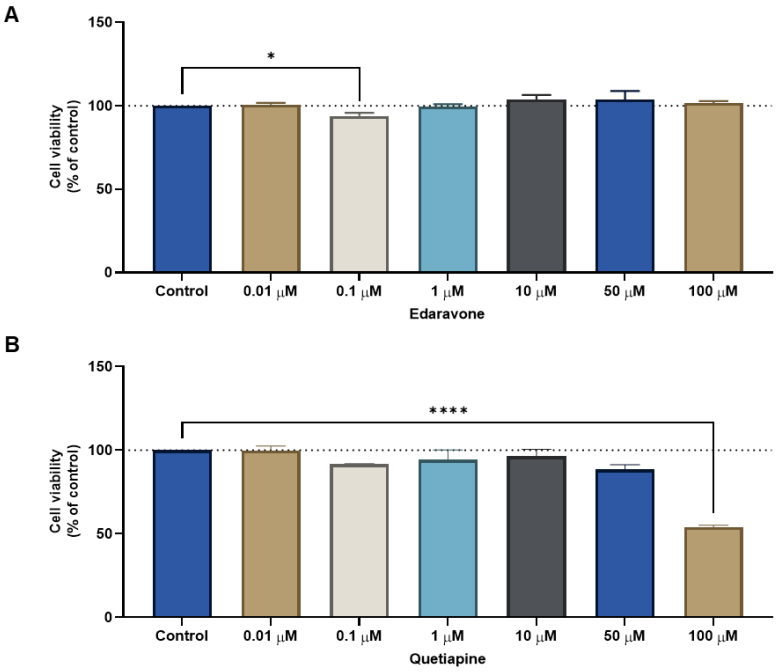

Figure S4. Cytotoxic effects of the CNS drugs (**A**) edaravone and (**B**) quetiapine on MCF-7 cells. Cells were cultured in the presence of increasing concentrations of the drug and after 48 h, the MTT assay was performed to measure cellular viability. Values are expressed in percentage of control and represent mean ± SEM. Each experiment was done three times independently (n = 3); * statistically significant vs. control at $p < 0.05$. **** statistically significant vs. control at $p < 0.0001$.

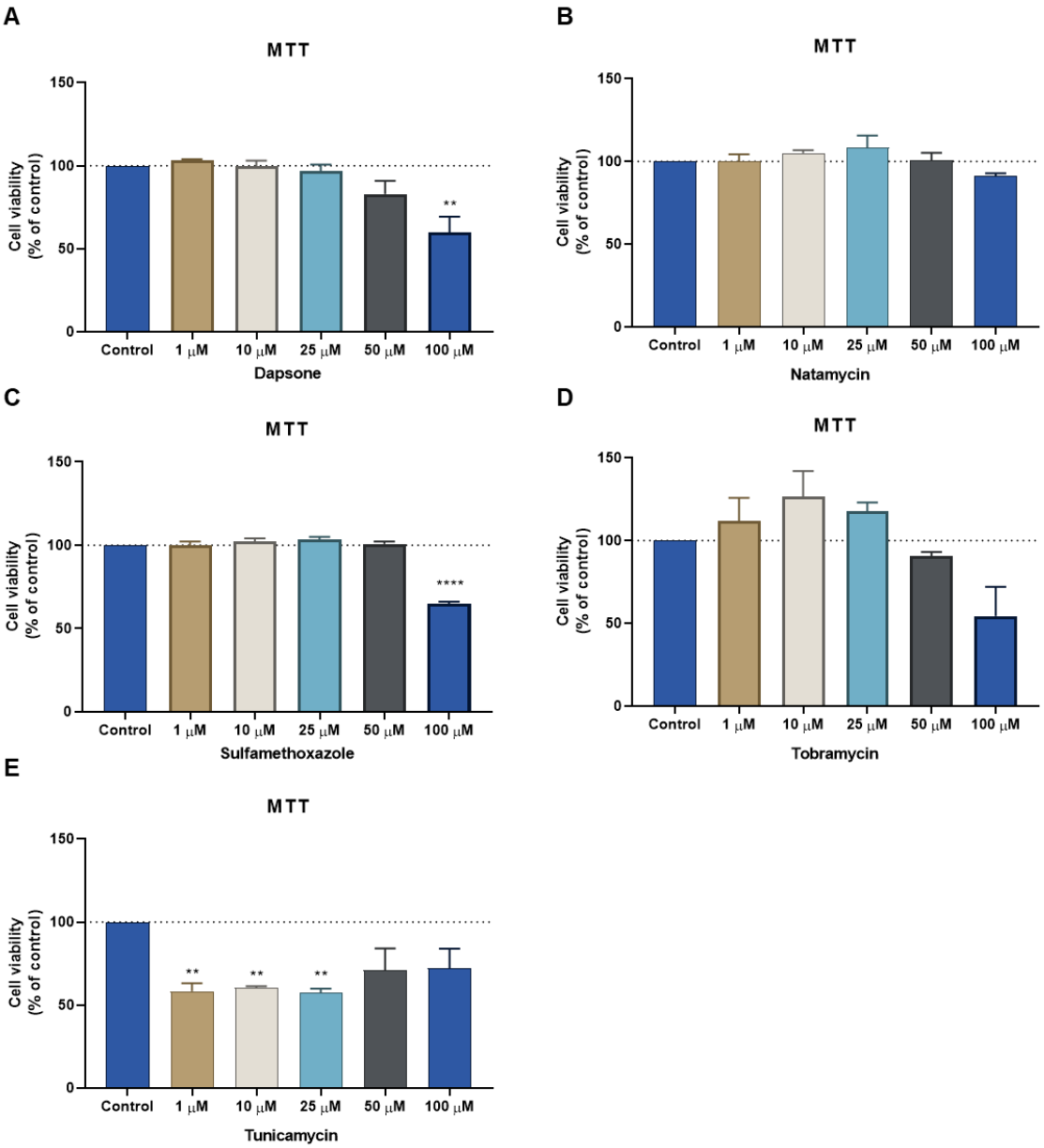

Figure S5. Cytotoxic effects of the antibiotic/antifungal drugs (**A**) dapsone, (**B**) natamycin, (**C**) sulfamethoxazole, (**D**) tobramycin and (**E**) tunicamycin on MCF-7 cells. Cells were cultured in the presence of increasing concentrations of the drug and after 48 h, the MTT assay was performed to measure cellular viability. Values are expressed in percentage of control and represent mean ± SEM. Each experiment was done three times independently (n = 3); ** statistically significant vs. control at $p < 0.01$. **** statistically significant vs. control at $p < 0.0001$.

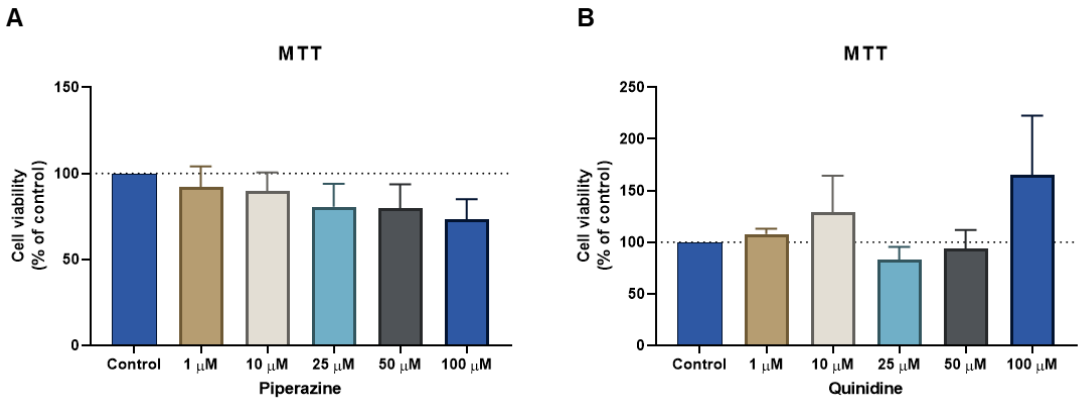

Figure S6. Cytotoxic effects of (**A**) piperazine and (**B**) quinidine on MCF-7 cells. Cells were cultured in the presence of increasing concentrations of the drug and after 48 h, the MTT assay was performed to measure cellular viability. Values are expressed in percentage of control and represent mean ± SEM. Each experiment was done three times independently (*n* = 3).

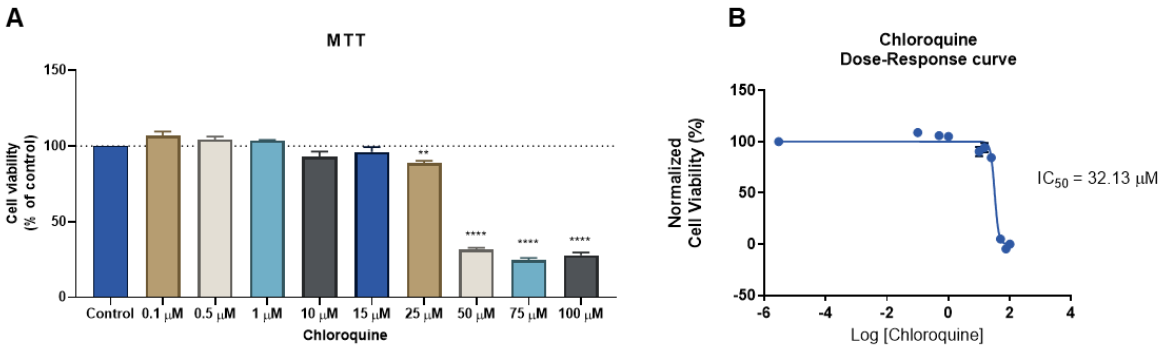

Figure S7. Effects of chloroquine on HT-29 cells. (**A**) Effect of chloroquine in cell viability and (**B**) dose-response curve. Cells were cultured in the presence of increasing concentrations of the drug and after 48 h, the MTT assay was performed to measure cellular viability. Values are expressed in percentage of control and represent mean ± SEM. Each experiment was done three times independently (*n* = 3); ** statistically significant vs. control at $p < 0.01$. **** statistically significant vs. control at $p < 0.0001$.

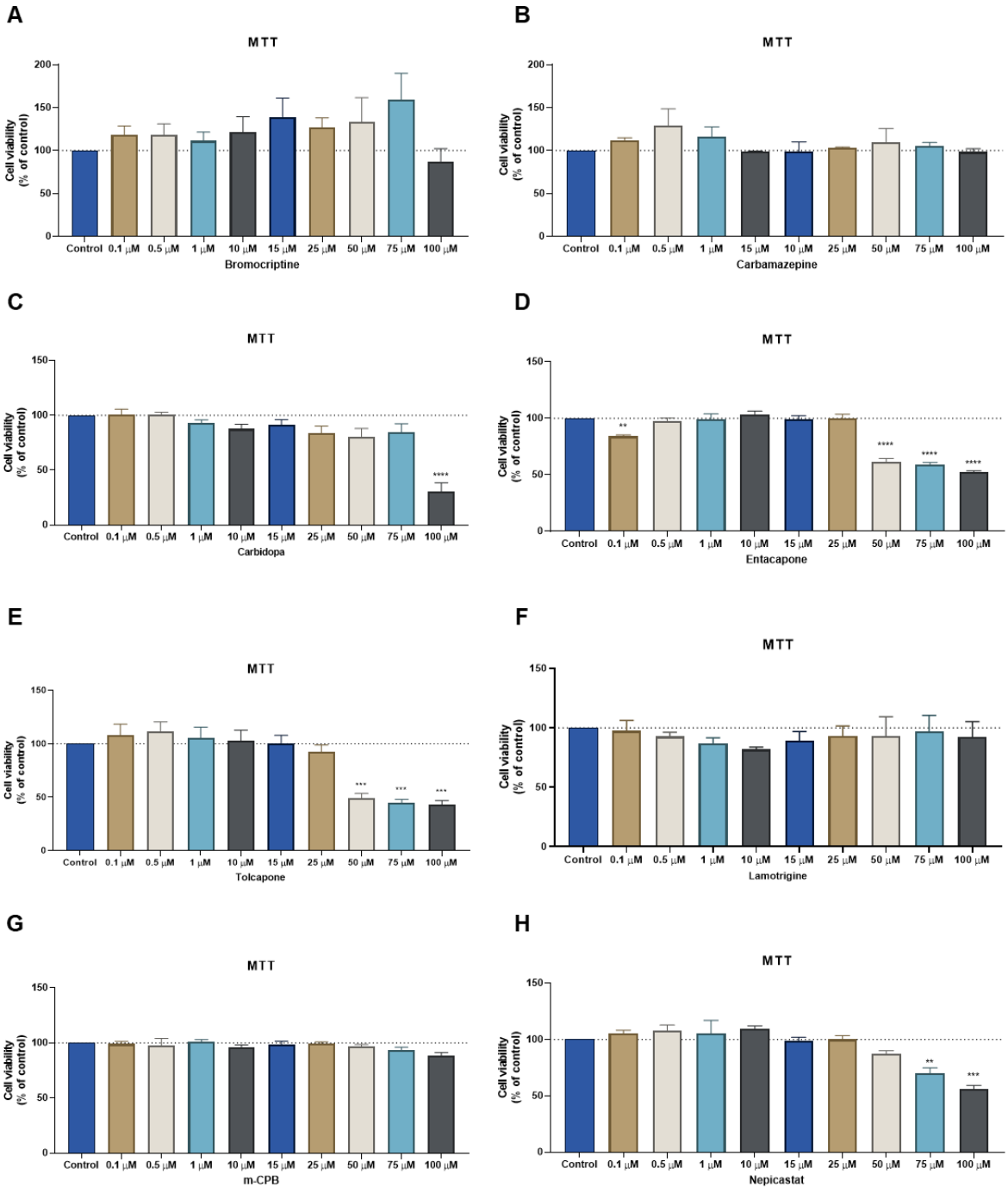

Figure S8. Cytotoxic effects of the CNS drugs (**A**) bromocriptine, (**B**) carbamazepine, (**C**) carbidopa, (**D**) entacapone, (**E**) tolcapone, (**F**) lamotrigine, (**G**) m-CPB and (**H**) nepicastat on HT-29 cells. Cells were cultured in the presence of increasing concentrations of the drug and after 48 h, the MTT assay was performed to measure cellular viability. Values are expressed in percentage of control and represent mean ± SEM. Each experiment was done three times independently (n = 3); ** statistically significant vs. control at $p < 0.01$. *** statistically significant vs. control at $p < 0.001$. **** statistically significant vs. control at $p < 0.0001$.

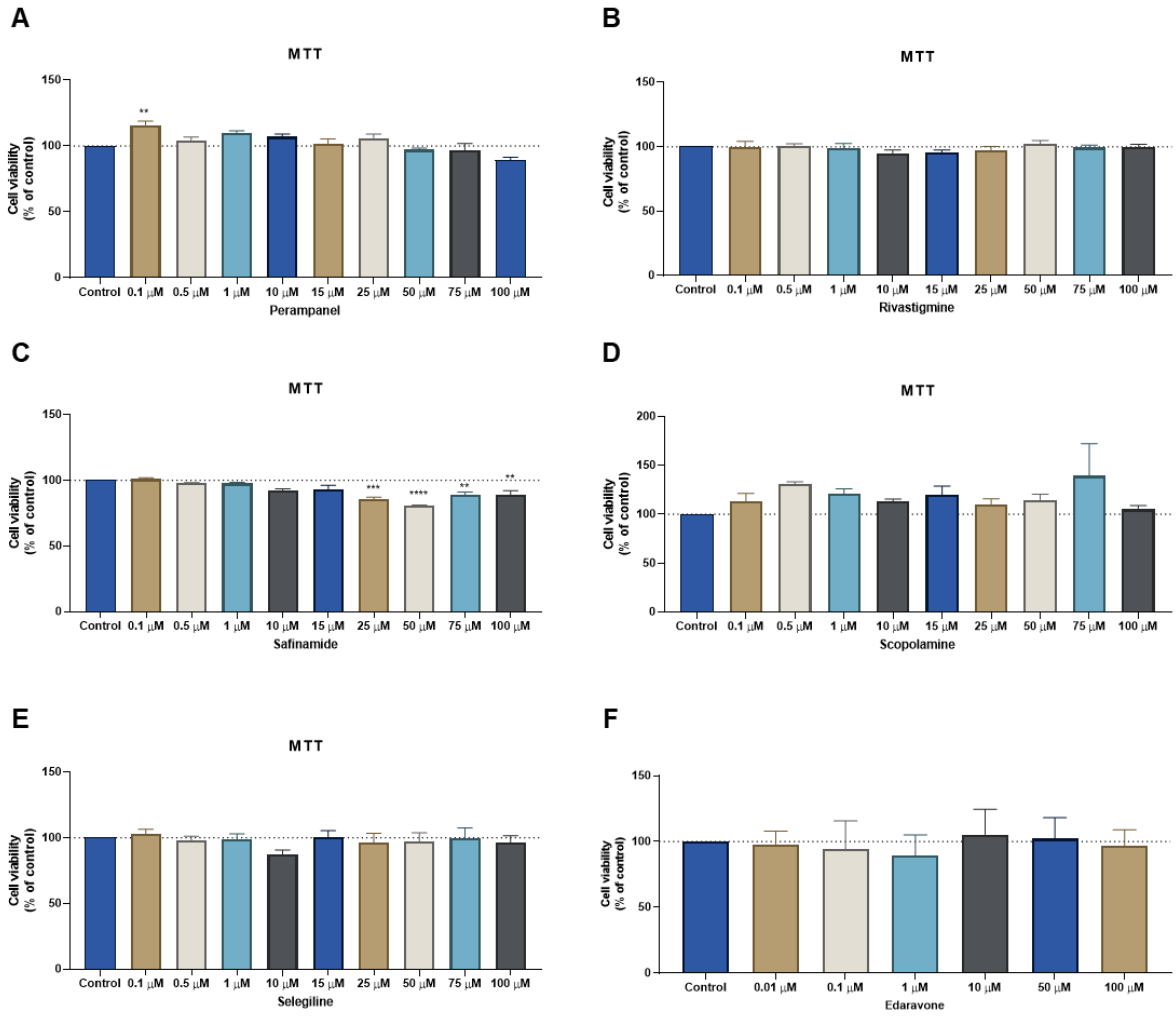

Figure S9. Cytotoxic effects of the CNS drugs (**A**) perampanel, (**B**) rivastigmine, (**C**) safinamide, (**D**) scopolamine, (**E**) selegiline and (**F**) edaravone on HT-29 cells. Cells were cultured in the presence of increasing concentrations of the drug and after 48 h, the MTT assay was performed to measure cellular viability. Values are expressed in percentage of control and represent mean ± SEM. Each experiment was done three times independently ($n = 3$); ** statistically significant vs. control at $p < 0.01$. *** statistically significant vs. control at $p < 0.001$. **** statistically significant vs. control at $p < 0.0001$.

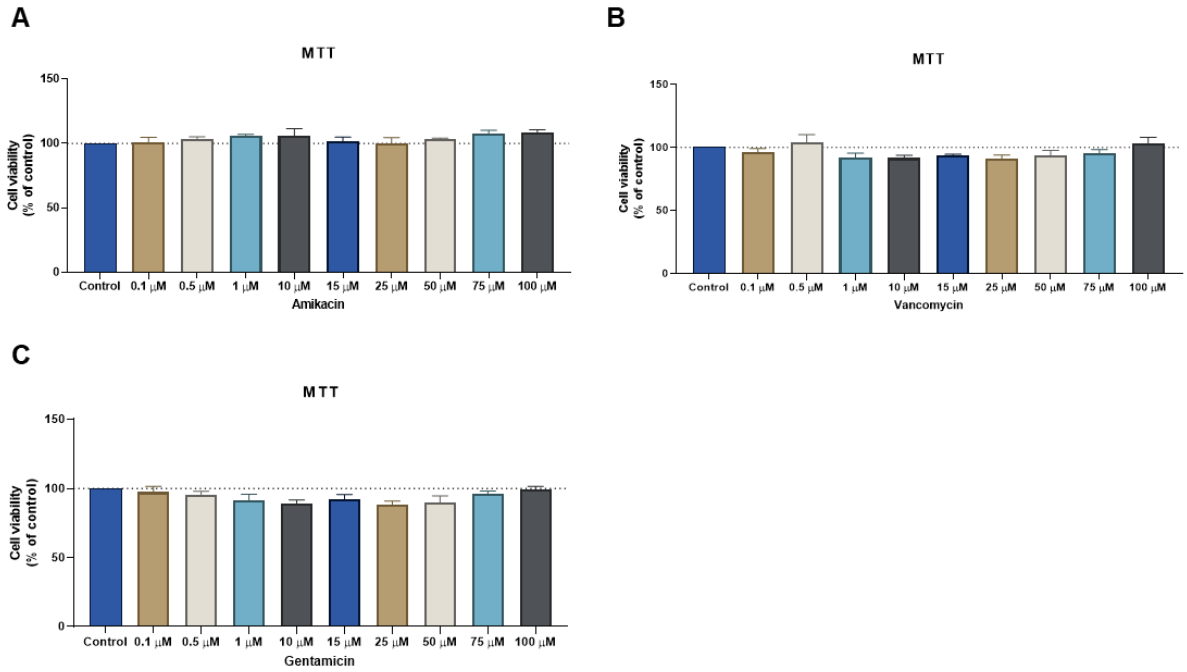

Figure S10. Cytotoxic effects of the antibiotic drugs (**A**) amikacin, (**B**) vancomycin and (**C**) gentamicin on HT-29 cells. Cells were cultured in the presence of increasing concentrations of the drug and after 48 h, the MTT assay was performed to measure cellular viability. Values are expressed in percentage of control and represent mean ± SEM. Each experiment was done three times independently (*n* = 3).

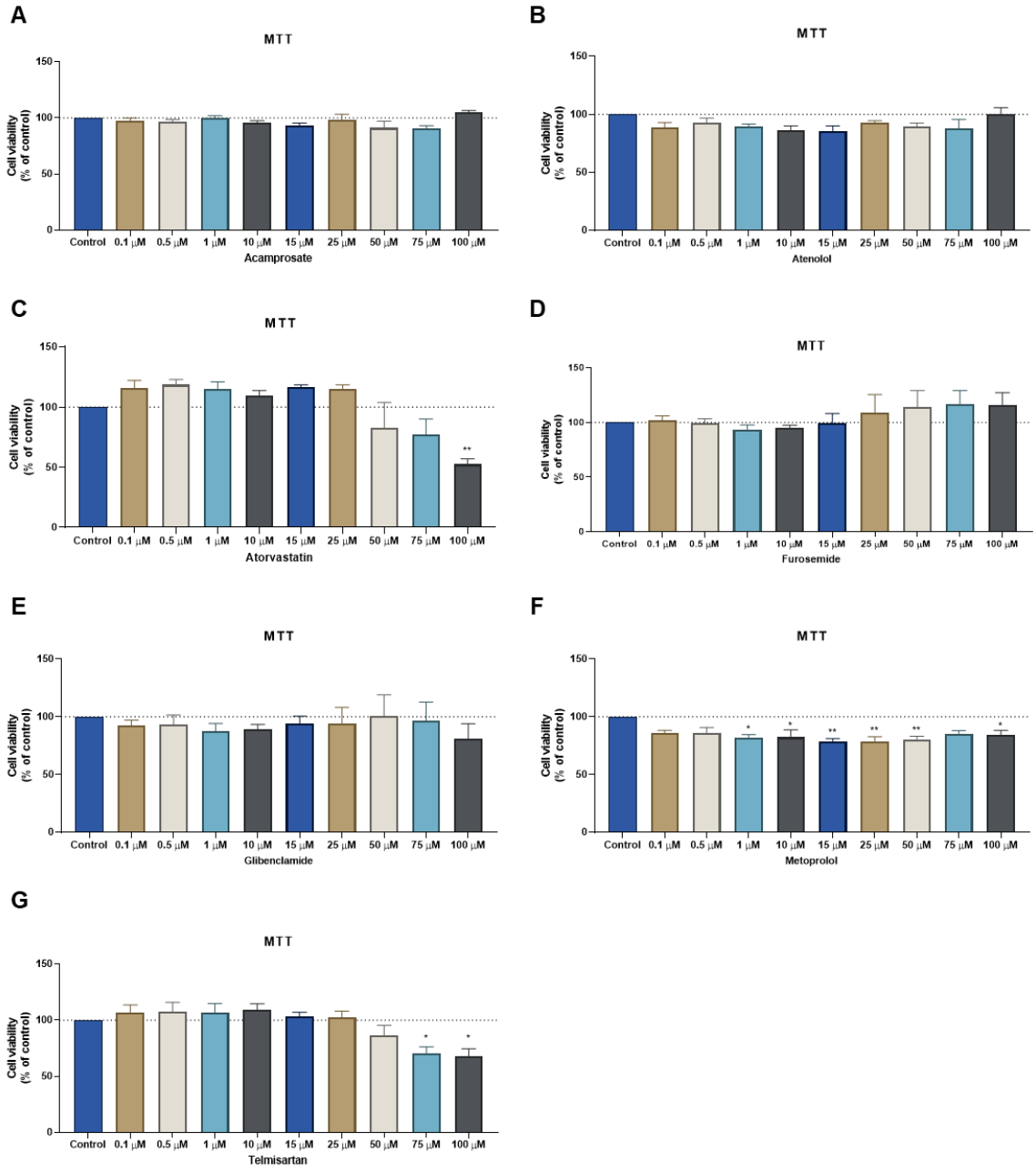

Figure S11. Cytotoxic effects of (**A**) acamprosate, (**B**) atenolol, (**C**) atorvastatin, (**D**) furosemide, (**E**) glibenclamide, (**F**) metoprolol and (**G**) telmisartan on HT-29 cells. Cells were cultured in the presence of increasing concentrations of the drug and after 48 h, the MTT assay was performed to measure cellular viability. Values are expressed in percentage of control and represent mean ± SEM. Each experiment was done three times independently (n = 3); * statistically significant vs. control at $p < 0.05$. ** statistically significant vs. control at $p < 0.01$.

REFERENCES

[1] Siegel RL, Miller KD, Fuchs HE, et al. Cancer statistics, 2022. *CA Cancer J Clin* 2022; 72: 7–33.

[2] Siegel RL, Miller KD, Jemal A. Cancer statistics, 2018. *CA Cancer J Clin* 2018; 68: 7–30.

[3] Weiss JR, Moysich KB, Swede H. Epidemiology of male breast cancer. *Cancer Epidemiol Biomarkers Prev* 2005; 14: 20–6.

[4] Tinoco G, Warsch S, Glück S, et al. Treating Breast Cancer in the 21st Century: Emerging Biological Therapies. *J Cancer* 2013; 4: 117–132.

[5] Fearon ER, Vogelstein B. A genetic model for colorectal tumorigenesis. *Cell* 1990; 61: 759–767.

[6] Simon A, Robb K. Cancer: breast. In: *Cambridge Handbook of Psychology, Health and Medicine*. Cambridge University Press, pp. 577–580.

[7] Hanby AM, Walker C. Pathology and Genetics: Tumours of the Breast and Female Genital Organs (WHO Classification of Tumours). *Breast Cancer Res* 2004; 6: 1–2.

[8] Odashiro AN. Cancer Staging. In: *Experimental and Clinical Metastasis*. New York, NY: Springer New York, pp. 275–278.

[9] Malhotra GK, Zhao X, Band H, et al. Histological, molecular and functional subtypes of breast cancers. *Cancer Biol Ther* 2010; 10: 955–960.

[10] Zardavas D, Irrthum A, Swanton C, et al. Clinical management of breast cancer heterogeneity. *Nat Rev Clin Oncol* 2015; 12: 381–394.

[11] Holliday DL, Speirs V. Choosing the right cell line for breast cancer research. *Breast Cancer Res* 2011; 13: 215.

[12] Hu LX, Du YY, Zhang Y, et al. Synergistic effects of exemestane and aspirin on MCF-7 human breast cancer cells. *Asian Pacific J Cancer Prev* 2012; 13: 5903–5908.

[13] Vargo-Gogola T, Rosen JM. Modelling breast cancer: one size does not fit all. *Nat Rev Cancer* 2007; 7: 659–672.

[14] Epstein MS, Lagios MD, Silverstein MJ. Ductal Carcinoma in Situ of the Breast. In: *The Breast*. Elsevier, pp. 562-575.e4.

[15] Choi DS, Rosato RR, Chang JC. Breast Cancer Stem Cells. In: *Molecular Pathology of Breast Cancer*. Cham: Springer International Publishing, pp. 133–151.

[16] Miller E, Lee HJ, Lulla A, et al. Current treatment of early breast cancer: adjuvant and

neoadjuvant therapy. *F1000Research* 2014; 3: 198.

[17] Marcom PK. Breast Cancer. In: *Genomic and Precision Medicine*. Elsevier, pp. 181–194.

[18] National Cancer Institute. Drugs Approved for Breast Cancer - National Cancer Institute. *National Cancer Institute*, https://www.cancer.gov/about-cancer/treatment/drugs/breast (2019, accessed 3 April 2019).

[19] Dear RF, McGeechan K, Jenkins MC, et al. Combination versus sequential single agent chemotherapy for metastatic breast cancer. *Cochrane database Syst Rev* 2013; 2013: CD008792.

[20] Pagani O, Senkus E, Wood W, et al. International Guidelines for Management of Metastatic Breast Cancer: Can Metastatic Breast Cancer Be Cured? *JNCI J Natl Cancer Inst* 2010; 102: 456–463.

[21] Coley HM. Mechanisms and strategies to overcome chemotherapy resistance in metastatic breast cancer. *Cancer Treat Rev* 2008; 34: 378–390.

[22] Stegmeier F, Warmuth M, Sellers WR, et al. Targeted Cancer Therapies in the Twenty-First Century: Lessons From Imatinib. *Clin Pharmacol Ther* 2010; 87: 543–552.

[23] Siegel RL, Miller KD, Goding Sauer A, et al. Colorectal cancer statistics, 2020. *CA Cancer J Clin* 2020; 70: 145–164.

[24] Bray F, Ferlay J, Soerjomataram I, et al. Global cancer statistics 2018: GLOBOCAN estimates of incidence and mortality worldwide for 36 cancers in 185 countries. *CA Cancer J Clin* 2018; 68: 394–424.

[25] Mármol I, Sánchez-de-Diego C, Pradilla Dieste A, et al. Colorectal Carcinoma: A General Overview and Future Perspectives in Colorectal Cancer. *Int J Mol Sci* 2017; 18: 197.

[26] Lynch HT, de la Chapelle A. Hereditary Colorectal Cancer. *N Engl J Med* 2003; 348: 919–932.

[27] Stoffel EM, Kastrinos F. Familial colorectal cancer, beyond lynch syndrome. *Clin Gastroenterol Hepatol* 2014; 12: 1059–1068.

[28] Henrikson NB, Webber EM, Goddard KA, et al. Family history and the natural history of colorectal cancer: systematic review. *Genet Med* 2015; 17: 702–712.

[29] Steele SR, Park GE, Johnson EK, et al. The Impact of Age on Colorectal Cancer

Incidence, Treatment, and Outcomes in an Equal-Access Health Care System. *Dis Colon Rectum* 2014; 57: 303–310.

[30] Brenner H, Kloor M, Pox CP. Colorectal cancer. *Lancet* 2014; 383: 1490–1502.

[31] Conti L, Del Cornò M, Gessani S. Revisiting the impact of lifestyle on colorectal cancer risk in a gender perspective. *Crit Rev Oncol Hematol* 2020; 145: 102834.

[32] Zhu B, Wu X, Wu B, et al. The relationship between diabetes and colorectal cancer prognosis: A meta-analysis based on the cohort studies. *PLoS One* 2017; 12: e0176068.

[33] Rossi M, Usman A, Keshavarzian A, et al. Colorectal Cancer and Alcohol Consumption—Populations to Molecules. *Cancers (Basel)* 2018; 10: 38.

[34] Akter S, Islam Z, Mizoue T, et al. Smoking and colorectal cancer: A pooled analysis of 10 population-based cohort studies in Japan. *Int J Cancer* 2021; 148: 654–664.

[35] Simon MS, Thomson CA, Pettijohn E, et al. Racial Differences in Colorectal Cancer Incidence and Mortality in the Women's Health Initiative. *Cancer Epidemiol Biomarkers Prev* 2011; 20: 1368–1378.

[36] Brocardo M, Henderson BR. APC shuttling to the membrane, nucleus and beyond. *Trends Cell Biol* 2008; 18: 587–596.

[37] Muzny DM, Bainbridge MN, Chang K, et al. Comprehensive molecular characterization of human colon and rectal cancer. *Nature* 2012; 487: 330–337.

[38] Munro AJ, Lain S, Lane DP. P53 abnormalities and outcomes in colorectal cancer: a systematic review. *Br J Cancer* 2005; 92: 434–444.

[39] Nassar D, Blanpain C. Cancer Stem Cells: Basic Concepts and Therapeutic Implications. *Annu Rev Pathol Mech Dis* 2016; 11: 47–76.

[40] Balchen V, Simon K. Colorectal cancer development and advances in screening. *Clin Interv Aging* 2016; 11: 967–976.

[41] Young A. ABC of colorectal cancer: Treatment of advanced disease. *BMJ* 2000; 321: 1278–1281.

[42] PDQ Adult Treatment Editorial Board. *Colon Cancer Treatment (PDQ®): Patient Version*, http://www.ncbi.nlm.nih.gov/pubmed/26389319 (2002, accessed 25 September 2019).

[43] Van Cutsem E, Cervantes A, Nordlinger B, et al. Metastatic colorectal cancer: ESMO

clinical practice guidelines for diagnosis, treatment and follow-up. *Ann Oncol* 2014; 25: iii1–iii9.

[44] National Cancer Institute. Drugs Approved for Colon and Rectal Cancer - National Cancer Institute. *National Cancer Institute*, https://www.cancer.gov/about-cancer/treatment/drugs/colorectal (2016, accessed 3 April 2019).

[45] Sun X, Yu Q. Intra-tumor heterogeneity of cancer cells and its implications for cancer treatment. *Acta Pharmacol Sin* 2015; 36: 1219–1227.

[46] Ray S, Das S, Suar M. Molecular Mechanism of Drug Resistance. In: *Drug Resistance in Bacteria, Fungi, Malaria, and Cancer*. Cham: Springer International Publishing, pp. 47–110.

[47] Wonders KY, Reigle BS. Trastuzumab and Doxorubicin-Related Cardiotoxicity and the Cardioprotective Role of Exercise. *Integr Cancer Ther* 2009; 8: 17–21.

[48] Naganuma M, Tahara K, Hasegawa S, et al. Adverse event profiles of solvent-based and nanoparticle albumin-bound paclitaxel formulations using the Food and Drug Administration Adverse Event Reporting System. *SAGE open Med* 2019; 7: 2050312119836011.

[49] Entezar-Almahdi E, Mohammadi-Samani S, Tayebi L, et al. Recent Advances in Designing 5-Fluorouracil Delivery Systems: A Stepping Stone in the Safe Treatment of Colorectal Cancer. *Int J Nanomedicine* 2020; 15: 5445–5458.

[50] Lindner JR, Link J. Molecular Imaging in Drug Discovery and Development. *Circ Cardiovasc Imaging* 2018; 11: 123–131.

[51] Hughes J, Rees S, Kalindjian S, et al. Principles of early drug discovery. *Br J Pharmacol* 2011; 162: 1239–1249.

[52] DiMasi JA, Hansen RW, Grabowski HG. The price of innovation: new estimates of drug development costs. *J Health Econ* 2003; 22: 151–185.

[53] Yu L, Zhao J, Gao L. Predicting Potential Drugs for Breast Cancer based on miRNA and Tissue Specificity. *Int J Biol Sci* 2018; 14: 971–982.

[54] Williams K, Bilsland E, Sparkes A, et al. Cheaper faster drug development validated by the repositioning of drugs against neglected tropical diseases. *J R Soc Interface* 2015; 12: 20141289–20141289.

[55] Mokhtari RB, Homayouni TS, Baluch N, et al. Combination therapy in combating cancer. *Oncotarget* 2017; 8: 38022–38043.

[56] Matsumura Y. Polymeric Micellar Delivery Systems in Oncology. *Jpn J Clin Oncol* 2008; 38: 793–802.

[57] Hay M, Thomas DW, Craighead JL, et al. Clinical development success rates for investigational drugs. *Nat Biotechnol* 2014; 32: 40–51.

[58] Kola I, Landis J. Can the pharmaceutical industry reduce attrition rates? *Nat Rev Drug Discov* 2004; 3: 711–716.

[59] Mullard A. 2016 FDA drug approvals. *Nat Rev Drug Discov* 2017; 16: 73–76.

[60] Mullard A. 2015 FDA drug approvals. *Nat Rev Drug Discov* 2016; 15: 73–76.

[61] Mullard A. 2017 FDA drug approvals. *Nat Rev Drug Discov* 2018; 17: 150–150.

[62] Ledford H. US drug approvals plummet in 2016. *Nature*.

[63] Kantarjian HM, Fojo T, Mathisen M, et al. Cancer Drugs in the United States: Justum Pretium —The Just Price. *J Clin Oncol* 2013; 31: 3600–3604.

[64] Jensen I, Zacherle E, Blanchette C, et al. Evaluating cost benefits of combination therapies for advanced melanoma. *Drugs Context* 2016; 5: 1–14.

[65] IQVIA. Global oncology trends. *Iqvia* 2018; 5: 15.

[66] Zheng W, Sun W, Simeonov A. Drug repurposing screens and synergistic drug-combinations for infectious diseases. *Br J Pharmacol* 2018; 175: 181–191.

[67] Shah RR, Stonier PD. Repurposing old drugs in oncology: Opportunities with clinical and regulatory challenges ahead. *J Clin Pharm Ther* 2019; 44: 6–22.

[68] Jourdan JP, Bureau R, Rochais C, et al. Drug repositioning: a brief overview. *J Pharm Pharmacol* 2020; 72: 1145–1151.

[69] Iwata H, Sawada R, Mizutani S, et al. Systematic drug repositioning for a wide range of diseases with integrative analyses of phenotypic and molecular data. *J Chem Inf Model* 2015; 55: 446–459.

[70] Sertkaya A, Wong HH, Jessup A, et al. Key cost drivers of pharmaceutical clinical trials in the United States. *Clin Trials* 2016; 13: 117–126.

[71] Yeu Y, Yoon Y, Park S. Protein localization vector propagation: a method for improving the accuracy of drug repositioning. *Mol Biosyst* 2015; 11: 2096–2102.

[72] Pantziarka P, Verbaanderd C, Sukhatme V, et al. ReDO_DB: the repurposing drugs in oncology database. *Ecancermedicalscience* 2018; 12: 886.

[73] Hernandez JJ, Pryszlak M, Smith L, et al. Giving Drugs a Second Chance: Overcoming Regulatory and Financial Hurdles in Repurposing Approved Drugs As Cancer Therapeutics. *Front Oncol* 2017; 7: 273.

[74] Laudisi F, Marônek M, Di Grazia A, et al. Repositioning of Anthelmintic Drugs for the Treatment of Cancers of the Digestive System. *Int J Mol Sci* 2020; 21: 4957.

[75] Keith A. The Economics Of Viagra. *Health Aff* 2000; 19: 147–157.

[76] Hennequin LF, Allen J, Breed J, et al. N -(5-Chloro-1,3-benzodioxol-4-yl)-7-[2-(4-methylpiperazin-1-yl)ethoxy]-5- (tetrahydro-2 H -pyran-4-yloxy)quinazolin-4-amine, a Novel, Highly Selective, Orally Available, Dual-Specific c-Src/Abl Kinase Inhibitor †. *J Med Chem* 2006; 49: 6465–6488.

[77] Shin DM, Khuri FR, Glisson BS, et al. Phase II study of paclitaxel, ifosfamide, and carboplatin in patients with recurrent or metastatic head and neck squamous cell carcinoma. *Cancer* 2001; 91: 1316–23.

[78] Gangadhar TC, Clark JI, Karrison T, et al. Phase II study of the Src kinase inhibitor saracatinib (AZD0530) in metastatic melanoma. *Invest New Drugs* 2013; 31: 769–773.

[79] Pushpakom S, Iorio F, Eyers PA, et al. Drug repurposing: progress, challenges and recommendations. *Nat Rev Drug Discov* 2018; 18: 41–58.

[80] Lotharius J, Gamo-Benito F, Angulo-Barturen I, et al. Repositioning: the fast track to new anti-malarial medicines? *Malar J* 2014; 13: 143.

[81] Miguel DC, Yokoyama-Yasunaka JKU, Uliana SRB. Tamoxifen Is Effective in the Treatment of Leishmania amazonensis Infections in Mice. *PLoS Negl Trop Dis* 2008; 2: e249.

[82] Machado PRL, Rosa MEA, Guimarães LH, et al. Treatment of Disseminated Leishmaniasis With Liposomal Amphotericin B. *Clin Infect Dis* 2015; 61: 945–949.

[83] D'Amelio P, Isaia GC. The use of raloxifene in osteoporosis treatment. *Expert Opin Pharmacother* 2013; 14: 949–956.

[84] Lankadasari MB, Aparna JS, Mohammed S, et al. Targeting S1PR1/STAT3 loop abrogates desmoplasia and chemosensitizes pancreatic cancer to gemcitabine. *Theranostics* 2018; 8: 3824–3840.

[85] Tanoli Z, Seemab U, Scherer A, et al. Exploration of databases and methods supporting drug repurposing: A comprehensive survey. *Brief Bioinform* 2021; 22:

1656–1678.

[86] Pantziarka P, Verbaanderd C, Huys I, et al. Repurposing drugs in oncology: From candidate selection to clinical adoption. *Semin Cancer Biol* 2021; 68: 186–191.

[87] Pantziarka P, Bouche G, Meheus L, et al. The Repurposing Drugs in Oncology (ReDO) Project. *Ecancermedicalscience* 2014; 8: 442.

[88] Drell TL, Joseph J, Lang K, et al. Effects of Neurotransmitters on the Chemokinesis and Chemotaxis of MDA-MB-468 Human Breast Carcinoma Cells. *Breast Cancer Res Treat* 2003; 80: 63–70.

[89] Yuan J, Tang Z, Yang S, et al. CRABP2 Promotes Myoblast Differentiation and Is Modulated by the Transcription Factors MyoD and Sp1 in C2C12 Cells. *PLoS One* 2013; 8: e55479.

[90] Liao X, Che X, Zhao W, et al. The β-adrenoceptor antagonist, propranolol, induces human gastric cancer cell apoptosis and cell cycle arrest via inhibiting nuclear factor κB signaling. *Oncol Rep* 2010; 24: 1669–1676.

[91] Sood AK. Stress Hormone-Mediated Invasion of Ovarian Cancer Cells. *Clin Cancer Res* 2006; 12: 369–375.

[92] Zhang D, Ma Q, Shen S, et al. Inhibition of Pancreatic Cancer Cell Proliferation by Propranolol Occurs Through Apoptosis Induction. *Pancreas* 2009; 38: 94–100.

[93] Sleire L, Førde-Tislevoll HE, Netland IA, et al. Drug repurposing in cancer. *Pharmacol Res* 2017; 124: 74–91.

[94] Zhao L, Zhao Y, Schwarz B, et al. Verapamil inhibits tumor progression of chemotherapyresistant pancreatic cancer side population cells. *Int J Oncol* 2016; 49: 99–110.

[95] Bouche G, Pantziarka P, Meheus L. Beyond aspirin and metformin: The untapped potential of drug repurposing in oncology. *Eur J Cancer* 2017; 72: S121–S122.

[96] Verbaanderd C, Meheus L, Huys I, et al. Repurposing Drugs in Oncology: Next Steps. *Trends in Cancer* 2017; 3: 543–546.

[97] Kasper B, Strobel P, Hohenberger P. Desmoid Tumors: Clinical Features and Treatment Options for Advanced Disease. *Oncologist* 2011; 16: 682–693.

[98] Rahim R, Strobl JS. Hydroxychloroquine, chloroquine, and all-trans retinoic acid regulate growth, survival, and histone acetylation in breast cancer cells. *Anticancer Drugs* 2009; 20: 736–745.

[99] Hooft van Huijsduijnen R, Guy RK, Chibale K, et al. Anticancer Properties of Distinct Antimalarial Drug Classes. *PLoS One* 2013; 8: e82962.

[100] Jiang P Du, Zhao YL, Shi W, et al. Cell Growth Inhibition, G_2/M Cell Cycle Arrest, and Apoptosis Induced by Chloroquine in Human Breast Cancer Cell Line Bcap-37. *Cell Physiol Biochem* 2008; 22: 431–440.

[101] Hamacher-Brady A, Stein HA, Turschner S, et al. Artesunate Activates Mitochondrial Apoptosis in Breast Cancer Cells via Iron-catalyzed Lysosomal Reactive Oxygen Species Production. *J Biol Chem* 2011; 286: 6587–6601.

[102] Kim J-HH, Choi A-RR, Kim YK, et al. Co-treatment with the anti-malarial drugs mefloquine and primaquine highly sensitizes drug-resistant cancer cells by increasing P-gp inhibition. *Biochem Biophys Res Commun* 2013; 441: 655–660.

[103] Cook KL, Warri A, Soto-Pantoja DR, et al. Chloroquine Inhibits Autophagy to Potentiate Antiestrogen Responsiveness in ER+ Breast Cancer. *Clin Cancer Res* 2014; 20: 3222–3232.

[104] Das A. Anticancer effect of antimalarial artemisinin compounds. *Ann Med Health Sci Res* 2015; 5: 93.

[105] Wong W, Bai X-CC, Sleebs BE, et al. Mefloquine targets the Plasmodium falciparum 80S ribosome to inhibit protein synthesis. *Nat Microbiol* 2017; 2: 1–9.

[106] YAN K-H, LIN Y-W, HSIAO C-H, et al. Mefloquine induces cell death in prostate cancer cells and provides a potential novel treatment strategy in vivo. *Oncol Lett* 2013; 5: 1567–1571.

[107] Sharma N, Thomas S, Golden EB, et al. Inhibition of autophagy and induction of breast cancer cell death by mefloquine, an antimalarial agent. *Cancer Lett* 2012; 326: 143–154.

[108] Hounkpatin AB, Kreidenweiss A, Held J. Clinical utility of tafenoquine in the prevention of relapse of Plasmodium vivax malaria: a review on the mode of action and emerging trial data. *Infect Drug Resist* 2019; 12: 553–570.

[109] Verbaanderd C, Maes H, Schaaf MB, et al. Repurposing Drugs in Oncology (ReDO)—chloroquine and hydroxychloroquine as anti-cancer agents. *Ecancermedicalscience* 2017; 11: 781.

[110] Thomé R, Lopes SCP, Costa FTM, et al. Chloroquine: Modes of action of an undervalued drug. *Immunol Lett* 2013; 153: 50–57.

[111] Choi J-HH, Yoon JS, Won Y-WW, et al. Chloroquine enhances the chemotherapeutic activity of 5-fluorouracil in a colon cancer cell line via cell cycle alteration. *Apmis* 2012; 120: 597–604.

[112] Sasaki K, Tsuno NH, Sunami E, et al. Chloroquine potentiates the anti-cancer effect of 5-fluorouracil on colon cancer cells. *BMC Cancer* 2010; 10: 370.

[113] Fan C, Wang W, Zhao B, et al. Chloroquine inhibits cell growth and induces cell death in A549 lung cancer cells. *Bioorganic Med Chem* 2006; 14: 3218–3222.

[114] Zheng Y, Zhao Y-LL, Deng X, et al. Chloroquine Inhibits Colon Cancer Cell Growth In Vitro and Tumor Growth In Vivo via Induction of Apoptosis. *Cancer Invest* 2009; 27: 286–292.

[115] Villanueva PJ, Martinez A, Baca ST, et al. Pyronaridine exerts potent cytotoxicity on human breast and hematological cancer cells through induction of apoptosis. *PLoS One* 2018; 13: 1–18.

[116] Baird JK, Hoffman SL. Primaquine Therapy for Malaria. *Clin Infect Dis* 2004; 39: 1336–1345.

[117] Baird JK, Fryauff DJ, Hoffman SL, et al. Primaquine for Prevention of Malaria in Travelers. *Clin Infect Dis* 2003; 37: 1659–1667.

[118] Camarda G, Jirawatcharadech P, Priestley RS, et al. Antimalarial activity of primaquine operates via a two-step biochemical relay. *Nat Commun* 2019; 10: 3226.

[119] Jha TK, Sundar S, Thakur CP, et al. A phase II dose-ranging study of sitamaquine for the treatment of visceral leishmaniasis in India. *Am J Trop Med Hyg* 2005; 73: 1005–11.

[120] Wasunna MK, Rashid JR, Mbui J, et al. A phase II dose-increasing study of sitamaquine for the treatment of visceral leishmaniasis in Kenya. *Am J Trop Med Hyg* 2005; 73: 871–6.

[121] Carvalho L, Luque-Ortega JR, López-Martín C, et al. The 8-Aminoquinoline Analogue Sitamaquine Causes Oxidative Stress in Leishmania donovani Promastigotes by Targeting Succinate Dehydrogenase. *Antimicrob Agents Chemother* 2011; 55: 4204–4210.

[122] Avina-Zubieta JA, Esdaile JM. Antimalarial Medications. In: *Dubois' Lupus Erythematosus and Related Syndromes*. Elsevier, pp. 650–660.

[123] Hughes W, Leoung G, Kramer F, et al. Comparison of Atovaquone (566C80) with

Trimethoprim-Sulfamethoxazole to Treat Pneumocystis carinii Pneumonia in Patients with AIDS. *N Engl J Med* 1993; 328: 1521–1527.

[124] Radloff P., Philips J, Nkeyi M, et al. Atovaquone and proguanil for Plasmodium falciparum malaria. *Lancet* 1996; 347: 1511–1514.

[125] Mather MW, Darrouzet E, Valkova-Valchanova M, et al. Uncovering the Molecular Mode of Action of the Antimalarial Drug Atovaquone Using a Bacterial System. *J Biol Chem* 2005; 280: 27458–27465.

[126] Ashton TM, Fokas E, Kunz-Schughart LA, et al. The anti-malarial atovaquone increases radiosensitivity by alleviating tumour hypoxia. *Nat Commun* 2016; 7: 12308.

[127] Gao X, Liu X, Shan W, et al. Anti-malarial atovaquone exhibits anti-tumor effects by inducing DNA damage in hepatocellular carcinoma. *Am J Cancer Res* 2018; 8: 1697–1711.

[128] Fiorillo M, Lamb R, Tanowitz HB, et al. Repurposing atovaquone: Targeting mitochondrial complex III and OXPHOS to eradicate cancer stem cells. *Oncotarget* 2016; 7: 34084–34099.

[129] Yang N-D, Tan S-H, Ng S, et al. Artesunate Induces Cell Death in Human Cancer Cells via Enhancing Lysosomal Function and Lysosomal Degradation of Ferritin. *J Biol Chem* 2014; 289: 33425–33441.

[130] Zhang P, Luo H-S, Li M, et al. Artesunate inhibits the growth and induces apoptosis of human gastric cancer cells by downregulating COX-2. *Onco Targets Ther* 2015; 8: 845.

[131] Greenshields AL, Fernando W, Hoskin DW. The anti-malarial drug artesunate causes cell cycle arrest and apoptosis of triple-negative MDA-MB-468 and HER2-enriched SK-BR-3 breast cancer cells. *Exp Mol Pathol* 2019; 107: 10–22.

[132] *Meyler's Side Effects of Drugs*. Elsevier, 2016.

[133] Rajesh Y, Biswas A, Kumar U, et al. Lumefantrine, an antimalarial drug, reverses radiation and temozolomide resistance in glioblastoma. *Proc Natl Acad Sci U S A* 2020; 117: 12324–12331.

[134] Roney MSI, Park S-K. Antipsychotic dopamine receptor antagonists, cancer, and cancer stem cells. *Arch Pharm Res* 2018; 41: 384–408.

[135] Fond G, Macgregor A, Attal J, et al. Antipsychotic drugs: Pro-cancer or anti-cancer?

A systematic review. *Med Hypotheses* 2012; 79: 38–42.

[136] Zong D, Zielinska-Chomej K, Juntti T, et al. Harnessing the lysosome-dependent antitumor activity of phenothiazines in human small cell lung cancer. *Cell Death Dis* 2014; 5: e1111–e1111.

[137] Munson JM, Fried L, Rowson SA, et al. Anti-Invasive Adjuvant Therapy with Imipramine Blue Enhances Chemotherapeutic Efficacy Against Glioma. *Sci Transl Med* 2012; 4: 127ra36-127ra36.

[138] Abdelaleem M, Ezzat H, Osama M, et al. Prospects for repurposing CNS drugs for cancer treatment. *Oncol Rev* 2019; 13: 37–42.

[139] Rajamanickam S, Panneerdoss S, Gorthi A, et al. Inhibition of FoxM1 -Mediated DNA Repair by Imipramine Blue Suppresses Breast Cancer Growth and Metastasis. *Clin Cancer Res* 2016; 22: 3524–3536.

[140] Yang W-H, Su Y-H, Hsu W-H, et al. Imipramine blue halts head and neck cancer invasion through promoting F-box and leucine-rich repeat protein 14-mediated Twist1 degradation. *Oncogene* 2016; 35: 2287–2298.

[141] Metts J, Bradley HL, Wang Z, et al. Imipramine blue sensitively and selectively targets FLT3-ITD positive acute myeloid leukemia cells. *Sci Rep* 2017; 7: 4447.

[142] Laidlaw KME, Berhan S, Liu S, et al. Cooperation of imipramine blue and tyrosine kinase blockade demonstrates activity against chronic myeloid leukemia. *Oncotarget* 2016; 7: 51651–51664.

[143] Ghorab MM, Alsaid MS, Samir N, et al. Aromatase inhibitors and apoptotic inducers: Design, synthesis, anticancer activity and molecular modeling studies of novel phenothiazine derivatives carrying sulfonamide moiety as hybrid molecules. *Eur J Med Chem* 2017; 134: 304–315.

[144] Wu C-H, Bai L-Y, Tsai M-H, et al. Pharmacological exploitation of the phenothiazine antipsychotics to develop novel antitumor agents–A drug repurposing strategy. *Sci Rep* 2016; 6: 27540.

[145] Kang SSS, Hong J, Lee JM, et al. Trifluoperazine, a Well-Known Antipsychotic, Inhibits Glioblastoma Invasion by Binding to Calmodulin and Disinhibiting Calcium Release Channel IP 3 R. *Mol Cancer Ther* 2017; 16: 217–227.

[146] Yeh C-T, Wu ATH, Chang PMH, et al. Trifluoperazine, an Antipsychotic Agent, Inhibits Cancer Stem Cell Growth and Overcomes Drug Resistance of Lung Cancer.

Am J Respir Crit Care Med 2012; 186: 1180–1188.

[147] Bertolesi GE, Shi C, Elbaum L, et al. The Ca 2+ Channel Antagonists Mibefradil and Pimozide Inhibit Cell Growth via Different Cytotoxic Mechanisms. *Mol Pharmacol* 2002; 62: 210–219.

[148] Ji MM, Wang L, Zhan Q, et al. Induction of autophagy by valproic acid enhanced lymphoma cell chemosensitivity through HDAC-independent and IP3-mediated PRKAA activation. *Autophagy* 2015; 11: 2160–2171.

[149] Chou YW, Chaturvedi NK, Ouyang S, et al. Histone deacetylase inhibitor valproic acid suppresses the growth and increases the androgen responsiveness of prostate cancer cells. *Cancer Lett* 2011; 311: 177–186.

[150] Terranova-Barberio M, Roca MS, Zotti AI, et al. Valproic acid potentiates the anticancer activity of capecitabine in vitro and in vivo in breast cancer models via induction of thymidine phosphorylase expression. *Oncotarget* 2016; 7: 7715–7731.

[151] Liu S, Liang B, Jia H, et al. Evaluation of cell death pathways initiated by antitumor drugs melatonin and valproic acid in bladder cancer cells. *FEBS Open Bio* 2017; 7: 798–810.

[152] Saha S, Yin Y, Kim K, et al. Valproic Acid Induces Endocytosis-Mediated Doxorubicin Internalization and Shows Synergistic Cytotoxic Effects in Hepatocellular Carcinoma Cells. *Int J Mol Sci* 2017; 18: 1048.

[153] Schuster C, Fernbach N, Rix U, et al. Selective serotonin reuptake inhibitors-A new modality for the treatment of lymphoma/leukaemia? *Biochem Pharmacol* 2007; 74: 1424–1435.

[154] Davies JA. Ethosuximide. In: *xPharm: The Comprehensive Pharmacology Reference*. Elsevier, pp. 1–4.

[155] Sills GJ, Rogawski MA. Mechanisms of action of currently used antiseizure drugs. *Neuropharmacology* 2020; 168: 107966.

[156] Abdul M, Hoosein N. Inhibition by anticonvulsants of prostate-specific antigen and interleukin-6 secretion by human prostate cancer cells. *Anticancer Res* 2001; 21: 2045–8.

[157] Frampton JE. Perampanel: A Review in Drug-Resistant Epilepsy. *Drugs* 2015; 75: 1657–1668.

[158] Tatsuoka J, Sano E, Hanashima Y, et al. Anti-tumor effects of perampanel in

malignant glioma cells. *Oncol Lett* 2022; 24: 1–9.

[159] Rose SR. Primidone. In: *Encyclopedia of Toxicology*. Elsevier, pp. 1066–1067.

[160] Findley LJ, Cleeves L, Calzetti S. Primidone in essential tremor of the hands and head: a double blind controlled clinical study. *J Neurol Neurosurg Psychiatry* 1985; 48: 911–915.

[161] *Primidone*, https://www.ncbi.nlm.nih.gov/books/NBK548512/ (2012, accessed 27 October 2022).

[162] Tandon S, Kaushal S, Chopra SC. Rufinamide. *J Anaesthesiol Clin Pharmacol* 2022; 26: 69–70.

[163] Deeks ED, Scott LJ. Rufinamide. *CNS Drugs* 2006; 20: 751–760.

[164] Davis C. Fluphenazine. In: *xPharm: The Comprehensive Pharmacology Reference*. Elsevier, pp. 1–7.

[165] Xu F, Xia Y, Feng Z, et al. Repositioning antipsychotic fluphenazine hydrochloride for treating triple negative breast cancer with brain metastases and lung metastases. *Am J Cancer Res* 2019; 9: 459–478.

[166] Davis C. Thioridazine. In: *xPharm: The Comprehensive Pharmacology Reference*. Elsevier, pp. 1–7.

[167] Zhang C, Gong P, Liu P, et al. Thioridazine elicits potent antitumor effects in colorectal cancer stem cells. *Oncol Rep* 2017; 37: 1168–1174.

[168] Arvanitis LA, Miller BG. Multiple fixed doses of 'seroquel' (quetiapine) in patients with acute exacerbation of schizophrenia: A comparison with haloperidol and placebo. *Biol Psychiatry* 1997; 42: 233–246.

[169] Wang Y, Huang N, Li H, et al. Promoting oligodendroglial-oriented differentiation of glioma stem cell: A repurposing of quetiapine for the treatment of malignant glioma. *Oncotarget* 2017; 8: 37511–37524.

[170] Bailly C. Potential use of edaravone to reduce specific side effects of chemo-, radio- and immuno-therapy of cancers. *Int Immunopharmacol* 2019; 77: 105967.

[171] Dash RP, Babu RJ, Srinivas NR. Two Decades-Long Journey from Riluzole to Edaravone: Revisiting the Clinical Pharmacokinetics of the Only Two Amyotrophic Lateral Sclerosis Therapeutics. *Clin Pharmacokinet* 2018; 57: 1385–1398.

[172] Ali ZK, Baker DE. Formulary Drug Review: Edaravone. *Hosp Pharm* 2017; 52: 732–

736.

[173] Zhang M, Teng C, Wu F, et al. Edaravone attenuates traumatic brain injury through anti-inflammatory and anti-oxidative modulation. *Exp Ther Med* 2019; 18: 467–474.

[174] Szczesny-Malysiak E, Stojak M, Campagna R, et al. Bardoxolone methyl displays detrimental effects on endothelial bioenergetics, suppresses endothelial et-1 release, and increases endothelial permeability in human microvascular endothelium. *Oxid Med Cell Longev* 2020; 2020: 1–16.

[175] Habib E, Linher-Melville K, Lin HX, et al. Expression of xCT and activity of system xc(-) are regulated by NRF2 in human breast cancer cells in response to oxidative stress. *Redox Biol* 2015; 5: 33–42.

[176] Tossetta G, Fantone S, Montanari E, et al. Role of NRF2 in Ovarian Cancer. *Antioxidants* 2022; 11: 663.

[177] Emanuelli M, Sartini D, Molinelli E, et al. The Double-Edged Sword of Oxidative Stress in Skin Damage and Melanoma: From Physiopathology to Therapeutical Approaches. *Antioxidants* 2022; 11: 612.

[178] Kokura S, Yoshida N, Sakamoto N, et al. The radical scavenger edaravone enhances the anti-tumor effects of CPT-11 in murine colon cancer by increasing apoptosis via inhibition of NF-κB. *Cancer Lett* 2005; 229: 223–233.

[179] Nonogawa M, Arai T, Endo N, et al. Reactive oxygen species generation through NADH oxidation by pterin derivatives. *Nucleic Acids Symp Ser* 2008; 52: 567–568.

[180] Arai T, Nonogawa M, Makino K, et al. The Radical Scavenger Edaravone (3-Methyl-1-phenyl-2-pyrazolin-5-one) Reacts with a Pterin Derivative and Produces a Cytotoxic Substance That Induces Intracellular Reactive Oxygen Species Generation and Cell Death. *J Pharmacol Exp Ther* 2008; 324: 529–538.

[181] Suzuki R, Gopalrao RK, Maeda H, et al. MCI-186 Inhibits Tumor Growth Through Suppression of EGFR Phosphorylation and Cell Cycle Arrest. *Anticancer Res* 2005; 25: 1131–1138.

[182] Corea N. Benztropine. In: *xPharm: The Comprehensive Pharmacology Reference*. Elsevier, pp. 1–4.

[183] Sogawa C, Eguchi T, Tran MT, et al. Antiparkinson Drug Benztropine Suppresses Tumor Growth, Circulating Tumor Cells, and Metastasis by Acting on SLC6A3/DAT and Reducing STAT3. *Cancers (Basel)* 2020; 12: 523.

[184] Bachurin S, Bukatina E, Lermontova N, et al. Antihistamine agent Dimebon as a novel neuroprotector and a cognition enhancer. *Ann N Y Acad Sci* 2001; 939: 425–435.

[185] Bharadwaj PR, Bates KA, Porter T, et al. Latrepirdine: molecular mechanisms underlying potential therapeutic roles in Alzheimer's and other neurodegenerative diseases. *Transl Psychiatry* 2013; 3: e332–e332.

[186] Bachurin SO, Shevtsova EP, Kireeva EG, et al. Mitochondria as a target for neurotoxins and neuroprotective agents. *Ann N Y Acad Sci* 2003; 993: 334–344.

[187] Chau S, Herrmann N, Ruthirakuhan MT, et al. Latrepirdine for Alzheimer's disease. *Cochrane database Syst Rev* 2015; 2015: CD009524.

[188] Dorsey ER. A randomized, double-blind, placebo-controlled study of latrepirdine in patients with mild to moderate Huntington disease. *JAMA Neurol* 2013; 70: 25–33.

[189] El Refaey H. Fluoxetine. In: *xPharm: The Comprehensive Pharmacology Reference*. Elsevier, pp. 1–9.

[190] Bowie M, Pilie P, Wulfkuhle J, et al. Fluoxetine induces cytotoxic endoplasmic reticulum stress and autophagy in triple negative breast cancer. *World J Clin Oncol* 2015; 6: 299–311.

[191] Sun D, Zhu L, Zhao Y, et al. Fluoxetine induces autophagic cell death via eEF2K-AMPK-mTOR-ULK complex axis in triple negative breast cancer. *Cell Prolif* 2018; 51: 1–10.

[192] Gwynne WD, Hallett RM, Girgis-Gabardo A, et al. Serotonergic system antagonists target breast tumor initiating cells and synergize with chemotherapy to shrink human breast tumor xenografts. *Oncotarget* 2017; 8: 32101–32116.

[193] Hallett RM, Girgis-Gabardo A, Gwynne WD, et al. Serotonin transporter antagonists target tumor-initiating cells in a transgenic mouse model of breast cancer. *Oncotarget* 2016; 7: 53137–53152.

[194] Abdul M, Logothetis CJ, Hoosein NM. Growth-Inhibitory Effects of Serotonin Uptake Inhibitors on Human Prostate Carcinoma Cell Lines. *J Urol* 1995; 154: 247–250.

[195] Španová A, Kovářů H, Lisá V, et al. Estimation of apoptosis in C6 glioma cells treated with antidepressants. In: *Physiological Research*, pp. 161–164.

[196] Levkovitz Y, Gil-Ad I, Zeldich E, et al. Differential Induction of Apoptosis by Antidepressants in Glioma and Neuroblastoma Cell Lines: Evidence for p-c-Jun,

Cytochrome c, and Caspase-3 Involvement. *J Mol Neurosci* 2005; 27: 029–042.

[197] Koch JM, Kell S, Aldenhoff JB. Differential effects of fluoxetine and imipramine on the phosphorylation of the transcription factor CREB and cell-viability. *J Psychiatr Res* 2003; 37: 53–59.

[198] Costa P, McCrae R, Cloninger C, et al. Kaplan and Sadock's Comprehensive Textbook of Psychiatry, Eighth Edition. *Am J Psychiatry* 2006; 163: 1458.

[199] Antoszczak M, Markowska A, Markowska J, et al. Antidepressants and Antipsychotic Agents as Repurposable Oncological Drug Candidates. *Curr Med Chem* 2021; 28: 2137–2174.

[200] Chiles C. Handbook of Psychiatric Drug Therapy, 5th ed. *J Clin Psychiatry* 2007; 68: 339.

[201] Jiang X, Lu W, Shen X, et al. Repurposing sertraline sensitizes non-small cell lung cancer cells to erlotinib by inducing autophagy. *JCI insight* 2018; 3: 1–16.

[202] Zinnah KMA, Seol J-W, Park S-Y. Inhibition of autophagy flux by sertraline attenuates TRAIL resistance in lung cancer via death receptor 5 upregulation. *Int J Mol Med* 2020; 46: 795–805.

[203] Amson R, Pece S, Lespagnol A, et al. Reciprocal repression between P53 and TCTP. *Nat Med* 2011; 18: 91–99.

[204] Gil-Ad I, Zolokov A, Lomnitski L, et al. Evaluation of the potential anti-cancer activity of the antidepressant sertraline in human colon cancer cell lines and in colorectal cancer-xenografted mice. *Int J Oncol* 2008; 33: 277–286.

[205] Lin C-J, Robert F, Sukarieh R, et al. The antidepressant sertraline inhibits translation initiation by curtailing mammalian target of rapamycin signaling. *Cancer Res* 2010; 70: 3199–3208.

[206] Gao Y, Shang Q, Li W, et al. Antibiotics for cancer treatment: A double-edged sword. *J Cancer* 2020; 11: 5135.

[207] Weng N, Zhang Z, Tan Y, et al. Repurposing antifungal drugs for cancer therapy. *J Adv Res*.

[208] Reyhanoglu G, Reddivari AKR. *Tobramycin*. StatPearls Publishing, 2022.

[209] Kotra LP, Haddad J, Mobashery S. Aminoglycosides: perspectives on mechanisms of action and resistance and strategies to counter resistance. *Antimicrob Agents Chemother* 2000; 44: 3249–3256.

[210] Kemnic TR, Coleman M. Trimethoprim Sulfamethoxazole. *Mayo Clin Proc* 2021; 74: 730–734.

[211] Kurien G, Jamil RT, Preuss C V. *Dapsone*. StatPearls Publishing, 2022.

[212] Kumar B. Re: Antimicrobial resistance in leprosy: results of the first prospective open survey conducted by a WHO surveillance network for the period 2009-2015. *Clin Microbiol Infect* 2019; 25: 644–645.

[213] Pillai V, Kadu R, Buch L, et al. Derivatives of Dapsone (dap): Synthesis and Study on In Vitro Anticancer Activity and DNA Laddering Against Hep G2 and C6 Human Cancer Cell Lines. *ChemistrySelect* 2017; 2: 4382–4391.

[214] Nami B, Donmez H, Kocak N. Tunicamycin-induced endoplasmic reticulum stress reduces in vitro subpopulation and invasion of CD44+/CD24- phenotype breast cancer stem cells. *Exp Toxicol Pathol* 2016; 68: 419–426.

[215] Wang X, Xiong W, Tang Y. Tunicamycin suppresses breast cancer cell growth and metastasis via regulation of the protein kinase B/nuclear factor-κB signaling pathway. *Oncol Lett* 2018; 15: 4137.

[216] You S, Li W, Guan Y. Tunicamycin inhibits colon carcinoma growth and aggressiveness via modulation of the ERK-JNK-mediated AKT/mTOR signaling pathway. *Mol Med Rep* 2018; 17: 4203–4212.

[217] Wang Y, Zhang L, He Z, et al. Tunicamycin induces ER stress and inhibits tumorigenesis of head and neck cancer cells by inhibiting N-glycosylation. *Am J Transl Res* 2020; 12: 541.

[218] De Freitas JCM, Silva BDRDA, De Souza WF, et al. Inhibition of N-linked glycosylation by tunicamycin induces E-cadherin-mediated cell-cell adhesion and inhibits cell proliferation in undifferentiated human colon cancer cells. *Cancer Chemother Pharmacol* 2011; 68: 227–238.

[219] Ling YH, Li T, Perez-Soler R, et al. Activation of ER stress and inhibition of EGFR N-glycosylation by tunicamycin enhances susceptibility of human non-small cell lung cancer cells to erlotinib. *Cancer Chemother Pharmacol* 2009; 64: 539–548.

[220] Shiraishi T, Yoshida T, Nakata S, et al. Tunicamycin enhances tumor necrosis factor-related apoptosis-inducing ligand-induced apoptosis in human prostate cancer cells. *Cancer Res* 2005; 65: 6364–6370.

[221] Patil A, Lakhani P, Majumdar S. Current perspectives on natamycin in ocular fungal

infections. *J Drug Deliv Sci Technol* 2017; 41: 206–212.

[222] Te Welscher YM, Ten Napel HH, Balagué MM, et al. Natamycin Blocks Fungal Growth by Binding Specifically to Ergosterol without Permeabilizing the Membrane. *J Biol Chem* 2008; 283: 6393–6401.

[223] Vasquez JL, Lai Y, Annamalai T, et al. Inhibition of base excision repair by natamycin suppresses prostate cancer cell proliferation. *Biochimie* 2020; 168: 241.

[224] An Y, Jiang J, Zhou L, et al. Peroxiredoxin 1 is essential for natamycin-triggered apoptosis and protective autophagy in hepatocellular carcinoma. *Cancer Lett* 2021; 521: 210–223.

[225] da Silva DM, Sanz G, Vaz BG, et al. Tert-butyl 4-((1-phenyl-1H-pyrazol-4-yl) methyl) piperazine-1-carboxylate (LQFM104)– New piperazine derivative with antianxiety and antidepressant-like effects: Putative role of serotonergic system. *Biomed Pharmacother* 2018; 103: 546–552.

[226] Gu ZS, Xiao Y, Zhang QW, et al. Synthesis and antidepressant activity of a series of arylalkanol and aralkyl piperazine derivatives targeting SSRI/5-HT1A/5-HT7. *Bioorg Med Chem Lett* 2017; 27: 5420–5423.

[227] Bassetto M, Leyssen P, Neyts J, et al. In silico identification, design and synthesis of novel piperazine-based antiviral agents targeting the hepatitis C virus helicase. *Eur J Med Chem* 2017; 125: 1115–1131.

[228] Dou D, He G, Mandadapu SR, et al. Inhibition of noroviruses by piperazine derivatives. *Bioorg Med Chem Lett* 2012; 22: 377–379.

[229] Wei ZY, Chi KQ, Wang KS, et al. Design, synthesis, evaluation, and molecular docking of ursolic acid derivatives containing a nitrogen heterocycle as anti-inflammatory agents. *Bioorg Med Chem Lett* 2018; 28: 1797–1803.

[230] Jain A, Chaudhary J, Khaira H, et al. Piperazine: A Promising Scaffold with Analgesic and Anti-inflammatory Potential. *Drug Res (Stuttg)* 2021; 71: 62–72.

[231] Berczyński P, Kładna A, Bozdağ Dündar O, et al. Preparation and in vitro antioxidant activity of some novel flavone analogues bearing piperazine moiety. *Bioorg Chem* 2020; 95: 103513.

[232] Patel R V., Mistry B, Syed R, et al. Chrysin-piperazine conjugates as antioxidant and anticancer agents. *Eur J Pharm Sci* 2016; 88: 166–177.

[233] Jeon SH, Shin CG. Effect of a novel piperazine compound on cancer cells. *Appl Biol*

Chem 2021; 64: 1–7.

[234] Jain A, Jack J. *Quinidine*. StatPearls Publishing, 2022.

[235] Grolleman JE, de Voer RM, Elsayed FA, et al. Mutational Signature Analysis Reveals NTHL1 Deficiency to Cause a Multi-tumor Phenotype. *Cancer Cell* 2019; 35: 256-266.e5.

[236] Davies JA. Bromocriptine. In: *xPharm: The Comprehensive Pharmacology Reference*. Elsevier, pp. 1–4.

[237] Seo E-J, Sugimoto Y, Greten HJ, et al. Repurposing of Bromocriptine for Cancer Therapy. *Front Pharmacol* 2018; 9: 1030.

[238] Tsuruo T, Iida H, Kitatani Y, et al. Effects of quinidine and related compounds on cytotoxicity and cellular accumulation of vincristine and adriamycin in drug-resistant tumor cells. *Cancer Res* 1984; 44: 4303–7.

[239] Davies JA. Carbidopa. In: *xPharm: The Comprehensive Pharmacology Reference*. Elsevier, pp. 1–5.

[240] Chen Z, Cai A, Zheng H, et al. Carbidopa suppresses prostate cancer via aryl hydrocarbon receptor-mediated ubiquitination and degradation of androgen receptor. *Oncogenesis* 2020; 9: 1–13.

[241] Ogura J, Miyauchi S, Shimono K, et al. Carbidopa is an activator of aryl hydrocarbon receptor with potential for cancer therapy. *Biochem J* 2017; 474: 3391–3402.

[242] Holm KJ, Spencer CM. Entacapone. A review of its use in Parkinson's disease. *Drugs* 1999; 58: 159–177.

[243] Enna SJ, Bylund DB. Tolcapone. In: *xPharm: The Comprehensive Pharmacology Reference*. Elsevier, p. 1.

[244] Grimes KL, Stuart CM, McCarthy JJ, et al. Enhancing the Cancer Cell Growth Inhibitory Effects of Table Grape Anthocyanins. *J Food Sci* 2018; 83: 2369–2374.

[245] Maser T, Rich M, Hayes D, et al. Tolcapone induces oxidative stress leading to apoptosis and inhibition of tumor growth in Neuroblastoma. *Cancer Med* 2017; 6: 1341.

[246] Forester SC, Lambert JD. Synergistic inhibition of lung cancer cell lines by (-)-epigallocatechin-3-gallate in combination with clinically used nitrocatechol inhibitors of catechol-O-methyltransferase. *Carcinogenesis* 2014; 35: 365–372.

[247] Sub Laban T, Saadabadi A. *Monoamine Oxidase Inhibitors (MAOI)*. StatPearls Publishing, 2022.

[248] Davies JA. Selegiline. In: *xPharm: The Comprehensive Pharmacology Reference*. Elsevier, pp. 1–4.

[249] Ryu I, Ryu MJ, Han J, et al. L-Deprenyl exerts cytotoxicity towards acute myeloid leukemia through inhibition of mitochondrial respiration. *Oncol Rep* 2018; 40: 3869–3878.

[250] Ziv K. Carbamazepine. In: *The Essence of Analgesia and Analgesics*. Cambridge University Press, pp. 301–305.

[251] Akbarzadeh L, Moini Zanjani T, Sabetkasaei M. Comparison of Anticancer Effects of Carbamazepine and Valproic Acid. *Iran Red Crescent Med J* 2016; 18: 37230.

[252] Meng QW, Zhao CH, Xi YH, et al. Inhibitory effect of carbamazepine on proliferation of estrogen-dependent breast cancer cells. *Ai Zheng* 2006; 25: 967–973.

[253] Meng Q, Chen X, Sun L, et al. Carbamazepine promotes Her-2 protein degradation in breast cancer cells by modulating HDAC6 activity and acetylation of Hsp90. *Mol Cell Biochem* 2011; 348: 165–171.

[254] Betchel NT, Fariba KA, Saadabadi A. Lamotrigine. *Essence Analg Analg* 2022; 306–309.

[255] Miles TF, Lester HA, Dougherty DA. Allosteric activation of the 5-HT3AB receptor by mCPBG. *Neuropharmacology* 2015; 91: 103–108.

[256] Schlicker E, Kathmann M, Exner HJ, et al. The 5-HT3 receptor agonist 1-(m-chlorophenyl)-biguanide facilitates noradrenaline release by blockade of α2-adrenoceptors in the mouse brain cortex. *Naunyn Schmiedebergs Arch Pharmacol* 1994; 349: 20–24.

[257] Narise K, Okuda K, Enomoto Y, et al. Optimization of biguanide derivatives as selective antitumor agents blocking adaptive stress responses in the tumor microenvironment. *Drug Des Devel Ther* 2014; 8: 701–717.

[258] Barbieri F, Verduci I, Carlini V, et al. Repurposed Biguanide Drugs in Glioblastoma Exert Antiproliferative Effects via the Inhibition of Intracellular Chloride Channel 1 Activity. *Front Oncol* 2019; 9: 135.

[259] Sakai T, Matsuo Y, Okuda K, et al. Development of antitumor biguanides targeting energy metabolism and stress responses in the tumor microenvironment. *Sci*

Reports 2021 111 2021; 11: 1–15.

[260] De La Garza R, Bubar MJ, Carbone CL, et al. Evaluation of the dopamine β-hydroxylase (DβH) inhibitor nepicastat in participants who meet criteria for cocaine use disorder. *Prog Neuro-Psychopharmacology Biol Psychiatry* 2015; 59: 40–48.

[261] Study of Safety and Potential Efficacy of SYN117 in Cocaine Dependent Volunteers - Full Text View - ClinicalTrials.gov, https://www.clinicaltrials.gov/ct2/show/NCT00656357 (accessed 31 October 2022).

[262] Pharmacogenetic Clinical Trial of Nepicastat for Post Traumatic Stress Disorder (PTSD) - Full Text View - ClinicalTrials.gov, https://www.clinicaltrials.gov/ct2/show/NCT00641511 (accessed 31 October 2022).

[263] Riad M, Hithe CC. *Scopolamine*. Springer Singapore, 2022.

[264] Ezzat SM, Salem MA, El Mahdy NM, et al. Rivastigmine. In: *Naturally Occurring Chemicals Against Alzheimer's Disease*. Elsevier, pp. 93–108.

[265] Sizar O, Rahman S, Sundareshan V. *Amikacin*. StatPearls Publishing, 2022.

[266] Wang YH, Chen YH, Shen WH. Amikacin Suppresses Human Breast Cancer Cell MDA-MB-231 Migration and Invasion. *Toxics* 2020; 8: 1–9.

[267] Chaves BJ, Tadi P. *Gentamicin*. StatPearls Publishing, 2022.

[268] Albi E, Cataldi S, Ceccarini MR, et al. Gentamicin Targets Acid Sphingomyelinase in Cancer: The Case of the Human Gastric Cancer NCI-N87 Cells. *Int J Mol Sci* 2019; 20: 4375.

[269] Codini M, Cataldi S, Ambesi-Impiombato FS, et al. Gentamicin Arrests Cancer Cell Growth: The Intriguing Involvement of Nuclear Sphingomyelin Metabolism. *Int J Mol Sci* 2015; 16: 2307.

[270] Patel S, Preuss C V., Bernice F. *Vancomycin*. StatPearls Publishing, 2022.

[271] Major. Vancomycin Treatment Increases Efficacy of Radiotherapy in Mice. *Cancer Discov* 2020; 10: 171.

[272] Waugh CD. Clotrimazole. In: *xPharm: The Comprehensive Pharmacology Reference*. Elsevier, pp. 1–4.

[273] S K, C S, CS K, et al. Clotrimazole as a Cancer Drug: A Short Review. *Med Chem (Los Angeles)* 2014; 4: 722.

[274] Samhsa, Csat, Kap. *Substance Abuse Treatment ADVISORY Breaking News for the*

Treatment Field Acamprosate: A New Medication for Alcohol Use Disorders, www.samhsa.gov (accessed 28 October 2022).

[275] Marraffa JM. Amiodarone. In: *Encyclopedia of Toxicology: Third Edition*. StatPearls Publishing, 2014, pp. 197–199.

[276] van der Graaf WTA, de Vries EGE, Timmer-Bosscha H, et al. Effects of Amiodarone, Cyclosporin A, and PSC 833 on the Cytotoxicity of Mitoxantrone, Doxorubicin, and Vincristine in Non-P-glycoprotein Human Small Cell Lung Cancer Cell Lines. *Cancer Res* 1994; 54: 5368–5373.

[277] Theodossiou TA, Galanou MC, Paleos CM. Novel amiodarone-doxorubicin cocktail liposomes enhance doxorubicin retention and cytotoxicity in du145 human prostate carcinoma cells. *J Med Chem* 2008; 51: 6067–6074.

[278] Ketchem CJ, Kucera C, Barve A, et al. The Antiarrhythmic Drug, Amiodarone, Decreases AKT Activity and Sensitizes Human Acute Myeloid Leukemia Cells to Apoptosis by ABT-263. *Am J Med Sci* 2018; 355: 488–496.

[279] Chang Y-L, Liu S-T, Wang Y-W, et al. Amiodarone promotes cancer cell death through elevated truncated SRSF3 and downregulation of miR-224. *Oncotarget* 2018; 9: 13390–13406.

[280] Gruetter CA. Metoprolol. In: *xPharm: The Comprehensive Pharmacology Reference*. Elsevier, pp. 1–7.

[281] Gruetter CA. Atenolol. In: *xPharm: The Comprehensive Pharmacology Reference*. Elsevier, pp. 1–6.

[282] Peixoto R, Pereira M de L, Oliveira M. Beta-Blockers and Cancer: Where Are We? *Pharmaceuticals* 2020; 13: 105.

[283] Carlos-Escalante JA, de Jesús-Sánchez M, Rivas-Castro A, et al. The Use of Antihypertensive Drugs as Coadjuvant Therapy in Cancer. *Front Oncol* 2021; 11: 1595.

[284] Khan TM, Patel R, Siddiqui AH. *Furosemide*. StatPearls Publishing, 2022.

[285] Shankar SS, Brater DC. Loop diuretics: from the Na-K-2Cl transporter to clinical use. *Am J Physiol Physiol* 2003; 284: F11–F21.

[286] Shiozaki A, Miyazaki H, Niisato N, et al. Furosemide, a Blocker of Na+/K+/2Cl− Cotransporter, Diminishes Proliferation of Poorly Differentiated Human Gastric Cancer Cells by Affecting G0/G1 State. *J Physiol Sci* 2006; 56: 401–406.

[287] Speers AG, Lwaleed BA, Featherstone JM, et al. Furosemide reverses multidrug resistance status in bladder cancer cells in vitro. *J Clin Pathol* 2006; 59: 912.

[288] Hardin MD, Jacobs TF. Glyburide. *Geriatr Med Today* 2022; 9: 63–64.

[289] Qureshi M, Gammoh E, Shakil J, et al. Update on Management of Type 2 Diabetes for Cardiologists. *Methodist Debakey Cardiovasc J* 2018; 14: 273–280.

[290] Qian X, Li J, Ding J, et al. Glibenclamide exerts an antitumor activity through reactive oxygen species-c-jun NH2-terminal kinase pathway in human gastric cancer cell line MGC-803. *Biochem Pharmacol* 2008; 76: 1705–1715.

[291] Núñez M, Medina V, Cricco G, et al. Glibenclamide inhibits cell growth by inducing G0/G1 arrest in the human breast cancer cell line MDA-MB-231. *BMC Pharmacol Toxicol* 2013; 14: 6.

[292] Yasukagawa T, Niwa Y, Simizu S, et al. Suppression of cellular invasion by glybenclamide through inhibited secretion of platelet-derived growth factor in ovarian clear cell carcinoma ES-2 cells. *FEBS Lett* 2012; 586: 1504–1509.

[293] Kim JA, Kang YS, Lee SH, et al. Glibenclamide induces apoptosis through inhibition of cystic fibrosis transmembrane conductance regulator (CFTR) Cl(-) channels and intracellular Ca(2+) release in HepG2 human hepatoblastoma cells. *Biochem Biophys Res Commun* 1999; 261: 682–688.

[294] Valentovic M. Atorvastatin. In: *xPharm: The Comprehensive Pharmacology Reference*. Elsevier, pp. 1–6.

[295] Longo J, van Leeuwen JE, Elbaz M, et al. Statins as anticancer agents in the era of precision medicine. *Clin Cancer Res* 2020; 26: 5791–5800.

[296] McClellan KJ, Markham A. Telmisartan. *Drugs* 1998; 56: 1039–1044.

[297] Matsui T, Chiyo T, Kobara H, et al. Telmisartan Inhibits Cell Proliferation and Tumor Growth of Esophageal Squamous Cell Carcinoma by Inducing S-Phase Arrest In Vitro and In Vivo. *Int J Mol Sci* 2019; 20: 3197.

[298] Khorsand M, Khajeh S, Eslami M, et al. Telmisartan anti-cancer activities mechanism through targeting N-cadherin by mimicking ADH-1 function. *J Cell Mol Med* 2022; 26: 2392–2403.

[299] Fujita N, Fujita K, Iwama H, et al. Antihypertensive drug telmisartan suppresses the proliferation of gastric cancer cells in vitro and in vivo. *Oncol Rep* 2020; 44: 339–348.

[300] Greish K, Fateel M, Abdelghany S, et al. Sildenafil citrate improves the delivery and

anticancer activity of doxorubicin formulations in a mouse model of breast cancer. *J Drug Target* 2018; 26: 610–615.

[301] Hu Q, Sun W, Wang C, et al. Recent advances of cocktail chemotherapy by combination drug delivery systems. *Adv Drug Deliv Rev* 2016; 98: 19–34.

[302] Frei E, Karon M, Levin RH, et al. The effectiveness of combinations of antileukemic agents in inducing and maintaining remission in children with acute leukemia. *Blood* 1965; 26: 642–56.

[303] Holohan C, Van Schaeybroeck S, Longley DB, et al. Cancer drug resistance: an evolving paradigm. *Nat Rev Cancer* 2013; 13: 714–726.

[304] Bardelli A, Siena S. Molecular Mechanisms of Resistance to Cetuximab and Panitumumab in Colorectal Cancer. *J Clin Oncol* 2010; 28: 1254–1261.

[305] Hochhaus A, Kreil S, Corbin A, et al. Molecular and chromosomal mechanisms of resistance to imatinib (STI571) therapy. *Leukemia* 2002; 16: 2190–2196.

[306] Palmer AC, Sorger PK. Combination Cancer Therapy Can Confer Benefit via Patient-to-Patient Variability without Drug Additivity or Synergy. *Cell* 2017; 171: 1678-1691.e13.

[307] Odeh LH, Talib WH, Basheti IA. Synergistic effect of thymoquinone and melatonin against breast cancer implanted in mice. *J Cancer Res Ther* 2018; 14: S324–S330.

[308] Calaf GM, Ponce-Cusi R, Carrión F. Curcumin and paclitaxel induce cell death in breast cancer cell lines. *Oncol Rep* 2018; 40: 2381–2388.

[309] Mirzapur P, Khazaei MR, Moradi MT, et al. Apoptosis induction in human breast cancer cell lines by synergic effect of raloxifene and resveratrol through increasing proapoptotic genes. *Life Sci* 2018; 205: 45–53.

[310] Yao M, Yuan B, Wang X, et al. Synergistic cytotoxic effects of arsenite and tetrandrine in human breast cancer cell line MCF-7. *Int J Oncol* 2017; 51: 587–598.

[311] Oliveras-Ferraros C, Vazquez-Martin A, Colomer R, et al. Sequence-dependent synergism and antagonism between paclitaxel and gemcitabine in breast cancer cells: the importance of scheduling. *Int J Oncol* 2008; 32: 113–20.

[312] Vogus DR, Pusuluri A, Chen R, et al. Schedule dependent synergy of gemcitabine and doxorubicin: Improvement of in vitro efficacy and lack of in vitro-in vivo correlation. *Bioeng Transl Med* 2018; 3: 49–57.

[313] Chou TC. Drug combination studies and their synergy quantification using the chou-

talalay method. *Cancer Res* 2010; 70: 440–446.

[314] Chou T-CTC. Theoretical basis, experimental design, and computerized simulation of synergism and antagonism in drug combination studies. *Pharmacol Rev* 2006; 58: 621–681.

[315] Tsakalozou E, Eckman AM, Bae Y. Combination Effects of Docetaxel and Doxorubicin in Hormone-Refractory Prostate Cancer Cells. *Biochem Res Int* 2012; 2012: 1–10.

[316] Foucquier J, Guedj M. Analysis of drug combinations: current methodological landscape. *Pharmacol Res Perspect* 2015; 3: e00149.

[317] Lee MJ, Ye AS, Gardino AK, et al. Sequential Application of Anticancer Drugs Enhances Cell Death by Rewiring Apoptotic Signaling Networks. *Cell* 2012; 149: 780–794.

[318] Le Tourneau C, Lee JJ, Siu LL. Dose Escalation Methods in Phase I Cancer Clinical Trials. *JNCI J Natl Cancer Inst* 2009; 101: 708–720.

[319] Pereira DM, Simões AES, Gomes SE, et al. MEK5/ERK5 signaling inhibition increases colon cancer cell sensitivity to 5-fluorouracil through a p53-dependent mechanism. *Oncotarget* 2016; 7: 34322–34340.

[320] Lou S, Zhao Z, Dezort M, et al. Multifunctional Nanosystem for Targeted and Controlled Delivery of Multiple Chemotherapeutic Agents for the Treatment of Drug-Resistant Breast Cancer. *ACS Omega* 2018; 3: 9210–9219.

[321] Khalil DN, Smith EL, Brentjens RJ, et al. The future of cancer treatment: immunomodulation, CARs and combination immunotherapy. *Nat Rev Clin Oncol* 2016; 13: 273–290.

[322] Zhu B, Strada S. The Novel Functions of cGMP-Specific Phosphodiesterase 5 and its Inhibitors in Carcinoma Cells and Pulmonary/Cardiovascular Vessels. *Curr Top Med Chem* 2007; 7: 437–454.

[323] Mei XL, Yang Y, Zhang YJ, et al. Sildenafil inhibits the growth of human colorectal cancer in vitro and in vivo. *Am J Cancer Res* 2015; 5: 3311–3324.

[324] ClinCalc. Metformin Hydrochloride - Drug Usage Statistics, ClinCalc DrugStats Database. *ClinCalc*, https://clincalc.com/DrugStats/Drugs/MetforminHydrochloride (2017, accessed 21 August 2020).

[325] Rena G, Hardie DG, Pearson ER. The mechanisms of action of metformin.

Diabetologia 2017; 60: 1577–1585.

[326] Dulskas A, Patasius A, Linkeviciute-Ulinskiene D, et al. A cohort study of antihyperglycemic medication exposure and survival in patients with gastric cancer. *Aging (Albany NY)* 2019; 11: 7197–7205.

[327] Dong S, Ruiz-Calderon B, Rathinam R, et al. Knockout model reveals the role of Nischarin in mammary gland development, breast tumorigenesis and response to metformin treatment. *Int J Cancer* 2020; 146: 2576–2587.

[328] Libby G, Donnelly LA, Donnan PT, et al. New users of metformin are at low risk of incident cancer: A cohort study among people with type 2 diabetes. *Diabetes Care* 2009; 32: 1620–1625.

[329] Kisfalvi K, Eibl G, Sinnett-Smith J, et al. Metformin disrupts crosstalk between G protein-coupled receptor and insulin receptor signaling systems and inhibits pancreatic cancer growth. *Cancer Res* 2009; 69: 6539–6545.

[330] Hosono K, Endo H, Takahashi H, et al. Metformin suppresses colorectal aberrant crypt foci in a short-term clinical trial. *Cancer Prev Res* 2010; 3: 1077–1083.

[331] Tran LNK, Kichenadasse G, Morel KL, et al. The combination of metformin and valproic acid has a greater anti-tumoral effect on prostate cancer growth in vivo than either drug alone. *In Vivo (Brooklyn)* 2019; 33: 99–108.

[332] Mogavero A, Maiorana MV, Zanutto S, et al. Metformin transiently inhibits colorectal cancer cell proliferation as a result of either AMPK activation or increased ROS production. *Sci Rep* 2017; 7: 15992.

[333] Mussin N, Oh SC, Lee KW, et al. Sirolimus and metformin synergistically inhibits colon cancer in vitro and in vivo. *J Korean Med Sci* 2017; 32: 1385–1395.

[334] Miskimins WK, Ahn HJ, Kim JY, et al. Synergistic Anti-Cancer Effect of Phenformin and Oxamate. *PLoS One* 2014; 9: e85576.

[335] Léauté-Labrèze C, de la Roque ED, Hubiche T, et al. Propranolol for Severe Hemangiomas of Infancy. *N Engl J Med* 2008; 358: 2649–2651.

[336] Masur K, Niggemann B, Zanker KS, et al. Norepinephrine-induced migration of SW 480 colon carcinoma cells is inhibited by β-blockers. *Cancer Res* 2001; 61: 2866–2869.

[337] Chin CC, Li JM, Lee KF, et al. Selective β2-AR Blockage Suppresses Colorectal Cancer Growth Through Regulation of EGFR-Akt/ERK1/2 Signaling, G1-Phase

Arrest, and Apoptosis. *J Cell Physiol* 2016; 231: 459–472.

[338] Shaashua L, Shabat-Simon M, Haldar R, et al. Perioperative COX-2 and β-Adrenergic Blockade Improves Metastatic Biomarkers in Breast Cancer Patients in a Phase-II Randomized Trial. *Clin Cancer Res* 2017; 23: 4651–4661.

[339] Pasquier E, Ciccolini J, Carre M, et al. Propranolol potentiates the anti-angiogenic effects and antitumor efficacy of chemotherapy agents: Implication in breast cancer treatment. *Oncotarget* 2011; 2: 797–809.

[340] Fu X, Tan T, Liu P. Regulation of Autophagy by Non-Steroidal Anti-Inflammatory Drugs in Cancer. *Cancer Manag Res* 2020; 12: 4595–4604.

[341] Balkwill F, Mantovani A. Inflammation and cancer: back to Virchow? *Lancet* 2001; 357: 539–545.

[342] Brücher BLDM, Jamall IS. Epistemology of the origin of cancer: a new paradigm. *BMC Cancer* 2014; 14: 331.

[343] Dihlmann S, von Knebel Doeberitz M. Wnt/b-catenin-pathway as a molecular target for future anti-cancer therapeutics. *Int J Cancer* 2005; 113: 515–524.

[344] Ho C-C, Yang XW, Lee T-L, et al. Activation of p53 signalling in acetylsalicylic acid-induced apoptosis in OC2 human oral cancer cells. *Eur J Clin Invest* 2003; 33: 875–882.

[345] Brücher BLDM, Jamall IS. Eicosanoids in carcinogenesis. *4open* 2019; 2: 9.

[346] Ashktorab H, Dawkins FW, Mohamed R, et al. Apoptosis induced by aspirin and 5-fluorouracil in human colonic adenocarcinoma cells. *Dig Dis Sci* 2005; 50: 1025–1032.

[347] Jin S, Wu X. Aspirin inhibits colon cancer cell line migration through regulating epithelial-mesenchymal transition via wnt signaling. *Oncol Lett* 2019; 17: 4675–4682.

[348] Brücher BLDM, Jamall IS. Chronic inflammation evoked by pathogenic stimulus during carcinogenesis. *4open* 2019; 2: 8.

[349] May K, Eghbal B, Ahmadinejad M, et al. Evaluation of Effectiveness and Tolerability of Isosorbide Mononitrate during a Three-Year Period in Patients with Angina Pectoris. *Cardiology* 1991; 79: 46–50.

[350] Chen C, Hu JT, Tu YJ, et al. Effects of isosorbide mononitrate on the restoration of injured artery in mice in vivo. *Eur J Pharmacol* 2010; 640: 150–156.

[351] Pipili-Synetos E, Papageorgiou A, Sakkoula E, et al. Inhibition of angiogenesis, tumour growth and metastasis by the NO-releasing vasodilators, isosorbide mononitrate and dinitrate. *Br J Pharmacol* 1995; 116: 1829–1834.

[352] Wang X, Diao Y, Liu Y, et al. Synergistic apoptosis-inducing effect of aspirin and isosorbide mononitrate on human colon cancer cells. *Mol Med Rep* 2015; 12: 4750–4758.

[353] Cuzick J, Otto F, Baron JA, et al. Aspirin and non-steroidal anti-inflammatory drugs for cancer prevention: an international consensus statement. *Lancet Oncol* 2009; 10: 501–507.

[354] Rothwell PM, Fowkes FGR, Belch JF, et al. Effect of daily aspirin on long-term risk of death due to cancer: analysis of individual patient data from randomised trials. *Lancet* 2011; 377: 31–41.

[355] Erkisa M, Aydinlik S, Cevatemre B, et al. A promising therapeutic combination for metastatic prostate cancer: Chloroquine as autophagy inhibitor and palladium(II) barbiturate complex. *Biochimie* 2020; 175: 159–172.

[356] Eloranta K, Cairo S, Liljeström E, et al. Chloroquine Triggers Cell Death and Inhibits PARPs in Cell Models of Aggressive Hepatoblastoma. *Front Oncol*; 10.

[357] Sasaki K, Tsuno NH, Sunami E, et al. Resistance of colon cancer to 5-fluorouracil may be overcome by combination with chloroquine, an in vivo study. *Anticancer Drugs* 2012; 23: 675–682.

[358] Santos DM, Pantano L, Pronzati G, et al. Screening for YAP inhibitors identifies statins as modulators of fibrosis. *Am J Respir Cell Mol Biol* 2020; 62: 479–492.

[359] Brücher BLDM, Lang F, Jamall IS. NF- κ B signaling and crosstalk during carcinogenesis. *4open* 2019; 2: 13.

[360] Zhou M, Zheng J, Bi J, et al. Synergistic inhibition of colon cancer cell growth by a combination of atorvastatin and phloretin. *Oncol Lett* 2018; 15: 1985–1992.

[361] Wu X, Song M, Qiu P, et al. Synergistic chemopreventive effects of nobiletin and atorvastatin on colon carcinogenesis. *Carcinogenesis* 2017; 38: 455–464.

[362] Środa-Pomianek K, Michalak K, Palko-Łabuz A, et al. Simvastatin strongly augments proapoptotic, anti-inflammatory and cytotoxic activity of oxicam derivatives in doxorubicin-resistant colon cancer cells. *Anticancer Res* 2019; 39: 727–734.

[363] Jang HJ, Hong EM, Jang J, et al. Synergistic Effects of Simvastatin and Irinotecan

against Colon Cancer Cells with or without Irinotecan Resistance. *Gastroenterol Res Pract* 2016; 2016: 1–9.

[364] Środa-Pomianek K, Michalak K, Palko-Łabuz A, et al. The combined use of phenothiazines and statins strongly affects doxorubicin-resistance, apoptosis, and Cox-2 activity in colon cancer cells. *Int J Mol Sci* 2019; 20: 955.

[365] Van Wyhe R, Rahal O, Woodward W. Effect of statins on breast cancer recurrence and mortality: a review. *Breast Cancer Targets Ther* 2017; 9: 559–565.

[366] Fan X, Zhu M, Qiu F, et al. Curcumin may be a potential adjuvant treatment drug for colon cancer by targeting CD44. *Int Immunopharmacol* 2020; 88: 106991.

[367] Zhang P, Lai ZL, Chen HF, et al. Curcumin synergizes with 5-fluorouracil by impairing AMPK/ULK1-dependent autophagy, AKT activity and enhancing apoptosis in colon cancer cells with tumor growth inhibition in xenograft mice. *J Exp Clin Cancer Res* 2017; 36: 190.

[368] Xiao B, Si X, Han MK, et al. Co-delivery of camptothecin and curcumin by cationic polymeric nanoparticles for synergistic colon cancer combination chemotherapy. *J Mater Chem B* 2015; 3: 7724–7733.

[369] Zhao H, Liu Q, Wang S, et al. In vitro additive antitumor effects of dimethoxycurcumin and 5-fluorouracil in colon cancer cells. *Cancer Med* 2017; 6: 1698–1706.

[370] Ling G, Lamprecht S, Shubinsky G, et al. Mycophenolate mofetil alone and in combination with tacrolimus inhibits the proliferation of HT-29 human colonic adenocarcinoma cell line and might interfere with colonic tumorigenesis. *Anticancer Res* 2018; 38: 3333–3339.

[371] Adrian TE, Collin P. The Anti-Cancer Effects of Frondoside A. *Mar Drugs* 2018; 16: 64.

[372] Ma X, Kundu N, Collin PD, et al. Frondoside A inhibits breast cancer metastasis and antagonizes prostaglandin E receptors EP4 and EP2. *Breast Cancer Res Treat* 2012; 132: 1001–1008.

[373] Attoub S, Arafat K, Gélaude A, et al. Frondoside A Suppressive Effects on Lung Cancer Survival, Tumor Growth, Angiogenesis, Invasion, and Metastasis. *PLoS One* 2013; 8: e53087.

[374] Dyshlovoy SA, Menchinskaya ES, Venz S, et al. The marine triterpene glycoside frondoside A exhibits activity in vitro and in vivo in prostate cancer. *Int J Cancer* 2016;

138: 2450–2465.

[375] Attoub S, Arafat K, Khalaf T, et al. Frondoside a enhances the anti-cancer effects of oxaliplatin and 5-fluorouracil on colon cancer cells. *Nutrients* 2018; 10: 560.

[376] Liu Y, Bi T, Wang Z, et al. Oxymatrine synergistically enhances antitumor activity of oxaliplatin in colon carcinoma through PI3K/AKT/mTOR pathway. *Apoptosis* 2016; 21: 1398–1407.

[377] Zhu XH, Lang HD, Wang XL, et al. Synergy between dihydromyricetin intervention and irinotecan chemotherapy delays the progression of colon cancer in mouse models. *Food Funct* 2019; 10: 2040–2049.

[378] Zhang K, Zhang K, Li Y, et al. Silencing survivin expression inhibits the tumor growth of non.small.cell lung cancer cells in vitro and in vivo. *Mol Med Rep* 2015; 11: 639–644.

[379] Liu B, Zhou W, Chen X, et al. Dihydromyricetin induces mouse hepatoma Hepal-6 cell apoptosis via the transforming growth factor-β pathway. *Mol Med Rep* 2015; 11: 1609–1614.

[380] Roy K, Kanwar RK, Krishnakumar S, et al. Competitive inhibition of survivin using a cell-permeable recombinant protein induces cancer-specific apoptosis in colon cancer model. *Int J Nanomedicine* 2015; 10: 1019–1043.

[381] Sobral F, Sampaio A, Falcão S, et al. Chemical characterization, antioxidant, anti-inflammatory and cytotoxic properties of bee venom collected in Northeast Portugal. *Food Chem Toxicol* 2016; 94: 172–177.

[382] Wu G-S, Lu J-J, Guo J-J, et al. Synergistic anti-cancer activity of the combination of dihydroartemisinin and doxorubicin in breast cancer cells. *Pharmacol Rep* 2013; 65: 453–459.

[383] Thorn CF, Oshiro C, Marsh S, et al. Doxorubicin pathways. *Pharmacogenet Genomics* 2011; 21: 440–446.

[384] Dong Z, Zhang D, Yang R, et al. Paclitaxel: new uses for an old drug. *Drug Des Devel Ther* 2014; 8: 279.

[385] Markman M, Mekhail TM. Paclitaxel in cancer therapy. *Expert Opin Pharmacother* 2002; 3: 755–766.

[386] Jordan MA, Wilson L. Microtubules as a target for anticancer drugs. *Nat Rev Cancer* 2004; 4: 253–265.

[387] Gan L, Chen S, Wang Y, et al. Inhibition of the Androgen Receptor as a Novel Mechanism of Taxol Chemotherapy in Prostate Cancer. *Cancer Res* 2009; 69: 8386–8394.

[388] Alexandre J, Hu Y, Lu W, et al. Novel Action of Paclitaxel against Cancer Cells: Bystander Effect Mediated by Reactive Oxygen Species. *Cancer Res* 2007; 67: 3512–3517.

[389] Taxol, https://www.breastcancer.org/treatment/druglist/taxol (accessed 11 November 2020).

[390] Wehbe R, Frangieh J, Rima M, et al. Bee Venom: Overview of Main Compounds and Bioactivities for Therapeutic Interests. *Molecules* 2019; 24: 2997.

[391] Rady I, Siddiqui IA, Rady M, et al. Melittin, a major peptide component of bee venom, and its conjugates in cancer therapy. *Cancer Lett* 2017; 402: 16–31.

[392] Mahadevappa R, Ma R, Kwok HF. Venom Peptides: Improving Specificity in Cancer Therapy. *Trends in cancer* 2017; 3: 611–614.

[393] Xie J, Bi Y, Zhang H, et al. Cell-Penetrating Peptides in Diagnosis and Treatment of Human Diseases: From Preclinical Research to Clinical Application. *Front Pharmacol* 2020; 11: 697.

[394] GUPTA B, LEVCHENKO T, TORCHILIN V. Intracellular delivery of large molecules and small particles by cell-penetrating proteins and peptides. *Adv Drug Deliv Rev* 2005; 57: 637–651.

[395] Tripathi PP, Arami H, Banga I, et al. Cell penetrating peptides in preclinical and clinical cancer diagnosis and therapy. *Oncotarget* 2018; 9: 37252–37267.

[396] Pooga M, Langel Ü. Classes of Cell-Penetrating Peptides. In: *Cell-Penetrating Peptides: Methods and Protocols*. Humana Press, New York, NY, pp. 3–28.

[397] Derakhshankhah H, Jafari S. Cell penetrating peptides: A concise review with emphasis on biomedical applications. *Biomed Pharmacother* 2018; 108: 1090–1096.

[398] GUO Z, PENG H, KANG J, et al. Cell-penetrating peptides: Possible transduction mechanisms and therapeutic applications. *Biomed Reports* 2016; 4: 528–534.

[399] F M. Cell-penetrating peptides: classes, origin, and current landscape. *Drug Discov Today* 2012; 17: 850–860.

[400] PA W, DJ M, K P, et al. The design, synthesis, and evaluation of molecules that enable or enhance cellular uptake: peptoid molecular transporters. *Proc Natl Acad*

Sci U S A 2000; 97: 13003–13008.

[401] JC M, H S, SC W, et al. Efficiency of protein transduction is cell type-dependent and is enhanced by dextran sulfate. *J Biol Chem* 2002; 277: 30208–30218.

[402] Verdurmen WPR, Brock R. Biological responses towards cationic peptides and drug carriers. *Trends Pharmacol Sci* 2011; 32: 116–124.

[403] Siegel RL, Miller KD, Jemal A. Cancer statistics, 2020. *CA Cancer J Clin* 2020; 70: 7–30.

[404] P A, S B, SS U, et al. CPPsite 2.0: a repository of experimentally validated cell-penetrating peptides. *Nucleic Acids Res* 2016; 44: D1098–D1103.

[405] Yamada T, Das Gupta TK, Beattie CW, et al. P28, an anionic cell-penetrating peptide, increases the activity of wild type and mutated p53 without altering its conformation. *Mol Pharm* 2013; 10: 3375–3383.

[406] Warso MA, Richards JM, Mehta D, et al. A first-in-class, first-in-human, phase I trial of p28, a non-HDM2-mediated peptide inhibitor of p53 ubiquitination in patients with advanced solid tumours. *Br J Cancer* 2013; 108: 1061–1070.

[407] Kondo E, Saito K, Tashiro Y, et al. Tumour lineage-homing cell-penetrating peptides as anticancer molecular delivery systems. *Nat Commun* 2012; 3: 951.

[408] Duarte D, Fraga AG, Pedrosa J, et al. Increasing the potential of cell-penetrating peptides for cancer therapy using a new pentagonal scaffold. *Eur J Pharmacol* 2019; 860: 172554.

[409] Tang J, Wennerberg K, Aittokallio T. What is synergy? The Saariselkï¿½ agreement revisited. *Front Pharmacol* 2015; 6: 1–5.

[410] Lederer S, Dijkstra TMH, Heskes T. Additive dose response models: Defining synergy. *Front Pharmacol* 2019; 10: 1–15.

[411] Roell KR, Reif DM, Motsinger-Reif AA. An Introduction to Terminology and Methodology of Chemical Synergy-Perspectives from Across Disciplines. *Front Pharmacol* 2017; 8: 158.

[412] Geary N. Understanding synergy. *Am J Physiol Metab* 2013; 304: E237–E253.

[413] Nieuwenhuis S, Forstmann BU, Wagenmakers EJ. Erroneous analyses of interactions in neuroscience: a problem of significance. *Nat Neurosci* 2011; 14: 1105–1107.

[414] Lehár J, Zimmermann GR, Krueger AS, et al. Chemical combination effects predict connectivity in biological systems. *Mol Syst Biol* 2007; 3: 80.

[415] Vlot AHC, Aniceto N, Menden MP, et al. Applying synergy metrics to combination screening data: agreements, disagreements and pitfalls. *Drug Discov Today* 2019; 24: 2286–2298.

[416] Slinker BK. The statistics of synergism. *J Mol Cell Cardiol* 1998; 30: 723–731.

[417] Caudle RM, Williams GM. The misuse of analysis of variance to detect synergy in combination drug studies. *Pain* 1993; 55: 313–317.

[418] BLISS CI. THE TOXICITY OF POISONS APPLIED JOINTLY. *Ann Appl Biol* 1939; 26: 585–615.

[419] Greco WR, Bravo G, Parsons JC. The search for synergy: a critical review from a response surface perspective. *Pharmacol Rev* 1995; 47: 331–85.

[420] Berenbaum MC. What is synergy? *Pharmacol Rev* 1989; 41: 93–141.

[421] Goldoni M, Johansson C. A mathematical approach to study combined effects of toxicants in vitro: Evaluation of the Bliss independence criterion and the Loewe additivity model. *Toxicol Vitr* 2007; 21: 759–769.

[422] Berenbaum MC. Synergy, additivism and antagonism in immunosuppression. A critical review. *Clin Exp Immunol* 1977; 28: 1–18.

[423] LOEWE S. The problem of synergism and antagonism of combined drugs. *Arzneimittelforschung* 1953; 3: 285–90.

[424] Loewe S. Die Mischarznei - Versuch einer allgemeinen Pharmakologie der Arzneikombinationen. *Klin Wochenschr* 1927; 6: 1077–1085.

[425] Loewe S, Muischnek H. Über Kombinationswirkungen - Mitteilung: Hilfsmittel der Fragestellung. *Arch für Exp Pathol und Pharmakologie* 1926; 114: 313–326.

[426] Tallarida RJ. Revisiting the Isobole and Related Quantitative Methods for Assessing Drug Synergism. *J Pharmacol Exp Ther* 2012; 342: 2–8.

[427] Chou TC, Talalay P. Analysis of combined drug effects: a new look at a very old problem. *Trends Pharmacol Sci* 1983; 4: 450–454.

[428] Chou T-C, Talalay P. Quantitative analysis of dose-effect relationships: the combined effects of multiple drugs or enzyme inhibitors. *Adv Enzyme Regul* 1984; 22: 27–55.

[429] Grabovsky Y, Tallarida RJ. Isobolographic Analysis for Combinations of a Full and

Partial Agonist: Curved Isoboles. *J Pharmacol Exp Ther* 2004; 310: 981–986.

[430] Sidorov P, Naulaerts S, Ariey-Bonnet J, et al. Predicting Synergism of Cancer Drug Combinations Using NCI-ALMANAC Data. *Front Chem* 2019; 7: 1–13.

[431] Zhao W, Sachsenmeier K, Zhang L, et al. A New Bliss Independence Model to Analyze Drug Combination Data. *J Biomol Screen* 2014; 19: 817–821.

[432] Rodea-Palomares I, González-Pleiter M, Martín-Betancor K, et al. Additivity and interactions in ecotoxicity of pollutant mixtures: Some Patterns, Conclusions, and open questions. *Toxics* 2015; 3: 342–369.

[433] Yadav B, Wennerberg K, Aittokallio T, et al. Searching for Drug Synergy in Complex Dose–Response Landscapes Using an Interaction Potency Model. *Comput Struct Biotechnol J* 2015; 13: 504–513.

[434] Ma J, Motsinger-Reif A. Current Methods for Quantifying Drug Synergism. *Proteomics Bioinforma Curr Res* 2019; 1: 43–48.

[435] Ocana A, Amir E, Yeung C, et al. How valid are claims for synergy in published clinical studies? *Ann Oncol* 2012; 23: 2161–2166.

[436] Shafer SL. All models are wrong. *Anesthesiology* 2012; 116: 240–241.

[437] Cokol M, Chua HN, Tasan M, et al. Systematic exploration of synergistic drug pairs. *Mol Syst Biol* 2011; 7: 544.

[438] Lehár J, Krueger AS, Avery W, et al. Synergistic drug combinations tend to improve therapeutically relevant selectivity. *Nat Biotechnol* 2009; 27: 659–666.

[439] Wientjes MG. Comparison of methods for evaluating drug-drug interaction. *Front Biosci* 2010; E2: 86.

[440] Zhao L, Wientjes MG, Au JLS. Evaluation of Combination Chemotherapy. *Clin Cancer Res* 2004; 10: 7994–8004.

[441] Borisy AA, Elliott PJ, Hurst NW, et al. Systematic discovery of multicomponent therapeutics. *Proc Natl Acad Sci* 2003; 100: 7977–7982.

[442] US FDA. Guidance for Industry: Codevelopment of Two or More New Investigational Drugs for Use in Combination. *Fda* 2013; 1–5.

[443] European Medicines Agency Committee for Human Medicinal Products. Committee for Human Medicinal Products (CHMP) Guideline on clinical development of fixed combination medicinal products, www.ema.europa.eu/contact (2017, accessed 18

March 2022).

[444] World Health Organization. Annex 5 Guidelines for registration of fixed-dose. *WHO Tech Rep Ser* 2005; 94–142.

[445] Ram R. Extrapolation of Animal Research Data to Humans: An Analysis of the Evidence. In: *Animal Experimentation: Working Towards a Paradigm Change*. BRILL, pp. 341–375.

[446] Woodcock J, Griffin JP, Behrman RE. Development of Novel Combination Therapies. *N Engl J Med* 2011; 364: 985–987.

[447] Keith CT, Borisy AA, Stockwell BR. Multicomponent therapeutics for networked systems. *Nat Rev Drug Discov* 2005; 4: 71–78.

[448] Hand DJ. Synergy in Drug Combinations. Springer, Berlin, Heidelberg, pp. 471–475.

[449] Sinzger M, Vanhoefer J, Loos C, et al. Comparison of null models for combination drug therapy reveals Hand model as biochemically most plausible. *Sci Rep* 2019; 9: 1–15.

[450] Di Veroli GY, Fornari C, Wang D, et al. Combenefit: an interactive platform for the analysis and visualization of drug combinations. *Bioinformatics* 2016; 32: 2866–2868.

[451] Twarog NR, Stewart E, Hammill CV, et al. BRAID: A Unifying Paradigm for the Analysis of Combined Drug Action. *Sci Rep* 2016; 6: 25523.

[452] Schindler M. Theory of synergistic effects: Hill-type response surfaces as 'null-interaction' models for mixtures. *Theor Biol Med Model* 2017; 14: 1–16.

[453] Zheng S, Wang W, Aldahdooh J, et al. SynergyFinder Plus: Toward Better Interpretation and Annotation of Drug Combination Screening Datasets. *Genomics Proteomics Bioinformatics* 2022; 20: 587–596.

[454] Meyer CT, Wooten DJ, Paudel BB, et al. Quantifying Drug Combination Synergy along Potency and Efficacy Axes. *Cell Syst* 2019; 8: 97-108.e16.

[455] Zimmer A, Katzir I, Dekel E, et al. Prediction of multidimensional drug dose responses based on measurements of drug pairs. *Proc Natl Acad Sci U S A* 2016; 113: 10442–10447.

[456] Lambert RJW, Dawson DA. New models for the time dependent toxicity of individual and combined toxicants. *Toxicol Res (Camb)* 2019; 8: 509.

[457] Boik JC, Newman RA, Boik RJ. Quantifying synergism/antagonism using nonlinear mixed-effects modeling: a simulation study. *Stat Med* 2008; 27: 1040–1061.

[458] Hennessey VG, Rosner GL, Bast RC, et al. A Bayesian approach to dose-response assessment and synergy and its application to in vitro dose-response studies. *Biometrics* 2010; 66: 1275–1283.

[459] Fu J, Zhang N, Chou JH, et al. Drug combination in vivo using combination index method: Taxotere and T607 against colon carcinoma HCT-116 xenograft tumor in nude mice. *Synergy* 2016; 3: 15–30.

[460] Skeberdytė A, Sarapinienė I, Krasko JA, et al. Salinomycin and dichloroacetate synergistically inhibit Lewis lung carcinoma cell proliferation, tumor growth and metastasis. *Biochem Biophys Res Commun* 2020; 523: 874–879.

[461] Xu Y, Zong S, Gao X, et al. Combined treatment of ABT199 and irinotecan suppresses KRAS-mutant lung cancer cells. *Gene* 2019; 688: 1–6.

[462] Ghosh S, Pal A, Ray M. Methylglyoxal in combination with 5-Fluorouracil elicits improved chemosensitivity in breast cancer through apoptosis and cell cycle inhibition. *Biomed Pharmacother* 2019; 114: 108855.

[463] Buocikova V, Longhin EM, Pilalis E, et al. Decitabine potentiates efficacy of doxorubicin in a preclinical trastuzumab-resistant HER2-positive breast cancer models. *Biomed Pharmacother* 2022; 147: 112662.

[464] Shen N, Yang C, Zhang X, et al. Cisplatin nanoparticles possess stronger anti-tumor synergy with PD1/PD-L1 inhibitors than the parental drug. *Acta Biomater* 2021; 135: 543–555.

[465] Damaraju VL, Bouffard DY, Wong CKW, et al. Synergistic activity of troxacitabine (Troxatyl™) and gemcitabine in pancreatic cancer. *BMC Cancer* 2007; 7: 1–11.

[466] Sánchez BG, Bort A, Mateos-Gómez PA, et al. Combination of the natural product capsaicin and docetaxel synergistically kills human prostate cancer cells through the metabolic regulator AMP-activated kinases. *Cancer Cell Int* 2019; 19: 1–14.

[467] Robles AJ, Kurmasheva RT, Bandyopadhyay A, et al. Evaluation of Eribulin Combined with Irinotecan for Treatment of Pediatric Cancer Xenografts. *Clin Cancer Res* 2020; 26: 3012–3023.

[468] Palmer AC, Izar B, Hwangbo H, et al. Predictable Clinical Benefits without Evidence of Synergy in Trials of Combination Therapies with Immune-Checkpoint Inhibitors.

Clin Cancer Res 2022; 28: 368–377.

[469] Kang Y-K, Chen L-T, Ryu M-H, et al. Nivolumab plus chemotherapy versus placebo plus chemotherapy in patients with HER2-negative, untreated, unresectable advanced or recurrent gastric or gastro-oesophageal junction cancer (ATTRACTION-4): a randomised, multicentre, double-blind, placebo-contr. *Lancet Oncol* 2022; 23: 234–247.

[470] Jain N, Keating M, Thompson P, et al. Ibrutinib Plus Venetoclax for First-line Treatment of Chronic Lymphocytic Leukemia. *JAMA Oncol* 2021; 7: 1213.

[471] Cousin S, Cantarel C, Guegan J-P, et al. Regorafenib-Avelumab Combination in Patients with Microsatellite Stable Colorectal Cancer (REGOMUNE): A Single-arm, Open-label, Phase II Trial. *Clin Cancer Res* 2021; 27: 2139–2147.

[472] Curigliano G, Martin M, Jhaveri K, et al. Alpelisib in combination with everolimus ± exemestane in solid tumours: Phase Ib randomised, open-label, multicentre study. *Eur J Cancer* 2021; 151: 49–62.

[473] Lim K-H, Opyrchal M, Acharya A, et al. Phase 1 study combining alisertib with nab-paclitaxel in patients with advanced solid malignancies. *Eur J Cancer* 2021; 154: 102–110.

[474] Hong DS, Moore KN, Bendell JC, et al. Preclinical Evaluation and Phase Ib Study of Prexasertib, a CHK1 Inhibitor, and Samotolisib (LY3023414), a Dual PI3K/mTOR Inhibitor. *Clin Cancer Res* 2021; 27: 1864–1874.

[475] Amin M, Gao F, Terrero G, et al. Phase I Study of Docetaxel and Temsirolimus in Refractory Solid Tumors. *Am J Clin Oncol* 2021; 44: 443–448.

[476] Ianevski A, Giri AK, Aittokallio T. SynergyFinder 2.0: Visual analytics of multi-drug combination synergies. *Nucleic Acids Res* 2021; 48: W488–W493.

[477] Shu C-H, Yang WK, Shih Y-L, et al. Cell cycle G2/M arrest and activation of cyclin-dependent kinases associated with low-dose paclitaxel-induced sub-G1 apoptosis. *Apoptosis* 1997; 2: 463–470.

[478] Jänicke RU. MCF-7 breast carcinoma cells do not express caspase-3. *Breast Cancer Res Treat* 2009; 117: 219–221.

[479] O'Brien FE, Dinan TG, Griffin BT, et al. Interactions between antidepressants and P-glycoprotein at the blood-brain barrier: clinical significance of in vitro and in vivo findings. *Br J Pharmacol* 2012; 165: 289–312.

[480] Kapoor A, Iqbal M, Petropoulos S, et al. Effects of Sertraline and Fluoxetine on P-Glycoprotein at Barrier Sites: In Vivo and In Vitro Approaches. *PLoS One* 2013; 8: e56525.

[481] Abou El Ela A, Härtter S, Schmitt U, et al. Identification of P-glycoprotein substrates and inhibitors among psychoactive compounds — implications for pharmacokinetics of selected substrates†. *J Pharm Pharmacol* 2010; 56: 967–975.

[482] Kashif M, Andersson C, Mansoori S, et al. Bliss and Loewe interaction analyses of clinically relevant drug combinations in human colon cancer cell lines reveal complex patterns of synergy and antagonism. *Oncotarget* 2017; 8: 103952–103967.

[483] Ben-Hamo R, Zilberberg A, Cohen H, et al. Resistance to paclitaxel is associated with a variant of the gene BCL2 in multiple tumor types. *NPJ Precis Oncol* 2019; 3: 12.

[484] Parasuraman S. Toxicological screening. *J Pharmacol Pharmacother* 2011; 2: 74–79.

[485] Krewski D, Acosta D, Andersen M, et al. Toxicity testing in the 21st century: a vision and a strategy. *J Toxicol Environ Health B Crit Rev* 2010; 13: 51–138.

[486] Samutprasert P, Chiablaem K, Teeraseranee C, et al. Epigallocatechin gallate-zinc oxide co-crystalline nanoparticles as an anticancer drug that is non-toxic to normal cells. *RSC Adv* 2018; 8: 7369–7376.

[487] Talevi A, Bellera CL. Challenges and opportunities with drug repurposing: finding strategies to find alternative uses of therapeutics. *Expert Opin Drug Discov* 2020; 15: 397–401.

[488] Cao J, Chen Z, Chi J, et al. Recent progress in synergistic chemotherapy and phototherapy by targeted drug delivery systems for cancer treatment. *Artif Cells, Nanomedicine Biotechnol* 2018; 46: 817–830.

[489] Duarte D, Cardoso A, Vale N. Synergistic Growth Inhibition of HT-29 Colon and MCF-7 Breast Cancer Cells with Simultaneous and Sequential Combinations of Antineoplastics and CNS Drugs. *Int J Mol Sci* 2021; 22: 7408.

[490] Duarte D, Vale N. New trends for antimalarial drugs: Synergism between antineoplastics and antimalarials on breast cancer cells. *Biomolecules* 2020; 10: 1–20.

[491] Santos Ramos F, Wons L, João Cavalli I, et al. Epithelial-mesenchymal transition in

cancer: An overview. *Integr Cancer Sci Ther* 2017; 4: 1–5.

[492] Guo F, Parker Kerrigan BC, Yang D, et al. Post-transcriptional regulatory network of epithelial-to-mesenchymal and mesenchymal-to-epithelial transitions. *J Hematol Oncol* 2014; 7: 19.

[493] Steinestel K, Eder S, Schrader AJ, et al. Clinical significance of epithelial-mesenchymal transition. *Clin Transl Med* 2014; 3: 17.

[494] Acloque H, Adams MS, Fishwick K, et al. Epithelial-mesenchymal transitions: the importance of changing cell state in development and disease. *J Clin Invest* 2009; 119: 1438–1449.

[495] Rhim AD, Mirek ET, Aiello NM, et al. EMT and dissemination precede pancreatic tumor formation. *Cell* 2012; 148: 349–361.

[496] Ye X, Tam WL, Shibue T, et al. Distinct EMT programs control normal mammary stem cells and tumour-initiating cells. *Nature* 2015; 525: 256–260.

[497] Morel A-P, Lièvre M, Thomas C, et al. Generation of Breast Cancer Stem Cells through Epithelial-Mesenchymal Transition. *PLoS One* 2008; 3: e2888.

[498] Singh A, Settleman J. EMT, cancer stem cells and drug resistance: an emerging axis of evil in the war on cancer. *Oncogene* 2010; 29: 4741–4751.

[499] Mani SA, Guo W, Liao MJ, et al. The epithelial-mesenchymal transition generates cells with properties of stem cells. *Cell* 2008; 133: 704–715.

[500] Krebs AM, Mitschke J, Losada ML, et al. The EMT-activator Zeb1 is a key factor for cell plasticity and promotes metastasis in pancreatic cancer. *Nat Cell Biol* 2017; 19: 518–529.

[501] Thompson EW, Newgreen DF. Carcinoma invasion and metastasis: A role for epithelial-mesenchymal transition? *Cancer Research* 2005; 65: 5991–5995.

[502] Pickup M, Novitskiy S, Moses HL. The roles of TGFβ in the tumour microenvironment. *Nat Rev Cancer* 2013; 13: 788–799.

[503] Lamouille S, Xu J, Derynck R. Molecular mechanisms of epithelial-mesenchymal transition. *Nat Rev Mol Cell Biol* 2014; 15: 178–196.

[504] Vieira AF, Paredes J. P-cadherin and the journey to cancer metastasis. *Mol Cancer* 2015; 14: 178.

[505] Wang Y, Zhou BP. Epithelial-mesenchymal transition in breast cancer progression

and metastasis. *Chin J Cancer* 2011; 30: 603–611.

[506] Kalluri R, Weinberg RA. The basics of epithelial-mesenchymal transition. *J Clin Invest* 2009; 119: 1420–1428.

[507] Patel NA, Patel PS, Vora HH. Role of PRL-3, Snail, Cytokeratin and Vimentin expression in epithelial mesenchymal transition in breast carcinoma. *Breast Dis* 2015; 35: 113–127.

[508] Lehtinen L, Ketola K, Mäkelä R, et al. High-throughput RNAi screening for novel modulators of vimentin expression identifies MTHFD2 as a regulator of breast cancer cell migration and invasion. *Oncotarget* 2013; 4: 48–63.

[509] Mizushima N, Yoshimori T, Levine B. Methods in Mammalian Autophagy Research. *Cell* 2010; 140: 313–326.

[510] Mizushima N, Levine B. Autophagy in mammalian development and differentiation. *Nat Cell Biol* 2010; 12: 823–830.

[511] Russell RC, Yuan H-X, Guan K-L. Autophagy regulation by nutrient signaling. *Cell Res* 2014; 24: 42–57.

[512] Yun CW, Lee SH. The Roles of Autophagy in Cancer. *Int J Mol Sci*; 19.

[513] Rosenfeldt MT, Ryan KM. The multiple roles of autophagy in cancer. *Carcinogenesis* 2011; 32: 955–963.

[514] Scott RC, Schuldiner O, Neufeld TP. Role and regulation of starvation-induced autophagy in the Drosophila fat body. *Dev Cell* 2004; 7: 167–178.

[515] Kim J, Kundu M, Viollet B, et al. AMPK and mTOR regulate autophagy through direct phosphorylation of Ulk1. *Nat Cell Biol* 2011; 13: 132–141.

[516] Martina JA, Chen Y, Gucek M, et al. MTORC1 functions as a transcriptional regulator of autophagy by preventing nuclear transport of TFEB. *Autophagy* 2012; 8: 903–914.

[517] Maiuri MC, Tasdemir E, Criollo A, et al. Control of autophagy by oncogenes and tumor suppressor genes. *Cell Death Differ* 2009; 16: 87–93.

[518] Botti J, Djavaheri-Mergny M, Pilatte Y, et al. Autophagy Signaling and the Cogwheels of Cancer. *Autophagy* 2006; 2: 67–73.

[519] Gewirtz DA. The Four Faces of Autophagy: Implications for Cancer Therapy. *Cancer Res* 2014; 74: 647–651.

[520] Salminen A, Kaarniranta K, Kauppinen A. Beclin 1 interactome controls the crosstalk

between apoptosis, autophagy and inflammasome activation: Impact on the aging process. *Ageing Res Rev* 2013; 12: 520–534.

[521] Lim K-H, Staudt LM. Toll-Like Receptor Signaling. *Cold Spring Harb Perspect Biol* 2013; 5: a011247–a011247.

[522] Nahta R, O'Regan RM. Evolving Strategies for Overcoming Resistance to HER2-Directed Therapy: Targeting the PI3K/Akt/mTOR Pathway. *Clin Breast Cancer* 2010; 10: S72–S78.

[523] Pachow D, Wick W, Gutmann DH, et al. The mTOR signaling pathway as a treatment target for intracranial neoplasms. *Neuro Oncol* 2015; 17: 189–199.

[524] Ghidini M, Petrelli F, Ghidini A, et al. Clinical development of mTor inhibitors for renal cancer. *Expert Opin Investig Drugs* 2017; 26: 1229–1237.

[525] AZ drops midstage cancer drug vistusertib. 2018; 15: 2–4.

[526] Zhang Y, Cao Y, Sun X, et al. Chloroquine (CQ) exerts anti-breast cancer through modulating microenvironment and inducing apoptosis. *Int Immunopharmacol* 2017; 42: 100–107.

[527] Datta S, Choudhury D, Das A, et al. Autophagy inhibition with chloroquine reverts paclitaxel resistance and attenuates metastatic potential in human nonsmall lung adenocarcinoma A549 cells via ROS mediated modulation of β-catenin pathway. *Apoptosis* 2019; 24: 414–433.

[528] Mereddy GR, Ronayne CT. Repurposing Antimalarial Drug Mefloquine for Cancer Treatment. *Transl Med* 2018; 08: 8–11.

[529] Lin JH, Yamazaki M. Role of P-Glycoprotein in Pharmacokinetics. *Clin Pharmacokinet* 2003; 42: 59–98.

[530] Rebecca VW, Nicastri MC, Fennelly C, et al. PPT1 Promotes Tumor Growth and Is the Molecular Target of Chloroquine Derivatives in Cancer. *Cancer Discov* 2019; 9: 220–229.

[531] Koster KP, Yoshii A. Depalmitoylation by palmitoyl-protein thioesterase 1 in neuronal health and degeneration. *Front Synaptic Neurosci* 2019; 11: 1–10.

[532] Sapir T, Segal M, Grigoryan G, et al. The interactome of palmitoyl-protein thioesterase 1 (PPT1) affects neuronal morphology and function. *Front Cell Neurosci* 2019; 13: 1–14.

[533] Balouch B, Nagorsky H, Pham T, et al. Human INCL fibroblasts display abnormal

mitochondrial and lysosomal networks and heightened susceptibility to ROS-induced cell death. *PLoS One* 2021; 16: e0239689.

[534] Magalhães AC, Ricardo S, Moreira AC, et al. InfectionCMA: A Cell MicroArray Approach for Efficient Biomarker Screening in In Vitro Infection Assays. *Pathogens* 2022; 11: 313.

[535] Giridharan S, Srinivasan M. Mechanisms of NF-kB p65 and strategies for therapeutic manipulation. *J Inflamm Res* 2018; Volume 11: 407–419.

[536] Finch A, Pillans P. P-glycoprotein and its role in drug-drug interactions. *Aust Prescr* 2014; 37: 137–139.

[537] Jedlitschky G, Hoffmann U, Kroemer HK. Structure and function of the MRP2 (ABCC2) protein and its role in drug disposition. *Expert Opin Drug Metab Toxicol* 2006; 2: 351–366.

[538] Li LT, Jiang G, Chen Q, et al. Ki67 is a promising molecular target in the diagnosis of cancer (review). *Mol Med Rep* 2015; 11: 1566–1572.

[539] Wang L, Liang C, Li F, et al. PARP1 in Carcinomas and PARP1 Inhibitors as Antineoplastic Drugs. *Int J Mol Sci*; 18.

[540] Nunes M, Silva PMA, Coelho R, et al. Generation of Two Paclitaxel-Resistant High-Grade Serous Carcinoma Cell Lines With Increased Expression of P-Glycoprotein. *Front Oncol* 2021; 11: 4326.

[541] Zhang A, Wang X, Fan C, et al. The Role of Ki67 in Evaluating Neoadjuvant Endocrine Therapy of Hormone Receptor-Positive Breast Cancer. *Front Endocrinol (Lausanne)* 2021; 12: 1426.

[542] Schluter C, Duchrow M, Wohlenberg C, et al. The cell proliferation-associated antigen of antibody Ki-67: A very large, ubiquitous nuclear protein with numerous repeated elements, representing a new kind of cell cycle-maintaining proteins. *J Cell Biol* 1993; 123: 513–522.

[543] Chen A. PARP inhibitors: its role in treatment of cancer. *Chin J Cancer* 2011; 30: 463.

[544] Xia L, Tan S, Zhou Y, et al. Role of the NFκB-signaling pathway in cancer. *Onco Targets Ther* 2018; 11: 2063.

[545] Duarte D, Vale N. How Antimalarials and Antineoplastic Drugs can Interact in Combination Therapies: A Perspective on the Role of PPT1 Enzyme. *Curr Drug*

Metab 2021; 22: 1009–1016.

[546] Yap SQ, Mathavarajah S, Huber RJ. The converging roles of Batten disease proteins in neurodegeneration and cancer. *iScience* 2021; 24: 102337.

[547] Famta P, Shah S, Chatterjee E, et al. Exploring new Horizons in overcoming P-glycoprotein-mediated multidrug-resistant breast cancer via nanoscale drug delivery platforms. *Curr Res Pharmacol Drug Discov* 2021; 2: 100054.

[548] Cordon-Cardo C, O'Brien JP, Boccia J, et al. Expression of the multidrug resistance gene product (P-glycoprotein) in human normal and tumor tissues. *J Histochem Cytochem* 1990; 38: 1277–1287.

[549] Karthika C, Sureshkumar R, Zehravi M, et al. Multidrug Resistance of Cancer Cells and the Vital Role of P-Glycoprotein. *Life (Basel, Switzerland)*; 12.

[550] Khatoon E, Banik K, Harsha C, et al. Phytochemicals in cancer cell chemosensitization: Current knowledge and future perspectives. *Semin Cancer Biol* 2022; 80: 306–339.

[551] Turner AP, Alam C, Bendayan R. Efflux transporters in cancer resistance: Molecular and functional characterization of P-glycoprotein. In: *Drug Efflux Pumps in Cancer Resistance Pathways: From Molecular Recognition and Characterization to Possible Inhibition Strategies in Chemotherapy*. Elsevier, pp. 1–30.

[552] Guerra AR, Duarte MF, Duarte IF. Targeting Tumor Metabolism with Plant-Derived Natural Products: Emerging Trends in Cancer Therapy. *J Agric Food Chem* 2018; 66: 10663–10685.

[553] Erin N, Grahovac J, Brozovic A, et al. Tumor microenvironment and epithelial mesenchymal transition as targets to overcome tumor multidrug resistance. *Drug Resist Updat* 2020; 53: 100715.

[554] Zhang YK, Wang YJ, Gupta P, et al. Multidrug Resistance Proteins (MRPs) and Cancer Therapy. *AAPS J* 2015; 17: 802.

[555] Kranz J, Hessel S, Aretz J, et al. The role of the efflux carriers Abcg2 and Abcc2 for the hepatobiliary elimination of benzo[a]pyrene and its metabolites in mice. *Chem Biol Interact* 2014; 224: 36–41.

[556] Sharifi MJ, Bahoush G, Zaker F, et al. Association of -24CT, 1249GA, and 3972CT ABCC2 gene polymorphisms with methotrexate serum levels and toxic side effects in children with acute lymphoblastic leukemia. *Pediatr Hematol Oncol* 2014; 31: 169–

177.

[557] Yamasaki M, Makino T, Masuzawa T, et al. Role of multidrug resistance protein 2 (MRP2) in chemoresistance and clinical outcome in oesophageal squamous cell carcinoma. *Br J Cancer* 2011; 104: 707.

[558] Huisman MT, Chhatta AA, Van Tellingen O, et al. MRP2 (ABCC2) transports taxanes and confers paclitaxel resistance and both processes are stimulated by probenecid. *Int J cancer* 2005; 116: 824–829.

[559] Guo B, Tam A, Santi SA, et al. Role of autophagy and lysosomal drug sequestration in acquired resistance to doxorubicin in MCF-7 cells. *BMC Cancer* 2016; 16: 1–18.

[560] Li Y, Sun Y, Jing L, et al. Lysosome Inhibitors Enhance the Chemotherapeutic Activity of Doxorubicin in HepG2 Cells. *Chemotherapy* 2017; 62: 85–93.

[561] Sonee M, Barrón E, Yarber FA, et al. Taxol inhibits endosomal-lysosomal membrane trafficking at two distinct steps in CV-1 cells. *Am J Physiol* 1998; 275: C1630-9.

[562] Li Z, Zhu Y-T ting, Xiang M, et al. Enhanced lysosomal function is critical for paclitaxel resistance in cancer cells: reversed by artesunate. *Acta Pharmacol Sin* 2020; 42: 624.

[563] Lund K, Olsen CE, Wong JJW, et al. 5-FU resistant EMT-like pancreatic cancer cells are hypersensitive to photochemical internalization of the novel endoglin-targeting immunotoxin CD105-saporin. *J Exp Clin Cancer Res* 2017; 36: 187.

[564] Dongre A, Weinberg RA. New insights into the mechanisms of epithelial–mesenchymal transition and implications for cancer. *Nat Rev Mol Cell Biol* 2018; 20: 69–84.

[565] YU H, SHEN Y, HONG J, et al. The contribution of TGF-β in Epithelial–Mesenchymal Transition (EMT): Down-regulation of E-cadherin via snail. *Neoplasma* 2015; 62: 1–15.

[566] Ribeiro AS, Paredes J. P-Cadherin Linking Breast Cancer Stem Cells and Invasion: A Promising Marker to Identify an 'Intermediate/Metastable' EMT State. *Front Oncol* 2014; 4: 371.

[567] Nan JN, Kim OR, Lee MA. β-Catenin expression is associated with cell invasiveness in pancreatic cancer. *Korean J Intern Med* 2019; 34: 618–625.

[568] Satelli A, Li S. Vimentin in cancer and its potential as a molecular target for cancer therapy. *Cell Mol Life Sci* 2011; 68: 3033–3046.